THE
PHYSICAL REVIEW

A journal of experimental and theoretical physics established by E. L. Nichols in 1893

SECOND SERIES, VOL. 80, NO. 2 OCTOBER 15, 1950

On the Theory of Slow Neutron Scattering by Solid and Liquid Helium*

L. GOLDSTEIN AND D. W. SWEENEY
University of California, Los Alamos Scientific Laboratory, Los Alamos, New Mexico
(Received June 26, 1950)

The slow neutron scattering properties of solid and liquid helium are studied in this paper on the assumption that these condensed phases have similar crystal structures. It is shown that, according to this limiting solid model, liquid helium, in contrast with usual structures, should exhibit a smoothly increasing total scattering cross section from the lowest group of neutron energies available at present up to those higher energies at which the asymptotic, free atom cross-section value should be approached. Neutron transmission experiments at various energies should enable one to determine whether this liquid scatters slow neutrons as a solid or not, and if the two liquid modifications have similar or dissimilar slow neutron scattering properties.

IN view of the absence of a rigorous theory of liquid helium, it was thought that the theoretical investigations of the neutron scattering properties of this fluid according to extreme models might be of interest. This was carried out previously with the ideal Bose-Einstein fluid model,[1] and the extreme solid model has been studied in this paper. Some of the results thus obtained will be described below. It should be noted that the scattering of very low energy neutrons, in an energy range not available at present, by liquid HeII described by the hydrodynamic model has been studied previously by Akhiezer and Pomeranchuk.[2]

The x-ray analysis of solid helium has been made by Keesom and Taconis.[3] According to them the most probable structure of this solid is of the ideal hexagonal close-packed form. Using this result, the polycrystalline, total coherent cross section, per atom, can be written down as:

$$\sigma/\sigma_f=(1/\sigma_f)\sum_{d=\frac{1}{2}\lambda}\sigma_d, \qquad (1)$$

where $d(hkl)=\lambda/\{2\sin[\theta(hkl)/2]\}$ is the spacing of the set of crystal planes of index triplet (hkl), λ is the de Broglie wave-length of the incident neutrons, θ is the scattering angle (double the Bragg angle). The summation extends over all partial cross sections σ_d which at the wave-length λ cooperate in the coherent scattering, and σ_f is the free atom total scattering cross section. In hexagonal close-packed structure, with the axial ratio c/a equal to $2(2/3)^{\frac{1}{2}}$,

$$d(hkl)/a=[(4/3)(h^2+hk+k^2)+(3/8)l^2]^{-\frac{1}{2}},$$

a being the side of the basic hexagon, $d(hkl)$ the spacing of the planes (hkl) or those equivalent sets which result from this one by the allowed permutations of the first two indices and their negative sum. The number of these similar or cooperating sets in the polycrystalline material will be denoted by N_d. The unit cell of this structure is a parallelopiped having a rhombus of side a as base and a height c or $2(2/3)^{\frac{1}{2}}a$. Its volume is $2^{\frac{1}{2}}a^3$ and contains two atoms. This crystal has thus two characteristic vibration frequency spectra, the low frequency acoustical branch and the high frequency or optical one, with no forbidden frequency gap between them. The cell structure factor is then

$$F_d=2\{1+\cos 2\pi[\tfrac{1}{3}(h+2k)+l/2)]\}.$$

The specific total coherent cross sections $\sigma_{d(hkl)}$ are given by

$$\sigma_d/\sigma_f=[(A+1)^2/A^2](\lambda^2/8\pi B)N_dF_d d\exp(-2W_d), \qquad (2)$$

where B is the volume of the unit cell, A is the atomic number of the crystal atom, while the exponent W_d of the exponential factor, familiar from the theory of

* Reported at the Washington, D. C., meeting of the American Physical Society, April 29, 1950.

[1] L. Goldstein, Proc. Conf. Low Temperature Physics, M.I.T., Cambridge, September, 1949; and Goldstein, Sweeney and Goldstein, Phys. Rev. 77, 319 (1950).

[2] A. Akhiezer and I. Pomeranchuk, J. Phys. USSR 9, 461 (1945).

[3] W. H. Keesom, Helium (Elsevier Publishing Company, Inc., Amsterdam, Holland), pp. 368–373.

x-ray scattering, is essentially the square of the ratio of neutron momentum change in the coherent scattering to the average momentum of the vibrating crystal atom. Explicitly,

$$W_d=\frac{3h^2}{2MkΘd^2}\left[\frac{1}{4}+\left(\frac{T}{Θ}\right)^2 D\left(\frac{Θ}{T}\right)\right] \tag{3}$$

$$D(x)=\int_0^x (e^y-1)^{-1}y\,dy;\quad D(\infty)=\pi^2/6.$$

Here h is Planck's constant, M the mass of the scattering atom, $Θ$ the average characteristic temperature of the solid, k Boltzmann's constant, and T the absolute temperature of the crystal. The theory of coherent neutron scattering by crystals has been given repeatedly,[4] and we have tried, in the preceding lines, to indicate the manner in which it was applied to our specific problem of solid and liquid helium. The above theory is based on the applicability of the Born method to the description of the elastic or coherent collision between the neutrons and the assembly of the assumedly harmonically oscillating crystal atoms. The crystal is assumed to have the idealized Debye spectrum of its characteristic vibration frequencies. The artifice of the practically infinite but also sufficiently small crystal sample is also used, allowing thus for the omission of surface effects together with secondary extinction. The solid is supposed to be isotropic with respect to the propagation of the longitudinal and transverse elastic waves, they having no dispersion, while the temperature $Θ$ is an average of the two types of characteristic temperatures.

The solid[5] and liquid helium[6] $Θ$-values were taken to be 32.5°K and 11°K, respectively. Since solid helium has been studied at liquid helium temperatures, $T<4$°K, it is seen that in view of the practically constant solid density values in this temperature range the coherent scattering cross section of the solid is essentially independent of the temperature. The temperature dependent term in the exponential factor, in (2) or (1), can be neglected completely, and it then reduces to its first term due to the zero point motion of the crystal atoms. In liquid helium, while the temperature dependent term cannot be neglected, the zero-point term still predominates. Here the increasing thermal motion of the atoms makes itself felt in the usual way, reducing the coherent scattering cross section. Since the characteristic temperature of the solid is about three times that of the liquid, it is seen that liquid coherent cross sections are considerably smaller than those of the solid. It is fully realized, of course, that the solid model representation of liquid helium is a rather extreme one, but of opposite character to that of the other limiting model of the ideal Bose-Einstein fluid. While the latter tends to impose upon the fluid a relatively high degree of order in momentum space, the former over-stresses in it the degree of spatial order. These models are thus, to a large extent, mutually exclusive. As far as the solid model of the liquid is concerned it should be noted that the assumption of a Debye solid for this liquid is quite difficult to justify from the point of view of the liquid specific heat. It is not clear, at present, whether there is actually a temperature region in which the constant volume specific heat of the liquid could be represented by a Debye type of function.[7] Our main object, however, in the present paper, was to obtain a clear idea of another limiting behavior of the liquid, as to its slow neutron scattering properties, beside those resulting from the extreme Bose-Einstein model.[1]

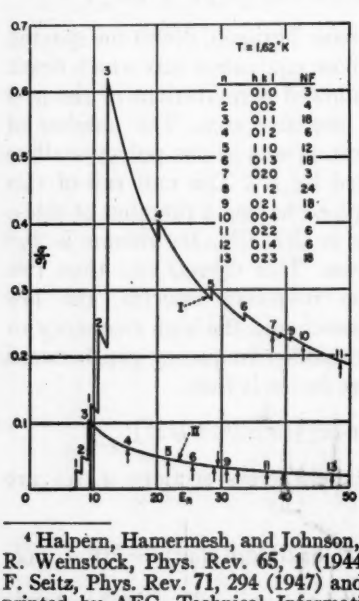

FIG. 1. Total polycrystalline coherent scattering cross sections σ_E in units of σ_f, the total free atom scattering cross section, *vs.* the kinetic energy E_n of the incident neutrons in units of kT_λ. I. Solid helium; II. Liquid helium.

Some of the results obtained in the coherent scattering cross-section calculations are given in Figs. 1 and 2. In Fig. 1, we give two total coherent polycrystalline cross-section ratio curves as a function of the neutron kinetic energy, E_n expressed in units of kT_λ, T_λ being the λ-point temperature of liquid helium, 2.19°K. Curve I represents the solid and curve II the liquid He cross section at a temperature of 1.62°K. It is to be remembered that σ_f, the helium free atom cross section, is about 1.25 barns.[8] The typical jagged character of the solid curve is quite prominent up to about the fifth set of cooperating crystal planes. The indices of these planes, ordered according to their decreasing separation, are given in the table on the figure, together with their NF values, the product of the number N of cooperating planes of equal spacing and the corresponding structure factor F. The smaller liquid cross sections compared with the solid cross sections, together with the rapid disappearance of the discontinuities are clearly shown.

[4] Halpern, Hamermesh, and Johnson, Phys. Rev. 59, 981 (1941); R. Weinstock, Phys. Rev. 65, 1 (1944); M. L. Goldberger and F. Seitz, Phys. Rev. 71, 294 (1947) and their MDDC-1036 paper printed by AEC, Technical Information Division, Oak Ridge, Tennessee.

[5] Reference 3, pp. 226–228.

[6] L. Tisza, Phys. Rev. 72, 838 (1947).

[7] See the discussion of the present status of this problem in Keesom's book quoted in reference 3.

[8] H. Carroll, Phys. Rev. 60, 702 (1941).

The discontinuities correspond to the sudden appearance in the series (1) of a new set of planes, which start to scatter coherently at a precise neutron energy or wave-length equal to their double spacing. The cross section decreases with increasing neutron energy, between two consecutive discontinuities, as E_n^{-1}, or as λ^2 with decreasing wave-length. At sufficiently high neutron energy in the case of the solid and at quite low energies, in the case of the liquid, the cross-section curves become smooth. We have indicated by arrows, the positions of the vanishingly small discontinuities on the liquid cross-section curve.

The temperature dependence of the liquid cross sections is exhibited in Fig. 2, where the 1.62°K liquid curve is replotted with a 3.27°K curve. The discontinuities on these curves correspond successively to the same sets of planes as those indicated in Fig. 1.

We should like to turn now to the discussion of the incoherent, or inelastic scattering processes. These are more complicated than are the coherent processes, for the rather trivial reason that they correspond to a change in state of the crystal oscillators as well as the linear momentum change occurring in the coherent scattering of the neutron. The neutron transfers now both energy and momentum to the solid or receives them from it in the inverse processes. In the direct processes where only one of the $3N$ oscillators forming the crystal of N atoms has been excited in the collision, the main difference between the probabilities of this incoherent process and the coherent one lies in the appearance of the phase-space factor for the emitted elastic quanta or phonon, this in a first approximation and omitting stimulated phonon emission. This is $12\pi(V/h^3)(h\nu)^2d(h\nu)/c^3$, where the already mentioned assumptions, as to the absence of dispersion of the elastic waves, isotropy of propagation, and an average velocity c of these waves, have been incorporated; V is the volume of the crystal. As long as the kinetic energy of the incident neutrons is small in comparison with the Debye energy $h\nu_D$, ν_D is the Debye frequency, or $k\Theta$, the probability of the inelastic collision is simply proportional to the volume of the phase space of phonons extending from $h\nu=0$ to $h\nu=E_n$, E_n being the kinetic energy of the neutrons. This leads at once to a factor of $(E_n/k\Theta)^3$ in the probability or cross section of those incoherent slow neutron scattering processes which are accompanied by the excitation of one phonon only. A more rigorous calculation confirms this energy dependence of the one-phonon total incoherent cross section.[9] A similar semiqualitative reasoning shows, approximately, that those incoherent processes in which two phonons have been excited simultaneously should have a cross section proportional to $(E_n/k\Theta)^6$. In other words, the total incoherent cross section, for slow

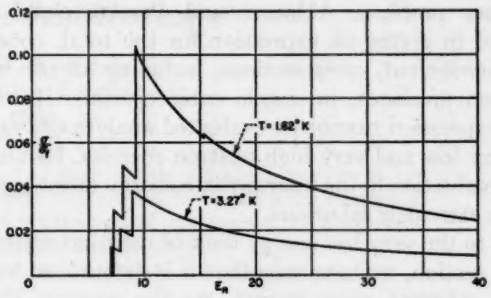

FIG. 2. Total polycrystalline coherent scattering cross-section ratios σ/σ_f of liquid helium *vs.* the kinetic energy E_n of the incident neutrons in units of kT_λ, at two temperatures.

neutrons with kinetic energy small in comparison with the characteristic energy of the crystal, appears to be given by a series of terms of ascending powers of the small quantity $(E_n/k\Theta)^3$. Successive terms in this series correspond to incoherent processes of increasing complexity, two-phonon, three-phonon, . . ., processes. At very low neutron energies only the first term of this series is of importance. The cross section of this process tends to vanish asymptotically as E_n^3 with decreasing neutron kinetic energy E_n. This contrasts with the energy dependence of the coherent scattering cross section which increases with decreasing energy, or one may say that the total slow neutron scattering cross section tends, the geometry of the crystal structure permitting, toward the "bound" atom total cross-section value.

It may be noted here that the energy and momentum conservation theorems tend to inhibit the incoherent processes in favor of the coherent ones at low energies. Indeed the fraction of the energy transferred by a neutron of mass m incident on a stationary nucleus of mass M is proportional, for $m \ll M$, to m/M. At low neutron energies the binding of the atoms in the crystal make these atoms seem to have a larger mass, and hence energy transfer from the neutron to the crystal is increasingly prohibited, in favor of momentum transfers only or coherent processes. This fact alone indicates that in crystals formed by heavy atoms, the incoherent scattering processes are of less importance then in those formed by light atoms. Hence, the problem of the incoherent slow neutron scattering processes in solid and liquid helium is particularly acute.

With increasing neutron energy the multiple phonon processes become more important. The evaluation of these, however, becomes also more complicated. Actually, the theory of these processes is complete as to their fundamentals, insofar as the quantum-mechanical matrix-elements describing these processes can be written down. The detailed analytical evaluation of the individual many-phonon incoherent collision cross sections presents considerable difficulties. Using a summation method first applied by Lamb[10] in connection with

[9] A. Akhiezer and I. Pomeranchuk, J. Exp. Theor. Phys. USSR 17, 770 (1947). We wish to thank here Dr. S. Pasternack, of the Brookhaven National Laboratory, for calling the attention of the senior author to this work.

[10] W. E. Lamb, Phys. Rev. 55, 190 (1939).

another problem, Akhiezer and Pomeranchuk[9] succeeded in giving an expression for the total, coherent and incoherent, cross sections, including all the many phonon processes, in simple cubic crystals. However, this expression cannot be evaluated analytically except at very low and very high neutron energies. Its numerical evaluation in the intermediate energy range appears to be extremely laborious.

As to the very low energy limit of the total scattering cross section, we have seen that it is determined by the total coherent cross section. As the neutron kinetic energy increases, the coherent cross section decreases while the incoherent one increases. At large enough energies the coherent cross section tends to vanish while the incoherent one predominates and increases, approaching the free or unbound atom total scattering cross section asymptotically. It is indeed clear that as the neutron kinetic energy increases, the collision time between the neutron and the oscillating crystal atom becomes small in comparison with the predominating periods of oscillations so that the atom tends to behave as free during the collision and hence should scatter as practically a free atom. The coherent and incoherent processes with cross sections having opposite energy dependence, seem to justify the conjecture[9] that the total scattering cross section of solids should be large at very low neutron energies, $E_n \ll k\Theta$, should decrease with increasing neutron energy, pass through a minimum, then increase and tend asymptotically towards the free atom total cross section at high neutron energies, $E_n \gg k\Theta$.

A glance at the coherent cross-section curves of Fig. 1 shows that as far as solid helium is concerned, the above indicated qualitative energy dependence of the total cross section is quite plausible. In liquid helium, which exhibits rather small coherent cross sections, one is more likely to have a somewhat different energy dependence of its total scattering cross section. In view of the rather great importance of incoherent processes in this light liquid, one should find here an almost smoothly increasing total scattering cross section over practically the whole slow neutron energy range, which is available with sufficient intensity at present. It is, indeed, seen on the liquid cross-section curve, of Fig. 1, that its maximum occurs for neutrons of about 20°K temperature, or already beyond the characteristic temperature of about 10°K of this structure. Since the incoherent cross section must increase from small neutron energies upward, it is expected that its value for 20°K neutrons be of the same order of magnitude as the coherent cross section. Hence, at energies somewhat higher than this, and which are usually available in abundance in the spectrum of thermal columns of fission piles, the increasing incoherent cross sections should predominate in liquid helium, and at the larger energies one should observe the approach toward the asymptotic free atom cross section. One cannot of course rule out a possible small hump in the total cross-section curve around the energy of the maximum of the coherent cross section. However, in view of the smallness of the liquid coherent cross sections, it is more likely that the smoothly increasing total cross section should be characteristic of this liquid over all the available neutron energy range. This result could hardly depend on the assumed crystal structure of the liquid. The smallness of the coherent cross section is due essentially to the small characteristic temperature of the liquid and its attendant open structure associated with its low density.

As a consequence of the preceding considerations the following simple experiment automatically suggests itself. It is seen that by measuring the transmission of liquid helium for slow neutrons, over a wide energy range, one should be able to determine whether this liquid scatters slow neutrons as a solid or not. The total scattering cross section remaining smaller than the free atom cross section would indicate a solid type behavior of this liquid as far as this physical property is concerned. It is to be recalled that a total scattering cross section slightly larger than the free atom cross section and approaching it asymptotically from above, was the behavior resulting from the extreme Bose-Einstein model.[1] Finally the investigation of the slow neutron scattering properties both above and below the λ-point should equally yield further information on the properties of the two modifications of this liquid.

It is planned to perform these experiments in this Laboratory.

Capture Cross Sections for Fast Neutrons*

R. L. HENKEL** AND H. H. BARSCHALL
University of Wisconsin, Madison, Wisconsin
(Received June 23, 1950)

The fast neutron capture cross section of Al^{27} was measured by observing the 2.3-minute activity of Al^{28} for neutron energies between 10 and 550 kev. Resonances were observed which showed some correlation with scattering resonances so that radiation widths of some of the levels could be estimated. Measurements of activation cross sections were also carried out for F, V, Cu^{65}, Ag, I, In^{115}, and Au.

I. INTRODUCTION

MEASUREMENTS of neutron cross sections have yielded a considerable amount of information about nuclear energy levels, in particular about their energies, their neutron widths, and the angular momenta of the incident particles and of the compound states. The present work is concerned with an attempt to obtain, in addition, information concerning the radiation widths of individual levels for light nuclei. In view of the small amount of data available on fast neutron capture cross sections and the inconsistencies in various determinations, further measurements of these cross sections appeared to be also of interest.

A summary of previous measurements of fast neutron capture cross sections is contained in a paper by Hughes *et al.*,[1] which describes the most recent determinations of the capture cross sections for fission neutrons. In almost all of the previous work, either neutrons with a large energy spread were used, or the determinations were carried out for heavy nuclei so that individual absorption resonances were not observed. It has been pointed out by Wigner[2] and Weisskopf[3] that radiation widths of levels can be deduced from measurements taken with poor neutron energy resolution, since the absorption cross section averaged over many levels can be calculated in terms of the radiation width. Nevertheless, it seemed desirable to obtain in a few cases direct measurements of the radiation widths which could be compared with the calculated values.

II. METHOD

Cross sections for the radiative capture of neutrons were determined through observations of induced radioactivities according to the method developed by Segrè[4] and Hughes.[1] In order to avoid the necessity for an absolute determination of neutron and of beta-particle counting efficiencies, the measurement consisted of a comparison of the activations induced by thermal and by fast neutrons in the same sample. A boron proportional counter served as a monitor to measure the relative neutron flux for the two types of activations. Since the variation of the boron disintegration cross section with energy[5] and the thermal activation cross sections of most elements are known, the fast neutron activation cross sections could be obtained.

III. APPARATUS

The samples to be activated consisted of hollow cylinders about 6 cm long and 2 cm in diameter which could be slipped over a Geiger counter. The cylinders were made of metal except in the cases of fluorine, where Teflon, $(C_2F_4)_n$, was used, and vanadium and iodine for which plastic cylinders were prepared from mixtures of NaI or V_2O_5 and polyethylene.

A BF_3 proportional counter served to monitor the neutron flux. The gas was contained between two thin concentric stainless steel cylinders. Four wires placed longitudinally between the cylinders formed the high voltage electrode. The cylindrical sample was inserted into this counter during the activations.

A thin-walled cylindrical Geiger counter was used for determining the induced beta-activity. In order to reduce the cosmic-ray background of the counter, it was surrounded by eight other identical counters mounted parallel to each other and the array was shielded with lead. By means of an anti-coincidence circuit,[6] pulses which were due to particles traversing an outer counter and the center counter were rejected. With this arrangement, the Geiger counter had a background of about six counts per minute.

IV. PROCEDURE

Fast neutrons were produced from the Li(p, n) reaction, using the electrostatic generator. These neutrons are monoenergetic in the forward direction with respect to the incident protons for energies of the main group between 120 and 650 kev. Monoenergetic neutrons below 120 kev could be obtained by carrying out measurements in a backward direction. Because of the low intensity of the neutrons under these conditions, small activation cross sections were difficult to measure below 120 kev, since the boron monitor count produced

* This work was supported partly by the AEC and partly by the Wisconsin Alumni Research Foundation.
** Now at the Los Alamos Scientific Laboratory, Los Alamos, New Mexico.
[1] Hughes, Spatz, and Goldstein, Phys. Rev. 75, 1781 (1949).
[2] E. P. Wigner, Am. J. Phys. 17, 99 (1949).
[3] Feshbach, Peaslee, and Weisskopf, Phys. Rev. 71, 145 (1947).
[4] MDDC-228, unpublished.
[5] R. K. Adair, Rev. Mod. Phys. 22, 249 (1950).
[6] R. Tangen, Det Kgl. Norske Videnskabers Selskabs Skrifter 1946 NR1.

by neutrons scattered from the floor became comparable to or larger than that caused by the neutrons coming directly from the target. The magnitude of this background could not be determined accurately. When the energy of the main neutron group is greater than 650 kev in the forward direction, Be^7 may be left in its 430-kev state[7] and furnish a group of low energy neutrons. Since most absorption cross sections increase with decreasing neutron energy, the small number of low energy neutrons from the $Li^7(p, n)Be^{7*}$ reaction will make the measurements above 650 kev somewhat unreliable. Nevertheless, measurements were made in this range as a check for comparison of the present work with previous results, some of which were obtained also by the use of $Li(p, n)$ neutrons.

For measurements above 120 kev, the boron proportional counter containing the sample was placed in front of the lithium target so as to have its axis coincide with that of the incident proton beam as shown in Fig. 1. Care was taken in positioning the sample so that the sample and the active counting volume of the monitor subtended the same angle at the target.

The effective energy spread of the neutrons depends on the thickness of the lithium target, on the energy spread of the protons (5 kev), and on the variation of neutron energy over the length of the counter and sample due to the angle of emission from the target. This latter effect amounted to about 6 kev in the geometry shown.

In spite of the fact that the counter was surrounded by cadmium, an appreciable fraction of the monitor counts was caused by neutrons which did not come directly from the target. The corresponding background in the induced activity amounted to less than 5 percent. In order to measure these backgrounds, the counter was moved sufficiently far away from the target so that a neutron absorber consisting of paraffin and boron could be inserted between the target and the counter. Both activation and monitor backgrounds were measured at various distances from the target and then extrapolated to the position actually used in the cross-section measurements.

Thermal neutrons were produced by slowing down neutrons from a 100-millicurie radium-beryllium source in a block of paraffin, as shown in Fig. 1. It was found that the thermal neutron flux was most constant over the counter and the sample when the source was placed at the center of the sample and the counter hole was extended throughout the paraffin. Activations and neutron monitor counts caused by epithermal and fast neutrons were corrected for by subtracting the values obtained when the counter and sample were surrounded by cadmium.

Usually the length of activations and beta-counting periods were two half-lives each. A 15-second delay was sufficient to transfer the sample to the Geiger counter. The same schedule was followed for both fast and slow neutron activations. All operations requiring accurate timing were performed by mechanical timers and relay control circuits.

V. RESULTS

In Table I the substances on which measurements were carried out are listed together with the half-life of

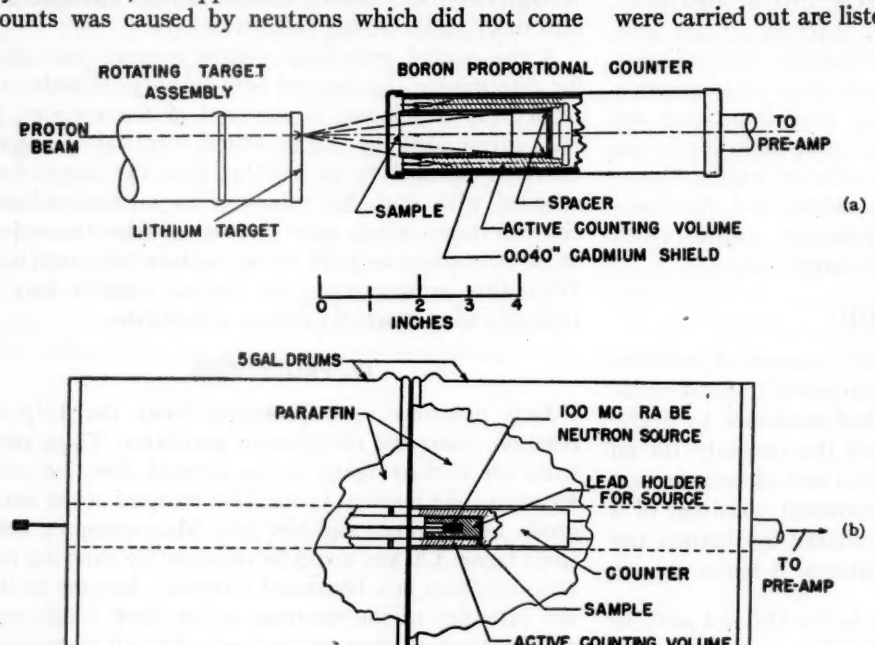

FIG. 1. Apparatus and geometry used for measurements of fast neutron activation cross sections. (a) Fast neutron activation. (b) Thermal neutron activation.

[7] Johnson, Laubenstein, and Richards, Phys. Rev. 77, 413 (1950).

the induced activity and the thermal activation cross section on which the present measurements are based. These substances were chosen because of the convenient half-lives of the induced activities, and because they absorb neutrons of energies below 1 Mev presumably only by radiative capture.

Comparison With Previous Results

Most of the previous measurements of capture cross sections were carried out for heavy elements which have high cross sections for fast neutrons; in particular, Ag^{107}, Ag^{109}, In^{115}, I^{127}, and Au^{197} were investigated carefully at Los Alamos.[4] As a check on the method used in the present work, data on these substances were compared with previous work. The most extensive measurements are available on gold, some of which are shown in the comparison of Fig. 2. Within the rather large uncertainty of both previous and present determinations, the agreement is good.

Similarly, good agreement with the data published in reference 4 was obtained for Ag^{107} and I^{127}. For Ag^{109} on the other hand, the present data give for neutron energies between 120 and 600 kev, cross sections about twice as high as those found by Segrè *et al.* In view of the fact that the measurement of such a short activity (24 sec.) offers some experimental difficulties, particularly because of the presence of the 2.3-min. activity of Ag^{107}, this discrepancy may not be too surprising. The 13-sec. activity of In^{115} gave a rather constant cross section varying from 140 millibarns at 15 kev to 90 millibarns at 1000 kev. The 1-Mev value agrees reasonably well with Hughes' data.

Aluminum

Aluminum appeared to be an element in which capture resonances might be relatively easy to observe. This element has a single isotope and the induced activity has a convenient half-life of 2.3 minutes. Previous measurements of the total cross section of aluminum indicated a sufficiently wide separation of energy levels that it could be expected that levels might be resolved with the energy spreads available in activation experiments.

In the lower part of Fig. 3, the absorption cross section of aluminum in millibarns is plotted against neutron energy in kev. The energy spread of the neutrons was about 10 kev below 100 kev and about 8 kev above this energy. Between 75 and 120 kev, measurements were difficult because of the relatively high background of neutrons scattered by the floor and the low value of the absorption cross section. In this energy range, evidence for at least one maximum was obtained, but because of the large uncertainty in the cross section the data are not shown in Fig. 3.

For comparison, the total cross section of aluminum in barns is shown in the upper portion of Fig. 3. In the total cross-section measurements, the energy resolution was about 10 kev below 50 kev, 25 kev between 50 and 130 kev, 2 kev between 130 and 200 kev, and 8 kev above this energy.

TABLE I. Thermal neutron activation cross sections.

Isotope	Percentage abundance	Induced half-life	Thermal activation cross section (barns)
F^{19}	100	10.7 sec.	0.01
Al^{27}	100	2.3 min.	0.22
V^{51}	100	3.7 min.	4.8
Cu^{65}	31	4.3 min.	2.05
Ag^{107}	51	2.3 min.	34
Ag^{109}	49	24 sec.	85
In^{115}	96	13 sec.	145
I^{127}	100	25 min.	6.1
Au^{197}	100	2.7 days	95

Fluorine

Measurements of the capture cross section for fluorine are complicated by the fact that its cross section is small and the half-life of the induced activity is so short (10.7 sec.). In the lower part of Fig. 4 the results of the investigations of two energy regions with an energy resolution of 20 kev are shown. The upper part of the figure gives the total cross section of fluorine, also measured with 20 kev energy spread.[8]

The mass values published in some of the literature[9,10] would lead to an exothermic $F^{19}(n,\alpha)N^{16}$ reaction which might be difficult to distinguish from the radiative capture process since the induced half-lives are 7.4 sec. for N^{16} and 10.7 sec. for F^{20}. However, recent work[11,12] has shown that the (n,α) reaction does not occur for fluorine in the energy range covered by this

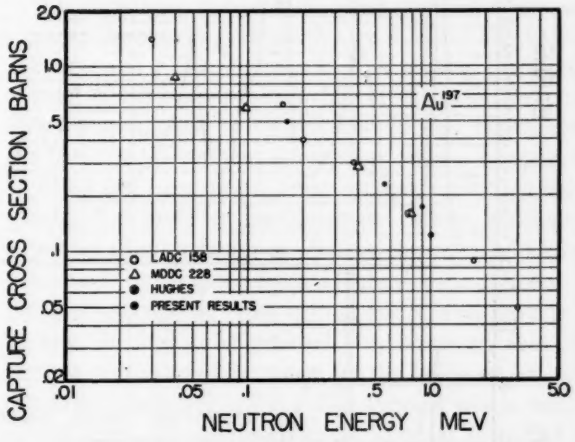

FIG. 2. Comparison of present results with previous values of neutron capture cross section for gold as a function of neutron energy.

[8] C. K. Bockelman (to be published).
[9] H. A. Bethe, *Elementary Nuclear Theory* (John Wiley & Sons, Inc., New York 1947), p. 124.
[10] J. Mattauch, *Nuclear Physics Tables* (Interscience Publishers, Inc., New York 1946), p. 126.
[11] H. S. Sommers and R. Sherr, Phys. Rev. **69**, 21 (1946).
[12] J. V. Jelley and E. B. Paul, Proc. Phys. Soc. London **63**, 112 (1950).

experiment, since the reaction energy is about −1.2 Mev.

Vanadium

According to measurements by Blair and Wallace,[13] energy resolutions of 5 to 10 kev are sufficient to find the effect of fast neutron resonances in vanadium but not to resolve the resonances fully. Determination of the capture cross section of vanadium carried out with 8-kev energy resolution indicated, in qualitative agreement with the total cross-section measurements, the presence of ten not fully resolved maxima between 120 and 650 kev. In view of the close spacing of the levels, it is difficult to judge whether the position of the resonances observed in total and capture cross sections agree, since the apparent spacing of the peaks is probably largely determined by the experimental resolution. The measured cross section of vanadium fluctuates by not more than 3 millibarns around a smooth curve which decreases from 16 millibarns at 120 kev, to 6 millibarns at 400 kev and to 3 millibarns at 650 kev.

Copper

With 8-kev resolution, the effect of individual levels on the capture cross section of copper could be noticed. Repetition of the measurements with 20-kev neutron resolution yielded a smooth curve. Observed values of the absorption cross section were 30 millibarns at 150 kev, 20 millibarns at 300 kev, and 13 millibarns at 500 kev. This cross section is for the Cu^{65} isotope only.

VI. SOURCES OF ERROR

The present determinations of fast neutron capture cross sections depend directly upon the boron disintegration cross section and the thermal activation cross sections, and are uncertain by at least the errors of these previous measurements. The probable error in the fast neutron boron cross section is about ±15 percent, while the probable error of most thermal activation cross sections is ±20 percent. An attempt was made to keep additional errors in the present comparison appreciably below 20 percent. In addition, the comparison used in the present determinations involves the assumption that both the boron cross section and the activation cross sections follow the $1/v$ law in the region of thermal energies. If the activation cross section deviated from this law, a small error is introduced for which no correction was made. It is estimated that the present data have a probable error of 30 percent.

VII. DISCUSSION

According to the Breit-Wigner theory of nuclear resonances, the resonance contribution to the cross sections for elastic scattering and radiative capture should be in the ratio of the neutron width to the

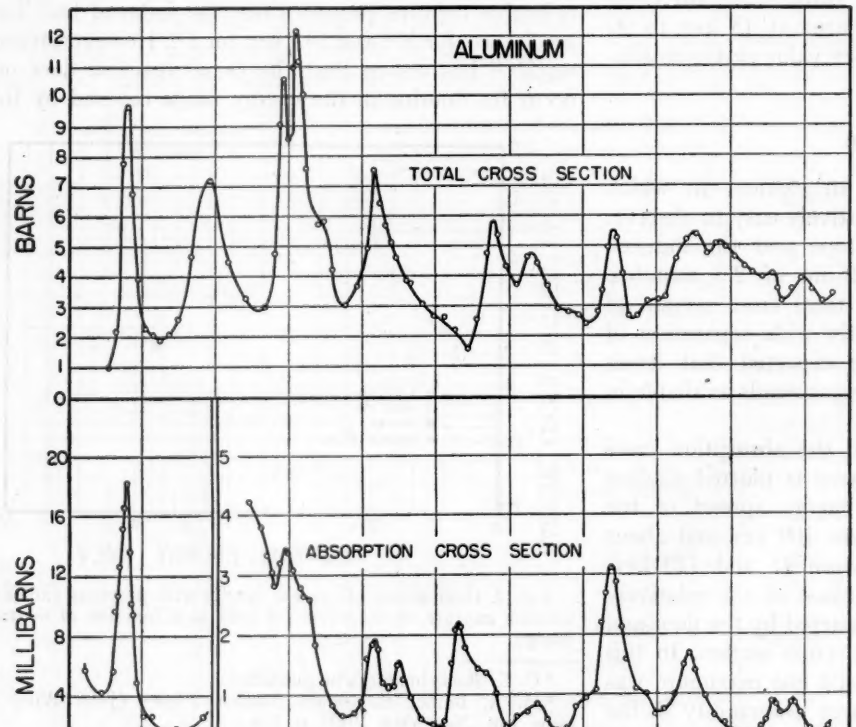

FIG. 3. Comparison of total cross section and capture cross section for aluminum as a function of neutron energy.

[13] J. M. Blair and J. R. Wallace, Phys. Rev. 79, 28 (1950).

radiation width of a level. For the nuclei for which the effect of individual levels were observed in the present investigation, the neutron widths are of the order of a thousand times larger than the radiation widths. As a consequence, the total widths of both scattering and radiative capture resonances should be practically equal to the neutron width. From the observed width of the resonance and the ratio of the scattering and absorption cross sections, it should then be possible to obtain values for the radiation widths. Factors which have to be taken into account in the evaluation are the following: For the energy region covered, if the observed resonance is due to *s*-neutrons, resonance and potential scattering will interfere in such a way as to shift the peak in the scattering cross section to a higher energy with respect to the absorption maximum by about half the width of the level. This energy shift will cause some uncertainty in correlating maxima in the two cross-section curves, if the peaks are closely spaced. On the other hand, this effect might be helpful in some cases in determining the angular momentum of the neutrons responsible for the resonance.

Another consideration which complicates the determination of radiation widths is the difference in the effect of finite energy resolution on the shape of the observed resonances in scattering and absorption. For both scattering and absorption measurements, the resonance peaks will be spread out if the energy spread of the neutrons is greater than the width of the resonance. Since the scattering cross sections were determined from transmission experiments, there is an additional hardening effect which will reduce the peak heights. While the area under a peak in the capture cross section is independent of the resolution used, the area under a peak in the scattering cross section increases as the resolution is improved. Therefore, estimates of radiation widths obtained from comparing peak heights will be reliable only if the maxima are fairly well resolved. By comparison of the observed height of a maximum in the total cross section with the theoretical maximum predicted by the Breit-Wigner theory it is possible to determine how well this condition is fulfilled.

It would be expected that every resonance should be observable in both the scattering and in the absorption cross sections. Neither in fluorine nor in aluminum is this correlation found for all the resonances.

For fluorine, the positions of the 280- and 590-kev maxima agree well on the curves shown in Fig. 4. Both resonances probably have natural widths not

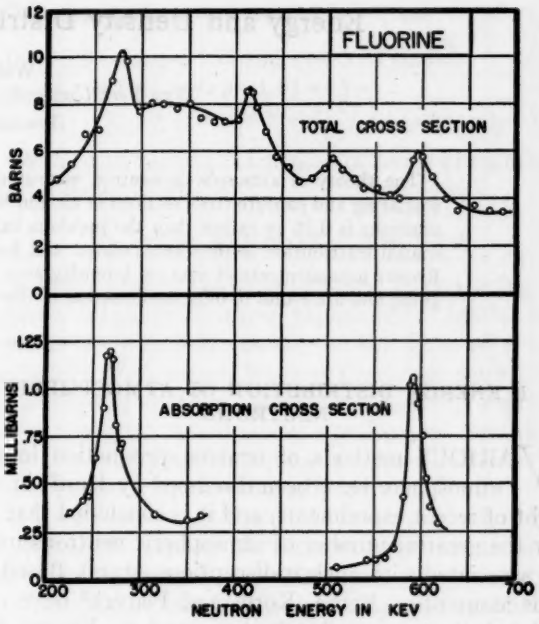

FIG. 4. Comparison of total neutron cross section and neutron capture cross section for fluorine.

appreciably smaller than the measured widths. A comparison of the peak heights for the two curves gives radiation widths of about 15 ev. No indications of peaks in the capture cross section were found, however, corresponding to the maxima shown at 340 and 510 kev in the total cross section. These latter two maxima are very broad so that the neutron widths may be too large compared to the radiation widths to give measurable peaks in the absorption cross section.

The aluminum curves show good agreement between some of the maxima, in particular those of the 40-kev, 215-kev, and 370-kev resonances. A reliable correlation of most of the other peaks is difficult since the structure is too complicated to be resolved in this experiment. For the three prominent absorption peaks a comparison of total and absorption cross section yields radiation widths of 5 to 15 ev for aluminum. These widths are larger by about a factor of 10 than the value of 1.25 ev calculated by Wigner from Hughes' measurement of the average capture cross section and a level spacing of 50 kev. It should be pointed out, however, that the present widths are determined for the levels which have the largest radiation widths. The average width, taking into account the narrower levels, appears to the of be same order of magnitude as the calculated value.

Energy and Density Distribution of Cosmic-Ray Neutrons*

WILLIAM O. DAVIS**
New York University, University Heights, New York
(Received June 7, 1950)

The theory of atmospheric neutron measurements is reviewed in the light of recent data on neutron scattering and capture cross sections in air and boron. It is concluded that the mean energy of atmospheric neutrons is 0.26 ev rather than the previous value of 0.06 calculated by Bethe, Korff, and Placzek. The spatial distribution is then recalculated and found to agree closely with earlier calculations by Flügge. Recent measurements of neutron intensity as a function of altitude are discussed in the light of the foregoing and are found to offer confirmation of the new calculations.

I. ENERGY DISTRIBUTION OF ATMOSPHERIC NEUTRONS

VARIOUS methods of neutron production in the atmosphere have been discussed by Korff[1] in the light of recent experiments, and it is concluded that by far the greatest number of atmospheric neutrons must be associated with nuclear disruptions (stars). Based on this assumption Bethe, Korff, and Placzek[2] have calculated the energy distribution, and S. Flügge[3] has calculated the expected density distribution of slow neutrons in the atmosphere. These distributions have been recalculated numerically by the author on the basis of more recent data on neutron cross sections in oxygen and nitrogen.

Using the Bohr model of the compound nucleus, Bethe, Korff, and Placzek[2] show that the mean diffusion length in the atmosphere for neutrons to be slowed down to 4 Mev by inelastic scattering is of the order of 36 g/cm². Below this energy, the lowest excitation level in oxygen or nitrogen, all further scattering is assumed to be elastic. When all scattering is elastic the fraction of neutrons which are slowed down to energy E without being captured is given by:[3]

$$N/N_0=\exp\left[-(M+1)\frac{\sigma_c(1\text{ ev})E^{-\frac{1}{2}}}{\bar{\sigma}_s}\right], \qquad (1)$$

where σ_c is the neutron capture cross section in air as a function of E and $\bar{\sigma}_s$ is the mean scattering cross section over the energy region concerned. This fraction differs appreciably from unity only at low energies and in this region the Columbia group gives the total cross section of nitrogen in the form:[4]

$$\sigma_t=(9.96+0.34E^{-\frac{1}{2}})\text{ barn}, \qquad (2)$$

where E is in ev. The constant term represents the scattering cross section, while the term in $E^{-\frac{1}{2}}$ is the capture cross section. On this basis the value of σ_c at 1 ev for nitrogen is 0.34 barn. Considering the capture cross section of oxygen to be negligible by comparison, we compute the effective cross section for air at 1 ev to be 0.28 barn.

In deriving Eq. (1) a constant value of σ_s was assumed throughout the region of integration. This is true for oxygen but not quite true in the case of nitrogen, although in the region where 99 percent of the value of the integral is developed (<40 ev), it holds very well.[5] By integrating the cross-section curves of Goldsmith, Ibser, and Feld, and again forming a weighted average for oxygen and nitrogen, a value of 8.6 barns for the mean scattering cross section of air over the entire region is obtained.

Using these values, and with $M=14.6$, the fraction of neutrons which get down to energy E without being captured is given by:

$$N/N_0=\exp(-0.509E^{-\frac{1}{2}}). \qquad (3)$$

In particular, the exponent becomes unity for

$$\bar{E}_c=0.26\text{ ev}. \qquad (4)$$

In other words, neutrons will on the average be slowed down to this energy before being captured.

The value originally computed in the same manner by Bethe, Korff, and Placzek[2] on the basis of earlier cross-section data was 0.06 ev. The calculation of absolute neutron intensities in the atmosphere shows the significance of this difference. If the average neutron energy had the lower value, then the use of a cadmium shield in the determination of atmospheric neutron intensities, would introduce little error, since a large percentage of the neutrons in the atmosphere would have energies below the cadmium cut-off (about 0.4 ev). On the other hand, if we accept the larger value, then a relatively larger number of neutrons will have energies above the cut-off and a substantial error will be introduced. From experimental observation the latter conclusion appears to be correct.

II. DENSITY DISTRIBUTION

Let us now consider the mean distance travelled before capture by a neutron slowing down in the atmos-

* This work was performed under contract with the Air Materiel Command, U.S. Air Force, and with the ONR.
** Major, USAF, now at Los Alamos Scientific Laboratory, New Mexico.
[1] S. A. Korff, Rev. Mod. Phys. 20, 327 (1948).
[2] Bethe, Korff, and Placzek, Phys. Rev. 57, 573 (1940).
[3] S. Flügge, Chapter 14, *Cosmic Radiation* (Dover Publications, New York, 1946), W. Heisenberg, editor.
[4] E. Melkonian, Phys. Rev. 76, 1750 (1949).
[5] Goldsmith, Ibser, and Feld, Rev. Mod. Phys. 19, 259 (1947).

phere, and the mean absorption depth. When the scattering is done by elastic collisions, i.e., at energies below 4 Mev, Bethe, Korff, and Placzek[2] give the mean square diffusion length as:

$$\langle r^2\rangle_{Av}=(M_{eff}+1)\int_{0.26\ ev}^{4\ Mev} l^2(E)dE/E, \tag{5}$$

where $l(E)$ is the total mean free path in g/cm² as a function of the neutron energy, and $M_{eff}=14.6$.

This integral can now be evaluated more accurately since $\sigma(E)$ over the entire range of energies has been measured quite accurately.[4,5] Performing the integration and assuming a mean diffusion length of 36 g/cm² above 4 Mev we find the total mean diffusion length to be:

$$[\langle r^2\rangle_{Av}]^{\frac{1}{2}}=154\ \text{g/cm}^2, \tag{6}$$

and the mean absorption depth

$$L=[\tfrac{1}{3}\langle r^2\rangle_{Av}]^{\frac{1}{2}}=89\ \text{g/cm}^2. \tag{7}$$

Because of the uncertainty at higher energies these figures are probably uncertain by plus or minus ten percent.

According to Bethe, Korff, and Placzek,[2] if all neutrons are produced at the very top of the atmosphere the slow neutron density will vary as follows:

$$N(v,x)=x\exp(-x^2/2L^2), \tag{8}$$

and will thus have a maximum at $x=L$. Since the maximum of neutron production presumably takes place at some depth between 0 and L, we should expect the measured maximum of slow neutron density to fall at a somewhat greater depth.

If we assume that neutrons are produced primarily in nuclear disruptions then Flügge[3] gives the distribution of neutrons after diffusion to the mean energy in the form of a Fourier series. Because of insufficient cross-section data, several assumptions had to be made originally in the numerical calculation of terms. In the light of new data[4,5] the author re-calculated terms. It was found that although the assumptions made did not in general turn out to be correct, several factors balanced out so that the new solution agreed with one of Flügge's quite closely. The general expression is:

$$\rho_0(p)=2J_0\sum_{n=1}^{\infty}\frac{n\pi}{\mu^2+n^2\pi^2}0.995^{n^2}\left[\frac{a(1-0.0166n^2)!}{\alpha^{2-0.0166n^2}}+\frac{b(1-0.0166n^2)!}{\beta^{2-0.0166n^2}}\right]\sin n\pi p. \tag{9}$$

Here $\rho_0(p)$ is the neutron density as a function of pressure in atmospheres; μ is found from experiment to be approximately 7 atmos.$^{-1}$; $a=0.178$; $b=6.16$ (both in arbitrary units); $\alpha=0.08$ Mev^{-1}; and $\beta=0.35$ Mev^{-1}. J_0 is an arbitrary normalization factor.

The first seven terms (with $2J_0=1$) are:

$$\rho_0(p)=3.96\sin\pi p+4.72\sin2\pi p+3.81\sin3\pi p+2.65\sin4\pi p+1.85\sin5\pi p+1.01\sin6\pi p+0.74\sin7\pi p+\cdots. \tag{10}$$

A plot of this function expressed in terms of millibarns will be found in Fig. 1.

III. SLOW NEUTRON DETECTION

We turn now to the detectors used in measuring the neutron intensity in these experiments. Let us first consider an idealized counter in the form of a thin unshielded $1/v$ detector. We have previously shown that the number of neutrons outside the $1/v$ energy region in air is negligibly small under equilibrium conditions. Under these conditions, then, we need only consider the region in which this law holds in air.

It then follows that there is a mass of air which will, at all energies, capture the same number of neutrons as the detecting element. Put another way, n captures per sec. in the entire mass of the detector implies q captures per gram per sec. in air. If the detector is a gas this relationship between the two capture rates is given to be:[2]

$$q=n(\sigma_a/\sigma_d)(780/V_d p_{0d})\ g^{-1}\ \text{sec.}^{-1}, \tag{11}$$

where V_d is the volume of the detector, p_{0d} is the filling

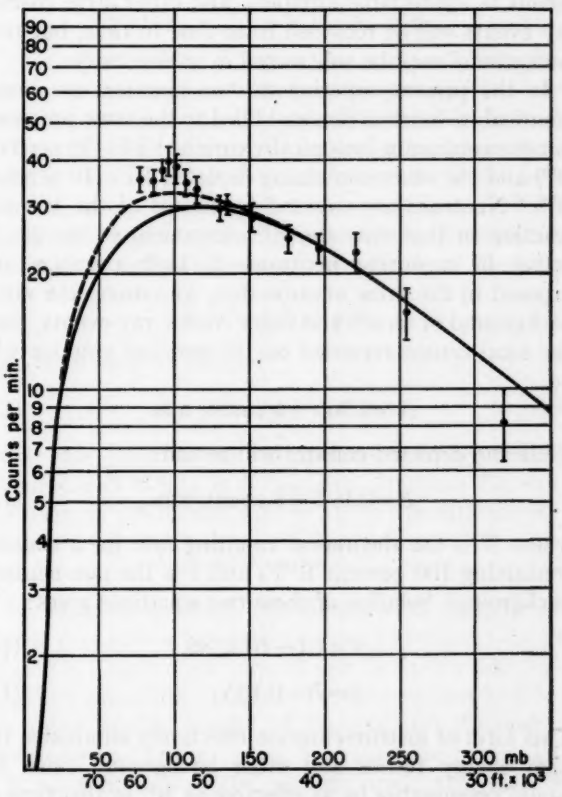

FIG. 1. Comparison of the data with theory. The theoretical curve is taken from reference 3 ($J_0=1.00$). The dashed curve is the same after correction for absorption in Pyrex.

TABLE I. Experimental neutron counting rates.

Pressure (mb)	N(Yuan) (c/min.)	N(Davis) (c/min.)	Absorption (percent)
300	13.6	11.6	15
250	19.3	16.5	15
150	34.7	31.0	11
100	39.0	36.0	8

pressure in atmospheres corrected to 0°C, and σ_a and σ_d are the capture cross sections of air and detector respectively. The ratio σ_a/σ_d is a constant since both are proportional to $1/v$.

Since the mean distance traveled by neutrons from the point of production is only about 150 g/cm², it follows that in a large region of the atmosphere the production rate will be in equilibrium with the absorption rate. In this region, which in practice lies between about 220 mb and 800 mb in the atmosphere (1 mb, $\cong 10^{-3}$ atmos.), the production rate is given directly by q.

On the basis of present day knowledge and proper instrumentation it is possible for us to consider an arrangement of BF_3 proportional counters as an excellent approximation to this theoretical detector. We now know the extension of the $1/v$ law for boron into higher energy regions[5] and find very slight variation in the important region. High energy neutrons will produce recoils in appreciable numbers, and other large cosmic ray events will be recorded from time to time, but this background may be subtracted in various ways.

In the present experiments two counters are used, identical in construction and filled to the same pressure, but one containing isotopically enriched BF_3 (96 percent B^{10}) and the other containing depleted BF_3 (10 percent B^{10}).[6] Neutrons are counted by means of the $B^{10}(n\alpha)$ reaction so that only the B^{10} component of the gas is active in capturing neutrons. If both counters are exposed to the same neutron flux, containing the same background of recoils and other cosmic-ray events, then the total counts recorded on the enriched counter will be:

$$A=0.96N+b \text{ count/min.}, \tag{12}$$

while the depleted counter will record:

$$B=0.10N+b \text{ count/min.}, \tag{13}$$

where N is the theoretical counting rate for a counter containing 100 percent $B^{10}F_3$ and b is the non-neutron background. Solution of these two equations gives:

$$N=(A-B)/0.86, \tag{14}$$

$$b=B-0.10N. \tag{15}$$

This form of instrumentation effectively eliminates the high energy recoils and other background since B^{11} would presumably be as effective as B^{10} in this type of event. It has a major advantage over the cadmium shield method in that all neutrons are counted rather than merely those in the slowest region.

Before the BF_3 counter can be regarded as an ideal $1/v$ detector corrections must be made for the envelope with which it is surrounded. If a glass envelope is used, it is important to ascertain its boron content, since the most common laboratory glasses, for example Pyrex, are usually boro-silicates. To a first approximation the percentage absorption by a thin envelope as a function of energy is:[7]

$$H=\sigma(E)A\rho Pt/M_N \text{ (percent)}, \tag{16}$$

where $\sigma(E)$ is the boron capture cross section in cm² as a function of E; A is Avogadro's number; ρ is the density of the glass used; P is the percentage by weight of boron in the glass; t is the thickness of the envelope; and M_N is the mean atomic weight of the glass.

For example, in the counters used in the present experiments (Pyrex): $\rho=2.23$; $P=4.4$ percent; $t=0.2$ cm; and $M_N=19.2$, so that:

$$H=6.1\times10^{-2}\times\sigma(E) \text{ (percent)}, \tag{17}$$

where $\sigma(E)$ is in barns.

If we assume the mean energy of neutrons in the atmosphere to be 0.26 ev as calculated, then the mean absorption

$$H=14 \text{ percent} \tag{18}$$

for the present experiments.

After appropriate corrections have been made it is then possible to consider the BF_3 counter as a nearly ideal $1/v$ detector and to use it to measure the rate of absorption of neutrons in the atmosphere.

IV. EXPERIMENTAL

The general method of instrumentation has already been described. Counters were filled with multiply-distilled BF_3 gas and were carefully matched as to plateau characteristics. All the counters used had approximately 150-volt neutron plateaus in the proportional region centered at 2050 volts. Contamination backgrounds were found to be less than $\frac{1}{4}$ c/min. in all cases.

To prevent spurious counts due to corona discharge at high altitudes the entire high voltage system including the counters was pressurized and units were tested at a simulated altitude of 100,000 feet for an extended time in the high altitude chamber at Mitchel Air Force Base, New York. In addition, extensive temperature and pressure tests on all elements of circuitry were made and revealed negligible effects within the range of temperatures normally encountered.

Pulses from the two counters were fed alternately through the same amplifying system and data were telemetered to two ground stations.

[6] Obtained from the Oak Ridge National Laboratory of the AEC.

[7] S. A. Korff, *Electron and Nuclear Counters* (D. Van Nostrand Company, Inc., New York, 1946).

Apparatus was flown by means of a General Mills polyethylene balloon 30 feet in diameter and ballast controls were added to cause the balloon to float nearly level at two successive altitudes. In this way it was possible to investigate the regions of the atmosphere which were specifically of interest. Details of this technique and a discussion of the electronic circuits will be published elsewhere. All flights were made in the vicinity of Rome, New York, geomagnetic latitude 55°8′ N.

V. COMPARISON WITH THEORY

In agreement with Yuan[8,9] a maximum in the neutron density as a function of altitude was found to exist. Under the conditions outlined by Bethe, Korff, and Placzek,[2] and Flügge[3] the maximum was found at about 100 g/cm² absorption depth (7.3 cm Hg). Yuan, counting only those neutrons with energies below the cadmium cut-off, found a maximum at 8.5 cm Hg or 113.5 g/cm². Since the two experiments did not measure the same thing it is to be expected that results will differ somewhat. Interpretation of Yuan's data in the light of the calculations described earlier in this paper shows his results to be in agreement generally with those of the author.

The primary source of disagreement between the two experiments was, of course, in the method of instrumentation used. Since at the higher elevations the percentage of more energetic neutrons increases, the counting rate as measured by the cadmium shield method will have its maximum at a lower altitude.

Another factor which must be considered in comparing Yuan's data with that of the author's is the effect of the boron in the Pyrex envelopes used by the latter. Yuan employed soft glass counters with negligibly small boron content.

By comparing the present results with those of Yuan it is possible to check the calculated value of the mean energy of neutrons in the atmosphere. Table I was prepared using data from three flights of Yuan[10] and one of the author's. Correction was made for the difference in counter volume and filling pressure between the counters used in the various experiments. Noncapture background was assumed to be the same for all apparatus, after efficiency corrections were made. In this table N is the neutron counting rate for 100 percent B^{10} content in the BF_3. Data from Yuan's experiments were taken only from the unshielded counters.

In view of the uncertainties in the relative counter calibrations this was taken as good agreement with the calculated absorption of 14 percent. The absorption of 29 percent which would have resulted if the mean energy were 0.06 ev does not seem to be indicated.

It will be noted that absorption is less at the higher altitudes. This is to be expected in view of the increasing proportion of higher energy neutrons at the higher elevations, and resultant higher mean neutron energy in Eq. (17).

An attempt was made to fit the observed data to the theoretical curve drawn from Eq. (10). This plot may be seen in Fig. 1. The solid curve represents the calculations with $J_0=1.00$. The curve was fitted by inspection. The dashed curve represents a correction for the changing absorption in Pyrex as observed experimentally. It will be noted that the effect of this changing absorption is to move the maximum to a higher altitude, which seems to agree with experiment. Although the statistical fluctuation is rather large it is felt that no basic disagreement between theory and experiment is shown in this curve.

For the counters used in these experiments the quanties in Eq. (11) are: $V_d=234$ cm³, $\sigma_d=585E^{-\frac{1}{2}}$ barn (based on 100 percent B^{10}); $\sigma_a=0.28E^{-\frac{1}{2}}$ barn; $p_{0d}=0.232$ atmos.; $n=N/60$ sec.$^{-1}$ when N is given in counts per minute, so that the production rate of neutrons in the atmosphere,

$$q=1.15\times10^{-4}\times N \text{ g}^{-1} \text{ sec.}^{-1}. \tag{19}$$

The production rate was calculated at two altitudes, namely those corresponding to 250 mb and 300 mb. The results were as follows:

$$\begin{aligned} &250 \text{ mb}, \quad q=2.2\times10^{-3} \text{ g}^{-1} \text{ sec.}^{-1}, \\ &300 \text{ mb}, \quad q=1.5\times10^{-3} \text{ g}^{-1} \text{ sec.}^{-1}. \end{aligned} \tag{20}$$

It is of interest to compare the neutron production rate in the atmosphere with that for protons. T. Coor[11] gives the proton production rate at 8.9 cm Hg (119 mb) in the copper-air mixture of an ionization chamber as 0.015 g^{-1} sec.$^{-1}$. In order to compare production rates it is necessary to extrapolate values obtained in the equilibrium region up to higher altitudes. If we assume in the lower region a pressure dependence of the form:

$$N=N_0 \exp(-\mu p), \tag{21}$$

then from data we obtain:

$$N=109 \exp(-0.007p). \tag{22}$$

Using this equation the extrapolated counting rate at 8.9 cm Hg (119 mb) is 47.5 c/min. Applying Eq. (19), the neutron production rate in air at this altitude is:

$$q=0.006 \text{ g}^{-1} \text{ sec.}^{-1}. \tag{23}$$

In order to compare this figure with that for the proton production rate it is necessary to correct for the copper in Coor's apparatus. It can be shown that for a spherical ionization chamber of copper as used by Coor, the mean atomic weight of the gas and chamber is effectively that of the copper, to at least one part in 100.

If we assume that the neutron production rate, R, at a given altitude may be represented empirically by

[8] L. C. L. Yuan, Phys. Rev. **74**, 504 (1948).
[9] L. C. L. Yuan, Phys. Rev. **76**, 165 (1949).
[10] L. C. L. Yuan, private communication.
[11] T. Coor, private communication.

the relation

$$R=CZ^{\alpha}, \tag{24}$$

where Z is the atomic weight and C is a constant, then from the data of Montgomery and Tobey[12] for carbon and aluminum we find α to be approximately 0.5. Using 14.6 for the mean atomic weight of air and 64 for copper we calculate the neutron production rate in copper at 119 mb to be

$$q_c=0.013\ \text{g}^{-1}\ \text{sec.}^{-1}. \tag{25}$$

[12] C. G. Montgomery and A. R. Tobey, Phys. Rev. 76, 1478 (1949).

When compared with the proton production rate at this altitude these data support the view that protons and neutrons are formed in approximately equal numbers in stars.

In conclusion the author wishes to extend grateful thanks to Professor S. A. Korff under whose direction this work was performed, and to the members of the New York University Cosmic-Ray Group: L. G. Collyer, H. A. C. Neuburg, M. Pavalow, W. P. Staker, and M. Swetnick.

The electronic equipment was designed and engineered by M. Pavalow and L. Hillman, and the author is indebted to the New York University Balloon Project for making the balloon flights for these experiments.

PHYSICAL REVIEW VOLUME 80, NUMBER 2 OCTOBER 15, 1950

The Penetration and Diffusion of Co^{60} Gamma-Rays in Water Using Spherical Geometry*

GLADYS R. WHITE
National Bureau of Standards, Washington, D. C.

(Received May 22, 1950)

Ionization and Geiger-Müller counter measurements of Co^{60} gamma-rays were made in effectively spherical geometry up to a distance of 252.8 cm (16 mean free paths of the primary radiation) corresponding to an exponential attenuation of the primary radiation by a factor of 8.8×10^6. The "build-up factor" was observed to climb up to 33.8 and approached closely the theoretically predicted trend of asymptotic variation $r^{1.4}$. Preliminary information on the spectral distribution of the radiation is included.

I. INTRODUCTION

MUCH experimental work has been done to measure absorption coefficients under narrow beam conditions in which no scattered radiation can reach the detector. In other absorption experiments singly or multiply scattered radiation can reach the detector but the geometry dictated by practical considerations hinders a detailed theoretical analysis of the results.[1] Some data are available from arrangements with simple geometry but only at small distances from the source.[2,3]

Therefore, in connection with the progress on the theory of the penetration and diffusion of x-rays,[4] it seemed advisable to conduct a new experiment in a large mass of water and in simple geometry. The Naval Gun Factory in Washington, D. C., kindly made available its large water tank which is 25 ft. in diameter and 60 ft. deep. Measurements were made using two Co^{60} sources with an apparent strength of 0.33 and 4.75

TABLE I. Data from the 4.75 curie source.

Distance (cm)	46	61	76	91	106	120.5	135.5	150.5	180.5
Mr/min.	125.4	36.6	12.8	4.09	1.39	0.500	17.80×10^{-2}	6.4×10^{-2}	8.3×10^{-3}
Standard error	1.3	0.3	0.2	0.06	0.01	0.009	0.02×10^{-2}	0.2×10^{-2}	—
Build-up factor	4.51	5.98	8.34	9.83	11.65	13.5	15.5	17.6	22.0
Distance (cm)	135.5	150.5	165.5	180.5	195.5	210.5	225.5	240.5	252.8
Counts/sec.[a]	1682	647.4	221.4	82.4	29.92	11.2	4.36	1.64	0.72
Standard error	1	0.8	2.5	0.5	0.08	0.1	0.10	0.01	—
Build-up factor[b]	14.7	17.9	19.2	21.7	23.6	26.2	29.6	32.5	33.8

[a] Corrected for coincidence counts and a background of 0.55 counts/sec.
[b] Counter data are scaled to match ionization data in the overlappingregion.

* Work supported by the Applied Mathematics Branch of the ONR.
[1] Kennedy, Wyckoff, and Snyder, J. Research Nat. Bur. Stand. 44, 157 (1950), RP2066.
[2] W. R. Faust, Phys. Rev. 77, 227 (1950).
[3] Levin, Weil, and Goodman, M.I.T. Tech. Rep. 22 (June 15, 1949).
[4] Phys. Rev. 76, 538, 739, 1843, 1885 (1949) and 77, 425 (1950).

curies[5] determined from a calibration in air. Dosage was measured at distances up to 180.5 cm with sealed Kelley-Koett pocket ionization chambers which were calibrated with a 25-mg radium source. A Cu Geiger-Müller counter of the type described by Faust and Johnson[6] was used as detector at distances from approximately 135 to 253 cm.

Figure 1 shows our experimental arrangement which insures effectively spherical geometry. A few measurements at large distances with both source and detector lowered from a depth of 6 ft. to 8 ft. confirmed that the geometry was adequate. Most exposure times were chosen to give a reading of approximately 160 mr. Leakage measurements in the absence of radiation were obtained for each exposure time. Leakage values were erratic and varied from 1 to 6 mr.

The data obtained with the 4.75 curie source are given in Table I. The data show that the dosage decreases with the distance less rapidly than a law of the form $\exp(-\mu_0 r)/r^2$, owing to the building up of secondary scattered radiation. The data are expressed in terms of a *build-up factor*. This factor is the ratio of the observed ionization to the ionization expected from the primary gamma-rays only, disregarding multiple scattering. The estimate of the expected ionization in the absence of scattering is based on (a) the results of measurements in air, where scattering is negligible, and

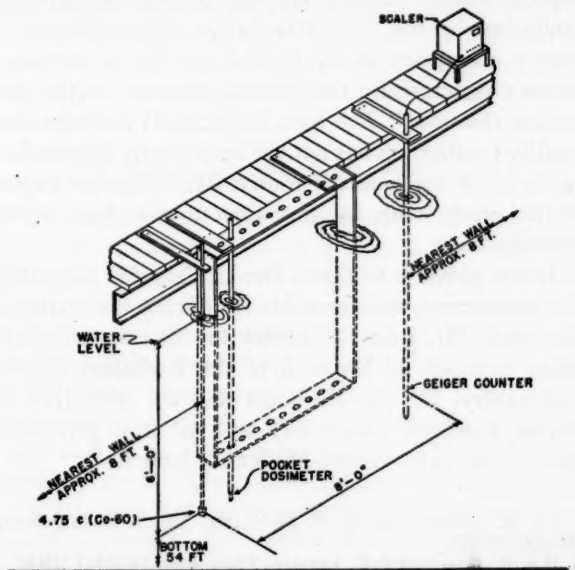

DISTANCE (CM)	46	61	76	91	106	120	135	150	165	180	195	210	225	240	252
TIME FOR 160 MR.	1'	4'	12'	35'	2"	5"	15"	36"	100"						
MR./MIN.	134	37	13	4.1	1.4	.50	.18	.084	.027	.008					
COUNTS/SECOND							1343	590	214	82	30	12	5	2	1

FIG. 1. Experimental arrangement.

[5] The apparent strength of a Co^{60} source in curies is determined by the ratio of its action on a standard ionization chamber to the action of another Co^{60} source of negligible self-absorption and of known strength in disintegrations per second. Thus the apparent strength of 4.75 curies means that the source gave a reading of 6.41 roentgen/hr. on a standard chamber at 1 meter distance at an average date during the experiment.

[6] W. R. Faust and M. H. Johnson, Phys. Rev. 75, 467 (1949).

TABLE II. Percentage absorption by 0.25 g/cm² shields with 4.75 curie source.

Distance (cm)	61	91	135.5	Very large (theoretical estimate)	
				Uncorrected for characteristic response of chamber	Corrected for characteristic response of chamber
Al	2.7	1.2	2.8		
Cu	9.9	9.1	17	21	26
Ag	20	20	26	32	40
Pb	23	25	30	38	46

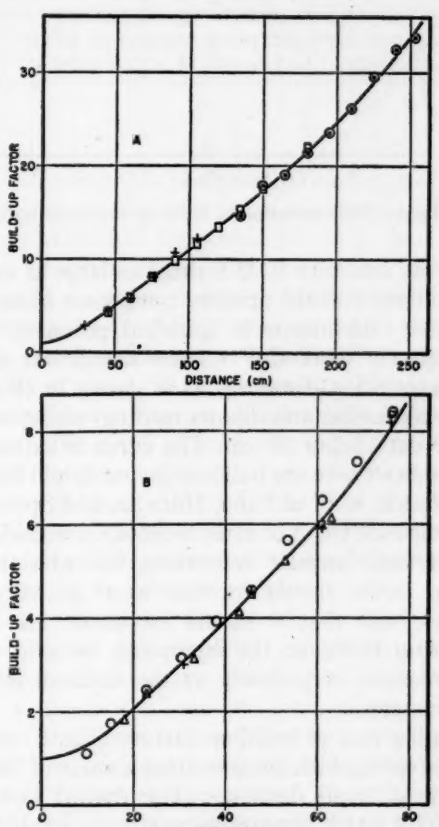

FIG. 2. The build-up factor as a function of distance. (A) Data from the present experiment. (B) Collection of data from various experiments for moderate penetration. + NBS, 0.33 curies, ionization data; □ NBS, 4.75 curies, ionization data; ⊙ NBS, 4.75 curies, counter data; ○ NRL, 0.04 millicurie, counter data; △ MIT, 1.9 curies, ionization data.

(b) a calculated attenuation in water according to the $\exp(-\mu_0 r)/r^2$ law. The calculation took into account the fact that different absorption coefficients pertain to the two Co^{60} lines. Only Compton absorption in water for 1.17 and 1.33 Mev was considered, since the contribution by pair production is of the order of 0.05 percent of the Compton absorption and the photoelectric effect is even smaller.

Figure 2 (A and B) shows data on the attenuation of Co^{60} gamma-rays in water. It is shown in (A) that the build-up factor increases with distance somewhat faster than linearly. At a distance of 252.8 cm the total

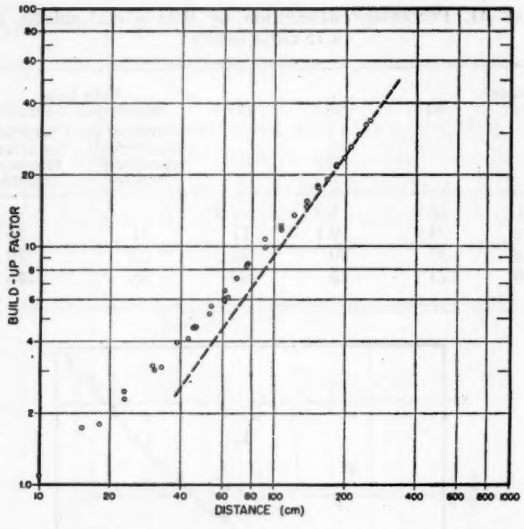

FIG. 3. Logarithmic variation of build-up factor with distance.

gamma-ray intensity is 33.8 times as large as the estimated intensity of the primary component alone. Data from other experiments in spherical geometry[2,3] with comparatively weak Co^{60} sources match our data at small penetration distances, as is shown in (B). Both ionization chamber and counter readings are represented in these data below 80 cm. The curve is extended to zero distance where the build-up factor should be unity.

Theoretical work of Fano, Hurwitz, and Spencer[7] on the asymptotic trend of x-ray intensities, including the effect of small angular deflections, indicates that the build-up factor should increase as r^k at very large distances, and that k should be about 1.4 in this experiment. However, the asymptotic behavior should be approached very slowly as the distance from the source increases.

A log-log plot of build-up factors (Fig. 3) shows a slope increasing with distance from a value of the order of unity at small distances. The dashed line has a slope of 1.4 which appears to match the latter portion of the experimental curve. It is expected, therefore, that the build-up factor will continue to increase beyond 253 cm as $r^{1.4}$ and will never reach a maximum value. This follows from the theory of Bethe, Fano, and Karr[8] according to which the intensity ratio of secondary to primary radiation increases beyond any limit. Spencer and Fano, in a paper to be published shortly, have calculated theoretically the build-up factor throughout the range of Fig. 2A. Their result agrees completely with the experimental data.

Some indication of the intensity of the soft radiation components at large distance from the source was obtained by shielding the ionization chambers with filters of various materials. Preliminary results are shown in Table II. The percentage decrease in the ionization when measured with shielded chambers has been variously used[9] to obtain an indication of the amount of soft radiation in the spectral distribution. Since the sleeve filters were approximately 0.25 g/cm² thick no appreciable amount of the hardest component was stopped. An indication of the spectral distribution of the radiation expected at very large distances is given by the "NRL distribution" of Karr and Lamkin,[10] that is, by the spectral distribution calculated for an infinite mass of water with a uniformly distributed Co^{60} source. The actual distribution for large penetration would be steeper on the high energy side than the "NRL distribution," since photons that have traveled large distances tend to have been scattered many times with little energy degradation. Nevertheless, the expected absorption by the Cu, Ag, and Pb filters was estimated using the "NRL spectral distribution." The spectral energy density for each photon energy was multiplied by the filter attenuation, the coefficient of energy absorption in air $(\tau+\sigma_a)$ and by a correction factor characterizing the spectral response of the ionization chamber.[11] The data in Table II indicate that quality equilibrium has not yet been closely approached up to 135.5 cm from the source. Much further experimental work is needed to complete this phase of the investigation.

It is a pleasure to thank Dr. U. Fano for suggesting the experiment and for guidance during the course of the work, Mr. John R. Howley for his assistance, and other members of the staff of the Radiation Physics Laboratory. Dr. W. R. Faust and his co-workers at Naval Research Laboratory lent us most generously their underwater Geiger-Müller equipment.

[7] Fano, Hurwitz, and Spencer, Phys. Rev. 77, 425 (1950). The difference in source geometry does not effect any change in the exponent in this case.

[8] Bethe, Fano, and Karr, Phys. Rev. 76, 538 (1949).

[9] E. H. Quimby and R. F. McNattin, Am. J. Roentgenology 28, 236 (1932).

[10] P. R. Karr and J. C. Lamkin, Phys. Rev. 76, 1843 (1949).

[11] Frank H. Day, "*X-ray calibration of radiation survey meters, pocket chambers and dosimeters*," Circular NBS (to be published)

Altitude and Latitude Dependence of Bursts in a Lead-Shielded Ionization Chamber*

ALLEN J. MCMAHON, BRUNO ROSSI,** AND W. F. BURDITT
Brookhaven National Laboratory, Upton, New York

(Received June 19, 1950)

The instrument used in this experiment consisted of a cylindrical ionization chamber covered by a half-cylindrical 15-cm thick lead (Pb) shell. Five trays of G-M tubes were placed around the shell and one tray directly below the ionization chamber. Various kinds of coincidences were recorded between bursts of ionization in the chamber and discharges of the G-M tubes. This equipment was flown in a B-29 at Rome, New York (geomagnetic latitude 55°N), and at Panama (geomagnetic latitude 20°N). The experiment provided information on the altitude, latitude, and angular dependence of the radiation responsible for the observed events. These were interpreted as due to nuclear interactions by nucleons of different energies. In particular, for events attributed to protons with an estimated minimum energy of about 5 Bev the intensity ratio between 55°N and 20°N at 30,500 feet was 1.17±0.04. In contrast, for events attributed to protons with an estimated minimum energy of about 0.4 Bev the latitude ratio at the same altitude was 1.96±0.18.

I. INTRODUCTION

THE work of Bridge, Rossi, and Williams[1] has shown that the observation of bursts in a shielded ionization chamber occurring in coincidence with discharges in trays of G-M tubes provides a convenient method for the detection of nuclear interactions of cosmic rays. This method was used by the authors mentioned above as well as by other experimenters[2–7] for the investigation of the dependence on altitude or depth and the absorption in various materials of the particles responsible for the nuclear interactions. The present experiment is designed to provide information on the latitude and angular dependence of these particles as well as to check the previous data on their variation with altitude.

II. EXPERIMENTAL ARRANGEMENT

The arrangement of the ionization chamber, G-M tubes and absorber is shown in Fig. 1. The ionization chamber (I) had a diameter of 7.5 cm and an effective length of 52 cm. It had copper walls $\frac{1}{32}$ in. thick (0.7 g cm^{-2}) and was surrounded by a $\frac{1}{4}$-in. (0.64 g cm^{-2}) Lucite electrical insulator. It was filled with pure argon at 4.0 atmos. pressure above vacuum (at 25°C) and it contained a polonium source of alpha-particles at the inner surface of the cylindrical wall. The pulses produced by the polonium alpha-particles (5.3 Mev) served as a standard for the measurement of the ionization bursts observed in the chamber. The size of these pulses will be designated as P_α. A pulse of this size corresponds to the amount of ionization produced by the passage through the chamber of about 100 electrons of 10 Mev traveling perpendicularly to the chamber axis.[4]

Each of the G-M tubes was 2.5 cm in diameter and had an effective length of 50 cm. These tubes were arranged in six trays, five trays consisting of five tubes (A), and one tray of four tubes (B). All tubes in any one tray were connected in parallel. The five trays A were placed above the lead absorber (Pb) and tray B was placed below the ion chamber in a tunnel in the absorber. The total amount of material between the sensitive volume of the ion chamber and of the G-M tubes B was about 2 g cm^{-2}. The lead absorber (Pb) separating the chamber from the upper trays A was 5 cm thick and it extended 9 cm beyond the sensitive volume of the chamber on each end.

The ion chamber pulses were amplified by a Los Alamos Model 100 amplifier and passed through a pulse-height discriminator selecting pulses greater than $0.6P_\alpha$. Coincidences between these pulses and a discharge of any one of the six G-M trays were selected by a circuit with about 15 μsec. resolving time and made to operate the horizontal sweep of an oscilloscope. The pulses of the chamber, properly delayed, were applied

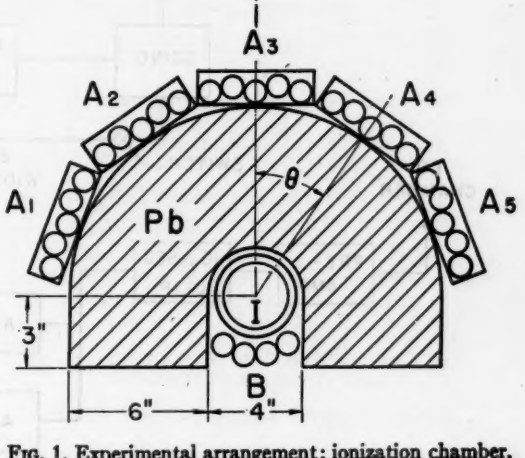

FIG. 1. Experimental arrangement; ionization chamber, Geiger-Müller tubes and absorber.

* Research carried out at Brookhaven National Laboratory under auspices of the AEC.

** At Massachusetts Institute of Technology, Cambridge, Massachusetts.

[1] Bridge, Rossi, and Williams, Phys. Rev. 72, 257 (1947).
[2] E. P. George, Nature 160, 327 (1947).
[3] Bridge, Hazen, Rossi, and Williams, Phys. Rev. 74, 1083 (1948).
[4] H. Bridge and B. Rossi, Phys. Rev. 75, 810 (1949).
[5] E. F. Fahy and M. Schein, Phys. Rev. 75, 207 (1949).
[6] D. Hudson, Cornell thesis (1950).
[7] R. H. Rediker, M.I.T. thesis (1950).

to the vertical deflecting plates of this oscilloscope, whose screen was photographed on a continuously moving film. A record of the trays which had been discharged in coincidence with pulses of the ion chamber was obtained on this same film. This was done by means of neon bulbs which were turned off in the event of a coincident discharge of a tray and of the ion chamber. To supplement the photographic record, electronically driven registers recorded the total number of chamber pulses greater than $0.6P_a$, and the total number of coincidences between these pulses and any of the G-M trays. A scaling circuit driving a third register could be connected to the separate trays of G-M tubes to determine their counting rates.

Bias curves of the alpha-particle pulses were measured periodically and served as a primary calibration for the setting of the discriminator. An electronic pulser was used as a secondary standard to record

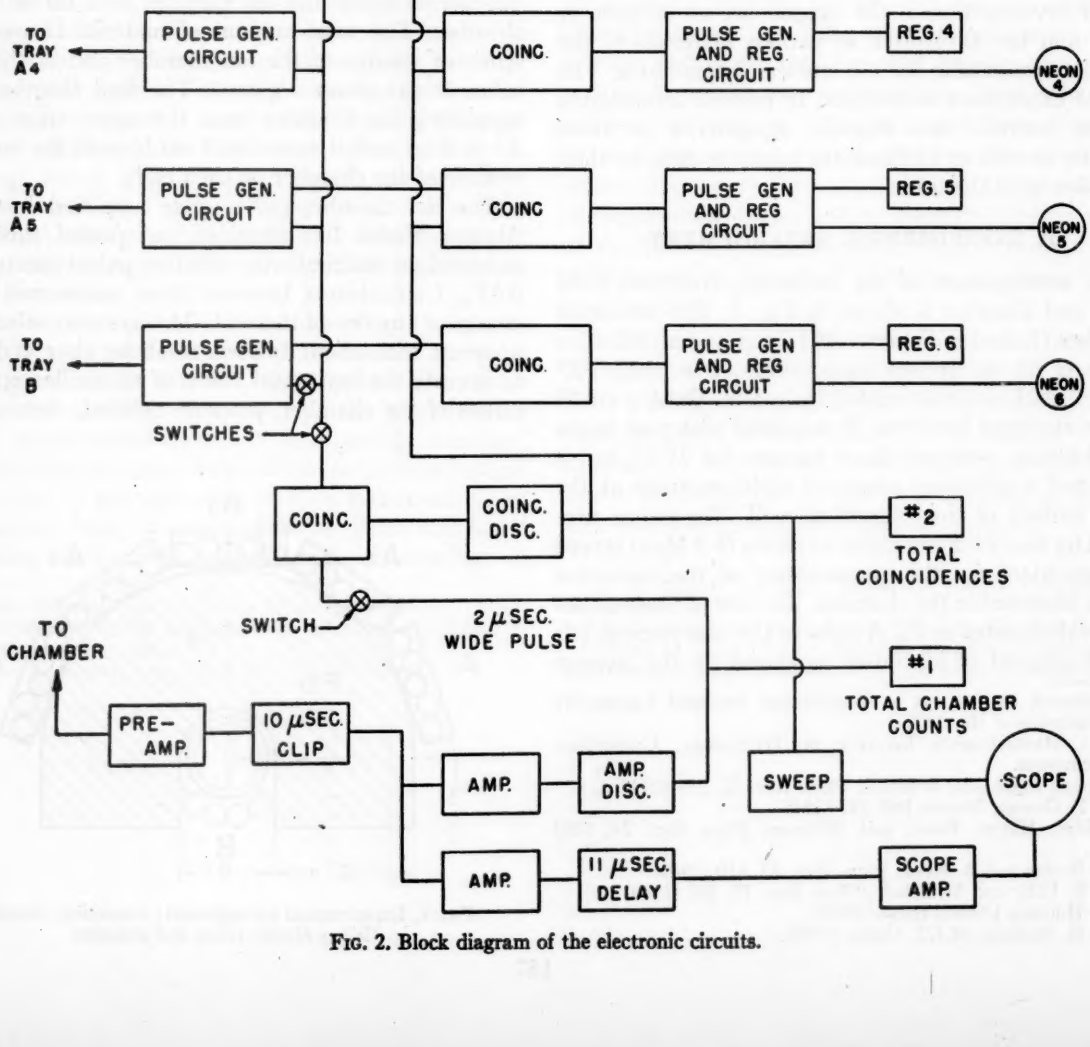

FIG. 2. Block diagram of the electronic circuits.

TABLE I. Counting rates per minute at various altitudes and latitudes. (Errors are standard statistical deviations.)

Atmospheric depth g cm^{-2}	Time (min.)	*AIB* Uncorr.	*AIB* Corrected	*AI–B* Uncorr.	*AI–B* Corrected	*IB–A* Uncorr.	*IB–A* Corrected	Remarks
				Geomagnetic latitude 55°N				
383	582	1.23	1.21 ±0.05	0.72	0.465±0.04	1.11	1.13±0.04	4 flights May '49
300	180	2.39	2.33 ±0.11	1.17	0.91 ±0.09	1.85	1.91±0.10	1 flights Sept. '49
273	285	3.00	2.92 ±0.10	1.66	1.102±0.09	2.41	2.47±0.09	3 flights May '49
				Geomagnetic latitude 20°N				
383	422	1.10	1.085±0.05	0.46	0.301±0.04	0.85	0.86±0.04	3 flights June '49
300	324	2.10	2.11 ±0.08	0.65	0.423±0.06	1.65	1.68±0.07	2 flights June '49
300	388	1.93	1.90 ±0.07	0.61	0.480±0.04	1.40	1.43±0.06	3 flights Sept. '49

pulses of known size on each film. The bias curves showed a flat plateau followed by a very steep drop indicating a spread of less than four percent in the size of the alpha-particle pulses. The gain of the amplifier was constant to better than two percent over the whole series of measurements.

A complete self-explanatory block diagram of the electronic circuits is shown in Fig. 2.

The equipment was installed in the rear pressure cabin of a B-29 airplane. At all times the axis of the chamber was perpendicular to the direction of flight.

III. EXPERIMENTAL RESULTS

Measurements were made with the airplane flying both in the east and in the west directions along geomagnetic parallels at 55°N and at 20°N geomagnetic latitude. For the flights at 55°N the plane was based at Rome, New York and for the flights at 20°N at Panama. From both bases, flights were made at 30,500 feet (300 g cm^{-2} atmospheric depth) and at 25,000 feet (383 g cm^{-2}). In addition, some flights were made at 32,500 feet (273 g cm^{-2}) from Rome, New York.

Table I lists the experimental results concerning three types of events which we shall designate as *AIB*, *AI–B*, and *IB–A*. The *AIB* event is a threefold coincidence between a discharge of trays *A*, a discharge of tray *B*, and a pulse larger than $0.6P_\alpha$ in the ionization chamber *I*. An *AI–B* event is a double coincidence between a discharge of tray *A* and a pulse greater than $0.6P_\alpha$ in *I* not accompanied by a pulse in tray *B*. An *IB–A* event is a double coincidence between a pulse greater than $0.6\ P_\alpha$ in *I* and the discharge of tray *B* not accompanied by a pulse in an upper tray *A*.

As is indicated in Table I, several flights were made at each altitude and latitude. The data from the different flights were consistent with one another within the experimental errors, except for some of those obtained during two groups of flights made at 20°N and 300 g cm^{-2} in June and in September, 1949, respectively. For this reason the results of these two groups of flights are shown separately in Table I. Since there is no objective ground on which to reject either one of the two experiments, we shall use the weighted averages of their results in our discussion.

During some of the flights at 55°N and 383 g cm^{-2} tray A_5 was removed from its normal position and placed horizontally with its center 184 cm from the chamber axis in order to test the effect of air showers. In a total of 300 minutes observation time, tray A_5 was discharged only four times in coincidence with the ion chamber and the lower tray *B*. This shows that only a negligible number of the events recorded by our arrangement can be due to air showers. The counting rates observed during the time that tray A_5 was displaced were, of course, corrected for the consequent decrease in the detection efficiency of the equipment.

Table I lists the observed counting rates as well as the counting rates corrected for accidentals. Accidentals include: (1) Chance coincidences between *AI* coincidences and unrelated *B* discharges; these turn out to be negligible. (2) Chance coincidences between *IB* coincidences and unrelated *A* discharges; these tend to increase slightly the *AIB* rate and correspondingly to decrease the *IB–A* rate. (3) Chance coincidences between discharges of the counter trays and uncorrelated pulses in the ion chamber. Most of these are due to the presence of the polonium source within the chamber, and their number decreases with time because of the decay of the polonium source (138.3-day half-life).[8] Such events increase the *AI–B* rate considerably and the *IB–A* rate very slightly. (4) Chance coincidences between *AB* coincidences and uncorrelated ion chamber

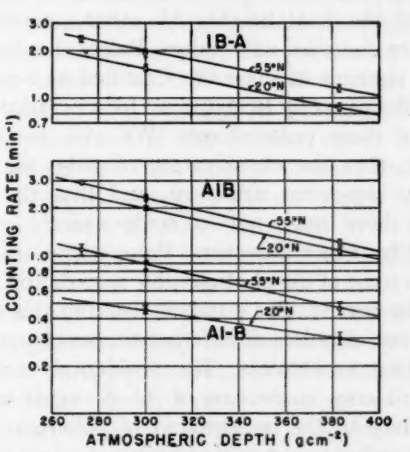

FIG. 3. Counting rates *vs.* atmospheric depth.

[8] W. H. Beamer and W. E. Easton, J. Chem. Phys. **17**, 1300 (1949).

TABLE II. Absorption thicknesses (L) and latitude effects. (Errors are standard statistical deviations.)

	Event		
	AIB	*AI–B*	*IB–A*
L—55°N	125± 8 (g cm^{-2})	127±30 (g cm^{-2})	143±10 (g cm^{-2})
L—20°N	135±11 (g cm^{-2})	198±50 (g cm^{-2})	143±11 (g cm^{-2})
$N_{55°}/N_{20°}$(300 g cm^{-2})	1.17±0.04	1.96±0.18	1.32±0.05

pulses; these result in a very slight increase of the *AIB* rate. One sees from Table I that the correction for accidentals is only important in the case of *AI–B* events. Because of this large correction, the experimental results concerning *AI–B* events are less reliable than those concerning either *AIB* or *IB–A* events.

In Fig. 3 the corrected counting rates listed in Table I are plotted on a logarithmic scale against atmospheric depth. The data obtained at 55°N are consistent with an exponential variation of the counting rate with depth. Least-square adjustments of this data to an exponential function of the form const.$\times\exp(-x/L)$ gives for L the values listed in Table II. The same table lists the values of the absorption thicknesses L at 20°N computed from the measurements at 300 g cm^{-2} and at 383 g cm^{-2} under the assumption of an exponential variation with depth. The ratios listed in the last line of Table II represent the latitude effect between 55°N and 20°N for the particles giving rise to *AIB*, *AI–B*, and *IB–A* events at 300 g cm^{-2}. The counting rates at 55°N were obtained from the least-square analysis and those at 20°N from direct measurement.

The pulses of the ion chamber show a variety of shapes corresponding to the different distribution of the ionization in the chamber. Following Bridge *et al.*[3] we have subdivided the pulses into three groups designated respectively as α, σ, and ν. Figure 4 shows sections of a typical record containing examples of the three different pulse shapes. A pulse is classified as an α-pulse if its height at one-half rise time is less than one-third the final height. All other smoothly rising pulses are classified as σ-pulses. Pulses showing discontinuous changes in slope are classified as ν-pulses. We refer to the paper by Bridge *et al.*[3] for a detailed interpretation of these pulse shapes. We wish to point out, however, that the classification of pulse shapes is by necessity somewhat arbitrary, and that the criterion adopted here may not coincide exactly with that adopted by other observers. Pulse shape analysis was made on some of the photographic records and Table III shows the results. The numbers listed in this table give the percent of pulses of different shapes computed after subtracting accidentals. The accidental correction is important only in the case of *AI–B* events where it is due mainly to the background of polonium particles. Background pulses resulting from polonium α-particles have shapes of the type called α in our classification. Of course, we took this into account in distributing the accidental corrections among pulses of different shapes.

The *AIB* events observed at 55°N during the flights at 273 g cm^{-2} and the *AIB* events observed at 20°N during part of the flights at 300 g cm^{-2} were analyzed for pulse height from the photographic records. The results obtained at the two latitudes are not significantly different. They are shown in Fig. 5 in the form of integral pulse-height distributions.

The records obtained at 55°N and most of those obtained at 20°N were also analyzed for single or multiple discharges of the A trays. The results obtained at the two latitudes and at the various altitudes were not significantly different. They are presented together in Fig. 6. The histograms in this figure give the total number of *AIB* and *AI–B* events in which one, two, three, four, or all five trays A were discharged. The data are corrected for accidentals, whose rate is appreciable only for events corresponding to single discharges of the A trays.

Events *AIB* and *AI–B* involving the discharge of only one of the A trays were sorted out according to which of these trays had been discharged in an attempt to study the angular dependence of the radiation responsible for the observed events. The results of this analysis are shown in Fig. 7 in which θ indicates the zenith angle of the line connecting the center of the ion chamber with the center of the tray. The points plotted at $\theta=0(\cos\theta=1)$ are the counting rates of events involving the discharge of tray A_3. The points plotted at

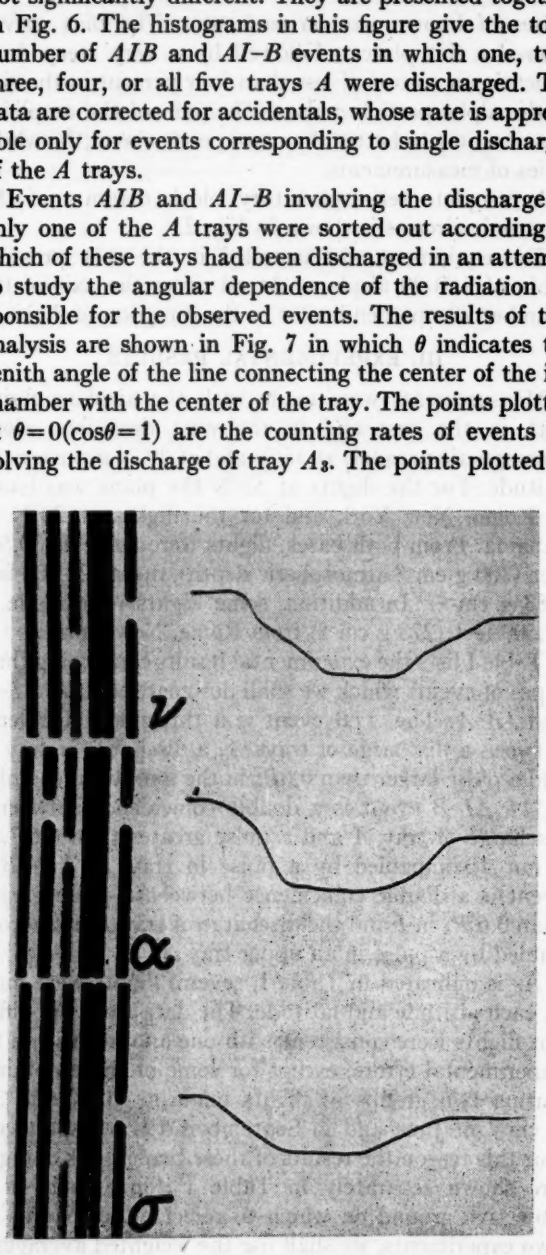

FIG. 4. Samples of photographic records showing a ν-pulse, an α-pulse, and a σ-pulse. The black lines on the left-hand side represent the images on continuous moving film of the neon bulbs recording discharges of the counter trays.

$\theta=35°(\cos\theta=0.82)$ are the averages of the counting rates for events involving trays A_2 and A_4. The points plotted at $\theta=70°(\cos\theta=0.342)$ are the averages of the counting rates for events involving trays A_1 and A_5. In the plane perpendicular to the axis of the chamber each tray subtends an angle of 32°. As an indication of the resolution of the instrument, horizontal lines are drawn through each experimental point to cover this angular interval. As shown by the solid lines, the experimental results are consistent with angular distributions of the $\cos^n\theta$-type. The significance of the dotted lines in the graphs shall be discussed later.

Lastly, we have analyzed the data for east-west asymmetry of the *AIB* and of the *AI–B* events. As noted above, the equipment was flown so that the axis of the chamber always pointed in the N–S direction. For each group of flights we have added together all events involving a discharge in one or both of the two *A* trays facing westward and all events involving a discharge in one or both of the two *A* trays facing eastward. From the numbers, N_W and N_E, thus obtained we have computed the E–W asymmetry, *R*, by means of the equation:

$$R=2(N_W-N_E)/(N_W+N_E).$$

The results are shown in Table IV. Note that the plane was flown for approximately equal times with trays A_1 and A_2 facing east and with trays A_4 and A_5 facing east, so as to minimize any possible error due to unequal efficiency of the G-M trays.

IV. DISCUSSION

AIB coincidences may be caused by electromagnetic interactions of high energy μ-mesons (knock-on showers, radiation showers), by nuclear interactions of high energy nucleons, or possibly by nuclear interactions of π-mesons. Previous experiments[1,4] have shown that the contribution of μ-mesons is important only near sea level. On the other hand, the number of π-mesons in the atmosphere is probably small compared with that of nucleons because of the very short mean life of π-mesons. One is thus justified in assuming that the events *AIB* observed in the present experiment are produced mainly by high energy protons and, to a considerably smaller extent, by high energy neutrons (in the latter case tray *A* is discharged by secondary ionizing particles ejected in the backward direction; see below).

Nuclear interactions of protons of several hundred Mev energy give rise mainly to stars of heavily ionizing particles (low energy protons and heavier nuclear fragments). Nuclear interactions of protons of greater energies produce heavily ionizing fragments and in addition showers of lightly ionizing particles. These are mainly electron showers initiated by photons arising from the nuclear interactions; they also contain relativistic mesons and protons. Individual heavily ionizing

TABLE III. Percent of pulses of α, σ, and ν shape.

Event	Time (min.)	Pulse shape α	σ	ν
		55°N, 300 g cm^{-2}		
AIB	180	16.6	77.0	6.4
AI–B	180	50.3	38.0	11.7
IB–A	180	33.1	60.2	6.7
		20°N, 300 g cm^{-2}		
AIB	120	26.8	67.9	5.3
AI–B	324	63.0	31.5	5.5
IB–A	324	32.2	59.8	8.0

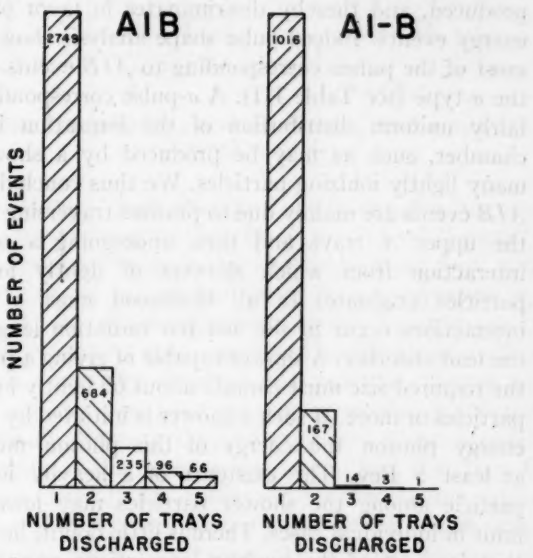

FIG. 6. Distribution of *AIB* and *AI–B* events according to numbers of *A* trays discharged. Data obtained at various latitudes and altitudes are included in this analysis.

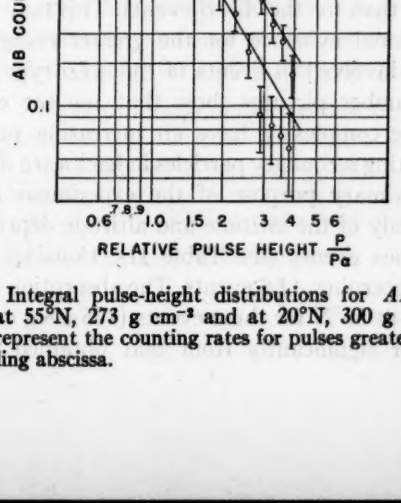

FIG. 5. Integral pulse-height distributions for *AIB* events observed at 55°N, 273 g cm^{-2} and at 20°N, 300 g cm^{-2}. The ordinates represent the counting rates for pulses greater than the corresponding abscissa.

TABLE IV. East-west effect: $R=[2(N_W-N_E)/(N_W+N_E)]$. (Errors are standard statistical deviations.)

	(AIB)	*(AI–B)*
55°N, 273 g cm^{-2}	$R=-0.25\pm0.11$	$R=-0.20\pm0.15$
20°N, 300 g cm^{-2}	$R=+0.10\pm0.10$	$R=+0.20\pm0.16$

particles as well as showers of lightly ionizing particles can produce detectable pulses in the ionization chamber. In the case of an *AIB* event the requirement of a discharge in tray *B* rules out nuclear interactions in which only short range, heavily ionizing particles are produced, and thereby discriminates in favor of high energy events. Indeed pulse shape analysis shows that most of the pulses corresponding to *AIB* events are of the σ-type (see Table III). A σ-pulse corresponds to a fairly uniform distribution of the ionization in the chamber, such as may be produced by a shower of many lightly ionizing particles. We thus conclude that *AIB* events are mainly due to protons traversing one of the upper *A* trays and then undergoing a nuclear interaction from which showers of lightly ionizing particles originate. In all likelihood most of these interactions occur in the last few radiation lengths of the lead absorber. A shower capable of giving a pulse of the required size must contain about 60 lightly ionizing particles or more. If such a shower is initiated by a high energy photon the energy of this photon must be at least 5 Bev. The existence of a heavily ionizing particle among the shower particles may lower this limit in individual cases. There is little doubt, however, that in most of the nuclear interactions recorded by the *AIB* coincidences the energy release is greater than 5 Bev. If the ionization pulses corresponding to *AIB* events are due mainly to electron showers, their number *vs.* size distribution is representative of the energy distribution of the photons arising from nuclear interactions.[4] As shown in Fig. 5 our experimental results are consistent with an integral pulse-height distribution represented by a power law with an exponent equal to about -1.60. This may be compared with the results of a similar experiment by Bridge and Rossi[4] giving the integral pulse-height distribution as a power law with exponent -1.55.

Events in which tray *B* fails to be discharged (*AI–B* events) must be due mainly to protons either entering the ionization chamber near the end of their range or producing stars whose heavily ionizing products traverse the chamber but fail to penetrate counters *B*. This is confirmed by the pulse shape analysis showing that more than one-half of the pulses corresponding to *AI–B* events are of the α or ν-type (see Table III). Pulses of these types correspond to a concentrated ionization such as is produced by a single or several heavily ionizing particles. Protons which enter the ionization chamber near the end of their range are those arriving at the absorber with approximately 0.4 Bev kinetic energy. Protons responsible for the production of low energy stars must have energies of the order of several hundred Mev after traversing the lead absorber, since most of the stars which give rise to ionization pulses are probably produced in the walls or the gas of the chamber. The energy of these protons before traversing the absorber is of the order of 0.5 Bev. (Protons incident upon 15 cm of lead with energies between 0.4 and 0.6 Bev emerge from the lead with energies between 0 and 350 Mev.) One thus concludes that the protons detected by the anticoincidences *AI–B* have a minimum energy of about 0.4 Bev and probably an average energy of the same order of magnitude.

Events in which all of the *A* trays fail to be discharged (anticoincidences *IB–A*) are interpreted as nuclear events initiated mostly by neutrons, but in small part by protons which miss the *A* trays. One might expect *a priori* that the average energy of the particles responsible for *IB–A* events is somewhat lower than that of the particles responsible for *AIB* events. In fact, it is reasonable to assume that the ratio of neutrons to protons increases as the energy decreases because the low energy end of the proton spectrum is depleted by ionization loss. On the other hand, the distributions of *AIB* and *IB–A* events according to pulse shapes do not show any significant difference (see Table III).

In agreement with the observations of Bridge and Rossi the present experiments show a fairly large proportion of cases in which more than one tray per event is discharged among those covering the lead shield. In the experiment of Bridge and Rossi events of this type were found to be caused in approximately equal numbers by nuclear interactions projecting ionizing particles upwards and by air showers. The contribution of air showers should be much smaller in our experiments than in those of Bridge and Rossi because of the more complete shielding of the ionization chamber. This conclusion is borne out by measurements taken with tray A_5 moved some distance away from the rest of the equipment. During these measurements we observed only three *AIB* events involving the discharge of tray A_5 and of one additional *A* tray against 34 similar multiple events involving the discharge of tray A_1. Figure 6 shows that the proportion of multiple discharges of the *A* tray is much greater for the *AIB* than for the *AI–B* events. This may be taken as additional evidence for the greater energy of the particles involved in events of the *AIB* type. In fact, cloud-chamber pictures show that nuclear events of increasing complexity have an increasing probability of projecting secondary particles in backward directions.

The primary purpose of the experiment described was a study of the latitude and altitude dependence of the various events (see Table II). Consider first the result concerning *AIB* events. The absorption thickness obtained at 55°N for these events (125 ± 8 g cm^{-2}) does not differ significantly from that obtained by other

authors for high energy nuclear interactions.[4,9] The absorption thickness at 20°N (135±11 g cm^{-2}) seems to be somewhat greater than that at 55°N but the difference is not outside of the statistical errors. At the 300 g cm^{-2} depth the intensity ratio between 55°N and 20°N is 1.17±0.04. This small latitude effect is consistent with our previous conclusion concerning the energy of the protons selected by the *AIB* coincidences. The geomagnetic cut-off for primary protons[10] is about 1.0 Bev at 55°N and 12 Bev at 20°N. The latter value is only twice the energy estimated to be the minimum necessary for the production of an *AIB* event. It is interesting to note that the latitude effect for *AIB* events found in the present experiment is not very different from the latitude effect for penetrating showers found by Walsh and Piccioni[11] between the same two latitudes (1.11±0.019).

The altitude dependence of the *AI–B* events at 55°N is not significantly different from that of the *AIB* events. There is an indication of an increase of the absorption thickness of *AI–B* events with decreasing latitude but the effect is not outside the experimental errors which, in this case, are very large. The intensity ratio between 55°N and 20°N at the depth of 300 g cm^{-2} amounts to 1.96±0.18 and is thus greater than the corresponding ratio for the *AIB* events. According to our previous discussion, most of the *AI–B* events are due to protons of energy not much greater than 0.4 Bev. The intensity ratio for these protons may be compared with the effect found by Conversi[12] for protons of approximately 15 cm Pb range (0.4 Bev energy) which amounts to about 2.1 between the latitude of 55°N and 20°N.

Events *IB–A*, which, according to our interpretation, are mainly due to high energy neutrons, have possibly a somewhat greater absorption thickness than events *AIB*. Their latitude effect (1.32±0.05) seems to be intermediate between those of the *AIB* and *AI–B* events.

For the discussion of the zenith angle dependence, consider that if there were no change of direction in the propagation of the nucleonic component through the atmosphere, the intensity $I(x, \theta)$ of this component at the depth x and the zenith angle θ would equal the vertical intensity at the depth $x/\cos\theta$. Under this assumption and with an exponential function, $\exp(x/L)$, to represent the dependence of the vertical intensity on depth, one obtains for $I(x, \theta)$ the expression

$$I(x, \theta) = I(x, 0)e^{-x/L[(1/\cos\theta)-1]}. \quad (1)$$

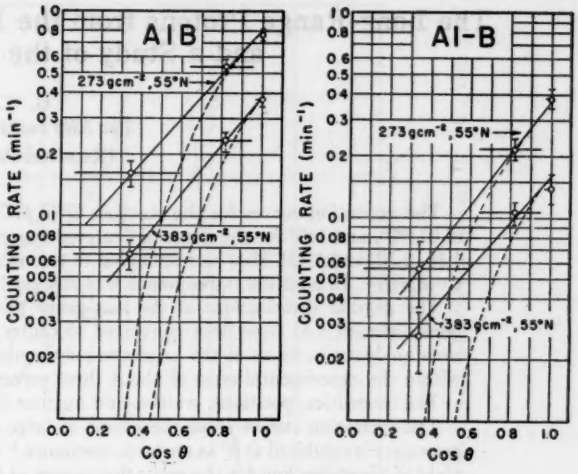

FIG. 7. Angular dependence of *AIB* and *AI–B* events observed at 55°N.

The dotted lines in Fig. 7 represent the angular dependence computed from Eq. (1) with $L = 125$ g cm^{-2}. One sees that whereas the observations at $\theta = 0$ and $\theta = 35°$ are not inconsistent with the law expressed by Eq. (1), the observations at $\theta = 70°$ indicate much greater intensities than one would anticipate according to this law. The observed discrepancies cannot be explained by the poor geometric resolution of the equipment. Nor can they be explained by an angular selectivity of the detector due to the fact that tray *B* is more likely to be discharged by the nuclear interactions of rays coming at a small zenith angle. This selectivity tends to increase the relative number of *AI–B* events observed at large zenith angles, but has the opposite effect on *AIB* events. It thus seems necessary to conclude that most of the nucleons observed at large zenith angles are the products of nuclear interactions occurring in the atmosphere above the instrument and in which high energy nucleons are emitted at wide angles to the direction of the primary particle.

The data on the E-W effect, unfortunately, was affected by large statistical errors. It is certain, however, that even at 20°N the asymmetry, if it exists at all, is small for both *AIB* and *AI–B* events. This may be due, at least in part, to a loss of directionality in the propagation of high energy nucleons through the atmosphere, such as is indicated by the measurements on the zenith angle dependence.

We wish to thank Herbert Bridge of the M. I. T. staff and William A. Higinbotham of the Brookhaven National Laboratory for advice and help in constructing the electronic equipment; the Air Materiel Command, United States Air Force, and to thank in particular the personnel of the 3171st Electronics Research Group. Rome, New York, who flew the B-29 airplane.

[9] J. Tinlot, Phys. Rev. **73**, 1476 (1948); **74**, 1197 (1948).
[10] M. S. Vallarta, Phys. Rev. **74**, 1837 (1948).
[11] T. G. Walsh and O. Piccioni, Echo Lake Conference on Cosmic Rays, 1949.
[12] M. Conversi, Phys. Rev. **76**, 444 (1949).

The Long-Range Protons from the Disintegration of Carbon by Deuterons and a Study of the Competing Reactions*

G. C. PHILLIPS
The Rice Institute, Houston, Texas
(Received February 27, 1950)

The excitation curves for the reaction $C^{12}(d,p)C^{13}$ have been determined at the three laboratory angles of 0°, 90°, and 150° for the range of deuteron energies 0.78 to 1.55 Mev. Resonances were observed at 0.91, 1.16, 1.30, and 1.435 Mev corresponding to resonances found previously for the competing $C^{12}(d,p)^*C^{13}$ and $C^{12}(d,n)N^{13}$. In addition, a resonance was observed for the long-range proton group at 1.13 Mev.

The angular distributions of the long-range proton group have been determined for eight energies of bombardment and have been converted to center of mass coordinates. These angular distributions have been analyzed in terms of the Legendre polynomials and show no terms higher than the fourth order to within the experimental error of about three percent.

The intensities, positions, widths, and angular distributions of the resonances are discussed.

The excitation curves show the effects of large amounts of interference between states. The 1.30-Mev resonance is exhibited at 0° as an "anti-resonance," while the 1.435-Mev resonance shows a shift of maximum yield of about ten kev for the excitation curves at 0° and 150°.

I. INTRODUCTION

RECENTLY, carefully determined excitation curves have been obtained in this laboratory,[1,2] and at several other laboratories,[3,4] for the production of gamma-rays and neutrons when C^{12} is bombarded by deuterons. These radiations occur according to the reactions:[2,5,6]

$$C^{12}+H^2\rightarrow{}^*N^{14}\rightarrow{}^*C^{13}+H^1-0.37\text{ Mev}$$
$$^*C^{13}\rightarrow C^{13}+\gamma(3.1\text{ Mev}), \quad (1)$$

$$C^{12}+H^2\rightarrow{}^*N^{14}\rightarrow N^{13}+n^1-0.281\text{ Mev}$$
$$N^{13}\rightarrow C^{13}+\beta^++\eta+1.20\text{ Mev}. \quad (2)$$

In addition, the neutron angular distributions have been determined at a number of bombarding energies.

The present report describes experiments that have been performed to investigate the excitation curves for the production of the long-range protons which leave C^{13} in its ground state according to the scheme:[6]

$$C^{12}+H^2\rightarrow{}^*N^{14}\rightarrow C^{13}+H^1+2.73\text{ Mev}. \quad (3)$$

Also the angular distributions of these protons have been determined at certain energies of bombardment.

It was hoped that a comparison of reactions (2) and (3) would be instructive as to the nature of the excited states of N^{14} and the validity of considering the emissions from the excited states as competing processes. Because of the identity of the spins of neutrons and protons and because of the assumed identity of the parities and spins of C^{13} and N^{13}, it would appear that no differences in the general features of yield and angular distributions could be anticipated, and that such differences as might appear would be accounted for by the penetration of the Coulomb and the centrifugal barriers by the particles. Also it appeared possible to determine the angular momentum quantum number and the parity of the resonant states by means of the angular distributions.

It was reported in reference 1 that the strong gamma-ray resonance of width 5.5 kev observed at 1.435-Mev deuteron bombarding energy does not appear with measurable intensity for the neutron reaction. Thus an investigation of this energy region for reaction (3) appeared of particular interest.

II. APPARATUS AND EXPERIMENTAL TECHNIQUES

To count the long-range protons of reaction (3) at various angles, a special target chamber was constructed. The chamber was formed of a brass cylinder 18 cm inside diameter and nine cm high. One-half inch diameter holes were drilled every 15° on one side of the cylinder, from 0° to 150°, where the 0° hole was in the direction of the deuteron beam. The holes were covered with aluminum foils of about six cm air equivalence. The target was on the axis of the cylinder and at the height of the exit holes and was carried by a ball bearing support so that it could be rotated by an external magnet to calibrated angles. Deuterons accelerated by the Rice Institute Van de Graaff generator were magnetically analyzed and collimated with apertures onto a small spot on thin carbon targets. The thin carbon targets were prepared by cracking benzene vapor on silver foils of about four cm air equivalence. The thickness of the silver foils was sufficient to stop the deuterons, but allowed the protons emitted in the forward direction to pass through and be detected.

The detection was accomplished by a proportional

* This project was also supported by the joint program of ONR and AEC.

[1] Bonner, Evans, Harris, and Phillips, Phys. Rev. 75, 1401 (1949).
[2] Bonner, Evans, and Hill, Phys. Rev. 75, 1398 (1949).
[3] Bailey, Freier, and Williams, Phys. Rev. 73, 274 (1948).
[4] Heydenburg, Inglis, Whitehead, and Hafner, Phys. Rev. 75, 1147 (1949).
[5] Seigbahn and Slatis, Arkiv. f. Mat. Astr. O. Fys. 32A, No. 9 (1945); Lyman, Phys. Rev. 55, 123 (1939); Townsend, Proc. Roy. Soc. A177, 357 (1941); Hornyak, Dougherty, and Lauritsen, Phys. Rev. 74, 1727 (1948).
[6] Buechner, Strait, Sperduto, and Malm, Phys. Rev. 76, 1543 (1949).

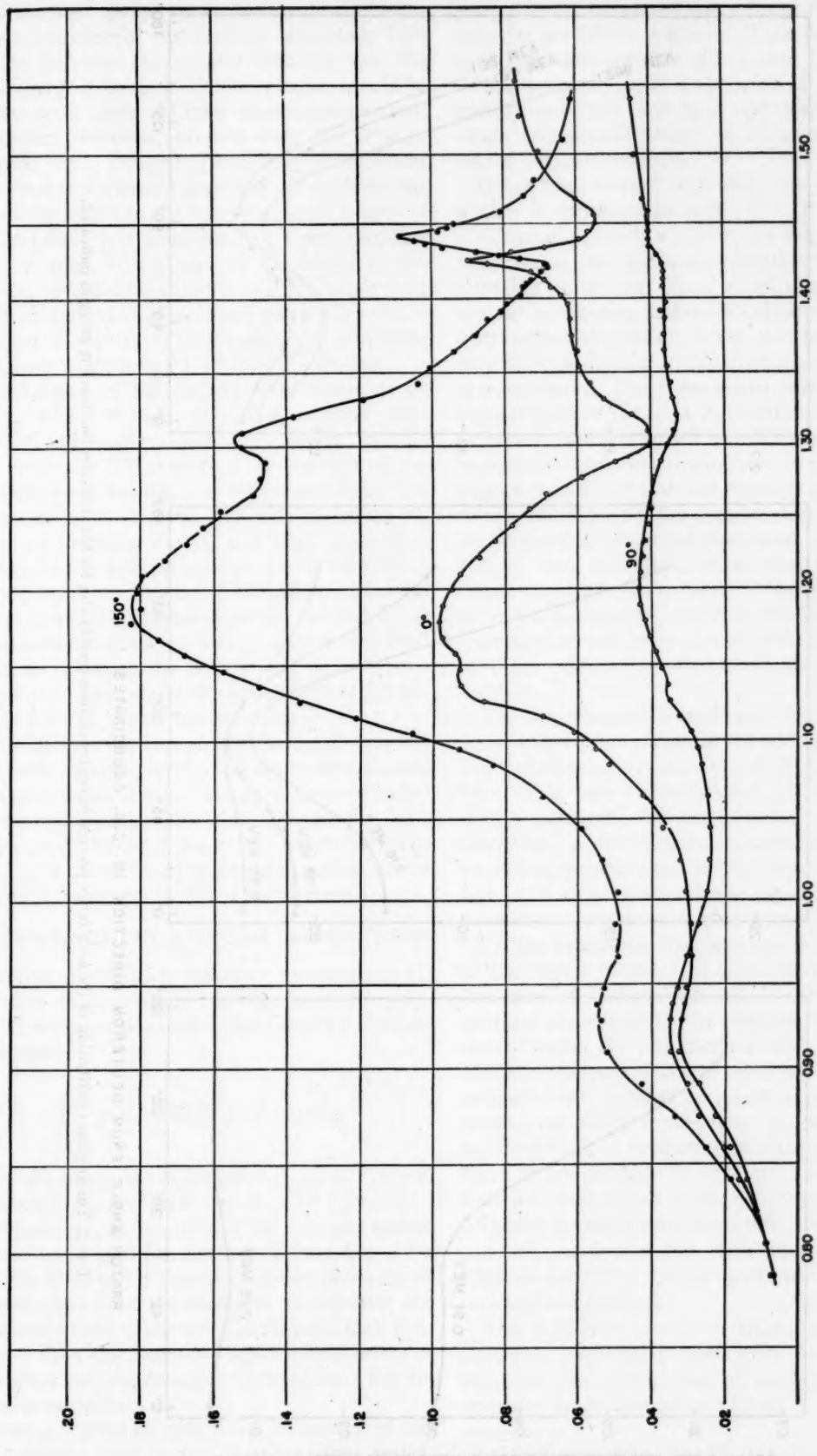

FIG. 1. The experimentally determined excitation curves for the production of long-range protons as a function of bombarding deuteron energy. The curves marked 0°, 90°, and 150° are cross sections determined at these laboratory angles.

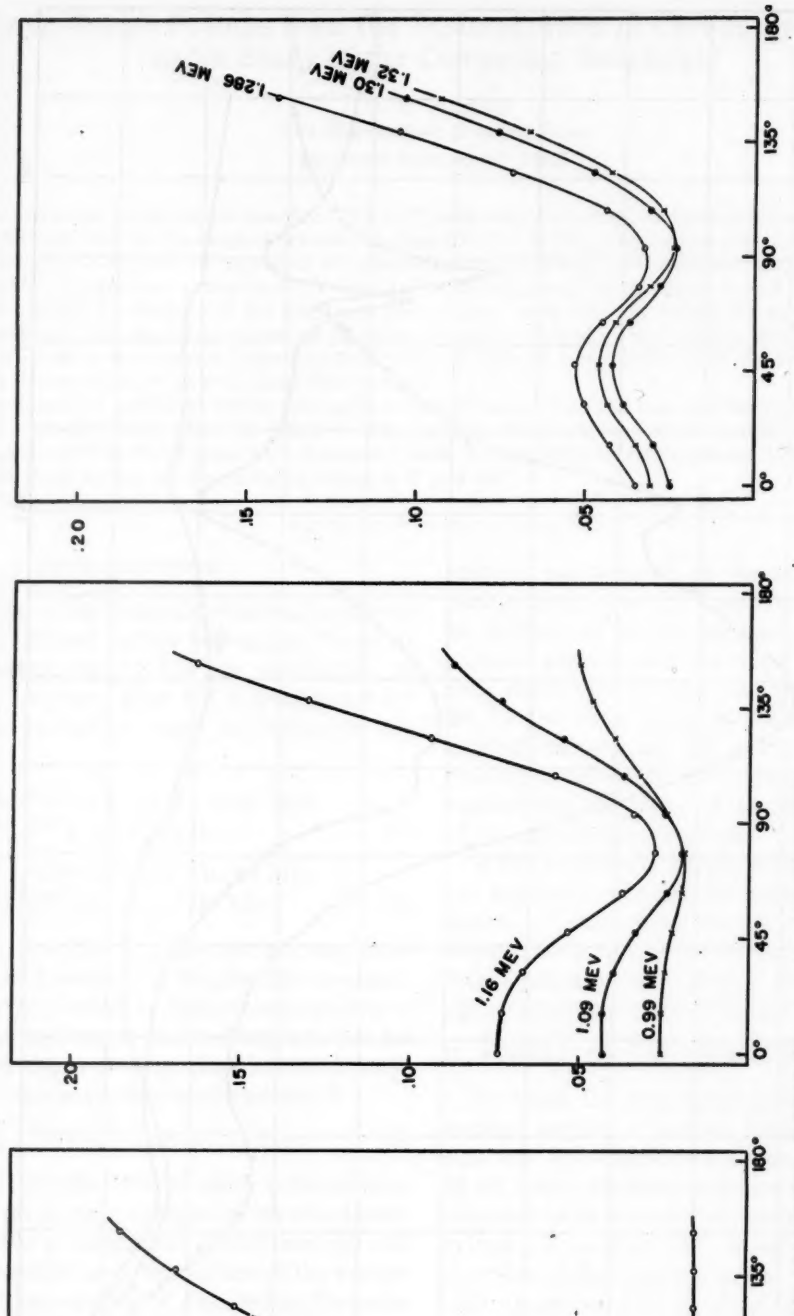

FIG. 2. The angular distribution of the long-range protons in center of mass coordinates for the deuteron bombarding energies indicated.

counter of standard design, which had a thin aluminum window for entrance of the protons. Absorbing foils were placed between the counter aperture and the target chamber exit holes so that the protons would be within a few cm of the end of their range when detected. This procedure prevented protons from the $O^{16}(d,p)$ reaction from being counted. These O^{16} protons would otherwise be a considerable source of error, since the exposure of the target to the beam produced a layer of oxygen. The pulses were amplified by a linear amplifier and were recorded with a scale of 64 circuit. In obtaining data, several foils of different thicknesses were used. Each datum point so obtained was always within a few percent of the others. The solid angle subtended by the counter window was 1.064×10^{-3} steradian.

The thicknesses of the targets were obtained[1] by comparison with reaction (2). The protons were counted at 0° at 1.30 Mev bombarding energy, and the positrons from the N^{13} remaining at the end of the bombardment were counted for several half-lives. Excitation curves were obtained with this apparatus for the laboratory angles of 0°, 90°, and 150°. These data are shown in Fig. 1, and are to be compared with Fig. 1 of reference 1, which shows the excitation curves for reactions (1) and (2). The resonance for reaction (3) at 1.435 Mev has been observed with thinner targets than those used in obtaining the data in Fig. 1. This resonance appears to have about the same width of 5.5 kev as reported for the gamma-ray resonance.[1]

The angular distributions shown in Fig. 2 were obtained by observing the proton yield at several stabilized bombarding energies. These data have been corrected for the center of mass motion, which changes the angle of emission and the solid angle of observation. The curves of Fig. 2 are to be compared with similar curves for reaction (2) as shown by Fig. 4 of reference 1.

III. DISCUSSION OF THE ANGULAR DISTRIBUTIONS

The angular distribution functions for reactions (2) and (3) have been expanded in the Legendre polynomials. These expansions were performed by evaluating the integrals

$$I_n=\int_{-1}^{+1}\sigma(E,\cos\theta)P_n(\cos\theta)d(\cos\theta),$$

so that for the expansion $\sigma(E,\cos\theta)=\sum A_n(E)P_n(\cos\theta)$ the coefficients A_n are given by $A_n(E)=\frac{1}{2}(2n+1)I_n$. The coefficients A_n, as functions of the deuteron energy E, are shown in Fig. 3 for reaction (2) and Fig. 4 for reaction (3). It is noted that no angular functions of order higher than four are necessary to describe the angular distributions analyzed. Coefficients that contributed less than the estimated experimental errors of ten percent for the neutrons and three percent for the protons were neglected.

Elementary arguments give some indication of the angular momenta and parity of the excited states, provided that the parity and spins of the incoming and outgoing particles are known. If the deuteron has spin 1, protons and neutrons spin $\frac{1}{2}$, and C^{12} has spin zero with even parity, and if the spins of C^{13} and N^{13} are one-half and they both have odd parity, one can calculate the allowed values of incoming and outgoing orbital angular momenta.

It has been shown[7] that when the differential cross section is expressed as $\sigma(\theta)=\sum A_nP_n(\cos\theta)$ that the coefficients A_n, with $n>2l^{\max}$, are zero; where $l^{\max}$, in this case, is the maximum orbital momentum of the incoming deuterons. Thus a finite number of total angular momentum states are indicated by the angular distributions. Analysis indicates that the coefficients A_n may show resonance or dispersion shapes in the region of a resonance. The cross section will have a general angular term of the form $P_{l_1}(\cos\theta)P_{l_2}(\cos\theta)$, which can be an odd function only if one of the outgoing angular momentum quantum numbers l_1 or l_2 are odd. This implies that if two states of opposite parity contribute to the disintegration the angular distributions will not be symmetrical about the equatorial plane in the C.M. system. Also, one might expect that when a resonant state competes in the emission of two groups of protons, or in the emission of neutrons and protons, then the cross sections will be governed by the probability of the particles penetrating the Coulomb and centrifugal barriers.

The Legendre polynomial coefficients shown in Figs. 3 and 4 have large values for the odd terms for the three first pronounced resonances: at 0.91, 1.16, and 1.30 Mev. This may be considered to indicate that the parity alternates for these states. Because of the similarity of the angular distributions and of the excitation curves in this energy region for reactions (2) and (3) it seems reasonable to assume that both reactions show resonances coming from the same states in $^*N^{14}$. The anomaly in the coefficient of the $P_2(\cos\theta)$ term in the region of the 1.16-Mev resonance shows that deuterons of at least one unit of orbital angular momentum contribute to the reaction. However, in this energy region the penetrability of d-deuterons is only about two percent of that of s-deuterons so that it seems unlikely that d-deuterons alone cause either of the states. Also p-deuterons cannot be mainly responsible for the 0.91-Mev resonance since there is no indication there of an anomaly in the term in $P_2(\cos\theta)$. These facts are most simply explained by assuming that the 0.91-Mev resonant state has a total angular momentum one unit and even parity, with the 1.16-Mev resonant state having one or two units of total angular momentum and odd parity.

The 1.30-Mev resonance shows anomalies in the Legendre polynomial coefficients up to A_4 and so indicates that d-deuterons, at least, are of some consequence in the formation of this state. The simplest

[7] L. Wolfenstein, Phys. Rev. 75, 1664 (1949).

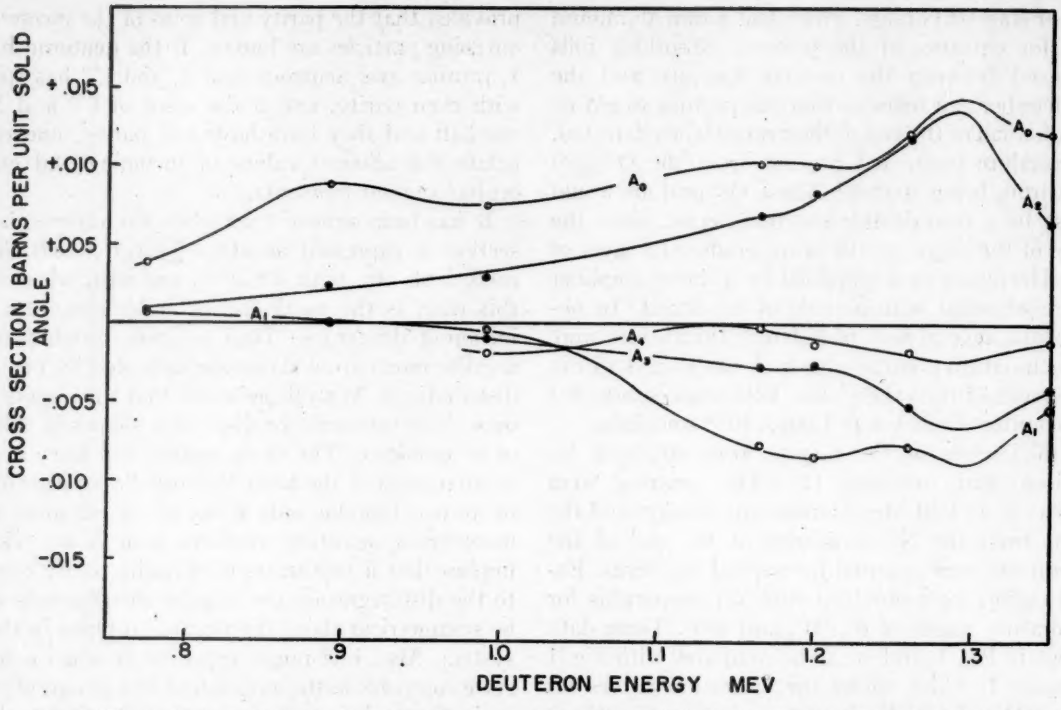

FIG. 3. The coefficients $A_n(E)$ in the expansion $\sigma_{\text{neutron}}(E, \cos\theta) = \Sigma_n A_n(E) P_n(\cos\theta)$ plotted as a function of the bombarding deuteron energy.

explanation of these facts is that the state in $^{*}N^{14}$ showing the 1.30-Mev resonance is of even parity and has one or two units of total angular momentum.

IV. THE INTENSITIES OF THE RESONANCES

The cross sections of the three reactions can be compared at the resonances by estimating each cross section above the background due to the overlapping resonances. The assignments of total angular momentum and parity for the first three large resonances of reactions (2) and (3) can be checked by comparison of the ratio of the total cross sections at resonance to the ratio of the penetrabilities of the two types of particles. The proton penetrabilities have been obtained from the curves of Christy and Latter,[8] and the neutron penetration of the centrifugal barrier has been calculated by the simple formulas of Weisskopf:[9]

$$P_1 = x^2/(1+x^2) (p \text{ neutrons}),$$
$$P_2 = x^4/(9+3x^2+x^4) (d \text{ neutrons}),$$

where $kR = x$, $R = e^2/2mc^2(1^{\frac{1}{3}}+13^{\frac{1}{3}})$ in this case, $k = \mu v/\hbar$, μ is the reduces mass, and v is the C.M. velocity. Since several outgoing angular momenta are important (as is witnessed by the complexity of the angular distributions), it was not possible to ascertain how to combine the penetrabilities. However, the intensity and penetrability ratios were found to be equal to within a factor of two when the lowest outgoing orbital angular momenta allowed were used. The approximate equality of these ratios may be taken to indicate that the nuclear part of the probability for long-range proton emission and neutron emission is nearly equal; or that the assignments of parity and angular momenta to the states, though far from certain, do not contradict the available data.

If reaction (1) is compared with reaction (3) in the same way for these three states, the agreement is not good. The intensity ratio of the short-range protons to long-range protons for these resonances in about unity. However, the ratio of the penetrabilities is very small (about 10^{-2} to 10^{-3}). Thus the short range protons are about one hundred times more intense than would be expected under the assumptions. It is perhaps significant that the disagreement is so large. This must mean that some mechanism other than that described by the simple assumptions is operating. A likely possibility is that the excited state in C^{13} formed by reaction (1) does not have the same parity and angular momentum as the ground state; and the short-range protons are emitted with less orbital angular momentum than the ground-state group has. However, at 0.91 Mev if s low energy protons are emitted (the most favorable case) and the high energy protons are p, the penetrability ratio disagrees with the intensity ratio by a factor of about fifteen. The same is true for the other resonances.

It is instructive to compare the rate of rise of the cross sections of the 0.91-Mev resonance for reactions (1) and (2). If these are the same levels, the ratio of the factor of rise should be the same as the ratio of the factor of rise of the penetrabilities since there appear to

[8] Christy and Latter, Rev. Mod. Phys. **20**, 185 (1948).
[9] V. Weisskopf, Lecture at Los Alamos, Summer, 1949.

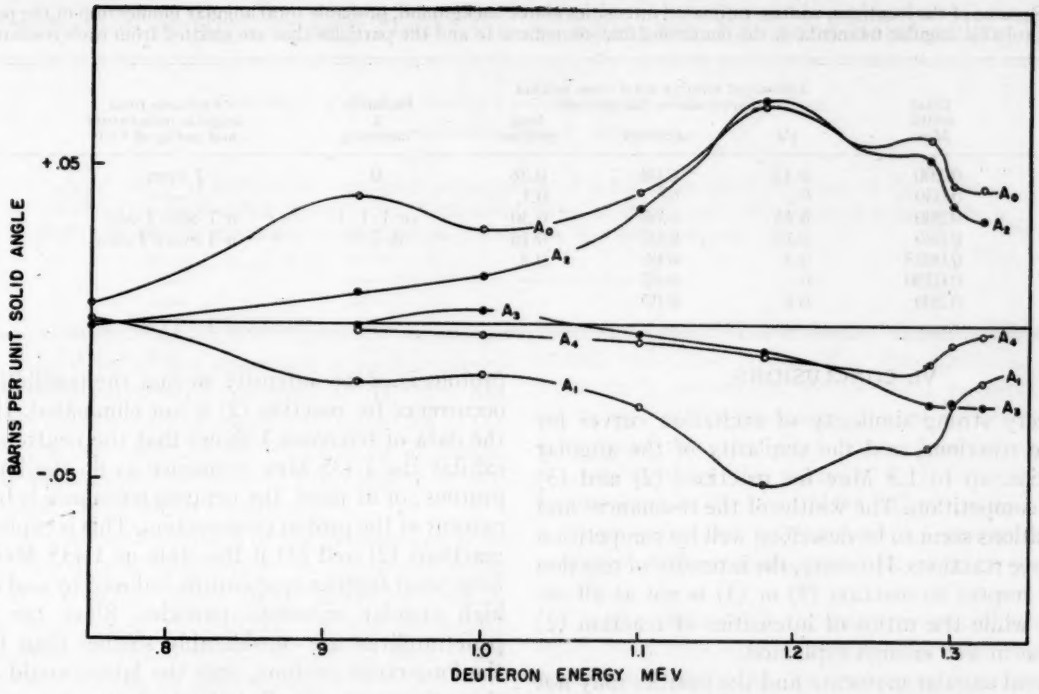

FIG. 4. The coefficients $A_n(E)$ in the expansion $\sigma_{\text{proton}}(E, \cos\theta) = \Sigma_n A_n(E) P_n(\cos\theta)$ plotted as a function of the bombarding deuteron energy.

be no resonances below. This ratio of rise of the experimental cross sections of reaction (1) to reaction (2) for the energy interval from 0.80 to 0.91 Mev is about unity. Now if p-particles are principally emitted by both reactions, the penetrability ratio of rise is about three, while if s short-range protons and p-neutrons are emitted, the penetrability ratio of rise is again about three. It is not obvious how the experimental cross sections could be in error by a factor of three.

V. THE POSITIONS AND WIDTHS OF THE RESONANCES

If the resonances that are shown by the three reactions are really competitive, one would expect them to coincide, except for small shifts due to the fact that the two proton groups of reactions (1) and (3) and the neutrons of reaction (2) do not have equal penetrabilities. Actually, not all the resonances have been found for all the reactions: the 1.13-Mev resonance is found only for reaction (3); the 1.435-Mev resonance only for reactions (1) and (3); however, this need not invalidate the theory of competition, but may point to unknown selection rules. However, Heydenburg, *et al.* have questioned the competition in this reaction.[4] The general similarity for the levels at 0.91, 1.16 and 1.30 for the three reactions and in particular the angular distributions for reactions (2) and (3) would lend credence to the hypothesis of competition.

The shift of a resonance due to the change of the penetrability across the resonance would be a maximum in the case of reaction (1). This shift would not be greater than 25 kev for the widths of the observed resonances of reaction (1). For reactions (2) and (3) they would be very small.

The levels at 0.91, 1.16 and 1.30 Mev show no shifting within the accuracy of the determinations. The excitation curves of the three reactions investigated at this laboratory were obtained with different targets, and and simultaneous experiments would be required to decide if the levels do not coincide. One can only say that the data, to the accuracy of the experiments, indicate no displacements.

The most striking examples of the shifting of resonance position occur when particles are observed at different angles across a resonance. The 1.435-Mev resonance shows a shift of about ten kev for reaction (3) from 0° to 150°. This shift may be due largely to the "interference" of the protons from this state with the overlapping states. The shape of the level is not entirely the Breit-Wigner shape, but has some of the shape of a dispersion curve.

The experimental widths of the resonances can be estimated from Figs. 1, 3, and 4, and from the data of reference 1. Each particular resonance, when shown by the different reactions, has widths that are closely the same. The only variation in width to be expected would be due to changes in penetration of the barrier in going across a resonance. Even for reaction (1) these changes are small percentage-wise. The small magnitude of the variation of widths for the three reactions give some support to the competing reaction hypothesis.

TABLE I. Resume of the locations, widths, estimated intensities above background, probable total angular momentum of the resonances, probable angular momenta of the deuterons that contribute to and the particles that are emitted from each resonance.

Deuteron energy at resonance Mev	Total width Mev	Estimated relative total cross section (barns) above background			Probable l incoming	Probable total angular momentum and parity of $*N^{14}$	Probable l outgoing
		γ's	neutrons	long protons			
0.91	0.200	0.12	0.08	0.36	0	1 even	1
1.13	0.030	0	0?	0.1	——	——	——
1.16	0.200	0.15	0.05	0.30	or 1/1, 3	or 1 odd/2 odd	or 0, 3/2
1.30	0.080	0.15	0.07	0.16	0, 2/2	or 1 even/2 even	or 1/1, 3
1.435	0.0055	0.3	0.01	0.2	——	——	——
1.62	0.0200	0	0.07	—	——	——	——
1.73	0.200	0.6	0.07	—	——	——	——

VI. CONCLUSIONS

The very strong similarity of excitation curves for the three reactions, and the similarity of the angular distribution up to 1.3 Mev for reactions (2) and (3) indicate competition. The widths of the resonances and their positions seem to be described well by competition of the three reactions. However, the intensity of reaction (1) with respect to reaction (2) or (3) is not at all explicable, while the ratios of intensities of reaction (2) and (3) seem well enough explained.

The total angular momenta and the parities may not be those deduced by consideration of the angular distributions and the penetrabilities, but these seem to be the simplest explanations of the experimental facts.

There are two aspects of the study that remain obscure: (*a*) What mechanism accounts for the unexpectedly large cross section for the short range protons; and (*b*) why do only the long-range protons exhibit the 1.13-Mev and the 1.435-Mev resonances, when otherwise reactions (2) and (3) are so similar;

It may be remarked on point (*a*) that the short-range protons act as if they did not need to penetrate the barrier.

The resonance at 1.13 Mev shown for the long-range protons is of low intensity so that the possibility of its occurrence for reaction (2) is not eliminated. However, the data of reference 1 shows that the neutrons do not exhibit the 1.435-Mev resonance as do the long range protons; or at most, the neutron resonance is but a few percent of the proton cross section. This is explicable for reactions (2) and (3) if the state at 1.435 Mev is of a large total angular momentum, induced by and emitting high angular momenta particles. Since the neutron penetrabilities are considerably smaller than those for the long-range protons, only the latter would strongly show the resonance. But this high angular momentum certainly would not be expected to allow the very strong resonance shown by the low energy proton group.

A tabulation of the best information on the resonances in given in Table I.

The author wishes to thank Professor T. W. Bonner for much help and encouragement on this project. He also wants to thank Professor W. V. Houston for discussions of the theory. The assistance of Mr. J. E. Richardson on the target preparations and of Mr. J. F. Vander Henst on the construction of apparatus is appreciated. During part of this research the author was the Humble Oil Company Fellow in Physics at the Rice Institute.

The Production of High Energy Deuterons by Energetic Nucleons Bombarding Nuclei

J. HEIDMANN*
Laboratory of Nuclear Studies, Cornell University, Ithaca, New York
(Received June 9, 1950)

A calculation is given of the cross section for production of fast deuterons ($\gtrsim$50 Mev) by fast nucleons ($\gtrsim$100 Mev) bombarding heavy nuclei. A corrected Fermi model is used. The dependence on energy is given and also the momentum wave function of a nucleon in a heavy nucleus.

I. INTRODUCTION

THE production of fast deuterons in nuclear events involving energies of the order of 100 Mev has been shown to take place in cosmic-ray stars[1] and in the Berkeley cyclotron experiments.[2-4] The most advanced study has been made by York in bombarding C, Cu and Pb targets with 90-Mev neutrons.

A semi-empirical calculation of the process has been made by Chew and Goldberger[5] in which the wave function of the nucleon which will be picked up is taken from the experiments themselves; another treatment using the Wheeler alpha-particle model has been given elsewhere[6] for the case of light nuclei.

In this paper we give a treatment for heavy nuclei which is a continuation of the Chew and Goldberger work, in the sense that no data essential for the calculation are taken from the deuteron production experiments. That will enable us to draw some conclusions concerning the energy dependence of the process.

II. FORMULATION OF THE PROBLEM

As we are dealing with energies of the order of 100 Mev we shall use the Born approximation. Let the indices 0 and 1 refer to the incident neutron and the proton of the nucleus which will be picked up to produce the deuteron. Let $\mathbf{r}_i$ be the position vector of the ith nucleon in the center of mass system of the nucleus, which we shall assume to be heavy enough to be used as a convenient reference system; let $\mathbf{k}$ and $\mathbf{K}$ be the propagation vectors of the incident neutron and of the produced deuteron in that system. Then the amplitude for the production of a deuteron of momentum $\hbar\mathbf{K}$ is:

$$A=-(1/4\pi)\Big[P\exp[i\mathbf{K}\cdot(\mathbf{r}_0+\mathbf{r}_1)/2]\psi_D(0,1)\psi_f(2,\cdots A)\times\sum_{n=1}^{A}V_{0n}\chi_0\exp(i\mathbf{k}\cdot\mathbf{r}_0)\psi_i(1,\cdots A)\Big], \quad (1)$$

where χ_0 is the spin wave function of 0, ψ_D the total wave function of the deuteron, ψ_i and ψ_f those of the initial and final nuclei, V_{0n} the potential between nucleons 0 and n. As we use as a perturbation the interaction before the rearrangement collision we must antisymmetrize the final wave function, which is accomplished by the operator P. It is seen that the contribution of the terms $n\neq 1$ will be negligible if $K/2$ is large compared to the internal momenta of the nucleons of the nucleus, which is roughly the case at 90 Mev.

For the term $n=1$ the antisymmetrization gives a small correction, as k is large compared to the internal momenta. Finally, as the final wave function is symmetric with respect to nucleons 0 and 1 in both spin and space coordinates, the P_x and P_σ exchange operators which occur in V are equivalent to unity. The amplitude is then simply:

$$A=-(1/4\pi)\Big[\exp[i\mathbf{K}\cdot(\mathbf{r}_0+\mathbf{r}_1)/2]\psi_D(0,1)\psi_f(2,\cdots A)\times V_{01}\chi_0\exp(i\mathbf{k}\cdot\mathbf{r}_0)\psi_i(1,\cdots A)\Big]. \quad (2)$$

Integrating over $\mathbf{r}_0-\mathbf{r}_1$ first we can separate the terms depending on the state of the nucleus from those depending on the nucleonic forces:

$$A=-(1/4\pi)\sum_{\text{spin}}\int\exp[i(\mathbf{k}-\mathbf{K}/2)\cdot(\mathbf{r}_0-\mathbf{r}_1)]\times\psi_D^*(0,1)V_{01}\chi_0\times\int\exp[i(\mathbf{k}-\mathbf{K})\cdot\mathbf{r}_1]\psi_f^*\psi_i. \quad (3)$$

The first factor is the Fourier component of $\psi_D V_{01}$, corresponding to the momentum change of the neutron. The second factor is the component of $\psi_f^*\psi_i$ corresponding to the total momentum change of the free particles (i.e., final deuteron momentum minus initial neutron momentum); if the ψ's were products, this would be exactly the momentum wave function of the proton, as was stated by Chew and Goldberger.

III. USE OF FERMI MODEL

If we make use of the statistical Fermi model, then restricting ourselves to the case of heavy nuclei, an opposing case to our previous treatment,[6] we can write the initial wave function of the nucleus as:

$$\psi_i(1,\cdots A)=v^{-\frac{1}{2}}\chi_1\exp(i\mathbf{p}\cdot\mathbf{r}_1)\phi_i(2,\cdots A)$$

* Attache de Recherches du C.N.R.S.

[1] Hoang, Jauneau, and Morellet, *Cosmic Radiation* (Butterworth's Scientific Publications Ltd., London, 1949).
[2] K. Brueckner *et al.*, Phys. Rev. **75**, 1274 (1949).
[3] H. F. York, Phys. Rev. **75**, 1467 (1949) and thesis, University of California, Radiation Laboratory, 1949.
[4] Cuer, Morand, and van Rossum, Comptes Rendus **228**, 481 (1949).
[5] G. F. Chew and M. L. Goldberger, Phys. Rev. **77**, 470 (1950).
[6] J. Heidmann, Phil. Mag. **41**, 444 (1950).

where χ_1 is the spin function of 1, $\mathbf{p}$ its propagation vector, v the volume of the nucleus.

Integration over nucleons $2\cdots A$ will give unity if these nucleons remain in the original states and integration over proton 1 will also give unity if $\mathbf{K}-\mathbf{k}\sim\mathbf{p}$. Since in a Fermi distribution p has a definite upper limit L, the differential cross section will be different from zero only for $|\mathbf{K}-\mathbf{k}|<L$. In reality, of course, momentum changes greater than L will occur; in fact, if the initial energy of the neutron is high, these are the only ones that *can* occur for energetic reasons. In this case, then, it is necessary to go beyond the Fermi model.

IV. CORRECTION TO FERMI MODEL

The correction we shall make consists in the introduction of an interaction between proton 1 and another nucleon 2 of the nucleus. We shall then write ψ_i as:

$$\psi_i(1,\cdots A)=v^{-\frac{1}{2}}\chi_{12}\exp(2i\mathbf{P}\cdot\mathbf{r})\psi_p(\varrho)\phi_i(3,\cdots A),$$

with

$$\mathbf{r}=(\mathbf{r}_1+\mathbf{r}_2)/2,\quad \varrho=\mathbf{r}_1-\mathbf{r}_2.$$

In the same way we shall write the final wave function as:

$$\psi_f(2,\cdots A)=v^{-\frac{1}{2}}\chi_2\exp(i\mathbf{p}'\cdot\mathbf{r}_2)\phi_f(3,\cdots A).$$

The antisymmetrization of that final wave function will give but a small correction (exchange term).

Integration over $\mathbf{r}$ gives $\mathbf{k}-(\mathbf{K}-2\mathbf{P})\sim\mathbf{p}'$ and a factor v, and integration over nucleons $3\cdots A$ gives unity. Then (3) reduces to:

$$A=-(1/4\pi)\int\exp[i(\mathbf{k}-\mathbf{K}/2)\cdot(\mathbf{r}_0-\mathbf{r}_1)]\times\psi_D^*(\text{space})V_{01}\times S\times G$$

with

$$G=\int\exp(i\mathbf{q}\cdot\varrho)\psi_p(\varrho)d^3\varrho,\quad \mathbf{q}=\mathbf{k}-\mathbf{K}+\mathbf{P}. \tag{4}$$

The spin factor is $S=(T_{01}\chi_2,\ \chi_0\chi_{12})$ where T_{01} is a triplet state of the final deuteron.

V. CHOICE OF ψ_p

The interaction we introduce between nucleons 1 and 2 will be pictured by the choice we shall make for ψ_p. The form of ψ_p will depend upon the nature and state of nucleon 2. If that nucleon is a proton and if we assume a Serber interaction, nucleons 1 and 2 must be in a singlet state, which will occur $w_1=Z/4$ times; if nucleon 2 is a neutron we shall have an even triplet state with $w_2=3(A-Z)/8$ or an even singlet state with $w_3=(A-Z)/8$. These three possible states will be denoted later by the index i, which, however, will be omitted in unambiguous cases.

S can be calculated; if we are interested in the formation of a deuteron of any spin by an incident neutron of undefined spin it is found that in the three cases outlined above S^2 is equal to 3/4.

The spatial part of ψ_p will then be an even state of small energy $(\hbar p)^2/M$, which we shall assume to be an S state. The wave function can be written approximately, following Hulthén, as

$$\rho\psi_p=B\alpha[\sin(p\rho+\delta)/\sin\delta-e^{-\mu\rho}]/(\alpha^2+p^2)^{\frac{1}{2}} \tag{5a}$$

where α^{-1} is the scattering length, μ^{-1} the range of the Yukawa potential and δ the phase shift given by:[7]

$$\cot\delta\sim-\alpha/p.$$

B is a normalization factor; as μ^{-1} is small compared with the radius of the nucleus, B will be determined by the condition that, for ρ of the order of the radius of the nucleus R and $\delta\to0$, ψ_p is the S-part of a plane wave. We have then:

from (5a):

$$\psi_p\to B\alpha\sin p\rho/p\rho$$

from the normalized plane wave:

$$v^{-\frac{1}{2}}\exp(i\mathbf{p}\cdot\varrho)\to v^{-\frac{1}{2}}j_0(p\rho)$$

hence:

$$B\alpha=v^{-\frac{1}{2}}.$$

For $\rho\gtrsim R$ we must have $\psi_p=0$. This will be achieved essentially by putting in (4) a convergence factor $\exp(-\beta\rho)$ with $\beta\sim6^{\frac{1}{2}}/R$. Integrating over the angular variables in (4) we get:

$$G=\frac{4\pi B\alpha}{q(\alpha^2+p^2)^{\frac{1}{2}}}\int_0^\infty\sin q\rho\left[\frac{\sin(p\rho+\delta)}{\sin\delta}-e^{-\mu\rho}\right]e^{-\beta\rho}d\rho$$

hence:

$$G=\frac{4\pi B\alpha}{(\alpha^2+p^2)^{\frac{1}{2}}}\left[-\frac{1}{q^2+(\mu+\beta)^2}+\frac{\beta^2+q^2-\alpha\beta-p^2}{(\beta^2+q^2+p^2)^2-4q^2p^2}\right]$$

of which a good approximation is, for $|\mathbf{q}-\mathbf{p}|\gg\beta$ and $\mu\gg\beta$:

$$G=\frac{4\pi B\alpha}{(\alpha^2+p^2)^{\frac{1}{2}}}\left(-\frac{1}{q^2+\mu^2}+\frac{1}{q^2-p^2}\right). \tag{5}$$

The first term of (3) is simply the Fourier transform of ψ_DV_{01}. Assuming a Yukawa potential and an approximate (Hulthén) wave function:

$$\psi_D(\rho)=A_D(e^{-\alpha_1\rho}-e^{-\alpha_2\rho})/\rho,\quad V_{01}(\rho)=Ve^{-\mu\rho}/\mu\rho$$

this term is:

$$F(\mathbf{l})=\frac{4\pi A_DV}{\mu l}\left(\tan^{-1}\frac{l}{\alpha_1+\mu}-\tan^{-1}\frac{l}{\alpha_2+\mu}\right),\quad \mathbf{l}=\mathbf{k}-\mathbf{K}/2.$$

VI. CROSS SECTION

The differential cross section for the production of a deuteron of momentum $\hbar\mathbf{K}$ while nucleons 1 and 2 are

[7] H. A. Bethe, Phys. Rev. 76, 38 (1949).

in the initial state described by $\mathbf{P}$ and $\mathbf{p}$ is:

$$\sigma_{Pp}=(K/2k)(2M_{\text{red}}/4\pi\hbar^2)^2\cdot S^2\cdot F^2\cdot\sum_i Zw_iG_i^2$$

where the index i refers to the three cases outlined in the preceding paragraph.

In order to get the cross section without any regard to the initial state of nucleons 1 and 2, we have to integrate G_i^2 with respect to $\mathbf{P}$ and $\mathbf{p}$ with a weighting factor given by the probability of getting given values of $\mathbf{P}$ and $\mathbf{p}$ and taking into account the limitations given by the energy conservation relation.

VII. ENERGY CONSERVATION RELATION

Let $\mathbf{p}_1$ and $\mathbf{p}_2$ be the propagation vectors of nucleons 1 and 2 in the initial state when the distance between them is large compared to μ^{-1}; we have the relations:

$$\mathbf{P}=(\mathbf{p}_1+\mathbf{p}_2)/2,\quad \mathbf{p}=(\mathbf{p}_1-\mathbf{p}_2)/2.$$

Assuming that the energy of a bound nucleons is given by its potential energy (assumed to be -29 Mev), plus the kinetic energy of a free particle of the given momentum, the energy conservation relation is:

$$-k^2-p_1^2-p_2^2+\frac{K^2}{2}+\frac{(29-2)\text{Mev}}{20.7\times10^{-26}}+(\mathbf{k}-\mathbf{K}+\mathbf{p}_1+\mathbf{p}_2)^2=0.$$

Here 2 Mev is the binding energy of the deuteron, and 20.7×10^{-26} converts Mev into cm^{-2}. From this relation it is deduced that $\mathbf{K}$ lies on a sphere of center $\mathbf{C}$ and radius R given by:

$$\mathbf{C}=2(\mathbf{k}+2\mathbf{P})/3$$
$$R^2=4[(\mathbf{k}-\mathbf{P})^2+3p^2]/9-2\times27\text{ Mev}/3\times20.7\times10^{-26}$$

with the restriction:

$$K^2/2<k^2+(2-8)\text{ Mev}/20.7\times10^{-26}$$

which means that the residual nucleus cannot have less energy than its ground state.

VIII. DISTRIBUTION OF P AND p

We shall calculate this distribution from the distributions of $\mathbf{p}_1$ and $\mathbf{p}_2$, which we shall assume to be Fermi distributions; as G depends on $\mathbf{p}$ only through its modulus, we can integrate immediately over the angular parameters of $\mathbf{p}$ and get:

$$\mathcal{P}(\mathbf{P},p)d^3\mathbf{P}dp=P^2dPd\Omega_P dp\times72p\mathfrak{C}/4\pi L^6$$

with

$$\mathfrak{C}=p \quad \text{if} \quad p<L-P,$$
$$\mathfrak{C}=(L^2-P^2-p^2)/2P \quad \text{if} \quad L-P<p<(L^2-P^2)^{\frac{1}{2}}$$

where L is the maximum of the Fermi distribution. $\mathcal{P}$ is normalized such that

$$\int\mathcal{P}d^3\mathbf{P}dp=1.$$

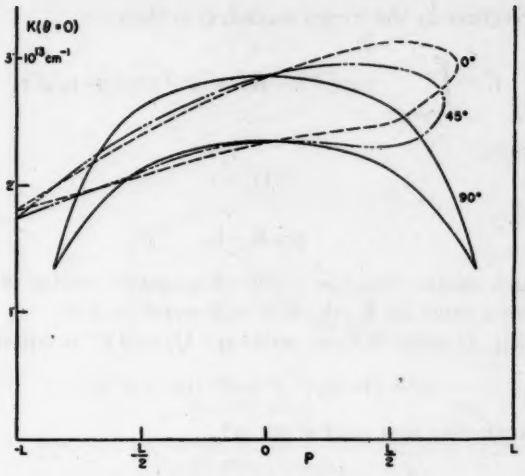

FIG. 1. Energy conservation relation.

The relation between $\mathbf{P}$ and $\mathbf{p}$ for a given $\mathbf{K}$ due to the energy conservation relation is very intricate, except in the asymptotic case $k\to\infty$. But as G^2 is not a too-rapidly varying function of K we can write (note the normalization of $\mathcal{P}$):

$$\left(\int G^2\mathcal{P}d^3\mathbf{P}dp\right)_K \text{ fixed}\sim\left(\int\mathcal{P}d^3\mathbf{P}dp\right)_K \text{ fixed}\times\left(\int G^2\mathcal{P}d^3\mathbf{P}dp\right)\text{ all space.}$$

From this equation we shall calculate the energy and angular distribution of the deuterons. The first term of the right-hand side is simply the distribution of $\mathbf{K}$ obtained from purely geometrical considerations. It can be estimated graphically (Fig. 1). For example, when the angle θ between $\mathbf{k}$ and $\mathbf{K}$ is zero and the angle between $\mathbf{k}$ and $\mathbf{P}$ is 45°, the modulus K of $\mathbf{K}$ must lie inside the contour labelled 45° in Fig. 1. From it, one can read the maximum and minimum value of K as a function of P, with p varying between 0 and $(L^2-P^2)^{\frac{1}{2}}$. Figure 1 also gives curves for an angle between $\mathbf{k}$ and $\mathbf{P}$ equal to 0 and 90°.

From the inspection of Fig. 1 and from the fact that the dependence of G on K will give greater probability to small values of K, we shall suppose that for any angle θ the energy distribution of the emerging deuterons (i.e., the distribution of K^2) is uniform between 40 and 80 Mev with zero probability outside that range. If an accurate calculation on the basis of Fig. 1 gives different results, it will only be necessary to correct the final result but not the calculation in the next section.

IX. CALCULATION OF $\Sigma_i Zw_i\int G_i^2\mathcal{P}d^3\mathbf{P}dp$

This is a function of $\mathbf{Q}=\mathbf{K}-\mathbf{k}$ which we set equal to $N(\mathbf{Q})$. We shall distinguish the three following cases:

(a). *Q small.* As stated above we can neglect the

correction to the Fermi model. G is then:

$$G=\int_{\text{nucleus}} \exp[i(\mathbf{k}-\mathbf{K})\cdot\mathbf{r}_1]v^{-\frac{1}{2}}\exp(i\mathbf{p}\cdot\mathbf{r}_1)d^3\mathbf{r}_1$$

hence:

$$N(\mathbf{Q})=v$$

and:

$$\mathbf{p}\sim\mathbf{K}-\mathbf{k},$$

which means that the initial propagation vector of the proton must be $\mathbf{K}-\mathbf{k}$. S^2 is still equal to 3/4.

(b). *Q large.* We can write $\mathbf{q}\sim\mathbf{Q}$, and G^2 is equal to:

$$G^2=(4\pi B\alpha)^2(p^2+\mu^2)^2/(\alpha^2+p^2)Q^8.$$

Integrating first over P we get:

$$\int\mathcal{P}d^3\mathbf{P}=12p^2(L-p)^2(2L+p)/L^6.$$

Then:

$$N(\mathbf{Q})=\sum_i 12(4\pi B\alpha)^2I_iZw_i/L^6Q^8$$

with:

$$I=\int_0^L p^2(\alpha^2+p^2)^{-1}(L-p)^2(2L+p)(p^2+\mu^2)^2dp$$

hence:

$$I=(\mu^2-\alpha^2)^2\left[\frac{\alpha^2}{2}(3L^2+\alpha^2)\ln\frac{\alpha^2+L^2}{\alpha^2}-2\alpha L^3\tan^{-1}\frac{L}{\alpha}\right.$$
$$\left.+\frac{3}{4}L^4-\frac{\alpha^2L^2}{2}\right]+\frac{L^8}{40}+\frac{L^6}{12}(2\mu^2-\alpha^2)$$

where the index i is omitted.

(c). *Q intermediate.* We shall restrict ourselves to the case in which G can be written in the form (5); i.e., $|\mathbf{Q}-\mathbf{L}|>\beta$. The calculation is simpler if we calculate first the distribution of the modulus of $\mathbf{Q}$; from it we shall get N by dividing the result by $4\pi Q^2$; we can do that as G^2 is proportional to the probability for the propagation vector of $\rho/2$ to be $\mathbf{q}$. We have then:

$$N(\mathbf{Q})=\sum_i\frac{Zw_i}{4\pi Q^2}\int_{q=Q-P}^{\infty}\int\int\frac{-2\pi q^2Q}{Pq}G_i^2\mathcal{P}dqdpd^3\mathbf{P},$$

i.e.,

$$N(\mathbf{Q})=-\sum_i 18(4\pi B\alpha)^2J_iZw_i/L^6Q$$

with, omitting again the index i:

$$J=\int\left\{\frac{Pp\mathfrak{C}}{\alpha^2+p^2}\left[\frac{1}{X^2+\mu^2}+\frac{1}{X^2-p^2}+\frac{2}{\mu^2+p^2}\ln\left|\frac{X^2-p^2}{X^2+\mu^2}\right|\right]\right.$$
$$\left.-\left[\frac{1}{2X(X-p)}+\frac{2}{X^2+\mu^2}\ln|X-p|\right]\frac{PX\mathfrak{C}_X}{\alpha^2+X^2}\right\}dpdP$$
$$+\int\frac{PX\mathfrak{C}_X}{\alpha^2+X^2}\left[\frac{1}{2X(X-p)}+\frac{2}{X^2+\mu^2}\ln|X-p|\right]dpdP,$$

where $X=Q-P$ and $\mathfrak{C}_X$ means that in $\mathfrak{C}$ we write $p=X$. In J the integration over q and the angular parameters of $\mathbf{P}$ has been performed. The second integral of J cancels the second term of the first integral; we introduced it in order to make the first integral calculable graphically by eliminating the poles occurring for $p=X$.

The integration over p in the second integral of J gives:

$$\int_0^L\left\{\frac{-P\mathfrak{C}_X}{2(\alpha^2+X^2)}\ln\left|\frac{X-(L^2-P^2)^{\frac{1}{2}}}{X}\right|\right.$$
$$\left.+\frac{2PX\mathfrak{C}_X}{(\alpha^2+X^2)(\mu^2+X^2)}(L-P)[\ln|L-P|-1]\right\}dP$$

where the subsequent integration over P will be performed graphically.

In case (c) we have carried out the calculation only for one value of Q, *viz.*, 1.3×10^{13} cm^{-1}; the value thus found can be joined to the results of cases (a) and (b), for instance by a Fermi distribution at suitably chosen temperature.

I_i and J_i depend upon the triplet or singlet character of the initial state of nucleons 1 and 2 only through the scattering lengths α_i^{-1}; but as the dependence is not very sharp we shall perform the calculation only for the triplet case; then we can separate the summation over w_i and, with $Z=A/2$, we get:

$$\sum_i w_i=3A/8.$$

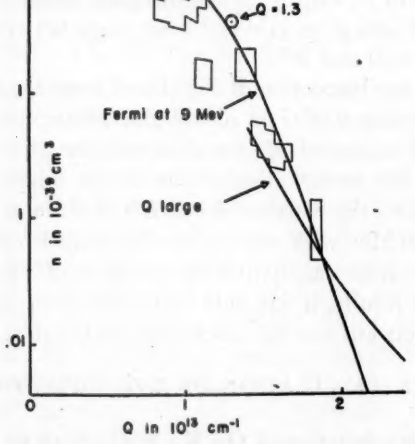

FIG. 2. Momentum distribution of a nucleon inside a nucleus (the odd contours are the result of the superposition of quadrangles representing York's data).

X. NUMERICAL RESULTS

We shall first deal with $N(\mathbf{Q})$ which is important as it is proportional to the momentum distribution of a nucleon inside a nucleus.

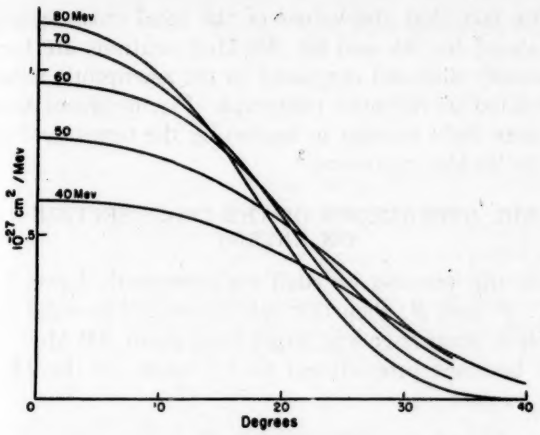

FIG. 3. Differential cross section per Mev and per nucleon for production of deuterons by 90-Mev nucleons.

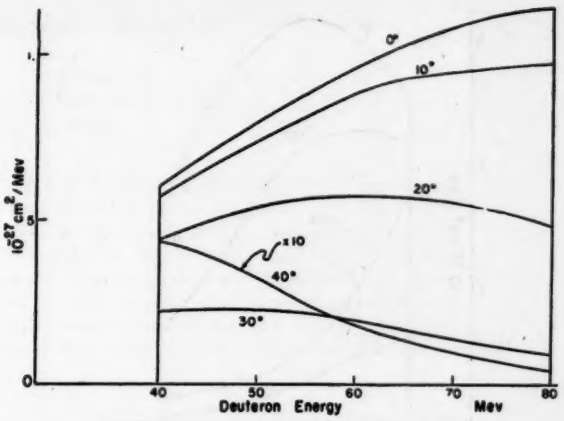

FIG. 4. Spectrum at various angles of the deuterons produced by 90-Mev nucleons.

The numerical values taken are:

$$L=1.0\times10^{13}\ \text{cm}^{-1} \qquad \mu=0.847\times10^{13}\ \text{cm}^{-1}$$
$$v=17\cdot A\times10^{-39}\ \text{cm}^3, \quad \alpha^{-1}=5.39\times10^{-13}\ \text{cm}.$$

Then for Q small we have:

$$n\equiv N(\mathbf{Q})/A=17\times10^{-39}\ \text{cm}^3,$$

for $Q=1.3\times10^{13}\ \text{cm}^{-1}$: $n=3.6\times10^{-39}\ \text{cm}^3$,

for Q large: $n=7.6\times10^{65}/Q^8\times10^{-39}\ \text{cm}^3$.

The n value for $Q=1.3$ is likely to be too high because $|\mathbf{Q}-\mathbf{L}|>\beta$ is only just satisfied, therefore we shall take $n=3.0$ instead. The temperature of the Fermi distribution joining these data is found to be 9 Mev, which is, within our uncertainties, in agreement with Watanabe's calculation.[8] The result of the calculation is shown in Fig. 2. Note that a Fermi distribution is used only for purpose of easy interpolation.

We can make a comparison with York's results. In his thesis York gives the cross section σ for production of deuterons ejected at given angles and of energy lying in given intervals. From these values we can plot σ/F^2 as a function of Q. That is done on Fig. 2 in arbitrary units from York's data on C. As a matter of fact, our calculations should not be too good for such a light nucleus as C, but we cannot compare them with York's results on Cu and Pb, first because the latter experiments are not so complete, and second because the internal scatterings of the incident neutron play a very important role in such heavy nuclei.[9] Even if our curve of Fig. 2 was rectangle-like it would be possible to account for a spread σ/F^2 through these internal scatterings.

XI. CROSS SECTION FOR 90-MEV NEUTRONS

The differential cross section per Mev and per nucleon is:

$$\sigma/A=\frac{K}{2k}\cdot\left(\frac{M}{\pi\hbar^2}\right)^2\cdot\frac{3}{4}\cdot F^2(\mathbf{k}-\mathbf{K}/2)\cdot n(\mathbf{K}-\mathbf{k})\cdot\frac{1}{40}.$$

[8] S. Watanabe, Zeits. f. Physik **113**, 482 (1939).
[9] M. L. Goldberger, Phys. Rev. **74**, 1269 (1948).

The numerical values involved in F are taken as:[10]

$$A_D^2=0.0613\times10^{13}\ \text{cm}^{-1}$$
$$\alpha_1=0.231\times10^{13}\ \text{cm}^{-1} \qquad V=67.8\ \text{Mev}.$$
$$\alpha_2=1.55\times10^{13}\ \text{cm}^{-1}$$

The differential cross section per Mev and per nucleon is shown in Fig. 3. The corresponding spectrum of the deuterons at various angles is shown in Fig. 4. It seems that our calculation accounts in a natural way, without the introduction of internal scattering, for the shift of the most probable deuteron energy to lower energies at larger angles which was observed by York. This shift is due to the fact that for large angle the values of K permitted by the energy conservation relation are such that $|\mathbf{K}-\mathbf{k}|$ can take the value L. By graphical integration we find that the total cross section is:

$$\sigma_T=1.94\times A\times10^{-26}\ \text{cm}^2.$$

This is a very large cross section; it is equal to r_0^2 where r_0 is the radius of the sphere containing one nucleon. This explains qualitatively the experimental result that the cross section of the pick-up process is considerable, a result which was surprising to most physicists because of the small binding energy of the deuteron. For a comparison with experiment, we should take into account that the deuteron can easily disintegrate again while escaping from the nucleus. We shall assume that the layer of the nucleus effective in the pick-up process has a thickness of r_0 (measured in the direction of motion of the deuteron and on the escape side of the nucleus only). The effective volume of the nucleus is then $\pi r_0(r_0A^{\frac{1}{3}})^2$ as compared to the total nuclear volume $(4\pi/3)r_0^3A$. This means the effective number of nucleons is about $\frac{3}{4}A^{\frac{1}{3}}$ instead of A. For C, this yields about 4, giving a theoretical cross section of about 8×10^{-26} cm^2. The observations of York give 2.6×10^{-26} cm$^2\pm25$ percent: our theoretical value is therefore about three times too high. An error in this direction is not unsatisfactory because (1) the "mean

[10] H. A. Bethe and C. Longmire, Phys. Rev. **77**, 647 (1950).

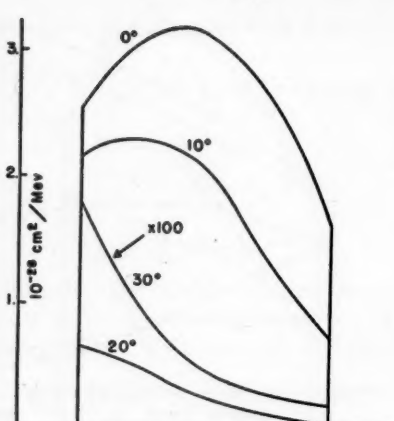

FIG. 5. Spectrum at various angles of the deuterons produced by 200-Mev nucleons.

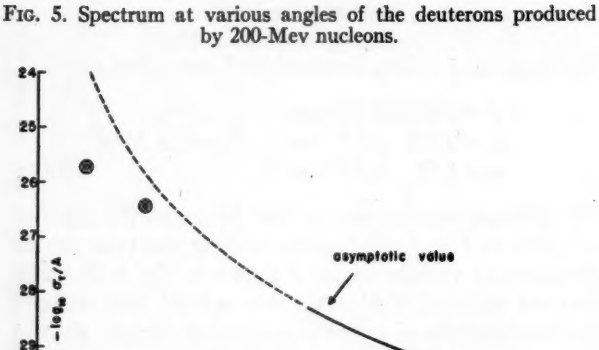

FIG. 6. Total cross section for production of deuterons as a function of the incident nucleon energy.

free path" of the escaping deuteron may be less than r_0, and (2) there are many competing processes for which our theory will also give large cross sections. The Born approximation customarily over-estimates cross sections. For heavier nuclei, there will be a further reduction because the incident neutron may be absorbed before it reaches the far side of the nucleus; the cross section should therefore increase less than $A^{\frac{1}{3}}$, in agreement with observation.

XII. CROSS SECTION FOR 200-MEV NEUTRONS

A similar procedure to that illustrated on Fig. 1 shows that the energy of the deuterons produced has a distribution nearly uniform in the range 120–194 Mev. Similarly to Fig. 4, we get a deuteron spectrum as shown in Fig. 5. By graphical integration the total cross section is:

$$\sigma_T = 0.37 \times A \times 10^{-26} \text{ cm}^2.$$

The fact that the values of the total cross section calculated for 90- and for 200-Mev neutrons are harmoniously disposed compared to the asymptotic value calculated in the next paragraph (Fig. 6) shows that we were right enough in neglecting the terms $n \neq 1$ in (1) for 90-Mev neutrons.

XIII. DEPENDENCE OF THE CROSS SECTION ON ENERGY

For this purpose we shall use asymptotic forms for G, C, F, and R; then this calculation will be valid for incident neutron energy larger than about 500 Mev.

F becomes proportional to l^{-2} where $l = |\mathbf{k} - \frac{1}{2}\mathbf{K}|$, and we get:

$$\sigma_{as} = \frac{K}{2k} \cdot \left(\frac{M}{\pi\hbar^2}\right)^2 \cdot \frac{3}{4} \cdot \left(\frac{4\pi A_D V}{\mu}\right)^2 \cdot (\alpha_1 - \alpha_2)^2 \cdot \frac{12(4\pi B\alpha)^2}{L^6} \cdot I \cdot \frac{3A}{8} \cdot Z \cdot l^{-4} Q^{-8}.$$

We have, moreover:

$$Q^2 \sim l^2 \sim k^2(5 - 4\cos 2\theta)/9$$

hence:

$$\sigma_{as} = \frac{K}{2k} \cdots Z \cdot 3^{12}/k^{12}(5 - 4\cos 2\theta)^6.$$

Thus we get the remarkable result that the angular distribution of the deuterons becomes independent of the energy of the incoming neutron and is characterized by a half-half width equal to 7°.

The spectrum of the deuteron becomes a sharp line at $8E/9$, E being the energy of the incident neutron.

The excitation given to the nucleus becomes $E/9$, in the form of recoil of the nucleon 2, which if $E/9$ is large enough will be ejected in the forward direction.

The total cross section is proportional to the inverse of the sixth power of the energy of the incident neutron, as in the corresponding case of the capture of an electron by an ion He^+ traversing a gas of H atoms.[11]* The explicit result in our case is:

$$\sigma_{as \cdot T} = 7.7 \times A \times 10^{-25} (100/E_{\text{Mev}})^6 \text{ cm}^2.$$

which is shown in Fig. 6.

It is a pleasure for the author to thank Professor H. A. Bethe who gave him, together with kind encouragement and constant advice, the path followed in working out this problem.

[11] Brinkmann and Kramers, K. Wet. Amst. 33, 973 (1930).

* Note added in proof: see explanation of that analogy given by Levinger and Bethe, Phys. Rev. 78, 115 (1950) in paragraph IV.

The Meson as a Composite Particle*

H. M. MOSELEY AND NATHAN ROSEN
University of North Carolina, Chapel Hill, North Carolina

(Received February 28, 1950)

Calculations are carried out along the lines of the work of Fermi and Yang in which the π-meson is considered as a composite particle formed from a proton and an anti-neutron. On the assumption of a vector interaction it is found that the $^1S_0$ state must be excluded because its energy goes to zero as the interaction goes to zero, while the $^3P_0$ state appears to give an acceptable solution. On the assumption of a tensor interaction it is found that $^1S_0$ and $^3P_0$ solutions both exist, but for opposite signs of the interaction. The tensor interaction must therefore be excluded since it would lead to the formation of a composite particle by a proton and a neutron. Using the vector interaction one finds that the ground state is a $^3P_1$, but that there are other states with $j=0$, 1 and 2 lying near it, the proximity depending on the interaction range assumed.

I. INTRODUCTION

SOME time ago the suggestion was made that particles of spin 0 and 1 are composite, consisting of two particles each of spin $\frac{1}{2}$, closely bound to each other.[1] The method of calculation used was essentially equivalent to that of Kemmer in his attempt at a relativistic treatment of the deuteron.[2] Recently this idea was applied by Fermi and Yang[3] to the case of a π-meson, regarded as a composite particle formed by a nucleon and an anti-nucleon. The present paper is devoted to a further consideration of this problem.

II. GENERAL TREATMENT

For two particles, individually satisfying the Dirac equation and interacting with each other directly, without any intermediary field, the wave equation can be written in the usual notation

$$\{-ihc\boldsymbol{\alpha}_1\cdot\nabla_1+m_1c^2\beta_1-ihc\boldsymbol{\alpha}_2\cdot\nabla_2 +m_2c^2\beta_2+H_{12}\}\psi=W\psi. \quad (1)$$

In order to have relativistic invariance,[2] the interaction term H_{12} must be of the form

$$H_{12}=-\delta(\mathbf{x}_1-\mathbf{x}_2)\textstyle\sum_i b_i\omega_i, \quad (2)$$

where the b_i are constants and

$$\begin{aligned}
&\omega_1=\beta_1\beta_2 && \text{(scalar interaction)},\\
&\omega_2=\tfrac{1}{2}(1-\boldsymbol{\alpha}_1\cdot\boldsymbol{\alpha}_2) && \text{(vector)},\\
&\omega_3=\tfrac{1}{2}\beta_1\beta_2(\boldsymbol{\sigma}_1\cdot\boldsymbol{\sigma}_2+\boldsymbol{\alpha}_1\cdot\boldsymbol{\alpha}_2) && \text{(tensor)},\\
&\omega_4=\tfrac{1}{2}(\boldsymbol{\sigma}_1\cdot\boldsymbol{\sigma}_2-\Gamma_1\Gamma_2) && \text{(pseudovector)},\\
&\omega_5=\beta_1\beta_2\Gamma_1\Gamma_2 && \text{(pseudoscalar)}.
\end{aligned} \quad (3)$$

Here $\boldsymbol{\sigma}$ is the spin vector ($\sigma_x=-i\alpha_x\alpha_y$, etc.) and $\Gamma=-i\alpha_x\alpha_y\alpha_z$.

The wave function ψ in (1) will have 16 components, which can be written ψ_{ij} ($i, j=1, 2, 3, 4$), the subscripts representing spinor indices associated with the two particles. However, in place of these spinor components, one can introduce linear combinations of them which will transform like components of tensors of various ranks. Thus, if one takes the Dirac matrices in the usual form,[4] one can write

$$\begin{aligned}
I&=\tfrac{1}{2}(\psi_{12}-\psi_{21}+\psi_{34}-\psi_{43}),\\
A_1&=\tfrac{1}{2}(-\psi_{13}+\psi_{24}+\psi_{31}-\psi_{42}),\\
A_2&=(i/2)(-\psi_{13}-\psi_{24}+\psi_{31}+\psi_{42}),\\
A_3&=\tfrac{1}{2}(\psi_{14}+\psi_{23}-\psi_{32}-\psi_{41}),\\
A_4&=\tfrac{1}{2}(-\psi_{12}+\psi_{21}+\psi_{34}-\psi_{43}),\\
B_{23}=G_1&=\tfrac{1}{2}(-\psi_{11}+\psi_{22}-\psi_{33}+\psi_{44}),\\
B_{31}=G_2&=(i/2)(-\psi_{11}-\psi_{22}-\psi_{33}-\psi_{44}),\\
B_{12}=G_3&=\tfrac{1}{2}(\psi_{12}+\psi_{21}+\psi_{34}+\psi_{43}),\\
J&=\tfrac{1}{2}(\psi_{14}-\psi_{23}+\psi_{32}-\psi_{41}),\\
U_1&=\tfrac{1}{2}(-\psi_{11}+\psi_{22}+\psi_{33}-\psi_{44}),\\
U_2&=(i/2)(-\psi_{11}-\psi_{22}+\psi_{33}+\psi_{44}),\\
U_3&=\tfrac{1}{2}(\psi_{12}+\psi_{21}-\psi_{34}-\psi_{43}),\\
U_4&=\tfrac{1}{2}(-\psi_{14}+\psi_{23}+\psi_{32}-\psi_{41}),\\
-iB_{41}=F_1&=\tfrac{1}{2}(-\psi_{13}+\psi_{24}-\psi_{31}+\psi_{42}),\\
-iB_{42}=F_2&=(i/2)(-\psi_{13}-\psi_{24}-\psi_{31}-\psi_{42}),\\
-iB_{43}=F_3&=\tfrac{1}{2}(\psi_{14}+\psi_{23}+\psi_{32}+\psi_{41}),
\end{aligned} \quad (4)$$

where I is a scalar, A_μ a four-vector, $B_{\mu\nu}$ an antisymmetric tensor (expressed in terms of two three-vectors $\mathbf{F}$ and $\mathbf{G}$), U_μ a pseudovector, and J a pseudoscalar.

Equation (1) can be rewritten as a set of equations for the above tensor components. It is convenient to introduce, in place of the coordinates $\mathbf{x}_1$ and $\mathbf{x}_2$, new variables $\mathbf{x}=\mathbf{x}_1-\mathbf{x}_2$ and $\mathbf{X}=\frac{1}{2}(\mathbf{x}_1+\mathbf{x}_2)$. However, it is easily seen that the total linear momentum of the system, i.e., the momentum conjugate to $\mathbf{X}$, will be a constant of the motion and by a Lorentz transformation can be made to vanish. In that case, derivatives with respect to components of $\mathbf{X}$ drop out of the equations and the resulting relations can be written as follows:

$$\begin{aligned}
(W+p\Omega)I+2ihc\nabla\cdot\mathbf{F}+2Mc^2A_4&=0,\\
(W-s\Omega)\mathbf{A}+2hc\nabla\times\mathbf{U}-2\mu c^2\mathbf{F}&=0,\\
(W+s\Omega)A_4+2Mc^2I&=0,\\
(W-v\Omega)\mathbf{G}+2ihc\nabla J-2Mc^2\mathbf{U}&=0,\\
(W+v\Omega)\mathbf{F}+2ihc\nabla I-2\mu c^2\mathbf{A}&=0,\\
(W+u\Omega)U_4+2\mu c^2J&=0,\\
(W-\mu\Omega)\mathbf{U}+2hc\nabla\times\mathbf{A}-2Mc^2\mathbf{G}&=0,\\
(W+q\Omega)J+2ihc\nabla\cdot\mathbf{G}+2\mu c^2U_4&=0,
\end{aligned} \quad (5)$$

* Part of this work was done while one of the authors (H.M.M.) held an AEC Predoctoral Fellowship.

[1] N. Rosen, Phys. Rev. **74**, 128(A) (1948). H. M. Moseley, Phys. Rev. **76**, 197(A) (1949). However it should be pointed out that a similar idea, although involving a different point of view, was proposed earlier by L. de Broglie, "Une Nouvelle Théorie de la Lumière" (Hermann, Paris, 1940) and "Théorie Générale des Particules à Spin" (Gauthier-Villars, Paris, 1943).

[2] N. Kemmer, Helv. Phys. Acta **10**, 48 (1937).

[3] E. Fermi and C. N. Yang, Phys. Rev. **76**, 1739 (1949).

[4] W. Pauli, *Handbuch der Physik* **24** (2nd ed.) Part 1, p. 219.

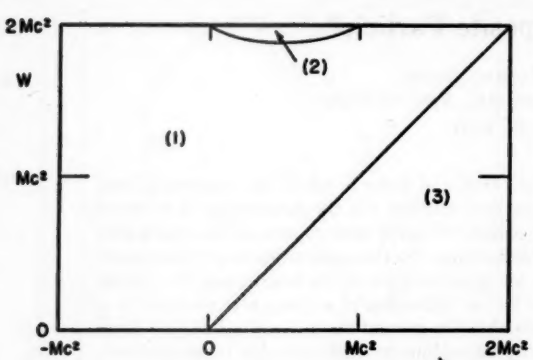

FIG. 1. The (W,b) plane, separated into regions according to the sign of T^2.

where the operator ∇ refers to the relative coordinates $\mathbf{x}$, $M=\frac{1}{2}(m_1+m_2)$, $\mu=\frac{1}{2}(m_1-m_2)$, $\Omega=\delta(\mathbf{x})$ and

$$\begin{aligned} p&=b_1 \quad +2b_2-3b_3-2b_4+b_5,\\ q&=-b_1+2b_2+3b_3-2b_4-b_5,\\ s&=b_1 \quad -b_2 \qquad -b_4 \quad -b_5,\\ u&=-b_1-b_2 \qquad -b_4 \quad +b_5,\\ v&=-b_1 \qquad -b_3 \qquad -b_5. \end{aligned} \tag{6}$$

Now Kemmer found in his deuteron calculation (taking $m_1=m_2$) that if the interaction involves $\delta(\mathbf{x})$, as is required for relativistic invariance, then there are no bound states of finite energy. Fermi and Yang, considering the problem from the standpoint of quantized fields, pointed out that the states of the system involving two particles are mixed with states in which additional particle pairs are formed. On the basis of this fact they were led to take for the effective interaction between a nucleon and an anti-nucleon a range of the order of $\hbar/Mc$, where M is the mass of a nucleon. On the other hand, if one accepts the idea of the existence of a universal length of the order of the classical electron radius as a limit to the accuracy of measurement of position,[5] one is led to a range of this order of magnitude (since it is large compared to $\hbar/Mc$). Hence in place of $\delta(\mathbf{x})$ we shall take hereafter

$$\Omega=\begin{cases}1, & r\leqslant\sigma,\\ 0, & r>\sigma,\end{cases} \tag{7}$$

where r is the inter-particle distance and σ a constant, the range of the interaction. This "square-well" potential is taken for simplicity; it is clear that its use can lead only to very approximate results.

III. THE MESON

As already mentioned, Fermi and Yang[3] assumed that the π-meson was composed of a nucleon and an anti-nucleon of equal rest-mass M. In this case then $\mu=0$ and Eqs. (5) can be transformed by a change of variables into the equations given by Kemmer.[2] Denoting the components of any one of the three-vectors $\mathbf{A}$, $\mathbf{U}$, $\mathbf{F}$, $\mathbf{G}$ by H_1, H_2, H_3 one takes instead

$$\begin{aligned} \mathfrak{C}_1&=-2^{-\frac{1}{2}}(H_1-iH_2), \quad \mathfrak{C}_2=H_3,\\ \mathfrak{C}_3&=2^{-\frac{1}{2}}(H_1+iH_2). \end{aligned} \tag{8}$$

With a suitable change of notation one then gets Kemmer's equations and one can use his method of solution.[6]

At this point is is desirable to make a more specific assumption concerning the nature of the interaction between the particles. Fermi and Yang pointed out that of the five types of interactions in (3), the vector and tensor interactions change sign if the anti-nucleon is replaced by a nucleon, whereas the other interaction terms remain unchanged. Hence, on the assumption that a proton and an anti-neutron form a composite particle, while a proton and neutron do not, they restricted the interaction to the vector and tensor types. While a linear combination of the two is possible, it is natural to take only one of them for simplicity. Fermi and Yang chose the vector interaction. However, the tensor interaction has *a priori* an equal claim. In the present paper both types of interactions will be considered.

Following Fermi and Yang, we shall restrict ourselves to the case $\mu=0$. These authors also restricted their discussion to the case of zero total angular momentum ($j=0$). To permit a ready comparison with their work, the next section deals with the case $j=0$, while the case of a general integral value of j is discussed in the following section.

IV. CASE $j=0$

There are two types of solutions for states with $j=0$. One will be labelled $^1S_0$. In the relativistic case it is a mixture of $^1S_0$ and $^3P_0$, but goes over into $^1S_0$ in the non-relativistic approximation. The other will be labelled $^3P_0$. It is also a mixture of $^3P_0$ and $^1S_0$ in the general case, but goes over in $^3P_0$ in the non-relativistic approximation. These two types of solutions differ in their behaviors under a reflection of coordinates.[2]

For the $^1S_0$ solutions the non-vanishing components are taken in the form:

$$I=f_1(r), \quad A_4=f_2(r), \quad \mathbf{F}=f_3(r)\mathbf{r}/r. \tag{9}$$

One obtains for $r>\sigma$

$$\begin{aligned} f_1&=Br^{-1}\exp(-kr), \quad f_2=-2Mc^2f_1/W,\\ f_3&=(-2i\hbar c/W)df_1/dr, \end{aligned} \tag{10}$$

and for $r<\sigma$

$$\begin{aligned} f_1&=Ar^{-1}\sin Tr, \quad f_2=-2Mc^2f_1/(W+s),\\ f_3&=-2i\hbar c(df_1/dr)/(W+v), \end{aligned} \tag{11}$$

[5] L. de Broglie, Comptes Rendus **200**, 361 (1935); A. March, Naturwiss. **26**, 649 (1938); N. Rosen, Phys. Rev. **72**, 298 (1947).

[6] The more general equations for $\mu\neq0$ and their solutions are discussed by H. M. Moseley, dissertation, University of North Carolina (in preparation).

where

$$k^2=(4M^2c^4-W^2)/4\hbar^2c^2,$$
$$T^2=(W+v)[(W+p)(W+s)-4M^2c^4]/4\hbar^2c^2(W+s), \quad (12)$$

and A, B are constants.

The boundary conditions at $r=\sigma$ determine the energy through the equation

$$T\sigma \operatorname{ctn}(T\sigma)=1-(1+k\sigma)(W+v)/W. \quad (13)$$

For the ${}^3P_0$ case, the non-vanishing components are

$$J=f_4(r), \quad \mathbf{G}=f_5(r)\mathbf{r}/r, \quad \mathbf{U}=f_6(r)\mathbf{r}/r. \quad (14)$$

One finds that, for $r>\sigma$

$$f_4=Br^{-1}\exp(-kr),$$
$$f_5=-2i\hbar cW(df_4/dr)/(W^2-4M^2c^4), \quad (15)$$
$$f_6=2Mc^2f_5/W,$$

while for $r<\sigma$

$$f_4=Ar^{-1}\sin Kr,$$
$$f_5=-2i\hbar c(W-u)(df_4/dr)/[(W-u)(W-v)-4M^2c^4], \quad (16)$$
$$f_6=2Mc^2f_5/(W-u).$$

Here

$$K^2=(W+q)[(W-u)(W-v)-4M^2c^4]/4\hbar^2c^2(W-u), \quad (17)$$

and the energy is determined by the boundary conditions through the equation

$$K\sigma \operatorname{ctn}(K\sigma)=1+(1+k\sigma)W[(W-u)(W-v)-4M^2c^4]/(4M^2c^4-W^2)(W-u). \quad (18)$$

From the preceding relations one can determine the energy for each of the two types of interactions.

(a) *Vector Interaction.* For the ${}^1S_0$ state, if we write b in place of the interaction constant b_2, then the relations (12) and (13) on the basis of (6) can be written

$$(T\sigma)^2=W\sigma^2[(W+2b)(W-b)-4M^2c^4]/4\hbar^2c^2(W-b), \quad (19)$$

$$T\sigma \operatorname{ctn}(T\sigma)=-k\sigma. \quad (20)$$

Let us now consider $(T\sigma)^2$ as a function of W and b, according to Eq. (19). Note that for $W=b$, $(T\sigma)^2=\infty$, and for $(W+2b)(W-b)=4M^2c^4$, $(T\sigma)^2=0$. The curves represented by these two equations divide up the (W, b) plot into three regions, as shown in Fig. 1. In the region marked (1) in this figure, $(T\sigma)^2<0$ so that Eq. (20) has no solution in this region, since $x \operatorname{ctnh} x\geq 1$. In the regions marked (2) and (3), $(T\sigma)^2>0$, so that solutions are possible. But if b is taken to lie in region (2), then $W>4\sqrt{2}Mc^2/3$, so that the energy is too large for the system to represent a π-meson. Hence only the region (3) remains.

Figure 2 shows a plot of the ground-state solution $W_1(b)$ and the solution for the first excited state $W_2(b)$ for values in the region (3) and with the range $\sigma=\hbar/Mc$. The lower curve passes through the point corresponding to the solution given by Fermi and Yang, i.e.,

$$W=Mc^2/6.46, \quad b=53.0Mc^2.$$

However, if we accept the criterion that only those solutions have physical significance for which the energy goes to $2Mc^2$ as the interaction is cut out adiabatically (in this case, as $b\to 0$), we see that no acceptable solution exists in this case. This conclusion is independent of what value one takes for the range σ, as can be seen from the shape of the region (3) in Fig. 1.

Let us now consider the ${}^3P_0$ state. The relations which determine the energy are

$$(K\sigma)^2=(W+2b)[W(W+b)-4M^2c^4]\sigma^2/4\hbar^2c^2(W+b), \quad (21)$$

$$K\sigma \operatorname{ctn}(K\sigma)=1+W[W(W+b)-4M^2c^4](1+k\sigma)/(W+b)(4M^2c^4-W^2). \quad (22)$$

By proceeding as above one finds that all solutions for which $b<0$ are of the type for which $W\to 0$ as $b\to 0$. On the other hand for $b>0$ acceptable solutions exist. Assuming that the ground state represents a π-meson, so that $W=Mc^2/6.46$ one obtains

$$\text{for } \sigma=\hbar/Mc, \quad b=286\,Mc^2, \quad (A)$$

$$\text{for } \sigma=2.8\cdot 10^{-13}\text{ cm}=a_0, \quad b=2.71\,Mc^2. \quad (B)$$

(b) *Tensor Interaction.* For the ${}^1S_0$ state, the conditions determining the energy are

$$(T\sigma)^2=(W-b_3)[W(W-3b_3)-4M^2c^4]\sigma^2/4\hbar^2c^2W, \quad (23)$$

$$T\sigma \operatorname{ctn}(T\sigma)=1-(W-b_3)(1+k\sigma)/W. \quad (24)$$

It is found that acceptable solutions exist only for $b_3<0$. For example, to get a ground-state energy corresponding to the mass of a π-meson one finds

$$\text{for } \sigma=\hbar/Mc, \quad b_3=-9.86Mc^2, \quad (C)$$
$$\text{for } \sigma=a_0, \quad b_3=-8.57Mc^2. \quad (D)$$

Finally, for the ${}^3P_0$ state the equations determining the energy are

$$(K\sigma)^2=(W+3b_3)[W(W+b_3)-4M^2c^4]\sigma^2/4\hbar^2c^2W, \quad (25)$$

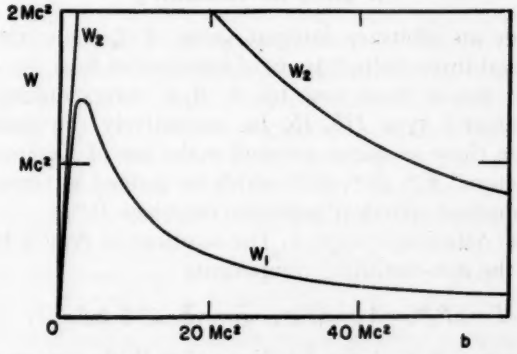

FIG. 2. The energies of the two lowest states of the ${}^1S_0$ type as functions of the interaction parameter b.

TABLE I. Energies of lowest states of various types.

State	W/Mc^2 $\sigma=\hbar/Mc$	W/Mc^2 $\sigma=2.8\times10^{-13}$ cm
$^3P_1$	0.1548	0.1548
$^3D_2$	0.166	0.15487
$^3P_0$	1.350	0.162
$^3S_1+^3D_1$	0.165	0.15486
$^3P_2+^3F_2$	0.180	0.15494

$$K\sigma\ \mathrm{ctn}(K\sigma)=1+[W(W+b_3)-4M^2c^4](1+k\sigma)/(4M^2c^4-W^2). \quad (26)$$

In this case acceptable solutions exist only for $b_3>0$, and to get the π-meson energy one finds

$$\text{for } \sigma=\hbar/Mc, \quad b_3=26.7Mc^2, \quad (E)$$
$$\text{for } \sigma=a_0, \quad b_3=25.7Mc^2. \quad (F)$$

The preceding results indicate that it is necessary to discard the tensor interaction. Since it has been found that bound states exist for both signs of b_3 it follows that if a proton and an anti-neutron form a composite particle, then a proton and a neutron will do likewise, in general. For example, if one accepts the solution (C) above for the $^1S_0$ state as describing a π-meson, then with a change in the sign of b_3 (corresponding to a change from an anti-neutron to a neutron) one can obtain a solution for the $^3P_0$ state. This is found to have an energy of $0.509Mc^2$. Similarly, if one accepts the solution (E) for the $^3P_0$ state, then changing the sign of b_3 leads to a solution for the $^1S_0$ state corresponding to a smaller mass than that of the π-meson. To avoid such neutron-proton systems one must discard the tensor type of interaction.

We see then that Fermi and Yang were justified in adopting the vector rather than the tensor interaction. However, it appears that one should take the $^3P_0$ solution rather than the $^1S_0$, as long as one restricts himself to states with $j=0$.

The question arises as to whether, for a given value of the interaction parameter, there may not be states with j different from zero lying below the ones considered previously. This is investigated in the next section.

V. CASE OF HIGHER j

For an arbitrary integral value of j, there are in general three distinct types of solutions of Eqs. (5). We shall denote them here by A, B, C corresponding to Kemmer's[2] type IIb, Ib, Ia, respectively. To characterize these solutions we shall make use of Kemmer's[2] "vectors" $\mathfrak{X}_j^m$, $\mathfrak{Y}_j^m$, $\mathfrak{Z}_j^m$, which he defined in terms of normalized spherical harmonic functions P_j^m.

(a) *Solutions of type A*. The solutions of type A have for the non-vanishing components

$$I=\alpha P_j^m, \quad A_4=\beta P_j^m, \quad \mathfrak{F}=\gamma\mathfrak{X}_{j-1}^m+\Delta\mathfrak{Z}_{j+1}^m, \quad (27)$$

where α, β, γ, Δ are functions of r. With respect to a reflection of coordinates through the origin the solution has a parity of $(-1)^j$. The $^1S_0$ solution found above is a special case of this type. It is found that, as in the $^1S_0$ case, the energy in general tends to zero rather than $2Mc^2$ as $b\to0$. Hence this type of solution will be discarded.

(b) *Solutions of type B*. The solutions of this type have for the non-vanishing components

$$\mathbf{A}=\epsilon\mathfrak{X}_{j-1}^m+\eta\mathfrak{Z}_{j+1}^m, \quad \mathbf{G}=\lambda\mathfrak{Y}_j^m, \quad \mathbf{U}=\zeta\mathfrak{Y}_j^m, \quad (28)$$

where ϵ, η, λ, and ζ are functions of r. Substituting into (5) enables one to express ϵ, η and λ in terms of ζ which satisfies the equations

$$\frac{d^2\zeta}{dr^2}+\frac{2}{r}\frac{d\zeta}{dr}+\left[k^2-\frac{j(j+1)}{r^2}\right]\zeta=0, \quad r>\sigma,$$
$$\frac{d^2\zeta}{dr^2}+\frac{2}{r}\frac{d\zeta}{dr}+\left[N^2-\frac{j(j+1)}{r^2}\right]\zeta=0, \quad r<\sigma, \quad (29)$$

where

$$N^2=(W+b)[W(W+b)-4M^2c^4]/4\hbar^2c^2W. \quad (30)$$

One can show that at $r=\sigma$, where the interaction has a discontinuity, ζ and $(W+b\Omega)^{-1}(d\zeta/dr+\zeta/r)$ must be continuous. The solutions of this type have a parity $(-)^j$ with respect to a reflection through the origin.

No solution of type B exists for $j=0$. For $j=1$, one gets solutions which will be denoted by $^3P_1$, but which in the relativistic case include also some $^3S_1$ and $^3D_1$. For these solutions one takes

$$\zeta=Ar^{-2}(Nr\cos Nr-\sin Nr), \quad r<\sigma,$$
$$\zeta=Br^{-2}(1+kr)\exp(-kr), \quad r>\sigma. \quad (31)$$

The boundary conditions at $r=\sigma$ give the relation which determines the energy,

$$N\sigma\ \mathrm{ctn}(N\sigma)=1+(N\sigma)^2(1+k\sigma)/[k^2\sigma^2+(b/W)(1+k\sigma+k^2\sigma^2)]. \quad (32)$$

A calculation shows that for the values of b determined in the previous section the lowest $^3P_1$ level lies below the $^3P_0$ level. Hence it is necessary to modify the interaction constant b so as to make the energy of the lowest $^3P_1$ state correspond to the mass of the π-meson ($0.1548Mc^2$). One finds that

$$\text{for } \sigma=\hbar/Mc, \quad b=28.3Mc^2,$$
$$\text{for } \sigma=a_0, \quad b=25.7Mc^2.$$

It follows then that the energy of the $^3P_0$ state in the first case is $1.350Mc^2$ and in the second case $0.162Mc^2$. There will also be a number of excited $^3P_1$ states, the first one in the first case ($\sigma=\hbar/Mc$) having an energy of $0.196Mc^2$.

In the case of $j=2$, one gets solutions labelled $^3D_2$. For the values of b chosen above one gets as the energy of the lowest state of this type for

$$\sigma=\hbar/Mc, \quad W=0.166Mc^2,$$
$$\sigma=a_0, \quad W=0.1549\,Mc^2.$$

(c) *Solutions of type C.* The solutions of this type have as non-vanishing components

$$J=\alpha P_j^m, \quad \mathsf{A}=\zeta \mathcal{Y}_j^m,$$
$$\mathsf{G}=\gamma \mathfrak{X}_{j-1}^m+\Delta \mathfrak{Z}_{j+1}, \quad \mathsf{U}=\epsilon \mathfrak{X}_{j-1}^m+\eta \mathfrak{Z}_{j+1}^m, \tag{33}$$

where α, ζ, γ, Δ, ϵ, and η are functions of r. This type of solution has a parity $(-1)^{j+1}$ under a reflection through the origin.

In the case $j=0$ the equations are fairly simple and one obtains the ${}^3P_0$ solution discussed in the preceding section. For larger values of j the equations, and also the boundary conditions giving the energy, are somewhat complicated and will therefore not be given here.[7]

For $j=1$ the solution is a mixture of ${}^3S_1$ and ${}^3D_1$ (with small amounts of ${}^3P_1$ and ${}^1P_1$, the proportions of these increasing as one goes to higher excited states). The lowest state of this type has an energy

$$\text{for } \sigma=\hbar/Mc, \quad W=0.165Mc^2,$$
$$\text{for } \sigma=a_0, \quad W=0.15486Mc^2,$$

where the value has been written with excessive precision to show its relation to the energy of the ground state. For $j=2$ the solution is largely a mixture of ${}^3P_2$ and ${}^3F_2$. The lowest state of this type has energy values $0.180Mc^2$ and $0.15494Mc^2$ for the above ranges, respectively. The preceding results are summarized in Table I.

In conclusion it should be emphasized that the numerical values for the energy levels are not significant because of the approximation introduced by the use of the square-well interaction. However, it is interesting that there are a number of different states lying close to the ground state with angular momenta 0, 1, and 2. These would be interpreted as particles with nearly equal masses and spins 0, 1, and 2. Further measurements and analysis of data on π-mesons should show whether variations in mass and spin actually occur.

[7] These will be found, in different notation, in reference 2. However, in Eq. (21b) of that paper there appears to be an error of sign in the third term of each of the two factors on the left-hand side.

PHYSICAL REVIEW VOLUME 80, NUMBER 2 OCTOBER 15, 1950

The Emission of Long-Range Charged Particles in the Slow Neutron Fission of Heavy Nuclei

K. W. ALLEN AND J. T. DEWAN
Atomic Energy Project, National Research Council of Canada, Chalk River, Ontario, Canada

(Received June 28, 1950)

Light charged particles with ranges greater than 6 cm of air produced in the slow neutron fission of U^{233}, U^{235}, and Pu^{239} have been studied in detail by coincidence counting methods. In each case particles with a continuous range distribution extending to about 50 cm of air were observed, the distribution showing a broad maximum in the neighborhood of 20 cm. Direct measurement of the energies of the light particles from U^{235} showed a fairly symmetrical distribution about 15 Mev with a maximum energy of about 26 Mev. Comparison of the energy and range distributions shows that all the long-range particles are α-particles. The frequency of emission of these α-particles was found to be

1 in 405±30 fissions for U^{233},
1 in 505±50 fissions for U^{235}, 1 in 445±35 fissions for Pu^{239}.

No protons were observed, although the apparatus would have detected any with ranges lying between 10 and 100 cm of air. The energy distribution of fission fragments coincident with long-range α-particles was also measured. The usual two peaks were observed indicating asymmetric division of mass, but each peak was shifted to a lower energy than is observed in binary fission. Quantitative comparison of the energies involved showed that, on the average, the total kinetic energy carried away in fission accompanied by α-emission is about equal to that liberated in binary fission. Possible explanations for α-emission in fission are discussed.

I. INTRODUCTION

THE occasional emission of light charged particles in the fission of uranium by slow neutrons seems to have been noticed first by Alvarez.[1] Subsequent investigations in several laboratories using coincidence counting techniques and uranium-loaded photographic emulsions have confirmed and extended the original observations. Farwell, Segrè, and Wiegand,[2] using a coincidence arrangement, reported that light particles with ranges up to 23 cm of air are produced in about 0.4 percent of fission events in U^{235} and in 0.2 percent of fissions in Pu^{239} by slow neutrons. By comparison of the ionization of the light particles with that of α-particles from polonium it was shown that they were probably α-particles, a conclusion in accord with the majority of measurements of grain density in photographic emulsions.[3–7] On the other hand, the work of Tsien and his associates[8] suggests that not all the light

[1] L. W. Alvarez, mentioned in reference 2. Earliest publications in the open literature are by Green and Livesey, Proc. Int. Conf., Cambridge, July, 1946, and Tsien, Chastel, Ho, and Vigneron, Comptes Rendus 223, 986 (1946).

[2] Farwell, Segrè, and Wiegand, Phys. Rev. 71, 327 (1947).

[3] P. Demers, Phys. Rev. 70, 974 (1946).

[4] Wollan, Moak, and Sawyer, Phys. Rev. 72, 447 (1947).

[5] L. L. Green and D. L. Livesey, Phil. Trans. A 241, 323 (1948).

[6] L. Marshall, Phys. Rev. 75, 1339 (1949).

[7] E. W. Titterton (unpublished). We are grateful to Dr. Titterton for communicating to us some of his results prior to publication.

[8] Tsien, Ho, Chastel, and Vigneron, J. de phys. et rad. 8, 165, 200 (1947).

particles are α-particles, but that some have masses as great as 9. In addition to the long-range particles, Cassels, Dainty, Feather, and Green[9] discovered the existence of a more abundant group of particles with ranges of about one cm of air accompanying the fission of uranium by slow neutrons. The observed frequency of emission of the short-range particles was about 1 in 25 fissions, assuming that they were emitted isotropically with respect to the direction of fission fragments. Subsequent angular distribution data indicate that this figure should be reduced to about 1 in 90 fission events.[5] Evidence for the emission of long-range particles in the photo-fission of uranium and thorium has recently been obtained by Titterton and Goward[10] and Titterton and Brinkley.[11]

A detailed investigation of light charged particles of all ranges emitted in the fission of U^{235} by slow neutrons has been made by Green and Livesey[5] and by Tsien, Ho, Chastel, and Vigneron.[8] These investigators observed fission events produced by slow neutrons in uranium-loaded photographic emulsions. It was found that both long-range and short-range particles are emitted preferentially at angles near 90° to the fission tracks, being slightly inclined towards the lighter fragment. The spread in angle of emission relative to the fission fragments is greater for the short-range particles than for the long-range particles,[12] although long-range particles are occasionally emitted at quite acute angles.[7] Only short-range particles have been observed in the fission of uranium and thorium by fast neutrons.[5,13]

The coincidence experiments of Farwell *et al.* and Cassels *et al.* show that the light particles are emitted within a time interval less than about 10^{-5} second of the instant of fission. Using a modified photographic plate in which the fissionable material was contained in a very thin film between two layers of emulsion, Demers[3] was able to show that the light particles are emitted within an interval less than 2×10^{-14} second after the fission has occurred. This result is consistent with the angular distribution observed, which suggests that the light particle is accelerated in the Coulomb field of the major fragments and must therefore be emitted within an interval not greater than about 10^{-21} second.

The relatively infrequent emission of light charged particles in fission makes the study of the process by the photographic plate method rather tedious if good statistical accuracy is to be obtained. Furthermore, owing to the desensitizing action on the emulsion of the uranyl ion, any energetic singly charged particles which may be produced in fission are unlikely to be observed. The use of the photographic plate method in the study of light charged particle emission in U^{233} or Pu^{239} is not practicable owing to fogging produced by the intense natural α-particle activity. For these reasons, coincidence counting methods were chosen for the experiments to be described. These experiments fall into four groups.

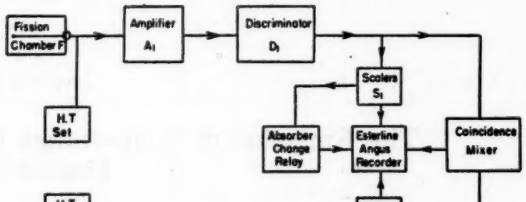

FIG. 2. Block diagram of electronic equipment for range measurements.

(1) Measurement of the range distributions of the long-range particles emitted in the fission of U^{233}, U^{235}, and Pu^{239} by pile neutrons.

(2) Search for singly charged particles and determination of the frequency of emission of the light particles in the fission of U^{233}, U^{235}, and Pu^{239} by pile neutrons.

(3) Measurement of the energy distribution of the light particles emitted in the fission of U^{235} by thermal neutrons.

(4) Measurement of the energy distribution of the major fragments coincident with long-range particle emission.

A brief account of part of this work has already been given.[14] A subsequent paper, now in preparation, will discuss in detail the short-range particles emitted in fission.[15]

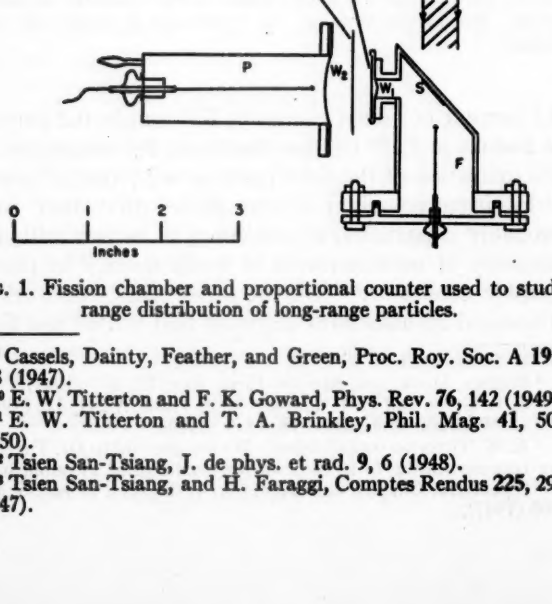

FIG. 1. Fission chamber and proportional counter used to study range distribution of long-range particles.

II. RANGE MEASUREMENTS

The range distribution of the light charged particles was studied by means of the apparatus shown in Fig. 1. A source of fissionable material S (U^{233}, U^{235}, or Pu^{239}), deposited on a platinum foil, was mounted in the fission

[9] Cassels, Dainty, Feather, and Green, Proc. Roy. Soc. A **191**, 428 (1947).
[10] E. W. Titterton and F. K. Goward, Phys. Rev. **76**, 142 (1949).
[11] E. W. Titterton and T. A. Brinkley, Phil. Mag. **41**, 500 (1950).
[12] Tsien San-Tsiang, J. de phys. et rad. **9**, 6 (1948).
[13] Tsien San-Tsiang, and H. Faraggi, Comptes Rendus **225**, 294 (1947).
[14] K. W. Allen and J. T. Dewan, Phys. Rev. **75**, 337 (A) (1949).
[15] J. T. Dewan and K. W. Allen, Phys. Rev. **76**, 181 (A) (1949).

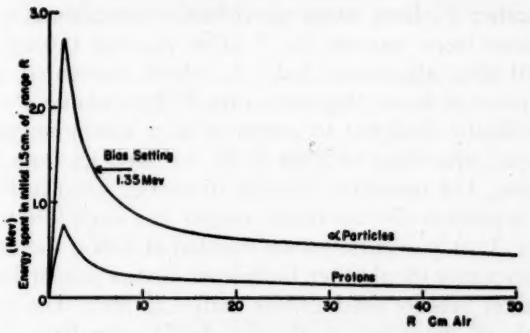

FIG. 3. *Calculated* energy spent in the proportional counter by protons and α-particles of initial range R.

chamber F and irradiated in a well-collimated beam of neutrons from an experimental hole of the Chalk River heavy water pile. A fraction of the long-range particles produced in the fission process was able to emerge through the mica window W_1 and pass into an end-window proportional counter P through a second mica window W_2. Aluminum absorbers A and B could be placed in the path of the light particles. Both the fission chamber and proportional counter were filled with a gas mixture consisting of 90 percent argon and 10 percent carbon dioxide to a pressure of 30 cm of mercury. This mixture resulted in very stable operation and in the production of pulses with rise times of 0.3 μsec. in both counters. In general, the proportional counter was operated with a gas multiplication of about 10.

The discriminator bias in the fission amplifier was set just above the level of the natural α-particles from the source; under these conditions all the fission fragments emerging from the source were counted, regardless of their directions of emission in the hemisphere. Thus there was, on the average, no angular correlation between fission fragments counted in F and long-range particles counted in P. Fission rates in excess of 10^6 counts per minute were generally employed.

A schematic diagram of the electronic equipment is shown in Fig. 2. Pulses from the fission chamber and proportional counter were amplified by similar systems each with a rise time of 0.2 μsec. The amplified pulses, after passing through pulse-height discriminators D_1 and D_2 were fed into a Rossi-type coincidence mixer with a resolving time of 0.56 μsec. Coincident pulses from the mixer were recorded on an Esterline-Angus pen recorder which also marked, after suitable scaling down, the numbers of fission pulses and proportional counter pulses. The final fission scaling unit contained a relay which controlled the position of a gravity-operated toothed wheel upon which were mounted fifteen aluminum absorbers B. In this way the absorber B could be changed automatically after a desired number of fissions, usually 256×10^6, the exact instant of change being indicated on the recording chart by a shift in the baseline. This method of recording had several advantages.

(a) All information was recorded on a single chart.

(b) A time scale was provided by the speed of the chart, which was quite constant, so that the time distribution of the pulses could be observed. Since the pile power was held steady to 0.1 percent, this served as a check on the stability of the counters as well as on the random distribution of the coincidences.

(c) The apparatus was self-recording, and could be operated without attention for long periods.

The fifteen absorbers B included four "infinitely thick" brass disks to stop all long-range particles and hence allow a direct determination of the background coincidence rate. The background obtained in this way agreed with that calculated from individual counting rates and the known resolving time of the coincidence mixer. It was generally less than 10 percent of the true coincidence rate. The aluminum absorbers B were spaced at intervals of about 3 mg/cm^2. Master aluminum absorbers, A, could also be inserted in the path of the particles thus enabling any desired portion of the range distribution to be studied in detail.

The effective length of the counter P, which was calibrated by a source of α-particles of known energy, was 1.5 cm of air. In Fig. 3, the *calculated* amount of energy spent in the counter by protons and α-particles of initial range R is plotted as ordinate against R as abscissa. Thus by suitable bias settings it was possible to distinguish between protons, α-particles, and heavier particles. Preliminary experiments with a source of uranium enriched in U^{235} showed that coincidences were observed only for absorber paths less than about 50 cm of air and for bias settings less than 2.7 Mev. This suggested that at least some of the long-range particles were α-particles with ranges up to 50 cm of air. No evidence was obtained for the existence of more heavily ionizing particles.

A detailed study of the range distribution of the particles was made with a bias setting equivalent to 1.35 Mev; at this setting, only α-particles with residual range on entering the counter lying between 0.75 cm and 4.75 cm were detected (Fig. 3). We may therefore say that the resolving power of the counter for α-particles was 4.0 cm. Furthermore, no singly charged particles could possibly be detected at this bias setting.

The range distribution obtained from a source of U^{235} is shown in Fig. 4. Corrections have been made for the

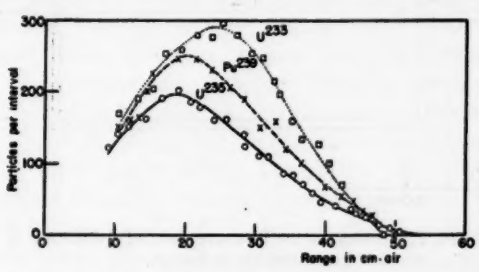

FIG. 4. Range distributions of long-range α-particles emitted in fission.

variation with α-particle energy of the stopping power of aluminum.[16] The total abundance of α-particles per fission was obtained by dividing the area under the curve by the resolving power of 4.0 cm and taking account of the solid angle of detection. This abundance, which was found to be approximately equal to that determined by setting the counter at low bias and detecting all particles passing through it in coincidence with fissions, was 1 in 600±80 fission events in U^{235}. Similar experiments were carried out with sources of U^{233} and Pu^{239}; the range distributions obtained are also shown in Fig. 4. In general, the curves for the three fissionable materials are similar in shape. Small differences are apparent in the positions of the peaks of the distributions and in the maximum ranges, which correspond to α-particles of about 25 Mev. The α-particle abundances were found to be 1 in 470±50 fissions of Pu^{239} and 1 in 370±50 fissions of U^{233} by pile neutrons. Since the abundances obtained by integration of the range distribution curves were equal to those obtained from the coincidence rates at very low bias settings, it seems unlikely that protons are produced in fission. However, protons, if produced in a manner analogous to the α-particles, might be expected to possess considerable energy and hence low specific ionization, so that they would have been difficult to detect in the experimental arrangement used. Further experiments were therefore undertaken to search for protons, and to obtain more accurate data on the frequency of emission of the α-particles.

III. ABUNDANCE MEASUREMENTS

The apparatus used for the abundance measurements is shown in Fig. 5. It consisted of a small fission chamber F placed over a large proportional counter P, the whole volume being filled with a 10:1 argon-carbon dioxide mixture to a pressure of one atmosphere. All fissions occurring in the thin source S were counted in the chamber F. Long-range particles in coincidence with fissions were counted in P after passage through a 0.001-inch aluminum foil, A, which prevented the entrance of fission fragments into P. The counter P was specifically designed to ensure a large minimum path length, equivalent to 3 cm of air, for particles from the source. The minimum amount of energy spent in P by an α-particle (50 cm initial range) was therefore 0.75 Mev. If only α-particles are emitted in fission the coincidence rate should then be independent of proportional counter bias for settings less than 0.75 Mev. The solid angle of detection in P, *viz.*, $4\pi/91$ steradians, was obtained by calculation and by counting α-particles from a U^{233} source of known strength placed at S, the two values agreeing within 1 percent. The standard source was also used to calibrate the discriminator bias in terms of energy released in the counter P. In order to ensure that no coincidences were lost because of too short a resolving time, a curve of coincidence rate *versus* resolving time was obtained (Fig. 6), and a conservative value of 1.25 μsec. chosen for subsequent measurements.

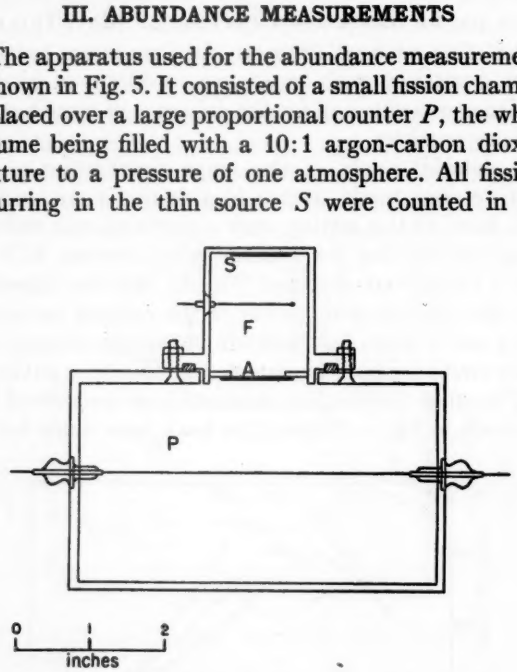

FIG. 5. Apparatus for measurement of frequency of α-emission in fission.

The integral abundance curves obtained for the three fissionable materials were very similar in nature, a typical one being shown in Fig. 7. There is no evidence for the emission of protons in fission as any significant number with ranges between 10 and 100 cm of air would have been indicated by a distinct rise in the curve below 0.75 Mev. Extrapolation of the bias curves leads to the following frequencies for α-emission in fission (after a correction has been made for those α-particles which are stopped in the aluminum foil):

U^{233}	1 in 405±30
U^{235}	1 in 505±50
Pu^{239}	1 in 445±35.

IV. ENERGY DISTRIBUTION OF LONG-RANGE PARTICLES

The experiments described above suggest that all of the energetic light particles emitted in fission are α-particles. This information is derived from specific ionization measurements which, however, are not sufficiently accurate to eliminate the possibility that at least some of the particles may be He^3, He^6, Li^6, etc. Furthermore, specific ionization measurements are particularly difficult to make and interpret in this case because of the wide spread in particle ranges.

If it is assumed that all of the particles are α-particles, then their energy distributions may be predicted uniquely from the range distributions shown in Fig. 4. We have therefore made a direct measurement of the energy distribution of the particles emitted in U^{235} fission for comparison with the predicted curve. This experiment utilized a back-to-back double ionization chamber, shown in Fig. 8, filled with argon at sufficiently high pressure to stop all the long-range particles in the sensitive region. The source S consisted of about 2.5 mg

[16] M. S. Livingston and H. A. Bethe, Rev. Mod. Phys. 9, 276 (1937).

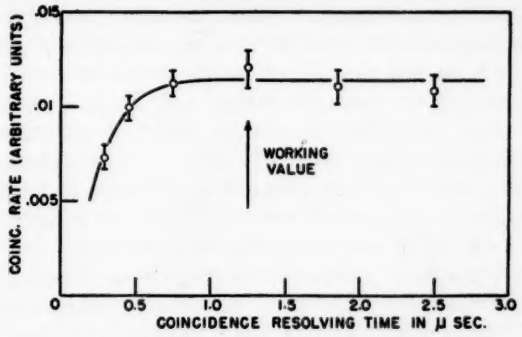

FIG. 6. Coincidence rate *versus* resolving time.

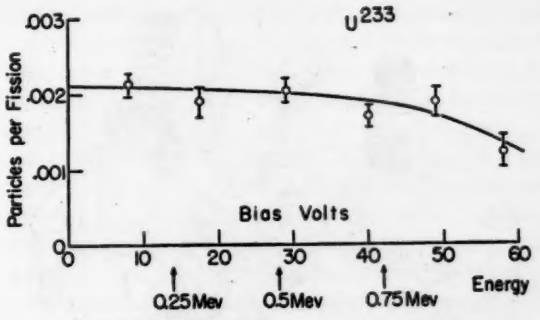

FIG. 7. Frequency of α-emission in fission of U^{233}.

of uranium oxide enriched in U^{235} deposited electrolytically on a 6 mg/cm^2 aluminum foil over a circular area 4 cm in diameter. It was mounted on the central electrode of the double chamber with the active material facing the fission chamber F. The aluminum foil was just thick enough to prevent fission fragments and natural α-particles from entering the chamber P. The long-range particles were collimated so that only those emitted at angles less than 45° to the axis of symmetry were able to enter the chamber. The product of collimator transmission and solid angle of detection was 1/92 of a sphere. The fission fragments were not collimated. The main body of the chamber was constructed from a 5-inch steel cylinder with $\frac{1}{4}$-inch walls, electrode assemblies being mounted on the two end plates for ease of access. A well-defined neutron beam passed axially through the chamber, entering and leaving through $\frac{1}{8}$-inch aluminum windows. Both fission chamber F and α-chamber P contained Frisch grids G_1 and G_2 designed to be about 96 percent efficient in shielding the electron collectors C_1 and C_2 from positive ion effects.[17] The plate-to-grid separation in chamber P was equivalent to 60 cm of air at a pressure of 10 atmos. of argon, so that all long-range particles were stopped in this region. For test purposes, a thin source of U^{233} was mounted in place of the source S, facing the chamber P. Studies of saturation and pulse rise time in the plate-grid region were carried out by connecting a fast amplifier to the grid G_2. With the chamber containing tank argon of 99.96 percent purity at a pressure of 10 atmos., saturation was achieved with a field of about 50 volts/cm. However the pulse rise time, which was about 25 μsec. even with a field strength as high as 500 volts/cm, was much too long for coincidence work. It was found that addition of 0.08 percent of CO_2 reduced this rise time to about 3 μsec., although saturation was then obtained only at fields greater than 250 volts/cm. The energy distribution of α-particles from the U^{233} source, obtained at a pressure of 0.6 atmos. and with electron collection at C_2, is shown in Fig. 9. At this pressure, the range of the α-particles is about the same as that of the most energetic long-range particles at a pressure of 10 atmos. The half-width of the α-particle distribution shows that the resolution of the chamber is about 5 percent. At higher pressures, the distribution was slightly broader, but the broadening could be accounted for by energy loss in the collimator.

The test source was removed and the fissile source S was inserted. In addition a very low activity Pu^{239} α-particle source was attached to the central electrode on the long-range particle side for energy calibration purposes. The source S was then irradiated in a beam of neutrons, and coincidences were sought between long-range particles and fission fragments. With the maximum neutron intensity, a large background of small pulses in the chamber P was encountered due to the effects of γ-rays and fast neutrons. This was an intrinsic difficulty of the experiment, since the extensive path length required to stop long-range particles in the chamber gas necessarily resulted in production of large pulses from the background ionization. Considerable reduction in the background was, however, effected by utilizing a neutron beam from the thermal column of the pile instead of one from an experimental hole. The effect was further minimized by working at low levels of intensity, and to this end a special circuit was developed for recording directly the sizes of individual α-particle pulses coincident with fission fragments. Thus good statistics were obtained with much lower counting rates than would otherwise have been possible. Only a brief account of the electronic arrangements (Fig. 10) will be given here as a detailed description is to be published elsewhere.

Amplified pulses from the chamber P were fed into a coincidence gating circuit. Those pulses coincident with a fission pulse passed through the gate unchanged; those not coincident with fissions were suppressed. Pulses passing through the gate were then lengthened in a two-stage peak voltmeter circuit and recorded on the chart of an Esterline-Angus recorder. The amplitude of the pulse finally written on the chart was proportional to the input pulse within 2 percent. The chart was calibrated in energy by means of α-pulses from the Pu source in the chamber P. Proper operation of the circuit required that there be no delay in the pulse triggering the gate; hence fission pulses were taken from the grid G_1 rather than from the collector C_1, the resulting loss

[17] Bunemann, Cranshaw, and Harvey, Can. J. Research A 27, 191 (1949).

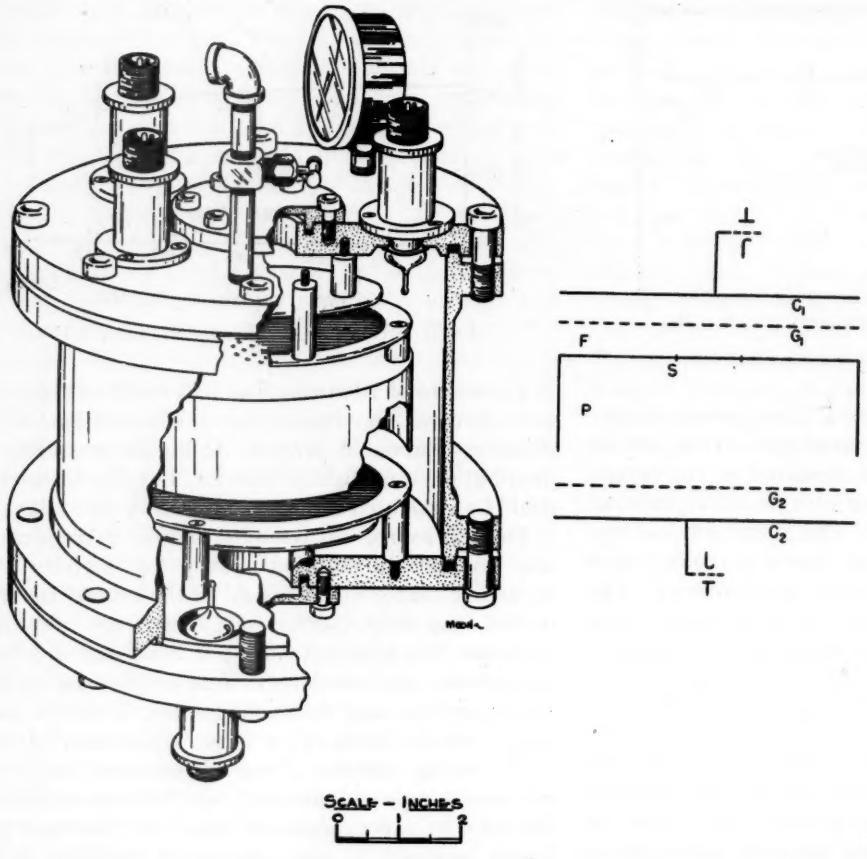

FIG. 8. High pressure double ionization chamber for energy measurements.

of amplitude due to positive ion effects being of no importance. Complete saturation of the fission pulses was also immaterial but care was taken to ensure that the α-pulses were saturated, the field in the region $S-G_2$ being about 400 volts/cm with a pressure of 10 atmos. The energy distribution of the long-range particles is plotted in Fig. 11. This curve was obtained from the analysis of 2000 pulses recorded in 87 hours. A very small correction for chance coincidences was made by substitution of artificial pulses for fission pulses and normalization to identical counting rates. This correction had the effect of reducing slightly the number of small coincident pulses recorded. The shape of the distribution, after correcting for spread due to background ionization, is shown by the solid line in Fig. 11. This correction, of the order of 5 percent, was estimated by feeding artificial pulses of constant amplitude into the α-particle amplifier system along with the background pulses from the chamber P and observing the spread in size of the artificial output pulses. The dotted curve, obtained by correcting the solid curve to allow for the energy spent in the aluminum source backing, is the final energy distribution of the fission α-particles. The points associated with the dotted curve are those predicted from the range measurements (Fig. 4) on the assumption that all the particles are α-particles. Agreement is good, verifying that all the long-range particles are indeed α-particles. The abundance was found to be 1 in 550 ± 30 fissions of U^{235}, in good agreement with that obtained from range experiments.

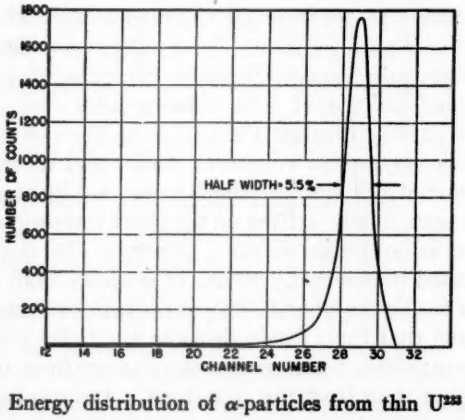

FIG. 9. Energy distribution of α-particles from thin U^{233} source.

V. ENERGY DISTRIBUTION OF FISSION FRAGMENTS COINCIDENT WITH LONG-RANGE α-PARTICLES

In principle, the method used to obtain the energy distribution of the long-range α-particles can be used to determine the energy distribution of the major fission fragments coincident with these α-particles. In this case the triggering pulses are supplied by the long-range α-particles, the sizes of coincident fission pulses being recorded on the Esterline-Angus chart. In practice, however, some changes were necessary.

(a) Owing to the extremely high electric field, of the order of 450 volts per cm *per atmosphere*, required to saturate the fission pulses in the mixture of $A+0.08$ percent CO_2, it was found necessary to reduce the pressure to 5 atmos. to obtain saturation with the maximum field available. At this pressure only about the first 30 cm of range of a very energetic fission α-particles was contained in the sensitive region of chamber P so that these particles produced smaller pulses than they would have done at 10 atmos. pressure. These smaller pulses, however, were still well above the threshold of detection.

(b) It was not feasible to collimate the fission fragments in an attempt to get better resolution for two reasons. Firstly, at 5 atmos. pressure the fission fragment tracks were so short that energy losses in the collimator itself introduced considerable straggling. Secondly, due to Coulomb repulsion, the fission α-particle is emitted preferentially in the same hemisphere as the light fragment; thus when collimation is used the heavier fragment is observed much more frequently in coincidence with an α-particle than is the lighter. This effect was encountered in the initial measurements and necessitated the removal of the collimator.

(c) Because a long-range α-particle may traverse P very obliquely when one of the major fragments proceeds directly across F, the triggering pulse may be delayed by as much as 2.5 μsec. with respect to the corresponding fission pulse. As the fission pulses decayed

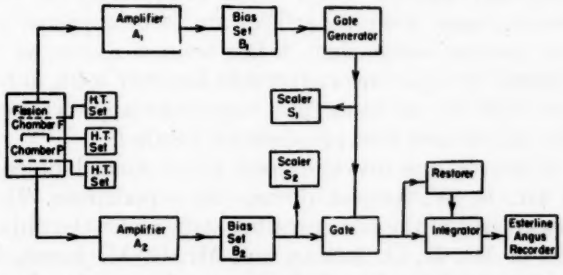

FIG. 10. Block diagram of electronic recording system used in energy measurements.

with a time constant of about 10 μsec. (necessary to minimize background effects and chance coincidences) the delay could result in some loss of amplitude of the fission fragment pulse in passing through the coincidence gate. In order to eliminate this effect the fission pulses, before passing into the coincidence gate, were shaped into flat-topped pulses of the proper amplitude and 15 μsec. duration. A direct measurement then showed that the loss in amplitude for triggering delays of 3 μsec. was less than 0.5 percent.

The method of the experiment was as follows. A very thin source of natural uranium, 0.02 mg/cm^2 in thickness, deposited uniformly on 0.001-inch aluminum foil, was placed over a hole in the common cathode facing the fission chamber F, and the energy distribution of fission fragments resulting from slow neutron bombardment was studied with a 30-channel pulse analyzer. When the electric field was high enough to saturate the pulses, the shape of the distribution was similar to that obtained by others under more nearly ideal conditions, although the resolution was not quite as good. By direct comparison with natural α-particles, the peak energies were found to be 58 and 92 Mev in good agreement with other work.[18] The normal fission fragment distribution was also obtained with fission pulses being recorded on the Esterline-Angus chart. This was done at a low neutron intensity giving about 15 fissions/min. The shape of the distribution was the same as that obtained with the pulse analyzer at the rate of 1000 fissions/min. The gating circuit was then brought into operation, and the sizes of fission pulses coincident with long-range α-particles were recorded. A series of runs was made over a period of five days, normal distributions being taken between triggered runs to check the constancy of the calibration. The final results are shown in Fig. 12, a total of about 1200 pulses being recorded for each distribution. The high energy peak is shifted by 10.5 Mev and the low energy peak by 8 Mev. The reduced amplitude of the high energy peak is due to the angular distribution effect mentioned above.

It is estimated that the triggering α-particles had a mean energy of about 15 Mev. Thus the average total energy released in fission accompanied by α-emission is $50+81.5+15=146.5$ Mev. This is to be compared with the average kinetic energy of the fragments in binary fission, *viz.*, $92+58=150$ Mev.

VI. DISCUSSION

The experimental results presented above show that the long-range particles emitted in the fission of U^{235} by slow neutrons are α-particles. The frequency of the process *viz.* 1 in 505 ± 50 fissions by pile neutrons and in 550 ± 30 fissions by thermal neutrons is rather less than that obtained by most other workers (about 1 in 300 fissions). The reason for the disagreement with earlier work is not understood, but may possibly be connected

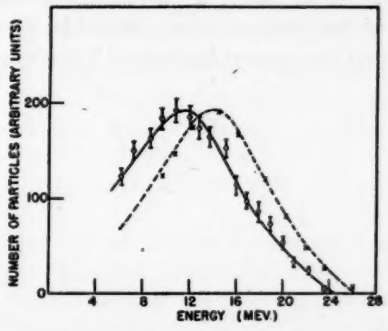

FIG. 11. Energy distribution of long-range α-particles emitted in fission of U^{235}. The broken line shows the distribution after correction for energy loss in the aluminum foil. Crosses indicate the curve predicted by the range measurements.

[18] D. C. Brunton and G. C. Hanna, Can. J. Research A 28, 190 (1950).

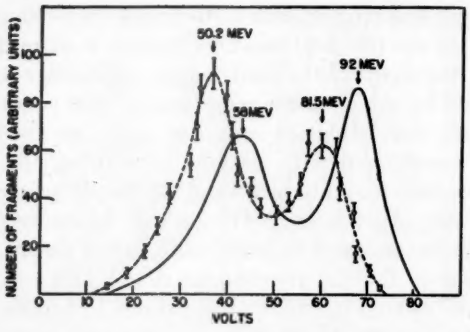

FIG. 12. Energy distribution of fission fragments. Solid curve is the normal distribution. Broken curve is the distribution in energy of fragments in coincidence with long-range α-particles.

with the energy spectrum of the neutrons producing fission. Tsien[12] has suggested that the greater the excitation of the compound nucleus, the less favored is the emission of long-range α-particles. The absence of such emission in the fast neutron fission of uranium and thorium substantiates this argument. Further experiments to determine the dependence on neutron energy of α-emission in fission are desirable.

From the similarity of the range distributions and specific ionizations, we conclude that the long-range particles emitted in the fission of U^{233} and Pu^{239} are also α-particles. In the case of U^{235} fission, the energy released in binary and ternary processes is about the same. No significant change in the mass ratio of the two main fragments is evident in the rarer mode of fission. This is in agreement with Marshall's conclusions.[6]

Tsien[12] has given a rather detailed discussion of the two main modes of ternary fission, *viz.*, fission accompanied by long-range α-particles, and fission accompanied by short-range charged particles. Using dynamical arguments based upon a simplified three-sphere model he has shown that it is possible to account for the energy and angular distributions of the light particles, independently of their precise nature and mass. As it has now been shown that all the *long-range* particles are α-particles, a rather more specific explanation of the process seems desirable, at the same time retaining the general features of Tsien's arguments.

Feather[19] has suggested that an α-particle may be evaporated from a highly excited fragment produced in a binary division if it lies in the particular range of nuclei which are unstable, or almost unstable, against α-emission in the ground state. The very considerable excitation of the fragment would account for the emission of α-particles within a time $\sim 10^{-21}$ sec. which is necessary to explain their angular distribution and energy. Because the region of maximum α-instability lies in the neighborhood of $Z \sim 40$ and $Z \sim 60$, this explanation predicts more asymmetry in the division of mass between the major fragments than in the average binary fission process. This does not appear to be supported experimentally, although it cannot be ruled out by our measurements.

Alternatively, it may be argued that the α-particle is emitted before the main division of the compound nucleus take place. For according to the Bohr-Wheeler nuclear model, excitations of the compound nucleus lasting for $\sim 10^{-14}$ sec. after a slow neutron is captured occur before the actual division takes place. If during this interval, the electrostatic α-particle barrier at some point of the nuclear surface is reduced to less than about 9 Mev (neutron binding energy ~ 4 Mev $+ \alpha$-disintegration energy ~ 5 Mev) an α-particle may be emitted. If fission occurs immediately after the α-emission, the α-particle will be accelerated in the Coulomb field of the two major fragments. Thus the process may be visualized as a special type of α-decay. A long-lived compound nucleus would favor this picture of the process, hence more α-particles are to be expected in slow neutron fission than in fast neutron fission, as is required by experiment. It would however seem to be very difficult to distinguish experimentally between this process and that proposed by Feather.

It is a pleasure to acknowledge the continued interest of Dr. B. W. Sargent during the experiments. The cooperation of the pile operating staff, under the direction of Mr. D. D. Stewart and Mr. G. M. James, is greatly appreciated, and thanks are also due Dr. J. G. MacHutchin for preparation of the sources of fissionable materials.

[19] N. Feather, Nature **159**, 607 (1947).

Distribution of Recoil Nucleus in Pair Production by Photons

R. JOST, J. M. LUTTINGER,* AND M. SLOTNICK†
The Institute for Advanced Study, Princeton, New Jersey
(Received May 22, 1950)

The angular and momentum distribution of the recoil nucleus in pair production by a photon is calculated covariantly by a method which utilizes the unitarity of the S matrix. The results are in disagreement with a recent experiment, particularly for small angles and high momentum transfers. The exact total cross section for pair creation is also given.

I. INTRODUCTION

RECENT attempts to measure the momentum and angular distributions of the recoil nucleus in pair production by energetic photons[1] have made a theoretical investigation of these effects desirable. There exists in the literature only an estimate of the momentum distribution.[2] An opportunity is also afforded of illustrating a method of calculation of somewhat more general applicability, which is based on the unitary character of the S matrix. A simplified and covariant calculation of the total pair production cross section and its asymptotic form (Bethe-Heitler formula[3]), is also carried through.

II. METHOD OF CALCULATION

In this discussion, the effect of the nucleus is represented by its static field

$$A_\mu(\mathbf{x})=\int \exp(-i\mathbf{q}\cdot\mathbf{x})A_\mu(\mathbf{q})d^3\mathbf{q}, \tag{1}$$

which is viewed as an external field. Higher radiative corrections are disregarded (see Appendix II), as is excitation of atomic states by the incident photon, and only the lowest term in the external field is computed (first Born approximation). The validity of some of these assumptions has been questioned,[4] but these effects are in any case not large.

The total cross section for pair production by a photon of energy k_0 (units in which $\hbar=c=1$ are used throughout) is then obtained in the form:

$$\sigma(k_0)=\int d^3\mathbf{q}A_\mu(\mathbf{q})A_\nu(-\mathbf{q})T_{\mu\nu}(\mathbf{q};k), \tag{2}$$

where $\mathbf{q}$ is the momentum transferred to the field and k is the energy momentum 4-vector of the photon, so that the integrand of (2) gives directly the differential cross section for obtaining a recoil nucleus of momentum $\mathbf{q}$.

To obtain $\sigma(k_0)$ we consider the scattering matrix, S, developed in a power series in the charge e:

$$S=1+eS_1+e^2S_2+\cdots. \tag{3}$$

If S^* is the Hermitian conjugate of S, the condition for the unitarity of S becomes

$$S^*S=1+e(S_1^*+S_1)+e^2(S_1^*S_1+S_2^*+S_2)+e^3(S_1^*S_2+S_2^*S_1+S_3^*+S_3)+e^4(S_1^*S_3+S_3^*S_1+S_2^*S_2+S_4^*+S_4)+\cdots=1, \tag{4}$$

so that each of the expressions in parentheses must vanish. Here, apart from mass terms,

$$e^nS_n=\frac{(-i)^n}{n!}\int_{1,\cdots,n} P[j_{\mu 1}(1),\cdots,j_{\mu n}(n)]\times P[A_{\mu 1}(1)+\phi_{\mu 1}(1),\cdots,A_{\mu n}(n)+\phi_{\mu n}(n)], \tag{5}$$

where $j_{\mu 1}(1)=ie\bar{\psi}(x_1)\gamma_{\mu 1}\psi(x_1)$, $\phi_{\mu 1}(1)$ is the electromagnetic field operator at x_1, etc., and the integral is taken over all the indicated 4-spaces.[5]

Consider next the expectation value for a state with a single photon of momentum k_0 of the e^4 term of (4), limiting ourselves to terms quadratic in the external field. If the external field cannot create pairs, which is true of a static field, the S_1 terms give zero. Furthermore, if the initial state in S_2 is a one-photon state, the final state can only have an electron-positron pair. The $e^4S_2^*S_2$ term is then the sum of the squares of all matrix elements between the initial state and all possible final states containing a pair; that is, the total probability for the creation of any pair by the photon. The cross section $\sigma(k)$ is thus given by $\sigma(k_0)=(k_0|e^4S_2^*S_2|k_0)$, which by virtue of (4) becomes

$$\sigma(k_0)=e^4(k_0|-S_4^*-S_4|k_0)=-2Re(k_0|e^4S_4|k_0). \tag{6}$$

This form is much more convenient for computational purposes than is the conventional non-covariant summation over final states.[6] It is to be noted that the absence of internal photon lines in the matrix elements of interest here makes unnecessary any explicit mass subtraction.

Employing the usual prescription of Feynman and Dyson[5] to evaluate the S_4 matrix element and averaging over the polarizations of the photon, one obtains

$$T_{\mu\nu}(q,k)=+(e^4/8\pi k_0)Re[A_{\mu\nu}(q,k)+B_{\mu\nu}(q,k)+B_{\mu\nu}(-q,k)+A_{\mu\nu}(q,k)+B_{\mu\nu}(q-k)+B_{\mu\nu}(-q,-k)]. \tag{7}$$

* Frank B. Jewett Fellow.
† AEC Postdoctoral Fellow.
[1] G. E. Modesitt and H. W. Koch, Phys. Rev. **77**, 175 (1950).
[2] H. A. Bethe, Proc. Camb. Phil. Soc. **30**, 524 (1934).
[3] H. A. Bethe and W. Heitler, Proc. Roy. Soc. **146**, 83 (1934).
[4] J. Wheeler and W. Lamb, Phys. Rev. **55**, 858 (1939).
[5] F. J. Dyson, Phys. Rev. **75**, 486 (1949); **75**, 1736 (1949).
[6] Some other applications of Eqs. (4)–(6) are discussed briefly in Appendix I.

$A_{\mu\nu}$ and $B_{\mu\nu}$ arise respectively from the Feynman diagrams (a) and (b) in Fig. 1, and are given by:

$$A_{\mu\nu}(q,k)=\int d^4p\frac{Sp[\gamma_\mu(i\gamma\cdot p-m)\gamma_\sigma(i\gamma\cdot(p-k)-m)\gamma_\nu(i\gamma\cdot(p-k-q)-m)\gamma_\sigma(i\gamma\cdot(p-q)-m)]}{(p^2+m^2)((p-k)^2+m^2)((p-k-q)^2+m^2)((p-q)^2+m^2)}, \tag{8}$$

$$B_{\mu\nu}(q,k)=\int d^4p\frac{Sp[\gamma_\mu(i\gamma\cdot(p+q)-m)\gamma_\nu(i\gamma\cdot p-m)\gamma_\sigma(i\gamma\cdot(p+k)-m)\gamma_\sigma(i\gamma\cdot p-m)]}{[(p+q)^2+m^2](p^2+m^2)^2[(p+k)^2+m^2]}, \tag{9}$$

where, for instance, p stands for the 4-vector p_μ, pq for $p_\mu q_\mu=\mathbf{p}\cdot\mathbf{q}-p_0q_0$, etc.

Terms arising from diagrams such as (c) of Fig. 1 all involve a photon self-energy operator acting on a free photon state, and hence give zero. Even the formally divergent momentum integrals associated with such operators will not be encountered here, since only real terms are carried in (7).

III. EVALUATION OF $T_{\mu\nu}(q;k)$

In calculating $T_{\mu\nu}$, we make use of the gauge invariance of $\sigma(k_0)$. If a gauge transformation is performed on the $A_\mu(x)$, it is seen from (2) that for gauge invariance

$$q_\mu T_{\mu\nu}(q;k)=0. \tag{10}$$

$T_{\mu\nu}$ must be of the form

$$T_{\mu\nu}=+(e^4/8\pi k_0)Re[I_1\delta_{\mu\nu}+I_2k_\mu k_\nu+I_3q_\mu q_\nu+I_4(q_\mu k_\nu+q_\nu k_\mu)], \tag{11}$$

where the I's are invariant functions of q and k. Equation (10) then yields the conditions:

$$I_1+I_3q^2+I_4qk=0,\quad I_2qk+I_4q^2=0, \tag{12}$$

so that only two of the I's need be computed. (Actually, three were computed as a check.)

We write

$$I_i(q,k)=A_i(q,k)+B_i(q,k)+B_i(-q,k)+(k\to-k)\quad(i=1,2,3,4)\cdots, \tag{13}$$

where $A_1(q,k)$ is the contribution from $A_{\mu\nu}(q,k)$, etc., cf. (8), (9), and similarly for the remaining I's. In the calculation, imaginary parts will be dropped freely, by virtue of (11).

An evaluation of the spur in (9), and use of the first of the relations:[7]

$$\frac{1}{abc^2}=3!\int_0^1 dx\int_0^x dy\frac{y}{[a+(b-a)x+(c-b)y]^4},$$
$$\frac{1}{abcd}=3!\int_0^1 dx\int_0^x dy\int_0^y dz\times\frac{1}{[a+(b-a)x+(c-b)y+(d-c)z]^4} \tag{14}$$

then yields:

$$B_2=-48\int d^4p\int_0^1 dx\int_0^x dy(x-y)y\frac{p^2(1+4(x-y)+2[(x-y)(Q^2+3m^2-2Qk)+Q^2+m^2]}{[p^2+m^2+q^2(1-x)-Q^2]^4}, \tag{15}$$

$$B_3=-48\int d^4p\int_0^1 dx\int_0^x dy(1-x)y\frac{p^2(1-4x)-2x(Q^2+3m^2-2Qk)}{[p^2+m^2+q^2(1-x)-Q^2]^4}, \tag{16}$$

where $Q=q(1-x)+k(x-y)$. Then, making use of:[7]

$$\int d^4p\frac{1}{[p^2+\lambda]^4}=\frac{\pi^2i}{6\lambda^2},\quad \int d^4p\frac{p^2}{[p^2+\lambda]^4}=\frac{\pi^2i}{3\lambda} \tag{17}$$

and the transformations $x-y=\eta$, $1-x=\xi$, it follows that

$$B_2=-16\pi^2i\int_0^1 d\xi\int_0^{1-\xi} d\eta\cdot\eta(1-\xi-\eta)\times\left[\frac{1+4\eta}{m^2+q^2\xi-Q^2}+\frac{\eta(Q^2+3m^2-2qk\xi)+Q^2+m^2}{(m^2+q^2\xi-Q^2)^2}\right], \tag{18}$$

$$B_3=-16\pi^2i\int_0^1 d\xi\int_0^{1-\xi} d\eta\cdot\xi(1-\xi-\eta)\times\left[\frac{4\xi-3}{m^2+q^2\xi-Q^2}-\frac{(1-\xi)(Q^2+3m^2-2qk\xi)}{(m^2+q^2\xi-Q^2)^2}\right], \tag{19}$$

with $Q=q\xi+k\eta$.

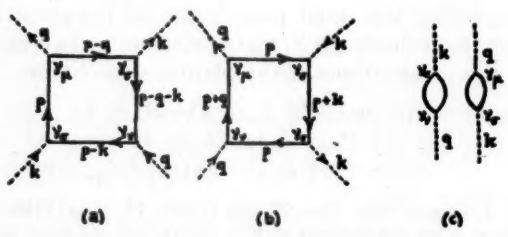

FIG. 1. Feynman diagrams for S_4.

[7] R. P. Feynman, Phys. Rev. 76, 769 (1949).

Consider first B_3: integrating (19) with respect to η, and dropping some purely imaginary terms, one obtains:

$$B_3=-\frac{16\pi^2 i}{\beta^2}\int_0^1 d\xi\frac{1}{\xi}[(3\xi-2)\{m^2+4r^2\xi(1-\xi)\}+4(1-\xi)(m^2+r^2\xi)]\{\ln[m^2+4r^2\xi(1-\xi)]-\ln[m^2+q^2\xi(1-\xi)]\}, \quad (20)$$

where

$$\beta=2qk \quad \text{and} \quad 4r^2=(q-k)^2. \quad (20a)$$

Since $q^2\geqslant 0$ for a static field, the term in

$$\ln[m^2+q^2\xi(1-\xi)]$$

may be dropped if the logarithm is chosen to be real at $\xi=0$. Equation (20) will then be purely imaginary unless

$$r^2<-m^2, \quad (21)$$

in which case $m^2+4r^2\xi(1-\xi)$ has two zeros in the range of integration, at

$$\xi_1=\tfrac{1}{2}(1-\omega), \quad \xi_2=\tfrac{1}{2}(1+\omega), \quad [\omega=(1+m^2/r^2)^{\frac{1}{2}}]. \quad (22)$$

Since m^2 must be thought to contain a small negative imaginary part, the path of integration for (20) is that of Fig. 2. For this branch of the logarithm we have

$$\ln[m^2+4r^2\xi(1-\xi)]=\begin{cases}\ln|m^2+4r^2\xi(1-\xi)| & \text{from } 0 \text{ to } \xi_1\\ \ln|m^2+4r^2\xi(1-\xi)|-i\pi & \text{from } \xi_1 \text{ to } \xi_2\\ \ln|m^2+4r^2\xi(1-\xi)| & \text{from } \xi_2 \text{ to } 1.\end{cases}$$

Then, if $f(\xi)$ is regular along the path,

$$Im\int_0^1 (d\xi/\xi)f(\xi)\ln[m^2+4r^2\xi(1-\xi)]=-i\pi\int_{\xi_1}^{\xi_2} d\xi(1/\xi)f(\xi). \quad (23)$$

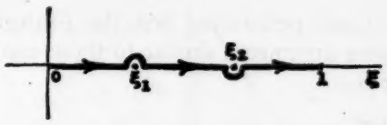

FIG. 2. Path of integration for B_3.

Then

$$B_3=-\frac{16\pi^2 i}{\beta^2}(-i\pi)\int_{\xi_1}^{\xi_2}\frac{d\xi}{\xi}[2m^2+\xi(-4r^2-m^2)+\xi^2(16r^2)+\xi^3(-12r^2)] \quad (24)$$

$$=\frac{32\pi^2m^2}{\beta^2}\left[\ln\frac{1-\omega}{1+\omega}+\omega\right].$$

In a completely analogous manner, one obtains from (18), after considerable calculation:

$$B_2=\frac{16\pi^3}{\beta^4}\Big\{q^2(12m^2q^2-8m^2\beta-\beta^2)\ln\left(\frac{1-\omega}{1+\omega}\right)+\omega[\beta^3+2\beta^2(m^2-q^2)+2\beta q^2(-8m^2+q^2)+2q^4(8m^2-q^2)]\Big\}. \quad (25)$$

Next, using the second of the relations (14) in Eq. (8), replacing $\int_0^1 dx\int_0^z dy\int_0^y dz\cdots$ by $\int_0^1 dy\int_0^y dz\int_y^1 dx\cdots$, and making the transformation of variables

$$z=(1-\xi)y-\zeta y, \quad x=y(1-\zeta)+\xi(1-y),$$

so that

$$\int_0^y dz\int_y^1 dx\cdots \text{ becomes } y\left[\int_0^{1-y} d\zeta\int_{\zeta y/(1-y)}^{1-\zeta} d\xi\cdots+\int_{-(1-y)}^{0} d\zeta\int_{-\zeta}^{1+\zeta y/(1-y)} d\xi\cdots\right],$$

we obtain after some algebra (putting $-\zeta$ for ζ in the second part of this integral, and then $\zeta=(1-y)t$):

$$A_{\mu\nu}(q,k)=6\int d^4p\int_0^1 dyy(1-y)\int_0^1 dt\left\{\int_{yt}^{1-(1-y)t} d\xi\frac{Sp[\ ]}{[(p-Q)^2+m^2+q^2y(1-y)+2qky(1-y)t]^4}+\int_{(1-y)t}^{1-yt} d\xi\frac{Sp[\ ]}{[(p-Q)^2+m^2+q^2y(1-y)-2qky(1-y)t]^4}\right\}. \quad (26)$$

Here, $Q=k\xi+qy$, and the spur is that appearing in (8). Now, evaluating the spur, putting $(1-y)$ for y in the second term of (26), and putting

$$A_2(q,k)=A_2'(q,k)+A_2'(-q,k), \qquad A_3(q,k)=A_3'(q,k)+A_3'(-q,k) \quad (27)$$

we obtain

$$A_2'(q,k)=-96\int d^4p\int_0^1 dyy(1-y)\int_0^1 dt\int_{(1-y)t}^{1-yt} d\xi\frac{-(p^2/2)-m^2+q^2y(1-y)-(2m^2+q^2)\xi(1-\xi)}{[p^2+m^2+q^2y(1-y)-2qky(1-y)t]^4},$$

$$A_3'(q,k)=-48\int d^4p\int_0^1 dyy(1-y)\int_0^1 dt\int_{(1-y)t}^{1-yt} d\xi\frac{p^2+2m^2(1-2y(1-y))}{[p^2+m^2+q^2y(1-y)-2qky(1-y)t]^4}. \quad (28)$$

Using (17) and performing first the ξ-integration, we obtain, using arguments similar to those used above in obtaining B_3,

$$A_3'=-\frac{16\pi^3}{\beta^2}[q^2-\beta+2m^2]\omega,$$

$$A_2'=\frac{16\pi^3}{\beta^4}\Big\{2(2m^2+q^2)q^2(\beta-q^2+2m^2)\ln\frac{1-\omega}{1+\omega}$$

$$-\omega[\beta^2+\beta^2(-q^2+2m^2)+(2m^2+q^2)6q^2(q^2-\beta)]\Big\}. \quad (29)$$

Collecting the results (24), (25), and (29), we have in view of (27) and (13)

$$I_2=\frac{64\pi^3q^2}{\beta^4}\Big\{\ln\frac{1-\omega}{1+\omega}[2(4m^4+6m^2q^2-q^4)$$

$$+2(-2m^2+q^2)\beta-\beta^2]$$

$$+\omega[4(q^2-\beta)(m^2-2q^2)-\beta^2]\Big\}, \quad (30)$$

$$I_3=\frac{64\pi^3}{\beta^2}\Big[2m^2\ln\frac{1-\omega}{1+\omega}+\omega(\beta-q^2)\Big], \quad (31)$$

if (21) is satisfied, and otherwise

$$I_2=I_3=0. \quad (32)$$

Then, from (12)

$$I_4=-(\beta/2q^2)I_2; \quad I_1=-q^2I_3+(\beta^2/4q^2)I_2. \quad (33)$$

Equations (30)–(33), substituted in (11), then complete the evaluation of $T_{\mu\nu}$. The distribution of the momentum vector $\mathbf{q}$ of the recoil nucleus, which is essentially $T_{\mu\nu}$, is thus given exactly and fairly concisely in terms of elementary functions by this method.

As a check on the correctness of the expression for $T_{\mu\nu}$, it is very easy to obtain from it the cross section for the production of pairs by two photons.[8] For this purpose, the momentum q must also be taken to belong to a photon (so that $q^2=0$) and the A_μ in (2) must be replaced by the creation operators ϕ_μ. Averaging over polarizations, the total probability for pair creation by the two photons is then proportional to

$$\frac{1}{2q_0}\cdot\frac{1}{2}T_{\mu\mu}(q,k)=\frac{e^4}{16\pi k_0q_0}(2I_1+kqI_4)\Big|_{q^2=0}$$

$$=\frac{e^4}{64\pi q_0k_0}\left(\frac{\beta^2}{q^2}I_2\right)\Big|_{q^2=0}$$

or

$$\sigma=\frac{\pi^2e^4}{\beta^2}\Big\{\ln\frac{1-\omega}{1+\omega}(8m^4-4m^2\beta-\beta^2)-\omega\beta(\beta+4m^2)\Big\},$$

which is the correct result.

[8] G. Breit and J. A. Wheeler, Phys. Rev. 46, 1087 (1934).

IV. THE MOMENTUM DISTRIBUTION OF THE RECOIL NUCLEUS

For a screened Coulomb field, $A_\mu(\mathbf{q})$ as computed from (1) is:

$$\mathbf{A}(\mathbf{q})=0; \quad A_0(\mathbf{q})=\frac{Ze}{(2\pi)^3}\frac{1}{\mathbf{q}^2}[1-F(\mathbf{q}^2)]. \quad (34)$$

Then, since $T_{00}=-T_{44}=-I_1+I_2k_0^2$ from (11) and (33), we have from (2)

$$\sigma(k_0)=\frac{-Ze^6}{4k_0(2\pi)^7}\int d^3\mathbf{q}\frac{(1-F(\mathbf{q}^2))^2}{\mathbf{q}^4}(I_1-I_2k_0^2) \quad (35)$$

where

$$I_1-I_2k_0^2=\frac{16\pi^3}{\beta^2}\Big[-4q^2\Big\{2m^2\ln\frac{1-\omega}{1+\omega}+\omega(\beta-q^2)\Big\}$$

$$-\frac{\beta^2-4q^2k_0^2}{\beta^2}\Big\{\omega[\beta^2-4(q^2-\beta)(m^2-2q^2)]$$

$$+\ln\frac{1-\omega}{1+\omega}[\beta^2+2(\beta-q^2)(2m^2-q^2)-8m^2(q^2+m^2)]\Big\}\Big] \quad (36)$$

if $r^2<-m^2$, and is zero otherwise.

Next, let us make the transformation of variables

$$2mQ=|\mathbf{q}|; \quad \mu=[k_0^2-|\mathbf{q}-\mathbf{k}|^2]/4m^2, \quad \alpha=k_0/2m. \quad (37)$$

Then $\int d^3\mathbf{q}$ over the region $r^2<-m^2$ or $|\mathbf{q}-\mathbf{k}|^2<k^2-4m^2$ becomes

$$\int_{\alpha-(\alpha^2-1)^{\frac{1}{2}}}^{\alpha+(\alpha^2-1)^{\frac{1}{2}}}dQ\int_1^{2\alpha Q-Q^2}d\mu\pi Q\cdot 4m^2/\alpha$$

and

$$\sigma(k_0)=\int_{\alpha-(\alpha^2-1)^{\frac{1}{2}}}^{\alpha+(\alpha^2-1)^{\frac{1}{2}}}dQP(Q,k_0). \quad (38)$$

$P(Q,k_0)$ is the distribution of the momentum Q of the recoil nucleus, in units of $2m$, and is given by

$$P(Q,k_0)=(Z^2e^6/32\pi^3k_0^2)[1-F(Q^2)]^2I(Q,\alpha)/Q^3,$$

$$I(Q,\alpha)=\{J_0+(1-2Q^2)J_1+(2Q^4-Q^2-4Q^2\alpha^2-\tfrac{1}{2})J_3$$

$$+2Q^2\alpha^2(1+6Q^2-4Q^4)J_4$$

$$+I_0+(1-4Q^2)I_1+[(4Q^2-1)Q^2-4Q^2\alpha^2]I_2$$

$$+4Q^2\alpha^2(8Q^2-1)I_3+4Q^4\alpha^2(1-8Q^2)I_4\}, \quad (39)$$

where

$$I_n=\int_1^y\frac{d\mu}{(Q^2+\mu)^n}\omega, \quad J_n=\int_1^y\frac{d\mu}{(Q^2+\mu)^n}\ln\frac{1-\omega}{1+\omega},$$

$$\omega=(1-1/\mu)^{\frac{1}{2}}, \quad y=2\alpha Q-Q^2. \quad (40)$$

With the exception of J_1, the integrals I_n and J_n are all elementary and for $n>1$ can be computed from I_1

and J_1 by differentiations with respect to the parameter Q^2. J_1 can be expressed, in terms of the functions[9]

$$R(t)=\int_0^t \ln(1+x)/x\,dx, \tag{41}$$

as

$$J_1=-R(1/Z\lambda)-R(\lambda/Z)+\pi^2/6+\tfrac{1}{2}(\ln\lambda)^2 +\tfrac{1}{2}(\ln Z)^2-(\ln Z)(\ln 8\alpha Q); \tag{42}$$

$$Z=[(y-1)^{\frac{1}{2}}+y^{\frac{1}{2}}]^2, \quad \lambda=[Q+(Q^2+1)^{\frac{1}{2}}]^2.$$

Then, after a lengthy calculation, one obtains:

$$I(Q,\alpha)=(1-2Q^2)J_1+\left(1-4Q^2-8Q\alpha+\frac{4Q^2-1}{3\alpha Q}\right)$$

$$\times\ln[(y)^{\frac{1}{2}}+(y-1)^{\frac{1}{2}}]+\left(3+\frac{2\alpha}{3Q}+\frac{2Q^2-1}{3\alpha Q}\right)(y(y-1))^{\frac{1}{2}}$$

$$+\left\{-2(1+Q^2)+\frac{2\alpha^2}{3}\left(-4+\frac{1}{Q^2}\right)\right\}\frac{1}{(1+1/Q^2)^{\frac{1}{2}}}$$

$$\times\ln\left\{\frac{(1+1/Q^2)^{\frac{1}{2}}-(1-1/y)^{\frac{1}{2}}}{(1+1/Q^2)^{\frac{1}{2}}+(1-1/y)^{\frac{1}{2}}}\right\}. \tag{43}$$

As a rather stringent test of (39), (38) was integrated asymptotically and found to give precisely the Bethe-Heitler formula.[10] Care must be taken because certain terms in (43) very nearly cancel over a large region. In fact, in the region where $y=2\alpha Q-Q^2\approx 2\alpha Q$ (i.e., $Q\ll\alpha$), a much more useful expression is:

$$I(Q,\alpha)\approx(1-2Q^2)J_1+\frac{1}{2}\left(1-4y-\frac{2}{3y}\right)\ln Z$$

$$+\frac{y^2(1-1/y)^{\frac{1}{2}}}{3}\left[11-\frac{13}{3}\left(1-\frac{1}{y}\right)-2\left(1-\frac{1}{y}\right)^2\right] \tag{44}$$

and if $Q\ll 1$,

$$(1-2Q^2)J_1\approx -2R(1/Z)-(\ln Z)(\ln 4y) +\tfrac{1}{6}\pi^2+\tfrac{1}{2}(\ln Z)^2. \tag{45}$$

In the latter region, it is therefore seen that $I(Q,\alpha)$ is a function only of $y\approx 2\alpha Q$.

In Fig. 3, the momentum distribution $P(Q,k_0)$ is plotted for several values of k_0 of possible experimental interest. The general behavior of the curves does not differ appreciably from that estimated by Bethe (reference 2, p. 537). The effect of screening may be taken into account by inserting appropriate values for

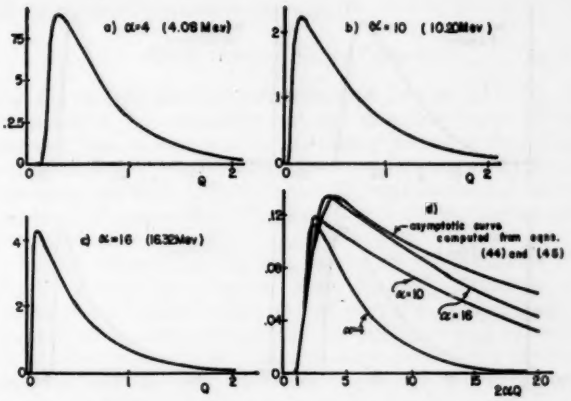

FIG. 3. Momentum distribution of recoil nucleus for several photon energies. Curves (a), (b), and (c): Ordinate: $P(Q,k_0)/(Z^2e^6/32\pi^3m^2)$. Abscissa: Q=momentum/$2m$. Curve (d): Ordinate: $P(Q,k_0)/(2\alpha Z^2e^6/32\pi^3m^2)$. Abscissa: $2\alpha Q$.

F in (39). It is easily verified, however, that for all Z and all energies considered in Fig. 3, the effect of screening is completely negligible.

V. ANGULAR DISTRIBUTION

Since, for the energies of interest here, screening may be omitted, F in Eq. (34) can be taken to be zero. We introduce in Eqs. (37) and (36) the variable Q of Eq. (37) and

$$\eta=\alpha\cos\theta=\alpha\mathbf{q}\cdot\mathbf{k}/qk_0, \tag{46}$$

θ being the angle the recoil nucleus makes with the direction of the incident photon. It then follows that

$$\sigma(k_0)=\frac{Z^2e^6}{16\pi^3k_0^2}\int_1^\alpha d\eta\int_{\eta-(\eta^2-1)^{\frac{1}{2}}}^{\eta+(\eta^2-1)^{\frac{1}{2}}}\frac{dQ}{Q^2}$$

$$\times\left\{\ln\frac{1-\omega}{1+\omega}\left[\left(1-\frac{\alpha^2}{\eta^2}\right)\left[1-\frac{1}{4\eta^2}+\frac{1}{2\eta Q}\right.\right.\right.$$

$$\left.-\frac{1}{8Q^2\eta^2}-\frac{Q}{\eta}+\frac{Q^2}{2\eta^2}\right]+\frac{\alpha^2}{2\eta^4}\Bigg]$$

$$+\omega\left[\left(1-\frac{\alpha^2}{\eta^2}\right)\left(1-\frac{1}{4\eta^2}+\frac{1}{2\eta Q}\right)\right.$$

$$\left.\left.+\frac{1}{\eta^2}\left(1-\frac{2\alpha^2}{\eta^2}\right)(-2Q\eta+Q^2)\right]\right\}, \tag{47}$$

where $\omega=[1-1/(2Q\eta-Q^2)]^{\frac{1}{2}}$.

Introducing the variable $\mu=2\eta Q-Q^2$, (47) becomes

$$\sigma(k_0)=(Z^2e^6/16\pi^3k_0^2)\int_1^\alpha d\eta I(\eta;\alpha),$$

[9] See W. Heitler, *Quantum Theory of Radiation* (Oxford University Press, London, 1944), second edition, p. 172. ($R(t)$ is there called $F(t)$). $R(x)$ is equal to the function $-\xi(1, 21-x)$ tabulated by K. Mitchell, Phil. Mag. **40**, 351 (1949).

[10] W. Heitler, reference 6, p. 200, Eq. (15).

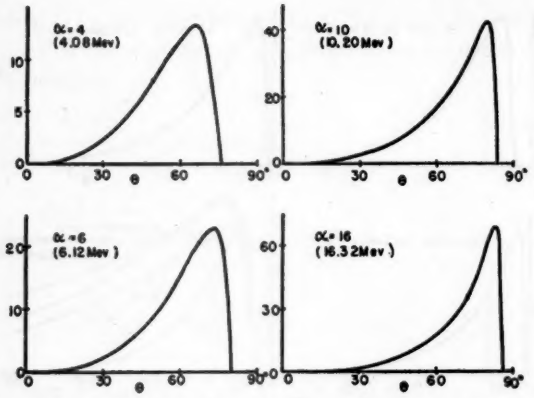

FIG. 4. Angular distribution of recoil nucleus for several photon energies. Ordinate: $P(\theta, k_0)/(Z^2e^6/64\pi^2m^2)$. Abscissa: Angle of scattering θ in degrees.

with

$$I(\eta;\alpha)=\int_1^{\eta^2}d\mu\frac{1}{(\eta^2-\mu)^{\frac{1}{2}}}\Big[\omega\Big\{\Big(1-\frac{\alpha^2}{\eta^2}\Big)\times\Big(\frac{2\eta^2}{\mu^3}+\frac{2(\eta^2-1)}{\mu^2}+\frac{(1/4\eta^2)-1}{\mu}\Big)+\Big(1-\frac{2\alpha^2}{\eta^2}\Big)\Big(-\frac{2}{\mu}+\frac{1}{\eta^2}\Big)\Big\}+\ln\frac{1-\omega}{1+\omega}\Big\{\frac{\alpha^2}{\eta^2\mu^2}-\frac{\alpha^2}{2\eta^4\mu}+\Big(1-\frac{\alpha^2}{\eta^2}\Big)\Big(+\frac{1}{2\eta^2}+\frac{1-8\eta^2}{4\eta^2\mu}+\frac{(2\eta^2-2-(1/8\eta^2))}{\mu^2}+\frac{2\eta^2+1}{\mu^3}-\frac{\eta^2}{\mu^4}\Big)\Big\}\Big]$$

with $$\omega=(1-1/\mu)^{\frac{1}{2}}. \tag{48}$$

We may then write

$$\sigma(k_0)=\int_0^{\cos^{-1}1/\alpha}d\theta P(\theta, k_0),$$

where

$$P(\theta, k_0)=(Z^2e^6\alpha/16\pi^2k_0^2)I(\eta;\alpha)\sin\theta \tag{49}$$

is the angular distribution of the recoil nucleus.

Integrating the term in $\ln[(1-\omega)/(1+\omega)]$ in (48) by parts and combining with the remaining terms, we obtain:

$$I(\eta, \alpha)=I_1(\eta, \alpha)+I_2(\eta, \alpha), \tag{50}$$

where

$$I_1(\eta, \alpha)=\frac{2}{\eta}\Big[\Big(\frac{37}{9}-\frac{14}{9}\eta^2\Big)E-\Big(\frac{11}{9}+\frac{4}{3\eta^2}\Big)F\Big]+\frac{2\alpha^2}{\eta^3}\Big[\Big(-\frac{73}{9}+\frac{14}{9}\eta^2\Big)E+\Big(\frac{29}{9}+\frac{10}{3\eta^2}\Big)F\Big], \tag{51}$$

and F and E are the complete elliptic integrals of the first and second kind, respectively, of modulus $(1-1/\eta^2)^{\frac{1}{2}}$:

$$F=\int_0^{\pi/2}\frac{d\phi}{\Big[1-\Big(1-\frac{1}{\eta^2}\Big)\sin^2\phi\Big]^{\frac{1}{2}}}=F\Big[\Big(1-\frac{1}{\eta^2}\Big)^{\frac{1}{2}}\Big],$$

$$E=\int_0^{\pi/2}d\phi\Big[1-\Big(1-\frac{1}{\eta^2}\Big)\sin^2\phi\Big]^{\frac{1}{2}}=E\Big[\Big(1-\frac{1}{\eta^2}\Big)^{\frac{1}{2}}\Big].$$

I_2 is not expressible in such simple form, and is:

$$I_2=\Big(1-\frac{\alpha^2}{\eta^2}\Big)\frac{1}{\eta}\int_1^{\eta^2}\frac{d\mu}{[\mu(\mu-1)]^{\frac{1}{2}}}\ln\frac{\eta-(\eta^2-\mu)^{\frac{1}{2}}}{\eta+(\eta^2-\mu)^{\frac{1}{2}}}=\Big(1-\frac{\alpha^2}{\eta^2}\Big)\frac{4}{\eta}F_1(\eta), \tag{52}$$

where

$$F_l(\eta)=\int_1^{\eta}\frac{d\xi}{\xi^l}F\Big[\Big(1-\frac{1}{\xi^2}\Big)^{\frac{1}{2}}\Big]. \tag{53}$$

Series expansions for the integral in (52) are easily obtainable, though numerical integrations proved more convenient for the actual calculations used to construct the graphs in Fig. 4.

It may be of interest to note that using (51) and (52) the integration indicated in (48) can be carried out in terms of complete elliptic integrals, F_1, and a simple integral over F_1. One obtains:

$$\sigma(k_0)=\bar{\phi}(1/\alpha^2)(W_1+W_2);\quad \bar{\phi}=(Z^2e^6/64\pi^2m^2), \tag{54}$$

where

$$W_1=\frac{2}{9}[37E_1-14E_{-1}-11F_1-12F_3+\alpha^2(-73E_3+14E_1+29F_3+30F_5)], \tag{55}$$

$$W_2=4\int_1^{\alpha}\frac{F_1(\eta)}{\eta}d\eta+2F_1(\alpha)+2F\Big[\Big(1-\frac{1}{\alpha^2}\Big)^{\frac{1}{2}}\Big]-2\alpha^2E\Big[\Big(1-\frac{1}{\alpha^2}\Big)^{\frac{1}{2}}\Big]. \tag{55}$$

W_1 can be further simplified[11] to

$$W_1=\frac{2}{9}\left\{-18F_1(\alpha)+\left(-\frac{64}{3}+\frac{82\alpha^2}{3}\right)E\left[\left(1-\frac{1}{\alpha^2}\right)^{\frac{1}{2}}\right]\right.$$
$$\left.+\left(\frac{98}{3}+\frac{2}{\alpha^2}+14\alpha^2\right)F\left[\left(1-\frac{1}{\alpha^2}\right)^{\frac{1}{2}}\right]\right\}. \quad (56)$$

(55) and (56) then yield the exact pair production total cross section:

$$\sigma(k_0)=\frac{\bar{\phi}}{\alpha^2}\frac{1}{}\left[4\int_1^\alpha\frac{F_1(\eta)}{\eta}d\eta+2F_1(\alpha)\right.$$
$$+\frac{2}{27}\left\{-(64+109\alpha^2)E\left[\left(1-\frac{1}{\alpha^2}\right)^{\frac{1}{2}}\right]\right.$$
$$\left.\left.+\left(125+\frac{6}{\alpha^2}+42\alpha^2\right)K\left(1-\frac{1}{\alpha^2}\right)^{\frac{1}{2}}\right\}\right]. \quad (57)$$

Using the following identities:

$$F(k)=(1+k_1)F(k_1),$$

where $k_1=[1-(1-k^2)^{\frac{1}{2}}]/[1+(1-k^2)^{\frac{1}{2}}]$

$$E(k)=[2/(1+k_1)]E(k_1)-(1-k_1)F(k_1).$$

(57) can be shown to be equivalent to a formula previously obtained by Racah.[12] This provides a very severe check on all the preceding algebra.

VI. COMPARISON WITH EXPERIMENT

The curves in Figs. 3 and 4 can be compared with the experimental data given by Modesitt and Koch.[1] Since these data give only relative intensities, the comparison is somewhat ambiguous. If the maxima of the experimental and theoretical curves are adjusted to agree approximately, the experimental curves are found to be too low for smaller angles and too high for high momentum transfers; the disagreement for the momentum distribution being particularly sharp.

APPENDIX I. OTHER APPLICATIONS OF THE UNITARITY CONDITION

An interesting application of Eqs. (4)–(6) seems to us to be the basis of an investigation by J. A. Wheeler and J. S. Toll,[13] the idea being to compute the imaginary part of S_4 from the real part, which is determined from (6) by $S_2^*S_2$. We shall illustrate the method for our case, and show also that the necessary assumptions are justified.

For this, we write the diagonal element of the gauge-invariant S_4 by the usual methods in the form (2):

$$S_4=\int d^3\mathbf{q}A_\mu(q)A_\nu(-q)T_{\mu\nu}(q,k).$$

For $T_{\mu\nu}$ we again have a decomposition of the type (11), (12), the invariants I_j now including real and imaginary parts. By expressing these invariants in the variables $q^2\gtrless 0$ and r^2 (Eq. (20a)), eliminating $\beta=q^2-4r^2$, and letting $r=-\zeta$ be a complex variable, one easily sees from (18), (19), and (28) that for fixed q^2, all the invariants I_j are analytic functions of ζ, with singularities only on the real axis.

It then follows that the real part of all the invariants is a regular potential function in either half-plane. Therefore, the values on the real axis define the real part of these invariants on one half-plane, and therefore also the imaginary part to within an additive constant. The constant is determined by the condition that the imaginary parts vanish for large real ζ. The formal connection reads, for real ζ:

$$Im[I(\zeta)]=\frac{1}{\pi i}P\int_{-\infty}^{\infty}\frac{Re[I(\zeta')]}{\zeta'-\zeta}d\zeta',$$

where $Re[I(\zeta)]=0$ for $\zeta<m^2$ (Eq. (21)). Physically, this means that we can deduce the *forward* scattering of light by a spherically symmetric static field (this restriction resulting from our summation over the polarizations of the light quantum) from the tensor $T_{\mu\nu}$ of (2), since this is the effect described by S_4.[14]

Of course, this procedure is widely generalizable. First, the restriction of (4) to diagonal matrix elements may be dropped, so that the full matrix S_4 may be computed from the second-order matrix S_2. Moreover, one can probably apply the same method to the calculation of radiative corrections. We do not believe, however, that the method is of great help for computation purposes, but it is certainly of interest in showing the interconnection between various parts of the S matrix.

APPENDIX II. ORDER OF MAGNITUDE OF RADIATIVE CORRECTIONS

To obtain an estimate of the order of magnitude of the radiative corrections to the total cross section for pair creation in a Coulomb field, we use the Weizsäcker-Williams method,[15] which is valid asymptotically for extremely high energies.

We transform to the Lorentz system in which the incoming photon, of energy k_0 in the rest system of the nucleus, has an energy m. As we assume $k_0\gg m$, the velocity of this system will be close to unity and

$$\xi=1/(1-\beta^2)^{\frac{1}{2}}\cong k_0/2m\gg 1.$$

The field of the fast-moving nucleus of charge Ze is decomposed into a suitable distribution of photons. The number of equivalent photons with an impact parameter S and an energy between ν and $\nu+d\nu$ reads

$$p(S,\nu)d\nu=(4Z^2e^2/\pi)\cdot\nu d\nu|K_1(S\nu/\xi)|^2/\xi^2,$$

where $K_1(Z)$ is that of Magnus and Oberhettinger.[16] The total cross section is therefore given by

$$\sigma(k_0)=2\pi\int_0^\infty d\nu\int_{S_{\min}}^\infty SdSp(S,\nu)Q(\nu,m),$$

where $Q(\nu,m)$ denotes the total cross section for pair-creation by the head-on collision of two photons with energies ν and m. ($Q(\nu,m)$ is given in lowest order by the Breit-Wheeler formula, see Section III.) $S_{\min}$ denotes a smallest impact parameter for the production of the electron pair, and will be of order $1/m$.

---

[11] Jahnke-Emde, *Tables of Functions* (Dover Publications, New York, 1945), pp. 73 ff.

[12] G. Racah, Nuovo Cimento **13**, 69 (1936).

[13] (To be published.) We are indebted to Professor Wheeler for showing us a preliminary draft, and for several discussions.

[14] Professor Wheeler informs us that Mr. Toll is applying their method to this effect.

[15] W. Heitler, reference 6, p. 263 ff. E. J. Williams, Kgl. Dansk Vid. Selsk. Math.-Fys. Medd. **13**, 4 (1935).

[16] Magnus and Oberhettinger, *Special Functions of Math. Phys.* (Chelsea Publishing Company, New York, 1949), p. 29.

The integration over S is straightforward and yields

$$\sigma(k_0)=-\frac{16Z^2e^2}{k^2}m^2\cdot S_{\min}{}^2\int_0^\infty \nu d\nu Q(\nu,m)\{K_1{}^2(\zeta_m)-K_0(\zeta_m)K_2(\zeta_m)\},$$

where $\zeta_m=S_{\min}\cdot 2m\nu/k_0\cong 2\nu/k_0$.

If $Q(\nu,m)$ is to contain radiative correction $\sim e^2$, one must include the possibility for the emission of a photon, besides the pair. The dependence of the cross section on the energy of this photon is uninteresting, and even a classical effect when the photon has a low energy. $Q(\nu,m)$ should therefore be the cross section for pair creation including possible emission of a photon. As $Q(\nu,m)$ must fall off for high energies ν (as is generally found for such cross sections in quantum electrodynamics), the main contributions to $\sigma(k_0)$ will come from small values of ν/m. We can therefore expand the bracket $\{\ \}$ with respect to ζ_m, obtaining

$$\sigma(k_0)=8Z^2e^2\int\frac{d\nu}{\nu}\left(\ln\frac{k}{2m}-\ln\frac{\nu}{2}-\ln\frac{\gamma}{2}-\frac{1}{2}\right)Q(\nu,m)$$
$$=A\ln(k_0/2m)+B,$$

where

$$A=8Z^2e^2\int Q(\nu,m)d\nu/\nu,$$
$$B=8Z^2e^2\int\frac{d\nu}{\nu}\left(\ln\frac{\nu}{m}+\ln\frac{\gamma}{2}+\frac{1}{2}\right)Q(\nu,m),$$
$$\ln\gamma=0.577\cdots.$$

The only change caused by the radiative corrections will therefore consist in a change of A and B of the order of 1/137, which is quite negligible.

PHYSICAL REVIEW VOLUME 80, NUMBER 2 OCTOBER 15, 1950

The Inelastic Scattering of High Energy Neutrons by Deuterons According to the Impulse Approximation

GEOFFREY F. CHEW
Department of Physics, University of California, Berkeley, California
(Received May 31, 1950)

The high energy $n-d$ inelastic scattering problem is formulated in such a way that the amplitudes for $n-n$ and $n-p$ scattering at the same energy appear explicitly. The formulation depends on: (1) the large radius of the deuteron compared with the range of nuclear forces and high energy scattering amplitudes; (2) the high velocity of the incident neutron compared to the zero point motion of the deuteron. The method does not depend on the weakness of nuclear forces compared to the kinetic energy of the neutron and is therefore not equivalent to the Born approximation.

I. INTRODUCTION

IN a previous paper[1] the author discussed the elastic scattering of 90- to 350-Mev neutrons by deuterons and pointed out that because elastic scattering may well represent a considerable fraction of the total n–d cross section, it is dangerous to assume that the latter is equal to the sum of the free n–n and n–p cross sections. This is because binding and interference effects play a large role in elastic scattering. They do not play so important a part in the inelastic scattering, however, and it is possible that experiments which concentrate on the latter rather than on the total n–d cross section may yet reveal the magnitude of the n–n interaction at high energies. Because of the similar properties of mirror nuclei it appears certain that n–n and p–p forces are equal for low relative energies. So many surprises have appeared in high energy scattering experiments, however,[2] that it is desirable, if possible, to measure the high energy n–n interaction independently.

It is the purpose of this first of two papers to formulate the n–d inelastic scattering problem in such a manner that from its measurement one can attempt to deduce the value of the free neutron-neutron cross section. The actual attempted deduction from Berkeley experiments will be carried out in the second paper. A secondary feature of this first part is the demonstration of a phenomenological approach to high energy nuclear reactions in light nuclei, using as a basis the experimentally measured values of nucleon-nucleon cross sections. It is hoped that this general method may eventually be extended to nuclei more complex than the deuteron.

The fundamental assumptions will be twofold: (1) the "collision" time in high energy n–d scattering is so short compared to the period of the deuteron that the change in the wave function of the latter during the collision can be described by an "impulse" approximation; (2) the deuteron has such a diffuse structure compared to the range of nuclear forces that the wave function of the incident neutron at one of the two scattering centers within the deuteron is not appreciably perturbed by the presence of the other center. Outgoing waves from both centers are present and must be added together, but individually they will be assumed to be the same as would be produced by a single neutron or proton. In this way the three-body problem is reduced to a superposition of the two-body problems.

It should be noted that these assumptions are not completely equivalent to the Born approximation,

[1] G. F. Chew, Phys. Rev. 74, 809 (1948).
[2] Hadley, Kelly, Leith, Segrè, Wiegand, and York, Phys. Rev. 75, 351 (1949); O. Chamberlain and C. Wiegand, Phys. Rev. 79, 81 (1950).

which has been used previously in this problem.[3,4] It will not be assumed here that the perturbation of the incident wave is small (which is true only at energies still unobtainable with accelerators) but only that the two perturbing centers act independently and "suddenly." The two-body scattering amplitudes can be treated as empirical quantities, and the calculations described in Sections III and IV simply have to do with the "quantum kinematics" of a three-body problem in which each of the three particles has spin one-half and two of the three are identical.

II. THE IMPULSE APPROXIMATION

The formulation of the approximation outlined in Section I is to be applied here to the non-relativistic case although the inclusion of relativistic effects should not be difficult. Before taking on all of the complications of the actual neutron-deuteron problem, it is instructive to consider a simplified situation in which the proton is bound to a fixed short-range force, $U(\mathbf{r}_p)$, which can accommodate one bound state $\varphi_0(\mathbf{r}_p)$ and which interacts with the incident neutron through a potential, $V(\mathbf{r}_n-\mathbf{r}_p)$. The interaction of the neutron with U will be ignored. The Schrödinger equation for this problem is

$$[-\hbar^2/2m\Delta_{r_n}-\hbar^2/2m\Delta_{r_p}+U(\mathbf{r}_p)+V(\mathbf{r}_n-\mathbf{r}_p)]\times\Psi(\mathbf{r}_n,\mathbf{r}_p)=E_0\Psi(\mathbf{r}_n,\mathbf{r}_p), \quad (1)$$

where $E_0=\hbar^2k_0^2/2m-B$, $\mathbf{k}_0$ being the wave number of the incident neutron and B the binding energy of the proton. A solution is desired of the form

$$\Psi(\mathbf{r}_n,\mathbf{r}_p)=(1/2\pi)^{\frac{3}{2}}e^{i\mathbf{k}_0\cdot\mathbf{r}_n}\varphi(\mathbf{r}_p)+\Psi_s(\mathbf{r}_n,\mathbf{r}_p), \quad (2)$$

where $\Psi_s(\mathbf{r}_n,\mathbf{r}_p)$ will contain various kinds of outgoing waves which represent elastic scattering, inelastic scattering, and pick-up processes.[5] Substitution into the wave equation and some rather conventional manipulations[6] allow one to derive an integral equation for $\Psi_s(\mathbf{r}_n,\mathbf{r}_p)$ into which the appropriate boundary conditions are incorporated. The asymptotic form of this equation for large $\mathbf{r}_n$, large $\mathbf{r}_p$, and large $|\mathbf{r}_n-\mathbf{r}_p|$ is

$$\Psi_s\rightarrow\frac{2m}{4\pi\hbar^2}\int d\mathbf{k}_p\varphi_{\mathbf{k}_p}(\mathbf{r}_p)\frac{e^{ik_nr_n}}{r_n}\int\int d\mathbf{r}_n'd\mathbf{r}_p'\varphi_{\mathbf{k}_p}{}^*(\mathbf{r}_p')\times e^{-i\mathbf{k}_n\cdot\mathbf{r}_n'}V(\mathbf{r}_n'-\mathbf{r}_p')\Psi(\mathbf{r}_n',\mathbf{r}_p'), \quad (3)$$

where $\varphi_{\mathbf{k}_p}(\mathbf{r}_p)$ is the continuum eigenfunction for the proton in the potential field $U(\mathbf{r}_p)$, which is normalized at infinity to $(1/2\pi)^{\frac{3}{2}}e^{i\mathbf{k}_p\cdot\mathbf{r}_p}$. The magnitude of $\mathbf{k}_n$ is determined by the energy equation, $\hbar^2k_n^2/2m=E_0-\hbar^2k_p^2/2m$. This is the part of the outgoing wave which corresponds to inelastic scattering with emission of the proton.

For the wave function which appears in the integrand of (3) the following approximation will now be made:

$$\Psi(\mathbf{r}_n,\mathbf{r}_p)\approx\Psi_a(\mathbf{r}_n,\mathbf{r}_p)=\int d\mathbf{k}_pg_0(\mathbf{k}_p)\psi_{\mathbf{k}_0,\mathbf{k}_p}{}^{np}(\mathbf{r}_n,\mathbf{r}_p), \quad (4)$$

where

$$g_0(\mathbf{k}_p)=(1/2\pi)^{\frac{3}{2}}\int d\mathbf{r}_pe^{-i\mathbf{k}_p\cdot\mathbf{r}_p}\varphi_0(\mathbf{r}_p),$$

and $\psi_{\mathbf{k}_0,\mathbf{k}_p}{}^{np}(\mathbf{r}_n,\mathbf{r}_p)$ is the wave function which represents the scattering of a neutron of momentum $\mathbf{k}_0$ by a free proton of momentum $\mathbf{k}_p$. $\Psi_a(\mathbf{r}_n,\mathbf{r}_p)$ clearly represents the scattering of a neutron of momentum $\mathbf{k}_0$ by a free proton wave packet which has the same momentum distribution as the bound proton function φ_0. The author believes that the replacement of Ψ by Ψ_a corresponds to assuming that for the "duration" of the proton's interaction with the neutron the proton does not interact with the force field $U(\mathbf{r}_p)$. The only effect of the latter is assumed to be the generation of the momentum distribution $g_0(\mathbf{k}_p)$, at a time much earlier than the arrival time of the neutron. It seems reasonable that if the range of the n–p force is ρ and the neutron velocity v_0, then the criterion for the validity of this approximation is essentially that the "collision time," ρ/v_0, be short compared to the period of the deuteron. (This ratio is, for instance, 1/10 for 90-Mev neutrons.) An attempt is now being made to verify this assertion by actually calculating the error made, and a discussion of the limitations of the impulse approximation in general will be given in a forthcoming paper by Wick and the author.

Two additional remarks about the approximate function Ψ_a may be added. In the first place it is always at least as good as the Born approximation, since in the limit of a very weak n–p force

$$\Psi_a\rightarrow(1/2\pi)^{\frac{3}{2}}e^{i\mathbf{k}_0\cdot\mathbf{r}_n}\varphi_0(\mathbf{r}_p).$$

Second, it will always represent correctly the limiting case of a very low binding energy of the proton, since in that case $g_0(\mathbf{k}_p)$ becomes a delta-function and one automatically gets free n–p scattering. Even without the supporting argument above, therefore, Ψ_a might be looked on as an interpolation between these two limits.

Substitution of Ψ_a into (3) leads to a simple result, particularly if one employs the R matrix notation.[7] In this notation, the matrix

$$(\mathbf{k}_n',\mathbf{k}_p'|R_{np}|\mathbf{k}_n,\mathbf{k}_p)=-\frac{i}{(2\pi)^{\frac{3}{2}}}\int\int d\mathbf{r}_n'd\mathbf{r}_p'e^{-i(\mathbf{k}_n'\cdot\mathbf{r}_n'+\mathbf{k}_p'\cdot\mathbf{r}_p')}\times V(\mathbf{r}_n'-\mathbf{r}_p')\psi_{\mathbf{k}_n,\mathbf{k}_p}{}^{np}(\mathbf{r}_n',\mathbf{r}_p') \quad (5)$$

describes free neutron-proton scattering from the initial wave numbers $\mathbf{k}_n$ and $\mathbf{k}_p$ to the final wave numbers $\mathbf{k}_n'$ and $\mathbf{k}_p'$. Since the wave function $\psi_{\mathbf{k}_n,\mathbf{k}_p}{}^{np}(\mathbf{r}_n,\mathbf{r}_p)$

[3] Ta You Wu and J. Ashkin, Phys. Rev. 73, 986 (1948).
[4] F. DeHoffman, Phys. Rev. 76, 216 (1950).
[5] G. F. Chew and M. L. Goldberger, Phys. Rev. 77, 470 (1950).
[6] See, for example, G. Breit, Phys. Rev. 71, 215 (1947).
[7] C. Møller, Kgl. Danske, Vid. 23, No. 1 (1945).

may be factored, i.e.

$$\psi_{\mathbf{k}_n,\mathbf{k}_p}{}^{np}(\mathbf{r}_n,\mathbf{r}_p)=(1/2\pi)^{\frac{3}{2}}e^{i\frac{1}{2}(\mathbf{k}_n+\mathbf{k}_p)\cdot(\mathbf{r}_n+\mathbf{r}_p)}\times\varphi_{\frac{1}{2}(\mathbf{k}_n-\mathbf{k}_p)}{}^{np}(\mathbf{r}_n-\mathbf{r}_p), \quad (6)$$

one can also write (5) in the form

$$(\mathbf{k}_n',\mathbf{k}_p'|R_{np}|\mathbf{k}_n,\mathbf{k}_p)=\delta(\mathbf{k}_n'+\mathbf{k}_p'-\mathbf{k}_n-\mathbf{k}_p)(\mathbf{k}'|r_{np}|\mathbf{k}), \quad (7)$$

where $\mathbf{k}=\frac{1}{2}(\mathbf{k}_n-\mathbf{k}_p)$, $\mathbf{k}'=\frac{1}{2}(\mathbf{k}_n'-\mathbf{k}_p')$, and

$$(\mathbf{k}'|r_{np}|\mathbf{k})=-i\int d\mathbf{r}e^{-i\mathbf{k}'\cdot\mathbf{r}}V(\mathbf{r})\varphi_{\mathbf{k}}{}^{np}(\mathbf{r}). \quad (8)$$

To find the cross section for free n–p scattering into any wave number interval, $d\mathbf{k}'$, the formula

$$\sigma_{np}d\mathbf{k}'=2\pi/\hbar v_0|(\mathbf{k}'|r_{np}|\mathbf{k})|^2\delta(E_n'+E_p'-E_n-E_p)d\mathbf{k}'$$

is to be used, in which v_0 is the initial relative velocity, $E_n=\hbar^2k_n^2/2m$, etc., and where all energies and momenta are to be expressed in terms of $\mathbf{k}'$, via the momentum conservation condition.

Similarly one can describe the inelastic scattering by an R matrix. From Eq. (3) it is seen that, if

$$(\mathbf{k}_n,\mathbf{k}_p|R_{in}|\mathbf{k}_0,0)=-i\int\int d\mathbf{r}_nd\mathbf{r}_p\varphi_{\mathbf{k}_p}{}^*(\mathbf{r}_p)e^{-i\mathbf{k}_n\cdot\mathbf{r}_n}V(\mathbf{r}_n-\mathbf{r}_p)\Psi(\mathbf{r}_n,\mathbf{r}_p), \quad (9)$$

then the cross section for emission of the proton into $d\mathbf{k}_p$ while the neutron emerges in $d\mathbf{k}_n$ is

$$\sigma_{in}d\mathbf{k}_nd\mathbf{k}_p=2\pi/\hbar v_0|(\mathbf{k}_n,\mathbf{k}_p|R_{in}|\mathbf{k}_0,0)|^2\times\delta(E_n+E_p-E_0)d\mathbf{k}_nd\mathbf{k}_p \quad (10)$$

with no condition of momentum conservation. Replacing Ψ by Ψ_a, it follows from the definition (5) that

$$(\mathbf{k}_n,\mathbf{k}_p|R_{in}|\mathbf{k}_0,0)\approx\int\int d\mathbf{k}_p'd\mathbf{k}_p{}^0g_{\mathbf{k}_p}{}^*(\mathbf{k}_p')(\mathbf{k}_n,\mathbf{k}_p'|R_{np}|\mathbf{k}_0,\mathbf{k}_p{}^0)g_0(\mathbf{k}_p{}^0) \quad (11a)$$

$$=\int d\mathbf{k}_p'g_{\mathbf{k}_p}{}^*(\mathbf{k}_p')\left(\frac{\mathbf{k}_n-\mathbf{k}_p'}{2}|r_{np}|\frac{\mathbf{k}_0-\mathbf{k}_p{}^0}{2}\right)g_0(\mathbf{k}_p{}^0), \quad (11b)$$

where

$$g_{\mathbf{k}_p}(\mathbf{k}_p')=(1/2\pi)^{\frac{3}{2}}\int d\mathbf{r}_pe^{-i\mathbf{k}_p'\cdot\mathbf{r}_p}\varphi_{\mathbf{k}_p}(\mathbf{r}_p),$$

and in (11b), $\mathbf{k}_p{}^0=\mathbf{k}_n+\mathbf{k}_p'-\mathbf{k}_0$.

Equation (11a) is the formal expression of the impulse approximation as applied to inelastic scattering. Replacement of $g_{\mathbf{k}_p}{}^*(\mathbf{k}_p')$ by $g_0{}^*(\mathbf{k}_p')$ would give the expression for elastic scattering.[1] One further step is desirable to complete the phenomenological theory; the n–p scattering amplitude should be taken outside the integral. This is possible if one of two conditions is satisfied. (1) If v_{np} varies only a little over the important range of $\mathbf{k}_p'$ it is legitimate to replace it by the value it takes where $g_{\mathbf{k}_p}{}^*(\mathbf{k}_p')$ is singular, which will always be at $\mathbf{k}_p'=\mathbf{k}_p$. (2) If r_{np} depends only on the *difference* of initial and final relative momenta, rather than on the individual values, then it is independent of $\mathbf{k}_p'$. For $\frac{1}{2}(\mathbf{k}_n-\mathbf{k}_p')-\frac{1}{2}(\mathbf{k}_0-\mathbf{k}_p{}^0)=\mathbf{k}_n-\mathbf{k}_0$ in virtue of momentum conservation. There are experimental and theoretical reasons for expecting one or both of these conditions to be well satisfied in the n–d problem. They will be discussed later in the actual calculation.

It is asserted therefore that the scattering amplitude for the three-body problem may be approximated by the product of two factors, each of which has to do with a two-body problem:

$$(\mathbf{k}_n,\mathbf{k}_p|R_{in}|\mathbf{k}_0,0)\approx\left(\frac{\mathbf{k}_n-\mathbf{k}_p}{2}|r_{np}|\frac{\mathbf{k}_0-(\mathbf{k}_n+\mathbf{k}_p-\mathbf{k}_0)}{2}\right)\times\int d\mathbf{k}_p'g_{\mathbf{k}_p}{}^*(\mathbf{k}_p')g_0(\mathbf{k}_n+\mathbf{k}_p'-\mathbf{k}_0). \quad (12)$$

This factorization allows one to hope that the results of the three-body scattering experiment may be analyzable in terms of two-body scattering at the same energy.

It is interesting that the form (12) is exactly that deduced by Fermi[8] from somewhat different arguments to describe the scattering of slow neutrons by molecularly bound protons. The equivalence is more obvious if the integrand of the second factor of (12) is written in configuration space:

$$\int d\mathbf{k}_p'g_{\mathbf{k}_p}{}^*(\mathbf{k}_p')g_0(\mathbf{k}_n+\mathbf{k}_p'-\mathbf{k}_0)=\int d\mathbf{r}_p\varphi_{\mathbf{k}_p}{}^*(\mathbf{r}_p)e^{-i(\mathbf{k}_n-\mathbf{k}_0)\cdot\mathbf{r}_p}\varphi_0(\mathbf{r}_p).$$

In Fermi's case, r_{np} is a constant, proportional to the so-called scattering length. In the forthcoming general discussion of the impulse approximation, the relation of these two problems will be made clear.

III. APPLICATION OF THE METHOD TO THE NEUTRON-DEUTERON PROBLEM

The arguments of the preceding section will be generalized now to apply to the case of inelastic neutron-deuteron scattering. The additional complications are fourfold. In the first place, the initial binding center is not infinitely heavy. It is well known that this can be accounted for by a center-of-mass transformation in conventional treatments. The approach used here likewise encounters no difficulty. In the second place, the incident neutron interacts both with the proton and with the proton's binding center, i.e., the other neutron. This will introduce into the expressions analogous to (3) and (9) two sources of scattering which are propor-

[8] E. Fermi, Ricerca Scient. VII–II, 13 (1936).

tional to $[V_{np}(\mathbf{r}_1-\mathbf{r}_p)+V_{nn}(\mathbf{r}_1-\mathbf{r}_2)]\Psi(\mathbf{r}_1, \mathbf{r}_2, \mathbf{r}_p)$ if $\mathbf{r}_1$ is the coordinate of the incident neutron and $\mathbf{r}_2$ that of the initially bound neutron. The approximation now is to assume that when $\mathbf{r}_1$ is close to $\mathbf{r}_p$ the wave function has the form

$$\Psi_a^{np}=\int\int d\mathbf{k}_p d\mathbf{k}_2 G_0(\mathbf{k}_p, \mathbf{k}_2) e^{i\mathbf{k}_2\cdot\mathbf{r}_2}\psi_{\mathbf{k}_0, \mathbf{k}_p}^{np}(\mathbf{r}_1, \mathbf{r}_p),$$

where

$$G_0(\mathbf{k}_p, \mathbf{k}_2)=(1/2\pi)^{7/2}\int\int d\mathbf{r}_p d\mathbf{r}_2 \times e^{-i(\mathbf{k}_p\cdot\mathbf{r}_p+\mathbf{k}_2\cdot\mathbf{r}_2)}\varphi_0(\mathbf{r}_p-\mathbf{r}_2)$$
$$=\delta(\mathbf{k}_p+\mathbf{k}_2)g_0\left(\frac{\mathbf{k}_p-\mathbf{k}_2}{2}\right)$$

$\varphi_0(\mathbf{r}_p-\mathbf{r}_2)$ being the deuteron wave function and g_0 its Fourier transform. On the other hand, when $\mathbf{r}_1$ is close to $\mathbf{r}_2$, a superposition of neutron-neutron scattering functions will be used. The essence of this approximation is thus to ignore the perturbation of the wave function at one of the two scattering centers which is induced by the other center. Its validity rests on the smallness of the high energy two-body scattering amplitudes in comparison to the dimensions of the deuteron.

A little forethought will reveal that a straightforward application of the procedure outlined in Section II with this approximate function will give a recipe for calculating inelastic n–d scattering which is not quite self-consistent. Forgetting the Pauli principle and spin, for a moment, and labeling the final momentum of the incident neutron by $\mathbf{k}_1$ and that of the initially bound neutron by $\mathbf{k}_2$, the formula analogous to (11a) will be

$$(\mathbf{k}_1, \mathbf{k}_2, \mathbf{k}_p|R_{in}|\mathbf{k}_0, 0)$$
$$\approx\int\int\int\int d\mathbf{k}_p' d\mathbf{k}_2' d\mathbf{k}_p^0 d\mathbf{k}_2^0 G_{\mathbf{k}_p, \mathbf{k}_2}^*(\mathbf{k}_p', \mathbf{k}_2')$$
$$\times\{(\mathbf{k}_1, \mathbf{k}_p'|R_{np}|\mathbf{k}_0, \mathbf{k}_p^0)\delta(\mathbf{k}_2'-\mathbf{k}_2^0)$$
$$+(\mathbf{k}_1, \mathbf{k}_2'|R_{nn}|\mathbf{k}_0, \mathbf{k}_2^0)\delta(\mathbf{k}_p'-\mathbf{k}_p^0)\}G_0(\mathbf{k}_p^0, \mathbf{k}_2^0), \quad (13)$$

where $G_{\mathbf{k}_p, \mathbf{k}_2}(\mathbf{k}_p', \mathbf{k}_2')$ is the Fourier transform of the final continuum deuteron wave function. The inconsistency becomes apparent if we formally insert the additional factors $\delta(\mathbf{k}_1-\mathbf{k}_1')$ and $\delta(\mathbf{k}_0-\mathbf{k}_1^0)$ and integrate over $d\mathbf{k}_1'$ and $d\mathbf{k}_1^0$. This does not change the value of the integral but it allows the following rather obvious interpretation: One starts with a wave function, expressed in momentum space, which is $\delta(\mathbf{k}_1^0-\mathbf{k}_0)\times G_0(\mathbf{k}_p^0, \mathbf{k}_2^0)$ and which represents a free neutron with momentum $\mathbf{k}_0$ and a deuteron at rest in its ground state. The matrix $R_{np}+R_{nn}$ operates on this state (the integration over $\mathbf{k}_1^0$, $\mathbf{k}_2^0$, $\mathbf{k}_p^0$), producing a scattered wave which must then be resolved into its component parts. The resolution is carried out by computing the overlap of the outgoing wave with $G_{\mathbf{k}_2, \mathbf{k}_p}(\mathbf{k}_2', \mathbf{k}_p')\times\delta(\mathbf{k}_1'-\mathbf{k}_1)$, a function which takes into account the interaction between the two particles of which originally the deuteron was composed but not the interaction between the incident particle and either of the other two. The interaction with the proton is presumably already included in the matrix R_{np} and that with the neutron is in R_{nn}, but in each of the two terms the interaction of one of the three pairs of particles in the final state is omitted. Now it is obvious that one pair must be omitted if one is to avoid solution of a three-body problem, and in the spirit of the approximation which is being made such an omission is consistent. However for reasons of common sense, it seems that the following recipe is more appropriate than that expressed by (13): In resolving the scattered wave generated by R_{np}, compute the overlap integral with *either* $G_{\mathbf{k}_2, \mathbf{k}_p}(\mathbf{k}_2'-\mathbf{k}_p')\delta(\mathbf{k}_1'-\mathbf{k}_1)$ *or* $G_{\mathbf{k}_1, \mathbf{k}_2}(\mathbf{k}_1', \mathbf{k}_2')\delta(\mathbf{k}_p'-\mathbf{k}_p)$ according to whether $|\mathbf{k}_p-\mathbf{k}_2|$ or $|\mathbf{k}_1-\mathbf{k}_2|$ is the smaller. In other words, take into account that interaction which is the stronger. Because of conservation of energy and momentum $|\mathbf{k}_p-\mathbf{k}_2|$ and $|\mathbf{k}_1-\mathbf{k}_2|$ cannot *both* be small. If they are nearly equal then they must be sufficiently large that both pairs of interactions are negligible. In resolving the wave generated by R_{nn} a similar choice should be made, based on the relative magnitudes of $|\mathbf{k}_p-\mathbf{k}_2|$ and $|\mathbf{k}_p-\mathbf{k}_1|$.

The final two additional complications possessed by the actual n–d problem are the spin degrees of freedom and the identity of the two neutrons. Spin variables must be included in the arguments of initial and final wave functions and also in the matrices R_{nn} and R_{np}, and summations over spin must be added to the integrations over momenta. The Pauli principle is satisfied by antisymmetrizing the scattering matrix in the neutron variables.

If the combined momentum and spin variables $\mathbf{k}_i$, σ_i of a particle i be designated by ξ_i and a summation over ξ_i understood to include integration over continuous momentum variables, then according to the above arguments the complete unsymmetrized matrix for n–d inelastic scattering is to be written as follows

$$(\xi_1, \xi_2, \xi_p|R_{in}|\xi_0, \xi_0^D)=\sum_{\xi_1', \xi_2', \xi_p'}\sum_{\xi_1^0, \xi_2^0, \xi_p^0}\{H_{\xi_p\xi_1, \xi_2}^*(\xi_p', \xi_1', \xi_2')(\xi_1', \xi_p'|R_{np}|\xi_1^0, \xi_p^0)\delta_{\xi_2', \xi_2^0}$$
$$+H_{\xi_1\xi_2, \xi_p}(\xi_p', \xi_1', \xi_2')(\xi_1', \xi_2'|R_{nn}|\xi_1^0, \xi_2^0)\delta_{\xi_p', \xi_p^0}\}H_0(\xi_1^0, \xi_2^0, \xi_p^0). \quad (14)$$

In this formula,

$$H_0(\xi_1^0, \xi_2^0, \xi_p^0)=\delta_{\xi_1^0, \xi_0}G_{\xi_0^D}(\xi_2^0, \xi_p^0),$$

where ξ_0 represents the momentum and spin of the incident neutron, and $G_{\xi_0^D}$ is the wave function (in spin-momentum space) of a deuteron at rest with a

well-defined spin. The other symbol requiring definition is

$$H_{\xi_1\xi_p,\,\xi_2}(\xi_1',\,\xi_2',\,\xi_p') = \delta_{\xi_1',\,\xi_1} G_{\xi_p,\,\xi_2}(\xi_2',\,\xi_p') \quad \text{if } |\mathbf{k}_2-\mathbf{k}_p| < |\mathbf{k}_2-\mathbf{k}_1|$$
$$= \delta_{\xi_p',\,\xi_p} G_{\xi_1,\,\xi_2}(\xi_1',\,\xi_2') \quad \text{if } |\mathbf{k}_2-\mathbf{k}_p| > |\mathbf{k}_2-\mathbf{k}_1|$$

etc., where, for example $G_{\xi_1,\,\xi_2}(\xi_1',\,\xi_2')$ is the continuum wave function of two neutrons, normalized on the energy shell to $\xi_{\xi_1',\,\xi_1}\delta_{\xi_2',\,\xi_2}$ plus outgoing waves.

This recipe is quite complicated, but from the conventional point of view, in which one assumes that he knows the nature of the two-body interactions, the recipe can in principle be carried out. It contains nothing but the solutions of two-body problems. However, the integrations indicated would be hopelessly tedious if one could not neglect the variation of the R matrices and take them outside the integrals. The latter simplification is certainly essential if we wish to reverse the usual procedure and deduce two-body R matrices from the experimentally observed three-body scattering. It is difficult to make a general argument justifying this approximation which will apply to all terms. It turns out, however, that for all important terms, one or both of the criteria stated at the end of Section II are reasonably well satisfied.

The formulation of (14) is general enough to include any kind of two-body forces, but the very generality conceals most of the physically interesting features of the problem. Therefore it is now proposed to restrict attention to central forces so that spin is independently conserved in the scattering. Tensor forces very likely are important in high energy phenomena; but past experience indicates that most conclusions about scattering, which can be reached from consideration of central forces only, except those which specifically have to do with interchange of spin and orbital angular momentum, also turn out to be true with tensor forces. In the hope that future work will confirm this feature for the present case, and because something is to be learned even if the assumption is incorrect, the remainder of this first paper, and all of the second one, will refer to central forces only. It will be evident, however, that the forces need not be derivable from static potentials.

IV. THE CENTRAL FORCE PROBLEM

With no coupling between spin and orbital angular momentum, the total spin and also the z-component of spin will be constants of the motion. Therefore, instead of considering all six possible initial spin functions and eight possible final spin functions, it suffices to consider two initial states, one quartet and one doublet, and three final, one quartet, and two doublet. These spin states have been discussed by Ashkin and Wu[3] and we depart from their scheme in only one respect. Whereas the initial doublet state for a given z-component of total spin is unique because of the requirement of symmetry in the spins of the two particles making up the deuteron, the final doublet state for the same z-component is twofold degenerate. Ashkin and Wu resolved the degeneracy according to the spin symmetry of the two particles which originally formed the deuteron. Here the degeneracy will be resolved according to the spin symmetry of the two neutrons.

There are three essential scattering amplitudes to compute and these will be designated as follows, departing from the general notation of formula (14). $(\mathbf{k}_1, \mathbf{k}_2, \mathbf{k}_p|\,{}^4R_{in}{}^S|\,\mathbf{k}_0, 0)$ will be the non-antisymmetrized matrix for inelastic scattering in a quartet state. The latter is symmetric in the spins of the two neutrons, as indicated by the superscript S. Now ${}^4R_{in}{}^S$ must contain the factor $\delta(\mathbf{k}_1+\mathbf{k}_2+\mathbf{k}_p-\mathbf{k}_0)$, so let the co-factor of this delta-function be designated by $(\mathbf{k}_{12}, \mathbf{k}_p|\,{}^4r_{in}{}^S|\,\mathbf{k}_0, 0)$, where $\mathbf{k}_{12}=\frac{1}{2}(\mathbf{k}_1-\mathbf{k}_2)$. Then the cross section for quartet inelastic scattering is given by

$${}^4\sigma_{in}d\mathbf{k}_p d\mathbf{k}_{12} = 2\pi/\hbar v_0 |\,(\mathbf{k}_{12}, \mathbf{k}_p|\,{}^4r_{in}{}^S|\,\mathbf{k}_0, 0) - (\mathbf{k}_{21}, \mathbf{k}_p|\,{}^4r_{in}{}^S|\,\mathbf{k}_0, 0)|^2 \times\delta(E_1+E_2+E_p-E_0)d\mathbf{k}_p d\mathbf{k}_{12}, \quad (15)$$

where

$$E_1+E_2=\hbar^2/4m(\mathbf{k}_0-\mathbf{k}_p)^2+\hbar^2/mk_{12}{}^2,$$

since $\mathbf{k}_1+\mathbf{k}_2=\mathbf{k}_0-\mathbf{k}_p$, and

$$E_p=\hbar^2/2mk_p{}^2, \quad E_0=\hbar^2/2mk_0{}^2-B.$$

The choice of final variables to be $\mathbf{k}_p$ and $\mathbf{k}_{12}$ is made because the proton momentum is the experimental quantity most likely to be measured.

For the doublet case there will be two distinct matrices, corresponding to final states symmetric and antisymmetric in the neutron spins. These will be designated by ${}^2R_{in}{}^S$ and ${}^2R_{in}{}^A$, respectively. Following the same convention as above, the doublet cross section will then be

$${}^2\sigma_{in}d\mathbf{k}_p d\mathbf{k}_{12} = 2\pi/\hbar v_0\{|\,(\mathbf{k}_{12}, \mathbf{k}_p|\,{}^2r_{in}{}^S|\,\mathbf{k}_0, 0) - (\mathbf{k}_{21}, \mathbf{k}_p|\,{}^2r_{in}{}^S|\,\mathbf{k}_0, 0)|^2 + |\,(\mathbf{k}_{12}, \mathbf{k}_p|\,{}^2r_{in}{}^A|\,\mathbf{k}_0, 0) + (\mathbf{k}_{21}, \mathbf{k}_p|\,{}^2r_{in}{}^A|\,\mathbf{k}_0, 0)|^2\} \times\delta(E_1+E_2+E_p-E_0)d\mathbf{k}_p d\mathbf{k}_{12}. \quad (16)$$

The average cross section for unpolarized scattering would be given by two-thirds of (15) plus one-third of (16), the respective statistical weights of the quartet and doublet states.

The recipe stated in Section III permits an unambiguous calculation of the three required inelastic matrices in terms of the four two-body matrices which describe n–p and n–n scattering in triplet and in singlet states. In all cases, the two-body matrices will be taken outside the momentum integrals and evaluated at the final observed values of the momenta. To save space, the following shorthand notation for the two-body

matrices will be used:

$$\left(\mathbf{k}_{1p}|r_{np}{}^{t}|\frac{\mathbf{k}_0+\mathbf{k}_2}{2}\right)=r_{1p}{}^{t},$$
$$\left(\mathbf{k}_{1p}|r_{np}{}^{s}|\frac{\mathbf{k}_0+\mathbf{k}_2}{2}\right)=r_{1p}{}^{s},$$
$$\left(\mathbf{k}_{12}|r_{nn}{}^{t}|\frac{\mathbf{k}_0+\mathbf{k}_p}{2}\right)=r_{12}{}^{t},\tag{17}$$
$$\left(\mathbf{k}_{12}|r_{nn}{}^{s}|\frac{\mathbf{k}_0+\mathbf{k}_p}{2}\right)=r_{12}{}^{s}.$$

The superscripts t and s refer to triplet and singlet two-body interactions. This notation is really unambiguous since only these combinations of initial and final momenta, except for interchange of $\mathbf{k}_1$ and $\mathbf{k}_2$ can ever occur.

As an example of the procedure of calculation, consider the simplest case, the quartet, which is totally symmetric in all three spins. Only the triplet two-body interactions enter and no spin changes are induced. Because of the criteria for taking account of final state interactions the terms generated by R_{np} must be considered separately from those generated by R_{nn}. The contribution of the n–p interaction to ${}^{4}R_{in}{}^{S}$ is as follows, for $k_{2p}>k_{21}$:

$$\delta(\mathbf{k}_1+\mathbf{k}_2+\mathbf{k}_p-\mathbf{k}_0)\int d\mathbf{k}_{21}'g_{k_{21}{}^{t*}}(\mathbf{k}_{21}')$$
$$\times\left(\frac{\mathbf{k}_1-\mathbf{k}_p}{2}+\frac{\mathbf{k}_{21}'-\mathbf{k}_{21}}{2}|r_{np}{}^{t}|\frac{\mathbf{k}_0+\mathbf{k}_2}{2}-\frac{\mathbf{k}_{21}'-\mathbf{k}_{21}}{2}\right)$$
$$\times g_0\left(\frac{\mathbf{k}_0-\mathbf{k}_p}{2}+\mathbf{k}_{21}'\right).\tag{18}$$

This term corresponds to the case in which the incident neutron transfers most of its momentum to the proton so that in the final state the two neutrons are the most strongly interacting pair. The function $g_{k_{12}{}^{t}}(\mathbf{k}_{12}')$ is the triplet relative wave function (not antisymmetrized) in momentum space of two neutrons with relative momentum $\mathbf{k}_{12}$.

There are several reasons for thinking that the matrix $r_{np}{}^{t}$ which appears under the integral sign, does not in fact depend appreciably on $\mathbf{k}_{12}'$. If $\mathbf{k}_{12}$ corresponds to a relative energy greater than about 10 Mev, $g_{k_{12}{}^{t}}(\mathbf{k}_{12}')\approx\delta(\mathbf{k}_{12}'-\mathbf{k}_{12})$, so that the peak of the integrand occurs in a region in which the dependence of $r_{np}{}^{t}$ on $\mathbf{k}_{12}'$ vanishes. If k_{12} is small, this will usually be because both k_1 and k_2 are small. Energy and momentum conservation, together with the character of the function g_0, which is appreciable only for small arguments, make it very unlikely that as a consequence of an n–p collision the two neutrons should go off with high but equal momenta. This is also rather obvious physically, since neutron number two has no way to acquire a high velocity. Now if k_1 and k_2 are both small, then $\mathbf{k}_p$ must be large and will dominate the final argument of $r_{np}{}^{t}$. The initial argument is likewise dominated by $\mathbf{k}_0$, so that again $\mathbf{k}_{21}'$ plays only a small role. A different argument may be based on the experimentally observed fact[2] that for large momentum transfers $r_{np}{}^{t}$ depends much more sensitively on the sum of initial and final relative momenta than on the difference. The reverse appears to be true for small momentum transfers. Taking the sum of initial and final relative momenta in (18) just cancels out the dependence on $\mathbf{k}_{21}'$; and it turns out that when $k_{2p}<k_{21}$ (which corresponds to small momentum transfers), taking the difference would cancel out the dependence on $\mathbf{k}_{2p}'$, the variable of integration in that case.

Similar arguments can be made for the terms generated by the n–n interaction, so that in general, the removal of the two-body scattering matrices from the integrals is well justified. In the special case of (18), this leads to

$$\delta(\mathbf{k}_1+\mathbf{k}_2+\mathbf{k}_p-\mathbf{k}_0)r_{1p}{}^{t}$$
$$\times\int d\mathbf{k}_{21}'g_{k_{21}{}^{t*}}(\mathbf{k}_{21}')g_0\left(\frac{\mathbf{k}_0-\mathbf{k}_p}{2}+\mathbf{k}_{21}'\right).\tag{19}$$

Overlap integrals, such as that which appears in (19), will appear in every term of the complete matrix. It is therefore appropriate to introduce another abbreviation as follows:

$$I_{21}{}^{t}=\int d\mathbf{k}_{21}'g_{k_{21}{}^{t*}}(\mathbf{k}_{11}')g_0(\mathbf{k}_{0p}+\mathbf{k}_{21}')$$
$$=\int d\mathbf{r}\,\varphi_{k_{21}{}^{t*}}(\mathbf{r})e^{-i\mathbf{k}_{0p}\cdot\mathbf{r}}\varphi_0(\mathbf{r}),\tag{20}$$

where $\varphi_{k_{21}{}^{t}}(\mathbf{r})$ is the relative wave function of the two neutrons in configuration space. The other integrals will be designated by $I_{21}{}^{s}$, $I_{p2}{}^{t}$, $I_{p2}{}^{s}$, $I_{p1}{}^{t}$, etc., where the subscript identifies the pair of particles whose final interaction is being accounted for and the superscript gives their spin. If the pair ij is being considered, then the momentum occurring in the exponential of the configuration space integral is always $\frac{1}{2}(\mathbf{k}_i+\mathbf{k}_j)$, so that additional indices are unnecessary.

It is clear, then, that the complete inelastic scattering matrix can be expressed as a sum of products of the type, $r_{1p}{}^{t}I_{21}{}^{t}$. The origin of each term will be indicated by the superscripts and subscripts. This particular one, for instance, comes from a collision in the triplet state between neutron number one and the proton, leaving neutron number one with the smaller final momentum and in a triplet state with respect to neutron number two.

Evaluation of this sum of products is merely a matter

of bookkeeping and only the results will be given here.

$$(\mathbf{k}_{12}, \mathbf{k}_p|\,{}^4r_{in}{}^S|\,k_0, 0)=\begin{Vmatrix} r_{1p}{}^t & I_{21}{}^t \\ r_{1p}{}^t & I_{2p}{}^t \end{Vmatrix}+\begin{Vmatrix} r_{12}{}^t & I_{p2}{}^t \\ r_{12}{}^t & I_{p1}{}^t \end{Vmatrix}$$

$$(\mathbf{k}_{12}, \mathbf{k}_p|\,{}^2r_{in}{}^S|\,\mathbf{k}_0, 0)$$

$$=\begin{Vmatrix} -\frac{1}{4}(r_{1p}{}^t-3r_{1p}{}^s)I_{21}{}^t \\ \frac{1}{8}(r_{1p}{}^t+3r_{1p}{}^s)I_{2p}{}^t-\frac{3}{8}(r_{1p}{}^t-r_{1p}{}^s)I_{2p}{}^s \end{Vmatrix}$$

$$+\begin{Vmatrix} \frac{1}{8}(r_{12}{}^t+3r_{12}{}^s)I_{p2}{}^t+\frac{3}{8}(r_{12}{}^t-r_{12}{}^s)I_{p2}{}^s \\ \frac{1}{8}(r_{12}{}^t+3r_{12}{}^s)I_{p1}{}^t+\frac{3}{8}(r_{12}{}^t-r_{12}{}^s)I_{p1}{}^s \end{Vmatrix}, \quad (21)$$

$$(\mathbf{k}_{12}, \mathbf{k}_p|\,{}^2r_{in}{}^A|\,\mathbf{k}_0, 0)$$

$$=\begin{Vmatrix} \sqrt{3}/4(r_{1p}{}^t+r_{1p}{}^s)I_{21}{}^s \\ \sqrt{3}/8(r_{1p}{}^t+3r_{1p}{}^s)I_{2p}{}^t+\sqrt{3}/8(r_{1p}{}^t-r_{1p}{}^s)I_{2p}{}^s \end{Vmatrix}$$

$$+\begin{Vmatrix} \sqrt{3}/8(r_{12}{}^t+3r_{12}{}^s)I_{p2}{}^t-\sqrt{3}/8(r_{12}{}^t-r_{12}{}^s)I_{p2}{}^s \\ \sqrt{3}/8(r_{12}{}^t+3r_{12}{}^s)I_{p1}{}^t-\sqrt{3}/8(r_{12}{}^t-r_{12}{}^s)I_{p1}{}^s \end{Vmatrix}.$$

Of the two alternatives within each bracket, that one is to be chosen which takes account of the strongest interaction between a final pair of particles. It can be verified quickly that in case both final interactions are negligible, the two alternatives are equal. For example if $\varphi_{\mathbf{k}_{21}{}^t}(\mathbf{r})\approx(1/2\pi)^{\frac{3}{2}}e^{i\mathbf{k}_{21}\cdot\mathbf{r}}$, then

$$I_{21}{}^t\approx(1/2\pi)^{\frac{3}{2}}\int d\mathbf{r}e^{-i(\mathbf{k}_2-\mathbf{k}_1/2)\cdot\mathbf{r}}e^{-i(\mathbf{k}_2+\mathbf{k}_1/2)\cdot\mathbf{r}}\varphi_0(\mathbf{r})$$

$$=(1/2\pi)^{\frac{3}{2}}\int d\mathbf{r}e^{-\mathbf{k}_2\cdot\mathbf{r}}\varphi_0(\mathbf{r})=g_0(\mathbf{k}_2).$$

$I_{21}{}^s$, $I_{21}{}^t$, $I_{2p}{}^s$ all approach this same limit, while $I_{p2}{}^t$, $I_{p2}{}^s$, $I_{p1}{}^t$, $I_{p1}{}^s$ all approach the limit $g_0(\mathbf{k}_p)$. The formulas (21) simplify in this limit to

$$(\mathbf{k}_{12}, \mathbf{k}_p|\,{}^4r_{in}{}^S|\,\mathbf{k}_0, 0)\approx r_{1p}{}^t g_0(\mathbf{k}_2)+r_{12}{}^t g_0(\mathbf{k}_p),$$

$$(\mathbf{k}_{12}, \mathbf{k}_p|\,{}^2r_{in}{}^S|\,\mathbf{k}_0, 0)\approx -\tfrac{1}{4}(r_{1p}{}^t-3r_{1p}{}^s)g_0(\mathbf{k}_2)$$

$$+\tfrac{1}{2}r_{12}{}^t g_0(\mathbf{k}_p), \quad (21a)$$

$$(\mathbf{k}_{12}, \mathbf{k}_p|\,{}^2r_{in}{}^A|\,\mathbf{k}_0, 0)\approx\sqrt{3}/4(r_{1p}{}^t+r_{1p}{}^s)g_0(\mathbf{k}_2)$$

$$+\sqrt{3}/2r_{12}{}^s g_0(\mathbf{k}_p).$$

V. SUMMARY

A formula (21) has been derived for the complete n–d inelastic scattering matrix in the case of central forces only. Properly antisymmetrized with respect to the neutron variables, this matrix leads to the corresponding cross section through formulas (15) and (16). The impulse approximation which is the basis of (21) is believed to be better than the usual Born approximation, depending on the large radius of the deuteron, the high incident velocity of the neutron, and the short range of nuclear forces, but not on the weakness of nuclear forces. Appearing in (21) are two kinds of quantities, each of which refers to a two-body problem. The first kind are n–p and n–n scattering matrices, evaluated for the initial and final momenta which occur in the three-body problem. The second kind are overlap integrals between final continuum wave functions and the initial deuteron function.

If the theory of nuclear forces were on a firm basis, as it may be someday, it would be a straightforward procedure to solve the required number of two-body problems and substitute into (21). At the present time, it is perhaps more sensible to adopt an empirical approach in terms of experimental values for the two-body scattering matrices. In the second part of this report, which will follow when experiments at Berkeley are complete and have been analyzed, this author will attempt such an approach. In particular, an effort will be made to derive information about the high energy n–n interaction from the experimental observations.

It might seem that the overlap integrals which occur in (21) would preclude the empirical approach, but this is not so. The asymptotic form of these integrals for high final relative momenta depends only on the deuteron wave function, as seen in (21a): and at low relative energies the perturbation is important only in the S part of the final wave function. Low energy S-state interactions are very reliably described by the empirical theory of the effective range,[9] so no essential difficulty need be encountered there. Trouble could come from interference terms in the n–d cross section, and one of the chief tasks of the second part of this report will be to show that these terms are actually not likely to be large for inelastic scattering.

Preliminary stages of this investigation were made in collaboration with Dr. M. L. Goldberger while he was at the Radiation Laboratory. During later stages Professor Serber and Professor Wick have given much help and encouragement for which the author is extremely grateful.

[9] H. A. Bethe, Phys. Rev. 76, 38 (1949); J. M. Blatt and J. D. Jackson, Phys. Rev. 76, 18 (1949); G. F. Chew and M. L. Goldberger, Phys. Rev. 75, 1637 (1949).

On Spin-Orbit Interactions and Nucleon-Nucleon Scattering

K. M. CASE AND A. PAIS
Institute for Advanced Study, Princeton, New Jersey
(Received June 20, 1950)

It is shown that one way of explaining the high energy proton-proton scattering data is by means of a spin-orbit coupling introduced into the nuclear interaction. The radial dependence of this coupling should be such that it has a strongly singular behavior at $r=0$ and a small tail. It seems feasible to retain the charge independence of nuclear forces for all energies explored so far. A possible connection with M. Mayer's interpretation of the shell model of heavy nuclei is indicated.

I. INTRODUCTION

THE experiments recently performed in Berkeley on the scattering of high energy neutrons and protons by protons show the following striking qualitative features, even when due account is taken of the present experimental uncertainties.

n-p Scattering

(*a*) The total cross section is "small." By this is meant that any n–p interaction which is made to fit the low energy data also describes the high energy scattering to a good approximation, provided the latter were essentially only due to S-wave scattering. In this way, one may, for example, account for about 90 percent of the 90-Mev n–p cross section,[1] while the 260-Mev data[2] still show a similar trend.

(*b*) The differential cross section $\sigma(\theta)$ in the center-of-mass system has a tendency toward symmetry around 90°. It is at present not quite clear to what extent this is true, especially as few data are available below about 40° scattering angle. Yet qualitatively this symmetry is rather unexpectedly marked from the point of view of any of the customary "symmetrical," "charged," or "neutral" phenomenological approaches.

p-p Scattering

(*a*) At 350 Mev the cross section is quite large. In fact $\sigma(90°)$ is from two to four times larger than the corresponding quantity for n–p scattering at the lower energy of 260 Mev.

(*b*) At 350 Mev $\sigma(\theta)$ is rather isotropic from 90° down to angles of approximately 20°. This contrasts with the marked anisotropy of the 260-Mev n–p data over the same angular region.

(*c*) At 30 Mev $\sigma(\theta)$, after a rapid decrease away from small angles due to Coulomb effects, rises again to reach a rather flat behavior around 90°.

These aspects of the nucleon-nucleon scattering are particularly interesting in that at first sight they would seem to indicate a sizable difference between the n–p and p–p interaction. This is in contradistinction to the well-known low energy charge independence, according to which the n–p and p–p forces are the same in identical states; i.e., the ${}^1S$, ${}^3P$, ${}^1D\cdots n$–p forces should be the same as those for the p–p system. (Of course at these low energies only S scattering occurs.)

To see this, we first consider the theory of the n–p scattering given by Christian and Hart.[1] Using a mixture of central and tensor forces adapted to the low energy data, they propose an exchange dependence of such a kind that the interaction is zero (or very small) in states of odd orbital angular momentum L. This proposal, made by Serber, will in the following be referred to as the "even-theory." In this way the P phases, next largest to the S phases, are suppressed. This leads to the desired effects both of small σ as well as to symmetry around 90°, there being no interference between waves of even and odd L. As central forces give (for high energies) a negligible contribution at 90°, the large angle scattering is here entirely due to the tensor force acting in even triplet states. Now these states drop out in the p–p interaction, so that it is clear that the even-theory applied to p–p scattering would give a $\sigma(90°)$ of an order of magnitude smaller than that for the n–p case, in conflict with the experimental findings mentioned above. Moreover, the even-theory would not yield the observed p–p angular distribution at 30 Mev. In fact, due to the interference of singlet S- and D-waves, it would lead to a $\sigma(\theta)$ rising away from 90°.

An interpretation of the p–p data has been given by Christian and Noyes.[3] Renouncing charge independence, they introduce a strongly singular tensor force for the p–p system. This non-central coupling enables them to mask the drop in $\sigma(\theta)$ toward 90° at 30 Mev. Furthermore, the p–p tensor force is more strongly singular than is the Yukawa-type tensor force used in the above n–p interpretation. Hence, more high frequency Fourier components are present so that the possibility of relatively large momentum transfers exists. In this way the high 90° p–p scattering can be accounted for.

It may directly be remarked here that, whatever interpretation one is aiming at, the presence of a

[1] R. S. Christian and E. W. Hart, Phys. Rev. **77**, 441 (1950). This paper contains the experimental results for 40- and 90-Mev scattering.

[2] Communicated to us by Dr. Christian to whom we are greatly indebted for this, as well as other, information on the work performed in Berkeley. We also wish to thank Professor H. Feshbach for informing us of his work on the potential constants of the n–p interaction.

[3] Most of the data are taken from R. Christian and H. P. Noyes report, Phys. Rev. **79**, 85 (1950).

strongly singular force which is more effective for p–p than for n–p scattering seems to be a fact which is hard to escape on the basis of the present data. Another way of introducing such a singular force between protons has been suggested and analyzed by Jastrow.[4] It consists in assuming the nuclear p–p attraction to go over into a very strong repulsion at distances of about $0.6\cdot10^{-13}$ cm. As a consequence, high Fourier components are again provided to account for the high cross section at 350 Mev, while a resulting decrease in the ^1D phase at 30 Mev tends to flatten the cross section for this energy around 90°.

It is the aim of this paper to present an alternative qualitative interpretation of the scattering data; *viz.*, by the introduction of a spin-orbit coupling of the type familiar from atomic interactions:

$$V(r)\cdot(\mathbf{L}\cdot\mathbf{S}),\quad \mathbf{S}=\boldsymbol{\sigma}^{(1)}+\boldsymbol{\sigma}^{(2)} \tag{1}$$

where S is twice the spin operator of the two-body system and L its relative orbital angular momentum vector. Again, $V(r)$ has to be strongly singular (Eq. (18)).

As will be shown in the following, it would seem to be feasible to obtain a charge independent phenomenological description of nuclear forces for all energies explored so far. This is possible, despite the dissimilarity in the observed cross sections. Indeed, there are extra states present for the n–p system that do not occur in the case of similar particles. Thus, forces in the ^3S, ^1P, $^3D\cdots$ states may, at sufficiently high energy have considerable influence on n–p scattering, without affecting the corresponding p–p case. Second, owing to the Pauli principle, states of interest for p–p scattering are weighted differently in the n–p cross section. It will turn out in the subsequent sections that these two circumstances still give sufficient leeway to allow at least qualitatively for charge independence. In this connection it should also be noted that Jastrow's hard core model can be reconciled in principle with charge independence by appropriately choosing the exchange dependence of the forces involved.[4]

The condition of charge independence for all energies is a suggestive requirement in view of the close similarity of n–p and p–p interactions in the ^1S states, deduced from low energy scattering. Such a generalization is a reasonable extrapolation from the little that is known of nuclear forces. However this may be, the main interest in a phenomenological approach to nuclear forces lies in testing heuristic principles which might be a guide in the search for a satisfactory field theory. It must be remembered though that charge independence cannot be considered as imposed at the outset, either from the available experimental evidence or from first principles, which are now notoriously inadequate.

It should be mentioned that all forces which will be considered in the present investigation are of a type compatible with present field theories. Thus, the existence of a spin-orbit coupling (1) is to be expected as a Thomas effect accompanying static forces. However, it will be seen in the next section that we actually need a stronger coupling than that predicted as a Thomas phenomenon. Such stronger LS interactions are not irreconcilable with present theoretical views.[5] It may furthermore be remarked that a strong LS coupling might be of help in explaining the spin-orbit interactions in heavier nuclei postulated by M. Mayer[6] (Section IV(a)).

It has been pointed out by Wigner and Eisenbud[7] that LS coupling is not the only conceivable spin-orbit interaction in the nuclear two-body problem. In fact, one can have also interactions proportional to

$$\mathbf{L}\cdot(\boldsymbol{\sigma}^{(1)}-\boldsymbol{\sigma}^{(2)}),\quad \text{or}\quad \mathbf{L}\cdot(\boldsymbol{\sigma}^{(1)}\times\boldsymbol{\sigma}^{(2)}) \tag{2}$$

which, however, can be effective only between nucleons in different charge states. Thus, they cannot contribute to the p–p interaction which we have seen to be the primary cause for exploring modifications of the more customarily examined interactions.

Our program will now be as follows. First we shall examine the main qualitative features of an LS interaction (Section II), then we shall show that by superimposing this coupling on an interaction like that used in the even theory of n–p forces, one can understand the qualitative features of p–p scattering (Section III). Thereupon, we will investigate the charge independent features of this interaction and will see that, within the experimental uncertainties, the introduction of the additional LS coupling in the n–p interaction does not spoil the qualitative agreement with experiment obtained by Christian and Hart using the even-theory solely (Section IV). In the course of this part of the work we shall need some formulas which are generalizations of the standard Faxén-Holtsmark results to the presence of LS interactions. These formulas will be derived in Appendix I.

[4] R. Jastrow, Phys. Rev. 79, 389 (1950). This possibility is also being investigated by N. Kroll.

[5] Thus, the vector meson theory with both vector and tensor coupling can give large LS interactions. See, e.g., B. Holmberg, Kungl. Fysiogr. Sällskapets Förh., Lundies 14, Nr. 22 (1944). L. Rosenfeld, Kgl. Dansk Vid, Selsk. Math.-Fys. Medd. 23, Nr. 13 (1945). Moreover, such effects can be expected from a theory consistently taking account of the reactive phenomena.

[6] M. Goeppert-Mayer, Phys. Rev. 75, 1969 (1949); 78, 16, 22 (1950); Haxel, Jensen, and Suess, Phys. Rev. 75, 1766 (1949). It should of course not be forgotten that one cannot, from a spin-orbit interaction in the many-body problem, uniquely infer back to such an interaction between pairs of nucleons. Thus, for example, also tensor forces in the two-particle coupling may lead to spin-orbit effects in heavy nuclei, see A. M. Feingold and E. Wigner, Phys. Rev. 79, 22 (1950).

[7] L. Eisenbud and E. Wigner, Proc. Nat. Acad. Wash. 27, 281 (1941). It is readily seen that the two interactions (2) are effectively equivalent.

II. QUALITATIVE FEATURES OF SCATTERING CROSS SECTIONS

Consider the two-nucleon Schroedinger equation in the center-of-mass system:

$$[(\hbar^2/M)\Delta+E-O^{(1)}(A_1+A_2\sigma^{(1)}\cdot\sigma^{(2)}+A_3S_{12})\times(\hbar^2/Mr_0^2)\phi_1(r/r_0)-O^{(2)}A_4\phi_2(r/r_0)\mathbf{L}\cdot\mathbf{S}(\hbar^2/Mr_0^2)]\psi=0, \quad (3)$$
$$S_{12}=3r^{-2}(\sigma^{(1)}\cdot\mathbf{r})(\sigma^{(2)}\cdot\mathbf{r})-\sigma^{(1)}\cdot\sigma^{(2)}.$$

Here $O^{(1,2)}$ express the exchange character of the forces involved; we take this, as well as the radial dependence, to be the same for central and tensor forces. We omit the Coulomb force between protons as this is irrelevant for the energies and angles with which we will be concerned.

Let

$$P_\sigma=\tfrac{1}{2}[1+\sigma^{(1)}\cdot\sigma^{(2)}], \quad P_\tau=\tfrac{1}{2}[1+\tau^{(1)}\cdot\tau^{(2)}],$$
$$P_x=\text{space exchange operator.}$$

Then we decompose $O^{(1)}$ as follows:

$$O^{(1)}=\tfrac{1}{2}(1-P_\sigma)(a_sP_\tau+b_s)+\tfrac{1}{2}(1+P_\sigma)(-a_tP_\tau+b_t), \quad (4)$$

$a_s, \cdots, b_t$ depend on the specific exchange type of the forces. In (4) the charge independence is manifest. We normalize these quantities such that

$$a_s+b_s=1, \quad a_t+b_t=-3. \quad (5)$$

Then for the ^1S state, $O^{(1)}=1$, for the ^3S state, $O^{(1)}=-3$. In particular we have for the even-theory

$$a_s=b_s=\tfrac{1}{2}, \quad a_t=b_t=-\tfrac{3}{2}. \quad (6)$$

A decomposition of the type (4) need not be made for $O^{(2)}$, as the LS coupling vanishes in singlet states. Taking into account the exclusion principle we may therefore write

$$O^{(2)}=-\alpha P_\tau+\beta=\alpha P_x+\beta. \quad (7)$$

Introducing r_0 as unit of length and putting $r=xr_0$, (3) becomes

$$[\Delta+k^2-O^{(1)}(A_1+A_2\sigma^{(1)}\sigma^{(2)}+A_3S_{12})\phi_1(x)-O^{(2)}A_4\phi_2(x)\mathbf{LS}]\psi=0,$$
$$k=(ME_0r_0^2/2\hbar^2)^{\frac{1}{2}};$$

E_0 is the energy of the incident particle in the laboratory system.

Now it is clear that spin-orbit effects vanish in S states, so that the low energy data, due to $A_{1,2,3}$ can be taken over without modification.[8] We have therefore only to consider triplet states, $L>0$ in dealing with the A_4 term.

As a first orientation we consider its effect in the Born approximation in which no interference occurs with the scattering due to central and tensor forces. That this is so follows from

$$(\mathbf{L}\cdot\mathbf{S})_{Av}=0, \quad \{(\mathbf{L}\cdot\mathbf{S})(\sigma^{(1)}\cdot\mathbf{r})(\sigma^{(2)}\cdot\mathbf{r})\}_{Av}=0, \quad (8)$$

where Av means an averaging over the initial and a summation over the final spin states. In our units the LS-contribution to the n–p cross section is

$$d\sigma_{LS}^{np}=(r_0/4\pi)^2A_4^2\left|\int\exp(-i\mathbf{k}'\cdot\mathbf{x})(\alpha P_x+\beta)\times\phi_2(x)\mathbf{L}\cdot\mathbf{S}\exp(i\mathbf{k}\cdot\mathbf{x})d\mathbf{x}\right|^2_{Av}d\Omega, \quad (9)$$

where $\mathbf{k}$, $\mathbf{k}'$ are the initial and final wave vectors, respectively. Since $\mathbf{L}=\mathbf{x}\times\mathbf{p}$, it follows that the matrix element must be proportional to $\mathbf{k}\times\mathbf{k}'$ and hence

$$d\sigma_{LS}\sim|\mathbf{k}\times\mathbf{k}'|^2=k^4\sin^2\theta,$$

where θ is the scattering angle. This property of the LS interaction is, of course, significant in that it shows the tendency to give preference to 90° scattering. Our particular interest in this respect is focussed on the p–p cross section, however, and we must now find what the counterpart of (9) is for that case.

For this purpose we need merely replace $\exp(i\mathbf{k}\cdot\mathbf{x})$ in (9) by $(1-P_x)\exp(i\mathbf{k}\cdot\mathbf{x})$ to obtain the appropriate antisymmetrization as well as normalization. Hence, for p–p scattering

$$d\sigma_{LS}^{pp}=(r_0/4\pi)^2A_4^2\left|\int\exp(-i\mathbf{k}'\cdot\mathbf{x})(-\alpha+\beta)\times(1-P_x)\phi_2(x)\mathbf{L}\cdot\mathbf{S}\exp(i\mathbf{k}\cdot\mathbf{x})d\mathbf{x}\right|^2_{Av}d\Omega. \quad (10)$$

In (9) and (10) P_x may alternatively be regarded as an operator reversing the direction of $\mathbf{k}$. As the integrals are clearly odd functions of $\mathbf{k}$ for the case that $\mathbf{k}$ and $\mathbf{k}'$ are perpendicular to each other, one may, in considering the 90° scattering, replace P_x by -1. Hence,

$$\sigma_{LS}^{p-p}(90°)=4\sigma_{LS}^{n-p}(90°), \quad (11)$$

which is suggestive in view of the experimentally found ratio of 90° p–p and n–p scattering. It should be noted, however, that the connection (11) can be of help only if the charge dependence of the LS interaction is *not* that of the even-theory. Indeed, according to (6) we would have in that case $\alpha=\beta$ and σ_{LS}^{p-p} would vanish identically (not only in the Born approximation, but also rigorously).

To compare in more detail the n–p with the p–p cross section, we shall take as a simple model a mixture of central and tensor forces with the charge dependence (6) of the even-theory and an LS force with an as yet unspecified, though different, charge dependence. Then at high energies:

$$\sigma^{n-p}(90°)=\sigma_{\text{even}}{}^s(90°)+\sigma_{\text{even}}{}^{tr}(90°)+\sigma_{LS}{}^{n-p}(90°),$$
$$\sigma^{p-p}(90°)=4\sigma_{\text{even}}{}^s(90°)+4\sigma_{LS}{}^{n-p}(90°),$$

[8] We shall disregard here the influence of the A_4 term on the small $^3D_1$ portion of the deuteron ground state wave function. See also Section IV(a) and footnote 16.

where "s" and "tr" denote the singlet and triplet contributions, respectively. As already mentioned,

$$\sigma_{\text{even}}{}^{s}(90°) \ll \sigma_{\text{even}}{}^{tr}(90°)$$

so that the factor 4 occurring in the singlet p–p contribution is no great help. It is, however, possible to exploit the LS ratio to advantage as we shall now see.

III. p–p SCATTERING

In line with the model which we employ, it is possible to use the singlet contributions to the cross section as calculated by Christian and Noyes,[3] but of course not the triplet part, which in the present scheme is entirely due to the LS interaction.

(a) Scattering at ~30 Mev

For this energy it suffices to take into account only the ^1S-, ^1D- and ^3P-waves. In reference 3 curves are given describing the separate SD contribution for various shapes of the singlet potential.[9] We shall here not be concerned with the details of this radial dependence. We note that it is possible on the one hand to fit the experimental points at angles ~20–30°, while then on the other hand, the SD curves drop steadily instead of following the observed rise toward a rather flat relative maximum at 90°. We shall now show that this additional hump, having an estimated magnitude of about 2 mb at 90° can be described as a spin-orbit effect.

Indeed, as follows from the expression of $\sigma(\theta)$ given in Appendix I, the partial cross section for ^3P scattering due to LS coupling is given by

$$\begin{aligned}\frac{2r_0^2}{k^2}\Big\{&\frac{17}{4}\sin^2\delta(^3P_2)+\frac{9}{4}\sin^2\delta(^3P_1)+\frac{1}{2}\sin^2\delta(^3P_0)\\&+\frac{9}{2}\cos(\delta(^3P_2)-\delta(^3P_1))\sin\delta(^3P_2)\sin\delta(^3P_1)\\&+2\cos(\delta(^3P_2)-\delta(^3P_0))\sin\delta(^3P_2)\sin\delta(^3P_0)\\&-\sin^2\theta\Big[\frac{21}{8}\sin^2\delta(^3P_2)+\frac{9}{8}\sin^2\delta(^3P_1)\\&+\frac{27}{4}\cos(\delta(^3P_2)-\delta(^3P_1))\sin\delta(^3P_2)\sin\delta(^3P_1)\\&+3\cos(\delta(^3P_2)-\delta(^3P_0))\sin\delta(^3P_2)\sin\delta(^3P_0)\Big]\Big\}.\end{aligned}\tag{12}$$

Here $\delta(3Pj)$ denotes the phase shifts for ^3P states with total angular momentum j. It should be noted that we are interested in a large angle effect so that Coulomb interference is not relevant. In this connection it is, moreover, worth mentioning that in the Born approximation the Coulomb—LS—interference actually vanishes, owing to the first of the relations (8). As we will see, only small P phases will come into play for the energy under consideration. In the appropriate approximation, (12) then becomes

$$\begin{aligned}\sim\frac{2r_0^2}{k^2}\Big\{&\frac{17}{4}\delta^2(^3P_2)+\frac{9}{4}\delta^2(^3P_1)+\frac{1}{2}\delta^2(^3P_0)\\&+\frac{1}{2}\delta(^3P_2)\delta(^3P_1)+2\delta(^3P_2)\delta(^3P_0)\\&-\sin^2\theta\Big[\frac{21}{8}\delta^2(^3P_2)+\frac{9}{8}\delta^2(^3P_1)\\&+\frac{27}{4}\delta(^3P_2)\delta(^3P_1)+3\delta(^3P_2)\delta(^3P_0)\Big]\Big\}.\end{aligned}\tag{13}$$

To simplify this further we make use of the Born approximation in which the scattering phases are proportional to the potential strengths. Now we have for the eigenvalues of $\mathbf{L}\cdot\mathbf{S}$:

$$\mathbf{L}\cdot\mathbf{S}=j(j+1)-l(l+1)-2 \tag{14}$$

and hence

$$\delta(^3P_2):\delta(^3P_1):\delta(^3P_0)=1:-1:-2. \tag{14a}$$

Inserting this into (13), the ^3P-cross section becomes

$$\sim(18r_0^2/k^2)\delta^2(^3P_2)\cdot\sin^2\theta, \tag{15}$$

having an angular dependence which is just that suggested by our interpretation of the 30-Mev data. To get the desired 2-mb cross section at 90° we need a phase shift

$$\delta(^3P_2)\sim 3.7°. \tag{16}$$

Any $\phi_2(r)$ in (3) which yields (16) will therefore reproduce the desired effect. This evidently leaves much arbitrariness which, however, is considerably reduced by a simultaneous inspection of the 30- and the 350-Mev data.

(b) Scattering at 350 Mev

Here we consider the Born approximation for the entire potential. Neglecting again all Coulomb effects, we find

$$\begin{aligned}r_0^{-2}\sigma(\theta)=&\tfrac{1}{4}(A_1-3A_2)^2[a_s'Y_1(K_1)+b_s'Y_1(K_2)]^2\\&+\tfrac{3}{4}(A_1+A_2)^2[a_t'Y_1(K_1)+b_t'Y_1(K_2)]^2\\&+6A_3{}^2[a_t'{}^2Y_2{}^2(K_1)-a_t'b_t'Y_2(K_1)Y_2(K_2)+b_t'{}^2Y_2{}^2(K_2)]\\&+2A_4{}^2k^4\sin^2\theta[\alpha'Y_3(K_1)-\beta'Y_3(K_2)]^2,\end{aligned}\tag{17}$$

$$\begin{aligned}a_s'=b_s'=a_s+b_s,\qquad K_1=2k\cos\theta/2,\\a_t'=-b_t'=a_t-b_t,\quad K_2=2k\sin\theta/2,\\\alpha'=-\beta'=\alpha-\beta,\end{aligned}$$

[9] See reference 3, Fig. 10, the curves marked $V_t=0$.

and

$$Y_1(K)=K^{-1}\int_0^\infty r\phi_1(r)\sin Kr dr,$$

$$Y_2(K)=K^{-1}\int_0^\infty r\phi_1(r)\times[\sin Kr+3(Kr)^{-1}\cos Kr-3(Kr)^{-2}\sin Kr]dr,$$

$$Y_3(K)=K^{-3}\int_0^\infty r\phi_2(r)[\sin Kr-Kr\cos Kr]dr.$$

For that part of (17) which is due to central and tensor forces we refer to the work of Ashkin and Wu, and of Rohrlich and Eisenstein.[10] The spin-orbit term is obtained using (8) and

$$\{(\mathbf{S}\cdot\mathbf{K})^2\}_{Av}=K^2/2.$$

In estimating the 350-Mev cross section, one must consider the importance of relativistic corrections to a formula like (17). A consistent relativistic treatment falls, of course, outside the scope of the present work, where only phenomenological couplings are considered without reference to the dynamics of the interaction which generates them. Hence, the best we can do is to estimate the relativistic effects insofar as kinematical aspects alone are concerned. As will be shown in Appendix II, one obtains in this way corrections of around 20 percent to the non-relativistic value of σ. Clearly, therefore, it is hardly worth while to attempt to fit the 350-Mev data in too great detail as, moreover, corrections of that order due to the dynamical features neglected here may well be expected. Moreover, it follows that for still higher energies estimates of the present kind will be even less trustworthy. Thus the energy range covered till now in scattering experiments seems to extend about as far as one can analyze without a more refined theory of nuclear forces.

Using the first line of (17) and (18) we first estimate the contribution due to the singlet potential as given by the even-theory. For this purpose we take a Yukawa potential with range of $1.18\cdot10^{-13}$ cm and depth 45.8 Mev. In the present units this corresponds to $3A_2-A_1=1.58$, while for 350 Mev $k=2.44$. From this one obtains $\sim$0.2 mb /sterad at 90°, in contrast with the experimental value[11] of $\sim$4 mb. Thus, on the present assumptions, the latter has to be considered as entirely an effect of spin orbit coupling.

Remembering that we also wish to account for 2 mb at 90° and 30 Mev as being due to *LS* coupling the ratio of $\sigma_{LS}(90°)$ for the energies 350 and 30 Mev is about 2. If we use the Born approximation at both energies this ratio is independent of the strength of the *LS* coupling. We now show that it depends very sensitively on its range and shape.

(c) Shape and Magnitude of the *LS* Interaction

We first consider the examples of a square well, a Yukawa potential and an $r^{-2}\exp(-r/r_0)$ potential, respectively, with $r_0=1.18\cdot10^{-13}$ cm in each case. For the above ratio we obtain in this way: square well 26; Yukawa 0.066; $r^{-2}\exp(-r/r_0)$ 1. This behavior can easily be understood qualitatively. The square well has no tail; hence it gives too little scattering at 30 Mev so that the ratio comes out too large. The Yukawa potential has too much of a tail on the one hand (yielding too big a 30-Mev scattering), and is too weakly singular on the other hand, so that the 350-Mev cross section is too small. Hence, the ratio is much too small. For the $r^{-2}\exp(-r/r_0)$ case, the balance between the degree of singularity and the amount of tail is already much better. It is, in fact, possible here to get the right ratio of about 2 by decreasing the range by factor of approximately 2. The various *LS* parameters then turn out to have values sizably different from those of the central and tensor forces.

This is not the case if we take the radial dependence of the *LS* coupling to be

$$\phi_2(x)=\frac{1}{\lambda x}\frac{d}{d(\lambda x)}\frac{e^{-\lambda x}}{\lambda x}, \tag{18}$$

where λ is the ratio of the range $1.18\cdot10^{-13}$ cm of the central forces to that of the spin-orbit interaction. The choice (18) is in some way the most natural one to make from a field theoretical point of view. Also, we shall show presently that there is more experimental evidence which makes (18) preferable over other choices. For $\lambda\approx1.1$ (corresponding to a range of $\sim1.1\cdot10^{-13}$ cm) one actually obtains the desired ratio of 2. Then in order to fit the $\sigma(90°)$ at 350 Mev to its value of $\sim$4 mb one obtains for the strength of the interaction

$$A_4\alpha'\sim0.4$$

or $\sim$12 Mev in customary units. We note in passing that it is impossible in this way to find out anything about α' separately; i.e., about the precise exchange dependence of the spin-orbit interaction.

It should be emphasized that the *LS* contribution to the 30-Mev p–p scattering decreases very rapidly with increasing λ. The corresponding quantity at 350 Mev varies little with λ, so the ratio considered above is very sensitive to changes in the range occurring in (18). Indeed, one finds a ratio 1 for $\lambda=1$ and 4 for $\lambda=1.2$. Hence there are several reasons which make it premature to give here any but preliminary estimates for the parameters. First, there are the experimental uncertainties. Second, an inclusion of a relatively small amount of a central force in triplet states cannot be ruled out. This would lead to a contribution $\sim\cos^2\theta$ to

[10] J. Ashkin and T. Y. Wu, Phys. Rev. **73**, 973 (1948); F. Rohrlich and J. Eisenstein, Phys. Rev. **75**, 705, 1411 (1949).

[11] The values quoted in reference 3 are higher. The present value was communicated to us by Professor Chew.

the ^3P scattering cross section, and hence to an increase in the amount of 90° scattering one might like to account for as a spin-orbit effect. Finally, the Born approximation used here in estimating the effects of the LS coupling is rather crude (see below).

There is now a further feature of the p–p scattering which calls for our attention, namely the flatness of the differential cross section at 350 Mev. Here the radial dependence makes itself manifest in an even more striking way, as is exemplified by the following table which gives the ratio $\sigma(30°)/\sigma(90°)$ as a function of the shape:

(a) exponential 930; (c) $r^{-2}\exp(-r/r_0)$ 4.7;
(b) Yukawa 40; (d) ϕ_2 from Eq. (18) 1.6;
(e) square well 0.42.

The range has been taken $1.18\cdot10^{-13}$ cm with the exception of case (d), where again the range $1.1\cdot10^{-13}$ cm was used. Also, this ratio is independent of the potential strength (in the Born approximation). Its strong shape dependence shows again that we need a potential which is not only strongly singular, but which also has a small tail. This tail may, however, not be negligibly small, as we see from case (e) where the cross section decreases by a factor about 2 in going from 90° to 30°. Case (d) seems to be the most suitable one. Here, too, we have found a marked sensitivity to the value of λ, small increases of which tend to flatten $\sigma(\theta)$ even more.

Actually, it should be possible, when more experimental evidence will be available, to distinguish between the various cases in quite another manner. In case (d), $\sigma(90°)$ is, in the Born approximation,

$$\sigma(90°)\approx 8(A_4\alpha')^2k^4r_0^2/(\lambda^2+2k^2)^2, \qquad (19)$$

from which one infers that $\sigma(90°)$ for p–p scattering should vary but little over an energy range from ~150 Mev upward until relativistic effects make themselves strongly felt. This behavior contrasts with that which is to be expected for the cases (c) and (b), in which the corresponding energy dependence will be like E_0^{-1} and E_0^{-2}, respectively.

In all estimates made here we have used the Born approximation. It need hardly be said that this is a crude procedure, especially for the more singular potentials.[12] In particular, one must view with some trepidation the Born treatment of the potential (18) with its r^{-3} singularity. On the other hand, one need not take this singularity too seriously in order to obtain the qualitative results stated above. In fact, one may consider (18) to be valid only down to the nucleon Compton wave-length, and then to be cut off at smaller distances. Even for the 350-Mev data this will not cause a drastic change, since the corresponding wave-length is still about 2.5 times larger than $\hbar/Mc$. Thus it seems to us to be fair to say that the p–p scattering data can be understood by considering an LS interaction with a radial dependence which has a strongly singular behavior and a small tail.

So far we have not made any commitments as to the sign of the spin-orbit coupling. This will now be determined from the n–p interaction.

IV. LS EFFECTS IN THE N-P SYSTEM

(a) Bound States

It has been stated that low energy phenomena are essentially unaltered by the LS term. Here one point requires closer inspection; *viz.* the influence on the $^3D_1$ part of the deuteron ground state. If the spin-orbit coupling were attractive in the $^3D_1$ state, the strong singularity would greatly counteract the centrifugal repulsion. This would result in a large $^3D_1$ admixture in the deuteron, in contradiction with the information obtained from the magnetic moment and electric quadrupole moment measurements. However, if the LS coupling is repulsive in this state, it will add to the already large centrifugal repulsion and hence have little effect on the deuteron ground state. Therefore, it would seem to be most reasonable to assume the spin-orbit term repulsive in the $^3D_1$ state. With this choice it follows from Eq. (14) that for given orbital angular momentum, the LS-interaction is attractive for the state $j=l+1$ and repulsive for $j=l$ and $j=l-1$.

The existence of the LS-coupling will also modify the ^3P states. In particular, it is important to see whether the singular behavior might result in some of these states being bound.[13] From the above sign determination it follows that the $^3P_2$ potential is attractive, while the $^3P_1$ and $^3P_0$ are repulsive and of absolute magnitude once and twice as great, respectively. Thus, the problem is whether a bound $^3P_2$ state exists.

To investigate this we have considered as a simple model a square well which is so deep (namely corresponding to a strength $V_0\sim130$ Mev in the $^3P_2$ state, for $r_0=1\times10^{-13}$ cm) that it duplicates the results of our potential at 350 Mev. The model is relevant, since we have to examine whether a potential deep enough at small distances to account for the 350-Mev p–p data does or does not yield bound states. (The slight tail required at 30 Mev is not particularly significant in this connection.)

For a square well the condition for bound P-states is:

$$MV_0r_0^2/\hbar^2>\pi^2.$$

[12] As the LS interaction only is present for states with $L\geq1$, there is of course no question of divergence of the integrals. For example, in evaluating the P phases in the Born approximation for the dependence (19) one has

$$\int_0^\infty\left(\frac{1}{x}\frac{d}{dx}\frac{e^{-x}}{x}\right)J_{3/2}^2(kx)x\,dx = -\frac{1}{2\pi}\left[\frac{1}{2k}+k-\frac{1}{2k}\left(1+\frac{1}{4k^2}\right)\ln(1+4k^2)\right]$$

which varies as k^3 for small k.

[13] This was kindly pointed out to us by Professor Oppenheimer.

Hence, with the above values for the parameters a bound $^3P_2$ state cannot exist. It should be noted that in the $^3P_0$ state the absolute magnitude of the depth is $2V_0$. Therefore, had we chosen the other sign for the *LS*-interaction, the question of bound states would have been uncomfortably acute. Thus, the sign of the *LS*-coupling is such as to bind tighter states of highest total angular momentum (for a given value of l).

Here it is interesting to note a possible connection with the spin orbit interaction postulated by M. Mayer in her analysis of heavy nuclei.[6] The interpretation by this author also requires the sign of the *LS*-term to be such that states of highest j lie lowest. Furthermore, we have estimated how the present two-body spin-orbit coupling manifests itself in the interaction between a nucleon and a closed core in a heavy nucleus shell model.[14] Using a simple model according to which the nucleon moves in a homogeneous distribution of nuclear matter, it is found that intra-multiplet differences of the order of an Mev may be expected. This agrees in order of magnitude with M. Mayer's requirements.

With the sign as determined above, the ratio (for large l) of states in which the term is attractive to those in which it is repulsive is 1:2, and so tends to favor saturation. This is badly needed, since the even-theory involves only attractive forces. However, it should be borne in mind that this favorable effect may be counterbalanced by the strongly attractive force introduced in some states by the *LS*-coupling.

(b) *n–p* Scattering

The principal question here is how the addition of the *LS* interaction to the potential of the even theory will affect Christian and Hart's interpretation of the *n–p* data.

While the exchange dependence of the *LS* interaction now of course becomes relevant, there is one statement which still can be made independent thereof: the relation between $\sigma_{LS}(90°)$ for the *p–p* and the *n–p* systems as given by Eq. (11). Assuming the form (18) for the radial dependence and keeping in mind the approximate constancy of $\sigma(90°)$ for energies greater than 150 Mev mentioned above, $\sigma_{LS}(90°)$ is ~1 mb for the *n–p* scattering at 260 Mev, at which energy experimental results are now available.[2] The data are at present still beset with considerable experimental uncertainties; the 90° scattering seems to lie between 1 and 2 mb/sterad. A precise determination of $\sigma(90°)$ for the *n–p* case at high energies is of importance for the examination of the relative influences of tensor and spin-orbit forces. However, it would seem to be premature at the present stage to draw any quantitative conclusions on this point.[15]

It remains to consider the full angular dependence of the various types of forces. For this purpose the Born approximation (17) may again serve as a guide. Equation (17) is made to apply to the *n–p* problem by dropping the dashes on the quantities a', b', α', β'.

The exchange dependence of the *LS* interaction is described by the ratio of α to β. As an instructive example one may consider that choice of α and β which leads to a $\sigma_{LS}{}^{n-p}$ symmetric around 90°. This can be done by taking $\alpha:\beta=1:-1$. It is immediately seen that then $\sigma_{LS}{}^{n-p}(\theta)$ is one-fourth of $\sigma_{LS}{}^{p-p}(\theta)$ for all angles. Bearing in mind the flatness of the high energy *p–p* cross section, it follows that for angles not too close to 0° or 180°, the present determination[16] of α and β will give an approximately constant contribution of ~1 mb/sterad. From this simple consideration it is already clear that, in view of the scanty evidence on high energy *n–p* scattering and the remaining arbitrariness in the choice of the potential parameters, it is hardly possible to draw any conclusions about spin-orbit coupling from the *n–p* analysis.

It remains to consider the *n–p* scattering at the intermediate energies of 40 and 90 Mev. Here two points must be examined: the pure *P*-wave scattering and the *SP*-interference effect. As to the former, it is relatively small. Indeed, we must remember that $\sigma_{LS}{}^{p-p}(90°)$ is about 2 mb at 30 Mev and hence according to (11) and (15) $\sigma_{LS}{}^{n-p}(\theta)$ reaches a maximum at 90° which is ~0.5 mb at 40 Mev. This would be but a small contribution to the observed value of about 17 mb. Finally, it follows from the expressions given in Appendix I that the *SP* contribution to the *n–p* cross section, arising from interference in the triplet states is given by

$$\frac{3r_0^2}{2k^2}\sin\delta(^3S)\cdot\cos\theta\{(5/3)\sin\delta(^3P_2)\cos[\delta(^3P_2)-\delta(^3S)] + \sin\delta(^3P_1)\cos[\delta(^3P_1)-\delta(^3S)] + \tfrac{1}{3}\sin\delta(^3P_0)\cos[\delta(^3P_0)-\delta(^3S)]\}. \quad (20)$$

Now in the energy range considered the ^3S phase is large, while according to (16) the ^3P phases are still rather small. Hence, (20) can be approximately written as

$$(3r_0^2/2k^2)\sin\delta(^3S)\cdot\cos\theta\cdot\tfrac{1}{3}[5\delta(^3P_2)+{}^3\delta(^3P_1)+\delta(^3P_0)]$$

which is zero, however, according to (14a). This result is a consequence of the Born treatment of the *P* phase, due to *LS* interaction only (the *S* phase being computed rigorously). It can therefore also be considered to follow

[14] We are indebted to Dr. A. Bohr for a discussion on this subject.

[15] Qualitatively, an appreciable spin-orbit contribution will tend to shift the ratio of central to tensor forces in favor of the former. Such a change can be made without necessarily disturbing the interpretation of the low energy data. An increase in the relative amount of central force will tend to a larger differential scattering cross section around 0° and 180°.

[16] It should be noted that for this choice of α and β the spin-orbit interaction vanishes in states of even angular momentum. Thus, in particular, the deuteron ground state is then entirely unaffected. Cf. in this connection the comments of Blanchard, Avery, and Sachs (Phys. Rev. 78, 292 (1950)) on the magnetic moment of the deuteron.

essentially from the first of the relations (8). Thus, provided the P phase shifts are mainly due to a spin-orbit coupling only, the symmetry disturbing SP interference will be negligible. The arguments presented by Christian and Hart in favor of the even-theory would therefore seem to be in no way incompatible with the inclusion of a spin-orbit coupling in the n–p interaction.

V. CONCLUDING REMARKS

The introduction of a spin-orbit coupling of type (1) and with a strongly singular radial dependence thus offers a possibility of interpreting the available p–p scattering data. Its inclusion in the n–p interaction proposed by Christian and Hart does not change drastically the theoretical n–p cross section, hence allowing at least qualitatively for a charge independent nuclear interaction. It need hardly be stressed that from this point of view the possibility of introducing an LS coupling is not tied to the even-theory. More generally, it can be said that at present there still seems to be enough flexibility to fit a spin-orbit term into an otherwise satisfactory description of the n–p interaction.

While the present interpretation might seem to be not unreasonable, it can lay no claim to uniqueness. Indeed, the use of a strongly singular tensor force[3] or of a hard core[4] so far seem equally acceptable from a phenomenological point of view. Nor does the argument of charge independence single out the LS coupling, as it may well be possible to choose the exchange dependence in such a way that the alternative interpretations also can be fitted in principle into a charge independent description. It is to be hoped that further experimental evidence may lead to a discrimination among the various possibilities. As discussed in Section II(c), a test is the dependence of $\sigma^{pp}(90°)$ on energy. Furthermore, it is noteworthy that the hard core model predicts a minimum at about 180 Mev for the total σ^{pp} as a function of energy, see reference 4, Fig. 6. The present model yields a monotonic cross section. Thus, it would seem to be possible to distinguish between the hard core model and the LS coupling with an r^{-3} behavior. A differentiation between the latter and a tensor force with a similarity strong singularity needs more detailed considerations, however, since their qualitative features are very much the same.

It is a pleasure to acknowledge various communications from the Berkeley group which have greatly facilitated this investigation. We also wish to thank Professor J. R. Oppenheimer for valuable comments. One of us (KMC) is indebted to the Institute for Advanced Study for having supported his research by a grant of AEC funds.

APPENDIX I

We give here the main steps in the derivation of the cross section for the scattering due to a mixture of spin orbit and central forces. Proceeding in the standard way the triplet scattering amplitude is found to be

$$f_m(\theta)=(2/k)\sum_{l=0}^{\infty}(\pi(2l+1))^{\frac{1}{2}}\sum_{j=l-1}^{l+1}e^{i\delta_{lj}}\sin\delta_{lj}a_l{}^{jm}\Pi_l{}^{jm},$$

where k is the wave number and m denotes the magnetic substate. δ_{lj} is the phase shift for the state lj. $\Pi_l{}^{jm}$ are the normalized simultaneous triplet eigenfunctions of J^2, L^2 and J_z. (Of course it is not necessary for this problem to construct these explicitly.) $a_l{}^{jm}$ is defined by

$$Y_l{}^0\,{}^3\chi_m=\Sigma_j\,a_l{}^{jm}\Pi_l{}^{jm},$$

where ${}^3\chi_m$ are the triplet spin eigenfunctions and $Y_l{}^0$ is the normalized spherical harmonic of order l. With the help of the orthogonality properties of the Π's, one readily finds for the total triplet cross section

$$\sigma=(\pi/k^2)\sum_{lij}(2l+1)\sin^2\delta_{lj}\sum_m|a_l{}^{jm}|^2.$$

Using $Q=\mathbf{L}\cdot\mathbf{S}$ as a projection operator, one derives

$$a_l{}^{jm}\pi_l{}^{jm}=[\alpha_{\nu l}Q^2+\beta_{\nu l}Q+\gamma_{\nu l}]Y_l{}^0\,{}^3\chi_m,\quad j=l+\nu,$$

where

$$\mathbf{S}=\tfrac{1}{2}(\boldsymbol{\sigma}^1+\boldsymbol{\sigma}^2).$$

Here

$$\alpha_{\nu l}=\frac{2\nu^2}{(2l+1)(2l+\nu+1)}-\frac{1-\nu^2}{l(l+1)},$$

$$\beta_{\nu l}=\frac{\nu^2(2l\nu+\nu+3)}{(2l+1)(2l+\nu+1)}-\frac{1-\nu^2}{l(l+1)},$$

$$\gamma_{\nu l}=\frac{\nu^2(2l\nu+\nu+1)}{(2l+1)(2l+\nu+1)}+1-\nu^2,$$

with the understanding $\alpha_{\nu 0}=\beta_{\nu 0}=0$.

Using

$$Tr(\mathbf{L}\cdot\mathbf{S})=0,\quad Tr(\mathbf{L}\cdot\mathbf{S})^2=2\mathbf{L}^2,\quad Tr(\mathbf{L}\cdot\mathbf{S})^3=-\mathbf{L}^2,$$
$$Tr(\mathbf{L}\cdot\mathbf{S})^4=2(\mathbf{L}^2)^2,$$

where Tr denotes the trace with respect to the spin variables, one obtains for the differential cross section

$$\sigma(\theta)=\frac{\pi}{k^2}\sum_{ll}\sum_{\nu\nu'}[(2l+1)(2l'+1)]^{\frac{1}{2}}\cdot\cos(\delta_{l\nu}-\delta_{l'\nu'})\times\sin\delta_{l\nu}\sin\delta_{l'\nu'}F_{\nu\nu'}{}^{ll'}(\theta),$$

in which

$$F_{\nu\nu'}{}^{ll'}=P_{l0}P_{l'0}[3\gamma\gamma'+2\alpha'\gamma l'(l'+1)+2\alpha\gamma' l(l+1)+\tfrac{3}{2}\alpha\alpha' l(l+1)l'(l'+1)]$$
$$+P_{l1}P_{l'1}[(\alpha-\beta)(\alpha'-\beta')+\beta\beta'][l(l+1)l'(l'+1)]^{\frac{1}{2}}$$
$$+\tfrac{1}{2}P_{l2}P_{l'2}\alpha\alpha'[(l-1)l(l+1)(l+2)(l'-1)l'(l'+1)(l'+2)]^{\frac{1}{2}}.$$

Here the P_{lm} denote the orthonormal associated Legendre functions. We have used the notation $\alpha=\alpha_{\nu l}$, $\alpha'=\alpha_{\nu' l'}$, etc. Finally, one obtains for the total triplet cross section

$$\sigma=(\pi/k^2)\Sigma_{lj}(2j+1)\sin^2\delta_{lj}.$$

APPENDIX II

We give here without derivation the formulas needed to take into account relativistic corrections to the scattering cross section. As emphasized in Section II(b), only kinematic features will be dealt with. For a more detailed discussion of the following relations we refer especially to Møller's work on the relativistic electron-electron scattering.[17]

Let v be the velocity in the laboratory system of the incoming nucleon and $\gamma=(1-v^2/c^2)^{-\frac{1}{2}}$. For the angle θ_{lab} corresponding to a scattering angle θ^* in the system where the momenta are equal and opposite, we have

$$tg\theta=[2/(\gamma+1)]^{\frac{1}{2}}tg\theta^*/2.$$

For 350-Mev nucleons, $\gamma=1.37$. It follows that the relativistic distortion of the angular distribution as compared with the non-relativistic limit ($\gamma=1$) is about 5°, which can be considered

[17] C. Møller, Ann. d. Physik 14, 531 (1932).

negligible with the present experimental uncertainties. The relation between the elements of solid angle is:

$$4\cos\theta_{\rm lab}d\Omega_{\rm lab}=\frac{8(\gamma+1)}{[(\gamma+3)+(\gamma-1)\cos\theta^*]^2}d\Omega^*.$$

Again, within experimental accuracy it is sufficient to use the relation obtained by putting $\gamma=1$.

In the moving reference system each particle has a velocity u where

$$u=\gamma v/(\gamma+1).$$

The relative flux is then $2u$. The density of final states is

$$(p^*E_f^*/32\pi^3\hbar^3)d\Omega^*.$$

Here p^* is the momentum of one of the particles and E_f^* is the total final energy:

$$p^*=M\gamma v/[2(\gamma+1)]^{\frac{1}{2}},\quad E_f^*=2M[\tfrac{1}{2}(\gamma+1)]^{\frac{1}{2}}.$$

Inserting these quantities into the Born approximation formulae one finds the net effect is to multiply the non-relativistic expression for the cross section by $\frac{1}{2}(\gamma+1)$ and to replace the non-relativistic wave vector $\mathbf{k}$ by a wave vector $\mathbf{k}^*$ corresponding to the momentum $\mathbf{p}^*$. Even at 350 Mev the difference between $\mathbf{k}$ and $\mathbf{k}^*$ is very small. Hence, the total "kinematic" relativistic effect is to multiply the cross section by $\frac{1}{2}(\gamma+1)$. For 350 Mev this factor is 1.18, while at 260 Mev it is 1.14.

Since comparable dynamic relativistic effects are to be expected,[18] there is little point to try for anything better than about 20 percent accuracy.

Notes added in proof.—(1) It has been kindly pointed out to us by Dr. Christian that while the S–P interference vanishes the P–D does not. While small, this contributes an asymmetry to the n–p scattering which is of the same order as that observed. However, the sign of the interference term turns out to be the opposite of that observed. This suggests the above sign determination of the LS term is wrong. With the "odd" exchange dependence this will not affect the deuteron. However, the connection with the work of M. Mayer is then lost.

(2) Professor Serber has emphasized to us that irrespective of the p–p effects the LS term does not *lower* the n–p total cross section which calculation always gives as too large compared with experiment.

(3) Preliminary exact calculations indicate that a considerably smaller range of the spin-orbit term is needed to achieve a really flat 350-Mev cross section. This would mean the constants given in this paper may need large alteration and the possibility of simultaneously fitting the 30-Mev data may be lost. These exact calculations will be reported elsewhere.

[18] H. J. Bhabha, Proc. Roy. Soc. **A166**, 501 (1938); H. Snyder and R. Marshak, Phys. Rev. **72**, 1253 (1947).

PHYSICAL REVIEW VOLUME 80, NUMBER 2 OCTOBER 15, 1950

The Cross Section for Photo-Disintegration of the Deuteron at Low Energies

G. R. Bishop, C. H. Collie, H. Halban, A. Hedgran, K. Siegbahn, S. du Toit,* R. Wilson
Nobel Institutet för Fysik, Stockholm, Sweden and Clarendon Laboratory, Oxford, England

(Received June 16, 1950)

Precision measurements have been made of the photo-disintegration of the deuteron with the gamma-rays of Ga^{72} and Na^{24}. Relative cross sections have been measured at 2.51, 2.62, and 2.76 Mev. Calibration of the sources gave absolute cross sections at 2.62 and 2.76 Mev.

I. INTRODUCTION

THE variation with energy of the photoelectric and photo-magnetic cross sections of the deuteron is essential data for the determination of the parameters of the nuclear forces. So far measurements of the total cross sections $\sigma_T=\sigma_e+\sigma_m$ have been made by several groups [1–8] using γ-rays of quantum energy 2.62, 2.76, 6.3, and 17 Mev.

The measurement of these cross sections falls naturally in two parts: the determination of the number of γ-quanta emitted per unit time by the source and the number of photo-disintegrations produced by this source in a system containing heavy hydrogen.

The disintegrations are now usually counted by observing the photo-protons either in an ionization chamber counter or in a photographic plate. These methods have the advantage of being independent of a neutron standard needed for older methods relying on the counting of photo-neutrons. Recently, deuterium filled ionization chamber counters with electronic collection have been developed sufficiently to allow a precision of 1 percent in comparing the number of photo-protons produced by γ-rays of different energy.

Several methods can be used for determining the number of γ-quanta emitted from the source. In the case of the 2.62 Mev γ-rays emitted by RdTh, one can use the results of Ricoux[9] or Winand[10] giving the number of disintegrations per second of a RdTh source which gives the same ionization as 1 mg of radium in an ionization chamber of the Curie type. Unfortunately,

* Temporarily absent from the National Physical Laboratory, Pretoria, South Africa. Dr. du Toit is indebted to the South African Council for Scientific Research for enabling him to take part in this research.

[1] J. Chadwick and M. Goldhaber, Nature **134**, 237 (1933).
[2] H. Halban, Nature **141**, 644 (1938).
[3] Wilson, Collie, and Halban, Nature **162**, 185 (1948); **163**, 245 (1949).
[4] Snell, Barker, and Sternberg, Phys. Rev. **75**, 1290 (1949).
[5] Russell, Sachs, Wattenberg, and Fields, Phys. Rev. **73**, 545 (1948).
[6] J. Van Allen and N. Smith, Phys. Rev. **59**, 618 (1941).
[7] Barnes, Stafford, and Wilkinson, Nature **165**, 70 (1950).
[8] H. Wäffler and S. Youmis, Helv. Phys. Acta **22**, 414 (1949).

[9] J. Ricoux, J. de phys. et rad. **8**, 388 (1939).
[10] L. Winand, J. de phys. et rad. **10**, 361 (1939).

neither author indicated the accuracy of his measurements. The agreement however is good (~1 percent), but both methods involve an accurate knowledge of the branching ratio of ThC in order to obtain the number of 2.62 Mev γ-quanta.

The determination of the absolute number of γ-quanta produced by a source can be made with an accuracy of 1 to 2 percent in the case of the 2.76-Mev γ-line of radiosodium,[11] Na^{24}. The γ-ray spectrum is sufficiently simple[12] to allow standardization either by the coincidence method or by the ionization method developed by Gray.[13] For Na^{24} these two methods agree within the limits of measurement.

When using a radiosodium source standardized by the coincidence method and a radiothorium source standardized by the Ricoux-Winand method three of us found[3] the ratio for the total cross section of the photo-effect at 2.76 Mev and 2.62 Mev to be 1.05 ± 0.08.

An error was discovered in the radiothorium calibration, however, since the Ricoux factor of 1.09, which should be applied to convert the source strength in milligrams radium equivalent to millicuries, was omitted. The corrected ratio (taking into account the new value for the decay constant of radium) was 1.12 ± 0.08, a result lower than the value of 1.21 which is predicted by theory. This discrepancy seemed especially interesting since the ratio of the two cross sections turns out to be fairly independent of the range of force, and the refinements of different theories. Thus Hansson and Hulthén[14] obtain values varying between 1.19 and 1.22. Bethe and Longmire[15] have calculated σ_m and σ_e for γ-ray energies of 2.62 and 2.76 Mev. In their phenomenological treatment they make use of recent data for the binding energy of the deuteron, neutron-proton and proton-proton scattering cross sections. From their figures for σ_T one equally obtains $\sigma_{2.76}/\sigma_{2.62}=1.19$. Similar calculations have been made by Halpern and Woodward.[15]

For this reason it was felt that the measurements should be extended to lower energies.

Radiogallium, Ga^{72}, emits a γ-ray spectrum which includes as its highest member a γ-ray of energy 2.51 Mev.[16,17] Unfortunately, both the coincidence method and Gray's method of standardization fail in practice when the spectrum is complicated, so that hitherto this convenient source has not been available for absolute measurements.

At this point cooperation between a group of workers in the Nobelinstitut för Fysik in Stockholm and a group of the Clarendon Laboratory in Oxford seemed promising. The procedure which became possible through the collaboration of the two groups, and which will be described below, made measurements with the Ga^{72} line feasible. Furthermore, it will in future allow one to determine the relative number of γ-quanta of 2.51 Mev, 2.62 Mev, and 2.76 Mev emitted by any set of sources of RdTh, Ga^{72}, and Na^{24} by comparing them on the substandard ionization chamber.

Throughout the work two sources each of Ga^{72} and Na^{24} provided by the Isotope Division of A.E.R.E. Harwell were used. After irradiation they were placed in copper tubes identical with the container of the RdTh source of 13.2 mg radium equivalent described later. These sources were compared on the substandard ionization chamber to an accuracy of 0.1 percent. The number of photo-protons produced by the RdTh source and one of each of the Ga^{72} and Na^{24} sources in the same deuterium filled ionization chamber counter was determined in Oxford. Each source has only one γ-ray line with sufficient energy to produce photo-protons of *measurable energy*.

The other set of sources was flown to Stockholm where the relative number of γ-quanta of each of the three lines was determined with a β-ray spectrograph. The combination of the measurements on the β-spectrograph and deuterium filled ionization chamber give the relative cross sections for the photo-effect of the deuteron for the 2.51-, 2.62-, and 2.76-Mev γ-ray lines. Absolute values were obtained at 2.62 Mev and at 2.76 Mev by calibrating the sources.

II. THE CURIE-TYPE SUBSTANDARD IONIZATION CHAMBER

All of the sources used were compared with a radium standard, and where possible with each other, on a substandard ionization chamber. This chamber is a copy of that used in the Curie Institute in Paris,[18] it is a shallow chamber 52 cm in diameter with 1 cm of lead for filtration on top. The exact location of the source on top of the lead is of small importance; there is only a 0.1 percent change in ionization if the source is displaced by 5 cm. Thus the chamber is ideal for the reproducible measurement of the extended sources which have been used. The electrometer was used as a null instrument and has proved to be very stable;[19] it is possible to compare two sources of approximately equal strengths to an accuracy of 1 part in 10^4. Two sources of very unequal strength can be compared to an accuracy of 1 part in 10^3.

III. MEASUREMENT OF THE RELATIVE INTENSITIES OF THE γ-RAYS AT 2.504(Ga^{72}), 2.618 (ThC'') AND 2.757 Mev (Na^{24})

Since the hard γ-rays here concerned are emitted together with a rather large number of other γ-lines in the different γ-spectra it is necessary to use a method

[11] J. L. Putman, Brit. J. Radiol. **23**, 265 (1950).
[12] O. T. Seaborg and I. Perlman, Rev. Mod. Phys. **20**, 585, 1948.
[13] L. H. Gray, Brit. J. Radiol. **22**, 677 (1949).
[14] I. F. E. Hansson and L. Hulthén, Phys. Rev. **76**, 1163 (1949).
[15] H. A. Bethe and C. Longmire, Phys. Rev. **77**, 647 (1950). See also I. Halpern and W. M. Woodward, M.I.T. Report.
[16] S. K. Haynes, Phys. Rev. **74**, 423 (1948).
[17] Mitchell, Zaffarano, and Kern, Phys. Rev. **73**, 1424 (1948).
[18] E. Curie, J. de phys. et rad. **2**, 975 (1912).
[19] R. Wilson and G. R. Bishop, Proc. Phys. Soc. London **42**, 257 (1949).

which allows a complete separation of the different γ-components so that each γ-line can be studied separately. A high resolution β-ray spectrometer is naturally best suited for this purpose and if the photo-effect produced by the γ-rays in a thin metal foil is studied one has the advantage of dealing with well-defined electron lines. The other two effects, which could have been used, *viz.*, the Compton effect and the pair formation effect, give continuous secondary electron distributions and are less suited for very precise intensity measurements.

The photo-electron method has already been quite extensively used for γ-ray intensity measurements and was actually introduced by Ellis and Aston as early as 1930, but it should be pointed out that with a few exceptions these previous measurements have never aimed to reach an accuracy better than 10 or even 15 percent. One is faced with rather serious difficulties when the demand for accuracy, as in the present case, is raised to one or two percent. Some of these difficulties will be discussed here.[20]

A. Thickness of Electron Converter

Photo-electrons expelled from the converter will straggle during their passage through the converter due to inelastic collisions and radiation losses.[21] Apart from a general line shift the photo-lines get broader and soon the line width caused by this effect exceeds that of the spectrometer, if this is adjusted for the high resolving power necessary in this case. Some of the electrons may even be scattered out from the line and get lost in the continuous distribution of Compton electrons. The need for a thin converter is therefore obvious. On the other hand, at these high energies the photo-effect is so much reduced in magnitude that the necessary demands for high statistical accuracy on each point on the photo-line can only be satisfied if a compromise is made in choosing the converter thickness.

As shown by Ellis and Aston[22] and later by Richardson[23] the other extreme possibility, that of using a practically infinitely thick converter, has the advantage of being more easily calculable than is the method of using a thin converter. Though in many cases this circumstance may be useful, it is still difficult to know to what accuracy Richardson's formula can be applied without making special experimental checks. There is, however, still one good argument against the use of the thick converter method in the present case. It is experimentally well known that the *form* of the Compton electron distribution changes somewhat if a thick lead foil is placed above a converter of low Z value, for example, copper. Thus it is very hard to separate in an accurate way a photo-line from the continuous Compton distribution, when the line is not completely resolved from the latter distribution, even if the investigation is made with and without a lead foil.

It was found that a lead foil of 20 mg/cm^2 was of a suitable thickness. According to Fig. 1, showing the photo-lines of ThC'' at 2.62 Mev and obtained with the double focusing spectrometer, it is possible to resolve completely the K photo-line both from the L photo-line *and* from the corresponding Compton electron distribution, and still have a sufficiently good counting rate. The line width at this energy is only slightly more than that given by the spectrometer and the size of the sample.

B. Anisotropy in the Photoelectric Emission

The direction of emission of the photo-electron relative to the direction of the quantum, being 90° at $E_\gamma=0$, will be more and more forward as energy increases, since momentum is transferred from the γ-quantum to the electron. Since the spectrometer only accepts electrons with a large forward component the intensity of the harder γ-rays may be overestimated unless one uses the differential photoelectric cross section when evaluating the data. This may happen especially for low energy γ-rays with "good" geometry (canalized γ-rays and small dimensions of converter) and extremely thin lead foils, where no smearing-out effects occur. The most probable angle for emission can be calculated[24] and it is found, in agreement with experiment,[25] that this angle is small at the energies relevant to this work. Thus Latyshev[25] finds the angle to be 9° at 2.62 Mev. This angle varies very little inside our energy range from 2.52 to 2.76 Mev. Furthermore, the geometry of our sample and converter is able to

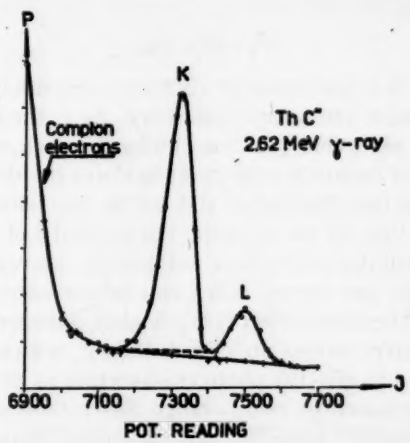

FIG. 1. Photo-lines of ThC''.

[20] For a more complete discussion see H. O. W. Richardson, Proc. Phys. Soc. London 63, 234 (1950), particularly dealing with the Ellis-Aston method. See also G. Latyshev, Rev. Mod. Phys. 19, 132 (1947) and Deutsch, Elliott and Evans, Rev. Sci. Inst. 15, 178 (1944).

[21] See W. Heitler, *The Quantum Theory of Radiation* (Oxford University Press, London, 1944), p. 219 (5) and p. 221 (9).

[22] C. Ellis and M. Aston, Proc. Roy. Soc. A129, 180 (1930).

[23] H. O. W. Richardson, reference 20.

[24] A. Sommerfeld, *Atombau und Spektrallinien* II, p. 494. Compare K. Siegbahn and H. Slätis, Arkiv. f. Mat. Astr. o. Fys. 32A, No. 9 (1945).

[25] G. Latyshev, Rev. Mod. Phys. 19, 132 (1947).

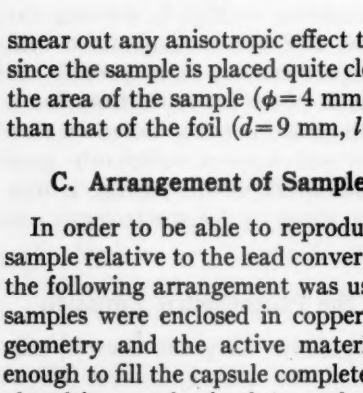

FIG. 2. Arrangement of sample and lead converter.

smear out any anisotropic effect to a fairly large extent, since the sample is placed quite close to the lead foil and the area of the sample ($\phi=4$ mm, $l=18$ mm) is smaller than that of the foil ($d=9$ mm, $l=20$ mm).

C. Arrangement of Samples and Converter

In order to be able to reproduce the position of the sample relative to the lead converter in an accurate way the following arrangement was used (Fig. 2). All three samples were enclosed in copper capsules of identical geometry and the active material in each case was enough to fill the capsule completely. The capsules were placed in a cavity in the sample holder and were held in the correct position by a spring. The lead converter, supported on a 0.2-mm aluminum plate, could be attached to the holder on a slide. In this way the position of the well-defined volume of the samples was always fixed relative to the lead converter within a tenth of a mm. Special checks were made to see if the intensity of the photo-lines were influenced by rotation of the samples or changed of ± 1 mm up or down, but no such effects could be observed.

D. Accuracy of the Theoretical Photoelectric Cross Section for Lead

If it is assumed that the experimental conditions are such that the complications due to straggling effects in the converter and the anisotropic photoelectric emission can be neglected, the intensity of a γ-line is simply given by:

$$J_\gamma = kJ_K/\sigma_K, \tag{1}$$

where k is a spectrometer constant, depending on the transmission and sample geometry, J_K is the intensity of the K photo-line (i.e., area under the peak, when the number of counts in each point has been divided by the corresponding $H\rho$ value and σ_K is the photoelectric cross section for the K shell. The accuracy of our final results will depend on how well known the variation of σ_K within our energy range can be considered to be. Though the photo-effect is in principle quite well understood, there exists no closed theory, which can be evaluated to give the photo cross section at all Z values and over the entire energy range. Several formulas have been deduced[26] based on various approximations, such as the Born approximation, which may be applied in different energy ranges and for different Z values, but most of these are fairly inaccurate in the energy region concerned here. An exact calculation by Hulme *et al.*[27] is valid for all Z values and energies, but cannot be evaluated numerically at energies greater than 2 Mev. There is still another formula due to Hall[28] which is mathematically not quite rigorous, but which was shown by Hume *et al.* to give very satisfactory results at sufficiently high energies. Thus, at 1.1 Mev the cross section deviates from the exact value of Hulme by only 6 percent. We are therefore inclined to trust the Hall formula as capable of giving accurately the *variation* of the cross section within our small energy range without introducing theoretical uncertainties. According to Hall's formula the cross sections for lead at 2.51, 2.62, and 2.76 Mev are 1.252, 1.184, and 1.113×10^{-24} cm^2, respectively. Evans and Evans[29] have given the cross section for lead based on a critical compilation due to Davisson.[30] The absolute value of the cross section at 2.62 Mev has been measured by Davidson and Latyshev[31] and it agrees well with that obtained from Evan's curve, which at this energy was calculated by means of Hall's formula. At lower energies the curve is based on other approximations.

In view of the fact that our lead converter could not be considered to be infinitely thin and also in view of our special geometry, an experiment was performed in order to check the validity of (1) for our particular case. The two sodium γ-lines are known to be emitted in cascade and to have the same intensity. By measuring the areas of the two photo-lines the relative values at the photo cross section at 1.38 and 2.76 Mev can be measured for our geometry, that is, we get an experimental check over a very much larger energy range than that with which our main experiment is concerned. We obtained consistently a value for $\sigma_{1.38}/\sigma_{2.76}$ which was 15 percent higher than that given by Evans' curve. The reason for this departure from the theoretical curve is somewhat puzzling, since any possible small influence of the converter thickness as well as the anisotropic emission should be expected to go in the other direction. We may therefore not disregard completely the possibility of a failure of Eq. (1) to yield accurate intensities over the entire energy range.[32] Even if we assume this to be the case it is evident that the correction would be very small within our narrow energy range. Instead of having a total variation of cross section between 2.51 to 2.76 Mev of 12 percent the sodium experiment could indicate an additional 2 percent. It is preferable, however, to use the theoretical values for our problem since

[26] See W. Heitler, reference 21, p. 125.

[27] Hulme, McDougall, Buckingham, and Fowler, Proc. Roy. Soc. **149**, 131 (1935).

[28] H. Hall, Phys. Rev. **45**, 620 (1934).

[29] R. D. Evans and R. O. Evans, Rev. Mod. Phys. **20**, 305 (1948).

[30] C. M. Davisson, thesis, M.I.T. We are very much indebted to Professor R. D. Evans for discussion on this point.

[31] Davidson and Latyshev, J. Phys. U.S.S.R. **6**, 15 (1942).

[32] It is interesting to note that the empirical relationship due to Gray (Proc. Camb. Phil. Soc. **27**, 103 (1931)) gives a value for $\sigma(1.38)/\sigma(2.76)$ which is 15 percent *higher* than our value. This relation is however based entirely on data below 1 Mev.

it must be assumed that the ideal conditions for the experiments are better satisfied at our high energies than at lower.

E. Experimental Procedure and Results

The measurements were performed with the large double focusing spectrometer ($\rho=50$ cm), described elsewhere.[33] The magnetic field measuring system has now been considerably improved and permits an accuracy in the field setting of 0.01 percent. The current through the Helmholz coil is measured by compensating the voltage developed across a manganin resistance in a temperature-controlled oil bath.

The K photo-lines of the hard γ-lines of Ga^{72}, ThC″ and Na^{24} are shown in Figs. 3–5. One interesting new fact was immediately recognized. The 2.51-Mev Ga line is double. This is evident from the values of the half-width of the three photo-lines in Figs. 3–5. In the case of ThC″ and Na^{24} this is constantly the same in all measurements (1.10 percent), whereas a large departure from this value is found for Ga^{72} (1.42 percent). The two lines are situated 0.6 percent apart and it is possible to resolve them completely in the spectrometer by making suitable arrangements, which will be discussed by one of us on a later occasion.[34] In the term scheme worked out by Mitchell *et al.*[16,17] there is actually room for a transition of this energy, i.e., between the fourth excited level and the ground state, in addition to the one already given between the sixth and the first excited levels. The new line therefore to a certain extent confirms the complicated scheme presented by Mitchell *et al.*

The fact that the γ-line at 2.51 Mev is double will not introduce any complications for the interpretations of the experiments on the number of photo-protons performed in Oxford. It is necessary, however, to consider this circumstance when the areas under the K photo-lines of lead are not completely resolved, in the sense that the intensity in the valley between is not zero. Nevertheless, it was found practicable to let the dotted line in Fig. 1 correspond to the base of the K photo-lines. When comparing the lines of Na^{24} and ThC″ this small simplification could in principle not introduce any error. Because of the double line character with the correspondingly greater line widths for Ga^{72} the valley between the K and L lines is situated somewhat higher in that case giving too small an intensity for the photo-line. The correction for this was experimentally determined and was found to be very small (=1 percent).

The three samples were always measured twice and interchanged in the following sequence: RhTa, Na, Ga, Na, Ga, RaTh. The total time required for a series of measurements was about 14 hours.

Besides the intensities, the energies of the lines were determined relative to the 2.618 Mev of ThC″ in the following way. From the dotted base-line a vertical line was drawn to the apex of the line. On the half-height of this a horizontal line was drawn cutting the photo-line in two points. The midpoint between these two points was chosen as representing the position of the line. When this procedure was used, it was found that the accuracy in defining the lines was greatly enhanced as compared with the more direct ways of trying to find the top of the lines, for example. The reproducibility for the sodium and ThC″ lines in three independent measurements was actually found to be 1 in 10^4. In the case of ThC″ and sodium this made a very accurate energy comparison possible. In the case of the double gallium line, the measurement of the precise energy value is naturally less clear and should only be interpreted as some weighted mean value of the two lines. Those values are taken to calculate the theoretical photo-disintegration cross section. The energy loss due to straggling in the lead foil for the three lines is almost independent of energy in this range[35] and the correction can be neglected. Taking the energy of the ThC″ γ-line to be 2.618 Mev[35] the energies of the Na^{24} and Ga^{72} lines were found to be: $E_\gamma=2.757\pm0.001$ and 2.504 Mev, respectively.

IV. ABSOLUTE SOURCE CALIBRATIONS

A. Radiosodium (Na^{24})

The radiosodium source was calibrated by the β–γ-coincidence technique developed by Dunworth[36] and improved by Putman.[11] Some calibrations were made at A.E.R.E. Harwell, using Putman's apparatus and other using a similar apparatus in Oxford.

The dilutions were made by dissolving the sodium carbonate source and weighting out an aliquot of solution. The sources were calibrated by separate coin-

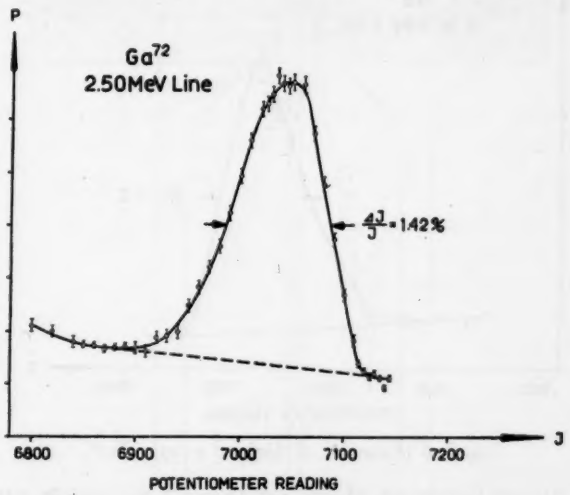

FIG. 3. K photo-line of the hard γ-ray of Ga^{72}.

[33] Hedgran, Siegbahn, and Svartholm, Proc. Phys. Soc. London (1950).
[34] A. Hedgran (to be published).
[35] Hornyak, Lauritsen, and Rasmussen, Phys. Rev. **76**, 731 (1949).
[36] J. R. Dunworth, Rev. Sci. Inst. **11**, 167 (1940).

cidence runs on 4 different aliquots. The over-all errors (statistical and weighing) are about 0.5 percent. There are several possible sources of systematic error. Multiple counts in the Geiger counter are suppressed by using a multivibrator quenching unit,[37] A.E.R.E. type 1014A. Other spurious counts probably introduce less than 0.1 percent error. The β–γ-angular correlation[38] is less than 1 percent. The 4.14-Mev cross-over γ-ray is not found[39] to 3 parts in 10^7 and there is less than 1 percent of a high energy β-ray.[12] If each of these effects were present to the limits given above they would together alter the absolute calibration by less than 0.5 percent.

Putman points out that the correction applied for the γ-rays counted by the β-counter is uncertain, since the efficiency of the β-ray counter for γ-rays changes when an aluminum absorber (used for suppressing the β-rays) is placed in front of the source. This effect is moreover dependent on the position of this aluminum absorber. This can cause an understimate of the source strength by 1 percent; an auxiliary experiment was performed to determine this correction more accurately.[39a] It was found that in our geometry this change of efficiency was 6 percent, which was exactly compensated by the absorption of γ-rays in the aluminium screen.

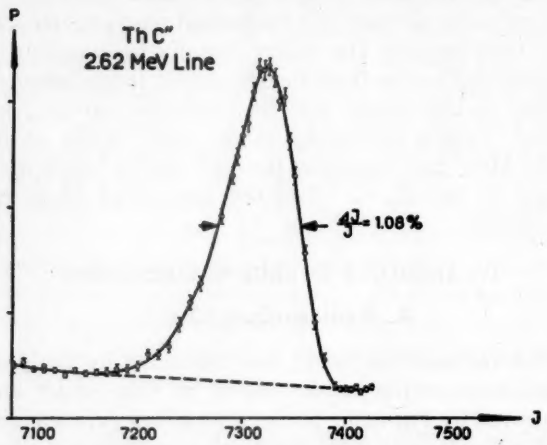

FIG. 4. K photo-line of the hard γ-ray of ThC''.

FIG. 5. K photo-line of the hard γ-ray of Na^{24}.

B. Radiothorium

The radiothorium source was calibrated by using the results of Ricoux[9] and of Winand[10] as reinterpreted by Bouchez[40] in the light of later values for various physical constants. Ricoux measured the total ionization produced by the α-particles from a Th(B−C′−C″) source and Winand measured the total heat produced by the α-particles. We compare the radiothorium source with a radium standard on our substandard ionization chamber (Section II). The accuracy of this calibration (in terms of the number of 2.62-Mev γ-ray quanta) we estimate to be about 2 percent; much of the error arises from the uncertainty in the branching ratio ThC′–ThC″. The branching ratio taken is 0.34 atom of ThC″ to 1 of ThC; this is a mean of the values of Albrecht[41] and Kovarik and Adams.[42]

C. Photo-Proton Counting. The Counter

The number of photo-protons was measured by placing the sources near an ionization chamber counter filled with deuterium to a suitable pressure. The rate of counting of photo-protons was measured with a statistical accuracy of 0.5 percent for each source. The counting rates were corrected for decay of the sources using the decay periods of 14.90 hr. for Na^{24} and 14.08 hr. for Ga^{72}.[16,39]

The counter used is shown in Fig. 6. The counting volume is defined by a spherical high voltage electrode, 4 cm diameter, 0.2 mm thick, spun from aluminium. The collecting electrode is shielded with glass except when inside this high voltage electrode. A plot of the field inside shows that the counting volume is equal to the geometrical volume of the sphere to within 0.1 percent. The geometrical volume was measured by filling with water and weighing. The outer pressure-containing cylinder acts also as a guard ring. Photo-protons produced in the gas between the pressure cylinder and the high voltage electrode are not counted; but there is a certain sensitivity for counting the photo-neutrons produced in this volume. A correction of 0.1 percent was subtracted from the count to allow for this effect.

The source is mounted rigidly on the counter and

[37] Cooke-Yarborough, Florida, and Davey, J. Sci. Inst. **26**, 124 (1949).
[38] Grace, Allen, and Halban, Nature **164**, 538 (1949).
[39] Bishop, Wilson, and Halban, Phys. Rev. **77**, 416 (1950). A new lower limit for the 4.14-Mev cross-over γ-ray has been found since publication.
[39a] R. W. Parsons and C. H. Collie, Brit. J. Radiol. (to be published).
[40] R. Bouchez, J. de phys. et rad. (1949).
[41] E. Albrecht, Zits. Akad. Wiss. Wien IIa **128**, 925 (1919).
[42] A. F. Kovarik and N. J. Adams, Phys. Rev. **54**, 40 (1938).

the distance can be measured to better than 0.1 percent. For the relative measurements, the sources were placed in a source holder which was in the same position for each source, so that even this small inaccuracy does not arise. A correction has to be made to the inverse-square law because of the finite sizes of the source and counter. A simple integration yields the formula.

$$\text{mean}\left(\frac{1}{p^2}\right)=\frac{1}{p^2}\left(1+\frac{a^2}{5p^2}-\frac{x^2+y^2}{3p^2}\right),$$

where p is the distance from the center of source to the center of the counter, a is the radius of the counter's spherical electrode, and $2x$ and $2y$ are the linear dimensions of the rectangular source. The sources used were smaller and more accurately defined than those used by some of us previously, due to the higher specific activity now available.

D. The Amplifier

The pulses of ionization are only just above the background noise from the amplifier when sources of radio-gallium (Ga^{72}) are used, so that a special low noise preamplifier was necessary.[43] This was used in conjunction with an amplifier A.E.R.E. type 1008. The pulses were analyzed by a single-channel kick-sorter, and the counter and amplifier were calibrated as a single unit by measuring the pulse-height distribution of the photo-protons from the disintegration of deuterium by radiothorium γ-rays. It was thus established that the pulse height distribution conformed to the distribution to be expected from the spread of energy of the protons,[44] and from spread of pulse height by noise, positive ion effects, and wall effect. These will be discussed individually later. Once the energy scale had been established the cross-section measurements were made by counting all photo-protons above a certain bias level with a simple discriminator. The counters were operated with about 5 kv between the electrodes, at which potential the pulse height was approximately saturated. Details of the counter testing and filling procedure adopted are described elsewhere.[45]

E. Pressure Measurement

The counter pressures used varied. For the absolute measurements only sources of radiosodium and radiothorium were used, and at 8 atmos. pressure the secondary electron background brought the amplifier noise up to the point where the pulses could be just separated from noise. The voltage pulse at the grid of the first tube has an average value of 60 μvolts. This is reduced to 30 μvolts by the pulse-shaping circuits while the r.m.s. noise is 12 μvolts. For the relative measurements with Ga^{72} (which gives photo-protons of lower energy)

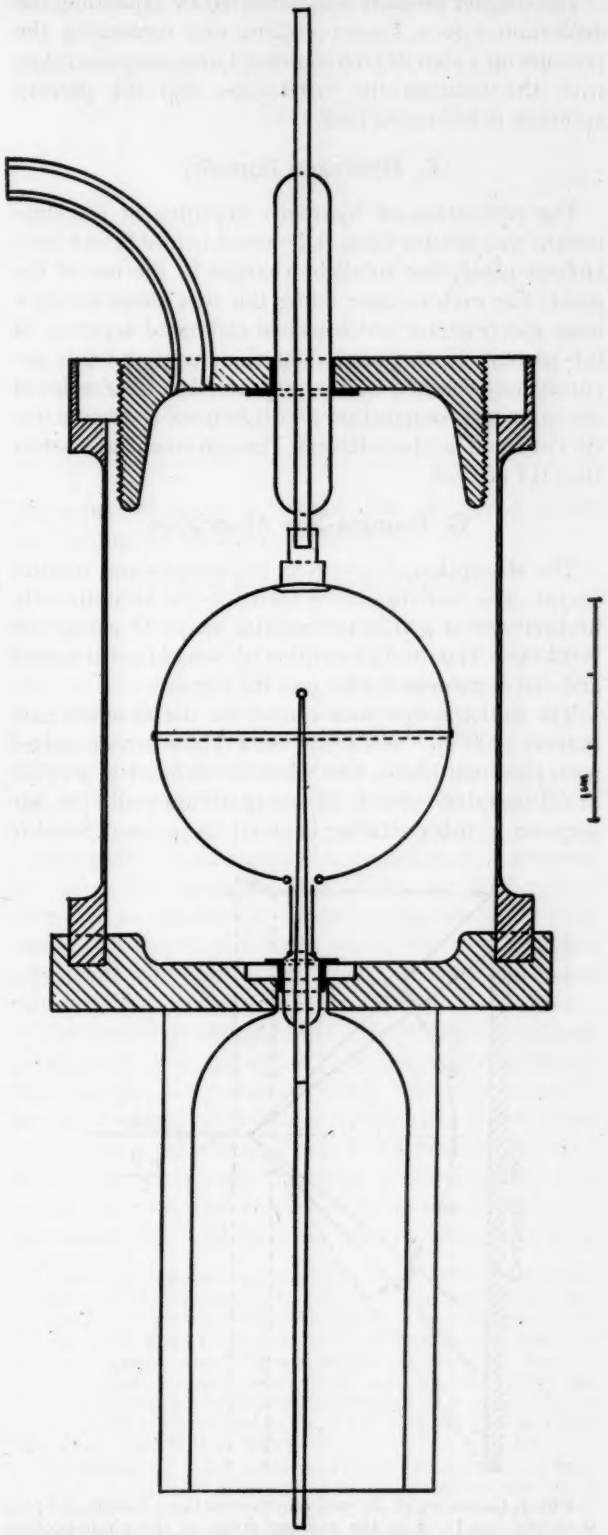

FIG. 6. Schematic diagram of the counter.

[43] R. Wilson, Phil. Mag. 41, 66 (1950).

[44] This spread in energy is due to the conservation of momentum. Photo-protons moving in the direction of the γ-ray have more energy than those moving in the opposite direction. We have found that the kick-size distribution represents at least qualitatively the angular distribution of the photo-protons. A quantitative development of this method is now being attempted.

[45] Wilson, Beghian, Collie, Halban, and Bishop, Rev. Sci. Inst. to be published (1950).

the pressure has to be reduced to 1.5 atmos. in order to reduce the background. (At the same time the pulse shaping time constants were readjusted to the optimum values.)

The counter pressure was measured by expanding the deuterium into a known volume and measuring the pressure on a mercury manometer. Great care was taken with the temperature corrections, and 0.1 percent accuracy is estimated here.

F. Hydrogen Impurity

The percentage of hydrogen impurity in the deuterium was greater than that found before in our electrolysis plant, due to slight changes in the use of the plant. For each counter filling this was measured on a mass spectrometer which has an estimated accuracy of 0.1 percent in the total deuterium content; this accuracy was checked by the measurement of samples of the same gas composition on other mass spectrometers (in Paris and in Chalk River). The agreement was better than 0.1 percent.

G. Gamma-Ray Absorption

The absorption of γ-rays in the sources and counter varied. The sodium source used for the absolute calibration was of a thin rectangular shape (2 cm$\times$2 cm $\times$0.4 cm). The total absorption of γ-rays for the source and the aluminum holder was 0.5 percent.

The radiothorium source used for the absolute calibration (200 mc) was made on a ThO_2 carrier, mixed with platinum black. The whole is enclosed in a cylindrical container with 1/10-mm platinum wall. The absorption in this container is about 10 percent. Some of this absorption is due to Compton scattering; not all degraded quanta from Compton scattering will produce photo-disintegration but all will produce ionization in the ionization chamber. The difference in the absorption for the calibration and for the use for photo-disintegration experiments is 1 percent and is applied as a correction.

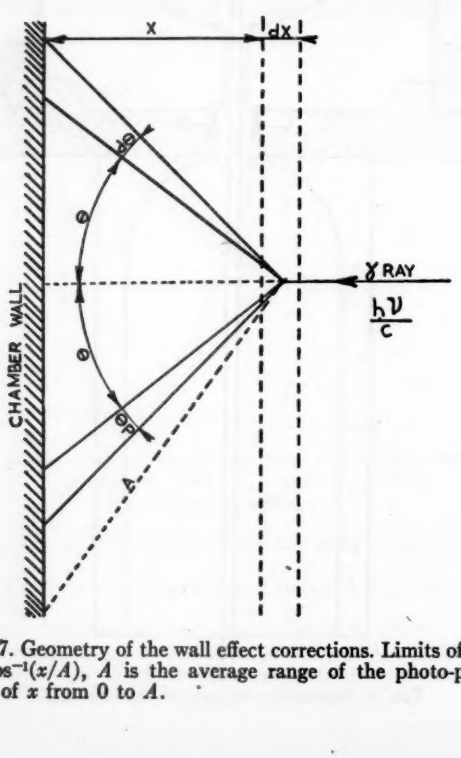

FIG. 7. Geometry of the wall effect corrections. Limits of θ from 0 to $\cos^{-1}(x/A)$, A is the average range of the photo-protons. Limits of x from 0 to A.

For the relative cross-section measurements, sources of sodium carbonate, gallium metal, and radiothorium (this time on Al_2O_3 as carrier) were placed in identical copper cylinders, 4 mm diameter and 18 mm long, with a wall thickness of 1.5 mm. The total absorption of γ-rays in the copper container is approximately the same (5 percent) for each source, but the absorption of γ-rays in the source material will differ (from 0.5 percent for sodium carbonate to 3 percent for gallium metal). However, we are only concerned with the number of γ-rays which escape from the source; the β-spectrometer calibration takes no account of those which are absorbed in the source or the source walls. This absorption enters thus into both the calibration and the use of the sources and can therefore be neglected. There is a difference in sensitivity of the β-ray spectrometer and the photo-disintegration counter for γ-rays slightly degraded by Compton scattering. This leads to a second-order correction of about 0.05 percent and has been neglected. The absorption of γ-rays in the wall of the counter has been reduced by making the walls of stainless steel 0.5 mm thick, soldered on to mild steel ends. The inner spherical electrode is of aluminium, 0.2 mm thick, 4 cm diameter. The absorption in these is calculated to an accuracy of 0.1 percent of the final intensity.

The ends of the counter, and the supporting rod from the counter to the source, are massive for rigidity; this and other massive material were so placed that any γ-rays scattered into the counter were scattered through more than 12° and were therefore degraded in energy below the threshold for photo-disintegration of deuterium.

H. Wall Effect Corrections

The correction due to the wall effect is considerable and must be considered carefully. At even the highest pressures used (8 atmos.) 6 percent of the photo-protons lost part of their range in the walls, and thus had less probability of being counted. When counting the low energy protons from radiogallium the pressure had to be reduced to 2 atmos. in order to reduce the background of secondary electrons, with a corresponding increase (to 15 percent) in the wall effect.

The problem can be approached in two ways. The theoretical value may be taken assuming the range-energy relationship for protons in deuterium. The form of this curve has been derived from measurements of the stopping power of H_2 or D_2 gas for protons made by Crenshaw.[46] This curve agrees well with the Livingston-

[46] C. M. Crenshaw, Phys. Rev. **62**, 54 (1942).

TABLE I. Sodium source Na^{24}.

Date of measurement	$[C_p s]$	V (cm³)	P (atmos.)	R	S
November 28, 1949	3.7701×10^{4}	28.59	7.663	0.1705	2.544×10^{-16}
December 19, 1949	4.119×10^{4}	28.59	7.107	0.2053	2.495×10^{-16}
February 27, 1950	6.213×10^{4}	28.54	4.927	0.4480	2.550×10^{-16}
March 6, 1950	8.894×10^{4}	28.54	7.236	0.4347	2.528×10^{-16}
Average $S=(2.529\pm0.017)\times10^{-16}$					

TABLE II. RdTh source.

Date of measurement	$[C_p s]$	V (cm³)	P (atmos.)	R	S
November 28, 1949	1.964×10^{5}	28.59	7.663	0.8723	2.603×10^{-16}
January 27, 1950	1.170×10^{5}	28.59	4.963	0.8198	2.590×10^{-16}
February 3, 1950	1.268×10^{5}	28.59	5.401	0.8141	2.582×10^{-16}
Average $S=2.592\times10^{-16}\pm0.012$					

TABLE III. Na Source.

Date of measurement	N	R	T
March 28, 1950	11.28×10^{10}	0.7107	15.87×10^{10}

Bethe curve for protons in air, using the relative stopping powers of H_2 and air, compiled by Gray.[47] Recent confirmation of this curve has come from the study of the $N^{14}(n,p)C^{14}$ reaction by Cornog.[48] The calculation is complicated by two factors: the energy spread of the photo-protons due to the conservation of momentum, and the form of the range-energy relation. However, assuming an isotropic distribution and a fixed range equivalent to the average energy of the photo-protons, we calculate the number of photo-protons having their range terminated by the wall. For a plane wall and range S, there are all those protons ejected into a cone defined by θ from 0 to $\cos^{-1}(x/S)$, (Fig. 7). The total number of protons affected is then found by integrating this expression from $x=0$ to $x=S$. This gives $\frac{1}{4}NS$ where N is the number of photo-protons formed per unit volume. For a spherical counter of radius R the percentage of ranges affected is then $(3S/4R)\times100$ which may be written

$$I=(\text{surface area/volume})\times\text{range}\times\tfrac{1}{4}.$$

A correction for the spherical geometry is easily evaluated and the expression found is

$$\text{percentage of counts affected}=\frac{3}{2R}\left(\frac{S}{2R}-\frac{S^3}{24R^3}\right)\times100.$$

Thus for $S\ll R$ (i.e., high pressure), the correction is negligible. A further calculation for spherical geometry, correcting for the energy spread and range-energy relation and using an analytic expression for the stopping power, yields results in agreement with the simple formula. If we count protons having an energy of ≥140 kev say, determined by the bias setting, and the average photo-proton energy is 290 kev, then the percentage of the photo-protons not counted is

$$[(3/4R)(S_{290}-S_{150})\times100](\text{percent}),$$

where S_{290} and S_{150} are the ranges for 290-kev and 150-kev protons respectively. The value S_{150} arises because protons which lose 150-kev range in the walls will *just* be counted. We must therefore subtract from the simple expression those protons which lose 150 kev or less. The energies of the photo-protons are calculated from the γ-ray energies, assuming a binding energy[49] of 2.23 Mev.

Alternatively, an empirical approach may be adopted, by using the measured wall effects at low counter pressures to correct the measurements at higher pressures. This empirical method yields results in complete agreement with the values expected from the above calculations.

The counters were operated at a sufficiently high potential to make the loss of pulse height due to incomplete positive ion collection small. This was shown by the shape of the pulse height distribution curve which was nearly symmetrical. There was a low energy "tail" to this curve but, over the range of discriminator bias values used for the cross-section measurements, this tail was entirely due to those protons which lost some

TABLE IV. Intensity measurements.

Date of measurement	Isotope	Run	Corrected area of photo-line	Relative γ-ray intensity
I November 14, 1949 9:00 GMT	Na^{24} (2.757 Mev)	1	262.1	
		2	277.2	1.591
	ThC″ (2.618 Mev)	1	180.2	
		2	180.4	1
	Ga^{72} (2.504 Mev)	1	655.2	
		2	659.5	3.450
II January 16, 1950 9:00 GMT	Na^{24}	1	185.1	
		2	180.3	2.302
	ThC″	1	83.6	
		2	86.0	1
	Ga^{72}	1	427.3	
		2	421.5	
			427.9	4.76
III March 20, 1950 9:00 GMT	Na^{24}	1	273.1	
		2	272.0	3.452
	ThC″	1	83.0	
		2	85.6	1
	Ga^{72}	1	423.3	
		2	423.7	4.76

[47] L. H. Gray, Proc. Camb. Phil. Soc. 40, 72 (1944).
[48] Corneg, Franzen, and Stephens, Phys. Rev. 74, 1 (1948).

[49] This value was sent to us by Dr. W. B. Lewis. It is a correction by R. E. Bell and L. B. Elliott of their value 2.237 Mev published in Phys. Rev. 74, 1552 (1948). This also agreed well with the value of the binding energy 2.224 Mev deduced from the neutron-hydrogen mass difference 782±2 kev found by Taschek, Argo, Hemendinger, and Jarvis, Phys. Rev. 76, 325 (1949) and other transmutation cycles, combined with the mass spectrographic doublet 2H−D found by T. R. Roberts and A. O. C. Nier, Phys. Rev. 77, 746 (1950).

For purposes of γ-ray measurements it is preferable to take the value of Bell and Elliott based on the energy of the ThC″ γ-ray line as a standard. A decrease in the binding energy of the deuteron would, however, reduce the discrepancy between theory and experiment.

TABLE V. Photo-proton counting rate and substandard comparisons.

Measurement		I.C.C. Measurements Photo-proton counting rate	Corrected photo-proton counting rate	Substandard comparisons Ionization Oxford source relative to radium source	Ratio Stockholm source to Oxford source
I	Na	81.1	92.1±1	3.244	0.9806
November 14, 1949	RdTh	45.1	50.2±0.5	1.610	1.000
9:00 GMT	Ga	128.1	139.5±1.4	1.982	1.058
II	Na	74.33	85.18±1	4.464	1.032
January 16, 1950	RdTh	——	32.80[a]	——	1.000
9:00 GMT	Ga	104.5	114.5±1.2	24.44	1.149
III	Na	140.3	164.1±1.6	6.248	1.027
March 20, 1950	RdTh	36.43	41.45±0.4	1.435	1.000
9:00 GMT	Ga	151.1	168.6±1.7	25.91	1.059
IV	Na	229.2	240.5±2	5.541	0.8314[b]
February 13, 1950	RdTh	69.7	72.44±0.7	1.480	1.028[b]
9:00 GMT	Ga	——	±	——	——

[a] Calculated from RdTh counting rate in experiment (I) using the known counter pressures and source distances; the RdTh source was still in Stockholm so no separate count was made.
[b] Ratio of the Stockholm source of experiment (II) calculated from the ratios to the radium standard (correct to 9:00 on the respective mornings). The ratio of cross sections was calculated using the Stockholm figures for experiment (II).

of their energy in the walls. The value of the "differential" counting rate at these bias values was in complete agreement with the value to be expected from the wall effect calculations. If any appreciable loss of pulse height by positive ions had been occurring, this agreement would not have been reached. We estimate, therefore, that we are justified in correcting by the wall effect calculations alone for those protons which give too small a pulse to be recorded.

For the absolute cross section all of these errors appear directly, but for the relative cross sections some of them tend to cancel. The positive ion effect was actually observed by comparing the rise and decay times of the pulses with equal time constants of differentiation and integration. The most significant source of error for the relative cross sections is the wall effect. By counting the photo-protons from each source at the same discriminator bias, the error is minimized. The correction would be zero if the range-energy relationship were linear; the small non-linearity introduces a difference of 1.5 percent (which can be assessed to 0.1 percent).

For the absolute measurements, the wall effect correction is about 6 percent which is assessed to within 0.2 percent.

V. RESULTS

A. Absolute Cross Sections

The results from individual measurements are given in the following tables. In Tables I and II we give the results of photo-proton counting using a parameter S given by the expression

$$S=\{4\pi[C_p{}^2]/2LVP\}\times(1/R),$$

where $[C_p{}^2]$=counting rate × inverse square of distance between source and I. C. C. corrected for finite size of source and sensitive volume, L=Loschmidt's number, V=volume of counter, P=pressure in the chamber reduced to 0° measured in atmospheres, R=ratio of total activities of the source and standard Radium source as measured on the Curie chamber. Corrections are applied for (a) atomic percent of H_2 in the deuterium gas, (b) wall effect for the particular measurement, (c) absorption in source, source container, and walls of I.C.C. In Table III we give the results for absolute calibration of the sodium sources, using a parameter T defined by $T=N/R$ where N is the number of disintegrations/min. of the source, and R is the same factor as described in Table I. Then the mean value of S divided by the mean value of T is the photo-disintegration cross section $\sigma_{2.76}$ for radiosodium γ-rays. For radiothorium we take the value of the parameter T, given by the results of Bouchez,[40] assuming the effective intensity of our radium standard (N.P.L. certificate RG 467) to be known.[50]

We have then,

$$\sigma_{2.76}=(15.9\pm0.4)\times10^{-28}\text{ cm}^2,$$
$$\sigma_{2.62}=(13.8\pm0.4)\times10^{-28}\text{ cm}^2$$

and

$$\sigma_{2.76}/\sigma_{2.62}=1.17\pm0.06.$$

TABLE VI. Relative cross sections.

Measurement	$\sigma_{2.76}/\sigma_{1.80}$	$\sigma_{2.76}/\sigma_{2.62}$	$\sigma_{2.62}/\sigma_{1.80}$
I	1.327	1.131	1.175
II	1.382	1.164	1.187
III	1.302	1.178	1.105
IV		1.166	
Mean	1.337	1.159	1.156

[50] A small correction must be applied; the National Physical Laboratory specifies the effective value of the radium source as measured on their ionization chamber in which the γ-rays pass normally through 5-mm Pb. In our chamber the γ-rays pass, some of them obliquely, through 10-mm Pb and the absorption of soft radiation in the source container and carrier is less important. We evaluated this correction of 1.8 percent from the results of Kaye, Aston, and Perry, Brit. J. Radiol. 7, 540 (1934).

The errors given here are those of the reproducibility of the measurements.

B. Relative Cross Sections

The results are presented in two sections; Table IV shows the results of the intensity measurements on the spectrometer in Stockholm and Table V shows the results of the photo-proton counting and the substandard comparisons. All figures are corrected for source decay to 9:00 GMT on the day of measurement (±10:00 Swedish time). By division of the figures in these tables, the relative cross sections of Table VI are obtained.

C. Discussion of Errors

(a) *Accuracy of Intensity Measurements*

The largest deviation between two intensity measurements on one line occurred in the first sodium measurements and amounted to ±3 percent from the mean value. In all other cases the reproducibility is much better. Taking into consideration the combined results from the substandard ionization chamber measurements and the corresponding spectrometer results at different times we estimate the non-systematic errors in the γ-ray intensity measurements to be 2 percent. Additional systematic errors may be difficult to eliminate but judging from our experiments on the two γ-lines of sodium it seems unlikely, according to the previous discussion, that systematic errors should exceed 2 percent within our small energy range. If a correction of this magnitude due to a small departure from Eq. (1) should be applied to our final results, the photo-disintegration cross section would have a somewhat *smaller* slope, thus accentuating the disagreement with theory which appears later. We believe, however, that this correction should not be applied, since the correction may very well be smaller. The small gallium correction (1 percent) discussed above is probably accurate to $\frac{1}{2}$ percent.

(b) *Consistency of Oxford Measurements*

This is best illustrated by comparison of the results of individual measurements; taking the ratios of photo-proton counts for each pair of sources and dividing by the corresponding ratio as determined on the substandard ionization chamber (Tables VII and VIII). Since the photo-porton comparison is made with the same source to counter distance, and the same counter pressure for each source in the same measurement, the errors incurred in the determination of these are eliminated. The agreement is 0.3 percent, which is within the statistical error of counting.

A further comparison has been made by a reduction of the individual counting rates (instead of the ratios) to unit pressure and distance. The agreement is better than 0.6 percent, showing that the measurement of distance, and counter pressure, D_2 content, and source decay errors are small. The errors due to wall effect uncertainty and γ-ray absorption will be systematic errors and will not enter into this calibration. The total uncertainty of the photo-proton counting is estimated as 1 percent.

TABLE VII. Relative photo-proton and ionization (Na/Ga) counts.

Measurement	Photo-protons Na/Ga	Ionization Na/Ga	Photo-protons/unit ionization Na/Ga
I	$\frac{92.1}{139.5}=0.6604$	$\frac{3.244}{19.82}=0.1636$	$\frac{0.6604}{0.1636}=4.035$
II	$\frac{85.72}{115.4}=0.7429$	$\frac{4.492}{24.44}=0.1839$	$\frac{0.7429}{0.1839}=4.041$
III	$\frac{164.1}{168.6}=0.9736$	$\frac{6.248}{25.91}=0.2411$	$\frac{0.9736}{0.2411}=4.037$

TABLE VIII. Relative photo-proton and ionization (Na/Th) counts.

Measurement	Photo-protons Na/Th	Ionization Na/Th	Photo-protons/unit ionization Na/Th
I	$\frac{92.12}{50.2}=1.835$	$\frac{3.244}{1.61}=2.006$	$\frac{1.835}{2.006}=0.9109$
IV	$\frac{214.5}{72.54}=2.956$	$\frac{4.935}{1.48}=3.334$	$\frac{2.956}{3.334}=0.9078$
III	$\frac{164.1}{41.45}=3.961$	$\frac{6.248}{1.435}=4.354$	$\frac{3.961}{4.354}=0.9097$

VI. FINAL RESULTS AND COMPARISON WITH THEORY

A. Theoretical Cross Sections

One can calculate the theoretical cross section either by a meson theory, as has been done by Hansson and Hulthén[14] or by the phenomenological theory of Bethe and Longmire.[15] If coherent neutron-proton scattering data are used to determine the meson mass or effective range respectively, both theories must give the same result. The best experimental data for these calculations are the following:

(a) meson mass[51] $=(277\pm7)m_e$,
(b) binding energy of the deuteron[49] $=2.231\pm0.005$ Mev,
(c) effective range of force in the $n-p$ triplet state[52] $r_t=(1.71\pm0.04)\times10^{-13}$ cm,
(d) free proton scattering cross section for neutrons[53] $=20.32\pm0.01$ barns,

[51] This was calculated by Professor Hulthén from the experiment of neutron reflection by a liquid mirror. Hughes, Burgy, and Ringo, Phys. Rev. 77, 291 (1950). It agrees well with the mass of the π-meson (276±6) em. Smith *et al.*, Phys. Rev. 78, 86 (1950).

[52] Also obtained from the experiment of neutron reflection by a liquid mirror. Hughes, Burgy, and Ringo, Phys. Rev. 77, 291 (1950).

[53] E. Melkonian, Phys. Rev. 76, 1744 (1950).

TABLE IX. Photo-disintegration cross section of the deuteron.

	Experiment	Theory
$\sigma_{2.757}\times10^{-27}$ cm^2	15.9±0.6	15.1±0.3
$\sigma_{2.618}\times10^{-27}$ cm^2	13.9±0.6	12.5±0.3
$\sigma_{2.757}/\sigma_{2.504}$	1.34±0.05	1.49±0.02
$\sigma_{2.618}/\sigma_{2.504}$	1.16±0.04	1.24±0.01
$\sigma_{2.504}\times10^{27}$ cm^2	11.9±0.8	10.1±0.3

(e) neutron-proton capture cross section[54]
$\sigma_{cap}=(0.310\pm0.02)$ barn,

(f) energies of γ-rays used (obtained from Table IV) 2.757, 2.618, 2.504 Mev.

For the meson theory we use (a), (b), (d), and (f) since the capture cross section can be uniquely determined, in a meson theory, by these data. For a phenomenological theory we use the data (b) to (f) inclusive.

We have taken Hansson and Hulthén's[14] results, for a zero interaction in the *P*-state, and have interpolated to obtain the result for a meson mass 277; we have also adjusted the values for the small changes in the γ-ray energies and the binding energy of the deuteron. Bethe and Longmire's calculations when adjusted for the new experimental data given above, lead to values of the total cross section lower by about 2 percent.

There remain some uncertainties in the theory. If a non-zero interaction in the *P*-state is assumed, the photoelectric component of the cross section would be altered by up to 2 percent, the direction depending on the sign of the interaction.[14,15] The contribution of exchange currents to the magnetic moment of the deuteron, which appear in a charged meson theory, would change σ_m and σ_{cap} by an uncertain amount. Hansson and Hulthén[14] have shown that this effect is negligible if the Møller-Rosenfeld theory is assumed, but for other charged meson theories no theoretical calculations are available; accurate calculations are difficult because a cut-off procedure must be adopted. Professor Hulthén informs us however that it is unlikely that the *energy dependence* of the photo-magnetic effect would be appreciably altered by the existence of exchange currents.

[54] W. J. Whitehouse and G. A. R. Graham, Can. J. Research **A25**, 261 (1947). Dr. Whitehouse informs us that he attributes a possible systematic error of 4 percent to this result due partly to the uncertainty of the boron composition and partly to the finite size of the boron chambers used as neutron detectors; the total uncertainty in σ_{cap} becomes 8 percent.

B. Tabulated Results

For our experimental results (Tables IX) we attribute in addition to statistical errors possible systematic errors of 3 percent to the absolute cross section using ThC″, 2 percent using Na^{24} and 2 percent to the relative cross section.

C. Discussion

Our results could possibly indicate a divergence from theory, increasing as the energy decreases. Better agreement would be obtained if the theoretical photo-magnetic cross section were increased (by exchange currents for example). This is also suggested by measurements of the angular distribution of photo-neutrons.[55–60]

A definite limit to this possibility is given by the capture cross section.[54] The experimental value (0.310 ±0.02 barn) is very close to the theoretical value (0.315±0.003 barn). An increase of σ_{cap} by 10 percent, the limit of uncertainty of the experimental value, would be permissible.

We are grateful to the many people who have assisted us in these experiments; Dr. Seligman, Mr. Wells and others of the Isotope division, A.E.R.E., who supplied the sources; Mr. Putman, Dr. Johnston, and Miss Wildblood of A.E.R.E. who advised us on absolute calibration of the sodium sources and Mr. R. Parsons who assisted in this calibration; Mr. K. Mayne at Oxford, M. Guéron at Paris, and Mr. Morrison at Chalk River who measured the deuterium samples on their mass spectrometers.

We are especially indebted to Professor Hulthén and Mr. Hansson for informing us of the results of their calculations before publication. We are also indebted to Professor Rosenfeld who advised us on the theoretical implications of the results, also to Professor Evans for discussions on the accuracy of the photo-electron cross section.

Finally we would like to thank Professor Siegbahn and Professor Lord Cherwell for extending to us the facilities of their respective laboratories.

[55] G. A. R. Graham and H. Halban, Rev. Mod. Phys. **17**, 297 (1945).
[56] N. O. Lassen, Phys. Rev. **74**, 1533 (1948); **75**, 1099 (1949).
[57] W. M. Woodward and I. Halpern, Phys. Rev. **76**, 107 (1949).
[58] E. P. Meiners, Phys. Rev. **76**, 259 (1949).
[59] B. Hamermesh and A. Wattenberg, Phys. Rev. **76**, 1408 (1949).
[60] F. Genevese, Phys. Rev. **76**, 1288 (1949).

Experiments on the Initiation of Electric Arcs

F. E. HAWORTH
Bell Telephone Laboratories, Murray Hill, New Jersey
(Received May 29, 1950)

Arcs have been struck in vacuum between widely spaced electrodes by positive ion charging of an insulating film on the cathode, at separations from 0.5 to 5 mm and at potentials from 34 to 2000 volts. The arc current must be allowed to grow initially at the rate of at least 10^6 amp./sec. for the arc to occur. These experiments constitute a test of one of the fundamental steps postulated to account for the initiation of an arc between electrodes coming together at low voltages.

I. INTRODUCTION

WHEN two electrodes are brought together to complete an electrical circuit, under some conditions an arc is formed between them before they make metallic contact.[1] A series of events by which this arc can be initiated has been postulated,[1] one step of this series being the emission of electrons due to the intense field across an insulating film on the cathode produced by positive ions resting on this film. This paper is an account of experiments to test this step in the development of the arc; specifically, to study conditions under which an arc can result from the field produced across an insulating film by positive ions resting on it.

For a normal arc,[2] Druyvesteyn[3] has suggested that *insulating material* on the cathode may become so highly charged with positive ions that electrons are drawn from the cathode by the high electric field which they produce. Langmiur[4] suggested this mechanism earlier as an explanation of "flash back" during the reverse cycle of mercury vapor rectifiers. This was studied in detail by Kingdon and Lawton.[5] A similar effect has been reported for other types of discharge by Guntherschulze[6] in the "Spritzentladung" of the glow discharge, in the Malter[7] effect, and by Paetow.[8] The "scintillations" described by Koller and Johnson[9] in experiments with Malter cathodes were probably minute arcs.

In the experiments reported in this paper insulating films are deposited on an electrode by exposure to organic vapors, or films are built up one layer of molecules at a time from monomolecular layers of barium stearate by the Langmuir-Blodgett[10] technique. By using a positive ion gun to charge up these films, arcs have been produced between electrodes at various separations from 0.5 to 5 mm at initiating potentials as low as 34 volts, when, without the positive ions, no breakdown occurs up to 6000 volts. Current densities greater than 10^6 amp./cm^2 have been observed.

II. EXPERIMENTAL ARRANGEMENT

Figure 1 shows the experimental arrangement. The circuit in which the arc discharge is observed consists of the condenser C, the inductance L, and the electrodes. The cathode consists, in most experiments, of a highly polished chromium plated brass plate, on which are deposited the various insulating films. The anode is a platinum rod with a hole drilled along its axis, and is mounted in the end of an ion gun with the hole serving as a window through which positive ions are directed to the cathode. The ion gun consists simply of a thermionic filament, a positive grid for accelerating the electrons which ionize gas molecules, and the electrode with the window. The circuit is mounted inside a chamber which can be evacuated. The cathode plate is perpendicular to the gun axis and can be rotated in its own plane about an axis offset from the gun axis, so that as the insulating film is damaged by the arcs it can be replaced by fresh film. Positive ion current passing through the anode and reaching the cathode is observed by the galvanometer.

The apparatus is operated with the chamber at a pressure of about 5×10^{-3} mm Hg, which is sufficiently low to prevent gas discharges and yet high enough to provide plenty of positive ions. The mean free path of the gas atoms at this pressure is about 1.0 cm. The anode to cathode separation is in the range 0.5 to 5 mm. When an arc occurs it draws charge from the condenser and charges it in the opposite direction during a half-period of the circuit. When the current reaches zero at

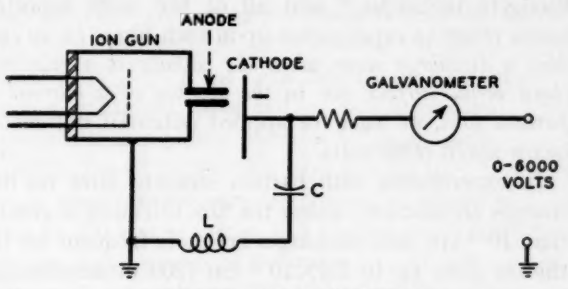

FIG. 1. Experimental circuit.

[1] L. H. Germer and F. E. Haworth, J. App. Phys. **20**, 1085 (1949).
[2] A good resume of the current theories is given by J. D. Cobine and C. J. Gallagher, Phys. Rev. **74**, 1528 (1948).
[3] M. J. Druyvesteyn, Nature **137**, 580 (1936).
[4] I. Langmuir, Zeits. f. Physik **46**, 283 (1928).
[5] K. H. Kingdon and E. J. Lawton, Gen. Elec. Rev. **42**, 474 (1939).
[6] A. Guntherschulze and H. Fricke, Zeits. f. Physik **86**, 820 (1933).
[7] L. Malter, Phys. Rev. **49**, 879; **50**, 48 (1936).
[8] H. Paetow, Zeits. f. Physik **117**, 399 (1941).
[9] L. R. Koller and R. P. Johnson, Phys. Rev. **52**, 521 (1937).
[10] K. B. Blodgett, J. Am. Chem. Soc. **57**, 1007 (1935). L. H. Germer and K. H. Storks, J. Chem. Phys. **6**, 280 (1938).

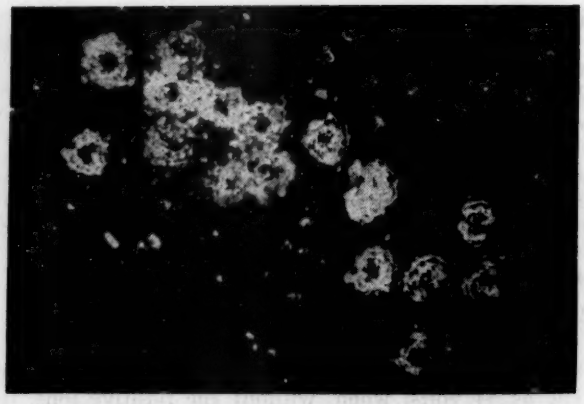

FIG. 2. Photograph of the damage to a 200-layer barium stearate film by a succession of arcs at an applied voltage of 700.×350. (The damaged spots produced by arcs at applied voltages of 200, Table I, are much smaller.)

the end of the half-period the arc stops. The condenser is immediately recharged, causing a ballistic swing of the galvanometer. The galvanometer thus serves two purposes—giving the steady value positive ion current, and, from the gallistic throw, the charge passed through each arc. The arc is completed before any appreciable recharge since the time constant of the charging circuit is about a thousand times as great as the maximum arcing time.

The occurrence of an arc is noted either by visual observation of the bright flash between the electrodes, by the galvanometer swing on recharging, or on the trace of an oscilloscope connected directly across the electrodes.

III. RESULTS

Experiments have been carried out on insulating films prepared in a number of different ways. Discharges have been found to occur at various low applied voltages after the metal electrodes had been exposed to vapors of turpentine, varnoline, or α-limonene, or after the cathode had been dusted with fine MgO powder. Discharges occur also when the cathode is of carbon rather than metal, but experiments with a carbon cathode have been found to be very erratic. The most reproducible experiments have been carried out with a cathode coated with barium stearate films deposited one layer of molecules at a time by the Langmuir-Blodgett technique,[10] and all of the work reported below refers to experiments upon such films. *In no case does a discharge occur when the cathode is a relatively clean metal surface nor in the absence of a current of positive ions*, at least for applied potential differences below about 6000 volts.

In experiments with barium stearate films no discharges are obtained unless the film thickness is greater than 10^{-5} cm, and discharges are more frequent for the thicker films up to 5.4×10^{-5} cm (200 monomolecular layers) which have been the thickest films studied. When a new film is bombarded by positive ions, discharges occur at irregular and progressively increasing intervals until they finally cease completely. The positive ion current which causes the discharges has been of the order of 10^{-8} amp., but no clear dependence of the frequency of discharge on the magnitude of the current has been established. The frequency of discharge has been found to increase with increasing voltage in the range from 34 to 700 volts but it is not clear that the frequency depends upon the electrode separation in the range which has been investigated between 0.5 and 5 mm.

Figure 2 is a photo-micrograph of the damage done by a number of discharges to a 200-layer film. Each spot of this photograph is caused by a discharge breaking down the film. The group consists of all the breakdowns occurring at one position of the cathode. When the barium stearate is removed from a damaged electrode by dissolving it in acetone, the surface of the chromium under each spot is found to be chewed up and pitted.

The photograph of Fig. 2 was obtained after arcs at an applied voltage of 700. After arcs at 200 volts the damaged spots have cross-sectional areas more than five times smaller than those of this photograph. From these areas it has been calculated that the maximum current densities in arcs at 200 volts and at the lower inductance are above 10^6 amp./cm^2 and may be above 10^7.

By means of a high resolution oscilloscope it has been determined that the discharges are actually arcs. Figure 3 shows photographs of oscilloscope traces for two values of inductance, keeping the other parameters the same. The calculated half-periods of the circuit are 0.26×10^{-6} sec. for 3(a) and 0.98×10^{-6} sec. for 3(b), which agree with the arc durations as measured on the traces of Fig. 3 within the accuracy with which the sweep time is known.

At each discharge the voltage drops abruptly from its initial value (indicated on the photographs of Fig. 3, for example, by the bright spots and the upper arrows) to the arc voltage, and at the end of the arc to a negative value, as shown in Fig. 3 by the horizontal retrace lines. The positions of zero voltage are indicated on the photographs by the lower arrows. Measured arc voltages and final voltages averaged from 52 oscilloscope traces are given in Table I.

During each arc at the lower inductance the arc voltage was steadily decreasing and the measured value of the table was the approximate mean. In each arc at the higher inductance there was an initial high voltage lasting on the average 0.11×10^{-6} sec., followed by the main arc at a comparatively constant voltage. The resistances given in the sixth column of Table I are the high frequency resistances calculated from the applied, arc, and final potentials.[11]

[11] See Eq. (4), page 1094 of reference 1.

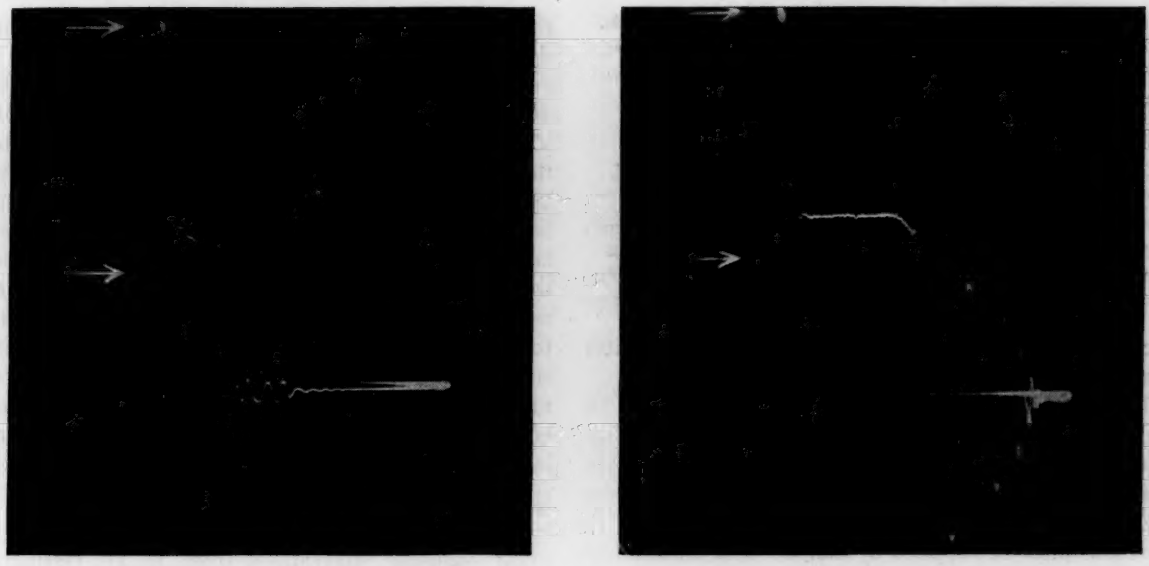

(a) (b)

FIG. 3. Oscilloscope traces of electrode potential during arcing. $V_0=200$ volts, $C=2\times10^{-9}$ f, electrode separation 1 mm, sweep time 2×10^{-6} sec. The 200-volt applied potential makes the spot at upper left, marked by the upper arrows; the positions of zero potential are marked by the lower arrows. (The open circuit oscillations occurring after the end of the arc are of no interest in the present investigation. The horizontal line represents the path of the oscilloscope spot on its return trace.)

(a) $L=3.3\times10^{-6}$ hr. The arc potential averages 33 volts.
(b) $L=48.3\times10^{-6}$ hr. The arc has two stages, the first at 60 volts, then the main arc at 34 volts.

Each of the two series of measurements of Table I was made on a new film of barium stearate. The *initial* arc voltage at the higher inductance (column 2) varies considerably between different observations, in general becoming steadily higher throughout the course of a series of observations; the voltages represented by the numbers of columns 3, 4, and 5 remain substantially unchanged for different arcs of a single series. It was also observed that the frequency of the discharges decreases with successive measurements on a single film until no arcs can be obtained *even from areas which have not been used*. The increase in initiating arc potentials (column 2) thus probably results from a progressive change in the insulating layer caused by the action of the positive ions. The initial arc potentials seem to be determined by the insulating layer, while the main arc potentials (columns 3 and 4) are characteristic of the metal only.

Calculations of the transit times across the gap for ions and vapor molecules lead to some interesting considerations. The transit time for air ions across the 1 mm gap of the arcs of Fig. 3 and Table I is 0.09×10^{-6} sec., which is nearly the same as the duration of the initial arc (0.11×10^{-6} sec.), suggesting that the initial arc lasts until the arrival of positive ions obtained from adsorbed gas on the anode. The transit time for platinum ions from the anode is 0.23×10^{-6} sec. The transit time for platinum vapor atoms at the boiling point of platinum (4300°C) is 1.6×10^{-6} sec., for chromium atoms from the cathode 1.1×10^{-6} sec., and for any vaporized atoms or molecules from the insulating layer perhaps about the same. Since the whole period of the arc is shorter than these vapor transit times, the observations apparently rule out any process which requires the filling of the gap by vaporization from the electrodes.

This conclusion is supported by visual observation of the arc, for there is a visible discharge only very close to the electrodes. A concentrated, brilliant flash occurs at the cathode, and at the smaller gaps a duller, diffuse glow at the anode. At 1 mm these occupy perhaps a quarter of the gap length. At 2 mm the anode glow has faded out, leaving the tiny cathode flash extending less than a tenth of the way across.

If the inductance L of the circuit is increased a value is soon reached for which the arc will not occur. This value varies with the applied voltage V_0, and a series of measurements was made in which, for each value of L, V_0 was slowly increased until the first arc occurred. It was found that above the arc voltage, v, this minimum V_0 increases approximately linearly with L, thus making $(V_0-v)/L$ nearly constant. Since in the arc the initial rate of increase of current $(dI/dt)_{t=0}$ is also equal to $(V_0-v)/L$ the data indicate that for an arc to form a minimum value of that rate is required. From the data this minimum value is 10^6 amp./sec.

With $L=48.3\times10^{-6}$ hr. and $C=2\times10^{-9}$ f, oscilloscope observations have been made at values of V_0 as high as 400 and as low as 100. In this range there is no change in the voltage of the main arc. At 100 volts the arcs occur very infrequently and calculation shows that

TABLE I. Averages of measurements from oscilloscope records.

Applied potential 200 volts $C=2\times10^{-3}$ f Electrode separation 1 mm							
(1)	(2)	(3)	(4)	(5)	(6)	(7)	(8)
Inductance	Arc voltage Initial	Mean	Main	Final voltage	Circuit res.	Max. current	Max. current density
(10^{-6} h)					(ohms)	(amp.)	(amp./cm²)
3.3		33.5		− 98	6	4.0	4×10^{6}
48.3	76		37	−109	12	1.0	1×10^{6}

the initial rate of current increase is only slightly greater than the above value of 10^{6} amp./sec.

In these arcs it is of course necessary that there be enough positive ions produced to prevent space charge limitation of the current density. Langmuir[12] has shown that ions produced at the anode can increase the maximum current density by a factor of only 1.8, so that ions must be supplied by ionization of the residual gas. For an arc like that of Fig. 3(b) (1 amp. maximum current, 1×10^{-6} sec. duration, and 5×10^{-3} mm Hg pressure) calculations indicate that the number of molecules entering the electron stream, assuming it to have the same breadth as the cathode spot, is of about the right size to provide sufficient ionization. At higher applied voltages and lower inductances, however, arcs have been produced with maximum currents much larger and lasting much shorter times, and it appears that the ionization produced (if the electron stream is no larger than the cathode spot) is orders of magnitude too small. Perhaps the arc can start at small current, small diameter, and high voltage, and then expand rapidly in size and current, with a rapidly decreasing voltage. Some evidence supporting this theory is found in Fig. 3(a), which shows the arc voltage decreasing throughout the arc's lifetime.

During the course of this work the author received many valuable suggestions from L. H. Germer, to whom he expresses sincere thanks.

[12] I. Langmuir, Phys. Rev. 33, 954 (1929).

PHYSICAL REVIEW VOLUME 80, NUMBER 2 OCTOBER 15, 1950

On the Symmetry of Graphite

JOSEPH S. LUKESH
Knolls Atomic Power Laboratory, General Electric Company, Schenectady, New York*
(Received June 29, 1950)

X-ray diffraction evidence indicates that the symmetry of graphite can be no higher than twofold. Evidence consists of twin observations and the occurrence of satellite reflections, both of which are incompatible with sixfold symmetry. Both phenomena strongly suggest that the classical concept of equivalent carbon-carbon bonds must be discarded in favor of one involving unequal bond lengths and bond angles.

I. INTRODUCTION

RECENTLY, considerable interest has been shown in the conductivity and the band structure of graphite.[1–4] The theoretical studies and calculations have been based on the classical crystal structure determined by Bernal,[5] where the symmetry is considered to be hexagonal holohedral. The structure consists of planar sheets of carbon atoms arranged in equilateral and equiangular hexagonal rings. The atoms in the planes are separated by a distance of $1.42kx$ units and the planes by $3.348kx$. Hexagonal symmetry is consistent with early x-ray diffraction studies and with most morphological examinations. Goldschmidt,[6] however, depicts a crystal which can have no higher than twofold symmetry. This is an isolated example and, apparently, has been regarded as a curiosity. Recently, Hoerni, and Weigle[7] have described extra reflections in electron diffraction patterns, which appear to double the a-axis. Finally, Pauling and the writer[8] have presented evidence based on certain twin relations which indicate a symmetry lower than hexagonal. It is the purpose of this communication to discuss this evidence and some of its implications, as well as to outline recently obtained x-ray diffraction data which appear to demonstrate conclusively that the symmetry of graphite cannot be higher than twofold. Although the study is not complete, it is felt that publication of the preliminary data is warranted because of its possible influence on theoretical studies.

II. TWIN OBSERVATIONS

Weissenberg and precession photographs, rotation and precession about the c-axis, have been taken of some hundred or more graphite crystals. These include

* The Knolls Atomic Power Laboratory is operated by the General Electric Company for the AEC.

[1] C. A. Coulson, Nature **159**, 265 (1947).
[2] R. P. Wallace, Phys. Rev. **71**, 265 (1947).
[3] D. Bowen, Phys. Rev. **76**, 1878 (1947).
[4] S. Mrozowski, Phys. Rev. **77**, 838 (1950).
[5] J. D. Bernal, Proc. Roy. Soc. (A) **106**, 749 (1924).
[6] V. Goldschmidt, *Atlas der Kristallformen* (Carl Winter's Universitatbuchhandlung, Heidelberg, 1915), Vol. IV.
[7] J. Hoerni and J. Weigle, Nature **164**, 1088 (1949).
[8] J. S. Lukesh and L. Pauling, Am. Mineral. **35**, 125 (1950). Read before the Crystallographic Society of America, Ann Arbor, Michigan, April 7, 1949.

natural material from six localities as well as that produced synthetically during the pouring operation at an iron blast furnace. The common characteristic of all the crystals is lack of singularity. With few exceptions, all showed two or more individuals with a common c-axis. It was at first believed that this phenomenon was a result of the loose bonding between layers and had no structural significance. However, the fact that certain angular relations appeared with such frequency as to eliminate coincidence made it evident that there must be structural control. Several such relations were observed but, for the purpose of this discussion, attention will be focused on one which relates the individuals by approximately two and one-half degrees. This relation has been found in specimens from all localities studied; in those separated from clear, white calcite found in Low Township, Quebec, it has been found in nearly fifty percent of the crystals. It would appear, therefore, that this phenomenon is not an unusual one but is the rule rather than the exception. Examples of this twin relation are shown in Figs. 1 and 2 illustrated by c-axis precession photographs. In both cases, the "a" illustrations show the photograph as taken; several twin laws are evident. In the "b" illustrations, all diffraction spots except those belonging to the twin pair under consideration have been blocked out for clarity.

An angular relation of two and one-half degrees is difficult to rationalize on the basis of a structure con-

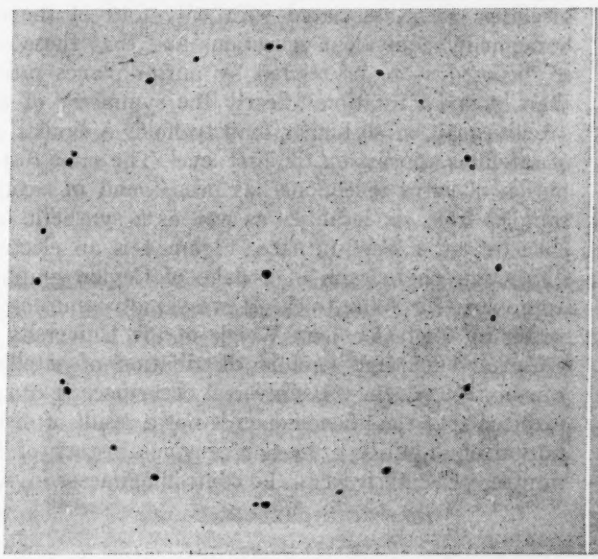

FIG. 1(a). 0-level, c-axis precession photograph of graphite, copper $K\alpha$-radiation, illustrating twinning. Crystal from Bouthillier Township, Labelle County, Quebec.

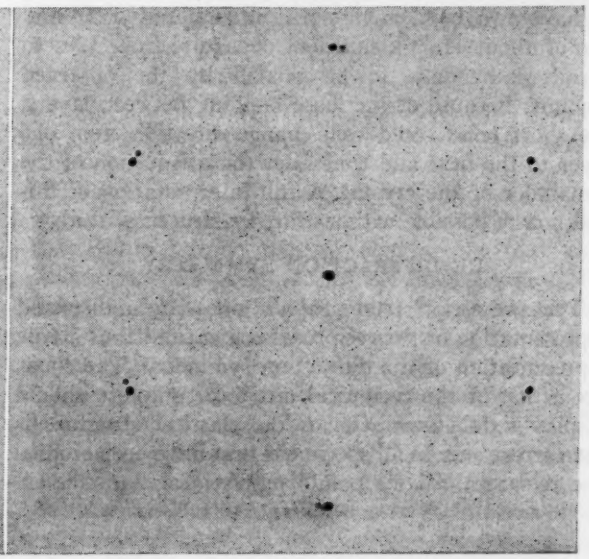

FIG. 1(b). Same as Fig. 1(a) with all individuals other than the pair separated by rotation of two and one-half degrees masked out.

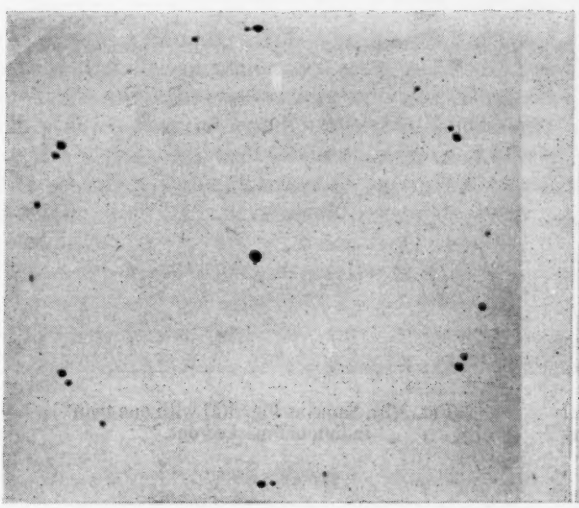

FIG. 2(a). Same as Fig. 1(a). Crystal from Low Township, Quebec.

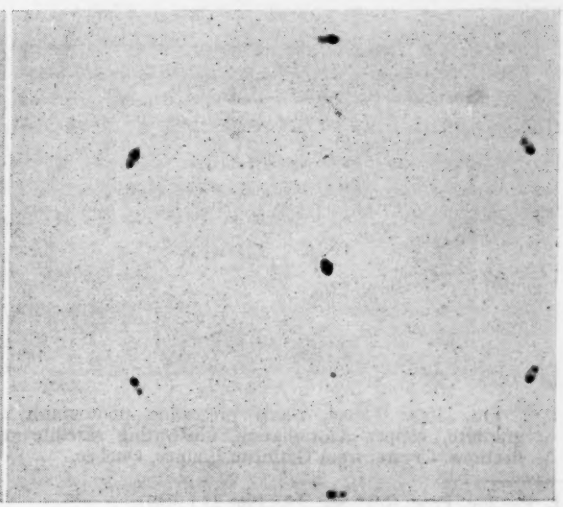

FIG. 2(b). Same as Fig. 1(b). Crystal from Low Township, Quebec.

sisting of equiangular and equilateral hexagonal rings of carbon atoms. For this reason, the writer was led to postulate a non-equivalence of the three carbon to carbon bonds of each carbon atom. Only by destroying the regularity of the hexagon could a mechanism be found which would permit such a relation, and this, of course, degrades the symmetry.

Non-equivalence of bonds in a resonating system is consistent with the recent suggestion of Pauling[9] where he has shown that, in such a system, bond numbers tend to be a simple rational fraction with a preference for one-half. In the case of graphite, this would give, ideally, one bond of order one-half and two of one-quarter. To conform with the lattice dimensions, each carbon atom in the hexagonal ring would be required to have two bond angles of approximately 121° and one of about 118°, a sufficient departure from 120° to permit individuals to be related by the observed amount. Because of the loose bonding between layers, the short bond could well change direction from one layer to the next and thus alter the orientation of the remainder of the crystal. A full interpretation of this will not be possible without further structural study.

III. DIFFRACTION SYMMETRY

The precession photograph[10] gives an undistorted representation of the reciprocal lattice, and thus a true representation of the diffraction symmetry. The c-axis projection of the reciprocal lattice of graphite should display sixfold symmetry if the classical structure is the correct one. In all specimens that have been studied the reciprocal lattice points representing the conventional hexagonal lattice show complete sixfold symmetry. However, in a majority, if not all, of the cases there is evidence of a superstructure which has only twofold symmetry. This is shown in Fig. 3 which is the c-axis zero level of the reciprocal lattice, taken by the precession method, of a naturally occurring graphite crystal found in calcite from Gatineau County, Quebec. The radiation employed was copper $K\alpha$, filtered through nickel foil. Because of the small size of the simple, conventional, cell, only the $10\bar{1}0$ group of reflections appears. It will be noted that two individuals are present. In Fig. 3b diffraction spots due to one individual have been masked out in order that the symmetry of the satellite reflections of the other individual may be seen more clearly. It is important to note that satellites occur associated with only four of the six hexagonally equivalent reflections and that these are so disposed as to be related by mirror planes rather than by axial rotation. Clearly the symmetry of the satellites can be no higher than twofold. A similar set of satellites appears on the first level. The same distribution of extra reflections has been found in natural samples from six localities as well as a synthetic one collected at a blast furnace. Figure 4 is an electron diffraction photograph of a flake of Ceylon graphite approximately 800A thick. It was kindly sent to the writer by Professor Jean Weigle of the University of Geneva. The same twofold distribution of satellites can be seen. From this universal occurrence it can be deduced that the phenomenon is not a result of distribution of impurity atoms or previous history of the sample.[11] Even if it were, the controlling factor in, say,

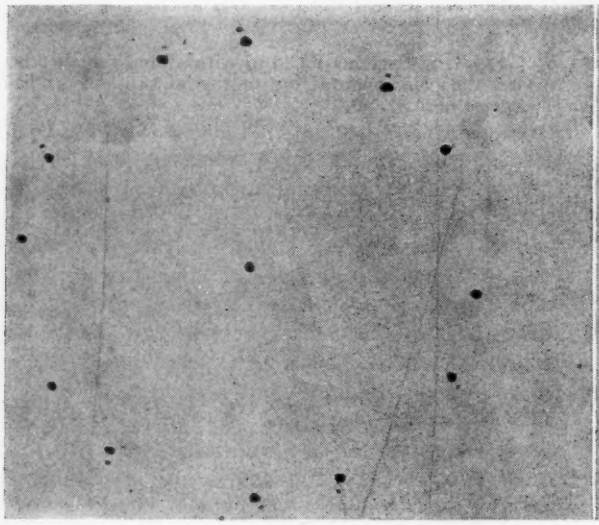

FIG. 3(a). 0-level, c-axis precession photograph of graphite, copper $K\alpha$-radiation, illustrating satellite reflections. Crystal from Gatineau County, Quebec.

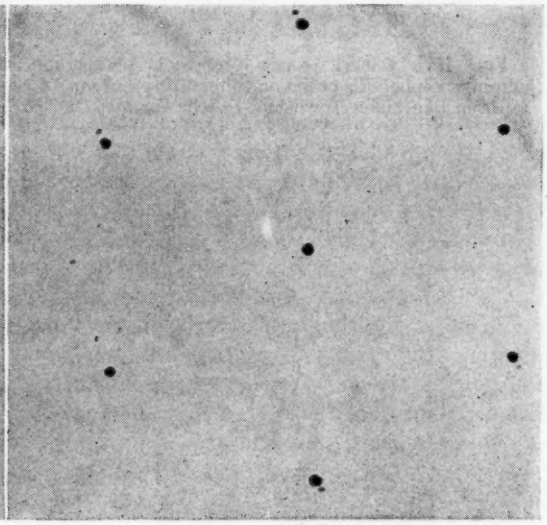

FIG. 3(b). Same as Fig. 3(a) with one twin individual masked out.

[9] L. Pauling, Proc. Roy. Soc. (A) **196**, 23 (1949).
[10] M. J. Buerger, "The photography of the reciprocal lattice," ASXRED Monograph No. 1 (1944).
[11] Examination of Figs. 1 and 2 does not reveal the existence of the satellite reflections. They are, however, present on the original film but were lost in the photographic reproduction, which was designed to emphasize the twinning.

the arrangement of impurity atoms would necessarily be symmetry of the graphite itself and one would expect a hexagonal array of satellite reflections were the symmetry hexagonal.

A further point of very considerable importance is that the spacing (in direct space) represented by the distance between the satellite reflection and its parent is exactly thirty times that between the parent and its hexagonally equivalent reflection at 120°. This leads to an increase in the hexagonal a_0 of 15 times, if one assumes the existence of a superstructure. The unit cell then becomes, compared with the orthohexagonal cell of the classical structure

Orthohexagonal (classical)	Orthorhombic (new cell)
$a_0=2.456kx$	$a_0=36.840kx$
$b_0=4.254$	$b_0=4.254$
$c_0=6.696$	$c_0=6.696$

or, transforming axes to the more conventional form,

$$a_0=4.254kx$$
$$b_0=36.840$$
$$c_0=6.696.$$

Because of the scarcity of data concerning the distribution of the superstructure reflections it is not possible to assign a space group. However, those reflections which are present appear to conform to a symmetry not higher than $D_{2h}^{23}-Fmmm$ and probably lower. It is to be emphasized that interpretation of the satellites as representing a superstructure is tentative. The important point is the obvious lack of hexagonal symmetry.

IV. DISCUSSION

The evidence cited in the preceding paragraphs can be explained only on the basis of a structure consisting of non-equiangular and non-equilateral carbon rings. The observed twin relation requires that the bond angles be other than 120°. The superstructure suggests a perturbation within the plane with a fifteen ring periodicity. (No evidence has been found that the atoms within a given sheet are not co-planar.) In order to explain these experimental observations, it is necessary to postulate non-equivalence of the three bonds of each carbon atom. It is because of the possible bearing

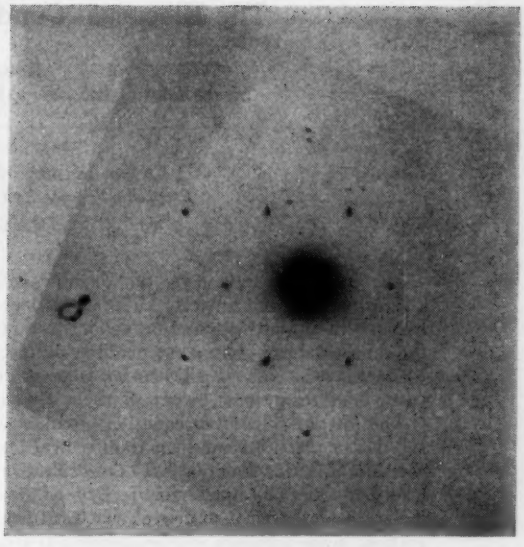

FIG. 4. Electron diffraction photograph of Ceylon graphite (courtesy Professor Jean Weigle).

of the non-equal bond lengths on the band structure and Brillouin zone pattern of graphite that these observations are presented at this time. X-ray diffraction data are, so far, inadequate to allow a determination of the nature of the departure of the crystal structure from the classical one.

It is of interest to note why the two observations described herein have not been reported before. The twinning cannot, of course, be detected in powder photographs. The reflections from the individuals of the twins are, further, superimposed in rotation photographs about the c axis and nearly so about other axes. The oscillation method, employed by Bernal[5] will not resolve them unless the oscillation range is of the order of one or two degrees. (The range normally employed is ten to twenty degrees.) The superstructure reflections are weak and can easily be overlooked in rotation and oscillation photographs. In regard to the powder method, the stronger satellite reflections are, coincidentally, superimposed on normal hexagonal reflections. For example, the reflection indexed on the basis of the new cell as 1·16·0 has nearly the same spacing as 1·15·1 ($10\bar{1}1$, hexagonal cell) and 1·14·1 has a d value nearly identical with 1·15·0 ($10\bar{1}0$, hexagonal cell).

The Electrical Conductivity of an Ionized Gas*

ROBERT S. COHEN**
Sloane Physics Laboratory, Yale University, New Haven, Connecticut

AND

LYMAN SPITZER, JR., AND PAUL MCR. ROUTLY
Princeton University Observatory, Princeton, New Jersey

(Received April 3, 1950)

The interaction term in the Boltzmann equation for an ionized gas is expressed as the sum of two terms: a term of the usual form for close encounters and a diffusion term for distant encounters. Since distant encounters, producing small deflections, are more important than close encounters, consideration of only the diffusion term gives a reasonably good approximation in most cases and approaches exactness as the temperature increases or the density decreases. It is shown that in evaluating the coefficients in this diffusion term, the integral must be cut off at the Debye shielding distance, not at the mean interionic distance.

The integro-differential equation obtained with the use of this diffusion term permits a more precise solution of the Boltzmann equation than is feasible with the Chapman-Cowling theory. While one pair of coefficients in this equation has been neglected, the remaining coefficients have all been evaluated, and the resultant equation solved numerically for the velocity distribution function in a gas of electrons and singly ionized atoms subject to a weak electrical field. Special techniques were required for this numerical integration, since solutions of the differential equation proved to be unstable in both directions. For high temperatures and low densities the computed electrical conductivity is about 60 percent of the value given by Cowling's second approximation.

INTRODUCTION

QUANTITATIVE analyses of non-uniform gases have naturally been developed along lines relevant to laboratory experiments. The theory of Enskog and of Chapman, systematically expounded by Chapman and Cowling,[1] is primarily concerned with the properties of gases composed predominantly of neutral atoms. While this theory has been applied[1-3] to the conductivity of a completely ionized gas (a gas containing no neutral atoms), the theory is in fact not well suited to handle inverse-square forces between the particles in a gas, and the accuracy of the results obtained is uncertain. In view of the great astrophysical importance of completely ionized gases, as, for example, in stellar interiors, stellar envelopes, and interstellar matter, a reconsideration of this problem has been undertaken.

A new approach to this subject is provided through the work of Chandrasekhar[4] on stellar dynamics. This work is based on the fact that when particles interact according to inverse-square forces, the velocity distribution function is affected primarily by the many small deflections produced by relatively distant encounters. There will be many such encounters during the time a particle travels over its mean free path, and the change in the particle velocity can be computed in the same way as is the change of the position of a particle in Brownian motion. On the assumption that the large deflections produced by the relatively close encounters may be neglected, Chandrasekhar therefore employs a diffusion equation for the velocity distribution function, similar to the equations describing the spatial distribution function in Brownian motion. A similar but incomplete approach was made somewhat earlier by Landau.[5] As we shall see below, the appropriate generalized diffusion equation may be solved numerically when a completely ionized gas is subject to a small electric field or a small temperature gradient.

In Part I, prepared by L. Spitzer, the basic principles of the present paper are developed. Part II, prepared by R. S. Cohen, applies this analysis to a singly ionized gas in a weak electric field, and evaluates certain coefficients in the appropriate integro-differential equation. In Part III, prepared by P. McR. Routly, the numerical solution of the resultant equation is briefly summarized. The final formulas for the electrical conductivity are given in Part IV.

I. GENERAL PRINCIPLES

The velocity distribution function f_r for particles of type r, interacting with particles of different types s, is determined by Boltzmann's equation (reference 1, Eq. (8.1$_1$))

$$\frac{\partial f_r}{\partial t}+\sum_i v_{ri}\frac{\partial f_r}{\partial x_i}+\sum_i F_{ri}\frac{\partial f_r}{\partial v_{ri}}=\sum_s\left(\frac{\partial_c f_r}{\partial t}\right)_s, \qquad (1)$$

where the notation is similar to that used by Chapman

* This work has been supported in part by the ONR.

** National Research Council Predoctoral Fellow (1946-48); now with the Department of Philosophy, Yale University. This material was submitted in part to Yale University in partial fulfillment of the requirements for a Ph.D. degree.

[1] S. Chapman and T. G. Cowling, *The Mathematical Theory of Non-Uniform Gases* (Cambridge University Press, London, 1939).

[2] T. G. Cowling, Proc. Roy. Soc. **A, 183**, 453 (1945).

[3] R. Landshoff, Phys. Rev. **76**, 904 (1949).

[4] S. Chandrasekhar, Astrophys. J. **97**, 255, 263 (1943).

[5] L. Landau, Physik Zeits. Sowjetunion **10**, 154 (1936). In this reference, the important terms representing dynamical friction, which should appear in the diffusion equation, are set equal to zero as a result of certain approximations.

and Cowling, except that v_{ri} is used for the component of velocity of an rth particle in direction i; it should be noted that F_r is the force per unit mass on a particle of type r. The quantity $(\partial_s f_r/\partial t)_s$ gives the change in f_r produced by encounters of r particles with particles of type s.

1. Evaluation of $\partial_s f_r/\partial t$ for Inverse-Square Forces

In the classical theory of non-uniform gases, the assumption is made that only the relatively close encounters are important, and that the forces between particles at greater distances have no effect. On this basis, $(\partial_s f_r/\partial t)dv_x dv_y dv_z$ is the sum of two terms, one representing the number of encounters which place particles of type r in the volume element of velocity space $dv_x dv_y dv_z$, the other, the number taking particles out of this volume element. Thus we have (reference 1, Sections 3.5 and 3.52)

$$(\partial_s f_r/\partial t)_s = \int\int\int (f_r' f_s' - f_r f_s) g b db d\epsilon d\mathbf{v}_s, \qquad (2)$$

where g is the relative velocity $|\mathbf{v}_r - \mathbf{v}_s|$ of the two types of particle before the encounter, b is the so-called impact parameter,—the distance of closest approach if no interaction forces were present,—and ϵ is the angle between the orbital plane and the plane containing the velocities of the two particles before encounter. The corresponding quantities in Chandrasekhar's[6] analysis of stellar dynamics are V, D, and Θ. The quantities f_r' and f_s' are the values of f_r and f_s for velocities such that a particle of type r will be left after the encounter within the volume element $dv_x dv_y dv_z$.

When the force between two particles varies as the inverse square of their mutual separation, Eq. (2) is no longer appropriate. As has been shown by Jeans,[7] the cumulative effect of the weak deflections resulting from the relatively distant encounters is more important than the effect of occasional large deflections (relatively close encounters). To illustrate this effect, one may compute the cumulative squared value of the deflection angle χ produced during the time Δt by all those encounters for which the impact parameter b is less than some upper limit b_1. For collisions of electrons with heavy ions, whose space density is n_i per cubic centimeter, it may be shown that

$$\langle \sum_{b<b_1} \sin^2\chi \rangle_{Av} = 4\pi g n_i b_0^2 \Delta t \left\{ \ln\left(1+\frac{b_1^2}{b_0^2}\right) - \frac{1}{1+b_0^2/b_1^2} \right\}, \qquad (3)$$

where b_0 is the value of b for which χ equals $\pi/2$, and is given by

$$b_0 = Z_i e^2/g^2 m, \qquad (4)$$

where m is the electron mass. Values computed from Eq. (3) are given in Table I. It is evident from Table I that the relatively distant encounters outweigh the closer ones. For encounters between charged particles of comparable masses, the formula for $\sin^2\chi$, considered by Chandrasekhar,[6] becomes much more complicated, but the general behavior shown in Table I is not altered.

TABLE I. Cumulative mean-square deflection produced by encounters with $b<b_1$.

Impact parameter b_1/b_0	0	1	2	4	10	10^2	10^4	10^8
Mean-square deflection in arbitrary units	0.00	0.19	0.81	1.89	3.63	8.21	17.4	35.8

While Eq. (2) could possibly be salvaged in this case, this equation is not appropriate for inverse-square forces, and obscures the true physical situation. When $\partial_s f_r/\partial t$ is produced by many small deflections, the total deflection produced in an interval of time is similar to the total distance travelled by a particle in Brownian motion, and the change of f_r by such small collisions is described by a diffusion equation of the Fokker-Planck type.[8] In fact, the value of $\partial_s f_r/\partial t$ resulting from the relatively distant encounters depends almost entirely on the first and second derivatives of f_r, not on values of f_r over the entire range of velocities.

If occasional large deflections were entirely negligible, $\partial_s f_r/\partial t$ would be entirely given by a diffusion equation. Actually, Table I shows this is not the case. If we define as a close encounter one for which b is less than some critical value b_c, then the error introduced by the neglect of these encounters will be appreciable for low values of b_m/b_0 but will gradually decrease as b_m/b_0 increases.

The effects produced by the close encounters are best described by an equation of the form (2), with b integrated only up to b_c. The relatively distant encounters are best described by the Fokker-Planck equation.[8] Thus we have finally

$$(\partial_s f_r/\partial t)_s = -J(f_r f_s) - K(f_r f_s), \qquad (5)$$

with

$$J(f_r f_s) \equiv \int_{\mathbf{v}_s=0}^{\infty}\int_{\epsilon=0}^{2\pi}\int_{b=0}^{b_c} (f_r f_s - f_r' f_s') g b db d\epsilon d\mathbf{v}_s, \qquad (6)$$

and

$$K(f_r f_s) \equiv \sum_i \frac{\partial}{\partial v_i}(f_r \langle \Delta v_{i,s} \rangle) - \tfrac{1}{2}\sum_{i,j} \frac{\partial^2}{\partial v_i \partial v_j}(f_r \langle \Delta v_{i,s} \Delta v_{j,s} \rangle), \qquad (7)$$

where, in general, for any quantity x, $\langle x_s \rangle$ is defined by

$$\langle x_s \rangle = \int_0^{\infty} g f_s dv_s \int_0^{2\pi} d\epsilon \int_{b_c}^{b_m} x b db; \qquad (8)$$

evidently $\langle x_s \rangle dt$ represents the mean value of x resulting

[6] S. Chandrasekhar, *Principles of Stellar Dynamics* (University of Chicago Press, Chicago, Illinois, 1942), Chapter II.

[7] J. H. Jeans, *Astronomy and Cosmogony* (Cambridge University Press, London, 1929), p. 318.

[8] A thorough survey of such processes has been given by S. Chandrasekhar, Rev. Mod. Phys. 15, 1 (1943).

from all encounters with particles of type s during the time interval dt. The definition of $J(f_r f_s)$ differs from that given by Chapman and Cowling (reference 1, Eq. 7.11_2) in that only the close encounters are considered, the effect of the distant encounters entering into $K(f_r f_s)$.

The terms of third and higher order in Δv have been neglected in Eq. (7). It is readily shown that these terms are relatively small if b_c much exceeds b_0. Thus Eqs. (5), (6), and (7) should give moderately high accuracy in the evaluation of $\partial_c f_r/\partial t$.

To obtain the velocity distribution function in a first approximation $J(f_r f_s)$ may be neglected. This will involve an appreciable error, as shown in Table I, but should at least provide a considerably more accurate determination of f_r than has hitherto been available. It is probably best in this case not to neglect the close encounters altogether, and we shall therefore let b_c equal zero in the computation of $K(f_r f_s)$. To obtain a higher approximation, a finite b_c could be retained, and $J(f_r f_s)$ could be introduced as a small perturbation to the solution found below.

Accordingly, we derive an equation for f_r on the assumption that $(\partial_c f_r/\partial t)_c$ in Eq. (1) may be set equal to $-K(f_r f_s)$. We shall assume that the gas is in a steady state with no systematic motion, but with an electrical field $\mathbf{E}$ and a temperature gradient ∇T. Following Chapman and Cowling (reference 1, Section 7.1), we shall write

$$f_r = f_r^{(0)} + f_r^{(1)}, \tag{9}$$

where $f_r^{(0)}$ is the Maxwellian velocity distribution function, and obtain, finally (by use of expressions $(8.3_{8,10})$ of reference 1),

$$f_r^{(0)}\left\{\frac{m_r v_r^2}{2kT}-\frac{5}{2}\right\}\sum_i v_{ri}\frac{\partial T}{T\partial x_i}-f_r^{(0)}\frac{eZ_r}{kT}\sum_i E_i v_{ri}$$
$$+\sum_s K(f_r^{(1)}f_s^{(0)})+\sum_s K(f_r^{(0)}f_s^{(1)})=0. \tag{10}$$

The electrical field E_i and the electrostatic charge e are in e.s.u.; thus for electrons Z_r is -1. Quantities involving the square of $f^{(1)}$ have been neglected in Eq. (10). When Eq. (10) is applied to an electron gas, we shall omit all subscripts from quantities referring to electrons, such as $f^{(0)}$, $f^{(1)}$, m, and v.

2. The Cut-Off Parameter b_m

The quantities $\langle \Delta v_{i,s} \rangle$ and $\langle \Delta v_{i,s} \Delta v_{j,s} \rangle$ in Eq. (7) are expressible in terms of integrals over encounters with different values of b. As is well known, these integrals diverge logarithmically, and the integration must be terminated at some maximum b_m to give a finite result. According to Cowling,[2] Chandrasekhar,[4] Spitzer[9] and others, b_m should be set equal to the interionic distance, but according to Persico,[10] Landau[5] and others, b_m should equal the Debye distance, h, at which the electron-ion plasma shields any particular charge; this cut-off has also been discussed and used by Bohm and Aller.[11] For a gas composed of electrons with a particle density n_e and of ions with an average charge $Z_i e$

$$h^2 = kT/4\pi n_e e^2(1+Z_i). \tag{11}$$

The factor $1+Z_i$ in the denominator takes into account shielding by heavy ions as well as by electrons.

We shall show that h is almost certainly the proper cut-off distance. Let us consider the mean square value of the velocity change Δv for a single electron during the time Δt. We shall consider that the electrons and ions all move in straight lines, a legitimate assumption for the distant encounters. Under these assumptions we shall then show that for a particle initially at rest $\langle (\Delta v)^2 \rangle$ is given by an equation of the form (3), even for values of b arbitrarily large compared to the interionic distance. It follows that some further assumption is needed to give a finite result, and the introduction of shielding gives h as the natural value of b_m to be used.

To obtain this result we consider the general statistics of the electrostatic field, a subject similar to that already treated by Chandrasekhar and von Neumann.[12] If Δv is the change in velocity experienced by an electron of charge $-e$ and mass m during the time interval Δt, then

$$(\Delta \mathrm{v})^2 = (e^2/m^2)\int_0^{\Delta t}\int \mathbf{E}(t)\cdot\mathbf{E}(t')\,dt\,dt' \tag{12}$$

where $\mathbf{E}(t)$ is the electrical field acting on the particle. If now Δt becomes large and both sides are averaged over all complexions of the gas, the integrand of Eq. (12) is seen to involve the autocorrelation coefficient of the electrical field $\mathbf{E}(t)$. If each electron is assumed to move in a straight line, this autocorrelation coefficient can be evaluated exactly; averaging also over a Maxwellian velocity distribution for the electrons, we have, in an obvious notation,

$$(\mathbf{E}(t)\cdot\mathbf{E}(t+\tau))_{\mathrm{Av}} = 8\pi^{\frac{1}{2}} n_e e^2 j/|\tau|, \tag{13}$$

where n_e is the particle density of electrons, and where

$$j^2 \equiv m/2kT. \tag{14}$$

Finally we obtain for Eq. (12)

$$\langle (\Delta v)^2 \rangle = (16\pi^{\frac{1}{2}} n_e e^4 j/m^2)\ln(\tau_2/\tau_1). \tag{15}$$

Since the integral of the autocorrelation coefficient over $d\tau$ diverges at both limits of integration, we have replaced the limits 0 and ∞ by τ_1 and τ_2, respectively. Apart from the argument of the logarithm, Eq. (15) agrees exactly with the $\langle (\Delta v)^2 \rangle$ found by Chandrasekhar[13]

[9] L. Spitzer, Jr., M. N. R. A. S. **100**, 396 (1940).
[10] E. Persico, M. N. R. A. S. **86**, 294 (1926).
[11] D. Bohm and L. H. Aller, Astrophys. J. **105**, 131 (1947).
[12] S. Chandrasekhar and J. von Neumann, Astrophys. J. **95**, 489 (1941); **97**, 1 (1943).
[13] Reference 6. The sum of the two Eqs. (5.724) gives $\langle (\Delta v)^2 \rangle dt$; $(G+H)/v_2$ equals $2j/\pi^{\frac{1}{2}}$ when v_2 is small.

for a particle at rest. It is evident from the derivation that Eq. (15) is valid for particles whose distance of closest approach exceeds the interionic distance, and the correct upper limit for τ must be about the period of a plasma oscillation. The divergence for low τ_1 is the natural result of extending the assumption of straight-line motion to the very close encounters; evidently τ_1 should be about b_0/v.

A simple physical argument shows the reasonableness of this result. The effects produced by electrons beyond the interionic distance may be attributed to statistical fluctuations in the electron density; i.e., the electron density is greater on one side than on the other. For electrons outside a sphere of radius r, the effective number of electrons which contribute to the force at the center of the sphere will be proportional to $n_e r^3$, and the fluctuations in this number will vary as $n_e^{\frac{1}{2}} r^{\frac{1}{2}}$, yielding a net electrical field at the center which is proportional to $e n_e^{\frac{1}{2}} r^{-\frac{1}{2}}$, but which is random in direction. This field will not change appreciably in direction for a time somewhat less than r/v, but after a time somewhat greater than r/v will be in a new random direction. Greater fields last a shorter time, while fields produced by more distant electrons are smaller. Thus this field from electrons outside a sphere of radius r will be primarily responsible for the value of the autocorrelation coefficient of $\mathbf{E}$ when t equals r/v. It follows that this autocorrelation coefficient is proportional to $(e n_e^{\frac{1}{2}} r^{-\frac{1}{2}})^2$ or to $e^2 n_e/vt$, in agreement with Eq. (13).

While the proof has been carried through only for electrons at rest, it seems most improbable that the results will be qualitatively different for electrons in motion. We shall therefore set b_m equal to h in all integrals for the diffusion coefficients, and these coefficients will then contain as a factor $\ln(h/b_0)$. While the quantity h/b_0 will in fact vary with velocity, the effect of such variations is no greater than that of other neglected terms. For the interaction of electrons with particles of average charge $Z_i e$ we may write

$$\ln(h/b_0)=\ln(qC^2) \tag{16}$$

where C^2 is the mean square electron velocity and

$$q\equiv(m/2e^2Z_i)[kT/\pi n_e(1+Z_i)]^{\frac{1}{2}}. \tag{17}$$

At high temperatures one must consider the wave character of the electrons, an effect pointed out in this connection by Marshak.[14] An electron passing through a circular aperture of radius a will be spread out by diffraction through angles of about $\lambda/2\pi a$, where λ is the electron wave-length h/mv. If this angle exceeds the classical deflection angle for an electron passing by at a distance a from an ion of charge $Z_i e$, the deflections produced by the most distant encounters will be materially increased. The ratio of the quantum mechanical to the classical deflection is $2Z_i\alpha c/v$, where α is the fine-structure constant 1/137. If Z_i is unity, this ratio equals one for a velocity of 4.4×10^8 cm/sec., corresponding to an electron temperature of about 4×10^5 degrees. For lower temperatures one may conclude that the classical formulas are valid. The corrections introduced by quantum mechanics will not be large except at temperatures substantially above 10^6 degrees.

[14] R. E. Marshak, Ann. N. Y. Acad. Sci. 41, 49 (1941).

3. Diffusion Equation in Spherical Coordinates

Before Eq. (10) can be solved, $K(ff)$ must be expressed in spherical coordinates. The derivation of the Fokker-Planck equation by Chandrasekhar is readily carried over to the spherical case, provided we substitute for the particle density f the quantity h, defined by

$$h(\mathbf{v})\equiv f(\mathbf{v},t)v^2\sin\theta. \tag{18}$$

By standard methods it follows that

$$K(ff)=-[\partial_t f(\mathbf{v},t)]/\partial t$$

$$=\frac{1}{v^2\sin\theta}\left\{\sum_i\frac{\partial}{\partial x_i}(h(\mathbf{v})\langle x_i\rangle)-\tfrac{1}{2}\sum_{i,j}\frac{\partial^2}{\partial x_i\partial x_j}(h(\mathbf{v})\langle x_ix_j\rangle)\right\}, \tag{19}$$

where x_i stands for the changes in the three coordinates; i.e., for Δv, $\Delta\theta$, and $\Delta\phi$ as i goes from 1 to 3.

To apply Eq. (19), the coefficients $\langle x_i\rangle$ must be expressed in terms of the velocity shifts in rectangular coordinates, since it is these which can be evaluated by the theory of binary encounters. We consider rectangular axes ξ, η and ζ, where ξ is in the direction of the velocity $\mathbf{v}$ before the encounter, while η and ζ are in the directions of increasing θ and ϕ, respectively. Thus the η, ζ axes are tangent to the circles of constant θ and constant ϕ at the point $\mathbf{v}$. We let Δ_ξ, Δ_η, and Δ_ζ represent the velocity displacements in these local rectangular coordinates.

The complicated general relations between Δv, $\Delta\theta$, and $\Delta\phi$ on the one hand and Δ_ξ, Δ_η, and Δ_ζ on the other simplify when these quantities are averaged over all collisions. When a small electrical field is present, for example, then (reference 1, Section 8.31) $f^{(1)}(v)$ varies as $\cos\theta$, where θ is the angle between $\mathbf{v}$ and $\mathbf{E}$. In such a case it is evident from the symmetry of the problem that the coefficients $\langle\Delta_\zeta\rangle$, $\langle\Delta_\zeta\Delta_\xi\rangle$ and $\langle\Delta_\zeta\Delta_\eta\rangle$ all vanish.

We shall also show that under these conditions $\langle\Delta_\zeta^2\rangle$ equals $\langle\Delta_\eta^2\rangle$. Consider encounters between particles of velocity $\mathbf{v}$ and those of velocity $\mathbf{v}_1$. We shall keep the angle between these velocities fixed, but shall vary the angle Θ between the fundamental plane, containing $\mathbf{v}$ and $\mathbf{v}_1$, and the ξ, η plane fixed by the direction of $\mathbf{v}$ and $\mathbf{E}$. Let Δ_F be the change of $\mathbf{v}$ perpendicular to the original value of $\mathbf{v}$ and lying in the fundamental plane, and let Δ_G be the change of $\mathbf{v}$ perpendicular to the

fundamental plane. Evidently,

$$\Delta_\eta=\Delta_F\cos\Theta+\Delta_G\sin\Theta \tag{20}$$

$$\Delta_\xi=\Delta_F\sin\Theta-\Delta_G\cos\Theta. \tag{21}$$

As Θ varies, Δ_F and Δ_G per encounter remain unchanged since the relative velocity g, the impact parameter b, etc., are all unaffected. It follows that $\langle\Delta\eta^2\rangle$ will equal $\langle\Delta_\xi^2\rangle$ provided that $\langle\sin2\Theta\rangle$ and $\langle\cos2\Theta\rangle$ are both zero. Since $f^{(1)}$ will have components varying only as $\cos\Theta$, these averages are in fact zero, and the result follows. Similar results hold when a small temperature gradient is present.

The relations we require then reduce to the simple form

$$\begin{aligned}
\langle\Delta v\rangle&=\langle\Delta_\xi\rangle+(\langle\Delta_\eta^2\rangle/v),\\
\langle\Delta\theta\rangle&=\frac{\langle\Delta_\eta\rangle}{v}-\frac{\langle\Delta_\xi\Delta_\eta\rangle}{v^2}+\frac{\cot\theta}{2v^2}\langle\Delta_\eta^2\rangle,\\
\langle(\Delta v)^2\rangle&=\langle\Delta_\xi^2\rangle,\\
\langle(\Delta v)(\Delta\theta)\rangle&=\langle\Delta_\xi\Delta_\eta\rangle/v,\\
\langle(\Delta\theta)^2\rangle&=\langle\Delta_\eta^2\rangle/v^2.
\end{aligned} \tag{22}$$

If we substitute relations (22) into Eq. (19), we have, after some rearrangement,

$$\begin{aligned}
K(ff)=&\frac{1}{v^2}\frac{\partial}{\partial v}\left[v^2f\left\{\langle\Delta_\xi\rangle+\frac{1}{v}\langle\Delta_\eta^2\rangle-\frac{1}{2v^2}\frac{\partial}{\partial v}(v^2\langle\Delta_\xi^2\rangle)\right\}\right]\\
&+\frac{1}{v\sin\theta}\frac{\partial}{\partial\theta}\left[f\sin\theta\left\{\langle\Delta_\eta\rangle-\frac{1}{2v}\frac{\partial}{\partial\theta}\langle\Delta_\eta^2\rangle\right\}\right]\\
&-\frac{1}{2v^2}\frac{\partial}{\partial v}\left[v^2\langle\Delta_\xi^2\rangle\frac{\partial f}{\partial v}\right]-\frac{1}{2v^2\sin\theta}\frac{\partial}{\partial\theta}\left[\sin\theta\langle\Delta_\eta^2\rangle\frac{\partial f}{\partial\theta}\right]\\
&-\frac{1}{v^2\sin\theta}\frac{\partial}{\partial\theta}\left[f\sin\theta\langle\Delta_\xi\Delta_\eta\rangle+\frac{\partial}{\partial v}(vf\sin\theta\langle\Delta_\xi\Delta_\eta\rangle)\right].
\end{aligned} \tag{23}$$

Equation (23) will give $K(f_r^{(n)}f_s^{(m)})$, provided that on the right-hand side $f_r^{(n)}$ replaces f wherever this occurs explicitly, and the averages of Δ_ξ, Δ_η, etc., are evaluated over $f_s^{(m)}$ rather than over f.

When this analysis was first carried out, it was thought that the cross-product term $\langle\Delta_\xi\Delta_\eta\rangle$ would have no effect on the velocity distribution function, and this term has been ignored throughout the remainder of this paper. It now appears that this term may be appreciable; to evaluate this term, however, an extension of Chandrasekhar's analysis of two-body encounters does not suffice, and a new approach to the statistics of such encounters is required.

II. DERIVATION OF EQUATION

When the average energy imparted to the electrons between encounters is small compared with their kinetic energy, we may write (reference 1, Sections 7.31 and 8.31)

$$f^{(1)}(\mathbf{v})=f^{(0)}(v)D(jv)\cos\theta. \tag{24}$$

The function $f^{(0)}(v)$ is the Maxwellian distribution function, given by the equation

$$f^{(0)}(v)=(n_ej^3/\pi^{\frac{3}{2}})\exp(-j^2v^2), \tag{25}$$

where n_e is the number of electrons per cm^3 and j is defined by Eq. (14). For subsequent convenience, we define D to be a function of the dimensionless variable jv. The quantity θ is again the polar angle measured from an axis parallel to the electric field $\mathbf{E}$.

For an electron-proton gas, Z is -1 for electrons, and if no temperature gradient is assumed, Eq. (10) becomes, in the present notation,

$$(2j^2ef^{(0)}/m)Ev\cos\theta+K(ff_p)+K(ff)=0. \tag{26}$$

1. Electron-Proton Interaction

The proton interaction term $K(ff_p)$ is found from Eq. (23). We assume the protons are at rest; all the terms in Eq. (23) for $K(ff_p)$ then cancel out or vanish except one, and we have

$$K(ff_p)=-\frac{1}{2v^2\sin\theta}\frac{\partial}{\partial\theta}\left(\sin\theta\langle\Delta_{\eta,p}^2\rangle\frac{\partial f}{\partial\theta}\right). \tag{27}$$

The diffusion coefficient $\langle\Delta_{\eta,p}^2\rangle$ may be taken from Chandrasekhar.[15] If now we substitute Eq. (9) and (24) into (27), and carry out the differentiation with respect to θ, we have

$$K(ff_p)=[3Lf^{(0)}D(jv)\cos\theta]/2v^3, \tag{28}$$

where we have written

$$L\equiv(8\pi e^4n_e/3m^2)\ln(qC^2). \tag{29}$$

2. Electron-Electron Interaction

Derivation of $K(ff)$ from Eq. (23) is more lengthy. Adopting the terminology of Chandrasekhar,[16] we denote as "test" particles, with a velocity v, those electrons whose change of velocity is being considered, and as "field" particles, with velocity v_1, those of all velocities whose perturbing effect on the test particles is being investigated. The velocities of the field particles fall in the two ranges $0<v_1<v$ and $v<v_1<\infty$.

There are nine terms in Eq. (23), each involving one diffusion coefficient. The first, second, third, and sixth terms, upon use of (24), will each yield one part due to interaction of $f^{(0)}(v_1)$, the spherically symmetric component of the field particles' velocity distribution, with the asymmetric component, $D(jv)$, of the test distribution, and a second part due to the corresponding inter-

[15] See reference 6, Eq. (5.724); the quantity $\Sigma\Delta v_\perp^2/dt$ equals $\langle\Delta_\xi^2\rangle+\langle\Delta_\eta^2\rangle$ and is thus twice $\langle\Delta_\eta^2\rangle$. For electron-proton interaction x_0 is large and $H(x_0)$ equals unity.

[16] See reference 6, paragraph 2.3.

action of $D(jv_1)$ with the symmetric component $f^{(0)}(v)$ of the test distribution. The second of these parts each, in turn, consists of integrals over dv_1 of $D(jv_1)$, multiplied by functions of v_1. The fifth and seventh terms each yield one part only, and the eighth and ninth terms are neglected.

The fourth term can apparently not be evaluated directly by any simple extension of Chandrasekhar's analysis. To evaluate this term by an indirect method, we multiply Eq. (23) by $\cos\theta \sin\theta d\theta$ and integrate over all θ. If we first subtract a term $f\langle\Delta_\xi\rangle/v$, adding this same quantity to the first term, then the fourth term becomes $-P/v$, where

$$P\equiv\int_0^\pi f\sin\theta d\theta\{\cos\theta\langle\Delta_\xi\rangle-\sin\theta\langle\Delta_\eta\rangle\}, \tag{30}$$

which will be evaluated separately.

3. Evaluation of the Diffusion Coefficients

We follow Chandrasekhar's general method,[17] but we replace his spherically symmetric distribution $f^{(0)}$ by the modified function $f^{(0)}(1+D\cos\theta)$, in accordance with Eqs. (9) and (24). The integrals obtained are all straightforward. If we let

$$\begin{aligned}\langle\Delta_\xi^2\rangle&=p_0+p_1\cos\theta,\\ \langle\Delta_\eta^2\rangle&=q_0+q_1\cos\theta,\\ \langle\Delta_\xi\rangle&=r_0+r_1\cos\theta,\end{aligned} \tag{31}$$

we have, first, Chandrasekhar's results

$$\begin{aligned}p_0&=(3LjG(x)/x);\\ q_0&=(3LjH(x)/2x);\\ r_0&=-6Lj^2G(x);\end{aligned} \tag{32}$$

where $G(x)$ and $H(x)$ are functions defined by Chandrasekhar.[18] The terms p_1, q_1, and r_1 may be expressed in the form

$$p_1=\frac{12}{5\pi^{\frac{1}{2}}}Lj\left[\frac{I_5(x)}{x^4}+x\{I_0(\infty)-I_0(x)\}\right]; \tag{33}$$

$$q_1=\frac{2}{\pi^{\frac{1}{2}}}Lj\left[\frac{I_3(x)}{x^2}-\frac{3I_5(x)}{5x^4}+\frac{2x}{5}\{I_0(\infty)-I_0(x)\}\right]; \tag{34}$$

$$r_1=-\frac{4}{\pi^{\frac{1}{2}}}Lj^2\left[\frac{2I_3(x)}{x^3}-I_0(\infty)+I_0(x)\right]; \tag{35}$$

the quantities x and $I_n(x)$ are defined by

$$x\equiv jv, \tag{36}$$

$$I_n(x)\equiv\int_0^x y^nD(y)\exp(-y^2)dy. \tag{37}$$

[17] See reference 6, Chapter II, Section 2.3. We use, in place of his gravitational factor, $G^2m_i^2$, the electrical analog, e^4/m^2. In place of his q, Eq. (17) is used.

[18] See reference 6, pp. 63 and 73.

The integral P which arises from the fourth term of Eq. (23) can be interpreted as $2/m$ times the rate of transfer of momentum per second from the test particles of velocity v in a unit volume of velocity space to field particles of all velocities; the momentum in the direction of the electrical field is considered, and the rate of momentum transfer is averaged over the polar angle θ between v and E. This rate of momentum transfer can be expressed in terms of $D(jv)$, $D(jv_1)$ and the value of $\langle\Delta_\xi\rangle$ found for a spherical distribution of field particles. To obtain this result we note that no momentum transfer arises from the interactions of $f^{(0)}(v)$ and $f^{(0)}(v_1)$, and also that the interactions of $f^{(1)}(v)$ and $f^{(1)}(v_1)$ are assumed small and are neglected. The interaction of $f^{(1)}(v)$ with $f^{(0)}(v_1)$ can be computed by finding the rate of momentum change for a single test particle on interaction with a spherically symmetrical distribution of field particles, and then integrating this rate over θ. Similarly, the interaction of $f^{(0)}(v)$ with $f^{(1)}(v_1)$ can be obtained by considering the rate of momentum change for a single field particle interacting with a spherically symmetrical distribution of test particles of velocity v, and then integrating over both θ_1 and v_1. Since these rates involve $\langle\Delta_\xi\rangle$ only, we can thus evaluate P without evaluating $\langle\Delta_\xi\rangle$ explicitly. These calculations are much simplified by the fact, first noted by Chandrasekhar,[19] that a test particle loses no momentum on interaction with a spherically symmetrical distribution of field particles if the velocities of the field particles exceed that of the test particle. We obtain

$$P=4Lj^2f^{(0)}\left\{-D(x)G(x)+\frac{2}{\pi^{\frac{1}{2}}}[I_0(\infty)-I_0(x)]\right\}. \tag{38}$$

4. Final Equation for $D(x)$

If now Eqs. (28), (30)–(35), and (38) are substituted into Eq. (26), suitably integrated over $\cos\theta \sin\theta d\theta$, we obtain a final equation for $D(x)$. Before writing this equation we first express the infinite integral $I_0(\infty)$ in closed form. We multiply Eq. (26) by $2\pi v^3\cos\theta \sin\theta dvd\theta$ and integrate over all θ and v. The three terms in (26) then give the total change of momentum arising from the electric field, electron-proton interactions, and electron-electron interactions, respectively. The last term, involving $K(ff)$, must give zero on integration, since the mutual electronic interactions cannot change the total momentum of the electrons; the actual cancellation of all the component parts of this term, on integration, provided a check on the detailed form for $K(ff)$. The second term yields $I_0(\infty)$, and the integration of the first term, representing the effect of the electrical field, is simple; we find, after some straightforward substitution,

$$I_0(\infty)=\int_0^\infty D(x)\exp(-x^2)dx=(3\pi^{\frac{1}{2}}A)/8 \tag{39}$$

[19] See reference 4, p. 260.

TABLE II. Values of velocity distribution function $D(x)$.

x	$D(x)/A$	x	$D(x)/A$	x	$D(x)/A$
0.10	0.01487	0.34	0.2079	1.12	1.790
0.11	0.01840	0.36	0.2324	1.20	2.031
0.12	0.02237	0.38	0.2579	1.28	2.291
0.13	0.02676	0.40	0.2844	1.36	2.573
0.14	0.03159	0.44	0.3401	1.44	2.878
0.15	0.03685	0.48	0.3994	1.52	3.208
0.16	0.04254	0.52	0.4620	1.60	3.567
0.17	0.04865	0.56	0.5278	1.76	4.380
0.18	0.05517	0.60	0.5967	1.92	5.343
0.19	0.06208	0.64	0.6687	2.08	6.484
0.20	0.06940	0.68	0.7438	2.24	7.842
0.22	0.08517	0.72	0.8219	2.40	9.437
0.24	0.1024	0.76	0.9033	2.56	11.34
0.26	0.1210	0.80	0.9876	2.72	13.54
0.28	0.1409	0.88	1.166	2.88	16.13
0.30	0.1621	0.96	1.359	3.04	19.05
0.32	0.1844	1.04	1.566	3.20	22.40

where

$$A\equiv -mE/[2\pi j^2 e^3 n_e \ln(qC^2)]. \quad (40)$$

If Eqs. (39) and (40) are used, the final equation for $D(x)$ becomes

$$D''(x)+P(x)D'(x)+Q(x)D(x)=R(x)+S(x), \quad (41)$$

where

$$P(x)=-2x-\frac{1}{x}+\frac{2x^2\Phi'(x)}{\Lambda}, \quad (42)$$

$$Q(x)=\frac{1}{x^2}-2\frac{1+\Phi(x)-2x^3\Phi'(x)}{\Lambda}, \quad (43)$$

$$R(x)=\frac{-2.4x^2+1.6x^4-2.4x^6}{\Lambda}A, \quad (44)$$

$$S(x)=\frac{16}{\pi^{\frac{1}{2}}\Lambda}\left\{xI_3(x)-2\left(\frac{1+x^2+x^4}{5x^3}\right)I_5(x)+x^2\left(\frac{2-3x^2+2x^4}{5}\right)I_0(x)\right\}. \quad (45)$$

The quantity $\Phi(x)$ is the usual error function, while $\Lambda(x)$ is defined by

$$\Lambda\equiv\Phi(x)-x\Phi'(x). \quad (46)$$

5. Behavior of $D(x)$ for Small and Large x

When x is small, Φ and Φ' may be expressed as power series, and the system of Eqs. (41) to (45) admits a special series solution in ascending powers of x, which we shall denote by $D_{a1}(x)$. For large x, on the other hand, Φ' may be set equal to zero, while Φ equals unity, and we have a special series solution $D_{a2}(x)$ in descending powers of x. Both these series are asymptotic, and will diverge after a certain number of terms.

To obtain general solutions for $D(x)$ in each of these regions, solutions of the homogeneous equation, with $T(x)$ set equal to zero, must be added. As will be evident from the analysis in the next section, such solutions are of two sorts. When x is small, for example, one of these solutions goes to infinity as $\exp(\alpha/x^3)$, yielding an infinite conductivity, and obviously cannot represent a physical solution. The other goes to zero more rapidly than $D_{a1}(x)$, and therefore becomes negligible as x decreases. Similarly, for large x one of the solutions cannot represent reality, while the other goes to zero more rapidly than the leading term of $D_{a2}(x)$. Hence the boundary conditions on Eq. (41) to (45) are that $D(x)$ approach $D_{a1}(x)$ and $D_{a2}(x)$, respectively, as x approaches zero or infinity.

For a Lorentz gas,[20] in which electron-electron interactions are entirely neglected and the protons are again assumed at rest, $K(ff)$ may be ignored in Eq. (26). In this case we obtain the usual result

$$D(x)=Ax^4. \quad (47)$$

III. SOLUTION OF EQUATION

We wish to find the solution to Eq. (41) which is of physical interest and which therefore agrees with the asymptotic series $D_{a1}(x)$ and $D_{a2}(x)$ at zero and infinity, respectively. This solution will be denoted by the superscript c. The complexity of Eq. (41) is such that a closed analytical solution cannot be expected. It might appear that Eq. (41) could be solved by direct numerical integration, since starting values for small x are known from the asymptotic series and the integrals in $S(x)$ could be evaluated as the integration proceeded. Actually such a direct integration is not possible. The integration of Eq. (41) is in fact unstable for both increasing and decreasing x; i.e., a small deviation from the correct solution increases so very rapidly in the course of integration that any trace of the correct solution soon disappears. This behavior is associated with the singularity of $Q(x)$, which varies as $1/x^3$ for small x. A similar instability is introduced by the dominant term in $Q(x)$ for large x. To obtain $D^c(x)$ the approach described below was developed.

1. Decomposition of Basic Equation

To overcome the difficulties associated with the instability of the basic equation, we let

$$P(x)=P_0(x)+\Delta P(x); \quad Q(x)=Q_0(x)+\Delta Q(x), \quad (48)$$

where $P_0(x)$ and $Q_0(x)$ are chosen to represent the leading parts of $P(x)$ and $Q(x)$ and also to permit analytical solution of the following simplified reduced form of Eq. (41),

$$D''(x)+P_0(x)D'(x)+Q_0(x)D(x)=0. \quad (49)$$

In general, Eq. (49) has two solutions, which we shall denote by $U(x)$ and $V(x)$. We now write

$$D(x)=g(x)U(x)+h(x)V(x) \quad (50)$$

[20] H. A. Lorentz, Proc. Amst. Acad. 7, 438 (1905).

where $g(x)$ and $h(x)$ are functions to be determined. The simultaneous differential equations for $g(x)$ and $h(x)$, which are easily obtained by the standard methods of variation of parameters, may then be solved numerically without any basic difficulty.

Because the leading terms of $P(x)$ and $Q(x)$ are different in the cases of small and large x, it was necessary to consider separately the two ranges of x, $0.10 \leq x \leq 0.80$ and $0.80 \leq x \leq 3.20$. The formulas used in each specific range are given below.

(i). Range $0.10 \leq x \leq 0.80$

All quantities peculiar to this particular range will carry the subscript 1. The functions $P_{01}(x)$ and $Q_{01}(x)$ are defined as follows:

$$P_{01}(x)=2/x, \quad Q_{01}(x)=(-3\pi^{\frac{1}{2}}/2x^{\frac{3}{2}})-2/x^2; \quad (51)$$

Equation (49) then has the solutions

$$U_1(x)=x^{-\frac{1}{2}}I_3(\alpha/x^{\frac{1}{2}}), \quad (52)$$

$$V_1(x)=x^{-\frac{1}{2}}K_3(\alpha/x^{\frac{1}{2}}), \quad (53)$$

where

$$\alpha^2 \equiv 6\pi^{\frac{1}{2}}. \quad (54)$$

The numerical values of these functions and their derivatives were computed by interpolation with the aid of B.A.A.S. Tables.[21]

(ii). Range $0.80 \leq x \leq 3.20$

The corresponding quantities in this range carry the subscript 2 and have the following expressions.

$$P_{02}(x)=-2x, \quad Q_{02}(x)=-4, \quad (55)$$

$$U_2(x)=xe^{x^2}, \quad (56)$$

$$V_2(x)=1-2xe^{x^2}\int_x^\infty e^{-v^2}dy. \quad (57)$$

2. Description of Integration

As a first step, a starting value of $g_1(x)$ at $x=0.10$ was obtained by integration of the appropriate equation for $g_1(x)$ from $x=0$, where $g_1(x)$ vanishes, to $x=0.10$. In this integration the asymptotic series D_{a1} was used to compute g_1'. The "correct" value of $g_1(x)$ at 0.10 is denoted by $g_1^c(0.10)$. In the same way, the accurate determination of $g_2^c(3.20)$ was carried out, with $D_{a2}(x)$ used to compute g_2'.

The starting value $h_1^c(0.10)$ cannot be determined so simply. In general there will be one value of $h_1(0.10)$, which, together with $g_1^c(0.10)$, will yield on numerical integration the calculated value of $g_2(x)$ at $x=3.20$; i.e., $g_2^c(3.20)$. This will be the correct solution. In order to obtain this correct solution, advantage was taken of the linear properties of the above equations. Two arbitrary starting values of $h_1(x)$ at $x=0.10$ yield two linearly independent solutions, each with the correct starting value of $g_1(x)$ at $x=0.10$. The linear combination of these two solutions, which at $x=3.20$ gives $g_2^c(3.20)$, is then the correct solution.

The starting interval used in the integration was 0.01 and was doubled after every ten steps. Central difference formulas were employed throughout. From the difference tables it was possible to guess ahead the values of $S(x)$ and of the appropriate combination of $D(x)$ and $D'(x)$; then first approximations to $g(x)$ and $h(x)$ at the next integration point could be obtained. These values were then used to obtain more accurate values of $S(x)$, etc., and ultimately second approximations to $g(x)$ and $h(x)$. This cyclic process was carried out at each integration point, in some cases as many as four times, until the values of $g(x)$ and $h(x)$ arising from the last two cycles agreed to five significant figures.

The resulting values of $D^c(x)$ over the entire range from 0.10 to 3.20 are given in Table II. The maximum error in any of these values should not exceed unity in the last digit, except perhaps for the last ten values, where errors as great as two in the last digit are possible.

The integrals $I_n(x)$ were found in the course of numerical integration up to x equal to 3.20. As x increases further these integrals also increase slightly by amounts which obviously depend on the values of $D(x)$ for x greater than 3.20. The special solution $D_{a2}(x)$ was not sufficiently accurate, and a term in $V_2(x)$ was added to yield the approximate general solution in this range. The following values were obtained.

$$I_0(\infty)=0.66464\text{A}. \quad (58)$$

$$I_3(\infty)=1.470\text{A}. \quad (59)$$

$$I_5(\infty)=4.562\text{A}. \quad (60)$$

This computed value of $I_0(\infty)$ may be compared with the exact value, which according to Eq. (39) equals $3\pi^{\frac{1}{2}}\text{A}/8$, or 0.66467A.

TABLE III. Constant in electrical conductivity formula.

Lorentz gas	1.000
Reference 1, first approximation	0.295
Cowling, second approximation	0.578
Present work	0.490

IV. VALUES OF THE ELECTRICAL CONDUCTIVITY

The electrical conductivity σ is simply the total current flowing per cm³ divided by the electrical field strength E. Electrons with velocities between v and $v+dv$ and with directions between θ and $\theta+d\theta$ and between ϕ and $\phi+d\phi$ will contribute $d\sigma$ to the conductivity per unit volume of physical space, where

$$d\sigma=[-f(v)ev\cos\theta/E]v^2\sin\theta dv d\theta d\phi. \quad (61)$$

[21] Our sincere thanks are due to Dr. W. G. Bickley of the Imperial College of Science and Technology, London, England, who very kindly sent us the proof sheets of these very complete Bessel function tables, prepared by the Committee for the Calculation of Tables of the British Association for the Advancement of Science.

TABLE IV. Values[a] of $\ln(qC^2)$ and $\ln(q'C^2)$.

Kinetic temperature (°K)	Electron density n_e (cm^{-3})				
	1	10^6	10^{12}	10^{18}	10^{24}
10^2	16.3	9.36	—	—	—
	12.4	7.78	3.2		
10^4	23.2	16.3	9.36	—	—
	17.0	12.4	7.78	3.2	
10^6	30.1	23.2	16.3	9.36	—
	21.6	17.0	12.4	7.78	3.2
10^8	37.0	30.1	23.2	16.3	9.36
	26.2	21.6	17.0	12.4	7.78

[a] For each pair of values of n_e and T, the upper figure gives $\ln(qC^2)$, the lower, $\ln(q'C^2)$; the logarithms are to the base e.

The minus sign results from the negative electronic charge. According to Eqs. (9) and (24), $f(v)$ is the sum of a spherically symmetric term $f^{(0)}(v)$, which clearly makes no net contribution to the conductivity, and the term $f^{(0)}(v)D(jv)\cos\theta$. If we substitute this term for $f(v)$, integrate over v, θ, and ϕ, and substitute from Eq. (40) for A we obtain

$$\sigma=[2m/3\pi^{\frac{1}{2}}e^2j^3\ln(qC^2)][I_3(\infty)]/\mathrm{A}. \tag{62}$$

It is convenient to express σ in terms of the conductivity in a Lorentz gas, multiplied by some constant γ. Since $I_3(\infty)/A$ for a Lorentz gas equals three, as may be seen by combining Eqs. (37) and (48), we have

$$\sigma=2\gamma(2/3\pi)^{\frac{1}{2}}mC^3/[e^2\ln(qC^2)], \tag{63}$$

where

$$\gamma=[I_3(\infty)]/3\mathrm{A}. \tag{64}$$

It may be remarked that the mutual electronic interactions do not change the conductivity directly, since the total change of momentum in such interactions is zero. Nevertheless, they alter $D(x)$ and in this way modify the effect which electron-proton collisions have in impeding the current.

The values of γ obtained from various theories are given in Table III below. The value given here, readily obtained on combining Eqs. (59) and (64), is some 15 percent smaller than that found by Cowling[2] in his second approximation.

In addition, the constant q used here is greater than that used by Cowling, since, as was shown in Part I, the cut-off distance should be equated to the Debye shielding radius h, rather than the interionic distance. We shall denote Cowling's value, based on the interionic distance, by q'. If the usual formula for C^2 is taken, and the ionic charge Z_i is set equal to unity, Eq. (17) yields

$$qC^2=(3/\pi^{\frac{1}{2}}n_e^{\frac{1}{2}}e^3)(kT/2)^{\frac{1}{2}} \tag{65}$$

while for q' we have[22]

$$q'C^2=4kT/n_e^{\frac{1}{2}}e^2. \tag{66}$$

Since $\ln(qC^2)$ appears in Eq. (63) for the conductivity, values of $\ln(qC^2)$ are given in Table IV, together with values of $\ln(q'C^2)$ for comparison. For high densities and low kinetic temperatures, q falls below q'; the analysis leading to Eq. (65) breaks down, and q' may be used. For still higher values of $n_e^{\frac{1}{2}}/T$, no values are given in the table; the present theory breaks down completely under such conditions and, moreover, the electron gas tends to become degenerate. It is evident from Table IV that for low densities and high temperatures the change in the cut-off distance has a greater effect on the conductivity than does the change in the value of γ. For these conditions the resultant electrical conductivity is about 60 percent of the value obtained by Cowling.

It is hoped to extend these results in the near future to ionized gases with different average ionic charges, and also to compute thermal conductivities. Further analysis is needed, however, to evaluate the cross-product terms in Eq. (23) which have been neglected in the present work.

[22] See reference 1, Section 10.33. $\mathrm{Ln}(q'C^2)$ equals one-half the function $A_1(2)$ introduced by Chapman and Cowling.

Influence of Plastic Flow on the Electrical and Photographic Properties of the Alkali Halide Crystals

FREDERICK SEITZ
Department of Physics, University of Illinois, Urbana, Illinois
(Received June 5, 1950)

The influence of plastic flow on the ionic conductivity and darkenability of the alkali halides is discussed on the basis of the assumption that vacant lattice sites are generated during lattice flow and condense to form clusters during a subsequent period of time. These assumptions appear to lead to a reasonable interpretation of the available experiments on the changes in properties of the alkali halides which accompany plastic flow. The bleaching action of plastic flow on colored crystals is also discussed, although the mechanism appears to be much less apparent in this case.

I. INTRODUCTION

IN the decade or so around 1930, there were carried out in continental Europe a number of experiments on the influence of plastic flow on the electrical conductivity and darkenability of the alkali halide crystals. This work, which centered in part about a controversy between Smekal[1] and Joffe[2] on the importance of imperfections in determining the properties of ionic crystals, takes on particular new meaning at the present time since it provides a close link between the properties of dislocations, positive- and negative-ion vacancies and color centers. These imperfections are finally beginning to be understood in a definite manner. It has been emphasized by a number of investigators[3] in recent years that the behavior of atomic or ionic imperfections in solids should be conditioned by the presence of dislocations. The alkali halides appear to offer a new and somewhat spectacular example. The basic experimental facts and related interpretation seem to be as follows.

1. The Enhancement of Ionic Conductivity

The ionic conductivity of sodium chloride can be increased by a factor of 100 or so as a result of plastic flow with stresses above the yield point. This effect was observed initially by Gyulai and Hartly[4] at 38°C. It was first questioned by Joffe,[2] who believed that it was the result of a type of piezoelectric effect. However, it was then confirmed by Stepanow,[5] one of Joffe's co-workers, who observed the effect in a temperature range from 30° to 170°C. The conductivity immediately after plastic flow produced by stresses in the vicinity of 10^8 dynes/cm^2 at 38°C rises from about 10^{-16} ohm^{-1} cm^{-1} to at least 10^{-14} ohm^{-1} cm^{-1}. This additional conductivity gradually decreases with time and becomes negligible at the end of an hour or so. Stress below the yield point does not produce a further rise of the same type, although Quittner[6] has apparently found a transient effect for stresses as low as 1.5×10^6 dynes/cm^2 that vanishes when the load is removed. Gyulai[7] has observed far larger effects when pellets of sodium chloride powder are pressed under hydrostatic load. Such pellets show a conductivity as high as 7.4×10^{-7} ohm^{-1} cm^{-1} at 111°C after pressing. It seems likely that only a fraction of this increase in conductivity can be a volume effect; a large portion must originate in migration on surfaces or grain boundaries. The conductivity then drops with time and has been followed for a number of hours, at the end of which period it had reached a value of 1.6×10^{-10} ohm^{-1} cm^{-1}. The normal value of the ionic conductivity of single crystals at this temperature is about 10^{-14} ohm^{-1} cm^{-1}. Recrystallization also has the effect of increasing the conductivity by a large factor.

Most of the specimens of sodium chloride employed in the experiments described above probably had of the order of one part per million of divalent impurity atoms, which have positive-ion vacancies associated with them. Recent work of Etzel and Maurer[8] shows that the heat of combination of the positive-ion vacancy and a divalent impurity is of the order of 0.3 ev in KCl, and presumably in NaCl, so that the vacancies spend an appreciable fraction of their time free at room temperature and contribute to the conductivity. It follows that the rise in ionic conductivity found by Gyulai and Hartly and by Stepanow in single crystals near room temperature arises from a density of about 10^{18} per cc of positive-ion vacancies which are produced during plastic flow. If we assume that the density of dislocation lines increases from about 10^9 to 10^{11} per cm^2 during the plastic flow, this corresponds to the production of at least one vacancy per atomic length of each line in the

[1] A. Smekal, Zeits. f. Physik **55**, 289 (1929); **93**, 166 (1934); Physik. Zeits. **33**, 204 (1932).
[2] A. Joffe, Zeits. f. Physik **62**, 730 (1930).
[3] A. H. Cottrell, Conference on the Strength of Solids (The Physical Society, London, 1948), p. 30; J. R. Haynes and W. Shockley, Conference on the Strength of Solids (The Physical Society, London, 1948), p. 151; J. S. Koehler and F. Seitz, J. App. Mech. **14**, 217 (1947).
[4] Z. Gyulai and D. Hartley, Zeits, f. Physik **51**, 378 (1928).
[5] A. W. Stepanow, Zeits. f. Physik **81**, 560 (1933).
[6] F. Quittner, Zeits. f. Physik **68**, 796 (1931); **56**, 597 (1929); **74**, 344 (1932); O. Beran and Quittner, Zeits. f. Physik **64**, 760 (1930).
[7] Z. Gyulai, Zeits. f. Physik **78**, 630 (1932); **96**, 210 (1935); Z. Gyulai and J. Boros, Zeits. f. Physik **96**, 355 (1935); Z. Gyulai and P. Tomka, Zeits. f. Physik. **96**, 350 (1935).
[8] H. Etzel and R. J. Maurer (to be published). See also, C. Wagner and P. Hantelmann, J. Chem. Phys. **18**, 72 (1950); H. Kelting and H. Witts, Zeits. f. Physik **126**, 697 (1949).

final state. One need not look far to understand how the vacancies may be produced. Figure 1, which shows the cross-sectional pattern of an edge dislocation in an alkali halide, provides an explanation. The slip plane in the alkali halides appears[9] to be the (110) plane and the slip direction is apparently (1$\bar{1}$0). Figures 1(a) and 1(b) represent cases in which the "extra" plane associated with the edge dislocation extends to two different heights in the vertical direction, the dotted lines correspond to the slip plane in the two instances. The dislocation line extends normal to the diagram. Neighboring planes possess the same pattern with the signs of the charges reversed. Suppose the pattern (*a*) is maintained for a number of rows and then changes abruptly to (*b*) so that planes (*a*) and (*b*) face one another at the point at which the slip plane jogs. The positive-ion *a* in Fig. 1(b) will then face the "incipient" halogen ion vacancy □ in Fig. 1(a). The jog will move one atomic spacing in opposite directions along the dislocation line if the positive ion *a* is replaced by a vacancy or if the incipient vacancy □ is replaced by a halogen ion. These are diffusion processes which allow[10] the projection of the dislocation pattern in the plane normal to the displacement vector to alter.

Figure 1 shows the ease with which vacancies can be generated or absorbed at an edge dislocation in one of the alkali halides, so that that the surface of the crystal or large cracks are not needed, as Nabarro[11] has emphasized. It is not difficult to imagine that vacancies evaporate from jogs of the type shown in the figure if the dislocation is set in motion and if local heating occurs as the results of dissipation of energy by the dislocation. The experiments of Taylor and Quinney[12] show that over 90 percent of the energy expended in plastic flow reappears as heat during flow. We may expect the heat generated to appear in the vicinity of the dislocations where it will be in the best possible state to evaporate dislocations from jogs of the type considered here.

It is also possible that the vacancies are generated as the result of collisions of dislocations. For example, two Taylor dislocations of opposite sign which are moving in opposite directions in neighboring slip planes and meet will produce either a row of vacancies or a row of interstitial atoms depending, respectively, upon whether the "extra" planes associated with the two dislocations are separated by one atomic spacing or overlap by this distance. Vacancies (or interstitial atoms) can be generated in this way by dislocations which are not purely of the Taylor type, provided they have at least a component of Taylor character, that is, are not pure Burgers dislocations.

It should be remarked that Stepanow[5] appreciated the fact that the heat evolved during plastic flow could play a role of the type described here; however the theories of dislocations and of vacancies had not yet evolved so that these concepts were not available to implement Stepanow's intuitive ideas.

Since processes such as sintering and recrystallization probably involve the motion of dislocations and diffusion of vacancies, we may expect them to be accompanied by an augmentation of ionic conductivity, just as in the simple case described here. In fact, the experiments of Gyulai[7] with pressed pellets show that the

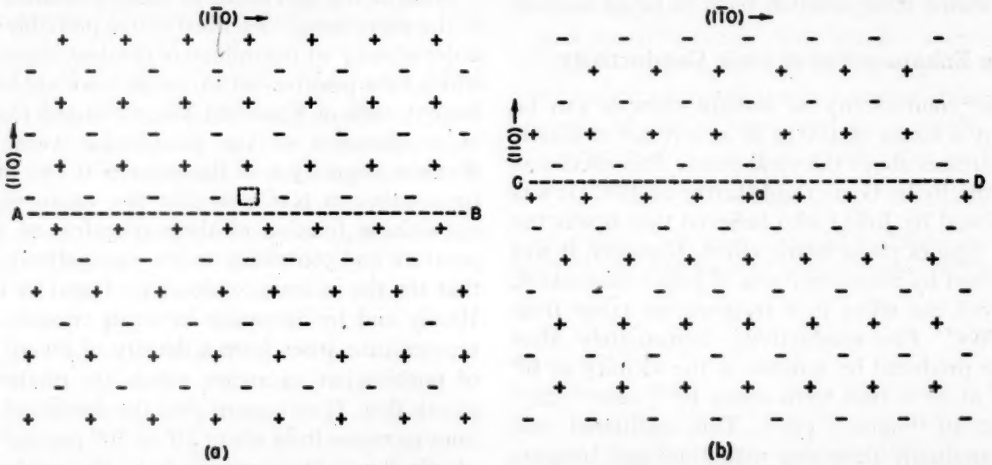

FIG. 1. Cross section through a Taylor dislocation in an alkali halide crystal at a point where the dislocation jogs from one slip plane to a neighboring plane. The slip plane is normal to the (110) direction and the slip direction is (1$\bar{1}$0). Figures (a) and (b) represent (100) planes which face one another at the position of the jog, so that the slip plane moves upward from the dotted line AB to CD. Planes beyond those shown in (a) and (b), along the continuous parts of the dislocation, resemble (a) and (b) although the sign of the charges alternate in neighboring planes. The incipient halogen-ion vacancy □ in Fig. (a) faces the positive ion *a* in Fig. (b).

[9] E. Schmid and W. Boas, *Kristallplastizität* (Verlag. Julius Springer, Berlin, 1936).
[10] See, for example, F. Seitz, "Review of the plastic properties of single crystals" (Conference on Plastic Deformation of Crystalline Solids, Pittsburgh, 1950).
[11] F. R. N. Nabarro, Conference on the Strength of Solids (The Physical Society, London, 1948), p. 75.
[12] G. I. Taylor and H. Quinney, Proc. Roy. Soc. **143**, 307 (1934); **163**, 157 (1937).

effects may be relatively enormous in the case of finely divided materials which contain relatively vast quantities of dislocations.

It is to be expected that vacancies can be generated in the same way in metals, however it would be far more difficult to detect their influence in the same, relatively unambiguous, manner. It is possible that the changes in density which accompany the production of vacancies could be detected, although there are at least two difficulties in evaluating such results quantitatively. First, the generation of new dislocations which accompany plastic flow should bring about density changes; second, it is possible, as mentioned above, that interstitial atoms as well as vacancies are produced so that the net change in density is smaller than if the vacancies alone were produced. The density changes associated with the generation of new dislocations could possibly be separated from those associated with the production of vacancies and interstitial atoms by annealing the specimens after cold working in such a way as to remove the vacancies without decreasing the additional hardening associated with the generation of new dislocations.

The vacancies produced during plastic flow will eventually recombine with one another to form clusters so that they will become immobile and cease contributing appreciably to the ionic conductivity.[13] The first stable cluster of this type is probably a pair of vacancies having opposite signs, although these may have a sufficiently small dissociation energy that they have only a transient existence. Pairs of this type may play a very important role, however, in transporting negative ion vacancies to regions where larger and more stable clusters are formed.[13] The positive-ion vacancy in sodium and potassium chloride probably[8,13] has a jump frequency in the neighborhood of 10 sec.$^{-1}$ at room temperature, whereas the free negative-ion vacancy has a value only about 10^{-5} as large, so that free negative-ion vacancies would not aggregate appreciably in 20 min. without assistance. On the other hand, pairs of vacancies probably have jump frequencies comparable to those for positive-ion vacancies[14] and could cause appreciable coagulation in a time of the order of 20 min. The clusters formed would probably dissolve in a long period of time and be precipitated in more stable form at dislocations. However, this process may take far longer periods of time than those required to form the first stable clusters, such as neutral quartets or octets. Clusters of this type could dissolve rapidly during plastic flow as a result of the thermal action of dislocations which pass nearby.

It may be remarked here that the fact that dislocations can act as sources or sinks for vacancies makes it unnecessary to assume that vacancies originate at the surface of the crystal in cases in which densities above 10^{18} per cc are produced by electron bombardment or x-ray irradiation, as the writer assumed in reference 13. However, it apparently is still necessary to assume that the positive-negative pair can diffuse at least as fast as a positive-ion vacancy to explain such things as the rapid coagulation of F-centers when the crystal is irradiated with light in the F-band (see Section II below).

II. THE ENHANCEMENT OF DARKENABILITY

The extent to which crystals of the alkali halides may be darkened by x-rays, or cathode rays, or ultraviolet light, lying in the long wave-length tail of the fundamental absorption band, is strongly dependent upon the mechanical history[15] of the specimen as well as upon other factors such as thermal treatment and impurity content. This fact appears to have been appreciated first by Przibram.[15] Exposure to these radiations produces F-centers, which are now presumed[13] with almost complete certainty to be halogen-ion vacancies to which electrons are bound, and V-centers which are believed to be positive-ion vacancies to which positive holes are bound. There is good evidence to suggest[16] that the V-centers observed at room temperature consist of a closely bound pair of positive-ion vacancies to which one or two holes are attached.

A certain amount of plastic flow increases markedly the amount by which the crystal may be darkened although very large amounts to flow seem to lead to an eventual decrease. The long wave-length tail of the fundamental absorption band is broadened as a result of plastic flow. The enhancement of the darkenability for ultraviolet light lying in this range is undoubtedly connected with this effect. It may be remarked that Smakula[15] has found that the quantum yield for darkening appears to be very close to unity during the early stages of darkening by ultraviolet light, although the yield eventually decreases. Photo-conductivity[17] is not observed during such darkening if visible light is excluded.

The influence of plastic flow on the darkenability can probably be ascribed to the large density of clusters of positive- and negative-ion vacancies which are formed during plastic flow, as discussed in Section I. The x-rays and cathode rays produce free electrons and holes and these undoubtedly have a solvent action on the clusters, as described elsewhere by the writer,[13] so that F- and V-centers are formed. These particles undoubtedly can also have a solvent action on the lines of incipient

[13] This topic has been discussed by the writer, Rev. Mod. Phys. 18, 384 (1936); see also, N. F. Mott and R. W. Gurney, *Electronic Processes in Ionic Crystals* (Oxford University Press, London, 1940). See also Estermann, Leivo and Stern, Phys. Rev. 75, 627 (1949).

[14] G. J. Dienes, J. Chem. Phys. 16, 620 (1948).

[15] See for example, K. Przibram, Zeits. f. Physik 41, 833 (1927); 68, 403 (1931) and many other papers by the same author; A. Smekal, Zeits. f. Physik 55, 289 (1929); Zeits. Ver. deut. Ing. 72, 667 (1928); E. Rexer, Physik. Zeits. 33, 202 (1932); Zeits. f. Physik 75, 777 (1932); A. Smakula, Zeits. f. Physik 59, 603 (1929); 63, 762 (1930).

[16] F. Seitz, Phys. Rev. 79, 529 (1950). E. Burstein and J. J. Oberly, Phys. Rev. 79, 903 (1950).

[17] R. Hilsch and R. W. Pohl, Zeits. f. Physik 68, 721 (1931).

vacancies along the edge of a dislocation. It requires as much energy to free these vacancies as to generate vacancies by transferring ions from the interior to the surface of the crystal. As a result, we might expect the "solvent action" of electrons and holes on the incipient vacancies at dislocations to be somewhat weaker than the action on the vacancies in small clusters, which are less stable. This view is in general agreement with the fact that it is relatively difficult to darken a well-annealed crystal for the first time, although it darkens more easily either after plastic flow or after it has been darkened and bleached without a prolonged annealing process at elevated temperatures.

In this connection it should be remarked that Harten[18] has recently described the results of darkening well-annealed single crystals of KCl with 60 kv x-rays and has found the following interesting facts, which duplicate almost exactly observations made on similar crystals by Estermann and Stern[19] with electron bombardment.

(a) Darkening is much more difficult at low temperatures than at temperatures near room temperature or above. For example, the energy required to produce an F-center rises from 100 ev near room temperature to 2000 ev near liquid air temperatures. This indicates that a thermal step is required in the production of color centers. This step is presumably the freeing of incipient vacancies from dislocations, or from clusters of vacancies near dislocations.

(b) The saturation darkening that may be achieved at low temperatures is much higher than at room temperature or above. This implies that the equilibrium darkening is determined by a balance between a forward and a reverse reaction, and that the latter decreases more rapidly than the former at lower temperatures.

(c) The darkenability of specimens which have been darkened and then bleached by the action of light and heat is not the same as that of virgin specimens, being markedly greater. This implies that the vacancies freed during the initial darkening are less tightly bound after bleaching.

The manner in which ultraviolet light lying in the tail of the fundamental absorption band produces F-centers (and presumably V-centers) is somewhat more obscure, since excitons, rather than free electrons and holes are formed. A possible explanation is as follows.

The ultraviolet light produces excitons which are trapped at clusters of vacancies if the light lies in the central portions of the fundamental band, or it produces trapped excitons directly in the vicinity of the cluster if the wave-length lies in the tail of the band. We may expect the width of the forbidden region of the energy spectrum to be altered in the vicinity of the clusters of vacancies so that excitons, which must remain in the vicinity of the cluster, can be formed with less energy there than in the center of the perfect crystal. The trapped exciton is probably metastable since irradiation in the fundamental absorption band does not appear to produce luminescent light.[20] We may assume that the electron becomes localized near a halogen-ion vacancy and the hole near a positive-ion vacancy. It is not easy to guess exactly what occurs next in the formation of F-centers and V-centers. It is possible that the positive-ion vacancy which has captured the hole wanders away immediately after the capture. This wandering would be aided by two factors. First, the negative charge of the vacancy would be neutralized by the hole so that it would not be so tightly bound, and, second, the thermal wave which is generated during readjustment of the nuclear coordinates to their new equilibrium positions may provide sufficient energy to supply the activation energy required. It is possible that once the positive-ion vacancy to which a hole is attached becomes free of the cluster it may wander about with an appreciable jump frequency carrying the hole with it. In fact, the experiments of Pringsheim[21] and his co-workers on the properties of alkali halides which are irradiated at low temperature suggest that this is the case and that single positive-ion vacancies with holes attached form normal V-centers at room temperature by a migration process of this kind.

The halogen-ion vacancy to which an electron is attached may also move somewhat away from the cluster, although we can be certain that it will not move very far, for F-centers are very stable at room temperature when light is excluded.[13]

The beautiful experiments of Apker and Taft[22] show almost conclusively that excitons formed by irradiation in the center of the fundamental absorption band of KI and RbI produce F-centers which act as the source of photoelectrons when the crystals are irradiated with light in the fundamental band or with longer wavelengths. Radiation lying in the center of the fundamental band is so strongly absorbed that only a very low surface density of F-centers is formed (*ca.* 10^{13} per cm^2). Although this represents a volume density near 10^{19} centers per cc, it is insufficient to detect by direct means; however, their observations fit in so well with other known facts that the over-all implications of their work appear to be unmistakable. It seems likely that

[18] H. Harten, Zeits. f. Physik **126**, 619 (1949).

[19] I. Estermann and O. Stern, Reports under Contract OEMsr-900, Division 14, NDRC.

[20] F. Seitz, Trans. Faraday Soc. **35**, 74 (1939); see also A. von Hippel, Zeits. f. Physik **101**, 680 (1936).

[21] Casler, Pringsheim and Yuster, Argonne Quarterly Reports (1949); J. Chem. Phys. **18**, 887 (1950). The writer is deeply indebted to these investigators for extensive discussions of their work. They have proposed that the V-band observed in the near ultraviolet in KCl when crystals are irradiated at liquid air temperature be termed the V_1-band and that the bands which are observed farther in the ultraviolet be termed V_2 and V_3. V_1, which is shown in Fig. 3 of the paper by these investigators, and which bleaches when the crystal is warmed above liquid air temperatures, is presumably formed by combination of an isolated positive-ion vacancy and a hole.

[22] L. Apker and E. Taft, Phys. Rev. (to be published). I am deeply indebted to these investigators for advance copies of their paper and a detailed discussion of their work.

clusters of vacancies or dislocations provide the agency for forming F-centers in these cases, as well as in those in which grosser darkening is obtained. There is a chance that the excitons produced in these cases decompose into trapped electrons plus free holes or into trapped holes plus free electrons, in the vicinity of the cluster, for sufficient energy is available; however, the effect of irradiation in the long wave-length part of the fundamental band shows that this assumption is not necessary.

It should be added that Alexander and Schneider[23] have suggested that a free hole possesses a very low mobility and will not contribute an observable component to conductivity. If this assumption is correct, it is possible to conclude that free holes (and bound electrons) may be produced by irradiation in the fundamental band either directly or by disintegration of excitons. This assumption does not appear to be essential for providing an explanation of the darkening of crystals by light absorbed in the fundamental band if it is assumed that a trapped exciton is metastable.

Plastic flow should have an influence on the speed with which the alkali halides can be darkened by the addition of a stoichiometric excess of the alkali metal from the vapor, in the manner employed by Pohl[24] and his co-workers (additive coloring). This process depends on the migration of electrons from the surface of the crystal to the interior where they join negative-ion vacancies, and, presumably the migration of positive-ion vacancies to the surface to compensate for the electronic charge. Pick[25] has found that the addition of divalent impurities greatly increases the rate of darkening, presumably because the density of mobile positive-ion vacancies is increased. Since plastic flow increases the density of both types of vacancies, we might expect it to have a similar if not even more pronounced effect in the case of very pure crystals.

III. BLEACHING EFFECT

Smekal[15] and Schroeder[26] have found that crystals of the alkali halides which have been darkened by x-rays in such a manner as to produce F- and V-centers undergo appreciable bleaching in the F-band when the crystals are deformed plastically. The influence of plastic flow on the V-band has not been examined. In the case of the F-band, Schroeder quotes cases in which the darkening was reduced by about 20 percent as a result of the application of uniaxial stresses of $4 \cdot 10^6$ dynes/cm^2 which is near the yield point, although stresses about ten times larger are usually needed. The amount of bleaching is critically dependent upon the history and purity of the specimen, being greatest for pure synthetic crystals.

The simplest explanation to offer of the bleaching effect of cold work is to assume that the region about the vacancies associated with the color centers become heated when a dislocation passes very close and that the electrons or holes evaporate and have an opportunity to recombine. The vacancies involved probably lie very close to dislocations, since the clusters from which they were formed were undoubtedly energetically more stable there. Thus the color centers produced in this way should be in an ideal position to experience the thermal effects which accompany the motion of dislocations. It is also possible that the color centers are induced to migrate without losing their electrons or holes and that recombination occurs in the bound state. It has also been suggested by Dr. F. C. Frank that the density of vacancies becomes sufficiently high in the vicinity of the dislocations immediately after plastic flow that the electron holes are able to wander about by tunnelling from vacancy to vacancy until they come sufficiently close to combine.

It is a pleasure to acknowledge the stimulation derived from discussion of this subject at the Pittsburgh Symposium on Plastic Deformation of Crystalline Solids (May 19 and 20, 1950) and to thank the participants for critical comments.

Note added in proof: Professor R. W. Pohl and Dr. H. Pick have kindly informed the writer that the specimens of natural crystal employed in the work of Gyulai and Hartly may have been very pure, containing only of the order of one part in ten million of divalent impurity. In this event, the rise of 100 or more in ionic conductivity during cold-work near room temperature, may imply the generation of 10^{17} mobile vacancies per cc and not the value 10^{18} estimated in part I. This lower value seems more consistent with the energy expended in cold work.

[23] J. Alexander and E. E. Schneider, Nature **164**, 653 (1949).
[24] R. W. Pohl, Physik. Zeits. **39**, 36 (1938).
[25] H. Pick, Ann. d. Physik **35**, 73 (1939); G. Heiland and H. Kelting, Zeits. f. Physik **126**, 689 (1949).
[26] H. J. Schroeder, Zeits. f. Physik **76**, 608 (1932).

Relations among the Crystal Structure Factors

H. HAUPTMAN AND J. KARLE
U. S. Naval Research Laboratory, Washington, D. C.
(Received March 30, 1950)

New relations among the structure factors and their magnitudes have been derived which take the form of inequalities. In the limiting case of point atoms, some of these reduce to equalities and many additional relations are also valid. The crystal structure problem for point atoms is discussed from the point of view of equivalent sets of algebraic equations. In this development no special symmetry relations are required. Because of the complexity of the results of this paper, their general application remains a problem to be solved.

I. INTRODUCTION

IN a previous paper,[1] the complete set of inequalities on the structure factors for crystals was derived on the basis that the Fourier series representing a crystal structure is a positive function.[2] Relations due to the more restrictive property of boundedness follow immediately from these, since $M-\rho(\mathbf{r})$ and $\rho(\mathbf{r})-m$ are non-negative if M and m are the upper and lower bounds, respectively, of the electron density function, $\rho(\mathbf{r})$. Further relations on the structure factors and their magnitudes are derived for the crystal structure problem involving N discrete points per unit cell. These are related to the problem for real atoms. The program is to derive the non-negative Hermitian forms associated with various functions of the structure factors and to illustrate the nature of the resulting equalities and inequalities. The problem for discrete atoms is discussed from the point of view of the solution of a system of algebraic equations. The possibility of adjusting the experimentally measured magnitudes to insure internal consistency making use of new relationships among the magnitudes alone is indicated.

The crystal structure problem for N point atoms is the problem of solving for ξ_j, η_j, ζ_j the system of equations[3]

$$\sum_{j=1}^{N} n_j \xi_j^h \eta_j^k \zeta_j^l = U_{hkl}, \tag{1}$$

where

$$\xi_j = e^{-2\pi i x_j}, \quad \eta_j = e^{-2\pi i y_j}, \quad \zeta_j = e^{-2\pi i z_j} \tag{2}$$

and in which, in addition to the constants n_j, only the magnitudes $|U_{hkl}|$ are assumed to be known. If we set

$$U_{hkl} = r_{hkl} \exp(i\varphi_{hkl}), \quad r_{hkl} \geq 0, \tag{3}$$

then

$$U_{\bar{h}\bar{k}\bar{l}} = r_{hkl} \exp(-i\varphi_{hkl}). \tag{4}$$

We choose $6(N-1)$ Eqs. (1) so that both U_{hkl} and $U_{\bar{h}\bar{k}\bar{l}}$ appear. These contain $3N$ unknowns ξ_j, η_j, ζ_j and $3(N-1)$ unknown phases, φ_{hkl}. It is evident that multiplying each ξ_j by an arbitrary phase factor $\exp(-2\pi i\xi_0)$, each η_j by $\exp(-2\pi i\eta_0)$, and each ζ_j by $\exp(-2\pi i\zeta_0)$ (which is equivalent to adding the constant ξ_0 to the x-coordinates of the atoms, η_0 to the y-coordinates, and ζ_0 to the z-coordinates, i.e., a translation of the coordinate frame) has the effect of multiplying U_{hkl} by $\exp[-2\pi i(h\xi_0+k\eta_0+l\zeta_0)]$ and leaving the magnitude $|U_{hkl}|$ unchanged. In other words, the phases φ_{hkl} are determined except for an additive term $-2\pi(h\xi_0+k\eta_0+l\zeta_0)$, where ξ_0, η_0, ζ_0 are arbitrary but fixed. The atomic coordinates are determined, once the origin is thus fixed, by the $6(N-1)$ Eqs. (1). Since $|U_{hkl}| = |U_{\bar{h}\bar{k}\bar{l}}|$, only $3(N-1)$ independent magnitudes r_{hkl} are needed. Since in general more than $3(N-1)$ independent magnitudes are known, the problem is overdetermined and we have the additional problem of adjusting the observed magnitudes in such a way that the complete system (1) is consistent.

In this paper we have defined each of the coordinates of the atoms in the unit cell as the roots of an algebraic equation involving the magnitudes of the U_{hkl} and the atomic numbers. For their general interest additional algebraic systems have been obtained. The approach to the problem by means of the Hermitian forms yields somewhat more general results than those obtained by Avrami[3] but shares the difficulty that the resulting equations define the atomic coordinates in terms of more than the algebraic minimum of $3(N-1)$ independent magnitudes. In addition, the equations are very complicated. It appears that the definition of each atomic coordinate in terms of the minimum number of magnitudes requires the use of general algebraic elimination theory which is being investigated at present. This, of course, does not guarantee that the solution so obtained will be simple enough to be of general use.

II. COMPLEX STRUCTURE FACTORS

The structure factor $F_{\mathbf{h}}$ is defined by means of

$$F_{\mathbf{h}} = V \int_V \rho(\mathbf{r}) \exp[-2\pi i \mathbf{h}\cdot\mathbf{r}] d\tau \tag{5}$$

where V is the volume of the unit cell and $\rho(\mathbf{r})$ is the electron density function. For N point atoms per unit

[1] J. Karle and H. Hauptman, Acta Crys. 3, 181 (1950).
[2] Systems of inequalities had been obtained previously by D. Harker and J. S. Kasper, Acta Crys. 1, 70 (1948); J. Gillis, Acta Crys. 1, 76 (1948).
[3] This problem has been considered by M. Avrami, Phys. Rev. 54, 300 (1938). In this paper new and more general results are obtained.

cell the F's are replaced by the unitary structure factors

$$U_{\mathbf{h}}=\sum_{j=1}^{N} n_j \exp[-2\pi i\mathbf{h}\cdot\mathbf{r}_j] \tag{6}$$

where $\mathbf{r}_j$ defines the position of the jth atom of atomic number Z_j and the normalized atomic numbers n_j are defined by

$$n_j=Z_j\Big/\sum_{\mu=1}^{N} Z_\mu>0. \tag{7}$$

A general system of relations valid for point atoms and involving the $U_{\mathbf{h}}$, n_j, and $\mathbf{r}_j$ will now be obtained and will be related to the inequalities previously found.[1] It will be seen that these new relations contain equalities which correspond to the inequalities which are valid for real atoms.

To derive these relations we construct a Hermitian form and reduce it to principal axes in order to find the rank of its determinant, as follows,

$$\begin{aligned}&\sum_{j=1}^{N}\frac{1}{n_j}X_j\bar{X}_j+\sum_{j=1}^{N}\sum_{\substack{\mathbf{h}'\\ N+1}}^{m}X_j\bar{X}_{\mathbf{h}'}\\ &\quad\times\exp[2\pi i(1-(N+1)/|\mathbf{h}'|)\mathbf{h}'\cdot\mathbf{r}_j]\\ &\quad+\sum_{\substack{\mathbf{h}\\ N+1}}^{m}\sum_{j=1}^{N}X_{\mathbf{h}}\bar{X}_j\exp[-2\pi i(1-(N+1)/|\mathbf{h}|)\mathbf{h}\cdot\mathbf{r}_j]\\ &\qquad+\sum_{\substack{\mathbf{h}\\ N+1}}^{m}\sum_{\substack{\mathbf{h}'\\ N+1}}^{m}X_{\mathbf{h}}\bar{X}_{\mathbf{h}'}U_{\mathbf{h}-\mathbf{h}'}=\sum_{j=1}^{N}\frac{1}{n_j}Y_j\bar{Y}_j\geq 0\end{aligned} \tag{8}$$

where

$$Y_j=X_j+\sum_{\substack{\mathbf{h}\\ N+1}}^{m}X_{\mathbf{h}}n_j\times\exp[-2\pi i(1-(N+1)/|\mathbf{h}|)\mathbf{h}\cdot\mathbf{r}_j]. \tag{9}$$

Since (8) is a diagonal form in N variables, the rank of the determinant of the original Hermitian form in (8) is N. This means that all minors of order $N+1$ or greater must vanish.

The determinant of (8) which is seen to involve $U_{\mathbf{h}}$, n's and $\mathbf{r}$'s may be written

$$\left\|\begin{matrix}(n_{jk}) & (\mu_{jk})\\ (\nu_{jk}) & (U_{jk})\end{matrix}\right\| \quad \text{(rank } N\text{)} \tag{10}$$

where

$$\begin{aligned}&n_{jk}=\delta_{jk}/n_j;\quad j,k=1,2,\cdots,N;\\ &\mu_{jk}=\exp[-2\pi i\mathbf{r}_j\cdot(\boldsymbol{\alpha}_{jk}+\mathbf{e}_j)];\\ &\qquad\qquad j=1,2,\cdots,N;\quad k=1,2,3,\cdots;\\ &\nu_{jk}=\bar{\mu}_{kj};\quad j=1,2,3,\cdots;\quad k=1,2,\cdots,N;\\ &U_{jk}=U_{\boldsymbol{\alpha}_{jk}};\quad j,k=1,2,3,\cdots,\end{aligned}$$

where

$$\boldsymbol{\alpha}_{jk}=\boldsymbol{\alpha}_{j1}+\boldsymbol{\alpha}_{1k},\quad \boldsymbol{\alpha}_{jj}=0,$$

and the ξ_j's are arbitrary.

An example of (10) is as follows

$$\left\|\begin{matrix}1/n_1 & \cdots & 0 & \xi_1^{0}\eta_1^{0}\zeta_1^{0} & \xi_1^{-1}\eta_1^{-2}\zeta_1^{0} & \cdots\\ \cdot & \cdots & \cdot & \cdot & \cdot & \cdot\\ 0 & \cdots & 1/n_N & \xi_N^{0}\eta_N^{0}\zeta_N^{0} & \xi_N^{-1}\eta_N^{-2}\zeta_N^{-2} & \cdots\\ \xi_1^{0}\eta_1^{0}\zeta_1^{0} & \cdots & \xi_N^{0}\eta_N^{0}\zeta_N^{0} & U_{000} & U_{\bar{1}\bar{2}0} & \cdots\\ \xi_1^{1}\eta_1^{2}\zeta_1^{0} & \cdots & \xi_N^{1}\eta_N^{2}\zeta_N^{0} & U_{120} & U_{000} & \cdots\\ \cdot & \cdots & \cdot & \cdot & \cdot & \cdot\end{matrix}\right\| \tag{11}$$

where

$$\xi_\rho=\exp(-2\pi ix_\rho),\quad \eta_\rho=\exp(-2\pi iy_\rho),\quad \zeta_\rho=\exp(-2\pi iz_\rho)$$

and x_ρ, y_ρ, z_ρ are the components of $\mathbf{r}_\rho$.

Since (10) is of rank N, the determinant

$$\|U_{jk}\| \quad \text{(rank } N\text{)} \tag{12}$$

is at most of rank N. It is possible to show[4] by a proof similar to (8) that the rank is exactly N. In view of (8) it follows that the principal minors of (10) and (12) are non-negative while those of order $N+1$ are zero. In the case of real atoms F_{jk} replaces U_{jk} giving

$$\|F_{jk}\|\geq 0, \tag{13}$$

and it has been shown[1] that all principal minors of (13) are non-negative.

Since all minors of (10) of order $N+1$ or greater are equal to zero, (10) represents a system of algebraic equations which define the atomic coordinates once the origin is fixed. However, the atomic coordinates are expressed in terms of the complex $U_{\mathbf{h}}$ whose phases are not known from experiment. Although (10) is sufficient to determine the phases, the relationships are highly implicit and involved and therefore the general application of (10) is at present not apparent.

Algebraic equations can be obtained which define the atomic coordinates in terms of the observed magnitudes of the structure factors. These have the obvious advantage that the unknown phases have been eliminated. However, they are very complicated and their general usefulness is not apparent.

[4] Formula (12) has been independently derived by J. Goedkoop (private communication).

III. MAGNITUDE RELATIONSHIPS

Again we construct an Hermitian form and reduce it to principal axes as follows,

$$\sum_{\substack{u<v\\1}}^{N} \frac{1}{n_u n_v} X_{(u-1)[N-(u/2)]+(v-u)} \bar{X}_{(u-1)[N-(u/2)]+(v-u)}$$

$$+ \sum_{\substack{\mathbf{h}'\\[N(N-1)/2]+1}}^{m} \sum_{\substack{u<v\\1}}^{N} X_{(u-1)(N-u/2)+(v-u)} \bar{X}_{\mathbf{h}'} \{\exp[2\pi i(1-[N(N-1)/2+1]/|\mathbf{h}'|)\mathbf{h}'\cdot(\mathbf{r}_v-\mathbf{r}_u)]$$

$$+\exp[2\pi i(1-[N(N-1)/2+1]/|\mathbf{h}'|)\mathbf{h}'\cdot(\mathbf{r}_u-\mathbf{r}_v)]\}$$

$$+ \sum_{\substack{\mathbf{h}\\[N(N-1)/2]+1}}^{m} \sum_{\substack{u<v\\1}}^{N} X_{\mathbf{h}} \bar{X}_{(u-1)(N-u/2)+(v-u)} \{\exp[2\pi i(1-[N(N-1)/2+1]/|\mathbf{h}|)\mathbf{h}\cdot(\mathbf{r}_v-\mathbf{r}_u)]$$

$$+\exp[2\pi i(1-[N(N-1)/2+1]/|\mathbf{h}|)\mathbf{h}\cdot(\mathbf{r}_u-\mathbf{r}_v)]\}$$

$$+ \sum_{\substack{\mathbf{h}\\[N(N-1)/2]+1}}^{m} \sum_{\substack{\mathbf{h}'\\[N(N-1)/2]+1}}^{m} X_{\mathbf{h}} \bar{X}_{\mathbf{h}'} \left\{ |U_{\mathbf{h}-\mathbf{h}'}|^2 + |U_{(1-[N(N-1)+2]/|\mathbf{h}+\mathbf{h}'|)(\mathbf{h}+\mathbf{h}')}|^2 - 2\sum_{\mu=1}^{N} n_\mu^2 \right\}$$

$$= \sum_{\substack{u<v\\1}}^{N} \frac{1}{n_u n_v} Y_{uv} \bar{Y}_{uv} \geq 0 \quad (14)$$

where

$$Y_{uv} = X_{(u-1)(N-u/2)+(v-u)} + n_u n_v \sum_{\substack{\mathbf{h}\\[N(N-1)/2]+1}}^{m} X_{\mathbf{h}} \{\exp[2\pi i(1-[N(N-1)/2+1]/|\mathbf{h}|)\mathbf{h}\cdot(\mathbf{r}_v-\mathbf{r}_u)]$$

$$+\exp[2\pi i(1-[N(N-1)/2+1]/|\mathbf{h}|)\mathbf{h}\cdot(\mathbf{r}_u-\mathbf{r}_v)\}. \quad (15)$$

Since (14) is a diagonal form in $N(N-1)/2$ variables the rank of the determinant of the original Hermitian form in (14) is $N(N-1)/2$. This means that all minors of order $N(N-1)/2+1$ or greater must be equal to zero.

We proceed to write the determinant of (14). Let v be the largest integer not exceeding N and such that $\Delta=4N^2-12N+1+8(v-j)$ is the square of a positive integer. Choose $u=(2N-1-\Delta^{\frac{1}{2}})/2$. Then $0<u<v\leq N$. The determinant of (14) is

$$\left\| \begin{matrix} (n_{jk}') & (\mu_{jk}') \\ (\nu_{jk}') & (U_{jk}') \end{matrix} \right\| \quad (\text{rank } N(N-1)/2), \quad (16)$$

where

$$n_{jk}' = \delta_{jk}/n_u n_v; \quad j,k=1,2,\cdots,N(N-1)/2;$$

$$\mu_{jk}' = \exp[2\pi i\alpha_{1k}\cdot(\mathbf{r}_v-\mathbf{r}_u)]+\exp[2\pi i\alpha_{1k}\cdot(\mathbf{r}_u-\mathbf{r}_v)];$$
$$j=1,2,\cdots,N(N-1)/2; \quad k=1,2,3,\cdots;$$

$$\nu_{jk}' = \mu_{kj}'; \quad j=1,2,\cdots; \quad k=1,2,\cdots, \quad N(N-1)/2;$$

$$U_{jk}' = |U_{\alpha_{j1}+\alpha_{1k}}|^2 + |U_{\alpha_{j1}-\alpha_{1k}}|^2 - 2\sum_{\mu=1}^{N} n_\mu^2;$$
$$j,k=1,2,3,\cdots;$$

and

$$\alpha_{j1}+\alpha_{1j}=0.$$

An example of (16) in one dimension is as follows

$$\left\| \begin{matrix} 1/n_1n_2 & 2 & \xi_1\xi_2^{-1}+\xi_1^{-1}\xi_2 & \xi_1^2\xi_2^{-2}+\xi_1^{-2}\xi_2^2 & \cdots \\ 2 & 2|U_0|^2-\sigma & 2|U_1|^2-\sigma & 2|U_2|^2-\sigma & \cdots \\ \xi_1\xi_2^{-1}+\xi_1^{-1}\xi_2 & 2|U_1|^2-\sigma & |U_0|^2+|U_2|^2-\sigma & |U_1|^2+|U_3|^2-\sigma & \cdots \\ \xi_1^2\xi_2^{-2}+\xi_1^{-2}\xi_2^2 & 2|U_2^2|-\sigma & |U_1|^2+|U_3|^2-\sigma & |U_0|^2+|U_4|^2-\sigma & \cdots \\ \cdot & \cdot & \cdot & \cdot & \cdot \end{matrix} \right\| \quad (17)$$

where

$$\sigma = 2\sum_{\mu=1}^{N} n_\mu^2.$$

Since (16) is of rank $N(N-1)/2$, the determinant

$$\|U_{jk}'\| \quad (\text{rank } N(N-1)/2) \quad (18)$$

is at most of rank $N(N-1)/2$, and it can be shown that the rank is exactly $N(N-1)/2$. In view of (14) it follows that the principal minors of (16) and (18) are non-negative while those of order $N(N-1)/2+1$ are zero.

Since the rank of (16) is $N(N-1)/2$, it constitutes a

system of algebraic equations which define the atomic coordinates in terms of the magnitudes of the structure factors. The high rank, however, appears to preclude general use.

IV. MISCELLANEOUS RELATIONS

It may be shown by proofs involving the construction of suitable Hermitian forms and their reduction to principal axes similar to the procedures in the previous sections that the following relationships hold. For the case of real atoms we have for the coefficients of the positive Patterson series.

$$\left\| |F_{\alpha_{j1}+\alpha_{1k}}|^2 \right\| \geq 0, \tag{19}$$

where

$$\alpha_{j1}+\alpha_{1j}=0. \tag{20}$$

For N point atoms we find the corresponding relations

$$\left\| |U_{\alpha_{j1}+\alpha_{1k}}|^2 \right\| \geq 0, \quad (\text{rank } N(N-1)+1) \tag{21}$$

and

$$\left\| |U_{\alpha_{j1}+\alpha_{1k}}|^2 - \sum_{\mu=1}^{N} n_\mu^2 \right\| \geq 0, \quad (\text{rank } N(N-1)), \tag{22}$$

where (20) holds. Relations (21) and (22) can be generalized to determinants like (16). These appear to be less valuable since their rank is at least twice that of (16).

Another type of relation is obtained from proving the non-negativity of the following Hermitian form.

$$G=\sum_{\mathbf{h}}^{m}\sum_{\mathbf{h}'} X_{\mathbf{h}}\bar{X}_{\mathbf{h}'}(|F_{\mathbf{h}-\mathbf{h}'}|^2 \mp |F_{\mathbf{h}+\mathbf{h}'+\mathbf{u}}|^2). \tag{23}$$

We find that

$$G=V^2\sum_{hkl}^{m}\sum_{h'k'l'} X_{hkl}\bar{X}_{h'k'l'}\int_{z=0}^{1}\int_{z'=0}^{z}\int_{y=0}^{1}\int_{y'=0}^{y}\int_{x=0}^{1}\int_{x'=0}^{x}[\Phi(x,y,z;x',y',z')+\bar{\Phi}(x,y,z;x',y',z')$$
$$+\Phi(x',y,z;x,y',z')+\bar{\Phi}(x',y,z;x,y',z')+\Phi(x,y',z;x',y,z')+\bar{\Phi}(x,y',z;x',y,z')$$
$$+\Phi(x,y,z';x',y',z)+\bar{\Phi}(x,y,z';x',y',z)]dx'dxdy'dydz'dz, \tag{24}$$

where

$$\Phi(x,y,z;x',y',z')=\rho(x,y,z)\rho(x',y',z')\{\exp -2\pi i[(h-h')(x-x')+(k-k')(y-y')+(l-l')(z-z')]$$
$$\mp\exp -2\pi i[(h+h'+u)(x-x')+(k+k'+v)(y-y')+(l+l'+w)(z-z')]\}$$

and u, v, w, the components of $\mathbf{u}$, are arbitrary integers. Then

$$G=4V^2\left[\int_{z=0}^{1}\int_{z'=0}^{z}\int_{y=0}^{1}\int_{y'=0}^{y}\int_{x=0}^{1}\int_{x'=0}^{x}\rho(x,y,z)\rho(x',y',z')\left|\sum_{hkl}^{m}X_{hkl}\begin{matrix}\sin\\ \cos\end{matrix}2\pi[(h+u/2)(x-x')+(k+v/2)(y-y')\right.\right.$$
$$\left.\left.+(l+w/2)(z-z')]\right|dx'dxdy'dydz'dz+\text{three similar terms}\right]\geq 0. \tag{25}$$

Therefore, we have for real atoms

$$\left\| |F_{\alpha_{j1}+\alpha_{1k}}|^2 \mp |F_{\alpha_{j1}-\alpha_{1k}+u}|^2 \right\| \geq 0 \tag{26}$$

and (20) holds.

For N point atoms we have

$$\sum_{\mathbf{h}}^{m}\sum_{\mathbf{h}'} X_{\mathbf{h}}\bar{X}_{\mathbf{h}'}(|U_{\mathbf{h}-\mathbf{h}'}|^2 \mp |U_{\mathbf{h}+\mathbf{h}'+\mathbf{u}}|^2)$$
$$=4\sum_{\mu<\nu}^{N} n_\mu n_\nu \left|\sum_{\mathbf{h}}^{N} X_{\mathbf{h}}\begin{matrix}\sin\\ \cos\end{matrix}2\pi[(\mathbf{h}+\mathbf{u}/2)\cdot(\mathbf{r}_\mu-\mathbf{r}_\nu)]\right|^2$$
$$+\sum_{\mu=1}^{N}(n_\mu^2 \mp n_\mu^2)\left|\sum_{\mathbf{h}}^{m} X_{\mathbf{h}}\right|^2 \geq 0. \tag{27}$$

Therefore the determinant for point atoms corresponding to (26)

$$\left\| |U_{\alpha_{j1}+\alpha_{1k}}|^2 \mp |U_{\alpha_{j1}-\alpha_{1k}+u}|^2 \right\| \geq 0,$$
$$\text{rank}\left\{\begin{matrix}N(N-1)/2\\ N(N-1)/2+1\end{matrix}\right\}. \tag{28}$$

Other relations which can be proven in a similar manner are

$$\left\| |U_{\alpha_{j1}-\alpha_{1k}+u+u'}|^2 + |U_{\alpha_{j1}-\alpha_{1k}+u-u'}|^2 + |U_{\alpha_{j1}+\alpha_{1k}+u}|^2 \right.$$
$$\left. + |U_{-\alpha_{j1}-\alpha_{1k}+u}|^2 - 4\sum_{\mu=1}^{N} n_\mu^2 \right\| \geq 0,$$
$$(\text{rank } N(N-1)/2), \tag{29}$$

$$\left\| |U_{\alpha_{j1}-\alpha_{1k}+u+u'}|^2+|U_{\alpha_{j1}-\alpha_{1k}+u-u'}|^2-|U_{\alpha_{j1}+\alpha_{1k}+u}|^2-|U_{-\alpha_{j1}-\alpha_{1k}+u}|^2 \right\| \geq 0, \quad (\text{rank } N(N-1)/2). \tag{30}$$

The interrelations among expressions (18), (21), (22), (28) are clarified by a factorization theorem for determinants.[5] By means of these (21) factors into (28), and (22) factors into (18) and (28). If $c_n = c_{-n}$,

$$\begin{Vmatrix} c_0 & c_{-1} & \cdots & c_{-(2n+1)} \\ c_1 & c_0 & \cdots & c_{-2n} \\ \cdot & \cdot & \cdots & \cdot \\ c_{2n+1} & c_{2n} & \cdots & c_0 \end{Vmatrix} = \begin{Vmatrix} c_0-c_1 & c_{-1}-c_2 & \cdots & c_{-n}-c_{n+1} \\ c_1-c_2 & c_0-c_3 & \cdots & c_{-(n-1)}-c_{n+2} \\ \cdot & \cdot & \cdots & \cdot \\ c_n-c_{n+1} & c_{n-1}-c_{n+2} & \cdots & c_0-c_{2n+1} \end{Vmatrix} \cdot \begin{Vmatrix} c_0+c_1 & c_{-1}+c_2 & \cdots & c_{-n}+c_{n+1} \\ c_1+c_2 & c_0+c_3 & \cdots & c_{-(n-1)}+c_{n+2} \\ \cdot & \cdot & \cdots & \cdot \\ c_n+c_{n+1} & c_{n-1}+c_{n+2} & \cdots & c_0+c_{2n+1} \end{Vmatrix} \tag{31}$$

$$\begin{Vmatrix} c_0 & c_{-1} & \cdots & c_{-2n} \\ c_1 & c_0 & \cdots & c_{-(2n-1)} \\ \cdot & \cdot & \cdots & \cdot \\ c_{2n} & c_{2n-1} & \cdots & c_0 \end{Vmatrix} = \tfrac{1}{2} \begin{Vmatrix} c_0-c_2 & c_{-1}-c_3 & \cdots & c_{-(n-1)}-c_{n+1} \\ c_1-c_3 & c_0-c_4 & \cdots & c_{-(n-2)}-c_{n+2} \\ \cdot & \cdot & \cdots & \cdot \\ c_{n-1}-c_{n+1} & c_{n-2}-c_{n+2} & \cdots & c_0-c_{2n} \end{Vmatrix} \cdot \begin{Vmatrix} c_0+c_0 & c_{-1}+c_1 & \cdots & c_{-n}+c_n \\ c_1+c_1 & c_0+c_2 & \cdots & c_{-(n-1)}+c_{n+1} \\ \cdot & \cdot & \cdots & \cdot \\ c_n+c_n & c_{n-1}+c_{n+1} & \cdots & c_0+c_{2n} \end{Vmatrix} \tag{32}$$

V. CONCLUDING REMARKS

Relations among the magnitudes and atomic numbers alone have been obtained and an adjustment procedure on the experimental data may be based on these equations. The most satisfactory procedure should involve relations which are complete; i.e., if, by means of them, $3(N-1)$ independent magnitudes determine all the others. The problem of developing such a procedure has not yet been worked out.

It should be noted that all relations derived in this paper are valid for the general crystal having no elements of symmetry. It is apparent however, that symmetry relations, when they exist, may be readily introduced.

In this paper it has been established that in the limiting case of point atoms, the atomic coordinates are determinate; in fact, they are generally over-determined. The case for real atoms does not differ greatly from that for point atoms inasmuch as the electron density is greatest close to the nucleus and, indeed, the experimental data can be "sharpened" by dividing through by average atom form factors. It has been shown that the determinantal inequalities of sufficiently high order resulting from positiveness are replaced by equations for point atoms. Since the problem for point atoms is completely determined, it is to be expected that the application of the inequalities resulting from positiveness to crystal structures should be quite restrictive.[6] Isolated inequalities by themselves need not be at all restrictive. However, positiveness requires that they be applied as a complete set and that conclusions be drawn consistent with the entire set. It would appear then that the difficulty is not that the infinite set of inequalities is not restrictive but that practical means for implementing them have yet to be developed.

[5] Equation (31) and (32) can be derived from the results of N. Achyeser and M. Krein, Comm. de la Soc. Math. de Kharkoff 11, 21 (1935).

[6] Such a statement cannot be made for arbitrary positive distributions not closely related to a point atom distribution.

Variation of Amplitude-Dependent Internal Friction in Single Crystals of Copper with Frequency and Temperature*

ARTHUR S. NOWICK**
Columbia University, New York, New York
(Received May 16, 1950)

The amplitude-dependent internal friction which originates in the motion of dislocations in single crystals of copper is studied as a function of frequency and temperature. Quantities are introduced which express the dependence of internal friction and of Young's modulus on strain amplitude and it is shown that these quantities are significant measures of the properties of a crystal. Measurements made between −60°C and +33°C show that the observed internal friction can be expressed as the product of a function of temperature and a function of amplitude alone. The data also indicate that the internal friction and elastic modulus are frequency independent when the structure sensitivity of the material is taken into account. The results are considered in terms of two viewpoints: a mechanism of *relaxation* by which dissipation is controlled through a rate process, and *simple hysteresis*, by which the stress-strain loop is independent of the rate of traversal. It is shown that the latter mechanism gives much better agreement with the experimental facts. Finally, simple hysteresis is interpreted in terms of the dislocation theory.

I. INTRODUCTION

THE internal friction of solid materials is usually studied by observing the behavior of a properly shaped specimen body which is vibrating in one of its normal modes. A coefficient of internal friction, Δ, can be defined by the formula

$$\Delta = w^d/2w^v, \tag{1}$$

where w^d is the energy dissipated per unit volume per cycle of vibration and w^v is the total vibrational energy per unit volume. There are numerous sources of dissipation in solids;[1] among these is the internal stress produced by cold-work. In a study of single crystals of copper and zinc in forced longitudinal vibration in the frequency range 30 to 100 kc/sec., Read[2] reports a characteristic amplitude-dependent internal friction which he relates to the internal stress by observing that the dissipation is increased by cold-work and decreased to a minimum by annealing at a high temperature. It is found that the internal friction increases and Young's modulus of the material decreases with increasing strain amplitude of vibration in both zinc and copper crystals. There is, however, a striking difference between the behavior of these two metals; in contrast to the behavior of zinc, the internal friction of copper crystals does not depend on the previous vibrational history of the material, nor is a persistent temporal variation of this quantity observed, following heat treatment or cold-work.

The internal stress associated with cold-work has long been related to the presence of linear lattice imperfections known as dislocations.[3] It is the stress-induced motion of these dislocations that is responsible for the dissipation observed by Read. Although great interest has recently been shown in the internal friction due to dislocations in zinc crystals[4] (probably because zinc contains only a single parallel set of slip planes) the dissipation in copper involves a considerably simpler situation. Inasmuch as the previous vibrational history has no effect on the copper crystals, it is reasonable to suppose that the vibrations cannot alter the distribution and number of dislocations; therefore, the dissipative mechanism is simply the *oscillatory motion of dislocations*, already present in the lattice, about their equilibrium positions. The present research is a contribution toward an understanding of this process. The significant factors here investigated are the effects of temperature and frequency on the manner in which both internal friction and elastic modulus vary with the strain amplitude.

II. EXPERIMENTAL METHOD

The method, which permits the measurement of both the internal friction and Young's modulus, E, of the specimen, is essentially that developed by Cooke and Brown[5] and Read,[2] so modified as to permit observations at various temperatures and on specimens in which the variation of Δ and E with strain amplitude is appreciable even at small strain amplitudes. The specimen, in the form of a right circular cylinder 5.3 mm in diameter and a few cm long, forms one part of a composite piezoelectric oscillator constructed by cementing to one end of the specimen an X-cut cylinder of crystalline quartz of identical cross section. This composite oscillator forms one arm of an alternating-current bridge, and measurements of the equivalent impedance of the composite oscillator near one of its resonant fre-

* Publication assisted by the Ernest Kempton Adams Fund for Physical Research of Columbia University.
** Now at the Institute for the Study of Metals, The University of Chicago, Chicago, Illinois.
[1] C. Zener, *Elasticity and Anelasticity of Metals* (University of Chicago Press, Chicago, Illinois, 1948).
[2] T. A. Read, Phys. Rev. **58**, 371 (1940); Trans. A.I.M.E. **143**, 30 (1941).
[3] An excellent review of dislocation theory by A. H. Cottrell appears in Chapter 2 of: B. Chalmers, *Progress in Metal Physics I* (Interscience Publishers Inc., New York 1949).
[4] T. A. Read and E. P. T. Tyndall, J. App. Phys. **17**, 713 (1946); I. H. Swift and J. E. Richardson, J. App. Phys. **18**, 417 (1947); C. A. Wert, J. App. Phys. **20**, 29 (1949).
[5] W. T. Cooke and W. F. Brown, Phys. Rev. **50**, 1158, 1165 (1936).

quencies yield the elastic and dissipative properties of the specimen.

It is found, as previously remarked, that Δ and E of the specimen material depend on the vibrational strain amplitude, which varies along the specimen cylinder. Therefore, the specimen cylinder is effectively inhomogeneous. The well-known results of the analysis in the case of homogeneous specimens are presented in the following section. It is then shown that under certain assumptions, the validity of which are demonstrated experimentally, a simple extension of these results correctly describes the inhomogeneous specimen.

Homogeneous Specimen; E and Δ Constant

The impedance, Z, of the composite oscillator near one of its resonant frequencies, f_0, can be written in the form $1/Z=i\omega C'+1/Z_m$, where ω is the angular frequency of the applied potential difference and the form of Z_m is precisely that of an electrical series resonant circuit, $Z_m=R+iX$. The resonant frequencies, for which $X=0$, are the solutions for f_0 of the equation

$$M_1 f_1 \tan(\pi f_0/f_1)+M_2 f_2 \tan(\pi f_0/f_2)=0, \tag{2}$$

where M_i=mass of a cylinder,

$$f_i=(E_i/\rho_i)^{\frac{1}{2}}(2L_i)^{-1}, \tag{3}$$

E_i=Young's modulus, ρ_i=density of a cylinder, L_i=length of a cylinder, and the subscripts 1 and 2 refer to the specimen and quartz cylinders respectively. The resistance and reactance near resonance are given by the expressions

$$R=Kf_0(M_1\Delta_1+M_2\Delta_2), \tag{4}$$

$$X=2\pi KM\delta f, \tag{5}$$

where K is a constant which must be obtained by experiment, $M=M_1+M_2$, and δf is the departure of the frequency of the applied potential difference from the resonant frequency, f_0. The quantities Δ_1 and Δ_2, called the "decrements" of the specimen and quartz cylinders respectively, are defined by the formula

$$\Delta_i=W_i^d/2W_i^v, \tag{6}$$

where W_i^d denotes the *total* energy dissipated per cycle of vibration and W_i^v the total vibrational energy, in a cylinder.

In the experiments here reported the lengths of the quartz and specimen cylinders are so adjusted that, when vibrating in the neighborhood of a resonant frequency, very nearly integral numbers of half-waves of vibration appear in both the quartz and specimen cylinders. Under these circumstances the variation of the *maximum* strain amplitude in the specimen cylinder with frequency is given by ϵ_{1m} where

$$\epsilon_{1m}^2=2\times10^7K(\rho_1/E_1)\mathcal{E}^2/(R^2+X^2) \tag{7}$$

and $\mathcal{E}$ is the r.m.s. voltage applied to the quartz. This formula is obtained by equating the electrical energy supplied to the oscillator in a cycle of vibration to the energy dissipated in the oscillator during the same time interval.

At any frequency near resonance, the composite oscillator can be replaced by a capacity and resistance connected in parallel. This effective resistance, $\mathfrak{R}$, of the composite oscillator is given by:

$$\mathfrak{R}=(R^2+X^2)/R. \tag{8}$$

The quantity $\mathfrak{R}$ is measured experimentally; at exact resonance $\mathfrak{R}=R$. When the reactance, X, is eliminated from Eq. (8) with the aid of Eq. (5), the following expression for the factor K results:

$$K^2=[(\mathfrak{R}/R)-1]\frac{R^2}{[4\pi^2M^2(\delta f)^2]}. \tag{9}$$

Accordingly, a measurement of $\mathfrak{R}$ at a known frequency departure, δf, from resonance yields the value of the quantity K; a separate measurement of the properties of the quartz crystal alone yields f_2 and Δ_2 and this information together with measured values of f_0 and R yields the elastic and dissipative properties of the specimen, after application of Eqs. (2), (3), and (4).

Homogeneous Specimen; E and Δ Variable with Vibration Amplitude

Modification of the foregoing theory necessary to obtain a description of the behavior of an inhomogeneous specimen is most easily obtained with the aid of an auxiliary concept; namely, that of a *fictitious specimen* which is homogeneous, but whose elastic and dissipative coefficients vary with the *maximum* strain amplitude in the specimen cylinder. For such a specimen the observed quantities are the resistance at

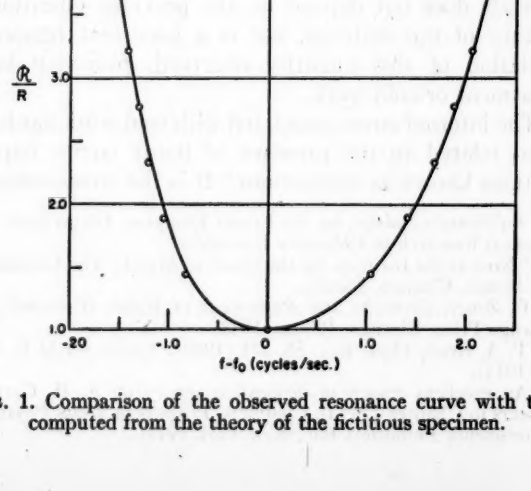

FIG. 1. Comparison of the observed resonance curve with that computed from the theory of the fictitious specimen.

resonance, R, and the resonant frequency, measured as a function of applied voltage. Quantities E_1 and Δ_1, which characterize the fictitious specimen at each amplitude of vibration, are calculated from the measured quantities f_0 and R exactly as in the earlier case, once the value of K is known. The maximum strain amplitude at resonance is related to $\mathcal{E}$ and R by Eq. (7), with X set equal to zero. The relation $\delta E_1/E_1=2\delta f_1/f_1$ connects the fractional changes, in the quantities f_1 and E_1, between zero amplitude and the strain amplitude of a given measurement.

In order to obtain the quantity K, Eq. (9) must be reinterpreted, for the variation, δf, in frequency near resonance is accompanied by a rapid decrease in the amplitude of vibration. Corresponding to a decrease in amplitude there is a change in Δ_1 and E_1 and hence in R and f_0. Let the applied potential difference, at which the measurement to determine K is made, be denoted by $\mathcal{E}$ and the corresponding (off resonance) resistance be denoted by $\mathfrak{R}$. Then the value to be inserted in Eq. (9) in place of R is the resistance R' which would be measured if the composite oscillator were vibrating at resonance with the actual off resonance amplitude; that is, if the oscillator were vibrating at resonance under a reduced voltage, say $\mathcal{E}'$. When the strain amplitude off resonance under a potential $\mathcal{E}$, obtained from Eq. (7) after elimination of the quantity (R^2+X^2) by means of Eq. (8), is equated to the strain amplitude at resonance under a potential $\mathcal{E}'$ the following expression is obtained

$$R'^{\frac{1}{2}}/\mathcal{E}'=\mathfrak{R}^{\frac{1}{2}}/\mathcal{E}. \tag{10}$$

This expression makes it possible to obtain $\mathcal{E}'$ and R' from the observed variation of resistance at resonance with applied voltage. It is necessary merely to plot the ratio, square root of the resistance at resonance divided by voltage at resonance, obtained from the data, as a function of voltage at resonance; $\mathcal{E}'$ is then the value of voltage at resonance at which this ratio equals $\mathfrak{R}^{\frac{1}{2}}/\mathcal{E}$.

Now consider the quantity δf in Eq. (9); it must now be re-interpreted as the frequency departure, not from the observed resonant frequency of the oscillator, but from the resonant frequency that the oscillator would have if the elastic modulus of the specimen retained the value characteristic of the vibration amplitude at resonance under an applied voltage $\mathcal{E}'$. Since $\mathcal{E}'$ is already determined, the desired frequency is obtained directly from the experimental curve of resonant frequency *versus* applied voltage.

The Resonance Curve

The behavior of the fictitious specimen is characterized by its "resonance curve," here defined as the variation of $\mathfrak{R}$ with frequency in the neighborhood of resonance. In accordance with Eq. (9) and the argument of the preceding section, a single determination of K, corresponding to a single value of δf, together with the data for variation of resonant frequency and of resistance at resonance with applied voltage, suffice uniquely to determine the entire course of the resonance curve characteristic of the fictitious specimen. Such a curve, corresponding to an applied voltage $\mathcal{E}=0.3$ volt, is shown in Fig. 1 together with the *observed* variation of $\mathfrak{R}$ with frequency for an actual specimen. Here R is the value of $\mathfrak{R}$ at resonance and the ordinates of the curve are the ratios $\mathfrak{R}/R$. The value of K employed in the computation is obtained from a resonance curve taken at an applied potential sufficiently small that Δ_1 and E_1 are very nearly constant over the entire range of strain amplitude present in the specimen, so that only the theory of the homogeneous oscillator is involved. Accordingly the close agreement between theory and observation demonstrated in Fig. 1 is obtained without the benefit of a single adjustable parameter.

The concordance exhibited in Fig. 1 means that the behavior of the actual specimen cannot be distinguished from that of a fictitious specimen whose elastic and dissipative coefficients vary with the maximum strain amplitude in the specimen cylinder in precisely the same manner as the quantities denoted by the symbols Δ_1 and E_1 are observed to vary when these are computed, from observations with the formulae of the theory. The sole remaining step in the argument is to relate the quanties Δ_1 and E_1 so defined to the physical properties of the actual specimen.

Relation of E_1 and Δ_1 to Properties of the Specimen Material

The form of the resonance curve of the fictitious specimen is a consequence of the fact that near resonance it vibrates in a single normal mode. In the actual specimen, the excitation of higher harmonics is to be expected whenever the dissipative coefficient varies with the strain amplitude, since such a behavior can only arise from a nonlinear dissipative term in the differential equation of motion of the bar. Accordingly, the physical significance of the agreement between the behavior of the fictitious specimen and the actual specimen is that, under the circumstances of measurement, higher harmonics appear to a negligible extent and hence that the specimen cylinder is, in fact, vibrating very nearly in a single normal mode.

The stress, σ, and strain, ϵ, in the fictitious specimen can be written as

$$\sigma=\sigma_{1m}\sin(\pi x/L_1)\cos\omega t=\sigma_m\cos\omega t, \tag{11}$$

$$\epsilon=(A\cos\omega t+B\sin\omega t)\sin(\pi x/L_1), \tag{12}$$

where ω is the angular frequency of the applied voltage. Here A and B are constants, for a given value of σ_{1m}, which are related to E_1 and Δ_1 by the formulas

$$1/E_1=A/\sigma_{1m}, \tag{13}$$

$$\Delta_1=\pi E_1 B/\sigma_{1m}. \tag{14}$$

Consider next an elementary length of the *actual* specimen cylinder located at a point x on the axis.

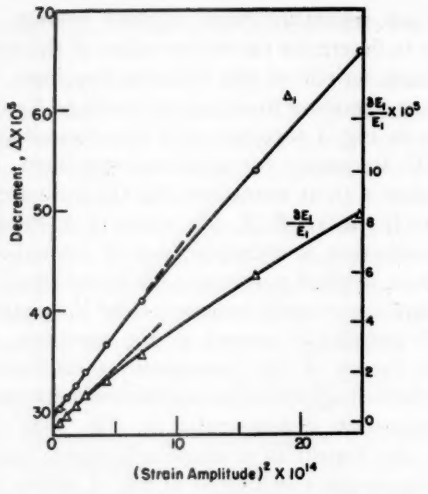

FIG. 2. Both Δ_1 and $\delta E_1/E_1$ are proportional to the square of the strain amplitude at low strain amplitudes.

When higher modes are neglected, the stress and strain at this point can be written as

$$\sigma = \sigma_m \cos\omega t, \tag{15}$$

$$\epsilon = a\cos\omega t + b\sin\omega t. \tag{16}$$

Here a and b are functions of σ_m and therefore of x. The local elastic modulus, E, of the material can be *defined* by

$$1/E = a/\sigma_m \tag{17}$$

and it follows from the definition of Δ, Eq. (1), that

$$\Delta = \pi E b/\sigma_m. \tag{18}$$

Now, whatever the nature of the variations of a and b with x, these quantities can be represented in the interval $0<x<L_1$, by Fourier series of the forms

$$a = \sum_n a_n \sin(n\pi x/L_1) \tag{19}$$

and similarly for b, with the usual Fourier inversions. The requirement that the vibration of the actual specimen is, very nearly, in a normal mode is equivalent to replacing a and b in Eq. (16) by the first terms only of the Fourier expansions, and it then follows by comparison of the resulting expression for ϵ with Eq. (12) that

$$A = a_1 \quad \text{and} \quad B = b_1. \tag{20}$$

Lastly, A and B are evaluated in terms of E_1 and Δ_1 by Eqs. (13) and (14) and a and b in terms of E and Δ by Eqs. (17) and (18). Accordingly, Eqs. (20) are equivalent to the formulas

$$\Delta_1 = (2/L_1)\int_0^{L_1} \Delta \sin^2(\pi x/L_1)dx, \tag{21}$$

and

$$1/E_1 = (2/L_1)\int_0^{L_1} (1/E)\sin^2(\pi x/L_1)dx, \tag{22}$$

where the assumption, justified experimentally, that the spatial variation of E is small of the order of 0.01 percent of its value, has been made.

III. EXPERIMENTAL DETAILS

Construction of the Composite Oscillator

The adhesive employed in the construction of oscillators on which measurements at room temperature are to be made is a thin film of phenyl salicylate (salol), a substance which melts at 43°C and supercools in the liquid state to room temperature. Because of this latter property it is possible to freeze the salol at room temperatures and in this way to prevent a differential thermal contraction at the quartz-specimen interface during cooling.

Strain due to differential thermal expansion at the interface has thus far defeated attempts to apply the composite-oscillator method of measuring the variation of internal friction with temperature.[6] In the present experiments this difficulty has been resolved by the use of a liquid adhesive in oscillators on which measurements below room temperature are to be made; the adhesive is a thin film of Dow Corning 50 centistoke silicone, DC200. This substance remains fluid to temperatures near that of solid CO_2.

A special apparatus is required to assemble an oscillator in which the adhesive is a liquid. The assembly procedure is as follows. Initially the component cylinders rest each upon four ball bearings which lie in parallel horizontal grooves cut in the base of the apparatus. The upper ends of a pair of fine wire loops, on which the oscillator is later supported, are cemented to a pair of parallel horizontal rods mounted above and parallel to the axis of the specimen. These rods are geared together, so that the loops can be shortened evenly by a rotational torque applied to one of them only. The lower parts of the loops are positioned very

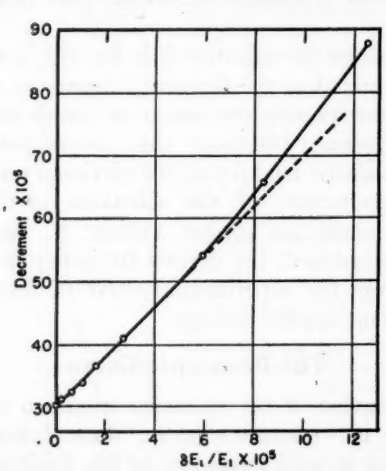

FIG. 3. Combination of the curves of Fig. 2 shows that the decrement is a linear function of $\delta E_1/E_1$ at small amplitudes.

[6] See C. A. Wert, reference 4; T. A. Read, private communication.

accurately beneath the respective centers of gravity of the two cylinders. A thin film of adhesive covers the end of the quartz cylinder proximal to the specimen. The two cylinders are forced together by a spring loaded pin, which is released from its retracted position by rotating a screw. Lastly, the pin is again retracted and the oscillator is elevated by rotating the geared rods, until the quartz lies in proper position between the electrodes. The latter are mounted in a frame constructed of Lucite. An oscillator so constructed and suspended, remains intact for several days.

The Cryostat

The cryostatic space is a horizontal glass tube two inches in diameter and three feet long with metal flanges and gasketed plates on the ends to permit evacuation. The working fluid of the cryostat is acetone which is circulated in coils through a slush of solid CO_2 in trichloroethylene and around the cryostatic space. Temperature is measured with a calibrated copper-constantan thermocouple.

Preparation of Specimens

Single crystals of copper are grown in graphite crucibles by the Bridgman method, in an oxygen-free atmosphere. Specimens are annealed at 600°C for four hours in vacuum to remove strains induced by cutting and lapping them to the desired length. Prior to certain measurements the crystals are subjected to a measurable amount of cold-work produced by application of a known longitudinal compressive stress.

Specimen Material

The specimen material is commercial copper rod. Spectrographic analysis reveals the presence of the following percentages of impurities: Al and Fe, 0.01 to 0.001; Pb, 0.0001; Ag, 0.003; traces of Ca, Mg, and Si.

IV. EXPERIMENTAL RESULTS

The data reported here are based on an extended series of experiments on five different copper crystals. The orientations of the cylinder axes of these crystals with respect to the crystal lattice are various, hence their lengths, which correspond to the same resonant frequency, vary between 3.5 and 5 cm.

Characteristics of the Variation of Young's Modulus and Decrement with Strain Amplitude

The purpose of this section is to point out certain general aspects of the variation of E_1 and Δ_1 with strain amplitude which characterize the behavior of single crystal specimens, within the ranges explored in the present experiments.

The Quantity Δ_1^0

This quantity is defined as the limiting value of Δ_1 as the strain amplitude approaches zero. All measured values of Δ_1^0 contain unspecifiable contributions ascribable to the adhesive and to the state of the surface of the specimen. The former are less than 10^{-5} when the adhesive is salol, and close to 10^{-4} when the liquid adhesive is used. Variations of Δ_1^0 between 10^{-5} and 5×10^{-5} can be produced by etching the surface of the specimen. Experiment proves, however, that the magnitudes of both of these spurious contributions to the internal friction are *independent of strain amplitude.*

TABLE I. Dissipative characteristics of specimens *A* and *B* at room temperature.

	$\Delta_1^0\times10^5$	$C_1\times10^{-4}$	r_1
Specimen *A*	14.0	0.26	3.4
Specimen *B*	29.4	1.61	4.0

The Quantity C_1

When Δ_1 and $\delta E_1/E_1$ are plotted as functions of ϵ_{1m}^2, graphs of the type shown in Fig. 2 are obtained. It thus appears that, at low amplitudes, both quantities vary linearly with the square of the maximum strain amplitude. The slope of the line which represents the variation of Δ_1 with ϵ_{1m}^2 is here denoted by C_1; thus

$$C_1=(d\Delta_1/d\epsilon_{1m}^2)_{\epsilon_{1m}=0}. \tag{23}$$

The quantity C_1 is the most significant for the description of the dissipative property of single crystals vibrating at low strain amplitudes, for the following reasons:

(*a*) C_1, which by definition is a measure of a property of the specimen cylinder, is closely related to the measure of the corresponding property of the specimen *material.* Thus, if

$$\Delta=\Delta^0+C\epsilon_m^2, \tag{24}$$

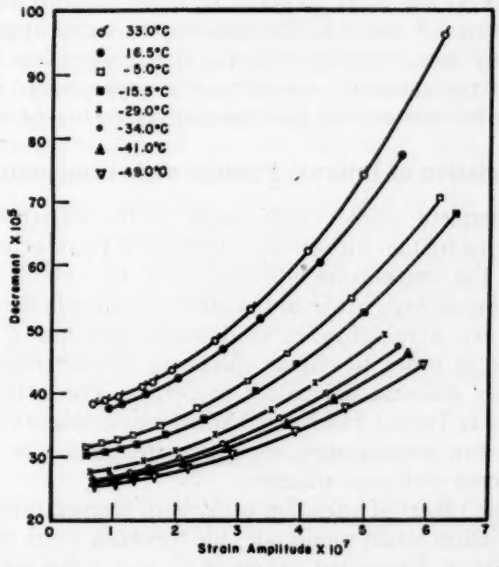

FIG. 4. Variation of internal friction with strain amplitude and temperature.

TABLE II. Variation of dissipative properties with temperature.

T, °A	$C_1\times10^{-9}$	r_1	T, °A	$C_1\times10^{-9}$	r_1
	Specimen *A*			Specimen *B*	
298.0	0.260	3.7	306.0	1.58	4.0
293.5	0.250	3.5	289.5	1.44	3.9
286.0	0.235	3.5	268.0	1.17	3.95
270.0	0.200	3.5	257.5	1.04	3.8
260.0	0.180	3.4	244.0	0.90	3.9
248.0	0.158	—	239.0	0.87	4.1
240.0	0.145	3.4	232.0	0.75	3.95
233.0	0.137	3.5	224.0	0.685	3.8
222.0	0.120	3.4			
215.5	0.110	3.3			

where $\epsilon_m=\sigma_m/E$ is the local strain amplitude, then from Eq. (21) it follows that $\Delta_1{}^0=\Delta^0$ and $C_1=\frac{3}{4}C$.

(*b*) C_1, unlike Δ_1, is free of error introduced by the adhesive and the state of the specimen surface; it is a measure of the dissipative property of the crystal lattice itself. Furthermore, it is an extraordinarily sensitive measure of this property; various values of C_1 observed in the course of these experiments differ by the factor 4000, while the corresponding values of $\Delta_1{}^0$ differ only by the factor 140.

The Quantity r_1

Corresponding values of Δ_1 and $\delta E_1/E_1$ obtained from Fig. 2, are plotted as ordinates and abscissae, respectively, in Fig. 3. The slope of the straight line obtained at small strain amplitudes is here denoted by r_1; thus

$$r_1=\left[d\Delta_1/d(\delta E_1/E_1)\right]_{\epsilon_{1m}=0}. \tag{25}$$

An analysis similar to the one which related C_1 to C shows that $r_1=r$, where r is the property of the material defined by an equation similar to Eq. (25) in which the subscript "1" is deleted throughout.

The values of r_1 observed in these experiments lie between 1.5 and 4.4. The quantity r_1 varies approximately monotonically with C_1; it is always less than three for annealed crystals and always greater than three for crystals that have been subjected to cold-work.

Variation of Internal Friction with Temperature

Complete studies were made of the variation of internal friction with strain amplitude in two specimens, over the temperature interval $+33$°C to -60°C. Both specimens were cut from the same crystal cylinder, but the two were subjected to different amounts of cold work in order to obtain specimens characterized by widely different dissipative properties. The latter are given in Table I which summarizes measurements made at room temperature on composite oscillators constructed with salol adhesive.

The observed variation of Δ_1 with temperature and maximum strain amplitude, for specimen *B*, is shown in Fig. 4. Computed values of C_1 and r_1 for the two specimens are given in Table II.

TABLE III. Results of measurements of internal friction at two frequencies.

No.	39 kc/sec. $\Delta_1{}^0\times10^5$	39 kc/sec. $C_1\times10^{-9}$	39 kc/sec. r_1	78 kc/sec. $\Delta_1{}^0\times10^5$	78 kc/sec. $C_1\times10^{-9}$	78 kc/sec. r_1
1	0.69	0.00074	—	0.81	0.00128	—
2	1.2	0.003	1.8	1.6	0.004	1.6
3	9.10	0.018	2.9	9.85	0.015	2.6
4	31.0	0.090	—	30.8	0.064	—
5	14.8	0.104	3.0	13.9	0.080	3.05
6	14.0	0.26	3.4	18.6	0.388	3.7
7	12.7	0.90	3.3	16.6	1.34	3.5
8	50.7	0.92	3.5	36.7	0.50	3.4
9	29.4	1.61	4.0	28.1	1.16	4.4
10	69.4	2.20	3.5	119.0	4.3	3.9

An analysis of curves such as those of Fig. 4 reveals the following: If due allowance be made for the uncertainty in the value of $\Delta_1{}^0$ by the addition of a suitable constant amount to the ordinates of each curve, then the entire family of curves for each specimen may be represented over the *entire range* of variation of temperature and strain amplitude by a function $F(T,\epsilon_{1m})$ which has the form

$$\Delta_1=F(T,\epsilon_{1m})=F_1(T)F_2(\epsilon_{1m}), \tag{26}$$

where

$$F_1(T)=Pe^{-\theta/T}, \tag{27}$$

and the value of P is chosen to be the same for both specimens. The value of θ has the same value, 700°A, for both specimens within the accuracy of these experiments, as is evident from Fig. 5, in which the natural logarithm of $F_1(T)$ is plotted as a function of $1/T$. It is clear from the form of Eq. (26) that the quantity C_1 differs from $F_1(T)$ by a constant factor.

It is worth noting specifically that the quantity r_1 is *independent of temperature.*

Variation of Internal Friction with Frequency

Measurements of the quantities $\Delta_1{}^0$, C_1, and r_1 were made upon various specimens at the fundamental frequency (39 kc/sec.) and the second harmonic frequency (78 kc/sec.). All such measurements were made at room temperature, on composite oscillators constructed with salol adhesive. Data are recorded in Table III; the first three measurements represent annealed specimens, the

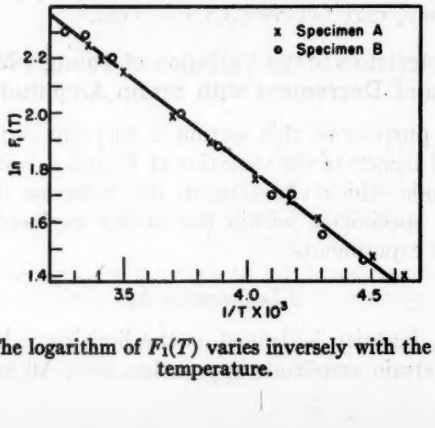

FIG. 5. The logarithm of $F_1(T)$ varies inversely with the absolute temperature.

remaining entries are for specimens which had been subjected to cold-work. The maximum compressive stress employed was 365 p.s.i.

The following general remarks summarize the results of this table. (*a*) Although both the quantities Δ_1^0 and C_1 increase with the degree of cold-work, there is no simple relationship between them. (*b*) In all but one case the changes in Δ_1^0 and C_1 between the fundamental and second harmonic are in the same direction. (*c*) Both C_1 and Δ_1^0 vary with frequency in an apparently random manner. It is particularly noteworthy that the specimens *A* and *B* which, as shown in the last section, obey almost identical laws of temperature dependence, vary with frequency in opposite directions. The data for these two specimens appear in Table III as numbers 6 and 9, respectively. (*d*) Since the experimental error in almost all measurements of r_1 is about ± 0.2, it appears that r_1 is independent of frequency within the accuracy of these experiments, over the entire range of values of C_1 and Δ_1^0 studied. Figure 6 illustrates this result for one of the measurements (No. 8) quoted in the table.

It is well known that the state of internal stress is very sensitive to previous history and to flaws in the crystal which result from accidents of growth; this "structure sensitivity" is reflected in the measured values of internal friction. It is in these terms that the apparently random results for the relative values of internal friction at the first two modes of vibration may be explained. In the fundamental mode of vibration, the maximum stress is located at the center of the specimen cylinder and the measurements obtained are primarily a result of the behavior of this part of the lattice. At the second harmonic stress loops are at $\frac{1}{4}$ and $\frac{3}{4}$ the length of the cylinder. Since the two measurements involve different parts of a highly structure-sensitive crystal lattice, it is not surprising that the frequency dependence of C_1 and of Δ_1^0 cannot be deduced from them. This argument does not apply to the quantity r_1 which is not very sensitive to history since it varies very slowly with C_1. The observation that r_1 is independent of frequency may therefore be regarded as one of the important results of these experiments.

V. DISCUSSION

A phenomenological discussion of two general dissipative mechanisms is presented in this section; the experimental results make it possible to select one of these to represent the behavior of the crystals investigated. The significance of the mechanism selected is then discussed in terms of dislocations. Since the dissipative and elastic properties of the specimen as a whole have been related to the properties of the material in an earlier section, it is necessary to consider only the behavior of an element of material under a stress, σ, which varies sinusoidally in time and produces a strain, ϵ.

In the presence of a source of dissipation (in the present case, dislocations) the strain may be written as the sum of two terms

$$\epsilon = \epsilon_1 + \epsilon_2,$$

where ϵ_1 is the purely elastic strain and ϵ_2, the contribution resulting from the presence of the dissipative process. Clearly,

$$\epsilon_1 = \sigma / E_t, \tag{28}$$

where E_t is the *true* Young's modulus of the material, to be distinguished from the measured value, E. If σ is given by Eq. (15), then ϵ, or at least its fundamental Fourier component, is given by Eq. (16), and E and Δ by Eqs. (17) and (18), respectively. The measured

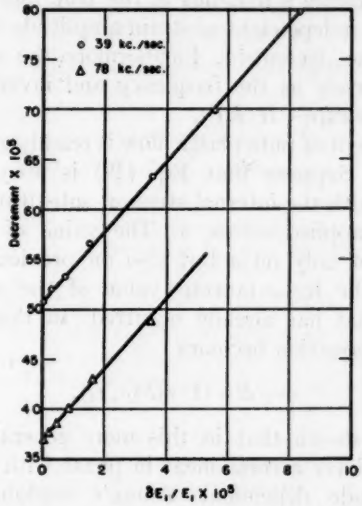

FIG. 6. The quantity r_1 is independent of frequency.

elastic modulus E will be equal to E_t if and only if the strain ϵ_2 is purely dissipative, i.e., contributes only to the factor b in Eq. (16) so that $a = \sigma_m / E_t$.

It is useful to distinguish two types of dissipative mechanisms. The first, a mechanism of *relaxation* is defined in terms of a stress-strain curve which depends on the rate of application of the stress. It is therefore characterized by the occurrence of creep at constant stress, or in vibration, by a stress-strain ellipse whose parameters depend on the frequency. The second mechanism, *simple hysteresis*, is defined in terms of a stress-strain loop that is independent of the rate of traversal. Under cyclic stress the strain may differ, for the same value of stress, during loading and unloading, but all values are independent of the frequency of the cycle. Inasmuch as all dissipative mechanisms studied to date fall into the category of relaxation (e.g., anelasticity[1] is a special case of relaxation) it seems natural to start by considering this mechanism.

The Mechanism of Relaxation

One example of relaxation is the behavior known as *pure plastic flow* in which the fundamental equation for ϵ_2 is

$$d\epsilon_2/dt = (1/\tau) f(\sigma), \tag{29}$$

where τ has the dimensions of time. This will generally be the equation of a rate process involving a Boltzmann factor which may be absorbed into the quantity τ, as follows:

$$\tau=\tau_0 e^{H/RT}, \tag{30}$$

where H is the *heat of activation* of the process. In view of the strong temperature dependence of the measured internal friction, the introduction of a heat of activation is not unreasonable. A special case of Eq. (29) is the Newtonian viscosity law, for which the equation becomes linear. It is readily shown that for pure plastic flow the strain ϵ_2 is purely dissipative so that the measured Young's modulus is the true modulus, and therefore is independent of strain amplitude and of the value of the decrement. Furthermore the decrement varies inversely as the frequency and inversely as τ, therefore as $\exp(-H/RT)$.

The concept of pure plastic flow is readily generalized as follows. Suppose that Eq. (29) is obeyed *microscopically* with the internal stress σ_i substituted for the externally applied stress, σ. The value of σ_i is dependent not only on σ but also on previous history, including the instantaneous value of the non-elastic strain ϵ_2 that has already occurred. In this case the relaxation equation becomes

$$d\epsilon_2/dt=(1/\tau)F(\sigma, \epsilon_2). \tag{31}$$

It can be shown that in this more general case the strain will have a component in phase with σ, so that an amplitude dependent Young's modulus will in general be observed.

The observed temperature dependence of internal friction as given by Eq. (27), suggests that the decrement varies very nearly inversely as τ, corresponding to the case of pure plastic flow, with a heat of activation equal to 1400 cal./mole. On the other hand, it is difficult to reconcile this temperature dependence with the experimental result that $\delta E_1/E_1$ is of the same order of magnitude as the decrement; i.e., that r is of the order unity.

The relaxation interpretation also fails to explain the frequency and temperature independence of r. As is shown in the Appendix, the expected variation is proportional to $\omega\tau$, in conflict with the experimental results.

It is possible to generalize to more complex relaxation mechanisms than that of Eq. (31), but such a generalization does not seem to lead to a resolution of the conflict between the theoretical predictions and the experimental results.

Mechanism of Simple Hysteresis

From the definition of simple hysteresis it is immediately predicted that all observable quantities are independent of frequency, if this is the mechanism that applies to the dissipative process under investigation. The experimentally observed frequency independence of the quantity r_1 is in agreement with this prediction. The fact that the ratio of C_1 at the fundamental to its value at the second harmonic is observed to lie on both sides of unity indicates that C_1 may actually be independent of frequency, when the explanation presented for the randomness of these data is taken into account.

The assumption that only fundamental Fourier components of strain are important means that the best possible ellipse is matched to the actual stress-strain loop. The effective modulus under periodic conditions, obtained from the slope of the major axis of this ellipse, is clearly less than the true modulus.

The slope of the stress-strain loop differs in the parts of the cycle where stress is increasing (loading) from its value when stress is being released (unloading); for example

$$\begin{aligned} d\epsilon_2/d\sigma &= g_1(\sigma)\text{(loading)}, \\ &= g_2(\sigma)\text{(unloading)}. \end{aligned}$$

Fourier analysis of this strain and the application of Eqs. (17) and (18) leads to the result

$$\Delta=2E\int_0^{\pi/2}[g_1(\sigma_m\cos\theta)-g_2(\sigma_m\cos\theta)]\times\cos\theta\sin\theta d\theta, \tag{32}$$

$$\frac{1}{E}-\frac{1}{E_i}=\frac{2}{\pi}\int_0^{\pi/2}[g_1(\sigma_m\cos\theta)+g_2(\sigma_m\cos\theta)]\sin^2\theta d\theta. \tag{33}$$

The experiments indicate that $g_1(\sigma)$ and $g_2(\sigma)$ are expressible in power series in which odd powers of σ do not appear. The constant terms leads to a decrement at zero amplitude and a deviation of the measured elastic modulus at zero amplitude from the true modulus; it is from the term in σ^2 that the quantities C and r result. If the function $g_i(\sigma)$ is written

$$g_i(\sigma)=\alpha_i+\beta_i\sigma_i^2 \quad (i=1, 2) \tag{34}$$

then

$$\Delta=E(\alpha_1-\alpha_2)+\tfrac{1}{2}E^3(\beta_1-\beta_2)\epsilon_m^2, \tag{35}$$

$$(E_i-E)/E=\tfrac{1}{2}E(\alpha_1+\alpha_2)+\tfrac{1}{8}E^3(\beta_1+\beta_2)\epsilon_m^2, \tag{36}$$

$$r=4[(\beta_1-\beta_2)/(\beta_1+\beta_2)], \tag{37}$$

where $\epsilon_m=\sigma_m/E$ is the strain amplitude. The most striking result is the prediction that r must lie between 0 and 4, in excellent agreement with experimental results. Only one observation (No. 9 of Table III, 78 kc) shows a value of r greater than 4.0 and the experimental error in this single case was sufficiently large to permit a true value of $r=4$. Numerous other data observed at room temperature and 39 kc, which are not tabulated here, always show values of r in the predicted range and closest to 4.0 for the most highly cold-worked crystals. This agreement with experiment indicates that the dissipative mechanism may be described, phenomenologically, in terms of simple hysteresis.

The following is a possible explanation for the observed dissipative mechanism in terms of the motion of dis-

locations. The activation energy for the release of dislocations from points at which they are restrained is sufficiently high so that at the high frequencies of these experiments negligible relaxation occurs. Instead, a distribution exists such that at each value of the stress a certain fraction of the dislocations will *snap loose* and move rapidly to another potential minimum, thereby contributing to the non-elastic strain. In terms of this description it is not surprising that corresponding measurements at lower frequencies[1] are of a different nature; e.g., no amplitude-dependent effects are observed. The strain caused by the time-dependent release of dislocations, a relaxation mechanism, can be expected to predominate over the time independent strain of simple hysteresis at sufficiently low frequencies. The present interpetation provides a link between the behavior of dislocations in two ranges of conditions which have hitherto been investigated independently of each other.

The large observed temperature dependence of internal friction may be explained in terms of dislocations when an auxiliary concept is introduced. Cottrell[7] has shown that a force of attraction exists between a solute (impurity) atom and certain preferred sites along a dislocation. Since the dislocations are anchored by impurity atoms located at these sites, the number of dislocations torn loose by an applied stress, and therefore the internal friction, is determined by the extent to which these favorable sites are occupied.[8] The extent of occupation, in turn, is determined by a Boltzmann factor $\exp(-V/kT)$, where V is the interaction energy between solute atom and dislocation, and is therefore a sensitive function of temperature.

The author wishes to express his appreciation to Dr. T. I. Taylor for the spectrographic analysis, to Dr. T. A. Read for valuable information about the apparatus and his own experiments, to Dr. C. Zener for helpful conversations, and to Dr. S. L. Quimby for his guidance throughout the course of this work.

APPENDIX

Calculation of the Frequency and Temperature Dependence of r from a Mechanism of Relaxation.

The observed temperature dependence of internal friction shows that if the dissipative mechanism is relaxation the behavior does not deviate greatly from pure plastic flow (Eq. (29)), so that the more general Eq. (31) can be expanded in a Taylor series

$$d\epsilon_2/dt=(1/\tau)\{F(\sigma,0)+\epsilon_2(\partial F/\partial\epsilon_2)_{\epsilon_2=0}+\cdots\}.$$

The fact that the observed decrement varies parabolically with strain amplitude at low amplitudes means that the above equation relating ϵ_2 and its time derivative to σ has only linear and cubic terms; thus

$$d\epsilon_2/dt=(1/\tau)\{c_1\sigma+c_2\sigma^3+\epsilon_2(c_3+c_4\sigma^2)\}.$$

If now the stress σ is sinusoidal, the internal friction and elastic modulus are obtained from the components of $d\epsilon_2/dt$ in phase and out of phase with the stress and from these quantities it is found that r is proportional to $\omega\tau$.

[7] A. H. Cottrell, *Rep. Conf. on Strength of Solids* (Phys. Soc. London, 1948), p. 30.

[8] The unusually high internal friction of spectroscopically pure copper observed by J. W. Marx and J. S. Koehler, Phys. Rev. 75, 1309A (1949), supports this interpretation.

High Temperature Plasma Properties from High Current Arc Stream Measurements

W. FINKELNBURG AND S. M. SEGAL
Engineer Research and Development Laboratories, Fort Belvoir, Virginia

(Received June 19, 1950)

The high current arc stream in air, operated at currents between 150 and 250 amperes, with an axial temperature between 10,000 and 12,000°K, is shown to be a very uniform high temperature plasma. Probe measurements of the potential gradient along the axis of the arc stream, and of its effective diameter, lead to the conclusion that its plasma has a constant electrical resistivity of 1/100 ohm-centimeter, widely independent of the arc current. From this resistivity, the current density, the potential gradient and the plasma temperature, empirical values of the electron mobility, their relaxation length, and the effective ion cross sections in the plasma are derived. The value of the ion cross section agrees well with that computed from a theoretical formula of Druyvesteyn, but is by a factor smaller than those generally considered correct.

I. INTRODUCTION

THE high current arc stream in air, operated at currents between 150 and 250 amp., with an axial temperature between 10,000 and 12,000°K, deserves special interest as an example of an apparently very uniform high temperature plasma. It will be shown in this paper that simple potential-probe measurements make it possible to determine, partly directly and partly indirectly, a number of important plasma properties, and to draw conclusions which are believed to be of general theoretical interest.

Earlier investigations by one of us have shown that the contracted high current arc stream which forms automatically[1] in air containing traces of carbon vapor at currents above 100 amp., consists of a bluish-white narrow column which is surrounded by well-defined zones of different colors and decreasing temperatures. The diameter of the central column increases from the cathodic foot point to a constant value of approximately twice its original value, at about 6 to 10 mm from the cathode, depending on the arc length (Fig. 1). From the strong continuous spectrum, the absence of molecular spectra, and the broadening of the few emission lines present, we had concluded[1] that the central column is the arc stream proper which, with its high degree of ionization, conducts virtually the total arc current. Though this conclusion has, in general, been accepted as reasonable, no direct measurement of the effective electrical diameter of the arc stream existed. Nor was the potential distribution along the arc stream and its dependence on the arc stream parameters known with sufficient certainty, though Höcker, Schulz, and the author[2] had used an old preliminary gradient determination of the author's for calculating an axial temperature of the contracted arc stream of 11,700±700°K, in satisfactory agreement with the spectroscopic estimate. Accurate determinations of both missing properties of the arc stream are reported in this paper, and it is a gratifying result that the original arc gradient measurement of 10 volts/cm proves to be correct for the main part of the arc stream, so that the temperature[2] based on it remains valid.

[1] W. Finkelnburg, J. App. Phys. **20**, 468 (1949); *Hochstromkohlebogen* (Springer-Verlag, Heidelberg, 1948).

[2] K. H. Höcker and W. Finkelnburg, Zeits. f. Naturforsch. **1**, 305 (1946); K. H. Höcker and P. Schulz, Zeits. f. Naturforsch. **4a**, 266 (1949). The theoretical results of the latter paper agree closely with those derived in this paper, more directly we believe, from our measurements.

II. MEASUREMENT OF POTENTIAL GRADIENT AND EFFECTIVE DIAMETER OF THE HIGH CURRENT ARC STREAM

For the measurement of the potential gradient and of the effective diameter for different distances from the cathode, a thin tungsten probe was whipped at a known constant speed through consecutive cross sections of the arc stream, each of which was one millimeter farther away (or closer to) the negative electrode than the preceding one. During each passage, the probe potential (with reference to one of the electrodes), the total arc voltage, and the arc current were recorded photographically by a Hathaway oscillograph. In passing through the arc stream plasma, the probe picks up a potential which, because of the high mobility of the electrons as compared to that of the positive ions, is always negative with respect to the actual plasma potential. However, because of the approximately constant temperature along the arc stream, this negative "contact potential" between probe and plasma is believed to be effectively constant for successive passages of the probe. The differences of the probe potential for successive passages consequently give the true arc stream gradient. The influence of the probe on the high current arc stream was studied by using a variety of probes and probe speeds. The amount of perturbation of the arc by the probe could be evaluated from the traces of arc voltage and arc current, which were recorded simultaneously with the probe voltage. As expected, the perturbation was the smaller the smaller the probe diameter. With a tungsten probe of 0.1-mm diameter which was covered by a thin glass tube (0.7-mm diameter) except for its point of 0.3-mm length, the perturbation of the arc remained within the accuracy of our recording device. Moreover, sequences of probe passages through the same cross section of the arc stream always gave the same probe potential, as did

passages at different probe speeds. From these observations we conclude that neither temperature effects nor gas turbulence caused by the probes being whipped through the arc stream have any appreciable disturbing effect on our results. In general, probe speeds between 50 and 100 cm/sec. were used.

Figure 2 shows the potential distribution along the axis of the arc stream. The potential of a point approximately 1 mm from the cathode tip has been chosen as the reference zero, because the potential drop within the last millimeter which includes the cathode drop is not known accurately enough. Figure 3 shows the potential gradient (volts/cm) determined by differentiation of Fig. 2, along the arc stream axis; it decreases from 40 volts/cm near the cathode to a constant value of 10 volts/cm in the main part of the arc stream.

The effective electric arc stream diameter could be determined, at least approximately, from the arc voltage record under the reasonable premise that the arc voltage is disturbed only when the probe is in the arc stream proper where the essential electric conduction takes place. This effective electrical diameter of the arc stream proved to be much smaller than the apparent optical diameter, in agreement with our previously stated opinion that only the contracted whitish part with its continuous spectrum is the arc stream proper which carries the current, whereas the outer luminous zones are essentially heated by conduction from the arc stream proper.

III. EXPERIMENTAL RESULTS

(1) The arc stream gradient, plotted in Fig. 3 as a function of the distance from the cathode tip, is independent of the positive carbon material, of the total arc length, and particularly independent of the arc current, at least in the range from 150 to 250 amperes.

(2) The arc stream gradient decreases from an initial value of 40 to 50 volts/cm near the cathode towards a constant value of 10 volts/cm which is reached from 5 to 10 mm from the cathode, depending on the more or less slender shape of the arc stream. The gradient increases again near the anode, due to the effect of the vapors emanating from the positive crater (disturbed part of the arc stream).

(3) The effective electrical diameter of the high current arc stream agrees, within the limits of our accuracy, with that of the whitish contracted arc stream proper, mentioned above with its spectral characteristics indicating its high degree of ionization. This diameter increases, for a 200-ampere arc, from a value of 2 mm near the cathode to a value of a somewhat above 4 mm which is reached from 6 to 10 mm from the cathode.

(4) From (2) and (3) it follows that the arc stream gradient is, to a first approximation, inversely proportional to the effective cross section of the contracted arc stream.

(5) From (1), (4), and the known current densities in the different regions of the contracted arc stream

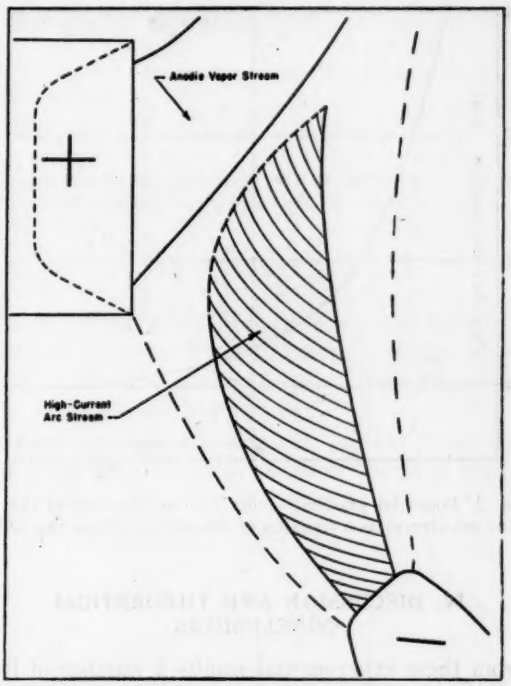

FIG. 1. Sketch of electrode arrangement and arc stream of the high current carbon arc.

(ranging between 5000 and 1000 amp./cm²) there follows a surprising and important conclusion: The plasma of the contracted high current arc stream behaves, independently of the arc stream diameter, the arc current and the arc length, as a uniform plasma with an approximately constant resistivity of 1/100 ohm-centimeter or, conversely, with a constant electric conductivity of 1×10^{14} e.s.u. The electric conductivity of this high temperature plasma, consequently, is of the same order as that of graphite and only one order of magnitude below that of many metals.

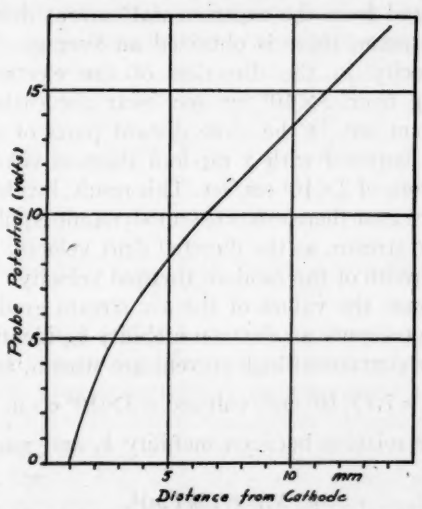

FIG. 2. Probe potential measured on the axis of the high current arc stream as a function of the distance from the cathode tip. The probe potential 1 mm from the cathode was chosen as the reference.

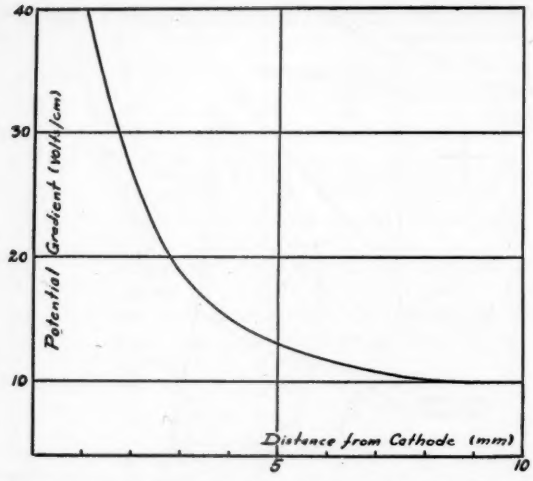

FIG. 3. Potential gradient (volts/cm) on the axis of the high current arc stream as a function of the distance from the cathode tip.

IV. DISCUSSION AND THEORETICAL CONCLUSIONS

From these experimental results a number of interesting conclusions can be drawn as to the behavior of this high temperature plasma if one last property is known; *viz.*, the degree of ionization. From the intensity of the continuous spectrum, which is a bremsspectrum of the discharge electrons,[3] it is apparent that the degree of ionization is by orders of magnitude higher than that of the low current arc stream. In agreement with this conclusion the Saha equation leads, according to a paper by Höcker and the author,[2] to a degree of ionization between 10 and 20 percent.

At atmospheric pressure and an average temperature of 10,000°K, we then have a gas density of 7×10^{17} atoms/cm³ and an electron and ion density of approximately 1×10^{17} per cm³. From this value of the electron density, and from the experimental current density in the arc stream, there is obtained an average electron drift velocity in the direction of the electric field decreasing from 3×10^{5} cm/sec. near the cathode to 7.5×10^{4} cm/sec. in the more distant parts of the arc stream, compared with a random thermal velocity of the electrons of 2×10^{7} cm/sec. This result, incidentally, is evidence that there exists thermodynamic equilibrium in the arc stream, as the directed drift velocity is only one hundredth of the random thermal velocity. Taking into account the values of the arc stream gradient of Fig. 3 we compute an electron mobility b_e, identical for the whole contracted high current arc stream, as

$$b_e=7.7\times10^{3}\ \text{cm}^2/\text{volt-sec.}=3\times10^{6}\ \text{e.s.u.}$$

From the relation between mobility b_e and mean free path λ_e

$$b_e/\lambda_e=e/(3kTm)^{\frac{1}{2}},$$

we get an empirical value of the mean free path of the electrons in the plasma of

$$\lambda_e=4\times10^{-4}\ \text{cm}.$$

Now we equate the mean free path λ_e of the electrons with the theoretical relaxation length, i.e., the average path for which an electron loses half of its kinetic energy[4] by interaction with the plasma partners,

$$s=\gamma(kT)^2/e^4N.$$

N is the density of electrons and ions, calculated above, and γ is a numerical factor which, according to different theoretical approaches to the problem has values between 0.01 and 2. By equating the theoretical relaxation length, s, with our empirical value of the mean free path, λ_e, we find an empirical γ-value, valid for our high temperature plasma, equal to unity, in fair agreement with the theoretical computation by Druyvesteyn,[5] but in sharp disagreement with the presently prevailing opinion that γ should be of the order of 10^{-2}.

This check on the theory of the relaxation length which seems possible by means of our arc stream measurements, is of general theoretical interest, because this relaxation length and the effective cross section, Q_i, of the positive plasma ions computed from it are essential, but hitherto unknown, properties of any plasma.

It seems to be a safe premise that in our plasma, where every seventh atom is ionized, the positive ions with their extended Coulomb fields alone play the dominant role in terminating the mean free paths of the electrons. Computations confirm that the cross sections of the neutral atoms are far too small to account for the empirical mean free paths of the electrons. We thus are justified in writing

$$s=\lambda_e=1/NQ_i.$$

where N is the ion density and Q_i is the effective cross section of the positive ions. Combining this with our result above that the factor γ is of the order of unity we have, for our high temperature plasma at least, the effective ion cross section

$$Q_i=e^4/(kT)^2.$$

Since the only existing experiments on relaxation lengths in a plasma have been made by Langmuir and Mott-Smith[6] in a low pressure mercury plasma of very low ion density (10^{9} compared to our 10^{17} ions/cm³) we believe that arc measurements like those reported here may contribute much to high temperature plasma research.

[3] W. Finkelnburg, *Kontinuierliche Spektren* (Verlag Julius Springer, Berlin, 1938).

[4] For this whole discussion compare the review of plasma physics by R. Rompe and M. Steenbeck, Ergeb. d. exakt. Naturwiss. **18**, 257 (1939).

[5] M. J. Druyvesteyn, Physica **5**, 561 (1938).

[6] I. Langmuir and H. Mott-Smith, Gen. Elec. Rev. **27**, 766 (1924).

On the Scattering Theory of the Dirac Equation*

GEORGE PARZEN†
Stanford University, Stanford, California
(Received June 8, 1950)

It is shown that for sufficiently strong potentials, the Born approximation is not valid even at very high energies. A variational principle is derived for the phase shifts and applied to a simple case. Two exact expressions for the phase shifts are also found.

I. INTRODUCTION

IN the course of an investigation on the problem of the scattering of high energy electrons from heavy nuclei, a number of results in the scattering theory of the Dirac equation were obtained. In the following paragraph, the limitations of the Born approximation in the Dirac theory are investigated. It is shown that for sufficiently strong potentials the Born approximation is not valid at very high energies. This is done by interpreting the Born approximation in terms of the phase shifts and then investigating the behavior of the phase shifts at high energies.

A variational principle is derived for the phase shifts. A simple application of the variational principle gives a result for the phase shift which is more accurate than the Born approximation. In addition, two exact expressions for the phase shifts are found.

II. DEFINITION OF THE PHASE SHIFTS

The phase shift method was first applied to the Dirac equation by Mott[1] in calculating the Coulomb scattering of fast electrons. We shall write the Dirac equation for an electron moving in an electric field only as[2]

$$(H+V)\psi=E\psi, \quad H=-(\alpha\cdot\mathbf{p}+\beta). \tag{1}$$

In (1) we have used relativistic units, $\hbar=m=1=c$.

As with the non-relativistic Schroedinger equation, we can decompose the wave function into spherical harmonics.[3] Let us denote the radial parts of the wave function by $f_l(r)/r$ and $g_l(r)/r$; these functions satisfy the differential equations,

$$(d/dr)f_l=-(l+1/r)f_l+(E-V-1)g_l, \tag{2-a}$$

$$(d/dr)g_l=-(E-V+1)f_l+(l+1/r)g_l. \tag{2-b}$$

If $V(r)$, the potential, goes to zero faster than $1/r$ at ∞, then the functions g_l and f_l have the asymptotic forms,

$$g_l\rightarrow(E+1)^{\frac{1}{2}}\cos[kr-\tfrac{1}{2}(l+1)\pi+\delta_l], \tag{3-a}$$

$$f_l\rightarrow(E-1)^{\frac{1}{2}}\sin[kr-\tfrac{1}{2}(l+1)\pi+\delta_l]. \tag{3-b}$$

The δ_l defined by Eqs. (3) are the phase shifts; they are zero if $V(r)\equiv 0$. If the potential goes like ze^2/r at infinity, then there is the additional logarithmic term just as in the Schroedinger theory.

In terms of these phase shifts, one can write down the cross section for an unpolarized incoming beam of electrons as[1]

$$\sigma(\theta)=|f_3(\theta)|^2+|f_4(\theta)|^2, \tag{4}$$

where

$$f_3(\theta)=\frac{1}{k}\sum_{l=1}\left\{(l+1)\left[\frac{e^{2i\delta_l}-1}{2i}\right]+l\left[\frac{e^{2i\delta_{-l-1}}-1}{2i}\right]\right\}P_l(\cos\theta) \tag{5}$$

and

$$f_4(\theta)=\frac{1}{k}\sum_{l=0}\left\{\frac{e^{2i\delta_{-l-1}}-e^{2i\delta_l}}{2i}\right\}P_l^1(\cos\theta). \tag{6}$$

Here

$$P_l^1=\sin\theta dP_l(\cos\theta)/d(\cos\theta),$$

and the δ_{-l-1} are also defined by Eqs. (2) and (3), where l is replaced by $-l-1$.

In the non-relativistic limit, $\delta_l=\delta_{-l-1}$, so that in (5) and (6), $f_3(\theta)$ becomes the usual Schroedinger scattering amplitude,

$$f_3(\theta)=\frac{1}{k}\sum_{l=1}(2l+1)\left[\frac{e^{2i\delta_l}-1}{2i}\right]P_l(\cos\theta),$$

and $f_4(\theta)\equiv 0$.

III. THE VALIDITY OF THE BORN APPROXIMATION IN THE DIRAC THEORY

It has already been noted that the Born approximation does not give good results in the Coulomb scattering from heavy elements, even at very high energies.[4,5] We shall show that this is a general property of the Dirac equation; if the potential is sufficiently strong,[6] then no matter how high the energy of the scattered particle, the Born approximation will not be valid. This

* Submitted in partial fulfillment of the Ph.D. requirements at Stanford University.
† Now at the Institute for Nuclear Studies, Chicago, Illinois.
[1] N. F. Mott, Proc. Roy. Soc. A 124, 426 (1949).
[2] L. I. Schiff, *Quantum Mechanics* (McGraw-Hill Book Company, Inc., New York, 1949), p. 311.
[3] C. G. Darwin, Proc. Roy. Soc. A 118, 654 (1928).
[4] Bartlett and Watson, Proc. Am. Acad. 74, 53 (1940).
[5] W. McKinley and H. Feshbach, Phys. Rev. 74, 1759 (1948).
[6] A criterion for "sufficiently strong" is given later.

is in contrast to the Schroedinger equation, where the Born approximation will always be valid if we take the energy of the incident particle large enough.

To investigate the validity of the Born approximation we shall first express it in terms of conditions on the phase shifts. In the non-relativistic theory one can show that the Born approximation is equivalent to the assumption that the phase shifts are given by,

$$(e^{2i\delta_l}-1)/2i=-k\int_0^\infty 2\cdot V(r)\cdot j_l^2(kr)\cdot r^2\cdot dr, \quad (7)$$

where $j_l(kr)$ is the spherical Bessel function.[7] We shall find a similar expression in the Dirac theory.

The Born approximation has been treated by others,[8] but we shall derive a somewhat different form of it which will be more useful for later work. Let us rewrite (1) as

$$(E+\boldsymbol{\alpha}\cdot\mathbf{p}+\beta)\psi=V\psi$$

and operate on both sides of the equation by

$$(E-\boldsymbol{\alpha}\cdot\mathbf{p}-\beta);$$

then because of the properties of the Dirac matrices we get

$$(\nabla^2+k^2)\psi=(E-\boldsymbol{\alpha}\cdot\mathbf{p}-\beta)\cdot V\psi, \quad (8)$$

where $k=(E^2-1)^{\frac{1}{2}}$ is the momentum. Now let us suppose we have an incoming plane wave represented by $a_{\mathbf{k}_0}\exp(i\mathbf{k}_0\cdot\mathbf{r})$, where $a_{\mathbf{k}_0}$ is a spinor. The plane wave has a momentum $\mathbf{k}_0$ and energy $E=(k^2+1)^{\frac{1}{2}}$. The solution of (8) is obtained by the usual procedure of using the Green's function

$$-\frac{1}{4\pi}\frac{e^{ik|\mathbf{r}-\mathbf{r}'|}}{|\mathbf{r}-\mathbf{r}'|}. \quad (9)$$

The solution of (2), giving the scattering due to the potential $V(\mathbf{r})$, is then

$$\psi=a_{\mathbf{k}_0}e^{i\mathbf{k}_0\cdot\mathbf{r}}-\int\frac{e^{ik|\mathbf{r}-\mathbf{r}'|}}{4\pi|\mathbf{r}-\mathbf{r}'|}\cdot[E-\boldsymbol{\alpha}\cdot\mathbf{p}'-\beta]\cdot V(\mathbf{r}')\cdot\psi(\mathbf{r}')\cdot d\mathbf{r}', \quad (10)$$

where $\mathbf{p}$ is the operator, $-i$ grad. We can bring the operator $(E-\boldsymbol{\alpha}\cdot\mathbf{p}'-\beta)$ outside the integral sign by first integrating by parts and then noting that

$$\frac{\partial}{\partial x'}\frac{e^{ik|\mathbf{r}-\mathbf{r}'|}}{|\mathbf{r}-\mathbf{r}'|}=-\frac{\partial}{\partial x}\frac{e^{ik|\mathbf{r}-\mathbf{r}'|}}{|\mathbf{r}-\mathbf{r}'|}. \quad (11)$$

Thus we get,

$$\psi=a_{\mathbf{k}_0}e^{i\mathbf{k}_0\cdot\mathbf{r}}-[E-\boldsymbol{\alpha}\cdot\mathbf{p}-\beta]\cdot\int\frac{e^{ik|\mathbf{r}-\mathbf{r}'|}}{4\pi|\mathbf{r}-\mathbf{r}'|}\cdot V(\mathbf{r}')\cdot\psi(\mathbf{r}')\cdot d\mathbf{r}'. \quad (12)$$

[7] Reference 2, p. 77.

[8] T. Sexl, Zeits. f. Physik 81, 178 (1933).

The asymptotic form of (12), which will yield the scattering amplitude, is

$$\psi\rightarrow a_{\mathbf{k}_0}e^{i\mathbf{k}\cdot\mathbf{r}_0}+\frac{e^{ikr}}{r}\cdot f(\theta,\varphi), \quad (13)$$

and

$$f(\theta,\varphi)=-\frac{1}{4\pi}(E-\beta-\boldsymbol{\alpha}\cdot\mathbf{k})\cdot\int e^{-i\mathbf{k}\cdot\mathbf{r}}\cdot V(\mathbf{r})\cdot\psi(\mathbf{r})\cdot d\mathbf{r}, \quad (14)$$

where $\mathbf{k}$ is the momentum vector in the direction θ, φ relative to the direction of $\mathbf{k}_0$. Here, of course, $f(\theta,\varphi)$ represents four functions, $f_i(\theta,\varphi)$, $i=1, 2, 3, 4$.

Equation (14) is a general expression for the scattering amplitude. To obtain the Born approximation from it, we replace $\psi(\mathbf{r})$ by its zero-order approximation $a_{\mathbf{k}_0}e^{i\mathbf{k}_0\cdot\mathbf{r}}$; thus in the Born approximation,

$$f(\theta,\varphi)=\tfrac{1}{2}(E-\beta-\boldsymbol{\alpha}\cdot\mathbf{k})\cdot a_{\mathbf{k}_0}\cdot f_{\text{n.r.}}(\theta,\varphi), \quad (15)$$

where

$$f_{\text{n.r.}}(\theta,\varphi)=\frac{-2}{4\pi}\cdot\int e^{-i\mathbf{k}\cdot\mathbf{r}}\cdot V(\mathbf{r})\cdot e^{i\mathbf{k}_0\cdot\mathbf{r}}\cdot d\mathbf{r} \quad (16)$$

and is the usual Born approximation for the non-relativistic Schroedinger equation.

From (15), we can obtain the differential cross section,

$$\sigma(\theta,\varphi)=|f(\theta,\varphi)|^2=\textstyle\sum_i|f_i(\theta,\varphi)|^2,$$

to check this expression for the scattering amplitude. Thus

$$\sigma=\tfrac{1}{4}\cdot a_{\mathbf{k}_0}^*\cdot[E-\beta-\boldsymbol{\alpha}\cdot\mathbf{k}]^2\cdot a_{\mathbf{k}_0}\cdot|f_{\text{n.r.}}|^2. \quad (17)$$

Now

$$[E-\beta-\boldsymbol{\alpha}\cdot\mathbf{k}]^2=2E\cdot(E-\beta-\boldsymbol{\alpha}\cdot\mathbf{k}) \quad (18)$$

since $\beta^2=1$, $\beta\boldsymbol{\alpha}+\boldsymbol{\alpha}\beta=0$ and $(\boldsymbol{\alpha}\cdot\mathbf{k})^2=k^2$. Thus

$$\boldsymbol{\alpha}a_{\mathbf{k}_0}^*[E-\beta-\boldsymbol{\alpha}\cdot\mathbf{k}]^2a_{\mathbf{k}_0}=2E[E+(1/E)+\mathbf{v}_0\cdot\mathbf{k}]; \quad (19)$$

since $a_{\mathbf{k}_0}^*\beta a_{\mathbf{k}_0}=-1/E$, and $a_{\mathbf{k}_0}^*\boldsymbol{\alpha}a_{\mathbf{k}_0}=-\mathbf{v}_0$, the initial velocity of the particle. Writing $vk\cos\theta$ for $\mathbf{v}_0\cdot\mathbf{k}$ in (19) and substituting into (17) we get for the cross section[9]

$$\sigma(\theta,\varphi)=\frac{1}{1-v_0^2}(1-v_0^2\sin^2\tfrac{1}{2}\theta)\cdot|f_{\text{n.r.}}|^2. \quad (20)$$

Returning now to expression (15) for the scattering amplitude $f(\theta,\varphi)$; we wish to derive an expression for the phase shifts from it. This we will do by comparison of Eq. (15) with the expression for $f(\theta)$ in terms of the phase shifts; namely, Eqs. (5) and (6).

In Eq. (14), let us introduce the explicit forms for the matrices $\boldsymbol{\alpha}$, β, and $a_{\mathbf{k}_0}$,

$$\boldsymbol{\alpha}=\begin{bmatrix}0 & \boldsymbol{\sigma}\\ \boldsymbol{\sigma} & 0\end{bmatrix},\quad \beta=\begin{bmatrix}1 & 0\\ 0 & -1\end{bmatrix},$$
$$\sigma_x=\begin{bmatrix}0 & 1\\ 1 & 0\end{bmatrix},\quad \sigma_y=\begin{bmatrix}0 & -i\\ i & 0\end{bmatrix},\quad \sigma_z=\begin{bmatrix}1 & 0\\ 0 & -1\end{bmatrix} \quad (21)$$

[9] A similar result was obtained by time perturbation by M. E. Rose, Phys. Rev. 73, 279 (1948).

and

$$a_{\mathbf{k}_0}=\begin{bmatrix}-k/(E+1)\\0\\1\\0\end{bmatrix}.$$

We have assumed the plane wave moving in the $+z$ direction and polarized with spin in the $+z$ direction. Then Eq. (15) gives for $f_3(\theta)$ and $f_4(\theta)$,

$$f_3(\theta)=\tfrac{1}{2}(E+1)\{1+(k/(E+1))^2\cos\theta\}\cdot f_{\text{n.r.}}(\theta), \quad (22\text{-a})$$

$$f_4(\theta)=\tfrac{1}{2}(E+1)\cdot(k/(E+1))^2\sin\theta\cdot f_{\text{n.r.}}(\theta). \quad (22\text{-b})$$

One may note that (22) has the correct non-relativistic limit. In this limit, $k\to 0$ to order v/c, $E\to 1$ to order $(v/c)^2$ and thus $f_3(\theta)\to f_{\text{n.r.}}(\theta)$ and $f_4\to 0$ to order $(v/c)^2$.

Now compare expressions (22-a) and (5) for $f_3(\theta)$. Using the orthogonal property of Legendre polynomials, we get

$$(l+1)\frac{e^{2i\delta_l}-1}{2i}+l\frac{e^{2i\delta_{-l-1}}-1}{2i}$$
$$=k\cdot\frac{2l+1}{2}\cdot\frac{E+1}{2}\cdot\int_0^\pi\left\{1+\left(\frac{k}{E+1}\right)^2\cos\theta\right\}$$
$$\cdot f_{\text{n.r.}}(\theta)\cdot P_l(\cos\theta)\sin\theta d\theta. \quad (23)$$

Now the expansion for $f_{\text{n.r.}}(\theta)$ in terms of $P_l(\cos\theta)$ is given by the Schroedinger theory as

$$f_{\text{n.r.}}(\theta)=\frac{1}{k}\sum_{l=0}(2l+1)\cdot\Delta_l\cdot P_l(\cos\theta), \quad (24)$$

where

$$\Delta_l=-k\int_0^\infty 2\cdot V(r)\cdot j_l^2(kr)\cdot r^2dr. \quad (25)$$

Δ_l is, as noted above, the non-relativistic Born approximation for $(e^{2i\delta_l}-1)/2i$.

Substituting (24) into (23), and using the relation

$$\int_{-1}^1 P_{l'}(x)\cdot P_l(x)\cdot x\cdot dx$$
$$=\begin{cases}2(l+1)/(2l+1)(2l+3), & l'=l+1\\ 0, & l'\neq l\pm 1\\ 2l/(2l-1)(2l+1), & l'=l-1,\end{cases} \quad (26)$$

we get

$$\frac{l+1}{2l+1}\frac{e^{2i\delta_l}-1}{2i}+\frac{l}{2l+1}\frac{e^{2i\delta_{-l-1}}-1}{2i}$$
$$=\frac{E+1}{2}\left\{\Delta_l+\left(\frac{k}{E+1}\right)^2\left[\frac{l}{2l+1}\Delta_l+\frac{l+1}{2l+1}\cdot\Delta_{l+1}\right]\right\}. \quad (27)$$

Equation (27) is one relation for δ_l and δ_{-l-1}; a second such relation will be obtained by treating $f_4(\theta)$ in a similar manner. As the functions $P_l'(\cos\theta)$ form an orthogonal set,

$$\int_{-1}^1 P_l^1\cdot P_{l'}^1\cdot dx=\delta_{ll'}\cdot\frac{2}{2l+1}\cdot l(l+1),$$

Eqs. (22-b) and (6) give,

$$\frac{e^{2i\delta_{-l-1}}-e^{2i\delta_l}}{2i}=\frac{k}{l(l+1)}\cdot\frac{2l+1}{2}\cdot\frac{E+1}{2}\cdot\left(\frac{k}{E+1}\right)^2$$
$$\times\int_0^\pi\sin\theta\cdot f_{\text{n.r.}}(\theta)\cdot P_l(\cos\theta)d(\cos\theta). \quad (28)$$

Again, substituting (24) for $f_{\text{n.r.}}(\theta)$ and now using the integral,

$$\int_{-1}^1(1-x^2)^{\frac{1}{2}}\cdot P_{l'}^1(x)\cdot P_l^1(x)$$
$$=\begin{cases}2l(l+1)/(2l+1)(2l-1), & l'=l-1\\ -2l(l+1)/(2l+1)(2l+3), & l'=l+1\\ 0, & l'\neq l\pm 1.\end{cases} \quad (29)$$

we get

$$\frac{e^{2i\delta_{-l-1}}-e^{2i\delta_l}}{2i}=\frac{E+1}{2}\cdot\left(\frac{k}{E+1}\right)^2\cdot\{\Delta_{l+1}-\Delta_l\}. \quad (30)$$

Equations (27) and (30) can be solved simultaneously for δ_l and δ_{-l-1}; thus,

$$(e^{2i\delta_l}-1)/2i=\tfrac{1}{2}(E+1)\{\Delta_l+(k/(E+1))^2\Delta_{l+1}\}, \quad (31\text{-a})$$

$$(e^{2i\delta_{-l-1}}-1)/2i=\tfrac{1}{2}(E+1)\{\Delta_l+(k/(E+1))^2\Delta_{l-1}\}. \quad (31\text{-b})$$

Use of the Born approximation in the Dirac theory is equivalent to calculating the phase shifts by means of Eqs. (31). In the non-relativistic limit, $E\to 1$, and we get $\delta_{-l-1}=\delta_l$ and $(e^{2i\delta_l}-1)/2i=\Delta_l$ as in the Schroedinger theory.

However, in the high energy limit, we get a result quite different from that expected in the Schroedinger theory. The phase shifts do not approach zero. If we assume the potential not to have a pole at $r=0$, then in Δ_l we can replace $j_l(kr)$ by its asymptotic form, $\sin(kr-\frac{1}{2}l\pi)/kr$. Equations (31) and (7) give,

$$\frac{e^{2i\delta_l}-1}{2i}\underset{k\to\infty}{\to}-\int_0^\infty V(r)\cdot dr. \quad (32)$$

That is to say, for a given fixed energy, no matter how high, then for increasing l the phase shifts, of course, approach zero. But if we hold l fixed, then with increasing energy, the phase shift approaches a definite constant, independent of l, given by (32).

Let us call the phase shift at infinite energy δ_∞. We will show in the next section, that if the potential $V(r)$

has no pole at $r=0$, then δ_∞ is actually given by

$$\delta_\infty = -\int_0^\infty V(r)\cdot dr \tag{33}$$

and not only in the Born approximation.

Now (32) agrees with (33) to first order in V, as the Born approximation should. However if $\int_0^\infty V\cdot dr$ is large, then the Born approximation can be considerably in error. A criterion for the validity of the Born approximation is then (in ordinary c.g.s. units),

$$|\delta_\infty| = \left|(1/\hbar c)\cdot\int_0^\infty V(r)\cdot dr\right| \ll 1. \tag{34}$$

As a practical example, consider a square well based on the mercury nucleus. Let the range of the well be the radius a of the nucleus, and its depth be given by Ze^2/a. Then for this wall, $\delta_\infty=0.6$, which is not small. However for a square well based on hydrogen, δ_∞ would be small and the Born approximation would be valid for such a well.

The difference in the behavior of the Born approximation in the Dirac and Schroedinger theories can be understood qualitatively in the following manner. The Born approximation gives good results if the potential is weak, that is, if the wave function of the scattered particle is almost that of a free particle. Now in the Schroedinger theory, as we increase the energy of the particle, the potential becomes effectively weaker, since the particle spends less time near the scatterer. Thus, even for strong potentials, we can find energies high enough that the potential is effectively weak. However in the relativistic Dirac theory, this is not the case. For if the energy is already such that the particle is moving with almost the speed of light, increasing the energy now will not appreciably shorten the time spent by the particle in the neighborhood of the scatterer. Thus, if the Born approximation is not valid at energies of, for example, 10 mc^2, it will not be valid at any higher energies.

The above argument should hold for any relativistic equation. The phase shifts for the Klein-Gordon equation also exhibit the same properties as the Dirac phase shifts at high energies, indicating the non-validity of the Born approximation for sufficiently strong potentials in the case of the Klein-Gordon equation.

IV. THE PHASE SHIFTS AT INFINITE ENERGIES

In this section we deal with the behavior of the phase shifts at high energies and establish the result used in the previous section. It is convenient to introduce here a transformation used by Gordon[10] in finding the energy levels of the hydrogen atom.

Let $S_l(r)$ and $\bar{S}_l(r)$ be defined by

$$g_l = \tfrac{1}{2}(E+1)^{\frac{1}{2}}(S_l+\bar{S}_l), \tag{35-a}$$

and

$$f_l = -i\tfrac{1}{2}(E-1)^{\frac{1}{2}}(S_l-\bar{S}_l). \tag{35-b}$$

where $\bar{S}_l$ is the conjugate of S_l. $S_l(r)$ then has the asymptotic form, because of Eqs. (3),

$$S_l(r) \underset{r\to\infty}{\longrightarrow} e^{i(kr-\frac{1}{2}(l+1)\pi+\delta_l)}. \tag{36}$$

Also, by substituting (35) in Eqs. (2) for g_l and f_l we can obtain the differential equations for S_l,

$$\frac{d}{dr}S_l = \left(ik - i\frac{V}{k}\cdot E\right)S_l + \left(\frac{l+1}{r} - \frac{iV}{k}\right)\bar{S}_l, \tag{37-a}$$

$$\frac{d}{dr}\bar{S}_l = \left(-ik + i\frac{V}{k}\cdot E\right)\bar{S}_l + \left(\frac{l+1}{r} + \frac{iV}{k}\right)S_l. \tag{37-b}$$

As both $f_l=g_l=0$ at $r=0$, $S_l=\bar{S}_l=0$ at $r=0$.

For purposes of later comparison between the Dirac and Schroedinger equations, we now show that the Schroedinger equation can be put in a form almost identical with that of Eqs. (37).

For the moment, let $g_l(r)/r$ denote the radial part of the wave function in the Schroedinger theory; then $g_l(r)$ satisfies the equation

$$\frac{d^2}{dr^2}g_l + \left\{k^2 - 2\cdot V(r) - \frac{l(l+1)}{r^2}\right\}g_l = 0. \tag{38}$$

In order to proceed in a manner analogous to that in the Dirac theory, we rewrite (38) as two first-order equations. We introduce a function $f_l(r)$ defined by

$$-kf_l(r) = \frac{d}{dr}g_l - \frac{l+1}{r}g_l. \tag{39}$$

If the singularity of $V(r)$ at $r=0$ is not stronger than $1/r$, then $f_l=0$ at $r=0$. Equation (38) becomes now

$$\frac{d}{dr}f_l = \left(k - \frac{2V}{k}\right)g_l - \frac{l+1}{r}f_l. \tag{40}$$

Equations (39) and (40) are two first-order equations involving two functions, and are equivalent to Eq. (38).

Again we introduce the complex function $S_l(r)$, now defined by

$$g_l = \tfrac{1}{2}(S_l+\bar{S}_l), \tag{41-a}$$

$$f_l = -i\tfrac{1}{2}(S_l-\bar{S}_l). \tag{41-b}$$

$S_l(r)$ has the asymptotic form

$$S_l \to \exp[i(kr - \tfrac{1}{2}(l+1)\pi + \delta_l)]$$

and can be shown to obey the equation,

$$\frac{d}{dr}S_l = \left(ik - \frac{iV}{k}\right)S_l + \left(\frac{l+1}{r} - i\frac{V}{k}\right)\bar{S}_l, \tag{42-a}$$

$$\frac{d}{dr}\bar{S}_l = \left(-ik + \frac{iV}{k}\right)\bar{S}_l + \left(\frac{l+1}{r} + \frac{iV}{k}\right)S_l. \tag{42-b}$$

Also, as $f_l=g_l=0$ at $r=0$, the $S_l=\bar{S}_l=0$ at $r=0$.

[10] W. Gordon, Zeits. f. Physik 48, 11 (1928).

It will be noted that Eqs. (37) in the Dirac theory become identical with Eqs. (42) in the Schroedinger theory if we put $E=1$ in (37). Equations (37) and (42) then make very clear the connection between the Dirac and Schroedinger equations. Also, any results we obtain in the Dirac theory using Eqs. (37) will likewise hold in the Schroedinger theory if we put $E=1$.

Returning now to the problem of calculating δ_∞, in Eq. (35), let

$$S_l(e)=e^{i\varphi(r)}S_l^0(r), \tag{43}$$

where $S_l^0(r)$ is the free particle wave function, a solution of (37) with $V\equiv 0$. Thus asymptotically, as $r\to\infty$, $\varphi(r)\to\delta_l$. Also, if $V(r)$ has no pole at $r=0$, S_l/S_l^0 is regular at $r=0$, so that $\varphi(r)$ and $d\varphi/dr$ are also regular at $r=0$.

By substituting (43) in (37), $\varphi(r)$ satisfies the equation,

$$\frac{d}{dr}\varphi=-\frac{V}{k}E+i\frac{l+1}{r}(\bar{S}_l^0/S_l^0)[1-e^{-i(\varphi+\bar{\varphi})}] -\frac{V}{k}(\bar{S}_l^0/S_l^0)e^{-i(\varphi+\bar{\varphi})}, \tag{44}$$

where $\bar{\varphi}$ is the complex conjugate φ.

Now if we assume $V(r)$ has no pole at $r=0$, then since $d\varphi/dr$ is regular at $r=0$, the $(l+1)/r$ term must be canceled. Thus we must have

$$\varphi+\bar{\varphi}=2Re(\varphi)=0, \text{ at } r=0. \tag{45}$$

Take the conjugate of (44) and add it to (42); this gives after integration,

$$\tfrac{1}{2}(\varphi+\bar{\varphi})\Big]_0^\infty=-\int_0^\infty\frac{V}{k}\cdot E\cdot dr +\left\{\frac{i}{2}\int_0^\infty\frac{l+1}{r}[1-e^{-i(\varphi+\bar{\varphi})}]\frac{\bar{S}_l^0}{S_l^0}dr+\text{cc}\right\} +\left\{-\int_0^\infty\frac{V}{2k}\frac{\bar{S}_l^0}{S_l^0}e^{-i(\varphi+\bar{\varphi})}\cdot dr+\text{cc}\right\}. \tag{46}$$

Note that $\frac{1}{2}(\varphi+\bar{\varphi})\big]_0^\infty=\delta_l$, so that (46) is an expression for the phase shift. Now in the limit $k\to\infty$, the second integral $\to 0$ at least as fast as $1/k$. For let

$$\frac{l+1}{r}[1-e^{-i(\varphi+\bar{\varphi})}]=h(r). \tag{47}$$

$h(r)$ has no pole at $r=0$. When $r\to\infty$, $\varphi+\bar{\varphi}\to$ a constant and $h(r)\to$const./r. So $h(r)$ is a smooth function. On the other hand $\bar{S}_l^0/S_l^0\to e^{-2ikr}$ for large k and r, and oscillates rapidly. Thus the integral $\int_0^\infty h(r)\cdot\bar{S}_l^0/S_l^0\cdot dr\to 0$ as least as fast as $1/k$ for high k.

Similarly the third integral in (46) $\to 0$ like $1/k^2$ for high k.

Thus,

$$\delta_l=-\int_0^\infty(V/k)\cdot E dr+O(1/k) \tag{48}$$

or

$$\delta_\infty=-(1/\hbar c)\int_0^\infty V(r)\cdot dr \tag{49}$$

(in ordinary c.g.s. units).

V. A VARIATIONAL PRINCIPLE FOR THE PHASE SHIFTS

In this section we derive a variational principle for the phase shifts. Let the integral I be defined by,

$$I=\frac{1}{2i}\int_0^\infty\left\{S_l\frac{d}{dr}\bar{S}_l-\bar{S}_l\frac{d}{dr}S_l+2iS_l\bar{S}_l\left(k-\frac{V}{k}\cdot E\right) +\left(\frac{l+1}{r}-\frac{iV}{k}\right)\bar{S}_l^2-\left(\frac{l+1}{r}+\frac{iV}{k}\right)\cdot S_l^2\right\}\cdot dr, \tag{50}$$

and let

$$J=\int_0^\infty S_l\left\{\frac{d}{dr}\bar{S}_l-\left(-ik+\frac{iV}{k}E\right)\cdot\bar{S}_l -\left(\frac{l+1}{r}+\frac{iV}{k}\right)\cdot S_l\right\}\cdot dr. \tag{51}$$

Then we have

$$I=-i\tfrac{1}{2}(J-\bar{J}), \tag{52}$$

where $\bar{J}$ is the complex conjugate of J. From (52) we observe that the integral I is real and that $I=0$ for the true wave function. Let us now introduce the trial junction $S_l(r)$ in I and J with the restrictions,

$$S_l(r)=0, \text{ at } r=0,$$
$$S_l(r)\underset{r\to\infty}{\to}\exp[i(kr+\eta_l)]=\exp i[kr-\tfrac{1}{2}(l+1)\pi+\delta_l], \tag{53}$$
$$\eta_l=\delta_l-\tfrac{1}{2}(l+1)\pi.$$

Forming the first variation of J, we get after integrating by parts

$$\delta J_l=S_l\cdot\delta\bar{S}_l\Big]_0^\infty+\int_0^\infty\left\{-\frac{dS_l}{dr}\cdot\delta\bar{S}_l-\left(-ik+\frac{iV}{k}\cdot E\right)\cdot S_l\cdot\delta\bar{S}_l-\left(\frac{l+1}{r}-\frac{iV}{k}\right)S_l\cdot\delta S_l\right\}\cdot dr. \tag{54}$$

But at infinity, $\delta\bar{S}_l=-i\delta\eta_l\exp(-ikr)$ and making use of Eq. (37) for S, Eq. (54) becomes

$$\delta J_l=-i\delta\eta_l-\tfrac{1}{2}\delta\cdot\int_0^\infty\left\{\left(\frac{l+1}{r}+\frac{iV}{k}\right)\bar{S}_l^2+\left(\frac{l+1}{r}-\frac{iV}{k}\right)S_l^2\right\}\cdot dr. \tag{55}$$

The last part is real and drops out in calculating δI_l which is the imaginary part of δJ_l. Thus we get our variational principle,

$$\delta\cdot\{I_l+\eta_l\}=0. \tag{56}$$

That is, if δ_l is the true phase shift, then as $I=0$ for the true wave function,

$$\delta_l=\text{extremum of }\{I_l+\delta_l\}. \tag{57}$$

Thus for any trial function S_l, obeying restrictions (53), we can calculate I_l and write, to first order,

$$\delta\cong I_l+\delta_l. \tag{58}$$

We might also point out that by simply putting $E=1$ in (50) and (56) we obtain a variational principle for the non-relativistic phase shift, where S is now the non-relativistic function defined in Section IV.

The simplest trial function to use is the solution $S_l(r)$ for some potential $V_l(r)$ and with the known phase shift δ_l. Putting $S_l(r)$ into (50) and (56) and using Eq. (37) for $S_l(r)$, obtain

$$\delta_l-\delta_l=-\frac{E}{k}\int_0^\infty (V-V_l)\times\left\{S_l\bar{S}_l+\frac{1}{2E}(S_l^2+\bar{S}_l^2)\right\}\cdot dr. \tag{59}$$

If we reintroduce the functions f_l and g_l, according to Eq. (41), then we can write (59) as

$$\delta_l-\delta_l=-\frac{E+1}{2k}\int_0^\infty 2\cdot(V-V_l)\cdot\left\{\frac{g_l^2}{E+1}+\left(\frac{k}{E+1}\right)^2\cdot\frac{f_l^2}{E-1}\right\}\cdot dr. \tag{60}$$

For the special case $V_l(r)\equiv 0$, $\delta_l=0$, the solutions for Eq. (2) can be shown to be,

$$g_l=(E+1)^{\frac{1}{2}}\cdot kr\cdot j_l(kr),\quad f_l=(E-1)^{\frac{1}{2}}\cdot kr\cdot j_{l+1}(kr),$$

and

$$g_{-l-1}=(E+1)^{\frac{1}{2}}\cdot kr\cdot j_l(kr),$$
$$f_{-l-1}=-(E-1)^{\frac{1}{2}}\cdot kr\cdot j_{l-1}(kr).$$

Thus,

$$\delta_l=\tfrac{1}{2}(E+1)\{\Delta_l+(k/(E+1))^2\Delta_{l+1}\}, \tag{61-a}$$

$$\delta_{-l-1}=\tfrac{1}{2}(E+1)\{\Delta_l+(k/(E+1))^2\Delta_{l-1}\}. \tag{61-b}$$

where the Δ_l are as defined in Section III,

$$\Delta_l=-k\int_0^\infty 2\cdot V(r)\cdot j_l^2(kr)\cdot r^2\cdot dr. \tag{62}$$

The variational result (61) is identical with the Born approximation except that $(e^{2i\delta_l}-1)/2i$ is replaced by δ_l. However (61) gives the correct limit for the phase shifts when $E\to\infty$, $\delta_\infty=-\int_0^\infty V\cdot dr$. Thus for a strong potential, where the phase shift may be large even at high energies, the variational results (60) and (61) are considerably better than the Born approximation.

As other writers[11] have already pointed out in connection with the Schroedinger theory, the variational principle for the phase shift provides neither an upper nor a lower bound. Thus it has the disadvantage that adding more parameters to the trial function does not necessarily give better results for the phase shift.

VI. SOME NUMERICAL RESULTS FOR THE PHASE SHIFTS OF A SQUARE WELL

In order to illustrate the behavior of the phase shifts in the Dirac theory, we shall do a numerical calculation for a square well of depth V_0 and range a. We shall calculate the phase shifts exactly and also by use of the variational formula (61), and compare the results.

For a constant potential $-V_0$, the solution of Eqs. (2) for f_l and g_l are

$$g_l=(E+V_0+1)^{\frac{1}{2}}\cdot kr\cdot j_l(pkr), \tag{63-a}$$

and

$$f_l=(E+V_0-1)^{\frac{1}{2}}\cdot kr\cdot j_{l+1}(pkr), \tag{63-b}$$

where

$$p=\left[1+2\cdot\frac{V_0}{k}\frac{E}{k}+\left(\frac{V_0}{k}\right)^2\right]^{\frac{1}{2}}.$$

By matching this solution at $r=a$ to the free particle solutions, we find the phase shift as

$$\tan\delta_l=\frac{((E+1)/(E-1))^{\frac{1}{2}}j_l(ka)-\gamma_l j_{l+1}(ka)}{((E+1)/(E-1))^{\frac{1}{2}}n_l(ka)-\gamma_l\cdot n_{l+1}(ka)}, \tag{64}$$

where

$$\gamma_l=g_l/f_l|_{ka}=\left(\frac{E+V_0+1}{E+V_0-1}\right)^{\frac{1}{2}}\cdot\frac{j_l(pka)}{j_{l+1}(pka)}$$

and $n_l(kr)$ is the spherical Bessel function,

$$n_l(x)=(\pi/2x)^{\frac{1}{2}}\cdot(-1)^{l+1}\cdot J_{-l-\frac{1}{2}}(x).$$

The phase shift at infinite energy can be found directly from (64) by substituting the asymptotic forms of the Bessel functions. We get

$$\delta_\infty=V_0a$$

which agrees with our more general result.

For our numerical calculation, we put $V_0=21.8$ Mev, which is approximately the Coulomb potential at the center of a uniformly charged lead nucleus, and let $a=8.09\times10^{-13}$ cm which is about the radius of a lead nucleus. As our scattered particles we take 100-Mev electrons.

With these figures $\delta_\infty=0.9$ radian, a rather large phase shift. Table I lists the exact phase shifts and those calculated by the variational result, (61). δ_0 has

[11] L. Hulthén, Arkiv. f. Mat., Astr. o. Fys. **35A**, No. 25 (1948).

very nearly its asymptotic value of $\delta_\infty = 0.9$. The phase shifts start out rather large, but decrease very rapidly with increasing l. The variational result gives good agreement for the first few δ_l and for the high δ_l. The agreement is worse for the intermediate δ_l.

VII. TWO EXACT EXPRESSIONS FOR THE PHASE SHIFTS

We shall now derive two exact expressions for the phase shift. If we multiply both sides of Eq. (35-a) by $\exp[-i(kr-\frac{1}{2}(l+1)\pi)]$ and note that

$$e^{-ikr}\frac{d}{dr}S_l=\frac{d}{dr}(e^{-ikr}S_l)+ike^{-ikr}S_l \tag{65}$$

then by integrating and using the property $S_l=0$ at $r=0$ we get

$$e^{i\delta_l}=\int_0^\infty e^{-i[kr-\frac{1}{2}(l+1)\pi]} \times\left\{-\frac{iV}{k}\cdot E\cdot S_l+\left(\frac{l+1}{r}-\frac{iV}{k}\right)\bar{S}_l\right\}\cdot dr. \tag{66}$$

The expression (66) for the phase shift differs from usual expressions for the phase shift, and is simpler in that instead of involving the product of two wave functions one of the wave functions is replaced by what is essentially its asymptotic form, the elementary function $\exp[-i(kr-\frac{1}{2}(l+1)\pi)]$.

Relation (66) will also hold in the Schroedinger theory if we put $E=1$. It is simpler to discuss (66) in this non-relativistic limit. If we substitute for S_l in (66), the solutions for $V(r)\equiv 0$, we get the approximate expressions for the phase shift,

$$\sin\delta_l\cong -k\int_0^\infty 2\cdot V(r)\cdot\frac{\cos[kr-\frac{1}{2}(l+1)\pi]}{kr} j_l(kr)\cdot r^2\cdot dr. \tag{67}$$

Equation (67) resembles the Born approximation for the phase shift: $(e^{2i\delta_l}-1)/2i$ is replaced by $\sin\delta_l$, which is not too important in the Schroedinger theory since δ_l is not large, and one of the spherical Bessel functions is replaced by its asymptotic form. Equation (67) does not give the phase shift correct to the first order in the potential, for then the term in the integrand of (66) involving $(l+1)/r$ would require that $\bar{S}_l(r)$ should be correct to first order in the potential. Also, one would not usually expect (67) to be better than the Born approximation as the asymptotic form of $j_l(kr)$ is a worse approximation to the true wave function near $r=0$ than is $j_l(kr)$.

However, the advantage of (66) would lie in using wave functions which are better approximations to the true wave function than are the free particle functions,

TABLE I. Phase shifts for a 100-Mev electron scattered from a potential well, depth 21.8 Mev and range 8.09×10^{-13} cm, according to the Dirac equation. The exact phase shifts are compared with those obtained by the variational result (61).

l	Exact δ	δ by relation (61)
0	0.857	0.864
1	0.823	0.844
2	0.723	0.525
3	0.273	0.179
4	0.0471	0.0369
5	0.0055	0.0050
6	0.00054	0.00049

and then making use of the simpler integrand to do the integration.

A second exact expression for the phase shift in the Dirac theory can be derived which is more analogous to the non-relativistic expression,

$$\sin\delta_l=-\int_0^\infty 2\cdot V(r)\cdot j_l(kr)\cdot g_l\cdot r\cdot dr.$$

Let us differentiate Eq. (2-b) and eliminate df_l/dr by means of (2-a); then we get the second-order equation for $g_l(r)$,

$$\frac{d^2}{dr^2}g_l+\left(k^2-\frac{l(l+1)}{r^2}\right)g_l=(2E-V)\cdot V\cdot g_l+\frac{dV}{dr}\cdot f_l. \tag{68}$$

Let $f_l^0(r)$ and $g_l^0(r)$ be the solutions of (2) for zero potential. By (68), $g_l^0(r)$ satisfies,

$$\frac{d^2}{dr^2}g_l^0+\left(k^2-\frac{l(l+1)}{r^2}\right)g_l^0=0. \tag{69}$$

Now multiply (68) by g_l^0, (69) by g_l, subtract and integrate. Then, using the asymptotic forms of g_l and g_l^0,

$$-(E+1)\cdot k\cdot\sin\delta_l=\int_0^\infty g_l^0(r)\left\{(2E-V)\cdot V\cdot g_l+\frac{dV}{dr}\cdot f_l\right\}\cdot dr. \tag{70}$$

If we now integrate the term involving dV/dr by parts, and eliminate df_l/dr and dg_l/dr by means of (2), we obtain finally

$$\sin\delta_l=-(1/2k)\int_0^\infty 2\cdot V(r)\cdot\{g_l^0g_l+f_l^0f_l\}\cdot dr. \tag{71}$$

Substituting the free particle wave functions given in Section VI, we get,

$$\sin\delta_l=-\tfrac{1}{2}(E+1)^{\frac{1}{2}}\int_0^\infty 2\cdot V(r)\cdot r\cdot\left\{j_l(kr)\cdot g_l(r)+\left(\frac{E-1}{E+1}\right)^{\frac{1}{2}}j_{l+1}(kr)\,f_l(r)\right\}\cdot dr, \tag{72-a}$$

$$\sin\delta_{-l-1}=-\tfrac{1}{2}(E+1)^{\frac{1}{2}}\int_0^\infty 2\cdot V(r)\cdot r\cdot\left\{j_l(kr)\cdot g_l(r)-\left(\frac{E-1}{E+1}\right)^{\frac{1}{2}}j_{l-1}(kr)\cdot f_{-l-1}(r)\right\}\cdot dr. \quad (72\text{-b})$$

The zeroth approximation to the wave functions will cause Eqs. (67) to yield a first-order approximation which will agree with the Born approximation in the Dirac theory except that $(e^{2i\delta_l}-1)/2i$ is replaced by $\sin\delta_l$.

A result similar to relation (66) will hold for potentials that go like Ze^2/r at infinity. We simply replaced in (66), the free particle solutions g_l^0 and f_l^0 by the Coulomb solutions and the potential $V(r)$ by the deviation from the pure Coulomb potential Ze^2/r.

I would like to express my gratitude to Professor L. I. Schiff for suggesting this problem and for advice and many discussions.

PHYSICAL REVIEW VOLUME 80, NUMBER 2 OCTOBER 15, 1950

The Evaluation of the Collision Matrix

G. C. WICK
University of California, Berkeley, California
(Received April 17, 1950)

Dyson's systematic approach to the reduction of the Heisenberg S-Matrix into a sum of "graph" terms can be simplified. A notation is introduced and an algebraic theorem is proved, which allow one to handle the reduction problem quite easily and in the same manner for any type of field.

I. INTRODUCTION

THE Feynman technique[1] for calculating transition probabilities is now so widely used that a full and satisfactory understanding of it by a wider circle is desirable. An important step in this direction has been Dyson's[2] direct derivation of the method from a simple expression for the S-matrix. One feels, however, that the *pedagogical* value of Dyson's proof is slightly marred by certain omissions and obscurities; moreover, some of the algebraic considerations seem more involved than should be necessary. The purpose of this note is to supply a simple and straightforward proof. The case of the electron-positron field interacting with a quantized electromagnetic field is sufficiently general to allow us to demonstrate all of the features of the method.

Let then $\psi(x)$ be the Dirac field operator at the space-time point x, $\psi^\dagger$ the hermitian-conjugate of ψ, $\bar\psi=\psi^\dagger\beta$ the adjoint, and $A_\mu(x)$ the μ-th component of the electromagnetic potential. The S-matrix for the system can be written:

$$S=1+S_1+S_2+\cdots \quad (1)$$

where S_n, the term of the n-th order in the electron charge ϵ is expressed by a multiple integral over a product of field factors ψ, $\bar\psi$, A [Eq. (18) below]. Our problem is the reduction of S_n to a sum of terms *à la* Feynman. To this end we notice that our fields ψ and A are linear combinations of creation and destruction operators. For example, $\psi(x)=\sum_r a_r\psi_r(x)$ where the ψ_r's are the normalized representatives of the states of a free Dirac particle, and a_r is a destruction (creation) operator if r is a positive (negative) energy state. Collecting all the positive energy states together into a term $u(x)$ and the negative states into a term $\bar v(x)$ we can write:

$$\psi(x)=u(x)+\bar v(x), \quad \bar\psi(x)=\bar u(x)+v(x), \quad (2)$$

where u ($\bar u$) destroys (creates) electrons, and v ($\bar v$) destroys (creates) positrons.[3] Similarly, we can write

$$A_\mu(x)=a_\mu(x)+a_\mu^\dagger(x), \quad (2')$$

where $a_\mu(a_\mu^\dagger)$ destroys (creates) photons.[4] Substituting such expressions into a product of fields, we can expand each product into a sum of products in which each factor is either a creation or a destruction operator.

Following an idea of Houriet and Kind,[5] we then proceed to rearrange such a product so as to carry all creation operators to the left of all destruction operators, writing for instance: $u(x)\bar v(y)=-\bar v(y)u(x)$, $u(x)\bar u(y)=\{u(x),\bar u(y)\}-\bar u(y)u(x)$ where the anticommutator $\{u,\bar u\}=u\bar u+\bar u u$ is a c-number. Thus one may transform a product of n creation and destruction operators into the "ordered" product of the same factors, plus extra terms in which some pairs of factors have been replaced by their commutators or anticommutators while the remaining factors are "ordered" in the above sense. The advantage of this is that when we take the matrix element of an ordered product between a final and an

[1] R. P. Feynman, Phys. Rev. 76, 749 (1949).
[2] F. J. Dyson, Phys. Rev. 75, 486 (1949).

[3] We set $\bar u=u^\dagger\beta$, $\bar v=v^\dagger\beta$ or $\bar v=\beta v^\dagger$; the asymmetry in the definition of $\bar u$ and $\bar v$ shall not cause any trouble here.
[4] $a_\mu^\dagger$ is the hermitian conjugate of a_μ (of $-a_\mu$ if $\mu=4$). As regards the treatment of timelike photons, see Section IV.
[5] A. Houriet and A. Kind, Helv. Phys. Acta 22, 319 (1949).

initial state, all the destruction operators must destroy particles actually present initially, and all creation operators must create particles actually present finally. The virtual creation-followed-by-destruction processes of the customary perturbation theory have been "digested" in the commutators and anticommutators, that appear in the course of the rearrangement. The main problem to be solved in carrying out this idea is one of algebraic technique, i.e., the development of a convenient notation to handle the rearrangement process easily and express the result in a compact way. This is achieved, we think, in the Theorems 1 and 2 below.

II. ALGEBRAIC PRELIMINARIES

Any "simple" factors in a product, like $\psi(x)$, $\bar{\psi}(y)$, $u(x)$, $\bar{u}(y)$, $\cdots$, $A(x)$, $a(y)$, $\bar{a}(z)$ will be denoted also by a capital letter like U, V, W, $\cdots$.

In the case of anticommutative fields (not considered by Houriet and Kind) the rearrangement of a product leads to changes in sign, as in the simple examples considered before. We call S-product, and denote by semicolons on both sides of the product, an "ordered product" symbol defined in such a way that the changes in sign are automatically taken into account. The symbol is then defined by the following rules:

Rule A: Distributive law:

$$:U\cdots V\psi(x)W\cdots Z: = :U\cdots Vu(x)W\cdots Z: + :U\cdots V\bar{v}(x)W\cdots Z:.$$

The S-product can thus be decomposed into a sum of S-products containing creation and destruction operators only.

Rule B: An S-product of the latter type is defined by:

$$:UV\cdots Z: = \delta_P XY\cdots W, \tag{3}$$

where the ordinary product on the right contains the same factors U, V, $\cdots$ ordered in the previously specified manner (creation operators to the left, destruction to the right) and δ_P is the signature, ± 1, of the permutation [between left-hand side and right-hand side of Eq. (3)] *of the electron-positron factors only.*

The δ_P factor takes care of the above-mentioned sign changes. The creation (or destruction) operators may be freely permuted amongst themselves, without affecting the right-hand side of Eq. (3).

Examples of S-products:

$$:\psi(x)\bar{\psi}(y): = :u(x)\bar{u}(y): + :u(x)v(y): + :\bar{v}(x)\bar{u}(y): + :\bar{v}(x)v(y): = -\bar{u}(y)u(x) + u(x)v(y) + \bar{v}(x)\bar{u}(y) + \bar{v}(x)v(y) \tag{4}$$

$$:\bar{\psi}(y)\psi(x): = :\bar{u}(y)u(x): + \cdots = \bar{u}(y)u(x) + v(y)u(x) + \bar{u}(y)\bar{v}(x) - \bar{v}(x)v(y).$$

Clearly

$$:\psi(x)\bar{\psi}(y): + :\bar{\psi}(y)\psi(x): = 0 \tag{5}$$

while the anticommutator:

$$\psi(x)\bar{\psi}(y) + \bar{\psi}(y)\psi(x) \equiv \{\psi(x), \bar{\psi}(y)\} \text{ is in general } \neq 0.$$

Note also that:

$$:\psi(x)\psi(y): = \psi(x)\psi(y), \quad :\bar{\psi}(x)\bar{\psi}(y): = \bar{\psi}(x)\bar{\psi}(y).$$

The reader can easily derive the result:

Rule C: Factors within an S-product symbol can be permuted "as if" all anticommutators $\{\psi, \bar{\psi}\}$, $\cdots$ and commutators $[A, A]$ etc., were zero.

One can write the Dirac current as an S-product

$$s_\mu = i\epsilon :\bar{\psi}\gamma_\mu\psi: = i\epsilon \sum_{\alpha\beta} (\gamma_\mu)_{\alpha\beta} :\bar{\psi}_\alpha\psi_\beta:, \tag{6}$$

where ϵ is the electron charge and γ_1, $\cdots$, γ_4 are the Dirac matrices. Writing the current as an S-product is equivalent to the customary prescription for removing the infinite charge of the negative sea.

Another kind of ordering that is useful occurs in the chronological product or T-product, with time running from right to left. This can be used, of course, only if the factors U, V, $\cdots$ of the product are specifically labeled with a time.

Rule D: The T-product is defined by:

$$T(UV\cdots Z) = \delta_P XY\cdots, \tag{7}$$

the factors U, V, $\cdots$ being rearranged in chronological order in the ordinary product on the right. Our T-product differs from Dyson's P-product in having the sign factor δ_P [same meaning as in Eq. (3)]. This simplifies the definition of the contraction symbol, Eq. (8) below.

Example:

$$T(\psi(x)\bar{\psi}(y)) = \psi(x)\bar{\psi}(y) \quad \text{if} \quad x_0 > y_0; \qquad = -\bar{\psi}(y)\psi(x) \quad \text{if} \quad x_0 < y_0. \tag{7'}$$

One has:

$$T(\psi(x)\psi(y)) = \psi(x)\psi(y), \quad \text{etc.}$$

Rule C′: The T-product obeys a rule quite similar to Rule C.

A further complication of the T-product occurs in the expression for the S-matrix, Eq. (18) below. If two or more "simple" factors in the product are labeled with the same time, the T-symbol does not prescribe their order. In the useful case, however, it turns out that either the order is irrelevant (independent fields) or it is prescribed by the S-rule as in (6). A symbol like

$$T(UV:WXY:\cdots Z), \tag{7''}$$

for example, will then mean that W, X, Y (bear the same time-label and) appear, in the form of an S-product, as a single factor in the chronological ordering. This may be called a mixed T-product.

We now turn to the basic problem of transforming the T-product in Eq. (18) into a sum of S-products. To this end we adopt Houriet and Kind's idea of a "contraction" symbol to represent the commutator or anticommutator which arises in switching two factors. The contraction will be denoted by appending a dot

superscript to both factors.[6] Thus, in the simplest case we write:

$$T(UV)=U^{\cdot}V^{\cdot}+:UV: \tag{8}$$

Houriet and Kind's definition, however, handles the reduction of an *ordinary* product into an ordered one. The definition (8) handles directly the reduction of a T-product, which is what we need, and avoids the complicated reassembly process which is otherwise necessary to arrive at the simple Feynman formulas. Contractions between independent fields, such as ψ and A, are zero. But also:

$$\psi^{\cdot}(x)\psi^{\cdot}(y)=\bar{\psi}^{\cdot}(x)\bar{\psi}^{\cdot}(y)=0. \tag{9}$$

On the other hand:

$$\psi^{\cdot}(x)\bar{\psi}^{\cdot}(y)=\{u(x),\bar{u}(y)\}=\sum_{r>}\psi_r(x)\bar{\psi}_r(y) \quad \text{if } x_0>y_0$$

and (10)

$$\cdots=-\{\bar{v}(x),v(y)\}=-\sum_{r<}\psi_r(x)\bar{\psi}_r(y) \quad \text{if } x_0<y_0,$$

where $r>$ (or $r<$) means that the sum extends over the positive (or negative) energy states only. The right-hand side of Eq. (10) is clearly the "mystical" kernel function which is variously designated with K_+ by Feynman,[7] $\frac{1}{2}S_f$ by Dyson,[2] etc.

We shall omit the $+$ in K_+ and write instead the spinor indices explicitly. Here are the main formulas:

$$\psi_{\alpha}^{\cdot}(x)\bar{\psi}_{\beta}^{\cdot}(y)=K_{\alpha\beta}(x-y), \tag{11a}$$

$$\bar{\psi}_{\alpha}^{\cdot}(x)\psi_{\beta}^{\cdot}(y)=-\psi_{\beta}^{\cdot}(y)\bar{\psi}_{\alpha}^{\cdot}(x)=-K_{\beta\alpha}(y-x), \tag{11b}$$

$$A_{\mu}^{\cdot}(x)A_{\nu}^{\cdot}(y)=\tfrac{1}{2}\delta_{\mu\nu}D_F(x-y), \tag{11c}$$

where D_F is defined, for example, by Dyson.[8]

One last convention about symbols. We want to give a meaning to an S-product with one or more contractions. In order to distinguish different contractions in a product, we shall use different superscripts, such as double dots, triple dots, etc. If a contraction is marked between two adjacent factors, it has the value given by (11) and may be regarded as a c-number; the remaining factors form the S-product proper. Contractions between non-adjacent factors are defined by:

Rule C″: Factors within an S-product with one or more contractions (including the contracted factors) obey a rule[9] similar to C. For example, if $U, V, \cdots$ etc. are all anticommutative fields, one has:

$$:U^{\cdot}VW^{\cdot\cdot}X^{\cdot\cdot}Y^{\cdot}Z:=-(U^{\cdot}Y^{\cdot})(W^{\cdot\cdot}X^{\cdot\cdot}):VZ: \tag{12}$$

$$:TU^{\cdot}VW^{\cdot\cdot}XY^{\cdot}Z^{\cdot\cdot}:=+(U^{\cdot}Y^{\cdot})(W^{\cdot\cdot}Z^{\cdot\cdot}):TVX:. \tag{13}$$

[6] Houriet and Kind's symbol is a line connecting the two factors like a string attached at both ends. It is very convenient for handwriting, but has been abandoned here for typographical reasons.

[7] See reference 1, Eq. (17).

[8] See reference 2, Eq. (42).

[9] The self-consistency of this rule is insured by Eq. (11b). Verify also that any two arrangements leaving the contracted fields together will give the same value.

And now let us prove the basic theorem. First let us show that if $:UV\cdots XY:$ is an S-product, and Z a factor *labeled with a time which is earlier than any of the times for* $U, V, \cdots, Y$ then

$$:UV\cdots XY:Z=:UV\cdots XY^{\cdot}Z^{\cdot}:+:UV\cdots X^{\cdot}YZ^{\cdot}:+\cdots+:U^{\cdot}V\cdots XYZ^{\cdot}:+:UV\cdots XYZ:. \tag{14}$$

It is clearly sufficient to prove Eq. (14) under the assumption that each simple factor is either a creation or a destruction operator, and furthermore that Z is a creation operator (if Z is a destruction operator the equation is trivial). Owing to the C-rules, the validity of Eq. (14) is invariant against a permutation of $UV\cdots XY$, and we may choose the order in such a way that $U, V, \cdots, X, Y$, are already an S-product *as they stand*. Let us then prove (14) on the assumption that $U, V, \cdots X, Y$ are all destruction operators; any number of creation operators may then be added on the left. The proof follows by induction. First (14) is true if there is only one factor:

$$YZ=T(YZ)=Y^{\cdot}Z^{\cdot}+:YZ:.$$

Then assume (14) is true for n factors, and multiply by another destruction operator T on the left:

$$T:UV\cdots XY:Z=T:UV\cdots XY^{\cdot}Z^{\cdot}:+\cdots+T:UV\cdots XYZ:.$$

Since $U, V\cdots Y$ are destruction operators, the colon between T and the rest can be moved to the left of T everywhere except in the last term. Now $:UV\cdots XYZ:=\delta_P ZUV\cdots XY$, δ_P being defined as usual. Since again (T being assumed "later" than Z)

$$TZ=T(TZ)=T^{\cdot}Z^{\cdot}+:TZ:=T^{\cdot}Z^{\cdot}+\delta_Q ZT$$

(Q being the permutation of electron positron operators in passing from TZ to ZT) one finds easily for the last term:

$$\begin{aligned}T:UV\cdots XYZ:&=\delta_P TZ(UV\cdots Y)\\&=\delta_P(T^{\cdot}Z^{\cdot}UV\cdots Y+\delta_Q ZTU\cdots Y)\\&=:T^{\cdot}UV\cdots YZ^{\cdot}:+\delta_P\delta_Q ZTU\cdots Y.\end{aligned}$$

Now $\delta_P\delta_Q=\delta_R$ where R belongs to the rearrangement from $ZTU\cdots Y$ to $TU\cdots YZ$, so that the last term is $=:TU\cdots YZ:$. This completes the proof for $(n+1)$ factors.

We may further generalize Eq. (14). If we mark a contraction between U, V *in all terms*, the equation will still be valid, since $U^{\cdot}V^{\cdot}$ will be merely a factor added on the left. Similarly one can add several such factors. Then, thanks to the C-rules, one can rearrange the order, and Eq. (14) is seen to hold even when any number of contractions (the same in every term!) is marked within $UV\cdots XY$.

Theorem 1. A T-product can be transformed into a sum of S-products as follows:

$$T(UV\cdots XYZ)=:UV\cdots XYZ:+:U^{\cdot}V^{\cdot}W\cdots YZ:+:U^{\cdot}VW^{\cdot}\cdots XYZ:+\cdots+:U^{\cdot}V^{\cdot\cdot}W^{\cdot\cdot}\cdots X^{\cdot\cdot}Y^{\cdot}Z^{\cdot\cdot}: \tag{15}$$

where the sum on the right includes all possible sets of contractions one can indicate. Of course, one can omit terms with contractions which are identically zero, such as $\psi\cdot\psi$, $\psi\cdot A$, etc.

Equation (8) is, of course, the simplest case of (15). The general case follows easily by induction. Suppose (15) is proved for n factors. Multiply on the right by an Ω belonging to an earlier time than any other factor:

$$T(UV\cdots Z)\Omega = :UV\cdots XYZ:\Omega + :U\cdot V\cdot W\cdots XYZ:\Omega + \cdots$$

they apply Eq. (14) to each term on the right and notice that

$$T(U\cdots Z)\Omega = T(UV\cdots Z\Omega).$$

The theorem is then seen to hold for $n+1$ factors. The restriction on the time label for Ω can be removed by rearranging the order of factors, using the C-rules.

Theorem 2. A mixed T-product, such as (7″) can be decomposed in a manner similar to Eq. (15) but omitting contractions between factors already S-ordered [for example contractions $W\cdot X\cdot$, $W\cdot XY\cdot$, $X\cdot Y\cdot$ in (7″)].

The reader can construct the general proof, after we have examined the case (7″) as an example. We may as usual assume that each factor W, X, Y is either a destruction or a creation operator. We then consider (7″) as the limit of:

$$T(UVWXY\cdots Z),$$

where the time label of the creation operators amongst W, X, Y is assumed later (by an infinitesimal amount) than that of the destruction operators. Equation (15) may then be applied. Furthermore the contractions to be omitted according to the statement of Theorem 2 are actually zero, so that the theorem follows.

III. PHYSICAL APPLICATIONS

The somewhat tedious details we have developed for the sake of clarity will not, we hope, obscure the fact that the whole method is quite simple, indeed somewhat trivial. Nevertheless it allows one to operate with considerable freedom on rather complex expressions.

Let us use for convenience the abbreviations:

$$\mathrm{A} = -i\gamma_\mu A_\mu, \quad \text{that is} \quad A_{\alpha\beta} = -i(\gamma_\mu)_{\alpha\beta}A_\mu \tag{16}$$

and

$$\bar\psi\mathrm{A}\psi(x) \quad \text{for} \quad \sum_{\alpha\beta}\bar\psi_\alpha(x)A_{\alpha\beta}(x)\psi_\beta(x). \tag{17}$$

As Dyson has shown, the n-th order term S_n in Eq. (1) can be written as a multiple integral over n points $x, y, \cdots, z$ in space time[10]

$$S_n = [(-i\epsilon)^n/n!]\int T(:\bar\psi\mathrm{A}\psi(x)::\bar\psi\mathrm{A}\psi(y):\cdots:\bar\psi\mathrm{A}\psi(z):) \times (dx)(dy)\cdots(dz), \tag{18}$$

[10] We use units $\hbar=1$, $c=1$.

where $(dx)=dx_1dx_2dx_3dx_0$, etc.$\cdots$. This integral involves a mixed T-product which can be reduced in the desired manner by means of Theorem 2. The rest of the analysis then proceeds very much in the same manner as in Section 7 of Dyson's paper,[2] Dyson's "associated pairs" of mutually annihilating factors being replaced here by the modified Houriet and Kind "contractions" that we have defined. There are, however, several simplifications. Thanks to the C-rules we can handle the S-products of Eq. (15) with great ease, so that nothing is to be gained now by reducing the procedure to a set of mechanical recipes. Here are, then, not recipes but a few suggestions as to how best to conduct the evaluation in any given case.

Suppose then, that (18) is decomposed according to Theorems 1 and 2 into a sum of terms, each term being an integral of an S-product with a number of contractions. For example, a term in S_3 will be:

$$[(-i\epsilon)^3/3!]\int :\bar\psi\cdots\mathrm{A}\psi\cdot(x)\bar\psi\cdot\mathrm{A}\cdot\cdot\psi(y)\bar\psi\mathrm{A}\cdot\cdot\psi\cdot\cdot\cdot(z): \times (dx)(dy)(dz). \tag{19}$$

If one applies a permutation to the $\bar\psi\mathrm{A}\psi$ groups (allowing the contractions to follow their factors according to rule C'') then one changes the names of the variables x, y, z, to restore their former order in the product, one will get in general another possible term in the development of S_3. The number of such "equivalent" terms is in the case of (19) precisely 3!, so that one can allow for them simply by omitting the factorial on the denominator. In the general case, however, the $n!$ permutations of the $\bar\psi\mathrm{A}\psi$ groups will not lead to $n!$ distinct terms[11] since a given set of possible contractions may be left completely unchanged by a subgroup of g permutations (automorphisms of the set), g being equal for two "equivalent" sets.[12] In this case, therefore, the number of distinct equivalent terms of a given kind will be $n!/g$, and their total contribution to S_n will be:

$$[(-i\epsilon)^n/g]\int S\text{-product}\cdot(dx)\cdots(dz), \tag{20}$$

the S-product being any one of the equivalent S-products, with contractions.

A "graph" is now simply a concise way of writing an S-product of the kind which interests us. In fact, once the points $x, y, \cdots, z$ are marked it is implicitly understood that there is a factor $:\bar\psi\mathrm{A}\psi:$ for each point. If there is a contraction between $A(x)$ and $A(y)$, say, draw

[11] Compare the similar discussion in reference 5, where, however, the expression "equivalent" has a slightly different meaning. The argument is reproduced here with appropriate modifications for the convenience of the reader.

[12] If P is an automorphism of the set s (we can write: $Ps=s$) and T transforms s into the equivalent set s' ($s'=Ts$) then: $s'=Ts=TPs=TPT^{-1}s'$, hence TPT^{-1} is an automorphism of s'. This establishes a one-to-one correspondence of a well-known type between the automorphisms of the two sets.

a dashed line between x and y and omit the A symbols. If there is a contraction between $\bar{\psi}(x)$ and $\psi(y)$, draw a directed full line from x to y and omit the ψ-symbols. The free factors ψ, $\bar{\psi}$, A, can be similarly disposed of by means of lines with a loose end, namely directed lines "into" the diagram (factor ψ), "from" the diagram (factor $\bar{\psi}$) or undirected dashed lines (factor A). For example (19) will be represented by the graph in which a directed line runs inwards to y, then from y to x, then from x to z, and thence outwards; a dashed line connects y and z.

At this stage, one will raise the question of *signs*. There are, indeed, signs involved in the values of the contractions, Eqs. (11a) and (11b), and in the δ_P-factors in Eq. (3), etc. One can, however, without memorizing any recipes, reduce such complications to a minimum, if one writes the $\bar{\psi}A\psi$-groups in a suitable order (this does not affect the over-all result). If an open polygon runs from point 1 to 2, to 3, $\cdots$, to m, one will write these points in the same order in the S-product, thus:

$$:\bar{\psi}\mathrm{A}\psi^{\cdots}(m)\cdots\cdots\cdots\cdots\bar{\psi}^{\cdots}\mathrm{A}\psi^{\cdot\cdot}(3)\bar{\psi}^{\cdot\cdot}\mathrm{A}\psi^{\cdot}(2)\bar{\psi}^{\cdot}\mathrm{A}\psi(1):.$$

All the contractions will then be between adjoining factors in the order of Eq. (11a) with no signs involved. If the points 1, $\cdots$, m, are in a closed loop, there will be a further contraction between $\bar{\psi}(m)$ and $\psi(1)$. One can carry over $\bar{\psi}(m)$ to the right of $\psi(1)$ by jumping an odd number of ψ or $\bar{\psi}$-factors. This will give a further factor: $-K(1, m)$ with one minus sign. In the end result there is a factor (-1) for each loop.[13] As regards the free factors ψ, $\bar{\psi}$ there will be, in the interesting cases, two, or at most, four of them. All questions of sign will be easily handled (after one has decided whether one wants to use the u or the $\bar{v}$ part of a ψ, the $\bar{u}$ or the v part of a $\bar{\psi}$) simply by using the easily remembered C-rules.

[13] This accounts for the $(-)^l$ factor in Dyson's formula (51) (reference 2). The $(-1)^n$ arises from a difference in sign between Dyson's S and our K kernel.

IV. LONGITUDINAL WAVES

In electrodynamics, longitudinal waves always require special considerations. In our case we must specify first that the destruction part a_μ is meant in the sense: part with an $e^{-i\omega t}$ $(\omega>0)$ dependence. As applied to a_4, this definition really implies *creation* of time-like photons; since these photons have negative energies, the term destruction is, nevertheless, quite proper. This is, at any rate, the convention leading to Eq. (11c).

The next and more important point is the following one. In Dyson's treatment, there is an ambiguity in the vacuum expectation value of $A_\mu(x)A_\nu(y)$ and one must show that this ambiguity is irrelevant. This has been done recently by Dyson.[14]

In our case, there is no ambiguity in the value of the contraction of $A_\mu(x)A_\nu(y)$, but the problem arises, of course, in another way. Consider, for example, a transition described by a graph involving a certain contraction between A_μ and A_ν. At first sight one can get a contribution to the *same* transition also from another term in the S-matrix, containing instead the S-product of A_μ and A_ν. This would not normally be the case but the complication arises out of the presence of an undetermined number of longitudinal and timelike photons both in the initial and final state. One has then to show that these extra terms are really zero. We have just learned, however, that this question is treated in detail in a forthcoming paper by Coester and Jauch[15] to which the reader may be referred.

[14] F. Dyson, Phys. Rev. 77, 421 (1950).

[15] This paper uses Houriet and Kind's method which is closely related to ours. I am indebted to Dr. K. M. Watson for showing me the manuscript in his possession. This paper has meanwhile appeared, Phys. Rev., 78, 149 (1950).

Ferromagnetism at Very High Frequencies. III. Two Mechanisms of Dispersion in a Ferrite

G. T. Rado, R. W. Wright, and W. H. Emerson
Naval Research Laboratory, Washington, D. C.
(Received May 22, 1950)

The magnetic spectrum of a ferrite is shown to contain two regions of pronounced dispersion. One occurs at radiofrequencies, resembles a resonance, and is proved to be due to domain wall displacements; the other occurs in the microwave range, exhibits typical resonance characteristics, and is attributed to domain rotations. The identification of the dispersion mechanisms is based primarily on a comparison of the complex permeability of solid samples with that of small particles of the same material. Several manifestations of single-domain behavior are reported, and a study of remanence by high frequency methods is presented. The wall effects are interpreted in terms of the concept of apparent wall inertia and it is shown that microscopic eddy currents cannot cause the damping. The rotational effects are interpreted on the basis of crystalline anisotropy. Previously used methods for identifying dispersion mechanisms are discussed.

I. INTRODUCTION

A NUMBER of experiments have shown that in several ferromagnetic oxides a pronounced dispersion of the permeability occurs at radio frequencies[1,2,*] or in the microwave range.[3,4] In all these experiments only *one* region of pronounced dispersion was observed in the magnetic spectrum of each substance studied, although the curve of Welch *et al.*[4] contains one experimental point below 300 Mc/sec. These dispersions were considered to be indicative of a broad resonance and were interpreted on the basis of the domain rotation theory originated by Landau and Lifshitz.[5] Their paper contains the fundamental idea that ferromagnetic anisotropy is equivalent to an internal magnetic field capable of producing a Larmor precession of the electron spins responsible for the spontaneous magnetization. Resonance absorption is to be expected, therefore, when the frequency of an applied alternating field equals the Larmor precession frequency.

While investigating the magnetic spectrum of several ferromagnetic ferrites we ascertained that in general there are *two* regions of pronounced magnetic dispersion at high frequencies. In "ferramic *A*,"[6] a substance which we have studied in some detail, one region occurs at radiofrequencies (~50 Mc/sec.) and resembles a broad resonance rather than a relaxation. The other region occurs in the microwave range (~2500 Mc/sec.) and has the appearance of a typical resonance. In the present paper the mechanisms responsible for the two dispersion regions are identified. This identification is based mainly on a comparison of the measured magnetic spectrum of ferramic *A* with that of very small particles of the same material. Additional evidence used in reaching our conclusions includes measurements of coercive force, the magnetic spectrum in the remanent state, as well as certain x-ray data and electron-microscopic observations.

Our experiments prove that in ferramic *A* the microwave resonance is caused by *domain rotations* (Larmor resonance) whereas the radiofrequency dispersion is primarily caused by *domain wall displacements*. These conclusions differ from the current view which is based on the observation of a single dispersion region and considers rotational processes solely responsible for the magnetic[7] losses in ferrites at frequencies above 1 Mc/sec. However, the existence of wall displacement effects at radiofrequencies is not unexpected. A theoretical treatment of such effects was given by Landau and Lifshitz[5] in the same article which contains the basic theory of domain rotations mentioned above. In paper II of the present series,[8] moreover, it was shown that in iron there are some experimental indications for wall displacements at 200 Mc/sec. even though the observed permeabilities are largely due to domain rotations, as first noted[9] in 1947.

Toward the end of this paper we shall discuss the methods used by other investigators in interpreting their experiments[10] on the magnetic dispersion in ferrites, and suggest possible reasons for the lack of evidence concerning wall displacements. In addition, we shall consider some predictions made by Döring[11] in his theoretical work on the apparent inertia of domain walls and show that our results provide some experimental confirmation for his ideas. It appears that

[1] J. L. Snoek, Physica **14**, 207 (1948); Nature **160**, 90 (1947).
[2] Brockman, Dowling, and Steneck, Phys. Rev. **77**, 85 (1950).
[*] In the present paper radiofrequencies are *not* understood to include microwave frequencies.
[3] J. B. Birks, Proc. Phys. Soc. London B **63**, 65 (1950). This paper contains references to Birks' earlier communications.
[4] Welch, Nicks, Fairweather, and Roberts, Phys. Rev. **77**, 403 (1950).
[5] L. Landau and E. Lifshitz, Physik. Zeits. Sowjetunion **8**, 153 (1935).
[6] Trade name for an iron-magnesium ferrite purchased from the General Ceramics and Steatite Corporation. A chemical analysis of the material used in our experiments gave the following composition: 45 percent Fe, 14 percent Mg, 3 percent Mn, 2 percent Ca, 1 percent Zn; the balance is presumably oxygen.
[7] We are not concerned with losses due to eddy currents and hysteresis.
[8] M. H. Johnson and G. T. Rado, Phys. Rev. **75**, 841 (1949).
[9] Johnson, Rado, and Maloof, Phys. Rev. **71**, 322 (1947).
[10] For a general discussion of ferromagnetic phenomena at microwave frequencies, see G. T. Rado, *Advances in Electronics* (Academic Press, Inc., New York, 1950), Vol. II, p. 251.
[11] W. Döring, Zeits. f. Naturforschung **3a**, 374 (1948).

TABLE I. Ferramic *A* at 1750 Mc/sec. All three sample dimensions are in inches. The dielectric constant, $\epsilon_1 - i\epsilon_2$, was measured at eight frequencies (fairly uniformly spaced) in the region of 50 to 10,000 Mc/sec. Throughout this frequency region ϵ_1 had a constant value of 8.5±10 percent; ϵ_2 was small throughout this region and did not exceed 0.7.

Outer diameter	Inner diameter	Thickness	μ_1	μ_2	ϵ_1
1.5	0.625	0.108	1.36	2.25	8.9
1.5	0.625	0.025	1.31	2.14	8.9
0.5	0.219	0.025	1.47	2.14	8.2
0.5	0.219	0.115	1.31	2.42	—

Döring's mechanism of resonance absorption by domain wall displacements is a possible explanation for our 50 Mc/sec. dispersion. We believe, however, that the high electrical resistivity (~10^9 ohm-cm) of our specimens excludes the possibility, proposed by Becker[12] and Döring, of attributing the fundamental damping processes to the action of microscopic eddy currents.

II. METHOD OF MEASUREMENT

At frequencies between 3.5 and 10,000 Mc/sec. we determined the complex permeability, $\mu = \mu_1 - i\mu_2$, and the complex dielectric constant, $\epsilon = \epsilon_1 - i\epsilon_2$, by means of coaxial line measurements. Since in ferramic *A* the skin effect is negligible, the elaborate method and technique[8, 9, 13] developed for the study of metals is not applicable in this case. Instead, we used a simple standing wave method which was developed by O. Halpern[14] and M. H. Johnson with particular reference to thin samples of magnetic insulators and dielectrics.

Our samples were toroids of rectangular cross section, and their radii were so chosen as to match those of the coaxial lines used. The permeabilities were determined by inserting a sufficiently thin sample into the line at a position adjacent to the shorted end, and measuring (1) the voltage standing wave ratio, ξ, and (2) the displacement, s, of the voltage minimum from its (previously observed) location in the shorted empty line. At the lowest frequencies the line had to be extended by means of coaxial cables. It may also be noted that ξ was obtained in the usual manner from a measurement of the width of the standing wave pattern near the voltage minimum. If the line losses are neglected it can be shown that

$$\mu_1 - 1 = s/L \qquad (1)$$

and

$$\mu_2 = 1/\xi k_0 L, \qquad (2)$$

where L is the thickness of the sample, $k_0 = 2\pi/\lambda_0$ is the propagation constant in the empty line, and λ_0 is the free-space wave-length. The dielectric constants were determined by placing the sample at a distance of $\lambda_0/4$ from the shorted end of the line, measuring ξ and s, and using Eqs. (1) and (2) with μ_1 replaced by ϵ_1, and μ_2 replaced by ϵ_2.

In order that these equations apply, the quantity $|\epsilon\mu|(k_0L)^2$ must be negligible compared to unity. This requirement was fairly well fulfilled by proper choice of the sample thicknesses used at the various frequencies. These thicknesses varied from 0.025 to 0.440 inch as the frequency was decreased. To make sure that no serious errors arose we checked our measurements on two (or more) suitable values of L at most frequencies. The resulting permeabilities agreed within the experimental error (±5 percent except for low frequency values of μ_2) and were averaged before being plotted on the final graphs. We also proved that the measured permeabilities are relatively independent of the radial dimensions of the samples. For this purpose we used two coaxial lines characterized by different radii. Table I contains data taken at 1750 Mc/sec. and shows, by means of an example, that our results are independent of all three sample dimensions. Similar comparisons were made at 50 and 3000 Mc/sec. and yielded equally satisfactory results. These experimental precautions are emphasized because they show that our data refer to *intrinsic* properties of the samples rather than to spurious effects. This point is particularly important since Brockman, Dowling, and Steneck[2] have called attention to the effect of "dimensional resonance" on the dispersion in ferrites.

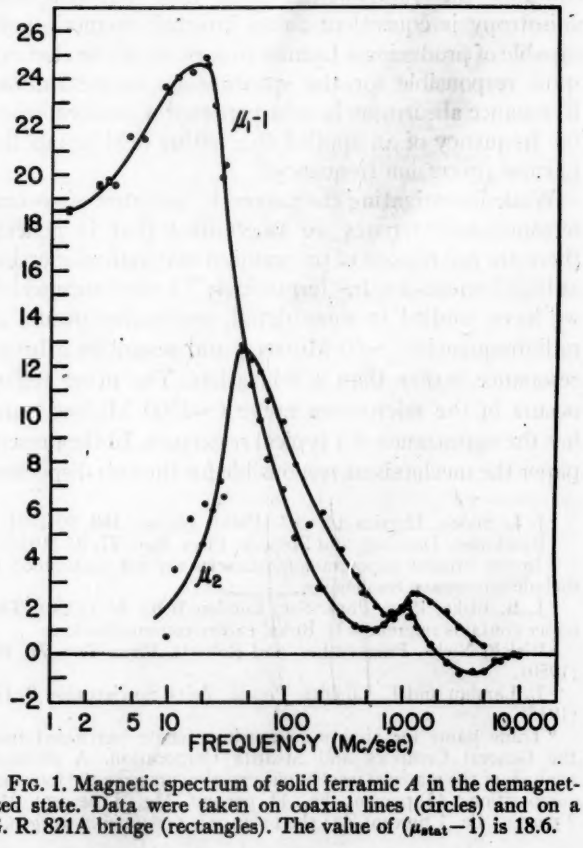

FIG. 1. Magnetic spectrum of solid ferramic *A* in the demagnetized state. Data were taken on coaxial lines (circles) and on a G. R. 821A bridge (rectangles). The value of $(\mu_{stat} - 1)$ is 18.6.

[12] R. Becker, Physik. Zeits. 39, 856 (1938); Ann. d. Physik (5) 36, 340 (1939).
[13] Rado, Johnson, and Maloof, Rev. Sci. Inst. 20, 927 (1949).
[14] O. Halpern, M.I.T. Radiation Laboratory Report VII-14S (1942), and unpublished work by M. H. Johnson.

The magnitude of the alternating magnetic field might also be expected to cause uncertainties in the results. However, the coaxial line measurements did not show any field dependence of the permeabilities, so that only *reversible* effects were detected. As an example, we cite measurements at 50 Mc/sec. where both μ_1 and μ_2 were constant within ± 3 percent for a field variation of 50 decibels.

At frequencies between 0.5 and 3.0 Mc/sec. we determined μ_1 by means of inductance measurements with a General Radio "twin-T impedance-measuring circuit, Type 821A." The samples were toroids of rectangular cross section and were wound with a convenient number of turns of insulated wire arranged in a single layer. Similar coils with a polystyrene core made it possible to check the inductance measurements. Since μ_2 appeared to be small we did not attempt to determine it accurately by measuring the high frequency resistance of the coils and separating out the eddy current effects due to the windings. It will be seen in the next section that in the frequency range of interest all of the results are based on coaxial line data; the inductance measurements merely served to extend the results to lower frequencies.

Similar inductance measurements on a Maxwell bridge were used to determine μ_1 at frequencies between 1 and 25 kc. The static reversible permeability, μ_{stat}, was obtained by a slight extrapolation (≈ 1 percent) of the μ_1 values to zero frequency and zero alternating field. This correction is not significant since it is about equal to the difference between the μ_1 values measured on different samples.

III. RESULTS AND INTERPRETATION

A. The Magnetic Spectrum

Figure 1 shows the complex permeability of ferramic *A* as a function of frequency. The measurements refer to the demagnetized state and cover the complete magnetic spectrum of this material. Up to a frequency of about 1 Mc/sec. the permeability is approximately constant and practically equal to the static value, μ_{stat}. At higher frequencies μ_2 reaches a conspicuous maximum in a region (≈ 50 Mc/sec.) where μ_1 decreases abruptly. It is interesting that μ_1 also passes through a maximum and becomes, in fact, larger than μ_{stat}. This indicates that the r-f dispersion is probably a resonance rather than a relaxation. However, the value of $(\mu_1 - 1)$ does not become negative at the minimum between the two dispersions. We cannot account for this fact by a simple superposition of two resonance curves; or by a magnetic interaction of the two mechanisms. At microwave frequencies the situation is again straightforward. Both μ_2 and $(\mu_1 - 1)$ exhibit a typical resonance behavior (including negative values of $(\mu_1 - 1)$) before approaching, in the vicinity of 10,000 Mc/sec., the value zero.

It is pertinent to inquire into the mechanisms responsible for the two observed dispersion regions. On the basis of the theoretical considerations presented in the following section we believe that the microwave dispersion is due to the now well-known mechanism of domain rotation resonance in the anisotropy field of the material. The r-f dispersion, on the other hand, may arise from domain wall displacements, or less likely, from domain rotations in those parts of the material where the anisotropy is conceivably very low. We shall now describe the experiments which proved the first alternative to be correct.

B. Identification of the Dispersion Mechanisms

In references 8 and 9 it was shown that the use of a static magnetic field parallel to the r-f field provides a possible method for distinguishing between the (relatively field-dependent) wall displacements and the (relatively field-independent) domain rotations in iron. Unfortunately, this method cannot be applied to ferramic *A* because the r-f dispersion could, in principle, be interpreted as a rotational resonance due to an internal field of about 16 oersteds, corresponding to a Larmor frequency of about 45 Mc/sec. But this field is comparable to the coercive field of the material (≈ 3 oersteds) so that rotations and wall displacements should be about equally field-dependent in the frequency range considered here.

We performed what appears to be a conclusive identification by using the results of the following alternative experiment. Ferramic *A* (which is a ceramic) was ground up in a ball mill and the relatively large particles were separated from the powder and discarded. The small particles were mixed with paraffin and molded to produce toroidal samples suitable for the coaxial lines and impedance measuring circuits described above.

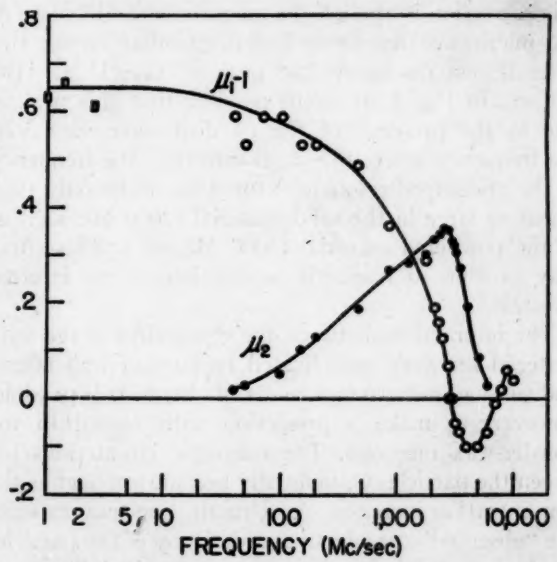

FIG. 2. Magnetic spectrum of 70 percent (by weight) mixture of ferramic *A* powder and wax. Data were taken on coaxial lines (circles) and on a G. R. 821A bridge (rectangles). The value of $(\mu_{stat} - 1)$ is 0.65.

Several solidified samples were then used in measuring the magnetic spectrum of a particular mixture containing 70 percent ferramic *A* by weight (36 percent by volume).

The results, plotted in Fig. 2 show that *the r-f dispersion is now absent whereas the microwave resonance is still present.* Similar results were obtained with a mixture of somewhat higher concentration (80 percent by weight). These facts clearly indicate that the r-f dispersion, unlike the microwave resonance, cannot be due to ferromagnetic anisotropy or any other fundamental property of the magnetic substance. Consequently the r-f dispersion cannot arise from domain rotations and must be attributed to wall displacements. It should be emphasized that the material used in the powder-wax mixture (Fig. 2) was obtained from the solid material (Fig. 1) without using a heat treatment or changing the chemical composition. The only factors capable of causing differences between the two sets of samples are particle size and shape, magnetic interactions, internal stresses, and possibly small impurities. Our argument is not concerned with these factors because it does not depend on the reason for the absence of the r-f dispersion in the powdered material; the only essential point is the *fact* of this absence *combined with* the presence of the relatively unmodified microwave resonance. It is nevertheless interesting to examine the factors mentioned above, and to consider their effects on the two dispersion mechanisms.

C. Factors that Influence the Dispersions

We shall discuss the *microwave resonance* first. In comparing this resonance in the cases of Figs. 1 and 2 it is necessary to take into account the change in volume concentration from 100 to 36 percent. After this correction is applied the magnitude (and width) of the microwave resonance is quite similar in the two cases if one disregards the peak of (μ_1-1) at 1100 Mc/sec. in Fig. 1; it seems possible that this peak is due to the presence of the r-f dispersion. However, the frequency where (μ_1-1) is zero (i.e., the frequency of the undamped resonance) turns out to be only two-thirds as large in the solid material (2000 Mc/sec.) as in the powdered material (3000 Mc/sec.). This effect may be due to magnetic interactions or to internal stresses.

The interactions between the crystallites of the solid material are very complicated because of wall effects and we shall not attempt to discuss them. It is possible, however, to make a prediction with regard to the powder-wax mixtures. The magnetic interactions between the particles undoubtedly become stronger as the concentration increases. As a result, one may expect[15] the "observed" (or effective) anisotropy of the particles to decrease with increasing concentration. The true crystalline anisotropy should correspond to the limiting case where the particles (assumed to be single crystals as well as single domains) are infinitely separated. Since the resonance frequency is proportional to the effective anisotropy, this explanation is in qualitative agreement with the following observations. We found that in ferrite-wax mixtures containing various concentrations of particles (whose internal stress was presumably constant) the microwave resonance frequency decreases with increasing concentration. This situation is similar to the known dependence[15,16] of the coercive force on the concentration of single-domain particles embedded in a non-magnetic matrix.

The role of the internal stresses is difficult to assess. The stresses in the solid material are small because the observed x-ray diffraction lines are sharp; the stresses in the particles, on the other hand, could not be estimated because the diffuseness of the observed lines is largely due to the smallness of the particle size mentioned below.

It remains to discuss the *r-f dispersion.* The most probable explanation for the absence of domain wall effects in the powdered material is that most of the particles are sufficiently small to be *single domains.* Electron-microscopic observations showed that the large majority of the particles is smaller than 0.4 micron in diameter. This value is to be compared with the approximate theoretical estimate of 0.4 micron for the critical diameter characterizing single domain behavior in ferramic *A*. Our estimate is based on Eq. (6.1.10) of Kittel's[15] review because the critical diameter exceeds the wall thickness [to be calculated in Section IVB] in this material. We used the following constants: saturation magnetization ($M_s=99$); Curie temperature ($T_c\approx 550°$K); spacing between the magnetic ions ($a\sim 4\times 10^{-8}$ cm); anisotropy constant ($K\sim 4\times 10^4$ ergs/cm^3). The wall energy per unit area was obtained from the approximate expression $(KkT_c/a)^{\frac{1}{2}}$, where k is Boltzmann's constant.

These considerations indicate that the particles are likely to be single domains. To obtain further evidence we determined the coercive force of the 70 percent ferramic *A*-wax mixture. The measured value ($H_c\approx 50$ oersteds) is considerably larger than that of the solid material ($H_c\approx 3$ oersteds) but decidedly smaller than the value ($\sim K/M_s$) expected on the basis of single-domain behavior. However, it is known[15,16] that the coercive force of a matrix containing single-domain particles does decrease rapidly with concentration, and it is also known[15] that complicated effects occur if single-domain behavior is not quite reached. Additional evidence consistent with the single-domain interpretation is provided by the fact that the static permeability of the 70 percent mixture changes but little (<1 percent) with the applied field even if the latter is as large as 30 oersteds. Since a very small amount of hysteresis was detected, however, some of the particles

[15] C. Kittel, Rev. Mod. Phys. 21, 541 (1949).

[16] L. Weil, Comptes Rendus (Paris) 225, 229 (1947).

may have transition properties between single-domain and ordinary behavior. It was also found that the static reversible permeability of the 70 percent mixture was the same at remanence as in the demagnetized state.

We can summarize the situation by stating that all of the evidence presented here favors the single-domain interpretation. It is nevertheless conceivable that the observed effects are due to internal stresses in the small particles; but this possibility is unlikely since ferramic *A* is rather brittle. A decisive experiment capable of demonstrating single-domain behavior in *some* substances has recently been reported by Kittel, Galt, and Campbell,[17] who have used nickel particles. However, their method is not applicable to ferramic *A* because in this substance the quantity K/M_s is not smaller than, but is comparable to, $4\pi M_s/3$. In view of this uncertainty we feel justified in mentioning again that our identification of the r-f dispersion as a domain wall effect does not depend on the single-domain interpretation or on any other detailed theoretical model.

D. Study of Remanence

Numerous ferromagnetic substances, possessing a sufficiently high anisotropy and reasonably small internal stresses, are known to have the interesting property that the remanence, M_r, of a *polycrystal* is roughly equal to half the saturation magnetization, M_s. The standard explanation[18] of this experimental fact may be formulated as follows. In a demagnetized polycrystal the magnetization vector of each domain is nearly parallel to one of the easy directions of magnetization determined by the crystalline anisotropy. Since in an isotropic polycrystal the axes of the crystallites are oriented at random, it follows that the magnetization vectors can point in all possible directions of the solid angle 4π. Consequently the net magnetization of the polycrystal vanishes. It may be noted that on account of internal demagnetizing fields and internal stresses the foregoing statement does not imply a truly random orientation of the magnetization vectors. The application of a sufficiently strong magnetic field causes the magnetization vectors to line up with the field and results in "technical saturation" of the polycrystal. Upon removal of the field the polycrystal assumes the state of remanence. This state must correspond to a minimum in the energy and is reached as a result of domain rotations and wall displacements. The distribution of the vectors is assumed to extend throughout that solid angle of 2π which includes the direction of the previously applied field and is located symmetrically with respect to it. To specify this distribution more accurately it is useful to introduce the angle θ between the field and an arbitrary magnetization vector. In terms of this angle the above assumption means that *each value of θ larger than $\pi/2$ occurring in the demagnetized state is replaced by $(\pi-\theta)$ at remanence.* An elementary calculation can now be used to show that the above assumption leads to $M_r=0.5M_s$.

It should be pointed out that the remanence problem in "normal" materials (defined by $M_r\approx 0.5M_s$) is not necessarily as straightforward as this simple theoretical model indicates. In view of the existence of internal demagnetizing fields (which were used by Bozorth[19] to discuss materials where $M_r \ll 0.5M_s$) it is clear that even in normal materials the reduction of the field from saturation toward remanence could, in principle, cause 180° wall displacements and thus lead to $M_r < 0.5M_s$. Wall displacements of this type are not considered in the simple theory because internal demagnetizing fields are neglected so that, even in the presence of stresses, the directions θ and $(\pi-\theta)$ are

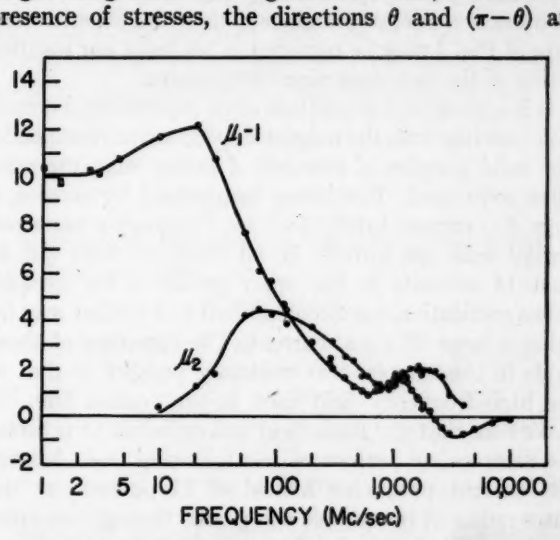

FIG. 3. Magnetic spectrum of solid ferramic *A* in a remanent state. Data were taken on coaxial lines (circles) and on a G. R. 821A bridge (rectangles). The value of $(\mu_{stat}-1)$ is 10.9.

energetically equivalent; consequently θ never exceeds $\pi/2$ as the field is decreased from saturation ($\theta=0$) toward remanence. The fact that the relation $M_r=0.5M_s$ is so closely fulfilled in many materials shows that the assumption used in the simple theory represents a good approximation. It is therefore interesting to discuss the following investigations which demonstrate by an independent experiment the remarkable applicability of the model described above.

The simple theory leads to the two following predictions for the (reversible) complex permeability. (1) If μ is *solely* due to domain rotations then the value of μ at remanence should be equal to that in the demagnetized state; this statement is based essentially on the equality of $\sin^2\theta$ and $\sin^2(\pi-\theta)$. (2) If μ is *primarily* due to wall displacements then the value of μ at remanence should be substantially smaller than that in the demagnetized state; this statement is based on the (deduced) presence of fewer types of "non-180°-walls" at remanence than in the demagnetized state. These

[17] Kittel, Galt, and Campbell, Phys. Rev. **77**, 725 (1950).

[18] R. Becker and W. Döring, *Ferromagnetismus* (Verlag. Julius Springer, Berlin, 1939), see pp. 111, 120, 160.

[19] R. M. Bozorth, Zeits. f. Physik **124**, 519 (1948).

predictions may be tested on ferramic *A* because in this material $M_r/M_s \approx 0.6$ and is thus reasonably close to the ideal value of 0.5. We now know, moreover, that the microwave resonance is due to domain rotations whereas the r-f dispersion is primarily due to wall displacements. Consequently the complex μ at microwave frequencies should be the same at remanence as in the demagnetized state. Throughout the r-f region, on the other hand, μ should be substantially smaller at remanence than in the demagnetized state.

A comparison of the experimental results given in Fig. 1 (demagnetized state) and Fig. 3 (remanence) shows that the theoretical predictions are confirmed in a satisfactory manner. If we now reverse the procedure mentioned above by *assuming* the correctness of the theoretical model of remanence, then the experimental data of Fig. 3 may be regarded as *verifying* our identification of the two dispersion mechanisms.

It is appropriate to mention some experimental details in connection with the magnetic spectrum at remanence. The solid samples of ferramic *A* rather than the mixtures were used. They were magnetized by passing a large d.c. current briefly (~5 sec.) through a brass rod coaxial with the toroids. In all cases the field was at least 14 oersteds at the outer radius of the sample. Demagnetization was accomplished in a similar way by using a large 60 c.p.s. current. The direction of these fields in the samples was evidently parallel to that of the high frequency field used in the coaxial line. To make sure that the static field was sufficient to saturate the samples we performed the following test. A large d.c. current producing a field of 11 oersteds at the outer radius of the sample was passed through the inner conductor of the coaxial line (using proper precautions to avoid shunting) and μ_1 was measured while the current was on. At the frequency used for this test (15 Mc/sec.) we obtained $\mu_1 = 1$ so that the field was indeed sufficient to produce true remanence.

IV. COMPARISON WITH THEORY

A. Domain Rotations

In all previously published experiments the single observed dispersion was interpreted by means of relations derived from the domain rotation theory of Landau and Lifshitz.[5] Their fundamental result for the resonance frequency, ν_0', is contained in the equation[20]

$$\nu_0' = (\gamma/2\pi)H_i, \tag{3}$$

where H_i is the effective internal field due to anisotropy and γ denotes the magneto-mechanical ratio. The numerical value of $\gamma/2\pi(=ge/4\pi mc)$ is 2.80 Mc/sec. oersted for a free electron spin ($g=2$); here g is the Landé splitting factor and e/mc is the specific electronic charge. Landau and Lifshitz were concerned with the special case of a uniaxial crystal exposed to an alternating field applied normal to the preferred axis. When expressed in current notation, their resonance condition (Eq. (41) of their paper) is

$$\nu_0' = (\gamma/2\pi)(2K/M_s), \tag{4}$$

where the symbols have the same meaning as elsewhere in this paper.

Snoek[1] applied Eq. (3) to a polycrystal containing randomly oriented crystallites and obtained

$$\nu_0' = (\gamma/2\pi)(M_s/\chi_0')(2/3), \tag{5}$$

where χ_0' is the static initial susceptibility *for rotations*. He found that Eq. (5) (with the measured χ_0 instead of χ_0') agrees within a factor of about two with a resonance frequency observed in the r-f region, and gave several possible reasons (neglect of internal stresses, damping, and magnetic interactions) for the residual discrepancy. However, Snoek simply *assumed* the absence of wall displacements and did not justify using the measured χ_0 in place of χ_0' in Eq. (5). It is therefore conceivable that the resonance discovered by Snoek is due to wall displacements rather than to rotations. Similar remarks apply to the interpretation of the results of Brockman *et al.*[2] who found a resonance at about 4 Mc/sec. after correcting their data for dimensional effects.

To illustrate the above statements we consider an example taken from our measurements. For ferramic *A* the measured values of M_s and χ_0 are 99 and $18.6/4\pi$, respectively; thus Eq. (5) yields a resonance frequency of 124 Mc/sec. *if* χ_0, rather than χ_0', is used. It is interesting that a resonance frequency of this order of magnitude (≈45 Mc/sec.) was actually observed (Fig. 1); but this approximate agreement is obviously a coincidence since the 45 Mc/sec. dispersion is definitely due to wall displacements rather than to rotations (Section IIIB). If we had not made microwave measurements, therefore, we might have concluded incorrectly that the 45 Mc/sec. resonance is due to rotations.

The microwave resonance (~1300 Mc/sec.), on the other hand, might be interpreted with Eq. (5) (as written) but this procedure would be of questionable value because χ_0' is not known. The measured χ_0 contains a contribution χ_0'' due to the wall effects (so that $\chi_0 = \chi_0' + \chi_0''$) and there is no unique way of separating χ_0' from χ_0 on the basis of Fig. 1 alone. It is possible, however, to use Eq. (5) in connection with the data of Fig. 2. Here the measured static initial susceptibility ($=0.65/4\pi$) of the mixture is solely due to rotations. Assuming for this purpose, that χ_0' is inversely proportional to the volume concentration (36 percent), $\chi_0' = 0.14$ is obtained. The resonance frequency ν_0' calculated this way is 1300 Mc/sec. and should be compared with the value 2500 Mc/sec. measured at the peak of μ_2 in Fig. 2. It seems probable that this discrepancy is due to the factors mentioned but neglected by Snoek in deriving Eq. (5).

The interpretation of the resonance shown in Fig. 2

[20] We adopt the convention of denoting quantities characteristic of domain rotations by a single prime (′) and quantities characteristic of domain wall displacements by a double prime (″).

may be based on Eq. (4) as well. This equation should apply to cubic crystals just as accurately as to uniaxial ones because the anisotropy energy density is the same ($=K\phi^2$) in both cases, provided the displacement, ϕ, of a domain magnetization vector from an easy direction is small. On this basis we obtain $K=4.4\times10^4$ ergs/cm^3 from the resonance at 2500 Mc/sec. This value represents an "effective" anisotropy constant (as mentioned in Section III) because demagnetizing effects have not been considered. The true anisotropy constant may differ from the above value by a factor of perhaps 2 or 3 but for our present purposes (Sections IIIC and IVB) only the order of magnitude of K is needed; the sign of K is not determined. (If K is negative, $H_i=-4K/3M_s$.)

It should be mentioned that Birks[3] reported a microwave resonance in several ferrite-wax mixtures. He attributed the effect to domain rotations because the measured permeabilities were relatively insensitive to a static magnetic field applied at an arbitrary angle with respect to the alternating field. In interpreting his data he used the relations of Landau and Lifshitz [Eq. (4)] and Snoek [Eq. (5)]. Birks' results represent the properties of a hypothetical substance obtained by extrapolating measurements performed on ferrite-wax mixtures. The r-f dispersion which we observed in the solid samples (Fig. 1), and proved to be due to wall effects, does not involve any extrapolation. We did not observe this dispersion even in our 80 percent mixture which represents a volume concentration of 49 percent and exceeds the highest concentration used by Birks.

B. Domain Wall Displacements

The first theoretical treatment of domain wall displacements at high frequencies was given by Landau and Lifshitz.[5] These authors attribute the damping of the wall motion to a certain interaction between the spins. They refer to this interaction as "relativistic interaction" and describe it by a phenomenological constant which is denoted[21] by η and has the same dimensions as M_s. Their treatment explicitly omits any consideration of hysteresis effects and results in a purely imaginary susceptibility which varies inversely with the frequency.

A somewhat different theory was proposed by Döring.[11] He shows that the motion of a domain wall requires, in general, the existence of an internal demagnetizing field. This field modifies the spin distribution and causes the energy of a moving wall to exceed that of the same wall at rest by a term proportional to the square of the wall velocity. The proportionality constant is interpreted by Döring as an apparent mass (or inertia) characterizing the moving wall. Since Döring (unlike Landau and Lifshitz) does take into account the restoring force acting on a wall, the apparent mass leads him to predict that resonance phenomena will occur when any given type of wall is exposed to an alternating field of the correct frequency.

Neither of these theories has yet been compared quantitatively with the experimental data[1–4] cited although Döring has tentatively suggested that Birks' results may be due to wall displacements as well as to rotations. Some of our experimental results, however, may be used for such a comparison because the r-f dispersion in ferramic A was shown to be primarily a wall effect. In the following presentation we shall follow Döring's theory but treat the damping according to the mechanism of Landau and Lifshitz.

The displacement, x, of an "average" domain wall is given by the equation of motion

$$m(d^2x/dt^2)+\beta(dx/dt)+\alpha x=M_sH, \tag{6}$$

where m is the apparent mass per unit wall area and $H=H_0\exp(i\omega t)$ is the applied field; the constants α and β will be discussed below. Using the abbreviations

$$\omega_0''=(\alpha/m)^{\frac{1}{2}} \tag{7}$$

and

$$\omega_c''=\alpha/\beta, \tag{8}$$

as well as the definition of the susceptibility due to wall displacements

$$\chi''=xM_s/Hd, \tag{9}$$

one obtains from Eq. (6)

$$\chi''=\frac{\chi_0''}{1-(\omega/\omega_0'')^2+i(\omega/\omega_c'')}, \tag{10}$$

where

$$\chi_0''=M_s^2/\alpha d \tag{11}$$

is the static susceptibility and d denotes the average domain size. (We omitted a factor whose magnitude is between one and two on the right-hand side of Eqs. (6) and (9) because its value depends on the type of wall under consideration.) Eq. (10) is a standard form of a resonance and differs from Döring's formulation only in that the solution of Eq. (6) is expressed in terms of χ'' rather than x.

We consider the resonance frequency first. The "stiffness constant," α, measures the restoring force and is given by Eq. (11) in terms of χ_0''. The apparent mass, m, was calculated by Döring and represents the fundamental contribution of his theory. Neglecting a factor of the order of unity, we may write his result[22] for 90° walls in the simple form‡

$$m=1/8\pi\gamma^2\delta, \tag{12}$$

where δ is the wall thickness parameter and is given by $\delta\sim(kT_c/Ka)^{\frac{1}{2}}$; γ denotes the magneto-mechanical ratio, as before. Combining Eqs. (7), (11) and (12), we obtain

$$\nu_0''=(\gamma/2\pi)(M_s/\chi_0'')(8\pi\chi_0''R)^{\frac{1}{2}}, \tag{13}$$

[21] Landau and Lifshitz use the symbol λ instead of η.

[22] Döring's theory contains an expansion retaining terms to the order of $(K/2\pi M_s^2)^2$. In our case this square is about 0.4.

‡ This factor equals unity if the wall normal is perpendicular to the spin directions of the adjacent domains.

where $\nu_0''=\omega_0''/2\pi$ is the resonance frequency due to wall displacements and R is a dimensionless ratio defined by

$$R=\delta/d. \tag{14}$$

Equation (13) was written to resemble Eq. (5) in all but the last factor. It is interesting to note that these two equations are based on completely different mechanisms and may nevertheless predict the same resonance frequency if R and the static permeability are of the order of unity; this possibility is particularly likely to arise if the measured static susceptibility, rather than χ_0', is used in Eq. (5). To compare Eq. (13) with our results we use $\chi_0=1.48$ (see Fig. 1) because the contribution of the rotations (i.e., χ_0') is only about 0.14 as estimated on the basis of Fig. 2 and the known volume concentration of 36 percent. We obtain $R=1.5\times10^{-3}$ if we take $\nu_0''=45$ Mc/sec. (i.e., the peak of μ_2) as the experimental resonance frequency. This is a rather arbitrary choice since ν_0'' should be the frequency where $(\mu_1-1)=0$; but we shall not attach any significance to factors of about 2 in our estimated domain size. The value of δ for ferramic A is about 7×10^{-6} cm. Thus Eq. (14) leads to $d=5\times10^{-3}$ cm; this appears to be of the right order of magnitude because x-ray data indicate that the crystallite size in solid ferramic A is between 5×10^{-3} and 5×10^{-4} cm.

Döring did not consider the damping due to spin-spin interaction but used Becker's[12] theory of microscopic eddy currents to obtain a value for ω_c''. This mechanism does not give any appreciable damping for ferramic A because in this substance the resistivity ($\rho\sim10^9$ ohm cm) is about 10^{15} times higher than in iron. For this reason we derive ω_c'' from the Landau-Lifshitz theory. It should be noted, however, that this is merely a formal step since the damping might influence the mass calculated by Döring; in addition, the damping (i.e., η) was introduced phenomenologically as mentioned above. Landau and Lifshitz have shown (their Eq. (29)) that

$$dx/dt=(\gamma M_s\delta/\eta)H. \tag{15}$$

Comparison of this result with Eq. (6) yields $\beta=\eta/\gamma\delta$, so that we obtain from Eqs. (8), (11) and (14)

$$\nu_c''=(\gamma/2\pi)(M_s/\chi_0'')(M_sR/\eta) \tag{16}$$

where $\nu_c''=\omega_c''/2\pi$ is the critical damping frequency. From Eq. (6) it follows that the oscillation is less than critically damped if $\omega_0''<2\omega_c''$; using Eqs. (13) and (16), this condition may be written

$$\eta/M_s<(R/2\pi\chi_0'')^{\frac{1}{2}}. \tag{17}$$

We are now in a position to set an upper limit on the unknown constant η by using the relation (17) as an equality and substituting the value $R=1.5\times10^{-3}$ derived from our r-f experiments which show a resonance effect due to walls. The resulting η/M_s is 1.3×10^{-2} and may be considered satisfactory in that the Landau-Lifshitz theory assumes $\eta\ll M_s$. There are, however, two difficulties. (1) As pointed out by Döring, the width of the absorption "line" due to the wall resonance is partly due to the *distribution* of α-values in an actual material. Consequently the value of η derived above not only describes the basic interactions between the spins but includes all other effects that broaden the line. (2) If we *arbitrarily* attach a fundamental significance to an experimentally determined η, as is sometimes done, we find that the Landau-Lifshitz theory of spin *rotations* (their Eq. (40)) predicts a much sharper microwave line (on the basis of $\eta/M_s=1.3\times10^{-2}$) than the one we observed. It therefore appears that the width of the microwave resonance is due even more to experimental effects (inhomogeneities, particle shape, stresses, etc.) than is the r-f resonance. These considerations indicate that the theories[23] available at present do not explain the line widths observed in our experiments on natural ferromagnetic resonance. The resonance frequencies, on the other hand, can be accounted for on the basis of these theories.

We wish to thank Messrs. F. J. Woodsmall, A. Terris, M. Maloof, and H. Rosenblatt for help with the experiments.

[23] C. Kittel, Phys. Rev. 79, 214 (1950), suggested independently that the dispersion in ferrites be interpreted in terms of domain rotations and wall displacements. He proposed using Landau and Lifshitz' equation (our Eq. (4)) for rotations and a relaxation frequency (similar to our Eq. (16)) for wall displacements, and showed this to be in qualitative accord with the data of Welch *et al.* (reference 4). It should be noted, however, that these data include only one point (100 Mc/sec.) below 300 Mc/sec. As mentioned by one of us during the discussion period for Kittel's talk, our experiments show a wall resonance and had been found to be consistent with Döring's theory (reference 11) of apparent wall inertia.

Letters to the Editor

PUBLICATION of brief reports of important discoveries in physics may be secured by addressing them to this department. The closing date for this department is five weeks prior to the date of issue. No proof will be sent to the authors. The Board of Editors does not hold itself responsible for the opinions expressed by the correspondents. Communications should not exceed 600 words in length.

The Soft X-Ray Valence Band Spectra and the Heat of Formation of Chemical Compounds and Alloys

K. DAS GUPTA
Department of Physics, University College of Science, Calcutta, India
March 31, 1950

THE soft x-ray K-valence emission spectra of Mg, Al, and Si in the pure metallic state, as well as in their oxides, of silicon in SiC and L_{III}-valence emission spectra of Fe in the alloy $AlFe_3$ have been investigated with bent gypsum and mica crystals in a vacuum spectrograph. The shift of K_β- or K-valence emission band of the constituent elements A and B of the compound or alloy A_mB_n toward the longer or shorter wave-length side with respect to the respective pure elements have been qualitatively, as well as semiquantitatively correlated with the heat of formation of the corresponding compound or alloy. The large values of the heat of formation for most of the compounds and the negligibly small values for the alloys and the homopolar compound like SiC, etc., cannot be explained from the consideration of the changes in the values of the specific heats of the constituent elements when forming a compound or alloy.

In the equation:

$$m\cdot V_A\cdot\Delta E_A \pm n\cdot V_B\cdot\Delta E_B = Q/23.02,$$
$$\leftarrow Q_A \rightarrow \quad \leftarrow Q_B \rightarrow$$

where V_A and V_B are the numbers of electrons in the outermost level of the elements A and B, respectively, involved in emission of the valence band spectra, e.g. 2 for Mg, 3 for Al, 4 for Si, 6 for oxygen, 8 for Fe, etc.; ΔE_A and ΔE_B are the shifts in electron volts of the valence band peak of elements A and B in the compound A_mB_n with respect to the respective pure elements A and B; Q is the heat of formation of the compound or alloy expressed in kilocalories per gram-formula weight and 23.02 is the conversion factor.

If in the equation ΔE_A and ΔE_B are individually zero or negligible, $Q=0$, or is negligibly small. If ΔE_A and ΔE_B are oppositely directed, the value of Q may be large or small or even negative (endothermic) according to the relative values of ΔE_A and ΔE_B. The data are given in Table I.

TABLE I. Soft x-ray valence band shifts and the heat of formation of the compounds and alloys.

Specimens A_mB_n	ΔE_A (ev)	Q_A (kcal.)	ΔE_B (ev)	Q_B (kcal.)	$Q_{A_mB_n}$	$Q_{A_mB_n}$ (thermochemical data)
MgO	4.5	207	0.52	72	135	145
Al_2O_3	4.48	618	0.52	215	403	400
SiO_2	3.9	359	0.52	144	215	200
MgS	(expected 5)	237	1.12	155	...	82
$AlFe_3$	2.0	138	0.24	132	6	(of the order of 10)
SiC	(no shift for Si)	0	(no shift for C)	0	0	(of the order of 1)

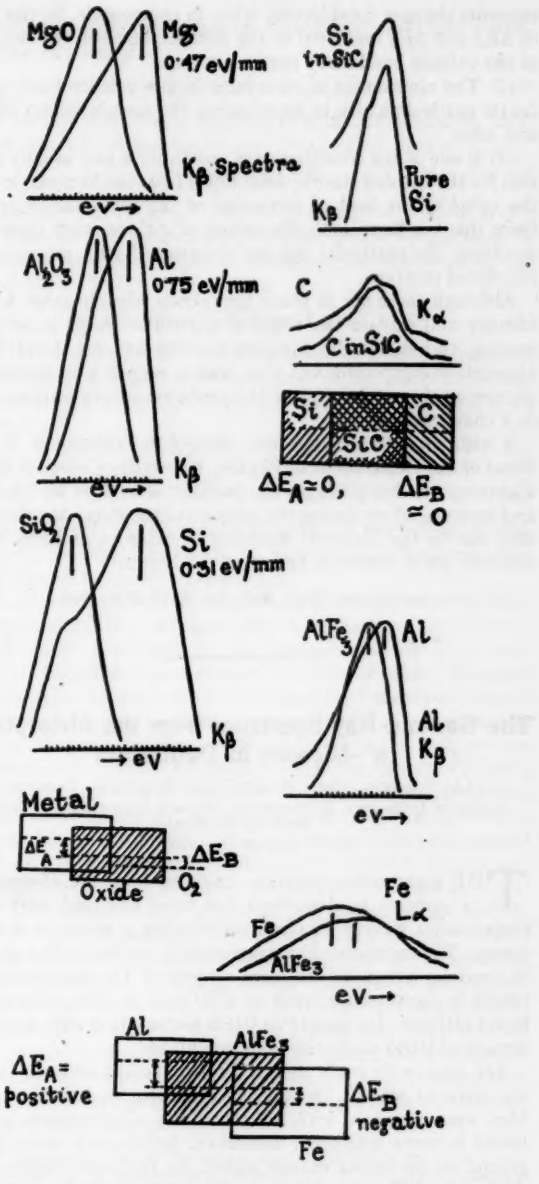

FIG. 1. Tracings of the original microphotometer records of the valence band spectra of elements in pure solid state, in compounds and in alloys.

The constant value of the shift 0.52 ev in the case of oxygen for which V_B is taken to be six is justified from the appearance in the same position of the peak of oxygen K_α-band for all these oxides taken by O'Bryan and Skinner.[1] For a shift towards the longer wave-length ΔE is positive, which is to be connected with the heat of evolution, and for a shift towards the shorter wave-length ΔE is to be counted as negative, which is to be connected with the heat of absorption.

The equation, although inadequate to give an exact value of the heat of formation, has been tested for a large number of compounds and alloys and found to indicate correctly the direction of the shift of valence band spectra of the constituent elements with respect to the spectra for the pure elements. Approximate calculation shows that the contribution of the specific heat factor is very small.

The uncertainties in the application of the equation are due to the following factors:

(1) The intensity distribution of the valence band spectra of the

elements changes considerably when in compounds. So the values of ΔE_A and ΔE_B measured as the distance between the two peaks of the valence bands may not be accurate.

(2) The appearance of structures in the valence band spectra create much difficulty in ascertaining the correct values for ΔE_A and ΔE_B.

(3) If one of the constituents is ordinarily a gas, usually a position for the gaseous state is determined from the formula, knowing the value of the heat of formation of the particular compound. Once this has been done, the values of ΔE for other compounds involving the particular gas are determined with respect to the calculated position.

Although there are so many limitations, the equation helps to identify and explain the origin of particular bands in soft x-ray spectra, to indicate the direction and the amount of shift for the elements in compounds and alloy, and to suggest a straightforward picture as the mechanism of the evolution or absorption of heat in a chemical reaction.

I wish to express my sincere thanks to Professor S. N. Bose, Head of the Department of Physics, University College of Science, Calcutta, who has given me the facilities of work in his laboratory and encouraged me during the progress of the work. My thanks are also due to the National Institute of Sciences of India for appointing me a Research Fellow of the Institute.

[1] O'Bryan and Skinner, Proc. Roy. Soc. **A176**, 229 (1940).

The Gamma-Ray Spectrum from the Absorption of π^--Mesons in Deuterium*

LEE AAMODT, JAMES HADLEY, AND WOLFGANG PANOFSKY
Radiation Laboratory, Department of Physics, University of California, Berkeley, California
August 25, 1950

THE gamma-ray spectrum resulting from the absorption of π^--mesons in deuterium has been analyzed with a pair spectrometer having 30 channels covering a range of 3 to 1 in energy. The experimental arrangement is similar to that discussed in previous letters by the same authors.[1,2] The deuterium is contained in the pressure vessel at 2700 p.s.i. at the temperature of liquid nitrogen. Its density[3] is 0.096 as compared with a hydrogen density of 0.046 under the same conditions.

Ten runs were made over a 72-hour period without changing the physical set-up. The regions centering on 130 Mev and 70 Mev were examined with full sensitivity. Comparisons were obtained between hydrogen, deuterium, helium, and vacuum background in the upper energy region. In the lower energy region deuterium, helium, and background were examined so that a limit might be set to the null effect observed there in deuterium.

The spectrum from π^--capture in hydrogen has been attributed to the reactions

(a) $\pi^- + p \rightarrow n + \gamma$ ($E_\gamma = 131$ Mev).
(b) $\pi^- + p \rightarrow n + \pi^0 \rightarrow n + 2\gamma$ ($E_\gamma = 70$ Mev).

In deuterium one or more of the following reactions are probable:

(c) $\pi^- + d \rightarrow 2n + \gamma$ ($E_\gamma = 0$ to 135 Mev).
(d) $\pi^- + d \rightarrow 2n + \pi^0 \rightarrow 2n + 2\gamma$ ($E_\gamma = 70$ Mev).
(e) $\pi^- + d \rightarrow 2n$.

By combining the channels in which a positive counting rate is observed we find the following total counting rates for the various processes:

(a) 0.470±0.046 c.p.m. } For a total of 0.925±0.1 c.p.m.
(b) 0.455±0.09 c.p.m. } in hydrogen.
(c) 0.275±0.034 c.p.m. } For a total of 0.275±0.04 c.p.m.
(d) −0.008±0.020 c.p.m. } in deuterium.

The ratio of the yield in deuterium to that in hydrogen is 0.30±0.04.

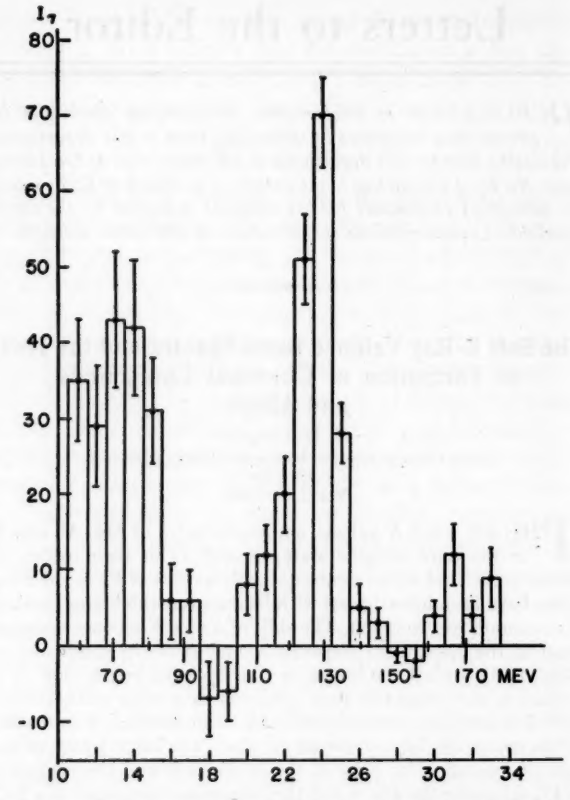

FIG. 1. Gamma-ray spectrum from absorption of π^--mesons in hydrogen. The lower numbers represent spectrometer channels.

(e) Attempts are being made to detect the fast neutrons from this process, but without conclusive results at this time. This process probably accounts for the remainder of the π^--captures in deuterium.

The runs with helium were made to see whether the background was increased by π^0-production from fast protons scattered into the deuterium, since it is known[4] that the cross section for production of π^0-mesons by protons on neutrons is much greater than for protons on protons. No counts above vacuum background

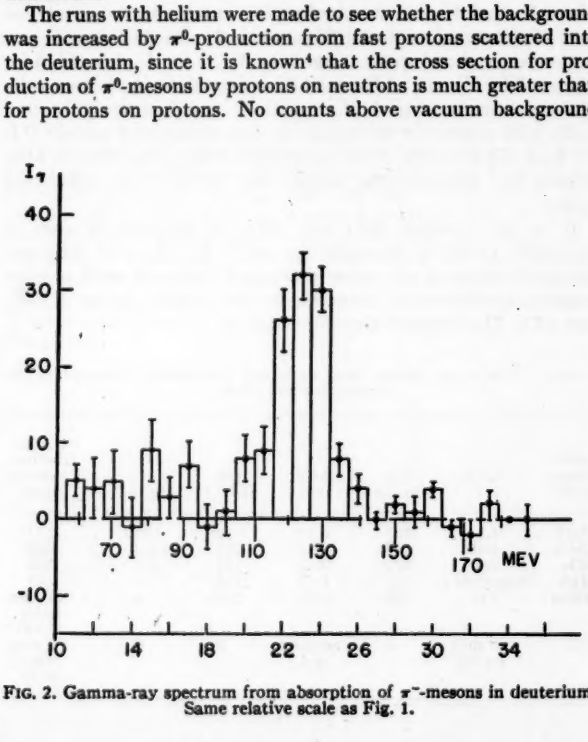

FIG. 2. Gamma-ray spectrum from absorption of π^--mesons in deuterium. Same relative scale as Fig. 1.

were observed from the helium, although the total number of counts was small (~120).

The observed spectrum from process (c) differs markedly from that calculated on phase space considerations alone, possibly because of the interaction of the outgoing neutrons. Process (d) is energetically possible; however, the yield is expected to be small, since energy available for the π^0 is small and selection rules require that the π^0 come off in the p state with respect to the two neutron system (assuming parity of π^0 same as π^- and capture from the S-state).

We wish to thank Mr. J. Vale and the cyclotron crew for providing the bombardments.

* The work described in this paper was performed under the auspices of the AEC.

[1] Panofsky, Aamodt, and York, Phys. Rev. 78, 825 (1950).
[2] Panofsky, Aamodt, Hadley, and Phillips, Phys. Rev. 80, 94 (1950).
[3] Johnston, Bozman, Rubin, Swanson, Corak, and Rifkin, MDDC 850, unpublished.
[4] Crandall, Moyer, and York (private communication).

On Advanced and Retarded Potentials

ALFRED LANDÉ
Ohio State University, Columbus, Ohio
June 26, 1950

WHEELER and Feynman[1] in their absorber theory of radiation have attempted to circumvent the classical infinities of point charges by introducing retarded and advanced potentials of interaction on an equal footing. Their theory has provoked much (unpublished) favorable as well as adverse comment. In view of the importance of the question whether a description of nature using advanced forces of interaction at a distance is possible, the following purely critical remarks may not be out of place.

That there are doubts about the consistency and physical applicability of the W-F theory is due to the dynamical incompleteness of the Maxwell-Lorentz theory, with fields determined by the world-lines of the charges, although the latter may be guided not only by self- and mutual electrodynamic forces and inertia but also by external forces, electromagnetic or mechanical, chosen at will, in short, by the arbitrary intervention of an experimenter. That the present motion of particles on a star 50 light years away should *actually* depend on whether a person on the earth arbitrarily will or will not decide to push a button in the year 2000 seems absurd, at least to our customary way of thinking. Closer analysis of the word "actually" shows that it could mean that the behavior of particles on the star in $(1950+n)$ for various n's shows a dependence on whether some one does or does not push a button on the earth in $(200+n)$ as established *post factum*. An "actual" dependence of the year 1950 on the year 2000 as confirmed by observation does not seem so absurd any more. It is quite a different question, however, whether waves converging on the "cause" are empirically acceptable. To reconcile us with this special form of retroaction, W-F wish to exclude arbitrary abrupt interventions, such as observers pushing buttons. They admit only built-in continuous mechanisms (W-F, II p. 427) which thereby become parts of the system itself. Thus they restrict their theory to closed deterministic systems in which "the distinction between cause and effect is pointless. The stone hits the ground because it was dropped from a height; equally well, the stone fell from the height because it was going to hit the ground" (W-F, II p. 428). The exclusion of arbitrary intervention, usually called an experimental test, for the sake of permitting a description by advanced and retarded potentials looks like a flight into unreality, however.

Wheeler and Feynman's reply to this objection is that their absorber theory permits a *consistent* derivation of the *tested* results of the usual retarded theory. In particular, they point out that the well known self-force experienced by a particle a under an acceleration (which may also be represented by Dirac's antisymmetric expression

$$F^a(a)=\tfrac{1}{2}[F^a{}_{\rm ret}(a)-F^a{}_{\rm adv}(a)],) \tag{1}$$

can be derived from the symmetric sum of half-advanced, half-retarded forces produced by the particles k other than a:

$$F^a(a)=\tfrac{1}{2}\Sigma_{k\neq a}[F^k{}_{\rm ret}(a)+F^k{}_{\rm adv}(a)]. \tag{2}$$

The equivalence of (1) and (2) which is the central point of W-F's theory rests on two assumptions, namely, *first*, that the body of all particles constitutes a "perfect absorber" characterized by the equation [W-F, I (37)]:

$$\Sigma_{\rm all\ }{}_kF^k{}_{\rm ret}(P)=\Sigma_{\rm all\ }{}_kF^k{}_{\rm adv}(P) \tag{3}$$

valid in all world points P including those of a particle; *second*, that the following initial conditions hold at the place of particle a at the instant when a alone is accelerated (by any test force whatsoever):

$$\tfrac{1}{2}\Sigma_{k\neq a}F^k{}_{\rm ret}(a)=0, \tag{4}$$

although

$$\tfrac{1}{2}\Sigma_{k\neq a}F^k{}_{\rm adv}(a)\neq 0. \tag{4'}$$

The left-hand side of (4') then is identical on the one hand with (2), and on the other hand with (1), by virtue of (3) and (4), thus proving the equivalence of (1) and (2).

Now, although there is no mathematical contradiction between the assumptions (3), (4) and (4'), nevertheless the following physical objection against the simultaneous validity of (3) and (4), (4') at the time of acceleration of a may be raised. Equation (4) implies that before and at the instant $t=0$ when particle a is accelerated, the other particles are in a state of disorder so that their retarded force contributions which arrive in a at $t=0$, average out to zero. At times $t>0$, however, the other particles are affected by what happens to a at $t=0$ and thus yield a non-vanishing advanced contribution (4') arriving at a at $t=0$. The privileged rôle of particle a at $t=0$ leads to the unsymmetric initial conditions (4) and (4'). The absorber hypothesis (3), however, implies and can be accepted only (a) when all particles are on an equal footing, thus excluding any privileged part played by the particle a, and (b) when we are assured that no particle has, or ever will be, subjected to an arbitrary disturbance; otherwise (3) would be self-contradictory, as is shown by the example of keeping all particles at rest before $t=0$, and on prescribed paths after $t=0$. Thus, although (3) alone, or (4) and (4') alone may be acceptable, it is physically *inconsistent* to couple the symmetric assumption (3) with the asymmetric initial conditions (4), (4'). It seems that other ways will have to be found in order to get rid of the classical infinities of point charges.[2]

[1] J. A. Wheeler and R. P. Feynman, Rev. Mod. Phys. 17, 157 (1945), Bohr commemoration number; Rev. Mod. Phys. 21, 425 (1949), Einstein number. Referred to as W-F, I and II.
[2] We mention in this connection M. Born's theory of reciprocity, Rev. Mod. Phys. 21, 463 (1949), Einstein number; also A. Landé, Phys. Rev. 76, 1176 (1949); 77, 814 (1950).

Collimated and Wide-Angle Meson Groups in a Hard-Shower Star

MAURICE M. SHAPIRO
Nucleonics Division, Naval Research Laboratory, Washington, D. C.
AND
HERMAN YAGODA
National Institutes of Health, Laboratory of Physical Biology, Experimental Biology and Medicine Institute, Bethesda, Maryland
August 10, 1950

SPRAYS of relativistic particles associated with cosmic-ray stars have been observed in ultrasensitive photographic emulsions by many workers.[1-6] These sprays are now known to consist principally of π-mesons,[7,8] and they can be identified with the penetrating showers observed in cloud chambers and with counter

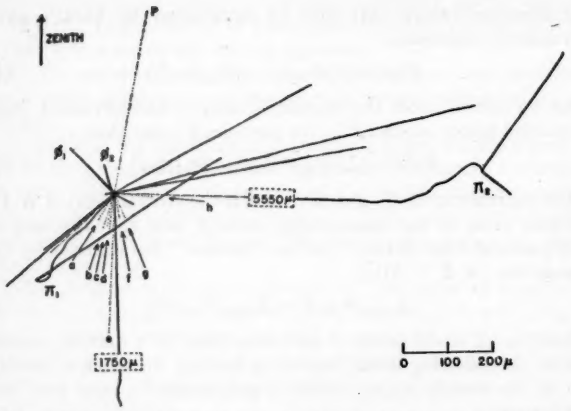

FIG. 1. Projection sketch of star, showing tracks due to: P, initiating particle; a to g, narrow-angle spray; h, another relativistic particle; π_1, π_2, slow π^--mesons terminating in stars; ϕ_1, ϕ_2, nuclear fragments. Number inside of each box denotes length in microns of portion of track omitted from drawing.

techniques.[9] Surrounding a narrow-angle spray, there appears fairly often a wider-angle shower of particles usually less energetic than those in the core.[10]

Bethe[11] has proposed a hypothesis to account for the simultaneous occurrence of wide-angle and collimated showers. He suggests that in a violent collision between nucleons, mesons can be produced either from the incident nucleon or from the target nucleon. The mesons arising from the incident nucleon might be emitted isotropically in the reference system of that particle, and mesons produced from the nucleon originally at rest may be isotropic in the system of that nucleon. The result in the laboratory frame of reference will be two groups of mesons, one collimated, the other spread out. Both will move predominantly into the forward hemisphere, for even the particles arising from the target nucleon, which move "backward" in the c.m. system, should usually, in the laboratory system, move in the general direction of the incident particle, though at larger angles with it than the core particles. If the incident nucleon is a proton, the collimated group is likely to have an excess of positive mesons, whereas no such excess (and perhaps even a π^--excess) might be expected for the wide-angle group.

In a 300μ Ilford G.5 emulsion exposed in the stratosphere[12] in Minnesota, we have observed an example of meson production in a high energy nuclear explosion which seems to fit the main features of Bethe's hypothesis. The star (reproduced as a projection sketch in Fig. 1)[13] shows: (1) a shower of eight tracks at minimum ionization, of which seven (a to g) form a relatively narrow downward spray, whereas the eighth (h) is emitted sidewise, at 96° with the zenith; (2) in the upper hemisphere, a single minimally ionizing track P, nearly collinear with the axis of the spray; (3) the characteristically scattered tracks of two slow π^--mesons (π_1, π_2) identifiable as negative by the secondary stars which they generate upon coming to rest; (4) ten dense "evaporation" tracks, including two due to heavy nuclear fragments (ϕ_1, ϕ_2), which display the usual "thin-down." These splinters emerge as a single fragment which breaks up into two after traveling 3μ.

From the number of dense tracks, the disintegration must have occurred in one of the heavier nuclei (Ag, Br, or I) in the emulsion. Of the two slow mesons, π_1 was emitted with an energy of 3.3 Mev, deduced from its range, and it generated a single charged secondary; π_2 had 18.4 Mev, and produced a two-prong star.

Track P and the narrow spray together form a "broom"[2] of roughly elliptic cross section, with P as the "handle." The major axis of the ellipse subtends 55° at the apex, the minor axis, 40°. The extension of P passes within 1° of the major axis, and 5° of the minor axis; i.e., it nearly coincides with the axis of the spray cone. Accordingly, there is little doubt that P is due to an incoming particle, probably a proton, which initiated the explosion. For the seven spray tracks, the average projected angle with their common axis is 14°; for the three tracks h, π_1, and π_2, the average angle with the same axis is 74°. In view of results by Fowler[7] and others, it is reasonable to attribute six to eight of the shower tracks to π-mesons, and the rest to protons.

We thus have a narrow-angle spray of five to seven relativistic mesons, and a wide-angle group of one relativistic particle and two slow π^--mesons. If a few additional fast mesons were emitted in the wide-angle group, these could be missed, since in a shower orientated like this one, the geometry discriminates against observation of the wide-angle tracks.[14] It will be seen that Bethe's hypothesis accounts rather satisfactorily for this event. By itself, the latter scarcely provides clear evidence, but considered together with Hornbostel and Salant's observations,[10] it lends plausibility to the two-group mechanism.[15]

Examples of single σ-mesons (slow, star-generating π^-) emerging from a star are not uncommon. On the other hand, observations of two σ-mesons from the same star are very rare.[16] This may be ascribed to two causes: (a) even the mesons in the wide-angle group are more likely to be fast than slow (our event is a somewhat special example in that the difference in velocities of the two meson groups is accentuated by the two slow σ's); (b) limitations of geometry.[14]

[1] Brown, Camerini, Fowler, King, Muirhead, Powell, and Ritson, Nature 163, 47 (1949).
[2] J. Hornbostel and E. O. Salant, Phys. Rev. 76, 468 (A) (1949); Osborne and Feld, Phys. Rev. 76, 468 (A) (1949).
[3] Leprince-Ringuet, Bousser, Tchang-Fong, Jauneau, and Morellet, Comptes Rendus 229, 163 (1949).
[4] Brown, Camerini, Fowler, Heitler, King, and Powell, Phil. Mag. 40, 862 (1949).
[5] J. J. Lord and M. Schein, Phys. Rev. 77, 19 (1950).
[6] P. Freier and E. P. Ney, Phys. Rev. 77, 337 (1950).
[7] P. H. Fowler, Phil. Mag. 41, 169 (1950).
[8] Camerini, Fowler, Lock, and Muirhead, Phil. Mag. 41, 413 (1950).
[9] O. Piccioni, Phys. Rev. 77, 1 (1950).
[10] J. Hornbostel and E. O. Salant, Phys. Rev. 76, 859 (1949).
[11] H. A. Bethe, Proceedings of the Echo Lake Symposium (June, 1949), p. 123 ff, unpublished.
[12] Balloon flight arranged by courtesy of ONR Project Skyhook.
[13] Thanks are due Mr. F. W. O'Dell for this drawing.
[14] When they are steep, near-minimal tracks are difficult to detect, and slow meson tracks are unlikely to terminate in the emulsion, and therefore are difficult to identify. The resulting discrimination affects a large fraction of the sprays which are most apt to be found in emulsions. Thus, if one observes, say, twice as many tracks in the core of a meson shower as in the surrounding portion, it is unsafe to conclude that a preponderant number of particles was actually emitted in the collimated group. Depending on the orientation of the shower cone, the two groups may in fact contain nearly equal numbers of mesons, as would be expected from Bethe's hypothesis.
[15] That at least two of three mesons in the wide-angle group are negative is also consistent with Bethe's hypothesis. However, the presence of π^- and the absence of identifiable π^+ is adequately explained by the infrequent occurrence of slow π^+-mesons in stars, since even when they are born slow, they acquire considerable, velocity in passing through the Coulomb field, and thus emerge fast. It is noteworthy in this connection, that of 24 nascent σ-mesons observed by one of us (H.Y.) 17 are actually emitted *backward*, i.e., into the upper hemisphere.
[16] In the only other example which has come to our attention there was no accompanying collimated spray. The latter, observed by E. O. Salant, is reproduced in F. Bitter's *Nuclear Physics* (Addison-Wesley Press, Cambridge), p. 89.

Some Properties of the 43-Day Isomer of Cd^{115}

P. S. GILL,* C. E. MANDEVILLE, AND E. SHAPIRO
Bartol Research Foundation of the Franklin Institute,† Swarthmore, Pennsylvania
August 25, 1950

AN activity of 43 days has been reported in cadmium.[1] The series of reactions[1] whereby it can be produced have identified it as an isomer of Cd^{115}. In the first investigation[1] of its properties, the activity was reported to decay by negatron emission, with a maximum beta-ray energy of 1.5 Mev, and a gamma-ray energy of 0.5 Mev. The early measurements also seemed to indicate that one gamma-ray accompanied each disintegration beta-ray.

A source of 43-day cadmium was prepared for the present researches when metallic cadmium was irradiated by slow neutrons in the Oak Ridge pile. The irradiated material was aged for more than a month to permit disappearance of any 2.5-day Cd^{115}. After this time, chemical separations were carried out for the removal of any lead, silver, antimony, or indium which might be present as

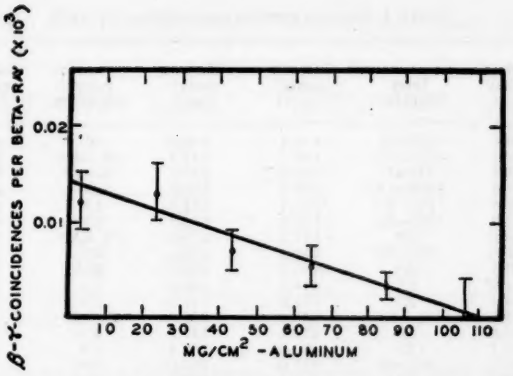

FIG. 1. Beta-gamma-coincidence rate of the 43-day cadmium as a function of the surface density of aluminum placed before the beta-ray counter.

radioactive contaminants. The beta-rays of the 43-day Cd^{115} were absorbed in aluminum. The absorption limit occurred at 600 mg/cm², corresponding to an energy of 1.41 Mev as calculated from Feather's equation.[2] An absorption curve in lead revealed the presence of two gamma-rays, having approximate energies of 0.10 and 2.0 Mev, the latter being of low intensity. A coincidence absorption curve gave a maximum gamma-ray energy of 1.10 Mev. It was also noted that the gamma-ray intensity was considerably less than one gamma-ray per beta-ray.

The results relating to gamma-rays were so markedly different from those of the earlier report that additional chemical purification was carried out for removal of any residual silver and indium. After completion of this chemical purification, the various absorption measurements on the beta-rays and gamma-rays were repeated. Two months had now elapsed since removal of the target material from the pile. The results were identical with those taken prior to the last chemical separation and one month previously.

A source of the highly purified Cd^{115} was placed in a beta-gamma-coincidence counting arrangement, and the beta-gamma-coincidence rate was observed as a function of the surface density of aluminum placed before the beta-ray counter. These data are shown in Fig. 1, where the beta-gamma-coincidence rate is observed to decrease from 0.014×10^{-3} coincidence per beta-ray at zero absorber thickness to zero at 110 mg/cm², indicating the presence of an inner beta-ray spectrum having a maximum energy of 0.38 Mev which is coincident with gamma-radiation. The harder beta-spectrum of 1.41-Mev maximum energy apparently leads to the ground state of the residual nucleus.

Assuming that on the average each beta-ray of the inner spectrum is followed by 1.10 Mev of gamma-ray energy, the calibration of the gamma-ray counter indicated that only one percent of the total beta-radiation is contained in the group of maximum energy 0.38 Mev.

A gamma-gamma-coincidence rate of 0.07×10^{-3} coincidence per gamma-ray was observed in Cd^{115}, showing that gamma-rays are present in cascade.

Bell, Cassidy, and Hughes of the Oak Ridge National Laboratory have independently reached conclusions similar to ours. Using a coincidence spectrometer employing scintillation counters, they find gamma-rays at 1.29, 0.93, 0.72, 0.50, 0.198, and 0.074 Mev and that 0.7 percent of the beta-rays are coupled with gamma-rays. They have also demonstrated that the gamma-ray at 2 Mev is associated with an impurity. Assuming that each beta-ray of the inner spectrum is followed by 1.29 Mev of gamma-ray energy, the beta-gamma-coincidence rate observed by the writers indicates that 0.85 percent of the total beta-radiation is contained in the low energy spectrum.

* Guest physicist, Bartol Research Foundation (1950). At present at University of Aligarh, India.
† Assisted by the joint program of the ONR and AEC.
[1] Seren, Engelkemeir, Sturm, Friedlander, and Turkel, Phys. Rev. 71, 409 (1947).
[2] N. Feather, Proc. Camb. Phil. Soc. 34, 599 (1938).

Energy Barrier for Asymmetric Fission in the Static Liquid Drop Model

J. JUNGERMAN*
Laboratory of Nuclear Studies, Cornell University, Ithaca, New York
August 24, 1950

WE have attempted to calculate the fission barrier for U^{236} by two approximate methods. As a first approximation a model was chosen which consisted of two tangent spheres of arbitrary radii joined by a frustrum of a cone which was tangent to each sphere. This configuration gives the sum of Coulomb and surface energies as 7.32 Mev greater than the parent nucleus if equal radii are chosen for the spheres. When the ratio of the radii is seven to eight (approximately a splitting in mass of two to three as is observed), the above energy is increased by 0.2_6 Mev. These results utilize 532.0 Mev for the surface energy and 799.8 Mev for the Coulomb energy of the U^{236} nucleus in agreement with Frankel and Metropolis.[1] Since the symmetric shape is quite similar to that given by the above authors, we feel that the barrier against asymmetric fission at the true saddle point should be of the above order of magnitude.

The second model used an arbitrary ellipsoid of revolution which was subjected to a deformation. We took the deformation to be:

$$r=a(\beta^2-\mu^2)^{\frac{1}{2}}\Sigma_l C_l\mu^l. \tag{1}$$

Here r is measured along the radius of the ellipsoid, R, in units of its major axis, a, μ is the cosine of the angle between R and a, and

$$\beta^2=a^2/(a^2-b^2), \tag{2}$$

where b is the minor axis of the ellipsoid. The C_l's are constants to be determined so that the deformation energy is a minimum. An expansion in powers of r/R permitted calculation of the surface energy, the mutual Coulomb energy between the deformation and the ellipsoid, and finally the self-Coulomb energy of the deformation to the order $(r/R)^2$. In this manner we obtained a quadratic expression for the deformation energy, ΔE, in terms of the C_l's for a given β. The energies were calculated as far as $l=4$, and in principle could be extended to higher l values without fundamental difficulty.

The equations

$$\partial\Delta E/\partial C_l=0, \quad l \text{ even} \tag{3}$$

together with the constant major axis condition

$$\Sigma_{l \text{ even}} C_l=0 \tag{4}$$

and the demand of zero volume change

$$\int_{-1}^{+1}(R^2r+Rr^2)d\mu=0 \tag{5}$$

determine the extremal values of the C_l's. This procedure does not determine the extremal values for odd l, since the corresponding C_l's enter only in second order in ΔE or condition (5).

For the choice $\beta^2=1.27$, $a/b=2.17$, the following minimal values of the C_l's were obtained: $c_0=-0.04558$, $c_2=+0.23567$, $c_4=-0.19009$; and these give $\Delta E=-1.0_2$ Mev. The difference in energy between this ellipsoid and the parent nucleus of the same

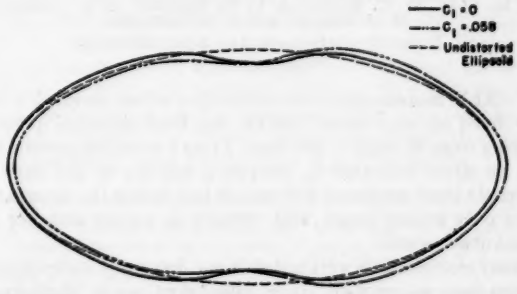

FIG. 1. Minimum energy configurations on the ellipsoid model for $\beta^2=1.27$.

volume is 8.64 Mev, so that the fission barrier is 7.6_2 Mev. If this calculation is repeated for several values of β, the maximum barrier found should be an approximate saddle-point value. Unfortunately, this procedure gives barriers that are much too high. When a plot is made of the shape of the nucleus produced by the above deformation, it shows a rather marked curvature in the equatorial region and is very close to the ellipsoid elsewhere. This can be seen in Fig. 1. The saddle-point curves of Frankel and Metropolis show a much smoother variation of nuclear surface. We believe this to be the root of our difficulty in obtaining a reasonable saddle point. An increase in the maximum value of l taken should ultimately remove this trouble. However, it probably would be better to start with $(\beta^2-\mu^2)^{\frac{1}{2}}$ or $(\beta^2-\mu^2)^{\frac{1}{4}}$ in the denominator of the expression for r so that the deformation would be accentuated in the region near the poles. The integrals for the deformation energy appear to be just as readily done for these choices of r.

The ellipsoid and tangent sphere models are complementary in that the former has marked curvature in the equatorial region whereas the latter has none. It is therefore interesting to compare the respective asymmetry barriers. In the introduction of asymmetry into the ellipsoid model again a somewhat arbitrary choice has to be made as to how the elongated drop will ultimately divide. On the assumption that the split will occur at the minimum of the constriction, the choice $c_1=0.05800$ will give roughly a two to three splitting of the above ellipsoid.

For minimum ΔE the other C_l's now become: $c_1=-0.04479$, $c_2=+0.22049$, $c_4=-0.17570$. This configuration is shown also in Fig. 1. The corresponding $\Delta E=-0.8_2$ Mev so that the barrier against this asymmetry is 0.2_0 Mev, in fair agreement with the tangent cone model. If the division of fragment masses is one to two, the asymmetry barrier becomes 0.61 and 0.75 Mev for the tangent cone and the above ellipsoid, respectively. The fact that the energy barrier disfavors asymmetric fission is in agreement with previous results.[1,2]

Since the barrier is not very great, the effects of non-uniformity of nuclear charge may be important. The model of two spheres in contact and the results of Feenberg[3] on increased nuclear binding due to non-uniform charge distribution give a crude estimate of 0.1 and 0.6 Mev in favor of asymmetric fission for two to three and one to two splittings, respectively. Thus the effect of non-uniformity appears to be of the same order of magnitude and opposite in sign to the barriers calculated above. The true influence of non-uniform charge would be obtained by including it systematically in the calculations of the Coulomb energy of a saddle-point configuration.

The author would like to thank Professor H. A. Bethe for many helpful discussions and for suggesting the models used.

* Now at Radiation Laboratory, University of California, Berkeley, California.

[1] S. Frankel and N. Metropolis, Phys. Rev. **72**, 914 (1947).
[2] Present, Reines, and Knipp, Phys. Rev. **70**, 557 (1946).
[3] E. Feenberg, Phys. Rev. **59**, 593 (1941).

Gamma-Rays from Ag^{110}

J. M. Cork, W. C. Rutledge, C. E. Branyan, A. E. Stoddard, W. J. Childs, and J. M. LeBlanc
*University of Michigan, Ann Arbor, Michigan**

August 24, 1950

EARLY measurements on radioactive silver revealed a long-lived activity whose half-life has been variously reported[1] as being from 90 days to 300 days. From a previous investigation here on silver activated in the pile a half-life of 282 days was reported.[2] Pool[3] has found 270 days as best fitting the observations taken over several years. This value is in accord with our continued observation.

Many electron lines were noted in our first study indicating four gamma-rays as reported. In a subsequent study Siegbahn observed[4] these four, together with six additional gamma-rays.

TABLE I. Electron energies from radioactive Ag^{110}.

Electron energy (kev)	Interpretation	Gamma-energy (kev)	Electron energy (kev)	Interpretation	Gamma-energy (kev)
90.6	$K^1(47)$	116.1	630.5	K^9	657.2
112.4	$L_{1,2}{}^1(47)$	116.1	632.4	$Ph-K^{12}$	720.0
115.3	$M^1(47)$	116.0	639.5	$Ph-L^9$	655.3
347.6	$Ph(Pb)K^2$	435.2	650.3	K^{10}	677.0
358.8	$Ph-K^3$	446.4	652.9	L^9	656.7
382.2	$Ph-K^4$	469.8	673.2	L^{10}	677.0
410.8	K^2	437.5	673.3	$Ph-K^{13}$	760.9
410.8	$Ph-K^5$	498.4	678.6	K^{11}	705.3
419.3	K^3	446.0	696.0	K^{12}	722.7
441.0	L^3	444.8	700.8	L^{11}	704.6
444.3	K^4	471.0	717.3	L^{12}	721.1
451.5	$Ph-K^6$	539.1	727.8	$Ph-K^{14}$	815.4
467.3	L^4	471.1	737.2	K^{13}	763.9
472.3	K^5	499.0	758.4	L^{13}	762.2
484.4	$Ph-K^7$	572.0	763.0	M^{13}	763.8
494.9	L^5	498.7	790.7	K^{14}	817.4
514.7	K^6	541.4	793.7	$Ph-K^{15}$	881.3
530.2	$Ph-K^8$	617.8	847.4	$Ph-K^{16}$	935.0
537.8	L^6	541.6	857.4	K^{15}	884.1
548.4	K^7	575.1	880.2	L^{15}	884.0
567.7	$Ph-K^9$	655.3	910.4	K^{16}	937.1
571.8	L^7	575.6	932.0	L^{16}	935.8
588.6	$Ph-K^{10}$	676.2	1293	$Ph-K^{17}$	1381
592.3	K^8	619.0	1357	K^{17}	1384
616.1	$Ph-K^{11}$	703.7	1377	K^{18}	1504

Continued investigation using photographic spectrometers and observing electrons due both to internal conversion and to photoemission from lead reveals a large number of previously unobserved electron lines. In order to have a source with greater specific activity, one irradiation was carried out in the Chalk River pile with its greater neutron flux. From measurements of the electron energies 18 gamma-rays can be identified and evaluated as associated with the radioactive decay. There is very good evidence that in the region from 400 to 600 kev additional gamma-rays exist but that their electron lines are too weak to be measured with sufficient accuracy, and hence they are not included in this report.

A summary of the electron energies together with their interpretation is presented in Table I. It is noted that the K–L–M differences for the first three electron lines are characteristic of silver and thus represent a gamma-ray emitted in a transition between isomeric states of silver. For all other conversion electron energies the K–L–M differences which fit best are those for cadmium. This indicates that competing decay processes occur, in one of which gamma-emission to a metsatable state is followed by beta-decay, whereas in the other decay mode beta-emission occurs

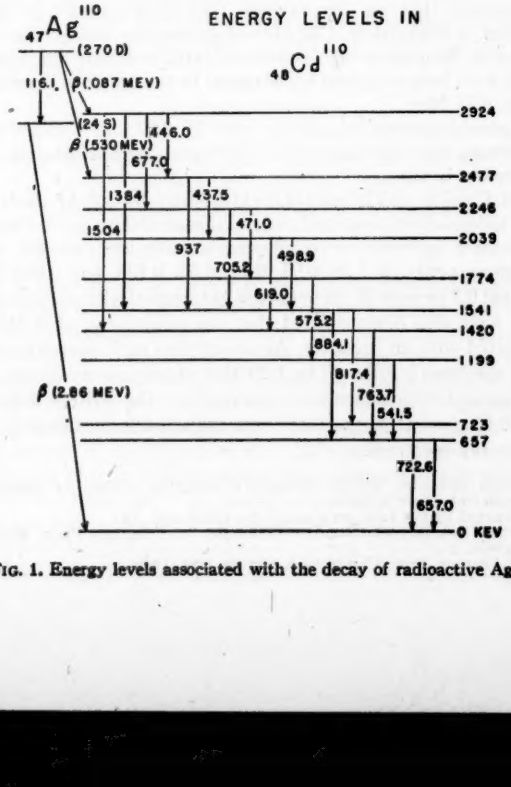

FIG. 1. Energy levels associated with the decay of radioactive Ag^{110}.

TABLE II. Summary of the gamma-rays associated with the decay of Ag^{110}. Legend: *S*—strong, *M*—medium, *W*—weak.

Arbitrary number	Energy (kev)	Intensity	Arbitrary number	Energy (kev)	Intensity
1	*116.1	*S*	10	677.0	*M*
2	437.5	*W*	11	705.2	*M*
3	446.0	*M*	12	722.6	*W*
4	471.0	*W*	13	763.7	*M*
5	498.9	*W*	14	817.4	*W*
6	541.5	*W*	15	884.1	*S*
7	575.2	*W*	16	937	*M*
8	619.0	*M*	17	1384	*W*
9	657.0	*S*	18	1504	*W*

* In silver.

first followed by multiple gamma-transitions. The many gamma-rays are assigned arbitrary numbers increasing in the order of increasing energy and are shown collectively in Table II. Every gamma-energy was derived from both photoelectric and conversion electron energies. The photoelectric energies are distinguished in Table I by the abbreviation "*Ph.*"

This many gamma-rays may be accommodated remarkably well by a level scheme as shown in Fig. 1. This arrangement utilizes the beta-energies and the gamma-rays observed by Siegbahn in somewhat the manner proposed except that certain of the energy values are modified by our measurements and the new transitions are added. The complex beta-spectrum, with upper limits at 0.087, 0.530, and 2.86 Mev, fits satisfactorily the proposed arrangement.

* This investigation was made possible by the joint support of the AEC and ONR.

[1] A. Mitchell, Phys. Rev. **53**, 269 (1938); J. Livingood and G. Seaborg, Phys. Rev. **54**, 88 (1938); K. Alexeeva, Comptes Rendus U.S.S.R. **18**, 553 (1938); H. Reddemann and F. Strassmann, Naturwiss. **26**, 187 (1938); Deutsch, Elliot, and Roberts, Phys. Rev. **61**, 389 (1942); **72**, 527 (1947); W. Rall and R. Wilkinson, Phys. Rev. **71**, 321 (1947).
[2] Cork, Shreffler, and Fowler, Phys. Rev. **74**, 1657 (1948).
[3] Gum, Thompson, and Pool, Phys. Rev. **76**, 184 (1949).
[4] K. Siegbahn, Phys. Rev. **75**, 1277 (1949); **77**, 233 (1950).

The $V^{51}(p,n)Cr^{51}$ Neutron Spectrum*

P. H. STELSON, W. M. PRESTON, AND CLARK GOODMAN
Laboratory for Nuclear Science and Engineering, Massachusetts Institute of Technology, Cambridge, Massachusetts
August 21, 1950

THE relatively low (p,n) threshold for vanadium[1] (1.564 Mev) and the ease of preparing thin and rugged evaporated targets of this metal suggest the use of the reaction $V^{51}(p,n)Cr^{51}$ as a monoergic neutron source at low energies.[2,3] From a study of the neutron spectrum at proton-bombarding energies well above the threshold, information can be obtained concerning the positions of excited levels of the residual nucleus, Cr^{51}, and the relative transition probabilities from the compound nucleus to these levels. These data allow conclusions concerning the monoergic nature of this source.

A 25-kev target on a tantalum backing was bombarded by 3.23- and 3.72-Mev protons from the Rockefeller electrostatic generator. Proton energies were measured by a generating voltmeter calibrated by the $Li^7(p,n)$ threshold at 1.882 Mev. The vanadium used contained 10 percent iron as impurity. This impurity was unimportant because: (a) the proton-bombarding energies were below the (p,n) threshold for the principal iron isotope (Fe^{56}: 91.6 percent),[4] and (b) the abundance of the other iron isotopes is small enough to be neglected in the present experiment.

Eastman NTB plates of 200μ thickness were placed a mean distance of 18 cm from the target in the forward direction. After the plates had been processed, proton recoil tracks within 10° of the neutron direction were measured with a microscope equipped with an oil immersion objective. The range-energy relation used to convert proton recoil track lengths to neutron energy E_n was obtained by measuring the $Li^7(p,n)$ spectrum at several bombarding energies. The resulting distributions for vanadium, corrected for the varying neutron-proton collision cross section to represent relative neutron intensities, are shown in Fig. 1.

TABLE I. Measured *Q*-values for the neutron groups shown in Fig. 1. The intensities are in each case relative to the ground-state peak *A*. The last column gives the excitation energy difference between *Q*-values for neutron groups, above the ground state, of levels in the residual nucleus Cr^{51}.

Neutron group	*Q*-values (Mev) $E_p=3.23$	$E_p=3.72$	Intensities $E_p=3.23$	$E_p=3.72$	Excitation energy (ΔQ in Mev)
A	−1.53	−1.55	1	1	
B	−2.30	−2.33	0.33±0.05	0.44±0.07	0.775±0.050
C	−2.69	−2.72	0.31±0.05	0.55±0.08	1.165±0.050
D		−2.97		0.30±0.05	1.420±0.080
E		−3.08		0.30±0.05	1.530±0.080

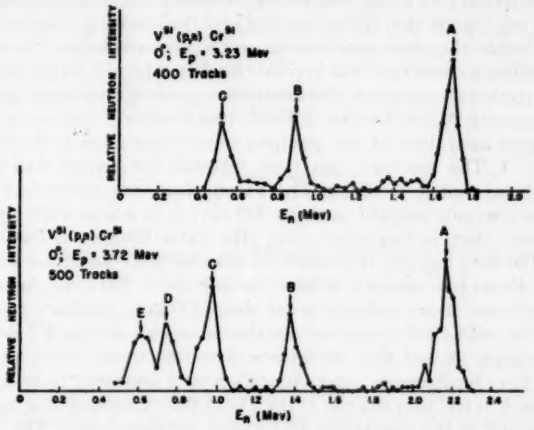

FIG. 1. Relative neutron intensity *vs.* neutron energy E_n for $V^{51}(p,n)Cr^{51}$ reaction using protons of energy E_p. Intensities include correction for variation of n–p scattering cross section with energy. Neutrons of known energy from the $Li^7(p,n)Be^7$ reaction were used to determine directly the range-energy relation for the photographic plates.

The peaks designated by *A* give *Q*-values which are in excellent agreement with that obtained from the threshold measurement of Smith and Richards.[1] Hence, the peaks at *A* correspond to neutrons which leave Cr^{51} in the ground state. Two additional peaks, designated by *B* and *C*, are of lower energy, have intensities comparable to *A*, and presumably indicate the existence of excited states in Cr^{51}. Two less well-defined groups, *D* and *E*, appeared with higher energy protons. The measured *Q*-values of these groups and the intensities relative to the ground state are given in Table I.

In Fig. 1, the curve for $E_p=3.23$ Mev gives almost 10 percent as the upper limit for the intensity, relative to the ground-state peak, of any possible neutron peak between *A* and *B*. Poor generator performance during this run may have increased the neutron background. The more satisfactory run at $E_p=3.72$ Mev gives approximately three percent as an upper limit for a peak between *A* and *B*. Therefore, the $V^{51}(p,n)$ reaction should furnish monoergic neutrons (within these limits) up to $E_n=775\pm50$ kev.

* Assisted by the joint program of the ONR, AEC, and BuShips.
[1] R. V. Smith and H. T. Richards, Phys. Rev. **74**, 1257 (1948).
[2] Hanson, Taschek, and Williams, Rev. Mod. Phys. **21**, 635 (1949).
[3] Vanadium consists of 99.75 percent V^{51} and 0.25 percent V^{50}; see D. C. Hess and M. C. Inghram, Phys. Rev. **76**, 1717 (1949); W. T. Leland, Phys. Rev. **76**, 1722 (1949).
[4] The $Fe^{56}(p,n)$ threshold is calculated to be 5.49 Mev from the disintegration scheme of Co^{56} (see A. C. G. Mitchell, Rev. Mod. Phys. **22**, 36 (1950)).

The Beta-Spectrum of P^{32}

S. D. Warshaw,* Joses J. L. Chen, and G. L. Appleton
University of Southern California,† Los Angeles, California
August 28, 1950

A RECENT measurement[1] of the P^{32} spectrum disagrees in several respects with previous investigations.[2] In view of the discrepancy between the shell model prediction in this case and the observation, and the experimental uncertainty itself, we thought it of interest to confirm the shape. The earlier investigations in reference 2 were subject to the usual thick source distortions and hence the disagreement here is not surprising. Siegbahn, however, used a source which was certainly thin enough to produce very little distortion (the actual thickness was not given, but is implied to be no more than 0.1 mg/cm² approximately) and Langer and Price took care to eliminate such distortions. Agnew's measurement, although apparently also made with care, resulted in a small but distinct deviation from the allowed shape which the other workers give; a new result was a pronounced rise in the momentum plot at energies less than 250 kev, which had not been observed with certainty before.

Our own work was done on carrier-free P^{32} from the Isotopes Division at Oak Ridge. Sources were deposited to thicknesses up to 0.2 mg/cm² on thin Nylon backing and the spectrum measured in a double thin lens spectrometer with good resolution. A small resolution correction[3] was applied; for this type of instrument the correction should make the observation come to even closer agreement with Agnew's result (a Fermi plot distinctly concave to the energy axis). One of our resulting momentum plots is shown in Fig. 1. The spectrum has been followed for several half-lives with no change in shape. The Fermi plots that result from all runs are quite straight to about 300 kev, or to a somewhat higher energy than in Siegbahn's case. (He states his plot is linear to <100 kev, but this is probably a misprint since an inspection of his Fermi plot shows it straight to only about 200 kev.) Agnew's result also shows a sharp rise at about 300 kev. Auxiliary experiments with Cs^{137} sources of the thickness used for the P^{32} determination showed that no serious distortion should occur above 80 kev; furthermore, since Agnew's source appeared to be quite thin, it is felt that the rise in the Fermi plot, corresponding to the "bump" in the momentum plot at low energies, is real. The end-point energy is 1.708±0.008 Mev, in excellent agreement with the other workers.

As has been pointed out by nearly all of the authors referred to, the result that nearly all of the spectrum has the allowed shape makes the interpretation quite difficult; the *ft* value of 8.5×10^7 places this decay in the second-forbidden class. While many of the first-forbidden correction factors may be energy independent, under certain conditions, only in very rare cases can the C_{21} become so. It is possible, of course, that the rise at low energy indicates a complex spectrum even though no gamma-ray is observed; this low energy component then might overlap the high energy component to the extent that the results appears to be, fortuitously, straight. If true, this would imply a level in S^{32} which would probably have $J=0$ to make the gamma-transition strictly forbidden. However, an analysis of the Fermi plot shows that if a low energy component is assumed, its end-point energy must be 330 kev, which is too low to distort the shape of the higher component. Furthermore, the lower component can account for no more than roughly five percent of the total activity. Hence, even this possibility does not make the beta-decay more interpretable, and the transition remains unexplained.

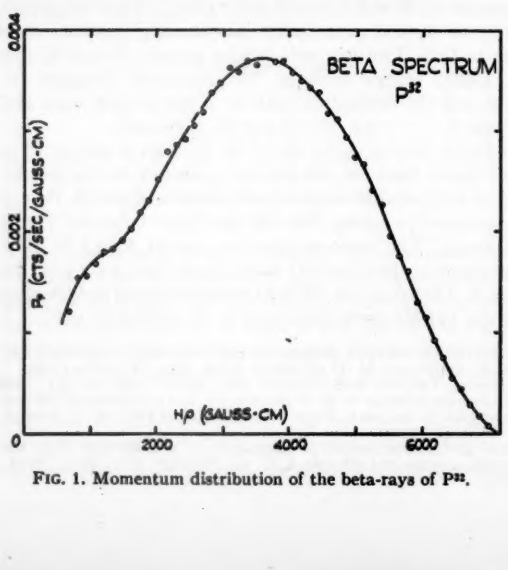

Fig. 1. Momentum distribution of the beta-rays of P^{32}.

* Now at the Institute of Radiobiology and Biophysics, University of Chicago, Chicago, Illinois.
† This work was assisted by the joint program of the ONR and AEC.
[1] H. M. Agnew, Phys. Rev. **77**, 655 (1950).
[2] E. M. Lyman, Phys. Rev. **51**, 1 (1937). J. L. Lawson, Phys. Rev. **56**, 131 (1939). K. Siegbahn, Phys. Rev. **70**, 127 (1946). E. J. Scott, Phys. Rev. **74**, 1240 (1948). L. M. Langer and H. C. Price, Phys. Rev. **76**, 641 (1949).
[3] G. E. Owen and H. Primakoff, Phys. Rev. **74**, 1406 (1948).

Nuclear Moment Discrepancies in Gallium and Indium

H. M. Foley
Columbia University, New York, New York
August 24, 1950

KUSCH[1] has pointed out the existence of a small discrepancy between the values of the nuclear magnetic moments of the gallium isotopes as determined in atomic beam experiments[2] and in nuclear magnetic resonance experiments.[3,4] The nuclear magnetic moments of the indium isotopes obtained from nuclear magnetic resonance experiments by Proctor and Yu[5] show similar differences from the atomic beam values.[6] Townes has suggested to the writer that the partial decoupling of the **L** and **S** vectors in the $^2P_{\frac{1}{2}}$ state by the applied field might affect the hyperfine interaction in such a way that the nuclear magnetic moment appears to be altered. This effect appears in the calculation as a cross term in second order between the matrix elements of the hyperfine interaction between the $^2P_{\frac{1}{2}}$ and $^2P_{\frac{3}{2}}$ states and the "Paschen-Back" matrix elements of the applied field. A non-relativistic one-electron wave function was used in developing an expression for the energy perturbation on the magnetic h.f.s. levels of the $^2P_{\frac{1}{2}}$ state. This perturbation is $[\Delta\nu/6(2I+1)]\mu_0 HM_I/\delta$ in the M_IM_J representation and will be added to the diagonal magnetic interaction term $-g_I\mu_0 HM_I$. $\Delta\nu$ is the hyperfine splitting in zero field and δ is the fine structure separation between the $^2P_{\frac{1}{2}}$ and $^2P_{\frac{3}{2}}$ states. The observed and calculated values of

$$R=1+\frac{\Delta\nu}{g_I\delta(2I+1)\delta}=\frac{\mu\ (\text{mag. res.})}{\mu\ (\text{atomic beam})}$$

are given below for gallium:

$$\text{Ga}^{69}:\ R=1.0080\pm0.0023,$$
$$\text{Ga}^{71}:\ R=1.0077\pm0.0017,$$
$$R_{\text{calc}}=1.0062,$$

and for indium:

$$R_{\text{calc}}=1.0043.$$

The calculated value of the ratio is somewhat too low, though within the assigned experimental error in the case of gallium. The remaining discrepancy may perhaps be accounted for by the well-known fact[7] that the ground states of such atoms as gallium, indium, and thallium are subject to configuration interaction mixing with some excited states of the outer three electrons, which affects strongly the observed hyperfine splittings in the $^2P_{\frac{1}{2}}$ state. There will be such effects in the off-diagonal hyperfine matrix elements employed here. Uncertainty in both the magnitude and the sign of this configuration interaction matrix element prevents an accurate estimate of this contribution.

It should be pointed out that exactly the same fractional correction to the magnetic interaction of the nuclear moment occurs in the FM_F (weak field) representation. Thus the Breit-Rabi formula for the energy levels in a $J=\frac{1}{2}$ state will still be obeyed formally in spite of the above second-order effects; however, the apparent nuclear moments must be corrected as indicated.

Mr. Robert Frosch obtained the off-diagonal hyperfine matrix elements employed in this calculation.

[1] P. Kusch, Phys. Rev. **78**, 615 (1950).
[2] G. Becker and P. Kusch, Phys. Rev. **73**, 584 (1948).
[3] R. V. Pound, Phys. Rev. **73**, 1112 (1948).
[4] Recent experiments by W. Knight and T. Wentinik with several gallium compounds confirm the result of Pound. Their results were communicated to the writer by Dr. Knight.
[5] Private communication to P. Kusch.
[6] P. Kusch and H. M. Foley, Phys. Rev. **74**, 250 (1948).
[7] E. Fermi and E. Segrè, Zeits. f. Physik **82**, 729 (1933).

The Disintegration of Hf^{181}

WILLIAM W. PRATT
*Institute for Atomic Research and Department of Physics, Iowa State College, Ames, Iowa**
August 21, 1950

THE radiations from Hf^{181} have been studied in this laboratory using the methods of coincidence spectrometry, in an attempt to determine the decay scheme of this isotope. A Hf^{181} source was taken from a standard unit (No. 31, Oak Ridge Catalog No. 3) of Hf_2O_3 bombarded for approximately 2½ months in the Oak Ridge pile. A spectrographic analysis of the material before bombardment indicated the only impurity in appreciable quantity to be 0.15 percent Zr. The measurements reported here were performed in a period between 4 and 7 months after removal of the Hf from the pile. The source was mounted on 2.5 mg/cm² mica and inserted into the beta-ray spectrometer,[1] which had been modified to use ring focusing.[2] A secondary counter was then placed directly behind the source; and coincidences were recorded between pulses in the spectrometer counter and the secondary counter. For $e-\gamma$-coincidence measurements, a platinum screen cathode Geiger counter with a copper wall was used as the secondary counter. A curve indicating gamma-counter efficiency as a function of quantum energy was obtained by determining points at 0.090 Mev, 0.238 Mev, and 1.25 Mev. The two low energy points were obtained by the coincidence method using the known decay scheme of ThB, and the high energy point was obtained by the coincidence method using the known decay scheme of Co^{60}. For $e-e$ coincidence measurements, a commercial end-window Geiger counter was used as the secondary counter.

When the gamma-counter was used as the secondary counter, coincidences were observed between the internal conversion electrons from the 130-kev transition[3,4] in Ta^{181}, selected by the spectrometer, and gamma-quanta actuating the secondary counter. Absorption of the gamma-quanta in lead indicated these coincidences to be caused by the 471-kev gamma-ray and in addition possibly to the 337-kev gamma-ray. No coincidences were observed between the 130-kev transition and any gamma-quanta when a 6-μsec. delay was introduced into either counter channel.

When the beta-counter was used as the secondary counter, coincidences were observed when the spectrometer was adjusted to select internal conversion electrons due to the 130-kev transition or to select electrons from the beta-spectrum alone. With the spectrometer adjusted to select internal conversion electrons due to the 130-kev transition, delayed coincidences were observed with a delay introduced into the secondary counter channel but not with a delay introduced into the spectrometer counter channel. With the spectrometer adjusted to select electrons from the beta-spectrum alone, the coincidence rate was increased when the resolving time was increased or when a delay was introduced into the spectrometer counter channel.

All of these results indicate that the beta-decay of Hf^{181} leads to the 20-μsec. metastable state which then decays via the 130-kev and 471-kev transitions in cascade. The work of Jensen[5] indicates that the 130-kev transition originates in the metastable state; and it is thus concluded that this transition precedes the 471-kev transition.

The measurements reported here do not serve to determine the positions in the decay scheme of the 337-kev or the 134-kev transitions. It has been suggested recently by Deutsch and Hedgran[6] that the 337-kev transition is due to an impurity rather than to Hf^{181} decay. The measurements reported here are consistent for the most part with either some such possibility, or with the complete decay scheme of Chu and Wiedenbeck.[3]

The writer is indebted to Dr. L. J. Laslett, Dr. E. N. Jensen, Mr. E. R. Rathbun, Jr., Mr. R. O. Lane, and Mr. J. Clement, all of the Physics Department; to Dr. A. Voigt and Mr. E. H. Dewell of the Chemistry Department; and to Mr. W. J. Mueller and the staff of the Electronics Shop, for valuable assistance in connection with various phases of the work.

* Contribution No. 120 from the Institute for Atomic Research and Department of Physics, Iowa State College, Ames, Iowa. Work was performed in the Ames Laboratory of the AEC.
[1] Jensen, Laslett, and Pratt, Phys. Rev. **75**, 458 (1949).
[2] Pratt, Boley, and Nichols (to be published in Rev. Sci. Inst.).
[3] K. Y. Chu and M. L. Wiedenbeck, Phys. Rev. **75**, 226 (1949).
[4] Since the spectrometer was operated at a low resolution of 4.9 percent in order to achieve as large a transmission as possible, the internal conversion electrons due to the 130-kev and 134-kev transitions were not resolved. However, both Chu and Wiedenbeck (see reference 3) and Jensen (see reference 5) have found the 134-kev transition to be considerably weaker than the 130-kev transition; and thus the effect of the former may presumably be neglected.
[5] E. N. Jensen, Phys. Rev. **76**, 958 (1949).
[6] M. Deutsch and A. Hedgran, Phys. Rev. **79**, 400 (1950).

The Structure of Methyl Bromide from Microwave Spectra*

JAMES W. SIMMONS AND WILLIAM O. SWAN
Department of Physics, Emory University, Atlanta, Georgia
August 21, 1950

SINCE the original publication[1] on the structures of the methyl halides a mistake in the calculations for methyl bromide has been called to our attention by Dr. A. H. Sharbaugh. Subsequent checking led to the conclusion that there was too small a percentage mass change from Br^{79} to Br^{81} to give satisfactory solutions of the methyl bromide structure equations using these two isotopes in combination with the value, derived from infra-red data, of the moment of inertia, I_A, about the figure axis of the molecule. Consequently, the microwave absorption spectra for the $J=1$ to $J=2$ rotational transition of $C^{13}H_3Br^{79}$ and $C^{13}H_3Br^{81}$ have been measured in this laboratory with the results shown in Table I.

A total of 18 lines was measured and values of frequencies for absorption lines for which $K=1$ as well as those for which $K=0$ were used in finding ν_0. In each case a constant stretching correction of 0.52 Mc/sec. was added to the observed frequency for lines of $K=1$, corresponding to the value of the stretching coefficient, D_{JK}, of 129 kc/sec. as found by Simmons and Anderson[2] for $C^{13}H_3Br$ using the equation[3]:

$$\nu_r=2B_0(J+1)-4D_J(J+1)^3-2D_{JK}(J+1)K^2. \qquad (1)$$

TABLE I. Frequencies of the hypothetical unsplit rotational lines, ν_0, for $C^{13}H_3Br^{79}$ and $C^{13}H_3Br^{81}$ and resulting moments of inertia from the rotational transition $J=1\rightarrow 2$.

Molecule	ν_0 (Mc/sec.)	B_0[a] (Mc/sec.)	I_B[b] ($\times 10^{-40}$ g-cm²)
$C^{13}H_3Br^{79}$	36477.67 ±0.09	9119.507	91.99_{03}
$C^{13}H_3Br^{81}$	36331.10	9082.860	92.36_{13}

[a] See text.
[b] Using $h=6.62373\times10^{-27}$ erg-sec. as given by J. W. M. DuMond and E. R. Cohen, Rev. Mod. Phys. **21**, 651 (1949).

TABLE II. Molecular dimensions of methyl bromide determined from different isotopic combinations.*

Molecular pair used	d_{CBr} (10^{-8} cm)	d_{CH} (10^{-8} cm)	∠HCH
$C^{13}H_3Br^{79}-C^{13}H_3Br^{79}$	1.9387	1.101	110°47′
$C^{13}H_3Br^{79}-C^{13}H_3Br^{81}$	1.9386	1.101	110°47′
$C^{13}H_3Br^{81}-C^{13}H_3Br^{79}$	1.9388	1.101	110°48′
$C^{13}H_3Br^{81}-C^{13}H_3Br^{81}$	1.9387	1.101	110°48′
Average values	1.9387	1.101	110°48′

* The constants used in these calculations were: $M_H=1.00813$, $M_{C^{12}}=12.00386$, $M_{C^{13}}=13.00761$, $M_{Br^{79}}=78.9417$, $M_{Br^{81}}=80.9400$, all in a.m.u.; $h=6.62373\times10^{-27}$ erg-sec., and the atomic mass unit $M=1.6599\times10^{-24}$ g.

The values of B_0 were then determined by using as a first approximation to the D_J values for $C^{13}H_3Br^{79}$ and $C^{13}H_3Br^{81}$, respectively, the values 11.1 kc/sec. and 10.7 kc/sec. found by Simmons and Anderson.

The data in Table I have been combined with the previous data obtained by Gordy, Simmons, and Smith[1] for the C^{12} compounds and with the infra-red I_A value, 5.496×10^{-40} g-cm², in the original equations,[1] yielding the results given in Table II. In contrast to the consistent values shown, the combination of data for $C^{12}H_3Br^{79}$ and $C^{12}H_3Br^{81}$ or for $C^{13}H_3Br^{79}$ and $C^{13}H_3Br^{81}$ gives unreliable values for d_{CBr} somewhat less than those listed.

The average structure constants given in Table II may be seen to fit well into the sequence of decreasing values of d_{CH} and increasing values of ∠HCH found for the methyl fluoride to methyl iodide series.[1]

* This work was supported by a Frederick Gardner Cottrell grant and by a grant-in-aid from the University Center in Georgia.

[1] Gordy, Simmons, and Smith, Phys. Rev. **74**, 243 (1948).
[2] J. W. Simmons and W. E. Anderson, Phys. Rev. (to be published).
[3] G. Herzberg, *Infra-Red and Raman Spectra of Polyatomic Molecules* (D. Van Nostrand Company, Inc., New York, 1945), p. 31.

Spin Dependence of Neutron Scattering by Na^{23}

W. SELOVE*
Argonne National Laboratory, Chicago, Illinois
August 24, 1950

FROM recent measurements[1] it has been found that the "potential scattering" of Na^{23} for slow neutrons appears to be very strongly spin-dependent. Na^{23} has a nuclear spin I of $\frac{3}{2}$, so that there are two states of $Na^{23}+n$. The $J=2$ state has a cross section $\sigma_+\sim0.8$ barn; for the $J=1$ state, $\sigma_-\sim8.8$ barns. (The $\pm$ denotes $J=I\pm\frac{1}{2}$.) These values do not include statistical spin factors (see below).

This result was obtained in the following way. The reaction $Na^{23}+n$ has its first resonance, predominantly a scattering resonance, at a neutron energy of 3 kev. This is a much smaller energy than the average spacing between resonances, which is of the order[2] of 100 kev. It is therefore probably a good approximation to interpret interference effects (between "potential scattering" and "resonance scattering") in the region below 3 kev in terms of the 3-kev resonance alone, neglecting the effect of other resonances. Since the "strength" $\sigma_0\Gamma^2$ of the 3-kev resonance is known ($\sim16\times10^6$ barn-ev²), the detailed nature of the interference effects gives the magnitude of the potential scattering for the spin state associated with the resonance, and also for the other spin state. The specific identification of the spin states is possible both from additional information on the 3-kev resonance and from coherent scattering data.[1]

In greater detail, the procedure is as follows. The cross section for a free Na nucleus can be written as $\sigma=g_+\sigma_++g_-\sigma_-$, where g is the statistical spin factor, $(2J+1)/2(2I+1)$. Now the 3-kev resonance is known to belong to the "+" spin state—i.e., $J=2$. Then from the experimental cross-section data one finds that near zero energy the destructive interference between this resonance and the corresponding potential scattering gives a resultant σ_+ almost equal to zero. From this, we have that near zero energy (1) the total scattering cross section is approximately $g_-\sigma_-$ alone, (2) the value of $(g_+\sigma_+)_{pot}$ is approximately equal to $(g_+\sigma_+)_{\text{due to 3-kev resonance}}$. The latter is $\sim\sigma_0\Gamma^2/4E_r^2$, thus ~0.5 barn. If we now interpret $g_-\sigma_-$ as $(g_-\sigma_-)_{pot}$ (i.e., we assume there are no nearby resonances for $J=1$), then $(g_+\sigma_+)_{pot}\sim0.5$b, $(g_-\sigma_-)_{pot}\sim3.3$b. Since $g_+=\frac{5}{8}$ and $g_-=\frac{3}{8}$, this gives the result stated above, $(\sigma_+)_{pot}\sim0.8$b, $(\sigma_-)_{pot}\sim8.8$b.

It is of interest to compare these values with $4\pi R^2$, where R is the nominal nuclear radius, $1.5\times10^{-13}A^{\frac{1}{3}}$ cm. For sodium, $R=4.3\times10^{-13}$ cm and $4\pi R^2=2.3$b. It is seen that the effective nuclear radius for σ_+ is ~0.6 the nominal value, and the effective radius for σ_- is about twice the nominal value. Sodium is such a comparatively light nucleus, only about three nucleons in "diameter," that it is not too surprising to find the effective nuclear radius differing so greatly from the nominal value. However, it is quite unusual, and therefore rather interesting, to find such a large spin dependence in the scattering, with $\sigma_-/\sigma_+\sim11$.

One can interpret the spin dependence in terms of potential wells which for the two spin states have different depths but the same range. Using the crude model of rectangular wells of radius[3] 4.3×10^{-13} cm, the only reasonable values for the well depths which give the observed "scattering lengths" [4] are $V_+\sim17$ Mev, $V_-\sim24$ Mev. (No other values of V_+ or V_- between ~4 Mev and ~50 Mev give the observed values of the scattering lengths.) With this model the observed spin dependence can be regarded as due to a near-resonant condition in the potential scattering. (A potential-scattering resonance,[5] as opposed to a resonance in the compound nucleus, does not involve intimate interaction and binding-energy-sharing between the incident neutron and the individual nucleons of the target nucleus.)

The numerical values resulting from the rectangular well model should not be taken too seriously, of course. However, there is certainly a moderate difference in the potential wells representing the two spin states of $Na+n$. The magnitude of the spin effect recalls the well-known strong spin dependence for neutron-proton scattering. There may well be a correlation between the two cases. In this connection one should note that in the spin-orbit-coupling nuclear model, the last odd proton alone would be responsible for the total nuclear spin[6] of Na. In the spin-orbit-coupling model, in other words, the nucleus would be considered to consist of a "core," even Z-even N and with zero spin, plus a single proton; thus the spin dependence of scattering by Na would be entirely due to the spin dependence of the n–p interaction. Although there may be some element of truth in this representation, however, a model quite this simple is not correct. Its principal failing is that this "last-odd-particle" model, in which the spin of an odd-A nucleus is determined entirely by the orbit of the single unpaired nucleon, is definitely not satisfactory for Na. Na is one of the relatively few odd-A cases for which the predicted spin from this model does not agree with experiment—rather it seems that several particles are involved.

One might hope that other odd Z-even N nuclei would show a similar strong spin dependence for neutron scattering, and it is planned to investigate nuclei of this type and of other types further. It may be difficult to obtain information as to the spin dependence of potential scattering in many cases, however. In Na, the effect is large and the analysis fairly simple because of two fortuitous circumstances: the effect is large because the potential scattering is nearly resonant, and the separation of "potential" and "resonance" effects is fairly simple because the neutron energy at the first (compound-nucleus-) resonance is much smaller than the average spacing between resonances.

* Harvard University, Cambridge, Massachusetts.
[1] Hibdon, Muehlhause, Selove, and Woolf, Phys. Rev. **77**, 730 (1950).
[2] Adair, Barschall, Bockelman, and Sala, Phys. Rev. **75**, 1,124 (1949).
[3] This value is taken from the approximation $1.5\times10^{-13}A^{\frac{1}{3}}$.
[4] E. Fermi and L. Marshall, Phys. Rev. **71**, 666 (1947).
[5] The term "potential-scattering resonance" may appear to be self-contradictory, but is not: such a resonance is very broad as compared to compound-nucleus-resonances, so that even near a potential-scattering resonance the value of σ_{pot} varies relatively slowly—e.g., σ_{pot} could very well not vary much over a range of tens or hundreds of kilovolts.
[6] M. G. Mayer, Phys. Rev. **78**, 16, 22 (1950).

Production of Positive Mesons by Photons on Hydrogen*

A. S. BISHOP, J. STEINBERGER, AND LESLIE J. COOK
Radiation Laboratory, Department of Physics, University of California, Berkeley, California
August 8, 1950

A SHORT time ago we reported some features of the production of mesons on carbon and hydrogen by photons.[1] The hydrogen cross sections had been obtained by a paraffin-carbon subtraction. The experiment has been repeated, using the same counting technique, but liquid hydrogen as a target. The new data have better energy resolution and statistical accuracy.

The reaction is $\gamma+P\rightarrow\pi^{+}+N$. The photons are produced in the Berkeley synchrotron with a bremsstrahlung spectrum of 330-Mev maximum energy. In the experiment both meson range and angle of production with respect to the beam are measured. The energy of the meson is computed by means of the range-energy relation, and that of the responsible photon by the conservation laws. It is possible, therefore, to measure cross sections as a function of photon energy, despite the continuous character of the x-ray spectrum.

Figure 1 shows the energy spectrum of mesons produced at 90° to the beam direction, as well as the number of photons as a function of the energy of the mesons which they produce. The

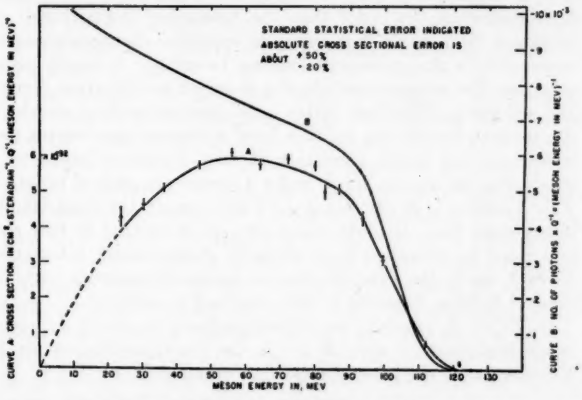

FIG. 1. Energy distribution of π^{+}-mesons at 90° from hydrogen. Also shown is the energy distribution of the photons responsible for meson production (see text). The quantity Q is defined to be the energy in the x-ray beam divided by the maximum photon energy.

x-ray spectrum is the theoretical bremsstrahlung spectrum[2] corrected for: (a) thickness of target producing the x-rays, (b) variation of electron energy due to variations in the magnetic field of the synchrotron during the 2×10^{-8}-sec. period of x-ray emission, (c) angular resolution of the meson production angle.[3]

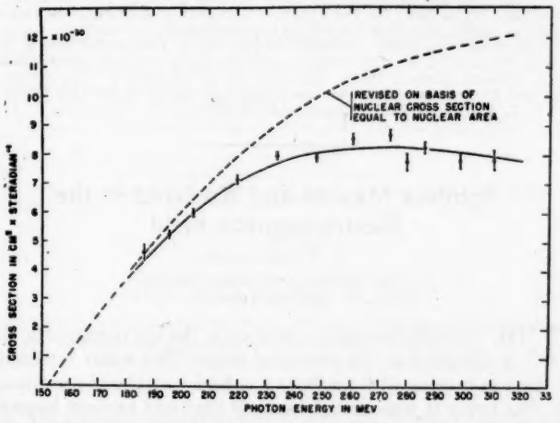

FIG. 2. Excitation function for the photo-production of π^{+}-mesons at 90° from hydrogen, with and without correction for nuclear absorption.

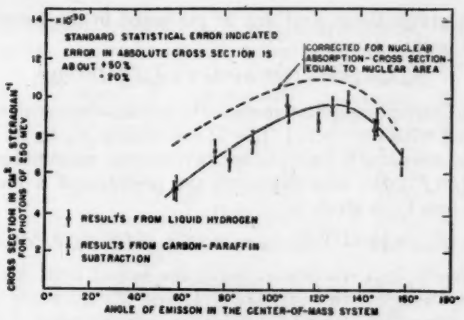
STANDARD STATISTICAL ERROR INDICATED
ERROR IN ABSOLUTE CROSS SECTION IS ABOUT +50% -20%
CORRECTED FOR NUCLEAR ABSORPTION - CROSS SECTION EQUAL TO NUCLEAR AREA
RESULTS FROM LIQUID HYDROGEN
RESULTS FROM CARBON-PARAFFIN SUBTRACTION
ANGLE OF EMISSION IN THE CENTER-OF-MASS SYSTEM

FIG. 3. Angular distribution (in center-of-mass system) of π^{+}-mesons produced in hydrogen by 250-Mev photons (laboratory system), with and without corrections for nuclear absorption.

Dividing the meson spectrum by the photon spectrum, one obtains the cross section for meson production at 90° in the laboratory system as a function of photon energy (Fig. 2) One source of error is the nuclear absorption of the mesons, which discriminates against the higher energy mesons. It is improbable that the nuclear absorption proceeds with larger cross section than nuclear area. To show the upper limit of this effect, we include in Fig. 2 the excitation function, revised on the basis that the nuclear absorption cross section is equal to the nuclear area.[4]

The angular distribution of mesons produced by 250-Mev photons is shown in Fig. 3 together with the older results.[1] Since no attempt has yet been made to obtain an accurate absolute cross section, the results from the two experiments were normalized in absolute magnitude to give the best fit. As has already been pointed out, the angular distribution shows clearly that photo-meson production is not a dipole photo-effect, as predicted by scalar meson theory, but that the interaction of the nuclear spin with the photon must play an important role.

A full account of these experiments, together with a discussion of their theoretical significance, is being prepared.

We are indebted to Dr. V. Z. Peterson for the use of his hydrogen target in the angular distribution measurements, and to Professor E. M. McMillan for stimulating discussions about this work. The bombardments were carried out by the synchrotron crew under the direction of W. Gibbins and G. McFarland.

* This work was performed under the auspices of the AEC.
[1] J. Steinberger and A. S. Bishop, Phys. Rev. 78, 494 (1950).
[2] This spectrum has been checked and shown to be correct within the accuracy of their experiment by Hartsough, Hill, and Powell (to be published).
[3] Since the meson production angle enters into the correspondence between photon and meson energies, any lack of angular resolution will result in a dispersion in the photon energy in this analysis.
[4] The cross section for producing nuclear events at high meson energies is approximately equal to the nuclear area, according to the experiments of Camerini, Fowler, Lock, and Muirhead, Phil. Mag. 41, 413 (1950).

On the Gravitational Self-Energy of Light

S. B. NILSSON AND K. V. LAURIKAINEN*
Institute of Mechanics and Mathematical Physics, University of Lund, Lund, Sweden
August 22, 1950

ONE of the well-known divergence difficulties in the quantum theory of fields relates to the gravitational effects of light. Indeed, Rosenfeld's result[1] for the self-energy of a photon due to its gravitational field is not only infinite, but the formal expression does not transform as the fourth component of a vector.

To elucidate this point, the problem was taken up using the invariant methods of Schwinger[2] and others, with the following results (in first approximation). (1) The vacuum expectation value of the energy-momentum tensor (properly, pseudotensor) of the

ensuing gravitational field can be expressed in the formally covariant form:

$$\langle t_{\mu\nu}\rangle_0=\tfrac{1}{2}\hbar^2c^2\kappa[(2\partial^2/\partial x^\mu\partial x^\nu)-d_{\mu\nu}\Box]D^{(+)}(0)^2, \quad (1)$$

κ being Einstein's gravitation constant and $d_{\mu\nu}$ the metrical tensor of special relativity ($=1, 1, 1, -1$; coordinates: $x_1, x_2, x_3, x_0=ct$). (2) The one-particle part of the gravitational momentum vector $P_\mu=(1/c)\int t_{\mu 0}dV$, resulting from the presence of a photon of momentum k_μ, is given by

$$\langle P_\mu\rangle_1=\tfrac{1}{2}\hbar c\kappa D^{(1)}(0)\cdot k_\mu+(\hbar^2c\kappa/2k_0)\partial^2D^{(1)}(0)/\partial x^\mu\partial x_0. \quad (2)$$

Evidently, in a relativistic theory the second term in (2) must vanish. Though both expressions (1) and (2) are really indeterminate (singular), a simple invariance argument, using $\Box D^{(1)}=0$, does indeed show that all second derivatives of $D^{(1)}$ should be chosen equal to zero at the origin. Unfortunately, we have no unique way of handling calculations with singular functions so as to insure the results demanded by invariance. Thus a straightforward evaluation in terms of momentum integrals will yield Rosenfeld's non-invariant expression.[1] A regularization in the sense of Pauli and Villars[3] is effective only if the regularized $D^{(1)}$-function satisfies $\Box D_R^{(1)}(0)=0$, which now appears as an additional assumption.

The remaining term in (2) corresponds to the mass-renormalization of the electron. In the present case this term can be made to vanish, either by symmetry arguments or by a suitable regularization. In all, we should then need the regularization conditions:

$$D_R^{(1)}(0)=0, \quad \Box D_R^{(1)}(0)=0 \quad (3)$$

(which entail those of Pauli and Villars, but are more restrictive). Anyway, a regularization of the vacuum part (1) is not so simple (for reasons of symmetry the value could be taken to be zero).

A more detailed account will be published in the *Arkiv för fysik*.

We wish to express our gratitude to Professor T. Gustafson, who has stimulated this investigation, and who has arranged to make it possible for one of us (K.V.L.) to visit his Institute.

* Permanent address: Technical Institute, Turku, Finland.
[1] L. Rosenfeld, Zeits. f. Physik **65**, 589 (1930).
[3] J. Schwinger, Phys. Rev. **74**, 1439 (1948); Phys. Rev. **75**, 651 (1949), *q.v.* for the definition of the singular functions used here.
[3] W. Pauli and F. Villars, Rev. Mod. Phys. **21**, 434 (1949).

Spinless Mesons in the Electromagnetic Field

P. T. MATTHEWS*
Clare College, Cambridge, England
May 19, 1950

THE use of renormalization in the S-matrix for spinless mesons in the electromagnetic field is considered by Dyson's method.[1]

The Hamiltonian is[2]

$$H=\frac{ie}{\hbar c}A_\mu\left(\phi^*\frac{\partial\phi}{\partial x_\mu}-\frac{\partial\phi^*}{\partial x_\mu}\phi\right)-\left(\frac{ie}{\hbar c}\right)^2\phi^*\phi A_\tau A_\rho\delta_{\tau\rho}-\left(\frac{ie}{\hbar c}\right)^2\phi^*\phi(A_\mu n_\mu)^2. \quad (1)$$

ϕ^* creates charge and ϕ annihilates charge, and (Dyson's notation is used throughout.)

$$\langle P[\phi(x),\phi^*(y)]\rangle_0=\tfrac{1}{2}\hbar c\Delta_F(x-y). \quad (2)$$

One can ignore,[3] without introducing any error, the n_μ-dependent term in (1) and in the equation corresponding to (2) but involving derivatives of both ϕ and ϕ^*. In a graph, the first term of H operates at a 3-vertex, the second term at a 4-vertex. The meson lines are directed. The corresponding S-matrix element is obtained by an argument similar to that for electrodynamics:[1]

(i) Each internal photon line gives a factor

$$\hbar c\delta_{\mu\nu}(2\pi)^{-3}\int D_F(p^i)d^4p^i.$$

(ii) Each internal meson line gives a factor

$$\hbar c(2\pi)^{-3}\int\Delta_F(p^i)d^4p^i.$$

(iii) Each 3-vertex gives a factor

$$ie(\hbar c)^{-2}(2\pi)^4(p_\mu{}^1+p_\mu{}^2)\delta(p^1-p^2+p^3),$$

where p^1 and p^2 are the 4-vectors of the meson lines entering and leaving the vertex, respectively.

(iv) Each 4-vertex gives a factor

$$-ie^2(\hbar c)^3(2\pi)^4\delta_{\tau\rho}\delta(p^1-p^2+p^3+p^4).$$

(v) Each external photon line gives $A_\mu(k^i)$, each external meson line entering or leaving gives $\phi(k^i)$ or $\phi^*(k^i)$, respectively.

(vi) The whole integral is multiplied by the number of different ways the operators can be paired off by interchanging the roles of the photon operators at the 4-vertices.[4]

The primitive divergents must satisfy

$$E_m+E_p<5. \quad (3)$$

The genuine primitive divergents are the same as in electrodynamics with the addition of $E_m=2$, $E_p=2$, to be called C-parts (Compton scattering), and $E_m=4$, $E_p=0$, M-parts (Møller interaction). The self-energy and vertex parts again modify the factors from single lines or single 3-vertices. The divergent C-parts can similarly be regarded as modifications of a 4-vertex. The quadratic divergences from meson self-energy parts are removed by mass renormalization. In order that the remaining (logarithmic) divergences from these four types of primitive divergents can be removed by a charge renormalization, to order e^4, it is only necessary that the infinite multiple of a 4-vertex coming from C-parts and self-energy insertions (after mass renormalization) should be the same as the infinite multiple from self-energy and vertex part insertions in a graph consisting of two 3-vertices joined by a meson line (since this graph and a 4-vertex are each of order e^2). *This condition is in fact satisfied.*[5] There remain the (logarithmic) divergences from M-parts which cannot be treated in this way, and must be cancelled by a suitably chosen direct interaction, $\delta\lambda\phi^2\phi^{*2}$, as in the case of spinless mesons interacting with nucleons.[6] A finite S-matrix is then obtained to order e^4.

If $(Z_1')^{-1}$, Z_2', and Z_3' are defined similarly to $(Z_1)^{-1}$, Z_2, and Z_3 in electrodynamics[1] and $(Z_4')^{-1}$ is the corresponding factor for 4-vertex parts, the general condition required is

$$(Z_1')^{-2}Z_2'=(Z_4')^{-1}. \quad (4)$$

We have shown that to order e^2, $Z_1'=Z_2'=Z_4'$.

* Now at the Institute for Advanced Study, Princeton, New Jersey.
[1] F. J. Dyson, Phys. Rev. **75**, 486, 1736 (1949).
[2] S. Tomonaga and S. Kanesawa, Prog. Theor. Phys. **3**, 1, 101 (1948). Alternatively, one can work in the interaction representation in the Heisenberg-Pauli formalism. In the calculation of the S-matrix this differs from the σ-formalism only in the form of the terms which can safely be ignored (reference 3).
[3] P. T. Matthews, Phys. Rev. **76**, 684, 1419 (1949).
[4] These rules are essentially the same as those given by Feynman [R. P. Feynman, Phys. Rev. **76**, 769 (1949)]. The author is grateful to Drs. D. Feldman and F. Rohrlich for helpful correspondence on rule (vi).
[5] This result was given non-relativistically by E. Corinaldesi and R. Jost [Helv. Phys. Acta **21**, 183 (1948)], and has been obtained relativistically by a different method by F. Rohrlich (to be published). The author is indebted to Professor Pauli for informing him of Dr. Rohrlich's result.
[6] P. T. Matthews, Phil. Mag. **41**, 185 (1950).

Spinless Mesons and Nucleons in the Electromagnetic Field

P. T. MATTHEWS
Clare College, Cambridge, England
May 19, 1950

THE S-matrix for spinless mesons in the electromagnetic field is discussed in the preceding letter.[1] The scalar interaction of spinless mesons with nucleons has been considered previously.[2] In that paper it was wrongly stated[3] that odd nucleon loops are excluded by a type of Furry theorem.[4] However, it follows from charge conservation that *the number of external charge bearing lines*

in any part must be even. Thus such parts, and in particular primitive divergents of this type, are excluded for *charged* mesons. But the general treatment of divergences in that paper is not complete, even for charged mesons, as there are secondary divergences from parts built up of $\delta\lambda$-vertices which have not been considered.[3] These difficulties arise only in high orders, (f^8), so that with the direct use of Dyson's work[5] it is now simple to set up in this way the combined interaction of charged spinless mesons, nucleons (scalar interaction), and the electromagnetic field.

The Hamiltonian for pseudoscalar mesons is

$$H=\Sigma H_i \quad (i=1, 2, 3),$$

where

$$H_1=\frac{ie}{\hbar c}A_\mu\left(\phi^*\frac{\partial\phi}{\partial x_\mu}-\frac{\partial\phi^*}{\partial x_\mu}\phi\right)-\left(\frac{ie}{\hbar c}\right)^2 A_\mu{}^2\phi^*\phi,$$

$$H_2=if\bar{\psi}\gamma_5(\tau_-\phi^*+\tau_+\phi)\psi+\delta\lambda\phi^{*2}\phi^2,$$

$$H_3=ie\bar{\psi}\gamma_\mu\tau_P\psi A_\mu.$$

The n_μ-dependent and mass renormalization terms have not been included. For scalar mesons $(\gamma_5)_{\alpha\beta}$ is replaced by $-i\delta_{\alpha\beta}$.

The primitive divergents must satisfy

$$\tfrac{3}{2}E_n+E_m+E_p<5.$$

This cannot be satisfied unless at least one term on the left-hand side is zero. Using the charge conservation rule, it can be shown that the genuine primitive divergents are the same as for the separate pairs of interacting fields,[1,2,5] but new internal structures are now possible. Since, for example, a proton-photon vertex part may depend on both e and f, the renormalized constants are double power series in e and f.

Considerations are now restricted to S-matrix elements of fourth order in the coupling constants. The $\delta\lambda$-term is chosen to cancel the (logarithmic) divergence from the scattering of mesons by mesons. All quadratic and linear divergences are removed by mass renormalization. In order that all the remaining (logarithmic) divergences can be removed by the renormalization of the constants e and f it is necessary that certain conditions be satisfied. The charge renormalization is determined by the infinite constants in Δ_F', D_F' and the meson photon 3-vertex parts. It must be shown that this renormalization is (i) identical with that determined by the infinite constants in S_F', D_F', and Γ_μ (the proton-photon interaction), and (ii) that it also removes the divergences from C-parts. Each of these conditions contains terms in e^2 and f^2, so they are together equivalent to four conditions. It must also be shown (iii) that the infinities from parts with two external neutron lines and one external photon line exactly cancel, since there is no simple vertex of this type and no renormalization is possible.[6] It has been checked by direct calculation that *all these conditions are satisfied both for scalar and pseudoscalar mesons.*

Although this result appears to be purely fortuitous in our work, it certainly suggests that some general principle is operative which might make renormalization effective to any order for this three-field mixture.

The author would like to thank Mr. Salam for stimulating discussions.

[1] P. T. Matthews, preceding letter.
[2] P. T. Matthews, Phil. Mag. **41**, 185 (1950).
[3] The author is further indebted to Dr. Feldman for pointing out these errors.
[4] W. H. Furry, Phys. Rev. **51**, 125 (1937).
[5] F. J. Dyson, Phys. Rev. **75**, 486, 1736 (1949).
[6] These graphs give the neutron magnetic moment and were discussed by K. M. Case, Phys. Rev. **76**, 1 (1949).

The Radioactivity of Am^{242}

G. D. O'KELLEY, G. W. BARTON, JR., W. W. T. CRANE, AND I. PERLMAN
Radiation Laboratory and Department of Chemistry, University of California, Berkeley, California*
August 28, 1950

THE neutron irradiation of 475-yr. Am^{241} results in the production of a pair of isomers,[1,2] Am^{242m} with 16-hr. half-life known to decay by β^--emission, and a long-lived ground state, Am^{242}, which is also a β^--emitter and has weak alpha-branching. Since fairly strong activities can be prepared by pile neutron irradiation of small quantities of Am^{241}, it became feasible to examine the radiations, particularly those of Am^{242m}, with beta-ray and x-ray spectrometers. When this was done only was the β^--transition characterized, but good evidence was obtained that in addition this isomer undergoes appreciable branching decay by isomeric transition and by electron capture.

The electron-capture branching results in the long-lived plutonium isotope, Pu^{242}, which was found with a mass spectrograph upon examination of the plutonium fraction from a sample of americium which had been subjected to long neutron irradiation.[3]

Much of the information on the modes of decay of Am^{242m} was derived from a bent crystal x-ray spectrometer used to analyze the L x-ray mixture. This instrument and its use in measuring the L-series x-rays accompanying radioactive decay in the heavy element region are described in another publication.[4] When the irradiated Am^{241} was observed with the x-ray spectrometer, L-series x-rays of curium (96), americium (95), plutonium (94), and neptunium (93) were identified, among which the $L\beta_1$-, $L\beta_2$-, $L\alpha_1$-, and $L\gamma_1$-lines were in greatest abundance. The curium, americium, and plutonium x-rays decayed with a 16-hr. half-life but the neptunium x-ray intensity did not decrease over a period of several days. The origin of the x-rays are presumably as follows: those of curium from an internal conversion process following the β^--transition, the americium x-rays from internal conversion in the isomeric transition of Am^{242m}, the plutonium x-rays following electron-capture decay, and the neptunium x-rays (which did not decay) following the internal conversion of a γ-ray known to exist in the alpha-decay[1] of Am^{241}. Table I lists the principal x-ray lines observed, their measured energies and relative intensities, and the energies calculated using the Moseley relation in a manner described elsewhere.[4] The complete x-ray spectra and other decay properties of Am^{242} will be discussed more fully at a later date. It is worth noting, however, that for a particular level vacancy, the ratios of intensities of different lines are about the same (as they should be), and that the relative incidence of L_{II} and L_{III} lines are roughly equal both for the plutonium and curium x-rays, but those from the isomeric transition (americium x-rays) show the L_{III} level x-rays to be about five times as abundant as those from the L_{II} level. Selection rules are probably in force here which are responsible for the selection of the L_{III} level (a $p_{\frac{3}{2}}$ state) and for a long lifetime of the metastable state.

TABLE I. Principal x-ray lines in decay of Am^{242m}.

X-ray line designation		Level transition	Measured energy	Relative intensity (corrected)[a]	Calculated energy
Pu	$L\alpha_1$	$L_{III}-M_V$	14.33 ±0.01	68	14.31
	$L\beta_2$	$L_{III}-N_{IV}$	17.32 ±0.02	22	17.29
	$L\beta_1$	$L_{II}-M_{IV}$	18.34 ±0.02	54	18.30
	$L\gamma_1$	$L_{II}-N_{IV}$	21.52 ±0.05	18	21.43
Am	$L\alpha_1$		14.66 ±0.02	39	14.66
	$L\beta_2$		[b]		
	$L\beta_1$		18.90 ±0.07	8	18.84
	$L\gamma_1$		[b]		
Cm	$L\alpha_1$		15.01 ±0.01	100	15.00
	$L\beta_2$		18.13 ±0.04	36	18.08
	$L\beta_1$		19.48 ±0.02	107	19.38
	$L\gamma_1$		22.78 ±0.07	33	22.68

[a] Estimated corrections for crystal and counter window absorption and reflection intensity variation with energy.
[b] Not resolvable from other lines.

The β^--ray spectrum of Am^{242m} was taken with a 255°-shaped magnetic field β-ray spectrometer using a resolution of three percent. The Fermi-Kurie plot of the continuous β^--spectrum showed an end point of 628±5 kev. Two sets of L conversion lines were seen corresponding to gamma-rays of 38 kev and 52 kev, assuming the former to be a plutonium γ-ray and the latter from curium. In attempting to assign these gamma-rays to the several transitions, the differences between L_{II} and L_{III} lines were matched with expected differences of the edges for plutonium, americium, and curium. The assignments on this basis are not

conclusive, since the differences in spacing between successive elements are about the same as the experimental uncertainties of electron energies. Tentatively, as indicated above, the 52-kev γ-ray is assigned to the β^--transition and the 38-kev γ-ray to the electron-capture transition. This leaves unaccounted for the origin of the x-rays of americium, so if the above assignments are to be taken seriously, the conversion electrons accompanying the isomeric transition must lie among the Auger electrons. There is some evidence that this is the case.

Lead and copper absorption curves showed no hard γ-rays or K x-rays and only the 50-kev soft γ-ray. When compared with the abundance of the conversion electrons, this γ-ray appears to be about 50 percent converted.

From arguments (not all consistent) based on relative abundances of x-rays, conversion electrons, and the β^--particles, Am^{242m} appears to decay about 60 percent by β^--emission, 20 percent by L-electron capture, and 20 percent by isomeric transition. All three of the modes of decay give rise to L-series x-rays which, when properly assigned and abundances measured, should aid materially in arriving at a decay scheme and in shedding light on the nuclear processes which result in the particular x-rays of this interesting nucleus.

The β^--particle of the ground state of Am^{242} has also been measured, but the accuracy of the end point has not yet been determined with desirable accuracy. The value obtained is 580 ± 30 kev which is consistent with the supposed 52 kev associated with the isomeric transition of Am^{242m}.

* This work was performed under the auspices of the AEC.

[1] Seaborg, James, and Morgan, *The Transuranium Elements: Research Papers* (McGraw-Hill Book Company, Inc., New York, 1949), Paper No. No. 22.1, National Nuclear Energy Series, Plutonium Project Record, Vol. 14B.

[2] W. M. Manning and L. B. Asprey, loc. cit., Paper No. 22.7.

[3] Thompson, Street, Ghiorso, and Reynolds, University of California Radiation Laboratory Report, UCRL-657 (June, 1950), to be submitted for publication.

[4] Barton, Robinson, and Perlman, to be submitted for publication.

On Sommerfeld's Surface Wave

C. J. Bouwkamp
Philips Research Laboratories, Eindhoven, Netherlands
October 24, 1949*

NUMEROUS papers on the theory of propagation of electromagnetic waves over plane earth have appeared, following Sommerfeld's celebrated paper[1] of 1909. Though it has been realized by subsequent authors that Sommerfeld's discussion of his basic equation for the vector potential of a vertical electric dipole in the presence of the earth is not quite satisfactory, this equation itself was generally accepted. However, in 1947 Epstein[2] proposed a new solution. As I have pointed out elsewhere[3] Epstein's expression for the vector potential is incompatible with the physical situation because it is singular along the whole axis of the dipole, whereas Sommerfeld's solution is regular outside the dipole. In fact, Epstein's solution is nothing but Sommerfeld's solution minus the surface wave.

The surface-wave problem was reconsidered by Kahan and Eckart. In their first note[4] these authors accepted Epstein's solution as being the only one compatible with Sommerfeld's radiation condition,[5] though they only showed that the surface wave does not fulfill this condition. It is, of course, immaterial whether some part (e.g., the surface-wave term) of Sommerfeld's solution does or does not satisfy the radiation condition. The behavior of the complete solution is conclusive.

In a second note,[6] Eckart and Kahan come to the conclusion that Epstein's solution is incorrect, though they fail to mention that they were of a different opinion in their first note.[4] They now accept Sommerfeld's original solution and point out that Sommerfeld's evaluation of the integral along the branch cut is in error. They stress that a correct evaluation would have yielded an expression that contains the surface wave with negative sign, so that the final result would have coincided with Weyl's result,[7] the negative surface-wave term being cancelled by the positive term due to the residue of the pole of the integrand. This explanation and clarification of the controversy is not at all new but has been known since 1937 through the work of Wise[8] and Rice.[9]

In two longer papers,[10,11] of which the last is apparently an English version of the first, Kahan and Eckart elaborate their previous discussions. In view of the foregoing arguments it will be evident that a detailed analysis of these papers is unfruitful. Let it be sufficient to mention, therefore, that the only new and interesting part of these two papers consists in an attempt to prove a uniqueness theorem on the basis of Sommerfeld's radiation condition, for real-valued wave numbers k_1 and k_2. Unfortunately, their proof breaks down, as one can demonstrate from Eq. (24) of reference 11. The left-hand member of this equation is a space integral of which the imaginary part is zero. The right-hand member is a surface integral of which the real part is zero. It is important to note that Eq. (24) is only valid in the limit $R\rightarrow\infty$. It is true that both members of Eq. (24) tend to zero as $R\rightarrow\infty$. Consequently, Ru_1 and Ru_2 tend to zero if R tends to infinity. This is the only important conclusion that can be drawn from Eq. (24). It cannot be inferred that u_1 and u_2 vanish identically, because the left-hand member, though equal to zero, consists of a sum of positive and negative terms. Whereas in many problems Sommerfeld's condition $\lim_{R\rightarrow\infty}R(\partial u/\partial R-iku)=0$ is sufficient, and $Ru\rightarrow0$ superfluous, this does not hold in the presence of an infinite plane earth, as is apparent from Rellich's paper.[12] If the earth is infinite, Sommerfeld's conventional form of the radiation condition does not apply at all, and even Rellich's theorem[12] is not applicable to a *plane* earth.

* Revised manuscript received August 28, 1950.

[1] A. Sommerfeld, Ann. d. Physik **28**, 665 (1909).
[2] P. S. Epstein, Proc. Nat. Acad. Sci. **33**, 195 (1947).
[3] C. J. Bouwkamp, Math. Rev. **9**, 126, 637 (1948).
[4] T. Kahan and G. Eckart, Comptes Rendus **226**, 1513 (1948).
[5] See A. Sommerfeld, Vorlesungen über theoretische Physik (Wiesbaden, 1947), Vol. 6, p. 192.
[6] G. Eckart and T. Kahan, Comptes Rendus **227**, 969 (1948).
[7] H. Weyl, Ann. d. Physik **60**, 481 (1919).
[8] W. H. Wise, Bell Sys. Tech. J. **16**, 35 (1937).
[9] S. O. Rice, Bell Sys. Tech. J. **16**, 101 (1937).
[10] T. Kahan and G. Eckart, J. de phys. et rad. **10**, 165 (1949).
[11] T. Kahan and G. Eckart, Phys. Rev. **76**, 406 (1949).
[12] F. Rellich, Jahresber. d. Deutsch. Math. Ver. **53**, 57 (1943).

On the Transport of Aluminum Atoms by a Gas

Michel Ter-Pogossian, Fred T. Porter, and C. Sharp Cook
Physics Department, Washington University, St. Louis, Missouri*
August 28, 1950

A SYSTEM which provides for the continuous flow of radioactive gas[1] between a duraluminum bombardment chamber at the cyclotron and a 14-cm radius of curvature magnetic spectrometer[2] has been in operation in this laboratory for several months. Because of the distance between the cyclotron building and the physics laboratory where the spectrometer is located, it is necessary to circulate the gas between these two buildings through underground copper pipes. The total length of pipe between the bombardment chamber at the cyclotron and the beta-ray spectrometer is 600 feet. An experimentally measured time of 16 seconds is required for the gas to travel through this length of pipe.

One of the most interesting facts discovered to date while using this system is that an activity which can be attributed to Al^{28} can be carried through the system in appreciable quantities. The fact that the activity belongs to aluminum has been verified in a number of ways. The maximum beta-ray end-point energy (2.8 Mev according to our measurements) and the half-life (127 seconds) of this activity as measured at the magnetic spectrometer end of the system agree quite closely with previously reported[3] values for Al^{28}. The activity appears to be produced because of the duraluminum construction of the bombardment chamber and the window separating the main vacuum system of the cyclotron from this chamber. The cyclotron beam (10 Mev, 100 μamp. for

these experiments) passes through this window. The largest percentage of the activity seems to come from the window since the substitution of a thin copper window reduces the negatron activity attributable to Al^{28} to negligible quantities. Aluminum atoms appear to enter the system's circulating gas as recoils ejected from the duraluminum by the cyclotron beam. So long as the duraluminum window is used, the existence of helium, nitrogen, oxygen, or carbon dioxide as the system's gas results in identical negatron spectra indicating that the source of the negatrons is in no way connected with the gas which is being circulated.

The method of transport of the aluminum atoms between the bombardment chamber and the spectrometer is still in doubt. It has been suggested that they may be carried on very small dust particles which act as a colloidal suspension in the circulated gas and which are too small to be removed from the gas by the filters used in the line.

The fact that no 5-min. Cu^{66} is present when a copper window is used in the cyclotron may mean that the transport phenomenon is characteristic of aluminum. Windows made from other elements have not been used as yet. However, a study of such effects for several types of windows is planned.

The work is continuing and further details will be published at a later date.

* Assisted by the joint program of the ONR and AEC.
[1] Ter-Pogossian, Porter, and Cook, Phys. Rev. **79**, 244 (1950).
[2] Ter-Pogossian, Cook, Goddard, and Robinson, Phys. Rev. **76**, 909 (1949).
[3] Benes, Hedgran, and Hole, Arkiv f. Mat. Astro. Fysik, **35A**, No. 12 (1948).

The Structure and Chemical Composition of Mars

HAROLD C. UREY
Institute for Nuclear Studies, University of Chicago, Chicago, Illinois
August 21, 1950

THE radius of Mars usually quoted[1] is 0.532 times that of the earth. The measured values of this quantity since Hartwig[2] have agreed rather closely with this value. Wright and Trumpler[3] showed that Mars has a substantial atmosphere by photographing the planet in infra-red, yellow, violet, and ultraviolet light, and the latter determined what he believed to be the radius of the planet's surface from the movement of the marking on its surface. His value for this radius is 0.521. The mass has recently been determined by Rabe[4] from the perturbations of the orbit of Eros. His value for the mass is 0.1069 times the earth's mass. Struve[5] deduced the oblateness of Mars from the orbital constants of the satellites and secured 1/190.4, which corrected for the smaller radii became 1/192. Thus, the ratio of the oblateness, ϵ, to the ratio of centrifugal to gravitational forces at the equator, Φ, can be calculated. The value using the larger radius is 1.13 and using the smaller radius is 1.21. The latter value is close to the value for a planet of uniform density, namely, 1.25.

The value of ϵ/Φ can be calculated for a planet of known or assumed density distribution.[6] From Bullen's[7] values for the density of the earth as a function of pressure one finds that

$$\rho=\rho_0+2.05\times10^{-12}p,$$

where ρ_0 depends on composition, and the coefficient of the pressure term is insensitive to composition.[8] The pressure within a planet of uniform density is, $p=(4\pi/6)G\rho_m^2(a^2-r^2)$, where G is the gravitational constant, ρ_m is the mean density, a is the radius of the planet, and r is the distance from the center. Substitution of this for the pressure gives ρ as a function of r. The expression for the mass is easily written down and determines ρ_0 as 3.96. The moment of inertia is 0.394 Ma^2 and it is now possible to calculate ϵ/Φ by well-known relations. The result using Trumpler's radius is 1.22. Brown[9] has calculated this quantity for a model of Mars with an iron core similar to that of the earth and found ϵ/Φ to be equal to 1.02, as compared with an observed value of 1.14, using the usually accepted value of the radius and older mass value. He concluded that the silicate and iron phases are not so completely separated as are those of the earth. Trumpler's smaller and more probable value for the radius thus indicates that Mars is a planet of grossly uniform composition and its density at zero pressure indicates that it contains about 30 percent of iron-nickel phase.

This calculation substantiates the suggestion made by the writer[10] that the primitive earth was composed of a grossly uniform mixture of iron-nickel metallic and silicate phases. The earth's core has grown during geological time and that of Mars has not. The difference is probably due to the difference in initial temperatures. That of the earth was high enough to permit convection currents which generated heat and melted its iron, which then flowed to the core, while the temperature of Mars was too low and it remains a fossil planet furnishing evidence in regard to the earth's past history. This as well as other evidence for this conclusion will be presented in greater detail elsewhere.

Trumpler's value for the oblateness, namely 0.0108(=1/93) determined from the measurements of the polar and equatorial diameters and also from observations on the movement of points on the surface agrees with other similar observations but not with Struve's value derived from the motions of the moons. He suggests that some atmospheric effects are responsible for the difference. If the equatorial regions are mountainous relative to the polar regions, the observations could be reconciled with Struve's value, since the moons would recognize the mean oblate spheroid only and Trumpler may have selected mountain tops as his point and the observed disk would be determined by mountains. Again, if the density is not spherically symmetrical and, say, higher in the polar regions and isostatic equilibrium has been attained, the non-rotating planet would be oblate but the moons would not recognize this oblateness. They would recognize only the oblateness due to rotation. A variation of 0.5 percent in the density would account for the disagreement. The atmospheric pressure at the polar surface would be twice that at the equatorial surface, but this probably would not be in disagreement with observation. A combination of these two effects is also possible and both might be caused by some spherically non-symmetrical character of the accumulation process that produced the planet. It appears to the writer that Struve's value is the correct one for the calculations reported here.

[1] Russell, Stewart, and Dugan, *Astronomy* (New York, 1945).
[2] E. Hartwig, Publ. der Astron. Gesell, **15**, 1–87 (1879). D. Reuyl, Astronomy J **49**, 125 (1941). P. van de Kamp, Astronomy J **38**, 61 (1928).
[3] W. H. Wright, Lick Obs. Bull. **12**, 48 (1925). R. J. Trumpler, Licks Obs. Bull. **13**, 19 (1927).
[4] E. Rabe, Astronomic J. **55**, 112 (1950).
[5] H. Struve, Astron. Nach. **138**, 217 (1895); Sitzungsber. Berlin Akad. **2**, 1056 (1911).
[6] H. Jeffreys, *The Earth* (Cambridge, 1929), p. 215, Eqs. (15) and (22).
[7] K. E. Bullen, Trans. Roy. Soc. New Zealand **67**, 122 (1938); Bulletin Seismological Soc. Am. **30**, 235 (1940); **32**, 19 (1942).
[8] This has been derived by the writer in connection with a study of the earth which will be published elsewhere.
[9] H. Brown, Astrophys. J. **111**, 641 (1950).
[10] H. C. Urey, Science **110**, 445 (1949).

Spectroscopic Value of the Magnetic Moment of $_{83}Bi^{209}$

F. M. KELLY, R. RICHMOND, AND M. F. CRAWFORD
McLennan Laboratory, University of Toronto, Toronto, Canada
August 18, 1950

PREVIOUSLY quoted values of the nuclear magnetic moment of Bi^{209} have been derived from hyperfine structure separations of only a few levels. The derivations have included an approximate Fermi-Segrè correction,[1] but no correction for the finite size of the nucleus.[2] Hyperfine structures in many lines of Bi II, III, IV, and V, excited in an electrodeless discharge, have been measured in this laboratory by Richmond[3] using a 21-ft. concave grating. From the separations of 14 levels of Bi III, IV, and V the nuclear magnetic moment has been calculated by the Goudsmit formula.[4] When the Fermi-Segrè correction evaluated by the

TABLE I. Nuclear magnetic moment of Bi^{209}.

Spectrum	Term	Interval factor cm^{-1}	$1-d\sigma/dn$	μ^0	μ	Average
Bi V	$6s$	2.6	1.14	3.57	4.2	
	$7s$	0.773	1.04	3.47	4.11	4.11
	$7p_{1/2}$	0.207		3.52	3.71	
Bi IV	$6s7s$	1.556		3.48	4.12	
	$6s8s$	1.429		3.55	4.21	
	$6s6d\ 5_1$	−0.589		3.30	3.91	4.14
	$6s6d\ 8_2$	0.422		3.45	4.09	
	$6s7d\ 14_1$	−0.646		3.57	4.24	
	$6s7d\ 17_2$	0.433		3.55	4.22	
Bi III	$7s$	0.472[a]	1.07	3.40	4.03	
	$8s$	0.182	1.009	3.45	4.09	4.06
	$6s6p_{3/2}6p_{3/2}8_{1/2}$	2.062		3.43	4.06	
	$7p_{1/2}$	0.104	3.62	3.62	3.81	
	$7p_{3/2}$	0.017		6.56		
					Final average 4.10 n.m.	

[a] H. Wittke, Zeits. f. Physik 116, 547 (1940). Wittke's factor agrees with our measurement.

method of Crawford and Schawlow,[5] the correction for the finite size of the nucleus[2, 5] and the correction for the volume distribution of the magnetic moment[6] are applied the mean of the spectroscopic values is in good agreement with the recently determined nuclear induction value.[7]

The levels and their interval factors are listed in Table I. The interval factor for the $6s$-electron of Bi V is taken from the work of Arvidsson.[8] The others were determined by Richmond and for all but the $7s$ of Bi V are the averages from two or more combinations. The experimental uncertainties are less than one percent for levels involving an s-electron, one percent for the $p_{\frac{1}{2}}$ levels and 8 percent for the $p_{\frac{3}{2}}$ level. The fourth column gives the Fermi-Segrè factor $(1-d\sigma/dn)$. The fifth column gives the value of the nuclear magnetic moment calculated by the Goudsmit-Fermi-Segrè formula. The sixth column gives the value of the magnetic moment obtained by applying the formula, $\mu=\mu^0/(1-\delta)(1-\epsilon)$, in which δ is the correction for the finite size of the nucleus and ϵ the correction for the volume distribution of the magnetic moment. For an s-electron in Bi $\delta=0.14$ and $\epsilon=0.020$, assuming that the nuclear charge is uniformly distributed.[9] For $p_{\frac{1}{2}}\delta=0.05$ and $\epsilon=0.007$.

The interval factor for the $6s$-electron of Bi V is determined from the separation of the two h.f.s. components measured by Arvidsson[8] in the transition $6s\ ^2S_{\frac{1}{2}}-6p\ ^2P_{\frac{1}{2}}$; but the experimental error is high so this value cannot be given much weight. The h.f.s. of the $7s$ level of Bi V is satisfactory for a calculation of the nuclear moment.

The variation in the values determined from the splitting of the various levels of Bi IV is fairly large because of the approximations which were made in determining the relative values of the interaction constants of the two electrons. For each configuration, except $6s7s$, a_{6s} was taken equal to $3.78g(I)$ where the numerical factor, including the Fermi-Segrè correction, was determined from the term values of the ns sequence of Bi V. In the $6s7s$ configuration a_{6s} was reduced by 3 percent to allow for the screening of the $6s$-electron by the $7s$-electron.[5] The contributions of the $7s$- and $8s$-electrons to the $6s7s$ and $6s8s$ interval factors were determined in terms of $g(I)$ by considering the outer electron as a one-electron system. The interaction constants for $6d$ and $7d$ were evaluated in terms of $g(I)$ by the Goudsmit formula and are small. The average of the nuclear moments obtained from the Bi IV levels is 4.14 n.m. and is essentially a determination of the nuclear moment from the interaction of a $6s$-electron of Bi V.

In principle the interval factors of $7s$ and $8s$ of Bi III afford two additional independent determinations of the moment, but as pointed out by Fermi and Segrè[1] and confirmed by a plot of the quantum defects they are perturbed by $6s6p_{\frac{1}{2}}6p_{\frac{3}{2}}8_{\frac{1}{2}}$. This level even in the limiting case of (jj) coupling is mainly a $^2S_{\frac{1}{2}}$ type. The values listed in the second last column of Table I were calculated neglecting perturbations. The formula for intermediate coupling[10] was applied to the $8_{\frac{1}{2}}$ level using a_{6s} reduced by 7 percent to allow for the screening of the $6s$-electron by the two p-electrons. This correction was estimated by interpolation from the corrections for screening of a $6s$-electron by a $6s$-, a $7s$-, and an $8s$-electron.[5] The effect of mutual perturbation can be eliminated to a first approximation by applying the sum rule, which gives essentially the same result as the average of the three values obtained neglecting perturbations.

The $7p\ ^2P_{\frac{1}{2}}$ levels of Bi V and III lead to lower values of the magnetic moment. This can be attributed to perturbations. An application of the Landé doublet formula leads to a value of Z_i greater than the nuclear charge. Without a corresponding increase in the h.f.s. interval factors due to the perturbations, the anomalously large doublet structure intervals would give low values of the magnetic moment when substituted in the Goudsmit formula. Thus these values are not included in the final average.

The gyromagnetic ratio of Bi has recently been determined by Proctor and Yu.[7] Their value of the nuclear moment is 4.0400 n.m. The diamagnetic correction raises this value by 1.04 percent to 4.082 n.m. The final average of the spectroscopic values is 4.10 ± 0.08 n.m. The good agreement between the spectroscopic and nuclear induction values of the magnetic moment further substantiates the assumption that the non-electrical forces between electrons and nucleons are negligible,[5] and favors a uniform charge distribution rather than a charge concentrated on the surface.[11]

[1] E. Fermi and E. Segrè, Zeits. f. Physik 83, 729 (1933).
[2] J. E. Rosenthal and G. Breit, Phys. Rev. 41, 459 (1932).
[3] R. Richmond, Ph.D. thesis, University of Toronto (1937).
[4] S. Goudsmit, Phys. Rev. 43, 636 (1933).
[5] M. F. Crawford and A. L. Schawlow, Phys. Rev. 76, 1310 (1949).
[6] A. Bohr and V. F. Weisskopf, Phys. Rev. 77, 94 (1950).
[7] W. G. Proctor and F. C. Yu, Phys. Rev. 78, 47 (1950).
[8] G. Arvidsson, Ann. d. Physik 17, 787 (1932).
[9] Aage Bohr, unpublished calculations.
[10] G. Breit and L. A. Wills, Phys. Rev. 44, 470 (1933).
[11] Schawlow, Hume, and Crawford, Phys. Rev. 76, 1876 (1949).

The Relative Neutron Capture Cross Sections of the Isotopes of Krypton and Xenon

J. MACNAMARA AND H. G. THODE
Hamilton College, McMaster University, Hamilton, Ontario, Canada
August 14, 1950

THE high neutron flux of the Chalk River atomic energy pile, together with the availability of high precision mass spectrometers in this laboratory, have made it possible to determine the relative neutron capture cross sections of the isotopes of xenon and krypton using both normal and fission product material.

The neutron capture cross sections of the isotopes of xenon and krypton are of special interest since they fall in the neighborhood of the 82 and 50 neutron shells, which are considered to be particularly stable nuclear structures. One might predict, therefore, that isotopes with closed shells would have very low capture cross sections. Also, nuclides having one neutron less than a closed shell, such as $_{36}Kr^{85}$ ($T_{\frac{1}{2}}=9.4$ yr.) would be expected to have a relatively high neutron capture cross section.

To date absorption cross sections of only a few of the isotopes of xenon and krypton have been determined using activation measurements. The total absorption cross section of those measured is only 0.1 barn for both elements. However, the total cross sections (absorption and scattering) of xenon and krypton are 40 and 27 barns, respectively.[1] This must mean that one or more of the other isotopes not yet investigated must have relatively high capture cross sections.

Small samples (10^{-2} cc at N.T.P.) of normal and fission product xenon and krypton were irradiated in quartz sample tubes at relatively high fluxes for a period of about three months in the Chalk River pile. In each case identical samples which were not irradiated were kept for comparison purposes. The relative abundances of the xenon and krypton isotopes in the irradiated

TABLE I. Isotopic composition of xenon and krypton before and after irradiation.

Mass	Normal krypton: Percent unirradiated	Normal krypton: Abundance irradiated	Normal krypton: Percent change	Fission product krypton: Percent unirradiated	Fission product krypton: Abundance irradiated	Fission product krypton: Percent change
80	2.27	2.24	−1.3±0.2			
82	11.52	11.45	−0.6±0.2			
83	11.48	11.12	−3.2±0.1	14.45	14.13	−2.3±0.1
84	57.29	57.67	+0.7±0.2	27.75	28.21	+1.7±0.2
85				5.85	5.83	−0.3±0.2
86	17.44	17.52	+0.5±0.2	51.96	51.85	−0.2±0.2
	Normal xenon			Fission product xenon		
128	1.89	1.90	+0.5±0.5			
129	26.41	26.24	−0.6±0.2			
130	4.03	4.17	+3.4±1.5			
131	21.24	20.85	−1.9±0.2	13.17	13.01	−1.2±0.1
132	27.00	27.34	+1.3±0.2	19.83	20.13	+1.5±0.2
134	10.49	10.52	+0.3±0.2	36.15	36.16	+0.1±0.1
136	8.93	8.97	+0.4±0.3	30.87	30.71	−0.5±0.3

and unirradiated samples were measured with a 180-degree direction focusing mass spectrometer. The results are given in Table I.

Assuming that only (n,γ) reactions are taking place and that we are concerned only with stable isotopes and Kr^{85} (9.4 yr.) the equation $n=n_0e^{-\sigma FT}$ can be used to calculate the isotopic absorption cross sections. F is the neutron flux, T is the time of irradiation, σ is the absorption cross section of the isotope, n_0 and n are the abundances of a given isotope before and after irradiation respectively. The data for both normal and fission product samples were used to calculate the neutron capture cross sections. The results are given in Table II. The relative cross-section values are more reliable than are the absolute values. This is due to the fact that the absolute values depend on the neutron flux and the time of irradiation, which are not accurately known, whereas the relative values depend only on the mass spectrometer measurements which are good to 0.5 percent or better.

The mass spectrometer analysis showed that less than 1:15,000 of Kr^{85} (9.4 yr.) was produced from Kr^{84} by neutron capture. This is further evidence that Kr^{84} has a very low capture cross section. Since 40 percent of the total capture of Kr^{84} produce 9.4-yr. Kr^{85}, it is possible to assume that no measurable change in the fission product Kr^{85} is due to a feeding in from Kr^{84}.

The results show that Kr^{80}, Kr^{83}, Xe^{129}, and Xe^{131} have relatively high absorption cross sections. It is interesting to note that Xe^{129}, Xe^{131}, and Kr^{83}, which have an odd number of neutrons, have the highest cross sections. Neutron capture cross-section data reported to date seem to indicate that this is a general rule. However, the low value for Kr^{85} is an exception to this rule.

It is apparent from these results that Kr^{85}, which has one neutron less than a closed shell, does not have an exceptionally high thermal neutron capture cross section. This, however, does not preclude the possibility of a high resonance cross section at higher neutron energies than are generally obtained in the Chalk River pile. The low cross sections found for Kr^{84}, Kr^{86}, Xe^{134}, and Xe^{136} are not surprising in view of the nuclear structure postulated for these isotopes.

TABLE II. Neutron capture cross sections of xenon and krypton.

Mass	Krypton: Isotopic cross section in barns	Mass	Xenon: Isotopic cross section in barns
78	(0.27)*	128	5 > 0
80	95±15	129	45±15
82	45±15	130	5 > 0
83	205±10	131	120±15
84	2 > 0.1 (0.156)	132	5 > 0 (0.02)
85	15 > 0	134	5 > 0 (0.02)
86	2 > 0 (0.064)	136	5 > 0 (0.15)
Total absorption cross section in barns			
Our results	30±5		37±5
Reported (absorption and scattering)	27		40

* The cross sections given in brackets are the known activation cross sections (reference 1).

We wish to thank W. E. Grummitt for his assistance in getting the samples irradiated. We also wish to thank the National Research Council of Canada for financial assistance and to acknowledge the use of the facilities of the Chalk River pile.

[1] W. H. Sullivan, *Trilinear Chart of Nuclear Species* (John Wiley and Sons, Inc., New York, 1949).

The Mobilities of Molecular and Atomic Rare Gas Ions in the Parent Gases: Helium, Neon, and Argon

JOHN A. HORNBECK
Bell Telephone Laboratories, Murray Hill, New Jersey
July 20, 1950

EXPERIMENT and theory disagree on the low field mobility (μ_0) of the ion He^+ in helium. Tyndall and Powell[1] obtained[2] $\mu_0=19.9$ cm²/volt-sec. after being dissatisfied with an earlier measurement[3] of 12. Biondi and Brown[4] from diffusion data obtained 12.8. Although classical kinetic theory[5] predicts $\mu_0=19.6$, a careful quantum-mechanical calculation of Massey and Mohr[6] predicts 11.

Meyerott[7] has suggested that these discrepancies are removed if (a) the value $\mu_0=19.9$ of Tyndall and Powell applies to He_2^+ rather than He^+, and (b) the superiority of the quantum-mechanical computation is recognized. The situation is further complicated, however, by Bates[8] suggestion that, because of ion age, Biondi and Brown also dealt partly with He_2^+.

Ion mobility measurements have been made in these Laboratories in the course of experiments on pulsed Townsend discharges. The transient current resulting from the liberation of a very short (0.1-μsec.) pulse of photo-electrons from the cathode of a gas-filled tube agrees well with the theory of Newton.[9] The predicted and observed discontinuity in current, corresponding to one ion transit time across the tube, permits measurement of the ion drift velocity (or mobility) as a function of E/p_0. In the gases studied, helium, neon, and argon, one discontinuity is observed over a range of E/p_0 from several hundred (units of volts/cm-mm Hg) to about 25. At lower E/p_0 two discontinuities have been observed consistently indicating the presence of two species of ions with different mobilities.

The ion appearing only at low E/p_0 in each gas has a mobility about twice that of the other ion. In the region where both ions were observed in helium, the age of the slow ion was never more than 30 μsec. and the fast ion never more than 15 μsec. At $E/p_0=10$ in helium the respective mobilities of the fast and slow ions were $\mu_{fast}=18$ and $\mu_{slow}=9.4$, and these values were increasing slowly as E/p_0 was decreased. Measurements at lower E/p_0 could not be carried out.

In this experiment the sharp time definition of the current discontinuity demands that the ions be formed within one microsecond after the photo-pulse and that the ions not change their identity during the transit across the tube.

The slow ion in each of the rare gases we identify as the atomic ion, He^+, Ne^+, and A^+, primarily on the basis that the slow ion is observed over the entire range of E/p_0. This implies, for example, an He^+ age of one μsec. at the highest E/p_0 obtained.

The identity of the fast ion might be (a) doubly charged atomic ion, (b) impurity ion, (c) molecular ion of the parent gas. Hypothesis (a) is unsatisfactory because the fast ion appears only at low E/p_0 and because the voltage applied to the electrodes was in some cases less than the appearance potential of the doubly charged ion. Time considerations suggest that an impurity concentration of the order of one percent or possibly more would be required to make hypothesis (b) reasonable. Mass spectrometer analyses of the gases used indicated no impurity within the limit

of sensitivity of the instrument (0.005 percent). Flashing additional Ba-Mg getters in the experimental tube did not alter the effect. The impurity hypothesis, therefore, appears to be untenable.

Turning to hypothesis (c), the proposed mechanism of formation of the molecular ions[10] (suggested to the author by C. Herring) is that atoms excited by the primary electron pulse to a high state above the metastable level may collide with neutral atoms before they radiate, giving the molecular ion and an electron.[11] The molecular ion hypothesis based on this formation process seems consistent in every respect. First, He_2^+, Ne_2^+, and A_2^+ are known to exist.[12] Second, the other factors that we have to consider, *viz.*, time of formation, energy of formation, pressure variation, and mobility, all agree with other experimental observations and theory to the extent that these are available or known.

The suggestion of Meyerott therefore seems to be well substantiated, namely, that the identity of the ion measured in some experiments has been confused, and that the calculation of Massey and Mohr for helium is essentially correct. From the present measurements of A_2^+, A^+, and Ne_2^+ and Ne^+, one concludes that the exchange force reduces the mobility of the atomic ions (making them slower than the molecular ions) by about the same factor that this force reduces the mobility of He^+ in helium. The results indicate, further, that the mobility measurements of Munson and Tyndall[13] presented as A^+ in argon and Ne^+ in neon actually are for A_2^+ and Ne_2^+.

I am greatly indebted to many of my colleagues, particularly Dr. J. P. Molnar, Dr. G. H. Wannier, and Mr. A. H. White, for their invaluable assistance and advice in the course of this work.

[1] A. M. Tyndall and C. F. Powell, Proc. Roy. Soc. **A134**, 125 (1931).
[2] All mobilities are quoted in these units for gas density at 0°C, 760 mm pressure. No temperature correction as such is implied.
[3] A. M. Tyndall and C. F. Powell, Proc. Roy. Soc. **A129**, 162 (1930).
[4] M. A. Biondi and S. C. Brown, Phys. Rev. **75**, 1700 (1949).
[5] H. R. Hasse and W. R. Cook, Phil. Mag. **12**, 554 (1931).
[6] H. S. W. Massey and C. B. O. Mohr, Proc. Roy. Soc. **A144**, 188 (1934).
[7] R. Meyerott, Phys. Rev. **66**, 242 (1944); **70**, 671 (1946).
[8] D. R. Bates, Phys. Rev. **77**, 718 (1950).
[9] R. R. Newton, Phys. Rev. **73**, 570 (1948).
[10] F. L. Arnot and M. B. M'Ewen, Proc. Roy. Soc. **A166**, 550 (1938), have suggested the same mechanism as a corollary to a formation process from a metastable atom-neutral atom collision.
[11] Evidence from this experiment indicates, in agreement with Meyerott, reference 7, that metastable He atoms cannot form He_2^+ by collision with a neutral atom, as proposed by Arnot and M'Ewen, Proc. Roy. Soc. **A171**, 106 (1939).
[12] O. Tüxen, Zeits. f. Physik **103**, 463 (1936). My thanks go to Professor W. P. Allis for pointing out this reference to me.
[13] R. J. Munson and A. M. Tyndall, Proc. Roy. Soc. **A177**, 187 (1941).

The Electric Field at a Thermionic Cathode as a Function of Space Current

PAUL L. COPELAND AND DELBERT N. EGGENBERGER
Illinois Institute of Technology and Armour and Company, Chicago, Illinois
June 5, 1950

THE work of Ivey[1] suggests that the field at the cathode of any diode is a simple function of $i \equiv I/I_s$, where I is the space current and I_s is the space-charge limited current in this diode. For simple symmetries (parallel planes, coaxial cylinders, and concentric spheres) the potential or the potential gradient are most easily expressed in terms of a harmonic coordinate z such that Laplace's equation takes the form $d^2V/dz^2=0$. The relationship between the "gradient" at the cathode in the absence of space charge $(dV/dz)_0$ and the "gradient" at the cathode when current flows $(dV/dz)_c$, we express as a Maclaurin's series in i as follows:

$$(dV/dz)_c=(dV/dz)_0(1-ai-bi^2-ci^3-\cdots). \quad (1)$$

From Eq. (17) of Ivey's paper we obtain $a=0.59259$, $b=0.10974$, and $c=0.052025$. If the conjecture put forward by Ivey is correct, a, b, and c do not depend on geometry.

We have expanded the potential $V(z)$ as a function of i by means of a Maclaurin's series, and through this series have evaluated the coefficient "a" in Eq. (1) for various ratios of the radii in the case of coaxial cylinders. The results of our calculations are summarized in Table I. These results suggest that the function expressing the ratio of the field at the cathode in the absence of current to that in the presence of current is not a universal one as Ivey tentatively suggests, but that the ratio $(dV/dz)_c/(dV/dz)_0$ is a slowly varying function of geometry.

TABLE I. Coefficient a in Eq. (1).

r/r_c	a
1.1	0.5926
5.0	0.5913
10.0	0.5896
100.	0.5729
1000.	0.5422

[1] H. F. Ivey, Phys. Rev. **76**, 554 (1949).

A Determination of the Speed of Light by the Resonant Cavity Method

KEES BOL
Department of Physics, Stanford University, Stanford, California
August 21, 1950

FOR the last several years an experiment has been in progress at Stanford University for the measurement of the speed of light, c, by the resonant microwave cavity method. The cavity consists of a cylinder 4.5 in. high and 9.8 in. i.d., which rests on one end plate, and three spacer rods inserted in the cylinder walls which support the top end plate. The TE_{012} and Te_{021} modes are both measured and are then used to eliminate the measurement of the absolute diameter. The height is found from the spacer rods, which are measured interferometrically.

The provisional result which has been obtained to date is

$$c=299{,}789.3\pm0.4 \text{ km/sec.}$$

The limits given do not include a possible systematic error due to a slight tarnish of the silver-plated walls of the cavity. On this account the result may be too low by possibly as much as, but probably less than, 0.5 km/sec. The experiment is being repeated at present in order to eliminate this difficulty, as well as some others of lesser importance. A detailed paper will be submitted on the completion of this work.

The experiment was devised by the late Dr. W. W. Hansen and was conducted under his supervision until his death.

The Structure of Lead Sulfide Films

J. A. JAMES, C. J. MILNER, AND B. N. WATTS
Research Laboratory, The British Thomson-Houston Company, Ltd., Rugby, England
August 28, 1950

IN the course of work on the development of lead sulfide photoconductive cells, mainly using the chemical method, we have examined the chemical precipitate by x-ray diffraction. We obtained powder patterns which, as reported by Doughty, Lark-Horovitz, Roth, and Shapiro,[1] showed, mainly, lines due to Pbs, with additional lines. In our case, these were definitely identified as being due partly to PbO, and partly to basic lead carbonate $Pb(OH)_2 \cdot PbCO_3$; and not to $PbO \cdot PbSO_4$ as the above authors consider probable.

We thank Mr. L. J. Davies, Director of Research, The British Thomson-Houston Company, Ltd., for permission to publish this note.

[1] Doughty, Lark-Horovitz, Roth, and Shapiro, Phys. Rev. **79**, 203A (1950).

Neutron Refraction in Ferromagnets

MELVIN LAX
Syracuse University, Syracuse, New York
September 1, 1950

THE disagreement between the results of Halpern[1] and of Ekstein[2] concerning the index of refraction of neutrons in ferromagnets can be summarized as follows. (1) Halpern claims that the change in neutron index of refraction is determined by the scattering amplitude in the forward direction. (2) Ekstein points out that Halpern's calculation of the forward scattering amplitude is incorrect and that the magnetic scattering of a neutron by an ion vanishes in the forward direction. (3) Ekstein shows that the change in index of refraction does not vanish but is determined by the magnetic field in the magnet.

I shall show here that *all* of these statements are correct. The procedure is based on a general theory of the multiple scattering of waves to be published soon. The chief result of this theory is that the coherent wave $\langle\psi(\mathbf{r})\rangle$ obeys an equation

$$(E-H-c\bar{T})\langle\psi(\mathbf{r})\rangle=0, \tag{1}$$

$$\bar{T}=\int_\tau T(\mathbf{r}_j)n(\mathbf{r}_j)d\mathbf{r}_j, \tag{2}$$

where $n(\mathbf{r}_j)$ is the density of scatterers. Here c is a correction factor for the relation between the "effective" and total neutron wave and for present purposes may be set equal to unity. $T(\mathbf{r}_j)$ is the transition operator[3] whose matrix elements $T_{ba}(\mathbf{r}_j)$ are proportional to the scattering amplitude from direction a to direction b for a scatterer at position $\mathbf{r}_j$. These differ by a phase factor from the case in which the scatterer is located at the origin:

$$T_{ba}(\mathbf{r}_j)=\exp[i(\mathbf{k}_a-\mathbf{k}_b)\cdot\mathbf{r}_j]T_{ba}(0). \tag{3}$$

$\bar{T}$ represents the sum of the scattering amplitudes of the scatterers in a volume τ equal to the volume of quantization. It follows from (2) and (3) that $\bar{T}$ is already diagonal and independent of τ if plane waves quantized in τ are used as the eigenfunctions. Since $E=\hbar^2k^2/2m$ and $H=-\hbar^2\nabla^2/2m=\hbar^2k'^2/2m$, the propagation constant k' in the magnet is related to the vacuum case by:

$$k'^2=k^2-c(2m/\hbar^2)(\bar{T})_{aa}. \tag{4}$$

This establishes the first point that the index of refraction k'/k is determined by the forward scattered amplitude.

Since both Halpern and Ekstein treat the scattering in Born approximation, we can replace T by the corresponding interaction potential:

$$T(\mathbf{r}_j)=V(\mathbf{r}-\mathbf{r}_j)-\mu\boldsymbol{\sigma}\cdot\mathbf{B}(\mathbf{r}-\mathbf{r}_j), \tag{5}$$

where $V(\mathbf{r}-\mathbf{r}_j)$ is the pseudopotential of the jth nucleus and $\mathbf{B}(\mathbf{r}-\mathbf{r}_j)$ is the magnetic field associated with the corresponding ion. The forward scattered amplitude of a single scatterer is then proportional to:

$$\lim_{\tau\to\infty}\int_\tau[V(\mathbf{r}-\mathbf{r}_j)-\mu\boldsymbol{\sigma}\cdot\mathbf{B}(\mathbf{r}-\mathbf{r}_j)]d\mathbf{r}. \tag{6}$$

The second term vanishes in the limit, since the complete space integral of a solenoid vector $\mathbf{B}$ vanishes,[4] providing $\lim r\mathbf{B}\to 0$ as $r\to\infty$. This establishes the second point that the Born approximation to the magnetic forward scattered amplitude vanishes.

We shall now show that (4) yields a non-vanishing magnetic contribution to the index of refraction providing we calculate $(\bar{T})_{aa}$ rather than $(T_{aa})_{Av}$. In other words, we must add the contributions of the individual scatterers before calculating the forward amplitude. Usually the two procedures would be in agreement, but here they differ because of the long-range nature of the magnetic forces:

$$(\bar{T})_{aa}=\frac{1}{\tau}\int_\tau d\mathbf{r}\int_\tau d\mathbf{r}_j[V(\mathbf{r}-\mathbf{r}_j)-\mu\boldsymbol{\sigma}\cdot\mathbf{B}(\mathbf{r}-\mathbf{r}_j)]n(\mathbf{r}_j) \tag{7}$$

$$=\lim_{\tau\to\infty}\frac{1}{\tau}\int_\tau d\mathbf{r}[V_i(\mathbf{r})-\mu\boldsymbol{\sigma}\cdot\mathbf{B}_i(\mathbf{r})] \tag{8}$$

$$=V_{Av}-\mu\boldsymbol{\sigma}\cdot\mathbf{B}_{Av}, \tag{9}$$

where $V(\mathbf{r})$ and $\mathbf{B}_i(\mathbf{r})$ represent the total potential and total magnetic field at $\mathbf{r}$ and V_{Av}, $\mathbf{B}_{Av}$ are the corresponding macroscopic average potential and field. Since the eigenvalues of $\boldsymbol{\sigma}\cdot\mathbf{B}_{Av}$ are $\pm|\mathbf{B}_{Av}|$ for neutrons polarized parallel or antiparallel to the magnetic field, we obtain Ekstein's result:

$$k'^2=k^2-(2m/\hbar^2)[V_{Av}\pm\mu|\mathbf{B}_{Av}|] \tag{10}$$

and establish the third point.

Equation (8) embodies carefully the principle that an index of refraction should be computed for a medium of infinite volume. The space integral of $\mathbf{B}_i(\mathbf{r})$ does not vanish for an infinite magnet because $r\mathbf{B}_i(\mathbf{r})$ does not vanish as $r\to\infty$.

[1] O. Halpern, Phys. Rev. **76**, 1130 (1949). Halpern, Hamermesh, and Johnson, Phys. Rev. **59**, 981 (1941).
[2] H. Ekstein, Phys. Rev. **78**, 731 (1950); **76**, 1328 (1949).
[3] M. Lax, Phys. Rev. **78**, 306 (1950).
[4] J. A. Stratton, *Electromagnetic Theory* (McGraw-Hill Book Company, Inc., New York, 1942), p. 111.

Cation Distribution in Copper Zinc Ferrite

JACOB L. SNOEK
Horizons Incorporated, Cleveland, Ohio
June 30, 1950

A NOTE in this Journal by Brockman[1] on the effect of low temperature heat treatment on the Curie temperature of copper zinc ferrite calls for comment.

The experimental results are not disputed; in fact, they agree with some qualitative observations made at an earlier date by the author of the present note.

The interpretation seems to me to be open to question, however. In view of the strong preference of zinc for the tetrahedral position, as shown by the fact that a quenching from 1200°C brings about only a weak ferromagnetism in pure zinc ferrite, and given the great sensitivity of the saturation magnetization of pure copper ferrite to variations in the heat treatment,[2] it seems to be much more likely that changes in the distribution of the copper atoms over the available positions in the lattice are responsible for the observed variations. Obviously, accurate measurements of the saturation magnetization would give the answer to this problem at once.

[1] F. G. Brockman, Phys. Rev. **77**, 841 (1950).
[2] L. Néel, Comptes Rendus **230**, 190 (1950).

Crystals and Geiger Counters for Scintillation Counting*

C. E. MANDEVILLE AND H. O. ALBRECHT
Bartol Research Foundation of the Franklin Institute, Swarthmore, Pennsylvania
September 5, 1950

IN three previous communications,[1-3] the writers have discussed the detection of alpha-, beta-, and gamma-rays by recording scintillations from crystals in photo-sensitive Geiger counters. A survey has been conducted wherein a large number of inorganic crystals have been produced with emphasis upon the silver-activated alkali halides. Some organic materials have also been considered. Using a scintillation Geiger counter as a detector, effects have been observed as shown in Table I.

TABLE I.

Scintillator	Particles detected in the photon Geiger counter
NaCl-Ag	alpha, beta, gamma
NaBr-Ag	alpha, beta
NaBr-Tl	alpha
Powdered durene	alpha
KCl-Ag	alpha
LiCl-Ag	alpha
LiBr-Ag	alpha

NaCl-Ag remains thus far the most satisfactory crystal for general purposes.

As often mentioned in the earlier communications, the counters have been of the gauze cathode-type and have been usually sensitized by a method described by Scherb.[4] However, counters are now being produced without sensitization of any kind which are sensitive enough to detect scintillations induced by alpha- and beta-rays. The discharge at liquid air temperatures does of course increase the counter sensitivity and hence efficiency of detection. It has always been necessary to sensitize the counters for detection of gamma-rays.

Several remarkable characteristics of treated photon counters have been observed in a qualitative fashion. For example, after the discharge treatment, the counters will withstand very high counting rates over a long period of time (greater than five hundred thousand counts per minute) without "breaking down." It is possible that points and rough spots on both the wire and the cathode are removed by the discharge. Although accurate observations have not been carried out, the counter sensitivity appears to remain constant over long time intervals. It also appears that photo-sensitivity increases as the diameter of the cathode of the counter is decreased. It is assumed, of course, that the operating voltage is kept constant by adjusting the counter pressure. The increased activity is explained by the fact that with smaller diameters, a stronger electric field is maintained adjacent to the cathode of the counter so that more of the soft ultraviolet photoelectrons are attracted into the counting volume of the counter.

Experiments with various counter geometries and crystals are continuing.

* Assisted by the joint program of the ONR and AEC.
[1] C. E. Mandeville and H. O. Albrecht, Phys. Rev. 79, 1010 (1950).
[2] C. E. Mandeville and H. O. Albrecht, Phys. Rev. 80, 117 (1950).
[3] C. E. Mandeville and H. O. Albrecht, Phys. Rev. 80, 300 (1950).
[4] M. V. Scherb, Phys. Rev. 73, 86 (1948).

The Detection of Gamma-Ray-Induced Scintillations from Crystals in a Photo-Sensitive Geiger-Müller Counter*

C. E. Mandeville and H. O. Albrecht
Bartol Research Foundation of the Franklin Institute, Swarthmore, Pennsylvania
August 30, 1950

In two previous communications,[1,2] the writers have discussed the detection in photon Geiger counters of scintillations from alpha-particles and beta-rays on NaCl-Ag. The photo-sensitive counters have been constructed of wire gauze cathodes and Corning 9741 glass. The cathode materials have been usually copper and tinned steel. Sometimes, the counters have been sensitized by a discharge technique previously described by Scherb,[3] formerly of this laboratory.

It has been shown[2] previously that short-lived fluorescent pulses are also produced in the deep ultraviolet when NaCl-Ag is irradiated by gamma-rays.[2] Scintillations from gamma-rays on NaCl-Ag have been detected until recently only in a 1P28 photomultiplier tube.[2] However, sufficient quantum efficiency has now been obtained to detect them in a photo-sensitive Geiger counter.

Photon counters have now been produced which are far more sensitive to the ultraviolet than are those used for detection of scintillations from alpha-particles and beta-rays. One of these very sensitive counters was placed within concentric cylinders of NaCl-Ag and Textolite, Textolite being innermost, and was irradiated by the million-volt gamma-rays of Sc^{46}. The wall thickness of the NaCl-Ag cylinder was 1.27 cm, and the wall thickness of the Textolite was 0.32 cm. When the Textolite shield was removed, the counting rate was observed to increase by a factor of 2.5. Precautions were taken to ascertain that the change in counting rate was a genuine effect and was not one brought about by stray light admitted with removal of the shield. The measurements were repeated subsequently with the use of a paper shield rather than Textolite, and the same result was obtained. When the cylinder of NaCl-Ag was removed, the effect disappeared. When the photon counter was replaced by an untreated one in a Nonex envelope, no effect was observed. All of these tests of the experimental arrangement point to the fact that the increased counting rate could be explained only by counting ultraviolet fluorescence when the crystals of NaCl-Ag were irradiated by gamma-rays.

The factor of 2.5 in increase of efficiency was obtained in a relatively poor geometric arrangement. For example, the inner diameter of the cylinder of NaCl-Ag was several times greater than the diameter of cathode of the photon counter. This unfavorable situation resulted from the shape of the counter at its ends and from the fact that sufficient space was allowed for easy removal of the Textolite light shield. It is estimated that were the side walls of the cylinder of NaCl-Ag contiguous with the counter, an efficiency factor of 4 or 5 would have been obtained.

The limit of photo-sensitivity has not yet been reached. It is anticipated that the efficiency factor for gamma-rays will be increased.

* Assisted by the join program of the ONR and AEC.
[1] C. E. Mandeville and H. O. Albrecht, Phys. Rev. 79, 1010 (1950).
[2] C. E. Mandeville and H. O. Albrecht, Phys. Rev. 80, 117 (1950).
[3] M. V. Scherb, Phys. Rev. 73, 86 (1948).

A Variational Principle for Time-Dependent Problems

Marcello Cini
Istituto di Fisica dell'Università di Torino, Italy
and
Luigi A. Radicati
Instituto di Fisica del Politecnico di Torino, Italy
August 29, 1950

Recently variational methods have been used particularly by Schwinger and his school[1] in connection with different kinds of physical problems.

It seems worth while to show that a similar variational principle holds for problems concerning the evolution of a quantum-mechanical system due to the action of an arbitrary time- and space-dependent potential. Let $f(\mathbf{x}, t)$ be the initial state of the system, $\psi(\mathbf{x}, t)$ the perturbed wave function, and $g(\mathbf{x}, t)$ an arbitrary final state. Then the probability amplitude for the transition from the state f to the state g is stationary with respect to small variations of $\psi(\mathbf{x}, t)$. This is easily seen using Feynman's[2] integral formulation, as the variational principle is derived by transformation of the differential equation into an integral equation containing a suitable Green's function.

Let us restrict ourselves for simplicity to the case of the motion of only one electron in a given potential $A(\mathbf{x}, t)$. (A is the four-vector matrix defined by Feynman[2].) If at time t_1 the electron is in the state f, the transition amplitude for finding the electron in the state g at time t_2 is

$$a=\int \bar{g}(2)\beta K^{(A)}(2,1)\beta f(1)d^3\mathbf{x}_1 d^3\mathbf{x}_2. \tag{1}$$

The potential acts on the electron transforming the initial wave function $f(1)$ into $\psi(2)$ which obeys the integral equation

$$\psi(2)=f(2)-i\int K_+(2,1)A(1)\psi(1)d\tau_1. \tag{2}$$

In a similar way we define the wave function $\chi(2)$ as

$$\bar{\chi}(2)=\bar{g}(2)-i\int \bar{\chi}(1)A(1)K_+(1,2)d\tau_1. \tag{3}$$

If g and f are orthogonal states, using Eqs. (2) and (3), Eq. (1) becomes

$$a=-i\int \bar{g}(2)A(2)\psi(2)d\tau_2=-i\int \bar{\chi}(2)A(2)f(2)d\tau_2. \tag{4}$$

From Eqs. (2)–(4) one easily obtains

$$\frac{1}{a}=\frac{\int \bar{\chi}(2)A(2)\psi(2)d\tau_2+i\int \bar{\chi}(3)A(3)K_+(3,2)A(2)\psi(2)d\tau_3 d\tau_2}{\int \bar{\chi}(2)A(2)f(2)d\tau_2\times\int \varphi(2)A(2)\psi(2)d\tau_2}. \quad (5)$$

The first-order variation of $1/a$, with respect to arbitrary independent variations of ψ and $\bar{\chi}$, vanishes.

In the particular case of a time-independent potential, starting from Eqs. (2) and (3) in which integration with respect to the time variable is performed, one obtains the variational principle for the scattering amplitude already used by Schwinger and his coworkers.[4]

It seems worth while to compare these results with the variational principle established by Schwinger[5] for the "reaction operator K."[6] Following Schwinger's notation it is useful to indicate the world-points 1 and 2 by x' and x, respectively. One has the relation[7]

$$K_+(2,1)=i\bar{S}(x-x')-\tfrac{1}{2}S^{(1)}(x-x'). \quad (6)$$

Solving Eqs. (2) and (3) by successive approximations and introducing the solutions in Eq. (4), one obtains an expression that can be compared with the analogous expansion of the reaction operator given in S III, Eq. (1.24).

One finds that a is the matrix element of the operator[8] $S-1$ taken between the initial and final state of the electron. The expansions of the two operators $\frac{1}{2}(S-1)$ and K are identical, except that in the former the function $K_+(2,1)$ given by Eq. (6) in term of functions $\bar{S}(x-x')$ and $S^{(1)}(x-x')$ appears, while in the latter only the function $i\bar{S}(x-x')$ is contained.

The fact that for the two operators the same variational principle holds follows from both functions $K_+(2,1)$ and $\bar{S}(x-x')$ being four-dimensional Green functions for Dirac's free electron equation.

The details of these calculations will be published elsewhere.

[1] J. Schwinger, Phys. Rev. **72**, 742 (1947); W. Kohn, Phys. Rev. **74**, 1763 (1948); J. M. Blatt and J. D. Jackson, Phys. Rev. **76**, 18 (1949).
[2] R. P. Feynman, Phys. Rev. **76**, 749 (1949).
[3] All symbols used are defined in Feynman's paper.
[4] See reference 1, Kohn, Section III.
[5] J. Schwinger, Phys. Rev. **74**, 1439 (1948); **75**, 651 (1949); **76**, 790 (1949); referred to as S I, S II, and S III.
[6] See reference 5, S I, Eqs. (4.15) and (4.22).
[7] The definitions of the functions $\bar{S}(x)$ and $S^{(1)}(x)$ are given in S II.
[8] See also F. J. Dyson, Phys. Rev. **75**, 1736 (1949).

Mass Assignment of Natural Activity of Samarium

BOYD WEAVER*
Oak Ridge National Laboratory, Y-12 Area, Oak Ridge, Tennessee
August 30, 1950

Sm^{147} has now been definitely established as the source of the natural alpha-radiation from this element. This was done by direct counting of each of the samarium isotopes, recently separated by the Isotope Research and Production Division at Y-12.[1]

Although previous reports had indicated that the alpha-active samarium isotope might be of mass 148[2] or 152,[3] Dr. A. J. Dempster's latest conclusions were "that the alpha emitting isotope is almost certainly the isotope at mass 147." [4]

Alpha-counting may be used for the approximate determination of the Sm^{147} content of enriched samarium isotopes. A comparison of 81.6 percent Sm^{147} with the other separated isotopes is given in Table I. Ten-milligram samples of samarium oxide were used in these determinations. Closer correlation with results from the mass spectrometer will probably be possible with improvement in the technique of sample preparation.

TABLE I. Counting rates of samarium samples.

Isotope collection	Natural Sm	144	147	148	149	150	152	154
Counts/min.	24.1	10.9	130.8	9.3	8.3	3.5	2.9	0.53
Mass 147 content in percent (by mass spectrometer)	15.07[a]	7.7	81.6	6.1	5.1	2.0	1.6	0.36
Sm^{147} content in percent (from alpha-counts)	15.0	6.8	—	5.8	5.2	2.2	1.8	0.33

[a] Inghram, Mark G., David C. Hess, Jr., and Richard J. Hayden, Phys. Rev. **73**, 180 (1948).

The method of preparing samples was as follows. Ten milligrams of pure Sm_2O_3 were placed on a stainless steel disk and dissolved in about 0.1 ml of concentrated nitric acid. The solution was dried over a low hot plate. Its tendency to contract toward the center of the disk was counteracted by spreading with a small glass rod until streaks were left in the thickening solution. The nitrate was ignited to oxide over a Meker burner. The sample covered about 20 cm^2 of disk area.

All samples were counted for at least an hour in proportional counters having backgrounds of only 5 to 10 counts/hr., after earlier measurements by other counters with higher backgrounds had revealed the activity from Sm^{147}.

Acknowledgement is made to C. P. Keim for his counsel in this research and to G. W. Keilholtz and H. R. Gwinn for their assistance in making the measurements.

* This report is based on work performed under contract for the AEC by the Y-12 Plant of the Carbide and Carbon Chemicals Division of Union Carbide and Carbon Corporation.
[1] C. P. Keim, H. W. Savage, and Boyd Weaver, Y-640.
[2] T. R. Wilkins and A. J. Dempster, Phys. Rev. **54**, 315 (1938).
[3] A. J. Dempster, Phys. Rev. **73**, 1125 (1948).
[4] A. J. Dempster (quotation from a private communication, 1949).

Single Crystal Magnetostriction Constants of an Iron-Cobalt Alloy

J. E. GOLDMAN*
Westinghouse Research Laboratories, East Pittsburgh, Pennsylvania
August 18, 1950

THE single crystal magnetostriction constants of iron-cobalt alloys have never been measured owing to the difficulty of obtaining large single crystals of a brittle material which undergoes a phase transformation, and the insensitivity of the usual measuring techniques which make them inapplicable to measurements on a small crystal. We have adapted the resistance strain gauge technique first employed by us for magnetostriction measurements on polycrystalline materials[1] to the measurement of magnetostriction in very small single crystals of iron-cobalt. The results reported below are for a crystal containing 30 percent cobalt very kindly loaned to us by Professor McKeehan of Yale University. The crystal is in the form of an oblate spheroid 3 mm in diameter and approximately 0.3 mm thick. For crystals of this size, the form effect can be neglected to a first approximation.[2] The orientation of the crystal was determined with x-rays by back reflection using white radiation from a tungsten target.[3] The plane of the sample is found to be approximately a (411) plane.

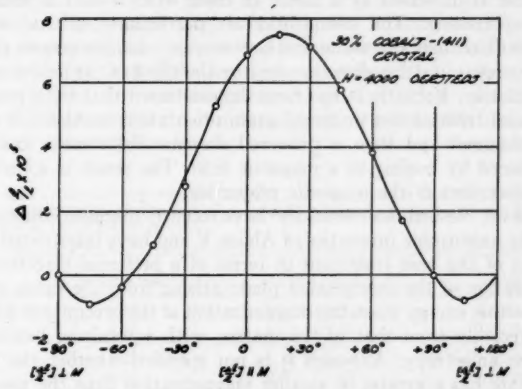

FIG. 1. $\Delta l/l$ in direction of gauge *vs.* angle between gauge and M.

A type A-19 advance wire strain gauge[4] with an effective length of $\frac{1}{16}$ in. was cemented onto the top surface of the crystal. This gauge is then made the active arm of a Wheatstone bridge in which all other arms are similar strain gauges and placed very near the crystal so as to minimize temperature and other effects. The detector is a Perkin-Elmer d.c. amplifier the output of which is connected to an Esterline-Angus d.c. milliampere recorder. The crystal was mounted in a unit which permits rotation of the crystal in the magnetic field. The change in magnetostrictive strain in a direction fixed relative to the crystal axes is then measured as the direction of magnetization is varied. The magnetic field employed is 4000 oersteds; thus the sample is always saturated and only differences in strain as a function of the direction of magnetization are measured. This eliminates the need for making any assumptions concerning the demagnetized state. The results are shown in Fig. 1 in which the strain in a fixed direction is plotted against the angle made by this direction with the applied field. The strain when the gauge is perpendicular to the field is arbitrarily set at zero. From this data, the constants in Becker's expression for the magnetostriction as a function of the direction cosines of the direction of strain and the direction of magnetization[5] can be obtained. In our case four terms in the series are required. Using Becker's notation we obtain for the magnetostriction in the principal crystal directions:

$$\lambda_{[100]}=1.5\times10^{-5}, \quad \lambda_{[111]}=8.5\times10^{-5}.$$

An extension of these measurements to other compositions is currently in progress. We are indebted to Mr. H. Plotkin for helpful assistance in making the x-ray measurements and to Professor Smoluchowski for discussions.

* Now at Carnegie Institute of Technology, Pittsburgh, Pennsylvania.
[1] J. E. Goldman, Phys. Rev. 72, 529 (1947); J. E. Goldman and R. Smoluchowski, Phys. Rev. 75, 149 (1949).
[2] R. Becker, Zeits. f. Physik 87, 547 (1934); also W. J. Carr, Jr. unpublished dissertation, Carnegie Institute of Technology (1950). We are indebted to Mr. Carr for discussions on this point.
[3] See, for example, C. S. Barrett, *Structure of Metals* (McGraw-Hill Book Company, Inc., New York, 1943).
[4] Available commercially from the Baldwin Southwork Division of the Baldwin Locomotive Works.
[5] Becker-Doring, *Ferromagnetismus* (Verlag. Julius Springer, Berlin, 1939), p. 275.

Theory of Magnetic Anisotropy in Alnico V

J. E. Goldman and R. Smoluchowski
Carnegie Institute of Technology, Pittsburgh, Pennsylvania
August 18, 1950

ALNICO V is the name given to an alloy of iron, cobalt, nickel, aluminum, and copper, which when cooled in a magnetic field shows unusual magnetic properties in the direction of the field. The energy product, $(BH)_{max}$, of an alloy treated in this manner is increased by a factor of three when a field is present during cooling. The composition is particularly critical with respect to cobalt and aluminum content; i.e., changes greater than two percent in either direction destroy the effect of the field almost completely. Recently it has been demonstrated that with proper thermal treatment a preferred grain orientation in Alnico V can be obtained and then a preferred domain distribution can be produced by cooling in a magnetic field. The result is a further improvement in the magnetic properties.

Kittel, Nesbitt, and Shockley[1] have recently discussed the origin of the anisotropic properties of Alnico V and have interpreted the effect of the heat treatment in terms of a preferred direction of nucleation of the precipitated phase arising from the extra magnetostatic energy when the magnetization of the precipitate differs appreciably from that of the matrix, with a resulting preferred shape anisotropy. Although it is not specified whether the precipitate has a greater or smaller magnetization than the matrix, it is apparent that it must be smaller in their theory, for otherwise it would require very large fields to saturate the alloy in directions other than the direction of the field present during the anneal. Specifically, a plate-like precipitate of the dimensions suggested by KNS with a magnetization *ca.* 1700 c.g.s. units requires a field of 15,000 oersteds to saturate it in a direction normal to the plate. It follows that in a direction perpendicular to the cooling field for reasonable volumes of precipitate compatible with the known saturation magnetization of the alloy (p in KNS notation), a field of the order of 10,000 oersteds would be required to attain saturation contrary to experimental evidence. On the other hand, to suppose thus that the precipitate is the more weakly magnetic constituent is contrary to the observations of Bradley and Taylor[2] and Dannohl[3] for FeNiAl, recently confirmed by Geisler[4] and by Went[5] for Alnico V. Moreover, the theory of KNS does not explain the unusual sensitivity of the Alnico V effect to small changes in composition[6] nor does it suggest a reason for the significant improvement obtainable by means of directional grain growth.

We propose to explain the Alnico V effect by considering the anisotropy of the elastic energy which accompanies the formation of nuclei of the precipitate during annealing in a magnetic field. This elastic deformation is due to magnetostriction of the strongly magnetic precipitate. The elastic anisotropy causes preferential growth of nuclei of given orientation. As shown below, this picture not only explains quantitatively the magnetic properties of Alnico V but also the sensitivity to composition and to grain orientation of the matrix. The very existence of the nuclei in the form of platelets in this and many other non-magnetic alloys reflects the influence of elastic strain at the temperature of nucleation.[7]

Alnico V differs from Fe_2NiAl (app. Alnico III) in the addition of cobalt and increased iron content. If one makes the plausible assumption that cobalt behaves as iron in solid solution, calculation shows that the precipitate is an iron-cobalt alloy containing approximately 30 percent cobalt. Comparison of the saturation moment and remanence of Alnico V with the moments of the assumed phases and of Alnico III confirms this assumption. (An extreme assumption that all the cobalt goes into precipitate does not alter the subsequent results significantly; any other assumption would be highly improbable.) It has been shown[8] that for an alloy of this composition, the magnetostriction is smallest in the cubic direction: $\lambda_{[100]}=1.5\times10^{-5}$, $\lambda_{[111]}=8.5\times10^{-5}$. Therefore, the elastic deformation due to magnetostriction is smallest when the nucleus is oriented with the [100] in the direction of the field. Such nuclei will, therefore, have a somewhat lower free energy and will grow preferentially. There will thus be a preponderance of volume of recipitate with a direction of easy magnetization ([100] axis) making a small angle with the field direction. According to our picture, therefore, the Alnico V effect which is essentially an increase in remanence is associated with the crystalline anisotropy of the precipitated magnetic phase and is consistent with recent results obtained by Geisler[4] with the electron microscope on single crystals of Alnico V. It appears, as Dr. Kittel has pointed out to us, that the orientational energy due to demagnetization is much greater than that due to magnetostriction. This is certainly true especially since ΔI appears to be about three times as great as the minimum value of 500 assumed by KNS. To be sure, this may influence the shape of the precipitate but, as indicated above, cannot alone explain the remanence or the field required to saturate in a direction perpendicular to the annealing direction.

On the basis of this theory we can now account for the unusual sensitivity of the Alnico V effect to composition. If the cobalt content is decreased, the Curie temperature of the precipitate is rapidly decreased to below the proper nucleation temperature. If the cobalt content is increased, the crystalline anisotropy of the precipitate is rapidly decreased and reverses its sign at a composition of 45 percent cobalt in the precipitate itself. Similarly, a decrease in aluminum content causes more nickel to go into the precipitate and reduce its Curie temperature.[9] An increase in aluminum content would tend to make cobalt enter the Ni-Al matrix with a similar effect on the Curie temperature of the precipitate.

We are indebted to Dr. Geisler and Drs. Kittel and Shockley for making available to us the results of their investigations in advance of publication.

[1] Kittel, Nesbitt, and Shockley, Phys. Rev. **77**, 839 (1950).
[2] A. J. Bradley and A. Taylor, *Physics in Industry: Magnetism* (Institute of Metals, London, 1938), p. 89.
[3] W. Dannohl, Arch. F. Eisenhuttenwesen **15**, 321, 379 (1942).
[4] A. H. Geisler (private communication to the authors).
[5] J. J. Went, Discussion at International Conference on Ferro- and Antiferromagnetism, Grenoble, France (July, 1950). We are indebted to Dr. Casimir for discussing this work with us.
[6] B. Jonas and H. J. M. van Embden, Philips Tech. Rev. **6**, 9 (1941).
[7] R. Smoluchowski, Physica **15**, 179 (1949).
[8] J. E. Goldman, Phys. Rev. **80**, 301 (1950), preceding letter.
[9] E. Both, Laboratory Report of Signal Corps Laboratories—communicated to the authors by J. F. Libsch.

On the Temperature Variations in Alcohol-Argon Filled G-M Counters

OM PARKASH
Punjab University Physics Laboratories, Government College, Hoshiarpur, Punjab, India
August 29, 1950

RECENTLY Tanyel[1] has noticed an improvement in plateau of a xylene-argon filled counter with rest period after filling. This is believed to be due to the formation of a continuous film on the cathode. The partial removal of the film, on heating the counter at 120°C and then cooling it slowly, produced an increase in slope of the plateau, which improved again with time. The effect, which the author[2] reported, in the case of ethyl alcohol-argon filled counters has also been attributed to the alteration of the film. However, our recent experiments, at even higher temperatures than those reported in the previous case, do not seem to confirm the above view, at least, in the particular case of alcohol-argon filled counters.

Counter *B* of the previous communication was successively raised to higher temperatures through 20° steps (up to 180°C) in a thermostat (±0.5°C) and kept at each temperature for 2 to 3 hr. Counting rate-voltage curves were obtained (Fig. 1) at different high temperatures and soon after each heating (within 30 min.) when the counter came to the room temperature. The curves obtained at room temperature before and after heating come out to be practically similar. A very large increase in counting rate and slope of the plateau is observed at high temperatures. Finally the plateau disappears. This is not in accord with the view of Tanyel in that he finds a semipermanent increase in slope which improves with time. If we consider the effect which we reported to be due to the partial removal of the film, then we must assume that either (a) this does not occur within the temperature range investigated or (b) the film removed on heating is restored soon after cooling.

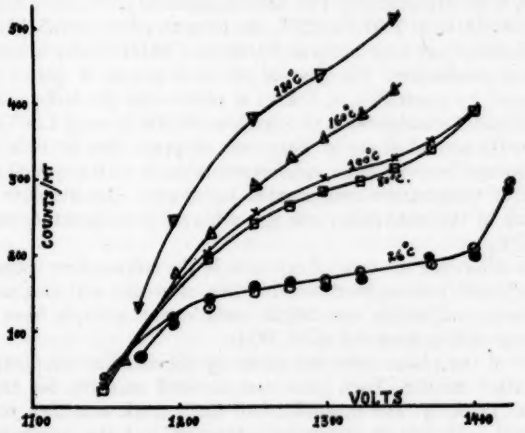

FIG. 1. Counting rate *vs.* voltage curves for counter *B* at different temperatures. Curves (●) before heating and (⊙) after heating at 26°C are exactly similar. Other repetitions have been omitted.

The large counting rate and greater slope at higher temperatures, together with the fact that there is a "residual slope"[3] always present with self-quenching G-M counters, may occur because of the spurious pulses which arise due to the positive ions[4] striking the cathode. If we assume that the secondary emmission from the cathode by the positive polyatomic ions is negligible at ordinary and even higher (?) temperatures, then the positive ions responsible for spurious pulses, and hence for the above-mentioned effects, may be of mercury. That mercury vapor can produce spurious pulses is not unexpected, since mercury has a low ionization potential (10.4 v) with the result that some ions are able to reach the cathode. (It may be mentioned that mercury vapor is always present in the counters owing to the mercury manometers, etc., which are connected with the filling apparatus.) However, the mercury ions are probably less effective at ordinary temperatures[5] but more important at high temperatures[6] and this explains the mentioned effects. Simpson[7] has recently reported an increase in slope in neon-argon counters from 0.035 to 0.11 percent per volt with mercury contamination and organic vapor impurities from greases. This supports the above view and further shows the effect of mercury vapor even at ordinary temperatures. The author's observations, therefore, seem to be a temperature effect rather than the cathode film effect. Detailed work on temperature effects in counters with and without mercury vapor contamination will be reported.

Thanks are due Dr. H. R. Sarna, Director of the Punjab University Physics Laboratories, for providing facilities for this work.

[1] B. Tanyel, Phys. Rev. **77**, 843 (1950).
[2] Om Parkash, Phys. Rev. **76**, 568 (1949).
[3] S. C. Brown and C. Maroni, Rev. Sci. Inst. **21**, 241 (1950).
[4] J. L. Putman, Proc. Phys. Soc. London **61**, 312 (1948).
[5] S. A. Korff, *Electron and Nuclear Counters* (D. Van Nostrand Company, Inc., New York, 1948), p. 115.
[6] I am grateful to Professor S. A. Korff of New York University for suggesting this explanation.
[7] J. A. Simpson, Jr., Rev. Sci. Inst. **21**, 558 (1950).

Multiple Scattering of Fast Electrons in Nuclear Emulsions*

DALE R. CORSON
Cornell University, Ithaca, New York
July 28, 1950

IN view of the increasing importance of multiple scattering in nuclear emulsion work[1] some preliminary scattering measurements on 115±5-Mev electrons in Ilford G-5 plates will be of interest. For each of 50 tracks the y-coordinate was measured with a calibrated eyepiece scale at 50μ-intervals along the x-coordinate. The angle between successive chords drawn between the ends of the intervals is given by $\alpha=D/X$ where D is the second difference $(2y_n-y_{n-1}-y_{n+1})$ and X is the interval length. The mean angle $\langle\alpha(X)\rangle_{Av}$ between chords for interval lengths X of 50, 100, 200, 300, and 400μ has been computed and is shown in Table I. The corresponding mean angle $\langle\alpha(100)\rangle_{Av}$ for a 100μ-interval (computed by assuming α proportional to $X^{\frac{1}{2}}$) is shown for each interval. For short intervals the measured mean angles

TABLE I. Second difference $\langle D(X)\rangle_{Av}$ and mean angle $\langle\alpha(X)\rangle_{Av}$ between successive chords for interval of length X. Also corresponding mean angle $\langle\alpha(100)\rangle_{Av}$ for a 100μ-interval.

X	$\langle D(X)\rangle_{Av}$	$\langle\alpha(X)\rangle_{Av}$	$\langle\alpha(100)\rangle_{Av}$
50μ	0.24μ	0.28°±0.01°	0.40±0.01
100	0.46	0.26 ±0.01	0.26±0.01
200	0.97	0.28 ±0.02	0.20±0.02
300	1.61	0.31 ±0.03	0.18±0.02
400	2.26	0.32 ±0.03	0.16±0.02

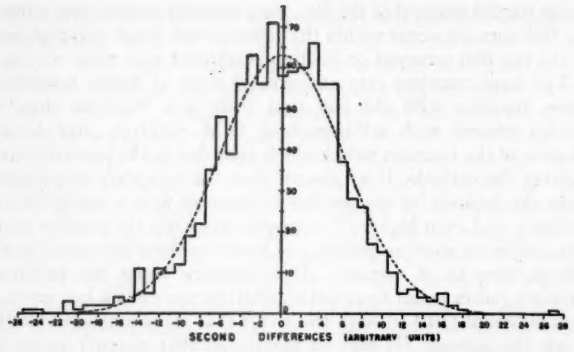

FIG. 1. Distribution curve of second differences (in units of 0.93μ) for 978 intervals of 100μ each. The dotted curve is the corresponding Gaussian distribution with the same mean as for the observed data out to second differences of 20 units.

are always larger than the true mean angles because (1) the observer records the coordinates of the track with an uncertainty Δy, (2) the emulsion may have distortions, and (3) the microscope stage motion may be more or less erratic. There is no evidence for systematic distortions (Fig. 1).

The observer uncertainties and the short-distance microscope irregularities can be treated in the following way. The coordinate y is assumed to be measured with an average uncertainty $\langle\Delta y\rangle_{Av}$. Then one can show that the measured second difference $\langle D_m(X)\rangle_{Av}$ for an interval X is related to the true value $\langle D_T(X)\rangle_{Av}$ by

$$\langle D_m(X)\rangle_{Av}^2=\langle D_T(X)\rangle_{Av}^2+6\langle\Delta y\rangle_{Av}^2.$$

One can show further that

$$\langle D_T(X)\rangle_{Av}=\langle\alpha_T(100)\rangle_{Av}X^{\frac{1}{2}}/(100)^{\frac{1}{2}}$$

so that a $\langle D_m(X)\rangle_{Av}^2$ *vs.* X^3 plot gives $\langle\alpha_T(100)\rangle_{Av}$ and $\langle\Delta y\rangle_{Av}$. Figure 2 is such a plot, giving $\langle\alpha_T(100)\rangle_{Av}=0.17°\pm0.020$ per 100μ. $\langle\Delta y\rangle_{Av}$ is about 0.1μ.

I have arbitrarily attributed all deflections greater than four times the mean to single scattering and therefore eliminated them from consideration here.

The simplest multiple scattering theory with which to compare these data is that of Williams,[2] as modified by Rossi and Greisen.[3] For a relativistic particle the mean projected angle between successive chords of length t (measured in radiation lengths) is given by $\langle\alpha\rangle_{Av}=(2t/3\pi)^{\frac{1}{2}}(21/E)=9.70t^{\frac{1}{2}}/E$ radians per radiation length for a particle of kinetic energy E (measured in Mev). The radiation length is 29,200μ.[4] Using microns and degrees, we have $\langle\alpha\rangle_{Av}$ $=3.25X^{\frac{1}{2}}/E°/X\mu$. For 115-Mev electrons this gives $\langle\alpha\rangle_{Av}=0.28°/100\mu$, which is appreciably greater than the measured value of $0.17°\pm0.02°/100\mu$. The major part of the disagreement probably lies in the maximum angle above which all scatterings are disregarded. As pointed out by Bethe[5] the finite size of the nucleus, which sets an upper limit to the scattering angle in Williams' theory, may not set the limit in such a measurement as this. In fact the angle corresponding to the nuclear radius in this case is 15° or 20° whereas angles greater than about one degree are disregarded.

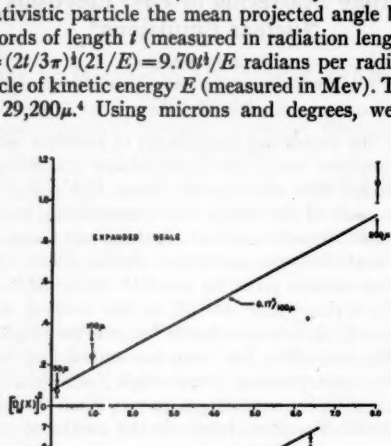

FIG. 2. Plot of second differences squared *vs.* the third power of the interval over which the corresponding second difference was observed. The upper curve is the same portion of the lower curve enclosed by dotted lines but plotted on an expanded scale. The slope of the straight line indicates a mean angle between chords of 0.17°/100μ.

A more satisfactory comparison can be made with the theory of Snyder and Scott.[6] The mean free path λ and the unit angle η_0 of this theory can be calculated for the emulsion to be $\lambda=1.6\times10^{-5}$ cm and $\eta_0=6.2\times10^{-3}$ degree. The mean angle $\langle\alpha\rangle_{Av}$ (considering only angles less than four times the mean) between chords can be computed to give $\langle\alpha\rangle_{Av}=0.20°/100\mu$, which is to be compared with the measured value of $0.17°\pm0.02°$.

I am indebted to Mrs. Margaret Keck for most of the observations on which these measurements are based and to Mr. J. E. Treat for some of the observations.

* This work was supported in part by the ONR.

[1] See Camerini, Fowler, Lock, and Muirhead, Phil. Mag. **41**, 413 (1950).
[2] E. J. Williams, Proc. Roy. Soc. **169**, 531 (1939); Phys. Rev. **58**, 292 (1940).
[3] B. Rossi and K. Greisen, Rev. Mod. Phys. **13**, 240 (1941).
[4] Reference 1 quotes a radiation length of 23,000μ, which I cannot account for unless it is based on some other definition of radiation length.
[5] H. A. Bethe, Phys. Rev. **70**, 821 (1946).
[6] H. Snyder and W. Scott, Phys. Rev. **76**, 220 (1949).

Diurnal Variation of Primary Cosmic-Ray Heavy Nuclei*

J. J. LORD AND MARCEL SCHEIN
Department of Physics, University of Chicago, Chicago, Illinois
September 5, 1950

SINCE the large decrease observed[1-3] in the flux of heavy nuclei at night is of interest in any theory concerning the origin of cosmic rays, additional measurements of greater accuracy and at higher elevations are reported in this paper.

Ilford G-5 photographic plates with emulsions located vertically were arranged in two separate stacks. The plates were placed in a large balloon gondola and covered with a considerable amount of thermal insulating material, since night temperatures in the stratosphere can be as low as −60°C. Several containers of water were placed below the plates so that the heat liberated in the formation of ice kept the temperature of the plates above 0°C.

A General Mills-type balloon was employed to expose the plates in the stratosphere and was launched at 6:00 P.M. on May 22, 1950, from Minneapolis. The balloon attained an altitude higher than 90,000 ft. at 7:50 P.M. CST, and from this time until 5:40 A.M. the balloon was kept between 90,000 and 94,000 ft. by a ballast release mechanism. The first of the two groups of plates was dropped by parachute at 5:45 A.M. After this the balloon rose slightly and remained almost exactly at 95,000 ft. until 12:05 P.M. when the second group of plates was dropped. The altitude was determined from pressure measurements made with a special new type of temperature-compensated barometer. The absolute accuracy of the instrument was ±1 mb over a temperature range of 60°C.

To determine the time of exposure in the stratosphere accurate corrections[2] were applied for the time of ascent and descent of plates as well as the very slight variations of altitude from the average ceiling elevation of 93,500 ft.

All of the plates were developed by the familiar temperature variation method. Each plate was scanned carefully for heavy nuclei tracks at low magnification. Each track was then re-examined with an oil immersion objective and the numbers of delta-rays longer than 1.1μ were enumerated along each track. The tracks were grouped according to their numbers of delta-rays

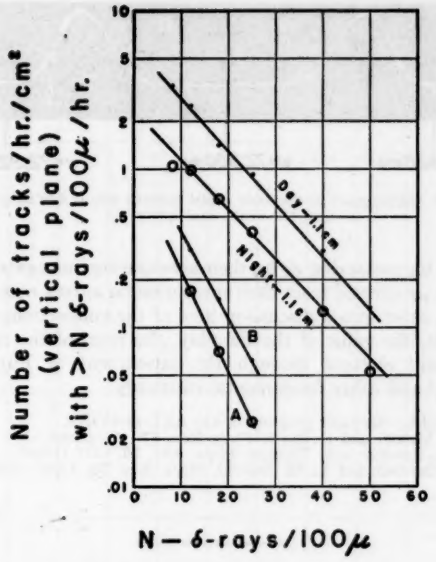

FIG. 1. Number of tracks/cm²/hr. having more than n delta-rays per 100μ. Note that the cm² is in the vertical plane.

per hundred microns. In order to show that temperature variations during the balloon flight could not affect the delta-ray intensities, measurements of the temperature sensitivity of the photographic plates were made which showed that all grain densities of tracks changed less than five percent in the interval of -15 to $+28$°C. At a temperature of -50°C the grain density of tracks of ionization energy loss 15 times the minimum value was reduced by 30 percent from the value at 20°C, while the tracks of minimum ionization were reduced by less than 10 percent in the same temperature interval. Thus the relatively small temperature change (20°C) occurring during the entire balloon flight could have no effect on the delta-ray intensity. This is substantiated further by the fact that the delta-ray intensity of primary nuclei of $Z\cong 26$ (iron nuclei) is the same on both the day and night portions of this balloon flight.

The flux of heavy nuclei having more than n delta-rays per hundred microns as a function of n is given in Fig. 1. In the interval from $n=10$ to $n=55$ the atomic number changes from $Z\cong 10$ to $Z\cong 26$. The upper two curves give the results of the measurements described in this paper. The ratio of the flux of heavy nuclei during the day to that at night is 2.55 ± 0.26, and within experimental error is the same for all atomic numbers from $Z\cong 10$ to $Z\cong 26$. As given previously[2] the two curves marked A and B (Fig. 1) give, respectively, the corresponding intensities during the night and during the day at an elevation of approximately 70,000 ft. The steeper slope of the curves, A and B, at 70,000 feet is the result of the increase of the absorption cross section of heavy nuclei with Z (atomic number).

The effect to be expected at sea level due to this observed diurnal variation of heavy nuclei can be estimated. Such an estimate is based on the known altitude variation of the rate of production of relativistic particles by nuclear interactions produced by the primary heavy nuclei, which will be published shortly. If approximately one-half of the relativistic particles produced are assumed to be mesons of high energy, then a change of the order of 0.1 percent would be produced in the total meson component at sea level by the observed diurnal variation of heavy nuclei. This is in agreement with the magnitude (0.3 percent) of the well-established diurnal variation of the total intensity of cosmic rays at sea level.[4,5] This diurnal variation of heavy nuclei would also account for the observed absence of any change with altitude in the time variation of the total cosmic-ray intensity.[6,7]

Measurements will need to be made at geomagnetic latitudes of less than about 40° in order to determine whether or not only low energy heavy nuclei are responsible for the observed diurnal effect. The evidence given above suggests strongly that the origin of the heavy nuclei is closely related to the sun.

Further experiments are now in progress in which two emulsions in contact are moved at a uniform rate with respect to each other, so that the time at which each heavy nucleus passes through the plates can be determined. This will make it possible to carry out a much more detailed study of the diurnal variation. In addition, the measurements are now being extended to include particles with $Z=6$ to $Z=10$.

The efforts of Mr. C. B. Moore of the General Mills Company in making possible such an excellent balloon flight and in arranging for highly accurate altitude determinations is gratefully acknowledged. We would also like to thank Mr. J. Litwin for his assistance in the measurements.

* Assisted by the joint program of the ONR and AEC.
[1] J. J. Lord and Marcel Schein, Phys. Rev. **78**, 321 (1950).
[2] J. J. Lord and Marcel Schein, Phys. Rev. **78**, 484 (1950).
[3] Freier, Ney, Naugle, and Anderson, Phys. Rev. **79**, 206 (1950).
[4] V. F. Hess and H. Th. Graziade, Terr. Mag. **41**, 9 (1936). W. Kolhorster, Physik. Zeits. **42**, 55 (1941). H. Alfven and K. G. Malmfors, Arkiv. f. Mat. Astr. Phys. **29**, A. No. 24 (1943).
[5] H. Elliot and D. W. N. Dolbear, Proc. Roy. Soc. **A63**, 137 (1950).
[6] D. W. N. Dolbear and H. Elliot, Nature **165**, 353 (1950).
[7] T. A. Bergstralh and C. A. Schroeder, Phys. Rev. **80**, 134(A) (1950).

A Direct Determination of the Magnetic Moment of the Proton in Nuclear Magnetons*

F. BLOCH AND C. D. JEFFRIES
Department of Physics, Stanford University, Stanford, California
September 5, 1950

THE method of Alvarez and Bloch[1] for reducing the measurement of a magnetic moment in units of the nuclear magneton μ_n to that of a frequency ratio has been applied to the magnetic moment μ_P of the proton. If ν_N and ν_R are the frequencies of nuclear resonance and orbital rotation, respectively, of a proton, both measured in the same homogeneous magnetic field H, one has

$$\nu_N = 2H\mu_P/h, \tag{1}$$

$$\nu_R = eH/2\pi Mc \tag{2}$$

(h = Planck's constant, e = elementary charge, c = velocity of light, M = mass of proton), and therefore

$$\mu_P/\mu_N = \mu_P/(eh/4\pi Mc) = \nu_N/\nu_R. \tag{3}$$

By means of relation (3) we have determined μ_P/μ_n with a relative accuracy better than 1/10,000; since nuclear induction makes it easily possible within a few parts in 100,000, both to measure ν_N and to ascertain the homogeneity of the magnetic field, the problem consisted essentially in an accurate determination of ν_R. This has been achieved by the arrangement schematically indicated in Fig. 1. A proton beam of 20,000 ev, originating from the arc source A passes through a tube T of 4 ft. length with three differential pumping stages before entering into the gap of the electromagnet M and the dee cavity of a very small decelerating cyclotron; the diameter of the dees is 8.5 cm and their width is 1.7 cm. Up to the injection region R, the path is held approximately straight by nine compensating electrodes C and the last injection

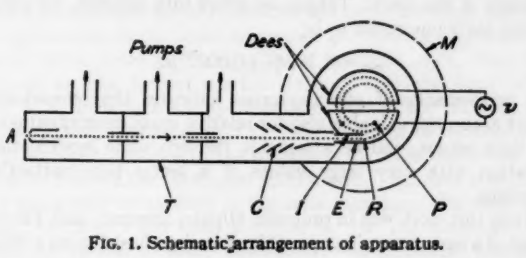

FIG. 1. Schematic arrangement of apparatus.

electrode E, which compensate the Lorentz force due to the motion of the protons in the magnetic field. Beyond R, the path becomes a slowly shrinking spiral with the dee voltage chosen slightly above the minimum of about 100 v, necessary to allow clearance of the injection plate I of 0.25 mm thickness after the first revolution. ν_R is determined from the dee frequency ν at which protons reach the inner probe P, protruding into the dee cavity. Since the magnetic field has to be shimmed to very great homogeneity and, therefore, could not provide magnetic focusing, we relied principally upon phase focusing to hold the protons within the dee cavity; it proved, indeed, sufficient to give probe currents of the order of 10^{-12} amp. after about 500 revolutions. This arrangement has the following advantages.

(1) Independently of the arc pressure, the pressure in the dee chamber can be made low enough so that gas collisions and ionization do not affect the measurement.

(2) Contrary to accelerating operation, the decelerating cyclotron can be operated not only at a dee frequency in the vicinity of $\nu=\nu_R$, but also of $\nu=n\nu_R$, where n is an odd integer. For a given number of revolutions, the higher multiples provide a correspondingly more accurate timing of the protons and the resonance band width is thereby reduced by $1/n$. A further reduction of the band width is due to the circumstance that the energy change of the protons per revolution becomes appreciably less when they have reached a radius sufficiently small so that the transit time between the dees becomes comparable to the period of the dee oscillation. Consequently, with the dee voltage still high enough to allow clearance of the injection plate, the number of revolutions which are necessary to reach the probe at a given position increases with increasing n, so that additional gain in resolution is obtained.

The measurements were carried out at a field $H\cong 5300$ gauss where the frequency of rotation is $\nu_R\cong 8.1$ Mc, and we have successfully operated the dees near all odd multiples of ν_R from the first to the eleventh. The consistency of the results obtained for the higher multiples gave a gratifying confirmation of our accuracy. Observations were made by applying a slight modulation with a period of 4 sec. to the dee frequency and by photographing the trace on an oscillograph whose vertical deflection gave a measure of the instantaneous probe current. Figure 2 shows a typical trace, taken around $\nu=9\nu_R$ with the same frequency interval covered twice as the small modulating condenser goes through a full revolution. The shape of the traces has been qualitatively understood in terms of the focusing action and its variation with ν. The relative half-width has been found to be about 1/200 for $n=1$; the expected gain in resolution was confirmed by the corresponding values 1/4000 and 1/10,000 found for $n=5$ and $n=11$, respectively. A marker was produced on each trace by the beat with a frequency meter, thus providing a highly precise record of the dee frequency. A small nuclear induction head, movable within the dee chamber, gave the nuclear resonance frequency ν_N of protons in water; the signal from this head was also used to hold H constant during runs and to ascertain homogeneity between the monitoring position and the inner region of the dees.

To insure an accurate result we have searched carefully for systematic errors: analysis showed that relativistic corrections were negligible; both by analysis and by experiment it was further shown that space-charge effects, collisions of the protons, fringing fields from the injection electrode, and distortions of the oscillating dee field by the probe likewise did not affect the accuracy of the result. Taking all errors into account, we can at present state our result to be

$$\mu_P=(2.79245\pm 0.0002)\mu_n. \quad (4)$$

The performance of our apparatus indicates that considerably higher accuracy, valuable also for relative mass determinations of the light atoms, will be attainable through some modifications; operation with very large values of n seems here particularly promising.

While this work was in progress, Hipple, Sommer, and Thomas[2] reported a new determination of the Faraday, based upon a similar principle for measuring ν_R by their accelerating "omegatron"; the value for μ_P derived from their measurement agrees with (4). We shall not enter into a discussion here of the connections between our result, the value of the Faraday, the ratio of the masses of proton and electron through the experiment of Purcell and Gardner,[3] and other fundamental constants.

FIG. 2. Oscillogram of detector probe current *versus* dee frequency near the ninth multiple of ν_R.

* Assisted by the joint program of the AEC and ONR.
[1] L. W. Alvarez and F. Bloch, Phys. Rev. **57**, 111 (1940).
[2] Hipple, Sommer, and Thomas, Phys. Rev. **76**, 1877 (1949).
[3] J. H. Gardner and E. M. Purcell, Phys. Rev. **76**, 1262 (1949).

Calculation of the Absorption and Emission Spectra of the Thallium-Activated Potassium Chloride Phosphor

FERD E. WILLIAMS
General Electric Research Laboratory, Schenectady, New York
August 25, 1950

PREVIOUS interpretations of solid-state luminescent phenomena have been either qualitative or phenomenological.[1] Therefore, it is important to calculate quantitatively the properties of a simple phosphor from first principles. The calculation of the peak absorption and emission energies for KCl:Tl has already been reported.[2] Improvements in the theory have permitted the determination of the absorption and emission spectra and their temperature dependence.

It is first recognized that the KCl:Tl phosphor is an ionic crystal[3] and that the luminescence arises from transitions characteristic of Tl^+ substituted in dilute concentration for K^+ ions.[4] The radial charge densities of free Tl^+ in the ground $^1S_0$ state and in the excited $^3P_1^0$ state are evaluated using the Sommerfeld modification[5] of the Fermi-Thomas method for the core and the Hartree self-consistent field method[6] for the two outer shell electrons. From these wave functions and from the known ionic radius r_0, polarizability α, and repulsion energy constant ρ for the ground state,[3] these parameters are evaluated for the Tl^+ in the excited state interacting with Cl^-. The method of Kirkwood[7] is used to determine α. The variation of repulsion energy with interatomic distance a is shown to be equal to the variation of S^2/a with a, where S is the overlap integral: $\int\Psi_{Tl^+}\Psi_{Cl^-}dV$. The Tl^+ in the $^1S_0$ and the $^3P_1^0$ states are substituted in dilute concentrations for the K^+ in the KCl, and the change in total energy of the system is calculated as a function of the change in the $Tl^+(000)$ nearest $Cl^-(100)$ distance Δr with the condition that the remainder of the lattice rearranges to minimize the total energy. A good approximation to this condition requires only displacement $\Delta r'$ of the $K^+(200)$ radially from the Tl^+ to the position $\Delta r_m'$ of minimum energy. Only symmetric displacements in Δr and $\Delta r'$ are considered. Madelung, exchange repulsion, van der Waals, and ion-dipole interactions are included. For the $^3P_1^0Tl^+$, the Coulomb overlap interactions determined from the free ion wave functions are included. After transformation to the $\Delta r_m'$ plane, the total energy *versus* the configuration coordinate Δr is plotted in Fig. 1 for the $^1S_0$ and $^3P_1^0$ states. It should be noted that the equilibrium Tl^+ nearest Cl^- distance is less for the excited than for the ground state. The energies are fitted to the plotted parabolas by mini-

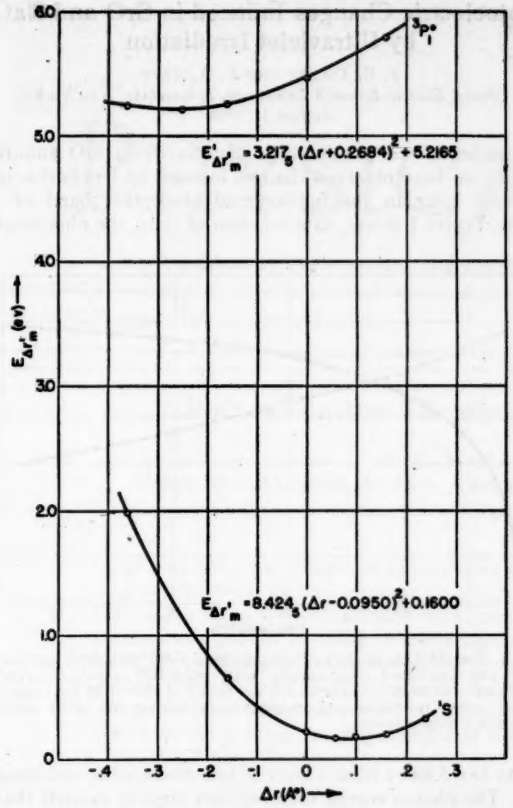

FIG. 1. Variation in total energy *versus* configuration coordinate for the $^1S_0$ and $^3P_1^0$ states of Tl^+ in KCl.

mizing the squared deviations. The absorption spectrum is computed by recognizing that the various atomic configurations of the system in the ground state have probabilities in accord with a Boltzmann function:

$$P(\Delta E) = C \exp[-(E-E_0)/kT] d(\Delta r)/d(\Delta E),$$

where $P(\Delta E)$ is the probability of the transition energy ΔE and C is a normalization constant. The emission spectrum is similarly determined using $E'-E_0'$. The calculated spectra are compared with experiment[8] on Fig. 2 for 298°K. The agreement is satisfactory. The broader theoretical emission spectrum may arise from using free ion wave functions for calculating the Coulomb overlap correction, or from neglecting the rearrangement energies of other

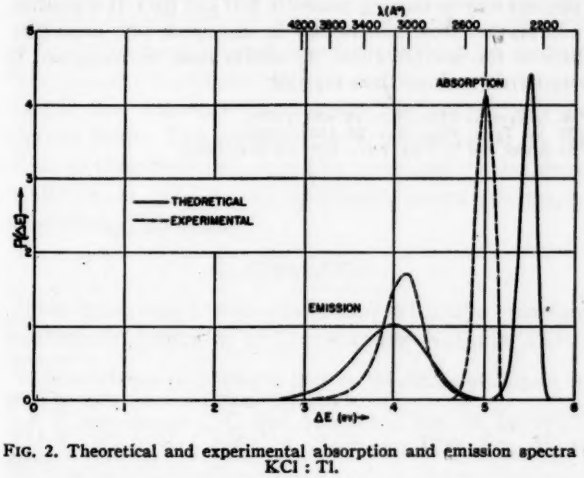

FIG. 2. Theoretical and experimental absorption and emission spectra of KCl : Tl.

neighbors for the configurations of large $|\Delta r|$. The theoretical temperature dependences of the spectra are also found to be in good agreement with experiment, the half-widths of both absorption and emission being halved in going to 80°K.

The author is indebted to E. Alden, C. Carter, D. Cusano, J. Marinace, J. Martens, R. Speck, and L. Stevens for performing the detailed calculations, and to M. H. Hebb for helpful suggestions. The complete manuscript on the detailed methods, calculations, and implications of this work is being assembled.

[1] F. E. Williams, J. Opt. Soc. Am. **39**, 648 (1949).
[2] F. E. Williams, Phys. Rev. **73**, 1257A (1948).
[3] J. E. Mayer, J. Chem. Phys. **1**, 270, 327 (1933).
[4] F. Seitz, J. Chem. Phys. **6**, 150 (1938).
[5] A. Sommerfeld, Zeits. f. Physik **78**, 284 (1932).
[6] D. R. Hartree, Proc. Camb. Phil. Soc. **24**, 89, 111 (1928).
[7] J. G. Kirkwood, Physik. Zeits. **33**, 57 (1932).
[8] W. Koch, Zeits. f. Physik **57**, 638 (1929); W. von Meyeren, Zeits. f. Physik **61**, 321 (1930); P. D. Johnson (unpublished data of this laboratory).

Photo-Disintegration of O^{16}

MELVIN A. PRESTON*
National Research Council of Canada, Chalk River, Ontario, Canada
August 31, 1950

THE reaction $O^{16}(\gamma,\alpha)C^{12}$ has been studied theoretically using an α-particle model of the O^{16} nucleus. Since the identity of charge and mass centers eliminates dipole transitions, the effect has been assumed to be quadrupole. The experiments of Millar and Cameron[1] show that the cross section of this reaction as a function of γ-energy is fairly sharply peaked and has a maximum between 16 and 18 Mev. Since this is well above the Coulomb barrier of C^{12}, it has been considered reasonable to treat the emitted particle as a plane wave and to apply a barrier penetrability factor for the lower energies. We assume that the wave function can be written as $\phi(\mathbf{r})\Psi$, where ϕ is a function of the coordinates of the ejected particle and Ψ depends on those of the other three. We consider the effect of the γ-ray on only the ejected particle, and we are led to matrix elements of the type $\int \Psi_f^* \exp(i\mathbf{p}\cdot\mathbf{r}/\hbar) x_3 \Psi_0 \phi_0(\mathbf{r}) d\tau$. Ψ_f is the wave function of the ground state of C^{12}; this should overlap Ψ_0 considerably. Moreover, it is reasonable to neglect the interaction of the γ-ray with the other particles, at least until there is sufficient energy to emit further α-particles; this threshold is at 18 Mev. Even then this interaction can be neglected until the cross section of the competing process is appreciable; results of Millar and Cameron indicate that this is still small at $E_\gamma = 21$ Mev. We put the integral of $\Psi_f^*\Psi_0 \doteq 1$; actually, it is smaller, but is energy independent in the region considered. [This model does not permit the calculation of the $(\gamma-n)$ and $(\gamma-p)$ processes, but their presence does not affect our results.]

We obtain

$$\sigma(\theta) = \pi(27me^2/\hbar^6c^3)E_\gamma^2 p \left| \int_0^\infty r^4 j_2(pr)\phi_0(r)dr \right|^2 \sin^2\theta \cos^2\theta$$

(m = proton mass). For energies below the Coulomb barrier ($E_\gamma < 12$ Mev), σ is multiplied by the penetration factor. For ϕ_0, we have used the forms: $\exp(-r/b)$, $\exp(-r^2/b^2)$ and modified Wheeler wave functions. Following Wheeler,[2] we have thought of O^{16} as a tetrahedron of four α-particles with a wave function

$$\prod_{i=1}^{4} \exp\{-\beta(1-\alpha)R_i^2\} \prod_{i<j} [\exp\{-\tfrac{1}{4}\beta\alpha R_{ij}^2\} - \exp\{-\tfrac{1}{4}\beta(\alpha+\epsilon)R_{ij}^2\}].$$

This insures that no two particles will come too close together, nor will any be too far from the center. By ignoring the vibrations of the other three particles a wave function, $\phi_0(\mathbf{r})$, has been deduced for the ejected particle. It is of the form $\exp(-r^2/b^2) \times f(r, a/b)$, in which a is the distance from a face centroid to a vertex of the tetrahedron. With this model it is reasonable to consider that the radius of the nucleus is $(3/4)(2a^2+b^2)^{\frac{1}{2}} = r_0$.

Figure 1 shows the total cross section $\sigma(E_\gamma)$. All the curves have been arbitrarily normalized to the same maximum. For each type of ϕ_0, the range b has been adjusted so that the maximum of σ occurs at $E_\gamma = 17.6$ Mev. Preliminary experimental points of

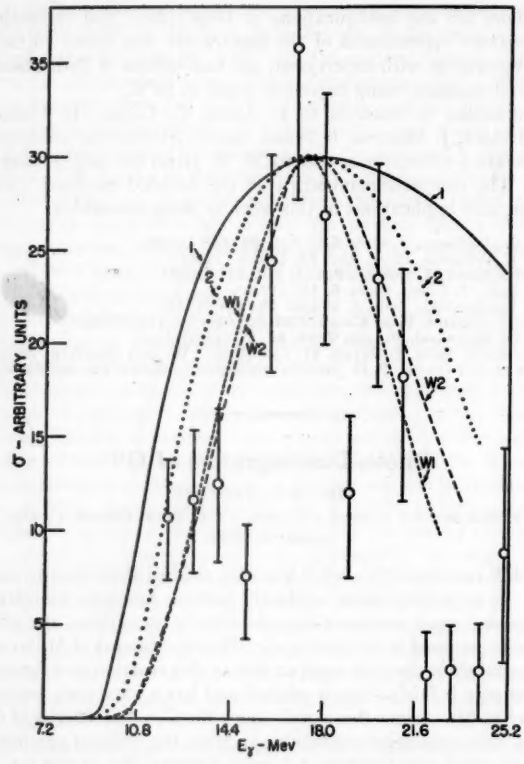

FIG. 1. $\sigma(E_\gamma)$ for various ϕ_1. 1. $\exp(-r/b)$, $b=0.8\times10^{-13}$ cm. 2. $\exp(-r^2/b^2)$, $b=2.45\times10^{-13}$. W1. $b/a=2^{\frac{1}{2}}$, $b=3.53\times10^{-13}$, $r_0=3.7\times10^{-13}$. W2. $b/a=2$, $b=5.19\times10^{-13}$, $r_0=4.7\times10^{-13}$.

Millar and Cameron are shown; the errors indicated are merely the statistical errors. The data represent 109 events. It will be observed that the tetrahedral function produces a narrow peak (which the data seem to indicate) and maximizes σ for a correct energy with a reasonable nuclear radius. However, the Gaussian wave function is much easier to use and gives only a slightly too wide peak.

Wäffler and Younis[3] give $\sigma(17.5\text{ Mev})=(1.8\pm0.6)\times10^{-4}$ barn. For the curve W1, the absolute value is $\sigma(17.6)=3\times10^{-3}$ barn. This is to be multiplied by

$$\left|\int\Psi_f^*\Psi_0\right|^2<1$$

and hence is an upper limit and an order of magnitude estimate only.

A more complete description of this work will be submitted to the *Canadian Journal of Research*. I am indebted to Dr. J. D. Jackson for discussions of this problem.

* Permanent address: Department of Physics, University of Toronto, Toronto, Canada.

[1] C. H. Millar and A. G. W. Cameron, Phys. Rev. **78**, 78 (1950) and private communication.

[2] J. A. Wheeler, Phys. Rev. **52**, 1083 (1937).

[3] H. Wäffler and S. Younis, Helv. Phys. Acta **22**, 614 (1949).

Photoelectric Changes Induced in SrO and BaO by Ultraviolet Irradiation

J. E. DICKEY AND E. A. TAFT
General Electric Research Laboratory, Schenectady, New York
August 31, 1950

IN studies of the photoelectric emission from SrO and BaO films, we have observed changes induced by irradiation with ultraviolet lying in the fundamental absorption band of the crystals. Figure 1 shows, as a function of time, the photoelectric

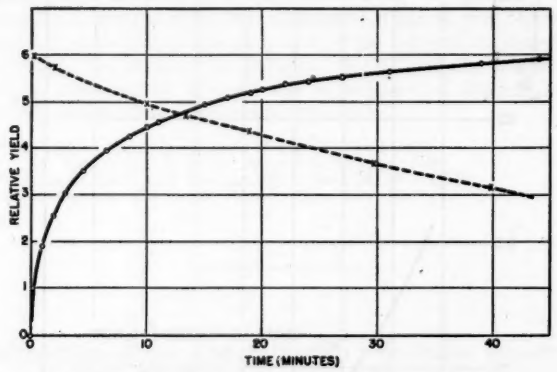

FIG. 1. The solid curve shows the increase of yield with time as a sample of SrO was irradiated continuously with $\sim2\times10^{12}$ quanta/sec./cm^2 at $h\nu=5.80$ ev. The broken curve shows the decay of this yield (at room temperature) when radiation was incident only during the short intervals necessary for measurement.

yield at $h\nu=5.80$ ev from a layer of SrO produced by oxidizing Sr metal. The photon energy involved here slightly exceeds that at the fundamental absorption edge of SrO as measured by Sproull.[1] Since the electron affinity of SrO is probably of the order of 1 ev, photoelectric ejection of electrons from the occupied energy band of the crystal is not possible at this $h\nu$-value. In agreement with this statement, the photoelectric yield was initially very small. It rose rapidly, however, as shown in Fig. 1, the initial increase being linear in time. After some minutes, the curves saturated. If the irradiation was stopped, the photoelectric yield measured in subsequent intervals decreased with time. Similar results[2] were obtained with BaO by irradiating with $h\nu>3.8$ ev. The initial yield in this case was usually measurable, however, and was probably due to excess Ba or other impurities.

These phenomena are very much like those observed when F-centers are formed in an alkali halide by irradiation in its fundamental absorption band.[3] The results given here suggest that excitions (or free electrons and holes) produced by the absorption of photons may be forming centers in SrO and BaO. It is possible, of course, that these centers may be associated with impurities. Whatever the interpretation, the effects must be recognized in photoelectric work on these crystals.

[1] R. L. Sproull, Phys. Rev. **78**, 630 (1950).

[2] W. W. Tyler, Phys. Rev. **76**, 1887 (1949).

[3] L. Apker and E. Taft, Phys. Rev. **79**, 964 (1950).